Volume XXIII

VIBRATIONS
IN PHYSICAL SYSTEMS

VIBRATIONS IN PHYSICAL SYSTEMS

Editor: Czesław CEMPEL
Co-Editor: Marian W. DOBRY
Secretary: Tomasz STRĘK

Editorial Committee

Czesław CEMPEL – chairman, Jarosław STEFANIAK –co-chairman, Jan AWREJCEWICZ, Roman BOGACZ, Marian W. DOBRY, Zbigniew ENGEL, Antoni GAJEWSKI, Stefan JONIAK, Jan KOŁODZIEJ, Krzysztof MARCHELEK, Bogdan MARUSZEWSKI, Stanisław MATYSIAK, Jan HOLNICKI–SZULC, Józef NIZIOŁ, Bogdan SKALMIERSKI, Tomasz SZOLC, Andrzej TYLIKOWSKI Franciszek TOMASZEWSKI, Józef WOJNAROWSKI, Czesław WOŹNIAK

Organizing Committee

Tadeusz WEGNER – chairman, Małgorzata WOJSZNIS – secretary, Czesław CEMPEL, Marian W. DOBRY, Bogdan MARUSZEWSKI, Marian OSTWALD, Jarosław STEFANIAK, Jacek KUBIAK, Piotr STASIEWICZ, Tomasz STRĘK, Elżbieta SZYMKOWIAK

Reviewers

Jan KICIŃSKI, Krzysztof MAGNUCKI, Zdzisław GOLEC, Roman BARCZEWSKI, Stefan JONIAK, Andrzej GARSTECKI, Marian OSTWALD, Marian W.DOBRY, Bartosz CZECHYRA, Marek IWANIEC, Roman BOGACZ, Janusz MIELNICZUK, Jarosław STEFANIAK, Zbigniew ENGEL, Józef NIZIOŁ, Józef WOJNAROWSKI, Jan KOŁODZIEJ, Franciszek TOMASZEWSKI, Jan AWREJCEWICZ, Bogdan MARUSZEWSKI, Tadeusz HOFFMANN, Andrzej MILECKI, Roman LEWANDOWSKI, Tadeusz UHL, Maria GOLEC, Jerzy ZIELNICA, Jacek BUŚKIEWICZ, Maciej TABASZEWSKI

Sponsors

Dean of Mechanical Engineering and Management Faculty
Foundations for Development of Poznan University of Technology

POZNAN UNIVERSITY OF TECHNOLOGY
MECHANICAL ENGINEERING AND MANAGEMENT FACULTY
INSTITUTE OF APPLIED MECHANICS
POLISH SOCIETY OF THEORETICAL AND APPLIED MECHANICS

Volume XXIII

VIBRATIONS
IN PHYSICAL
SYSTEMS

Editors
Czesław CEMPEL
Marian W. DOBRY

Poznan 2008

CONTENTS

INVITED PAPERS

PAPERS

INTRODUCTION TO THE VOLUME XIII OF COLLECTED PAPERS ON VIBRATIONS IN PHYSICAL SYSTEMS

As Heraclites said a long time ago: **'panta rei'-** all is moving, all is flowing, all phenomena behave dynamically, not always stationary, but sometimes having great oscillating component. Every two years some leading specialists in this field of investigation come to present the papers and discuss some important issues in such broad context of dynamics**.** This is possible in the frame of the "**Vibrations in Physical Systems**" Symposium, which has been organized since 1960 by the Poznań branch of the Polish Society of Theoretical and Applied Mechanics and the Institute of Applied Mechanics of Poznań University of Technology. This volume, entitled **Vibration in Physical Systems,** is the collection of delivered papers on this occasion.

The scope of these Symposia are not only dynamical problems of the pure mechanical systems, that means wave propagation, vibrations etc. in solids, fluids and mechanical constructions but also dynamical problems of heat conduction, electromagnetic waves and its influence on mechanical behavior of the medium. There are also some new and important areas of dynamic investigation like bio-systems including a human under motion and/or vibration. Finally, the important part of research nowadays is done by simulation, so some papers discuss this in terms of methodology, and/or obtained result.

In mechanics, these oscillations and / or vibration can be observed as the vibration of the structure of our interest and / or the surrounding environment. Depending on the medium of propagation (solid, gas, fluid) they can be observed as the vibration, sound or even the noise. In general they play at least three side roles.

First of all, they can carry information about the existence of the system, and also on its overall and technical condition and safe use. This is the cause they have been used more and more currently for the assessment of system condition, complex machines and equipment in particular. Some papers touch this problem directly or indirectly, considering some phenomena which can improve the reliability of the diagnostic decision.

Secondly and mostly, the influence of vibration on structures and the environment can be harmful. Of course, it depends on the characteristics of the vibration processes, the energy and its amplitude – frequency characteristics. For the structures and machines it gives mostly fatigue effects which degrade the system, its efficiency and safety. The most pronounced cases of large amplitude vibrations concerning large areas are the earthquakes, which can bring disaster to many buildings and the infrastructure. Prevention of such damaging effect is an area of intensive research. In some other cases of metrology and cutting machines the undisturbed position of some objects or its part are required as the conditions for the accuracy and quality of production process or service, the quality of work and life comfort of humans if the noise and vibration processes influence workers or inhabitants. Several papers investigating these important aspects of vibration are delivered in this volume.

Thirdly, vibration processes are carriers of energy in many cases of mechanical technology and civil engineering. They are used to transport the medium or some parts, as well as in crashing and cleaning processes. What is important in some other technological processes, is that the small additional vibration process can diminish the friction greatly, or enable to use much less energy to provide the needed operation. Some papers of this volume are dedicated to these, not new but important problems.

As it is usually, the papers were reviewed by the members of Scientific Committee, or in some cases by independent colleagues outside of committee, if our competence was too narrow. On the behalves of all participants of the Symposium, the user of our product, we would like to thank all reviewers for their contribution in bettering the quality of our discussion during the Symposium and the publication, as well.

<p style="text-align:center">Editors</p>

<p style="text-align:center">Czesław CEMPEL</p>

<p style="text-align:center">Marian W. DOBRY</p>

MODELLING AND SIMULATION OF TRIPLE PHYSICAL PENDULUM

Jan AWREJCEWICZ, Grzegorz KUDRA and Grzegorz WASILEWSKI
Technical University of Łódź, Department of Automatics and Biomechanics
1/15 Stefanowskiego St., 90-924 Łódź, Poland
Tel./fax: +48426312225, e-mail: awrejcew@p.lodz.pl, grekudra@p.lodz.pl

Abstract

Plane triple pendulum periodically forced is investigated both experimentally and numerically. Mathematical modeling includes details taking into account some characteristic features (real characteristics of joints built by the use of roller bearings) as well as some imperfections of the real system. Parameters of the model are obtained by estimation from the experimental data. Then the experimental and numerical analysis of the system is performed.

Introduction

A pendulum as a simple nonlinear systems is still a subject of interest of scientists from all the world. It is caused by simplicity of that system on the one hand, and due to many fundamental and spectacular phenomena exhibited by a single pendulum on the other hand. In mechanics and physics investigations of single and coupled pendulums are widely applied. Lately, even the monograph on the pendulum has been published [1]. This is a large study on this simple system also from the historical point of view.

Although a single or a double pendulum (in their different forms) are quite often studied experimentally [2,3], a triple physical pendulum is rather rarely presented in literature from a point of view of real experimental object. For example, in the work [4] the triple pendulum excited by horizontal harmonic motion of the pendulum frame is presented and a few examples of chaotic attractors are reported. Experimental rigs of any pendulums are still of interest of many researchers dealing with dynamics of continuous multi degrees-of-freedom mechanical systems. The model having such a properties has been analyzed in work [5]. It consists of a chain of N identical pendulums coupled by dumped elastic joints subject to vertical sinusoidal forcing on its base.

In February, 2005, in the Department of Automatics and Biomechanics, the experimental rig of triple physical pendulum was finished and activated. This stand has been constructed and built in order to investigate experimentally various phenomena of nonlinear dynamics, including regular and chaotic motions, bifurcations, coexisting attractors, etc.

In order to have more deep insight into dynamics of the real pendulum, the corresponding mathematical model is required. In the work [6] the suitable mathematical modeling and numerical analysis have been performed, where the viscous damping in the pendulum joints (constructed by the use of rolling bearings) has been assumed. In

the next step [7], we have also taken into account the dry friction in the joints with many details and variants. Here we present the model of friction taking into account only essential details.

1. Experimental rig
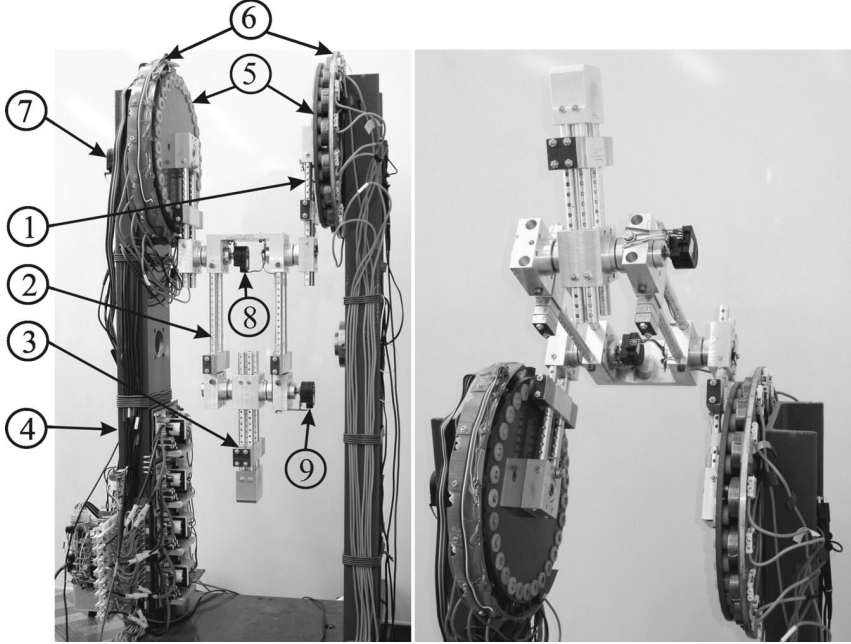
Figure 1. Experimental rig: 1, 2, 3 - links; 4 - stand; 5 - rotors; 6 - stators; 7, 8, 9 - rotational potentiometers.

The experimental rig (see Fig. 1) of the triple physical pendulum consists of the following subsystems: pendulum, driving subsystem and the measurement subsystem. It is assumed that the pendulum is moving in a plane.

The links (1, 2, 3) are suspended on the frame (4) and joined by the use of radial and axial needle bearings. The first link is forced by a special direct-current motor of our own construction with optical commutation consisting of two stators (6) and two rotors (5). The construction ensures avoiding the skewing of the structure and forming the forces and moments in planes different that the plane of the assumed pendulum motion. On the other hand the construction allows the full rotations of all the links of the pendulum.

The voltage conveyed to the engine inductors is controlled by the use of special digital system of our own construction together with precise signal generator HAMEG. As a result the square-shape in time forcing (but with some asymmetry - see the next sections) with adjustable frequency and desired amplitude is obtained.

The measurement of the angular position of the three links is realized by the use of the precise rotational potentiometers (7, 8, 9). Then the LabView measure-programming system is used for experimental data acquisition and presentation on a computer.

2. Mathematical model

Details on physical modeling, i.e. idealized physical concept (see Fig. 1) of real pendulum presented in Fig. 2 can be found in works [6, 7]. The system is idealized since it is assumed that it is an ideally plane system of coupled links, moving in the vacuum with the assumed model of friction in joints.
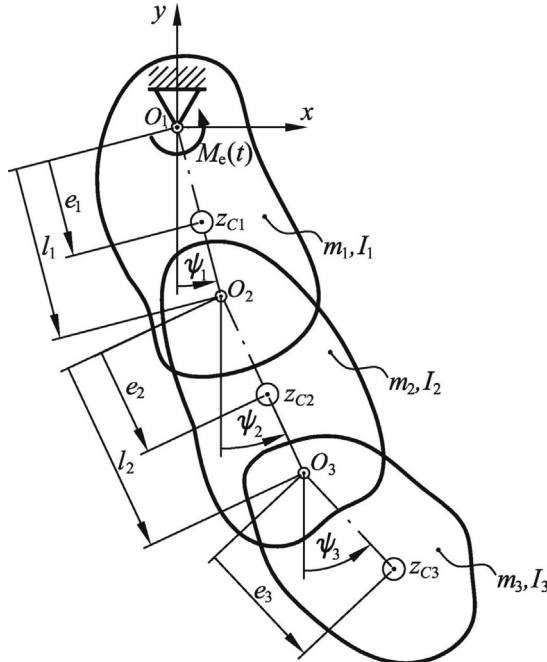
Figure 2. Physical model of triple pendulum.

The system is governed by the following set of differential equations:

$$
\begin{bmatrix}
B_1 & N_{12}\cos(\psi_1-\psi_2) & N_{13}\cos(\psi_1-\psi_3) \\
N_{12}\cos(\psi_1-\psi_2) & B_2 & N_{23}\cos(\psi_1-\psi_2) \\
N_{13}\cos(\psi_1-\psi_3) & N_{23}\cos(\psi_1-\psi_2) & B_3
\end{bmatrix}
\begin{Bmatrix}
\ddot{\psi}_1 \\
\ddot{\psi}_2 \\
\ddot{\psi}_3
\end{Bmatrix} +
$$

$$+\begin{bmatrix} 0 & N_{12}\sin(\psi_1-\psi_2) & N_{13}\sin(\psi_1-\psi_3) \\ -N_{12}\sin(\psi_1-\psi_2) & 0 & N_{23}\sin(\psi_1-\psi_2) \\ -N_{13}\sin(\psi_1-\psi_3) & -N_{23}\sin(\psi_1-\psi_2) & 0 \end{bmatrix}\begin{Bmatrix} \dot{\psi}_1^2 \\ \dot{\psi}_2^2 \\ \dot{\psi}_3^2 \end{Bmatrix}+ \tag{1}$$

$$+\begin{Bmatrix} M_{R1}(\dot{\psi}_1)-M_{R2}(\dot{\psi}_1,\dot{\psi}_2) \\ M_{R2}(\dot{\psi}_1,\dot{\psi}_2)-M_{R3}(\dot{\psi}_2,\dot{\psi}_3) \\ M_{R3}(\dot{\psi}_2,\dot{\psi}_3) \end{Bmatrix}+\begin{Bmatrix} M_1\sin\psi_1 \\ M_2\sin\psi_2 \\ M_2\,N_{13}/N_{12}\sin\psi_3 \end{Bmatrix}=\begin{Bmatrix} M_e(t) \\ 0 \\ 0 \end{Bmatrix}.$$

where the pendulum position is described by the use of three angles ψ_i ($i=1,2,3$) and where

$$M_{R1}=T_1\frac{2}{\pi}\arctan(\varepsilon\dot{\psi}_1)+2c\dot{\psi}_1,$$

$$M_{R2}=T_2\frac{2}{\pi}\arctan(\varepsilon(\dot{\psi}_2-\dot{\psi}_1))+c(\dot{\psi}_2-\dot{\psi}_1), \tag{2}$$

$$M_{R3}=T_3\frac{2}{\pi}\arctan(\varepsilon(\dot{\psi}_3-\dot{\psi}_2))+c(\dot{\psi}_3-\dot{\psi}_2),$$

are the moments of resistance in the corresponding joints and consisting of two parts: dry friction and viscous damping. The dry friction moment does not depend on the loading of the corresponding bearing and the sign function is approximated by the arctan function. The parameter c is the damping coefficient common for the second and third joint while in the first joint we assume damping two times greater (since the first joint is built by the use of four bearings, while each other joint contain two bearings).

In the work [7] more complex model of friction has been investigated where the dry friction moment consists of two part: the first one proportional to the normal loading in the bearing and the second one being constant (and present also in the lack of loading). Moreover the friction is a function of relative velocity due to the Stribeck's curve. As a result of those investigations we have concluded that in our case the model of friction can be simplified to the one presented by the Eq. 2, without any loss of precision.

The external excitation in the pendulum model can be an arbitrary time function, and in particular, it can be the same function as applied (and recorded to a file) in real system (it is useful in the parameter estimation process). On the other hand, it is possible to apply a forcing due to the following mathematical description:

$$M_e=\begin{cases} q & \text{if }(\omega t+\phi_0)\bmod 2\pi \le 2\pi a \\ -q & \text{if }(\omega t+\phi_0)\bmod 2\pi > 2\pi a \end{cases}. \tag{3}$$

which imitates the square-shape in time forcing (applied in the real pendulum), with adjustable angular velocity ω, initial phase ϕ_0 amplitude q and the coefficient a (for $a \neq 0.5$ there is an asymmetry in the forcing, as mentioned in section 1).

3. Model parameters

The model parameters are estimated by the global minimum searching of the criterion-function of the model and real system matching. The matching of model and real system is understood as the matching of the corresponding output signals ψ_i (i=1,2,3) from model integrated numerically and from the real pendulum, assuming the same inputs to both model and real system. The sum of squares of deviations between corresponding samples of signals from model and experiment, for few different solutions, serves as a criterion function. Together with the model parameters also initial conditions of the numerical simulation are estimated. A minimum is searched applying the simplex method. In order to avoid the local minima, the simplex method is stopped from time to time and a random searching is then applied. After random searching the simplex method is restarted again.

If we divide final value of criterion-function by the number of samples used in calculation of criterion-function, we obtain average square of deviation between two signals (obtained from the model and the experiment) - let us denote this parameter as F_{cr} . Now this parameter can be used for comparison of matching of different sets of experimental data and corresponding numerical solutions.

	A_1	B_1	C_1
B_1 [kg·cm^2]	1650.3	1634.7	1641.3
B_2 [kg·cm^2]	386.3	1378.7	1390.9
B_3 [kg·cm^2]	163.32	166.56	164.50
N_{12} [kg·cm^2]	1111.2	1104.5	1112.6
N_{13} [kg·cm^2]	198.99	201.47	199.92
N_{23} [kg·cm^2]	255.96	259.16	257.15
M_1 [N·cm]	879.76	874.38	875.00
M_2 [N·cm]	632.37	628.53	633.13
T_1 [N·mm]	56.83	72.73	97.53
T_2 [N·mm]	25.06	15.16	13.77
T_3 [N·mm]	11.07	4.58	6.61
c [N·mm·s]	*0*	1.057	0.532
ε [s]	*1000*	*1000*	6.77
F_{cr} [rad^2]	0.3255	0.3059	0.2809

Table 1. Parameter estimations.

In the Table 1 the part of the results of the parameter estimations performed in the work [7] is presented. Three different sets of parameters are presented, correspondingly to three variants of the model of resistance in the joints. The set A_1 corresponds to the model with

dry friction only. The model B_1 contains also viscous damping. The next model (C_1) is a development of the previous one (B_1): the parameter ε is added to the set of the identified parameters.

In all the identification processes, the same set of experimental solutions is used: five periodic solutions with the forcing frequencies ($f=\omega/2\pi$): $f=0.2, 0.35, 0.6, 0.85$ and 1.1 Hz (for each the solution the 20 sec of motion was recorded, after ignoring the transient motions) and one decaying solution, which starts from the periodic attractor with forcing frequency $f=0.5$ Hz (after few seconds of the recorded motion, the forcing was switched off and the total length of the recorded motion was 24 sec). Note that in our work, we do not measure actual value of the forcing, but only the control signal is recorded (determining the sign of the forcing), since we assume the constant forcing amplitude $q=1.718$ Nm (determined before the identification experiments).

4. Simulation results

The Figure 3 contains a bifurcation diagram for the mathematical model (C_1) with the forcing frequency f as a bifurcation parameter. The chaotic window for $f \in (0.698, 0.771)$ can be here observed, which is confirmed well by the experimental observations from which we have the chaotic zone for $f \in (0.695, 0.774)$.
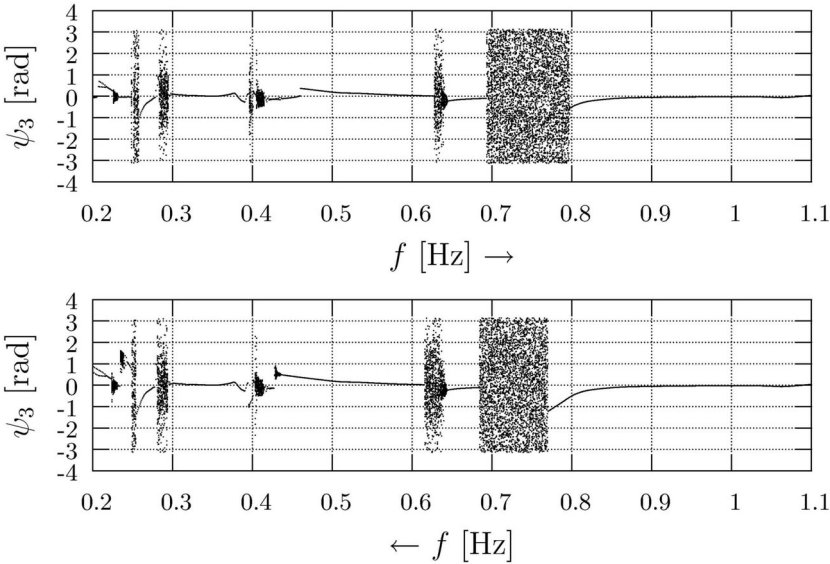
Figure 3. Bifurcation diagrams for the mathematical model C_1 with the parameter f growing ($\rightarrow$) and decreasing ($\leftarrow$).

In the upper part of Fig. 4 the final model (C_1) and real system matching for vanishing motion (started from the periodic attractor with the forcing frequency f=0.5 Hz), obtained during the identification process, is presented. In this scale we see almost perfect matching of the corresponding behaviours. The bottom part of Fig. 4 presents enlargement of the final phase of decaying of the same motion, where in addition the simulation of the model A_1 is shown. Here we can observe in details certain aspect of the difference between models A_1 and C_1.

Figure 5 shows results of investigation of the forcing frequency region 0.13-0.14 Hz. It is an example that the developed model with their parameters can predict real pendulum dynamics exhibited also for forcing frequencies f outside the region 0.2-1.1 Hz (containing all the periodic solutions taken to the identification process).
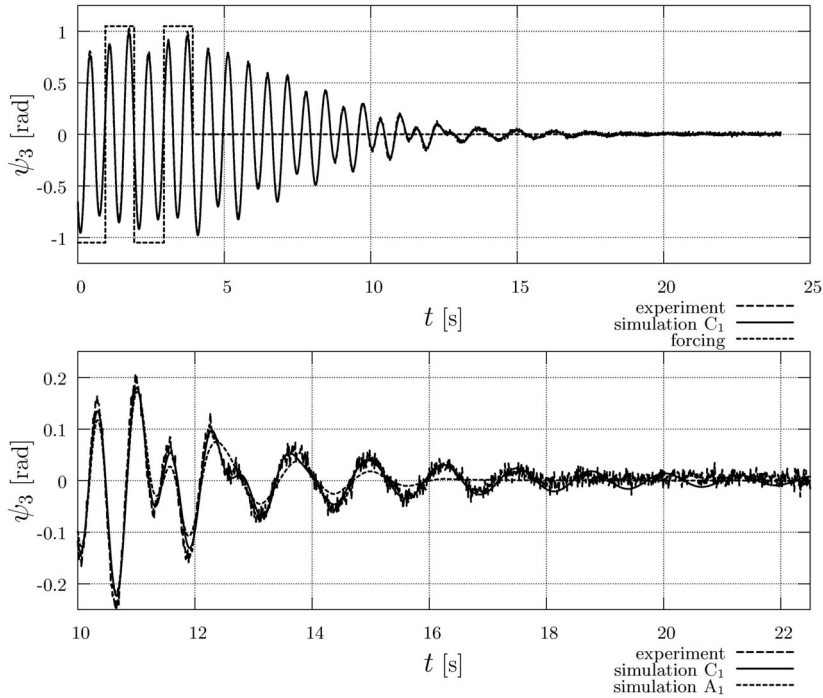
Figure 4. Final model (C_1 and A_1) and real system matching for vanishing motion
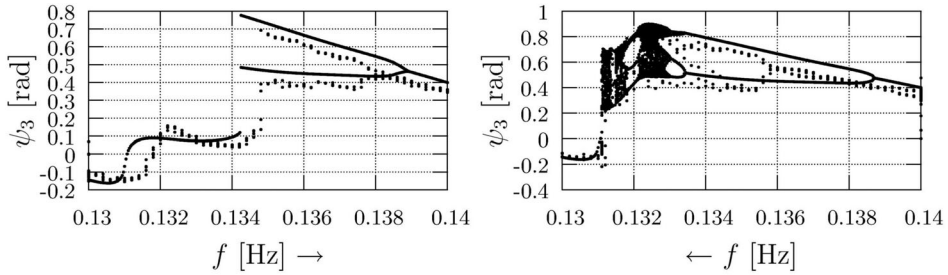
Figure 5. Bifurcation diagrams exhibited by experiment and model (C_1) with the parameter f growing ($\rightarrow$) and decreasing ($\leftarrow$).

5. Concluding remarks

Few versions of the model of resistance in the joints have been tested in the identification process. Good agreement between both numerical simulation results and experimental measurements have been obtained and presented, for all the variants of the friction model. However, one of them, namely C_1, seems to be optimal, since it gives relatively good results with simultaneous simplicity of the model itself, and high speed of the simulation.

The model C_1 is better for simulation (higher simulation speed) than others because the ε parameter is much smaller and the characteristic of the friction torque are is smooth. It is interesting that model C_1 give better results than models B_1, while the only modification is the parameter ε treated as identified one (the result is the smaller value of the parameter ε). We are not able to give a physical interpretation of that at this moment. But since it is important to have a model giving results close to experimental observations, we can accept even some artificial improvements of the model having only functional role, no physical sense, particularly if they speed up the simulation process.

I should be noted, that examples of numerical and experimental simulations presented is section 4 are selective. However, the presented examples show quite good agreement between numerical and experimental results. It leads to conclusion that the used mathematical model of triple pendulum with its parameters estimated can be applied as a tool for quick searching for various phenomena of nonlinear dynamics exhibited by a real pendulum as well as for explanation of its rich dynamics.

References

1. Baker G.L. and Blackburn J.A. The Pendulum. A Case Study in Physics. Oxford University Press, 2005.
2. Blackburn J.A., Zhou-Jing Y., Vik S., Smith H.J.T. and Nerenberg M.A.H. Experimental study of chaos in a driven pendulum. Physica D26(1-3), 1987, 385-395.

3. Bishop S.R. and Sudor D.J. The "not quite" inverted pendulum. International Journal of Bifurcation and Chaos 9(1), 1998, 273-285.
4. Zhu Q. and Ishitobi M. Experimental study of chaos in a driven triple pendulum   Journal of Sound and Vibration 227(1), 1999, 230-238.
5. Galan J., Fraser W.B., Acheson D.J. and Champneys A.R. The parametrically excited upside-down rod: an elastic jointed pendulum model. Journal of Sound and Vibration   280, 2005, 359-377.
6. Awrejcewicz J., Kudra G. and Wasilewski G. Experimental and numerical investigation of chaotic zones exhibited by the triple physical pendulum. Proceedings of the 8th Conference on Dynamical Systems - Theory and Applications. Łódź, Poland, 2005, 183-188.
7. Awrejcewicz J., Supeł, Kudra G., Wasilewski G. and Olejnik P. Numerical and experimental study of regular and chaotic motion of triple physical pendulum. International Journal of Bifurcation and Chaos 18(10), 2008, to appear.

NUMERICAL AND EXPERIMENTAL METHOD IN BIOMECHANICS

Romuald BĘDZINSKI
Wroclaw University of Technology
Lukasiewicza 7/9, 50-371 Wroclaw
e-mail: romuald.bedzinski@pwr.wroc.pl

Abstract

The analysis of the effort of structural components by calculation methods often encounters serious difficulties. Usually, aim of biomechanical research is determination displacement distribution of anatomical samples or physical models. Development of modern numerical method and computational techniques into field of biomechanics in recent years allow to solve highly complex problems encountered in the assessment of the strength and reliability of bone structures and implants. But they usually require experimentally determined boundary conditions or courses of the involved phenomena.

Key words: FEM, photoelsticty, elctronic speckle interferometry, holgraphic interferometry

1. Introduction

One of the most important line of the research in engineering biomechanics is the experimental and numerical analysis of the state of stress and strain existing in the organs which are most heavily loaded such the spine, the hip and the knee joint, or elements of human body which sustained an injury or in which pathological changes occurred. Clinical, experimental and numerical investigations of constructions supported human locomotion system, especially spine fixators, artificial human joints (hip and knee prosthesis) is also very important field of biomechanics. Discussions in this fields focuses on the problems of load models, using of different methods to investigations of biological objects in real and model conditions, interacting on biological tissues on changes of mechanical load.

In such investigations it is important to set oneself specific goals and determine what measured (or calculated) values will allow one to rich this goal. Physical and numerical models that are used should mirror as accurately as possible the studied object and take into account the influence of simplifications on the obtained results. As s rule, tests on models cannot reproduce the whole complexity of the ligamentous - muscular system, the nervous system, and the biological and biomechanical factors that occur in man's osteoarticular system. Even tests on anatomical specimens have these limitations. In the case of anatomical specimens, for instance, the time which passes since the taking of a specimen to the actual testing in crucial. As it was mentioned earlier, the main goal of experimental studies is to verify at some points theoretical models, or to confirm conclusion emerging from clinical practice. Still without tests and numerical investigations carried out on models and anatomical preparations it would be impossible

to determine the pathogenesis of some diseases or to evaluate the employed method of treatment, such as implantation.

The objectives of these paper include:

1. An analysis of the pathogenic mechanism of some diseases associated with the overloading of man's load-bearing system (e.g. the spine, the hip-tibial joint, the knee joint and the lower limbs). By man's load-bearing system we mean a complex of elements performing tasks chiefly in load-carrying and locomotion processes;
2. Clinical, experimental and numerical investigations of:
- spinal structures (an assessment of stresses, strains and displacements),
- the hip joint and the knee joint,
- the bone, ligament and muscular structures of the lower extremities;
3. An analysis of the optimum course of treatment in which some technological means such as endoprostheses, implants, stabilizers and so on are employed;
4. The creation of a basis for the selection and construction of implants and other treatment-aiding elements that meet such quality criteria as reliability, durability, biological compatibility, and ease of assembly and service.

2. Model of the pelvis bone

For solve problem analysis strain and strain in the human pelvis was investigated by used experimental and numerical method.

A geometric model of the bone was constructed on the basis of a series of cross – sections of the artificial pelvis bone. The model obtained in this way reflects accurately the actual geometry of the artificial pelvis bone. The computer programme ANSYS was used in numerical analysis (Fig. 1 a).

In numerical analysis were used three dimension, 10 – notes solid element. In the present case linear, isotropic material properties of the external cortical bone were assumed. The model of the human pelvis consisted of 59 000 elements with 98 247 nodes. The following material propertied were assumed: the elastic modulus E = 18 600 MPa, the Poission ratio $\nu = 0,3$.

Recently significant [11] improvements of laser doppler techniques gained interest for bone analysis. Laser speckle interferometry ESPI allows the full field and three-dimensional measurement of deformation and strain on complex surfaces. In electronic speckle pattern interferometry (ESPI) (Fig. 2 b) a speckle pattern is formed by illuminating the surface of the object to be tested, with laser light. This speckle pattern is imaged onto a CCD array where it is allowed to interfere with a reference wave, which may, or may not, be speckled. The resultant speckle pattern is then transferred to a frame grabber on board a computer where it issued in memory and displayed. When the object has been deformed, or displaced, the resultant speckle pattern changes due to the change in path difference between the wavefront from the surface and the reference wave. This second resultant speckle pattern is transferred to the computer and subtracted from, or added to, the previously stored pattern and the result is rectified.

Figure 1: Numerical model of the human pelvis (a) and results of experimental investigations of displacement distribution for model verification (b) by ESPI method. [11]

The loading conditions in the hip joint are a complex problem. Apart from the weight of the upper body, the muscles and ligaments forces operate onto the pelvis bone. Simple load models, which were based on Pauwels model [1], [5], were assumed in investigations. In the first model were considered only the interaction between femoral head and acetabulum, without muscles system. In the second model, the resultant force was a sum of the abductor muscles force like gluteus minimus and gluteus medius and the external force as a body weight.
Two cases of interaction between the head of the femur bone and the pelvis were investigated.

3. Experimental analysis of external fixator for femoral bone elongation

The interest in the external fixation system for limbs developed by Ilizarov has been growing in the last decade [2][4]. This is above all due to the high, in comparison with other fixators, effectiveness of treatment by the Ilizarov fixator of, e.g. complicated fractures of long bones, pseudarthrosis and limb axis correction or shortening. This high efficacy of the Ilizarov fixator results from, among other thing, its modular design that

allows one to create numerous configurations of the fixator and to modify its spatial arrangement during treatment depending on the needs. Another advantage is that the fixator's mechanical properties are conductive to the preservation of the optimal biomechanical conditions at the place of the joint of the bone fragments. The Ilizarov fixator is a flexible stabilizer. This mean that the load acting on the bone are carried both by the fixator's structure and the place of the join of the bone fragments, which ensures the axial dynamicsation of the latter.

The elongation of the lower limbs is one of the more interesting, but highly complex – both – in the clinical and mechanical aspects – cases of the application of the Ilizarov fixator. Though the clinical experience in the elongation of the lower extremities by means of the Ilizarov fixator is long, many disturbances and complications still frequently beset this process. This is particularly the case when the lower limbs are elongated in the thigh sections were complex conditions of a load acting an the femoral bone in the hip joint occur in usually strongly developed muscles groups surrounding the thigh begin elongated. The failures in the elongation are above all due to the still unexplained mechanisms of the effect of the fixator on the limb begin elongated and conversely the effect of the soft tissue surrounding the treated bone on the fixator's structure.

The aim of the work was to analyse the stability of the system formed by the Ilizarov fixator and the thigh being elongated [4]. The gaol of these studies was to determine the conditions of the load acting on the particular distance rods of the Ilizarov fixator and its changes during the elongation of the lower limbs in the thigh section. The tests were conducted in the distance rods of the stabilizer mounted on patients undergoing thigh elongation in clinical conditions. The forces were measured in all distance rods connecting the rings between which the bone's shaft had been cut. It was presumed that knowing the load pattern for the particular rods and their distribution around the bone being elongated, it would be possible to determine which groups of muscles acted stronger and which weaker on the system: the bone fragments – the Ilizarov fixator and how these actions change during the whole process of elongation.

Specially adapted extensometer converters built into the distance rods of fixator mounted on patients undergoing thigh elongation were used for the measurement of the forces acting in the distance rods (Fig 2.1).
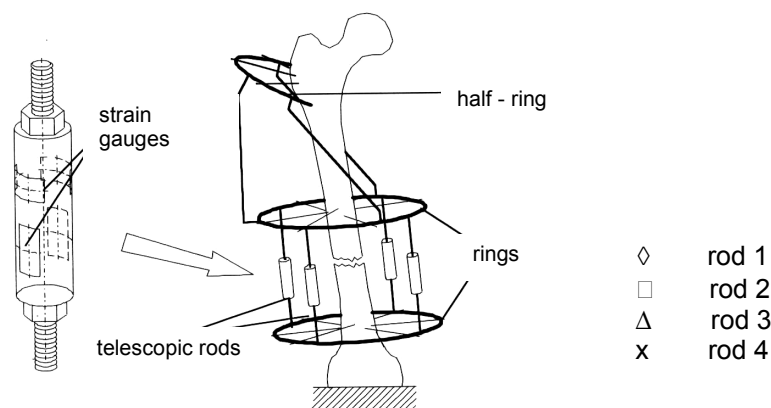
Figure 2.1. Force transducers and their localisation in distance rods of external fixator
[2][4]

The measurement covered ten cases of thigh elongation by the Ilizarov fixator. Measurements were made once o day at a fixed time, immediately before and after the application of a distance rod length increment.
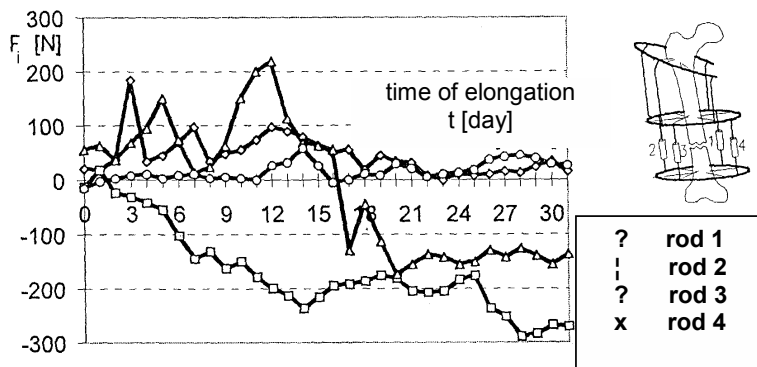
Figure 2.2.Distraction load measured in function of time: rate of elongation: 4x0.25 mm per day [4]

Figure 2.2 shows typical variations in distance rod load as a function of time recorded for selected cases. An analysis of the results recorded for the particular case shows that in most of them, the increments of forces in neighbouring rods were similar both in their character and in the variation of their values. The investigations have demonstrated that the stability of the system: the Ilizarov fixator - the thigh being

elongated, measured in values of the transverse displacements of the bone fragments, is a function of both the mechanical properties of the adopted fixator structure and the distribution of the forces acting on this system.

The clinical studies allowed determining the distribution of loads in the particular distance rods of the Ilizarov fixator and the variation of the loads as a function of the elongation time. The clinically developed and applied measuring method allows once to control continuously the correctness of the course of the elongation of the limb by analysing the conditions of the loading of the particular rods of the Ilizarov fixator and the changes of these loads as a function of the elongation time.

The studies conducted under clinical conditions have indicated that the preliminary assessment of the patient's physical condition – above all the degree to which the muscles surrounding the bone to be elongated are developed and trained, whether scars and pathological changes are present – is of major importance. When the mechanical properties of the soft tissue have been taken into account and the effect of the optimal spatial configuration of the fixator can be selected for the particular course of treatment. This means that in clinical practice the adopted goal will be achieved in the shortest time without complications.

4. Strain analysis in the intact femur bone and with implant

The loading conditions in the models of femur and femur with the stems implanted, respectively, were assumed after [2],[3],[5] for a single leg stance. Besides the resultant force of 2,47 BW (body weight), also the forces generated by three other muscles and tendon acting in this phase of gait were simulated; i.e., Gluteus medius – 0,535 BW, Gluteus minimums – 0,2 BW, Iliopsoas – 0,865 BW and Tractus iliotibialis 0,08 BW. The body weight for the considered model of femur was equal to 567 N. In the lower part of femur (on the condyles) the model was fully constrained.

Only the influence of stem shapes, geometrical and mechanical properties on the observed parameters were investigated. Because of numerical simulation simplifications only this kind of comparative analysis was possible. Thus, the Huber-Mises form of the strain energy was applied. The KERAMED stem generates considerably lower values of strain and stress, when compared with the values recorded for the intact bone changing strongly the strain and stress distribution. As a results only bending occurs in the lateral plane. The strain distribution shows concentrations in the subcollar region. However, both stems generate substantially different distributions of stress observed in the medial part of femur when compared with the intact femur.

Moreover, there is a non-uniform stress and strain distribution around the stem in a transverse cross-section. Analysis of the values of strain occurring in the bone in the bone/stem interface region indicates that both stem designs affect a strongly non-uniform and discontinuous strain distribution.
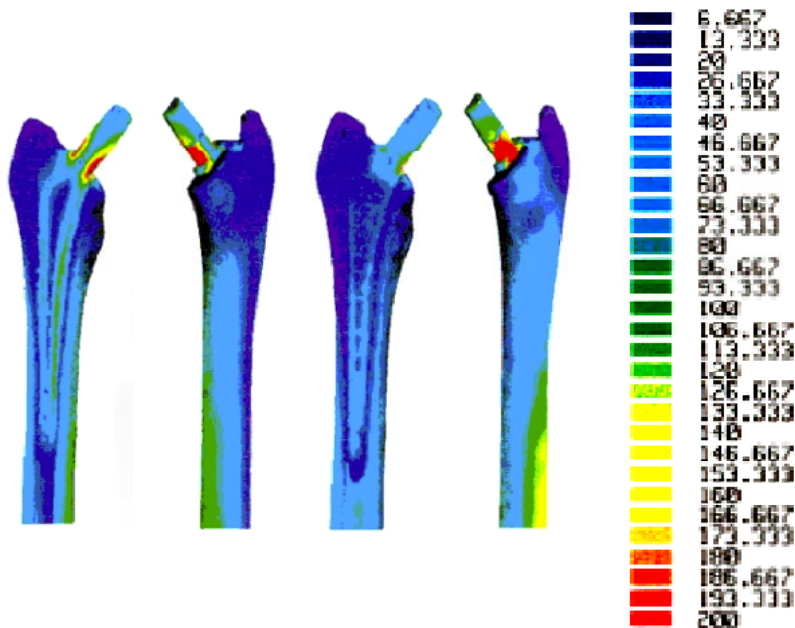
Figure 3: Stress and strain analysis in the hip join with endoprosthesis.

After a series of investigations the most important stem design features have been evaluated in the bone/stem system functioning perspective:

- Stem length. The stress and strain distribution is closest to that observed in the intact bone when short stems are applied, [3][5].

- It has been found that the collar plays a crucial role in achieving secondary stability of the stem. It produces, however, strain and stress concentrations in the subcollar region which, change decisively the implant/bone load transmission and contribute to an abnormality of the process of bone remodelling. A disadvantageous effect of the collar on the nature of stem/bone system functioning has been found in both the experimental investigations and numerical simulation. The investigations also show the occurrence of higher stresses in the bone in the proximal part of collarless stems when compared with those observed in stems with collars.

- The bending stiffness of the stems plays an important role in mechanical cooperation of stem and femur. Cross-sections of the objects without corners reveal a high regularity of strain and stress distribution in the bone. There is a lack, in literature, of the reports on the optimisation of endoprosthesis from the point of view of stem/bone stiffness relationship. It is unequivocally stated that this relationship is of crucial importance for maintenance of the normal bone/stem system functioning under physiological loading. The values of strains and stresses

in the bone decrease considerably with the increase of stem elastic modulus, Huiskes et al. [9][12]. Higher values of stem elastic moduli reduce strains in the proximal metaphysis of the hip bone. Materials with a low elastic modulus (e.g. titanium alloys) are much more suitable, from the mechanical point of view, for hip endoprosthesis stems than materials with a high Young modulus. None of the materials known so far meets simultaneously all the criteria.

5. Summary

The experimental methods, which are often use in analysis of the displacements and the stress distribution of the elements of human body, have a steady position in the biomechanical investigations. At the present the biomechanical studies are carried out in many scientific centers all over the world, in order to explaining reasons for course of orthopedics diseases and working out the optimal method in treatment of human's skeletal system. The scientific researches frequently concern one of the most loaded elements in human body like spine, hip joint and lower extremities. The experimental and numerical studies are mainly carried out at models and in the clinical conditions. The results of these investigations help to explain and understand both the formations of the degeneration changes in the skeletal system and elaborate efficient treatment methods.

The relative costs of developing and testing a design are an important consideration in the selection of a design analysis method [12]. The costs of calculation methods should be compared with those of experimental methods, considering the goal to be achieved. A selection of a research method should also be made on the basis of the relative costs due to the complexity of an investigated object [6].

The goal of the investigation and which methods enable to achieve this goal is the most important target in the biomechanical studies. Physical and numerical models should both represent the original models as well it is possible and estimate the influence of simplifications, which were made, on the final results.

Reference
[1] Beaupre, G.S. and Hayes W.C., Finite element analysis of a three-dimensional open-celled model for trabecular bone", *J. Biomech. Eng.*, 107 pp. 249-256, 1985.
[2] Będziński, R., *Biomechanical Engineering. Selected Problems (in Polish),* Oficyna Wydawnicza Politechniki Wrocławskiej, Wrocław, 1997.
[3] Bernakiewicz M., Będziński R., „Stress analysis in the human femur with different types o stems of the total hip endoprosthesis", Proceedings 9th International conference on Mechanics in Medicine and Biology, Ed. by D. Miklavcic et. Al. Lubljana 1996, p. 543-546.

[4] Będziński R., Filipiak J., „Experimental analysis of external fixators for femoral bone elongation", Acta of Bioengineering and Biomechanics, Vol.1, No. 2, 1999, 93 - 105

[5] Będziński, R., Bernakiewicz, M. and Ścigała, K., Biomechanical aspects of artificial joint implantation in lower limb, *Journal of Theoretical and Applied Mechanics*, Vol. 37, No 3, pp. 455-479, 1999.

[6] Borbas, L., *Elements of Experimental Stress Analysis*, Course *Design for Quality*, Forli, 1995.

[7] Cowin S.C., Bone stress adaptation models, J. Biomech. Eng. 115 pp.528-533, 1993

[8] Dalstra, M., Huiskes, R. and Erning, L., Development and validation of a three-dimensional finite element model of the pelvic bone, *J. Biomech. Eng.*, 117, pp. 272-278, 1995.

[9] Huiskes, R. and Chao, E.Y.S., A survey of finite element analysis in orthopaedic biomechanics, *Journal of Biomechanics*, 16, pp. 385-409 1983.

[10] Pilarski, W., Będziński, R., Trzaskacz, T. and Dulko, J. Experimental and numerical analysis of strain distribution in pelvis bone, *Proc. of III Sem. "Biomechanics of bone system"*, Warsaw, 2002.

[11] Prendergast, P.J., Finite elements models in tissue mechanics and orthopaedic implant design, *Clinical Biomechanics*, Vol. 12, No. 6, pp.343-366, 1997.

[12] Stupnicki, J., Trends of experimental mechanics, *Journal of Theoretical and Applied Mechanics*, Vol. 2, No. 34, pp. 207-233, 1965.

[13] Ścigała, K., FEM analysis of deformation and surgical correction of tibia bone, *Acta* No .1, pp.321-322, 2002.

RECENT INVESTIGATIONS IN DYNAMICS OF CONTINUOUS SYSTEMS SUBJECTED TO MOVING LOAD

Roman BOGACZ

Krakow University of Technology, Faculty of Civil Engineering and
Polish Academy of Sciences, Inst. of Fundamental Technol. Research Świętokrzyska
Str. 21, 00 049 Warsaw, Tel. 663 770086, rbogacz@ippt.gov.pl

Abstract
The paper is devoted to the study of continuous systems subjected to moving loads. Several cases of dynamical problems are considered, where the motion of elastically supported beams are excited by a moving concentrated force. In particular, we study interactions with periodic structure of the medium. Earlier results on one-dimensional structures are extended to the case of a set of plates.
Key words: dynamics, travelling loads,oscillation

Introduction

The development of modern technology of explosive bonding of layer materials or tracked high-speed transportation systems becomes more and more important. There is a strong need for simplified but reliable models of continuous systems in order to study various dynamical effects which influence comfort, durability of structures and damage of the environment. The first study of a beam on Winkler foundation subjected to simple force moving with constant speed was initiated by Timoshenko [1]. The first stationary solution of the simple case devoted to Bernoulli-Euler Beam on an elastic foundation was obtained in proper way by Ludwig [2]. The case of moving and oscillating force was formulated and partly solved by Mathews [3]. The first proper solution of Mathews problem was given by Bogacz and Krzyżyński in [4}.There are various extensions of this classic problem towards more realistic models of structures and loads. A great deal of new effects were recognize by authors of [5] studying the problem of oscillating load moving along a periodic (variable in space) structures. The dynamical effects for two or three-dimensional problems with moving load have an important practical engineering applications, [6]. Some problems connected with system of plates subjected to traveling load will be also presented in the paper.

1.1 Response of Beam to Normal Constant Force Moving at a Constant Speed

The classic problem of infinite Bernoulli – Euler beam on the Winkler foundation (flexural rigidity *EI,* mass density *m*, damping coefficient *d* foundation constant *c*) subjected to force F_0 moving with velocity V_0 is described by following equation of motion:

$$EI\, w,_{xxxx} + m\, w,_{tt} + d\, w,_t + c\, w = F_0\, \delta(x - V_0 t)\,, \qquad (2.1)$$

Where: δ denotes Dirac 'function', $w = w(x,t)$ is deflection of the beam, $-\infty < x < \infty$, $t > 0$.

The steady state solution for $V_0 < V_{cr}$, $V_{cr} = (4cEI/m^2)^{1/4}$ was obtained by Ludwig [2], looking for the stationary solution in the form of traveling wave with the velocity equal to the speed of moving force. In such a case the ordinary equation of motion has the form:

$$EI\, w^{IV} + mV^2\, w'' - d\, w' + c\, w = F_0\, \delta(X), \quad X = x - V_0 t. \qquad (2.2)$$

The stationary solution in the elastic case for subcritical range has the form:

$$w(X) = F_0 /[\, 4\, \alpha (c\, EI)^{1/2}\,]\ (\cos \beta X + \alpha/\beta \sin \beta\, |X|) \qquad (2.3)$$

where $\alpha = [1 - (V/V_{cr})^2]^{1/2}\, V_{cr}$, $\beta = [1 + (V/V_{cr})^2]^{1/2}\, V_{cr.}$.

The supercritical case yields waves expanding from the force location with smaller wave lengths and amplitudes in front of the load as behind it. Usual the sub-critical case is of technical importance. However, the critical speed can be reduced by the action of additional axial forces, as pointed out Kerr in ref. [7].

1.2 Response of Beam to Moving Oscillating Force

The more complicated case from the solution point of view but very important for the modelling of railway engineering track-train interaction is a system which is composed of a beam on an elastic foundation subjected to the moving force F_0, which oscillate harmonically with amplitude F_1. In this case the motion is described by the following equation:

$$EI\, w,_{xxxx} + T\, w,_{xx} + m w,_{tt} + c w = (F_0 + F_1\, \cos \omega t)\delta(x - V_0 t)\,, \qquad (2.4)$$

Such a problem for $F_0 = 0$ was formulated by Mathews [3]. The solution of the problem was expected in the form of standing waves in the system of coordinates moving, in the direction x with the velocity V_o. The equation (2.4) in the moving system of coordinates is equivalent to folowing equation:

$$EI\, w,_{XXXX} + T\, w,_{XX} + m(w,_{tt} - 2V_0\, w,_{Xt} + V_0^2\, w,_{XX}) + cw = (F_0 + F_1\, \cos \omega t)\delta(X)\,, \quad (2.5)$$

Looking for the solution in the form

$$w(X,\, t) = W_1(X)\, \sin \omega\, t + W_2(X)\, \cos \omega\, t \qquad (2.6)$$

one obtain the ordinary equation with respect X which ought to be solved using proper condition of radiation. The solution obtained in ref. [3] was valid in the first region of (Ω, V) plane only, $\Omega = \omega/\omega_0$, $V = V_O/V_{cr}$, ie. for the relatively small velocity of force motion and small frequency. The error made by Mathews was connected with the wrong way of use of the radiation condition. The correct solution of the Mathews' problem was obtained by Bogacz and Krzyżyński in [4}, and generalized for more complicated beam models in [8]. The traveling wave solution in the Bernoulli – Euler beam model has different form in the five regions of the frequency-velocity (Ω, V) plane. Corresponding number of regions in the case of the Timoshenko beam is twenty two. An example of the regions configuration for Rayleigh beam is shown in Fig 1. About the region in the neighborhood of frequency $\Omega = 1.0$ one can obtain information in ref. [8].

Exemplary case of wave propagation in the region II for the Rayleigh or Bernoulli-Euler beam is shown in Fig. 2 and Fig. 3. In Fig. 2 we can see the displacement of the beam in time- space plane excited by the moving and oscillating source, visible in the central line as displacement with higher amplitudes. In the left side of the figure we can see the ordinary case, the waves traveling from the source of excitation, and on the right side of plane waves traveling to the source of excitation. The case of frequency higher then the resonance frequency when on both side of the plane waves are propagating from the source of excitation is shown in Fig. 3.

The lines $V=0.1$ and $V=0.3$ on Fig. 1 are corresponding to the classic and high speed trains, respectively. This shows that above phenomena may occur in the real conditions. That is why such a study are important for engineering practice.
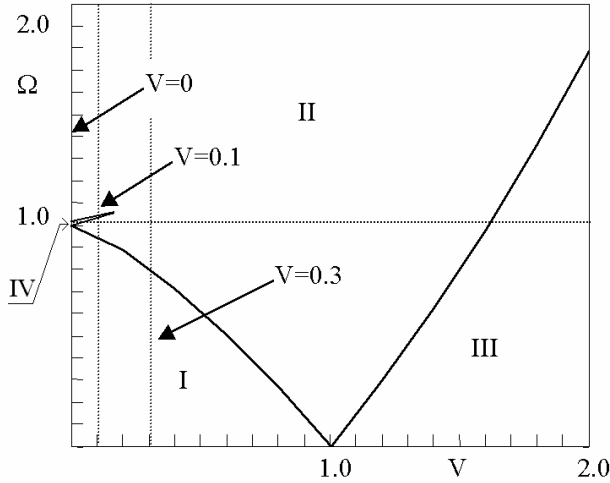
Fig. 1. Regions of solutions of characteristic equation for the Rayleigh beam on Ω-V plane. Region I: 4 complex roots, Region II: 2 complex and 2 real roots, Region III: real roots.
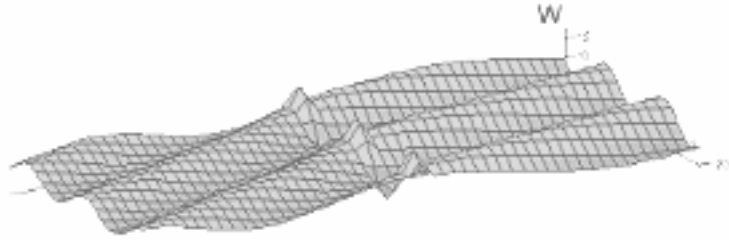
Fig.2 Displacement of beam on time- space plane excited by source moving in the central line, case of waves traveling to the source of excitation on right side of plane.
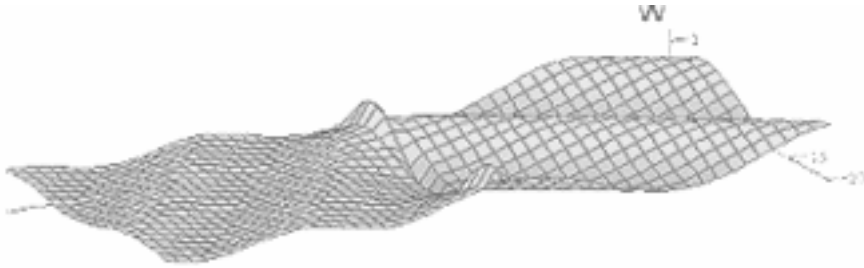
Fig. 3. Displacement of beam on time - space plane excited by source moving on the central line, case of waves traveling from the source of excitation on both sides of plane

1.3 Response of Beam to Moving Distributed Load

The problem of a flexibly supported beam vibration, when the beam is subjected to the moving distributed load can be composed of solution for the limiting case of load described by following Heaviside function $F_0 H(x - V_0 t)$:

$$EI\, w_{,xxxx} + T\, w_{,xx} + mw_{,tt} + hw_{,t} + cw = F_0 H(x - V_0 t) \qquad (2.7)$$

Such a case and the case of the beam on a visco-elastic semi-space was studied by Bogacz and Rozenbajgier in [9]. The superposition of the obtained solution for the Heviside function allows to obtain various kind of pice-wise constant load distributed on a finite-length segment. For example if we describe a load with given value F_1 distributed between $x = 0$ and $x = L$ at $t=0$, than it is possible to write as follows:

$$F(x,t) = F_1 [H(x - V_0 t) - H(x-L - V_0 t)] \qquad (2.8)$$

The boundary conditions take the form:

$$lim\ w(x) = 0\ \text{ for } |x| \rightarrow \infty, \qquad\qquad (2.9)$$

and the displacement $w(X)$, as well as $w_{,X}$, $w_{,XX}$, and $w_{,XXX}$ is continuous at $X = 0$ in the case of eq. *(2.7)* and *(2.8)* and additionally at $X = L$ in the case of load *(2.8)*.

The case of Timoshenko beam on an elastic foundation subjected to uniformly distributed moving loads has been studied by several authors, ie: refs.[10], [11].

$$EI\ \varphi_{,xx} + k'AG\ (w_{,x} - \varphi) - mI\ \varphi_{,tt} = 0,$$
$$k'AG(w_{,xx} - \varphi_{,x}) - m\ w_{,tt} - h\ w_{,t} - c\ w = - F_0\ H(x - V_0 t) \qquad\qquad (2,10)$$

where: φ - angel of rotation of beam due to pure shear, k' – shear coefficient, G – modulus of elasticity in shear, A – cross-sectional area and h – damping coefficient.
 The first stationary solution obtained for the case of the Timoshenko beam on an elastic foundation was obtained by Achenbach and Sun in [12]. The solution obtained is valid in full range of velocity, but only for the set of parameters fulfilling following inequality:

$$E > k'G\ (1 + k'G\ A^2\ (Ic)^{-1}) \qquad\qquad (2.11)$$

The discussion of qualitatively different traveling wave solution depending on the beam parameters is presented in [13].
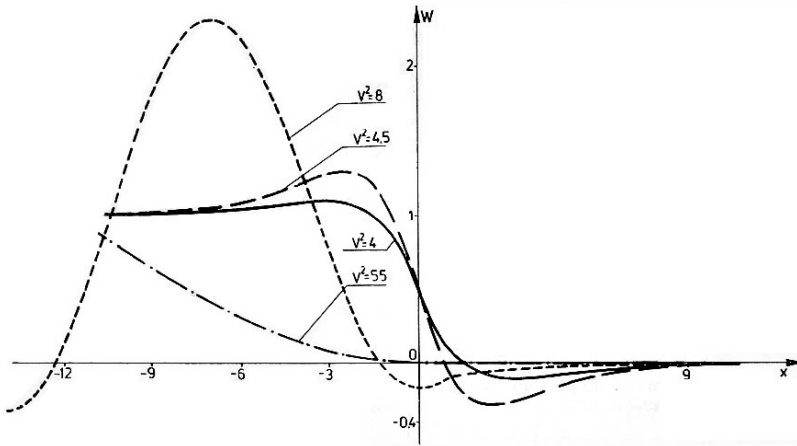
Fig. 4. Displacements of Timoshenko beam wish parameters not fulfilling inequality (2.11) for chosen value of velocity. Qualitatively similar solution is given in ref. [12]
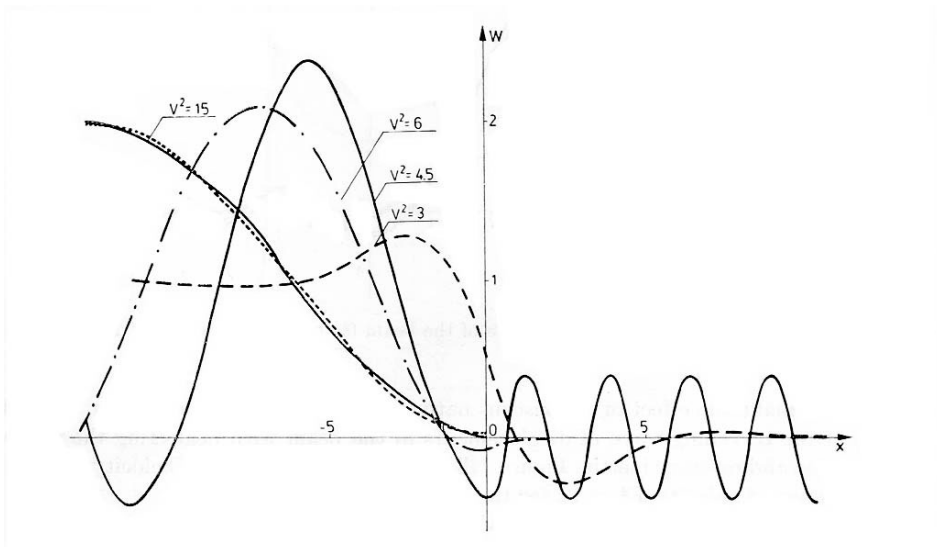
Fig. 5. Displacements of Timoshenko beam wish parameters fulfilling inequality (2.11) for chosen value of velocity, see ref. [13]

1.4 Response of Periodic Beam Structure to Moving Loads

The guideways for high-speed vehicles are composed of repetitive elements or cells which forms a periodic structure. The track is usually modeled as one dimensional system but sometimes the study concerns two dimensional system, [5]. The steady-state system response is determined for a moving disturbances source in the form of constant and periodic concentrated force *(2.4)*.

$$w(nl_+, t) = w(nl\text{-}, t); \quad w_{,x}(nl_+, t) = w_{,x}(nl\text{-}, t); \quad w_{,xx}(nl_+, t) = w_{,xx}(nl\text{-} , t); \qquad (2.6)$$

$$w_{,xxx}(nl\text{-},t) - w_{,xxx}(nl_+,t) = R(nl,t) \qquad (2.7)$$

The equation of motion is completed by interface conditions at the supports which depend on the model assumed, e.g. for the railway track is required condition of continuity *(2.6)* and equilibrium of vertical forces *(2.7)*, while for the supports of maglev model, they require continuity of displacements (position), vanishing bending moment and equilibrium of vertical forces.

The solution method proposed in such a case consists in the direct application of the Floquet's theorem, cf. ref. [14], to the differential equations of motion with periodic parameters, [5].

The very important phenomenon connected with periodic system dynamics is connected with passing and stopping bands. Because in the elastic case, or case of small damping

small differences in the system parameters can qualitatively change the solution of the system.
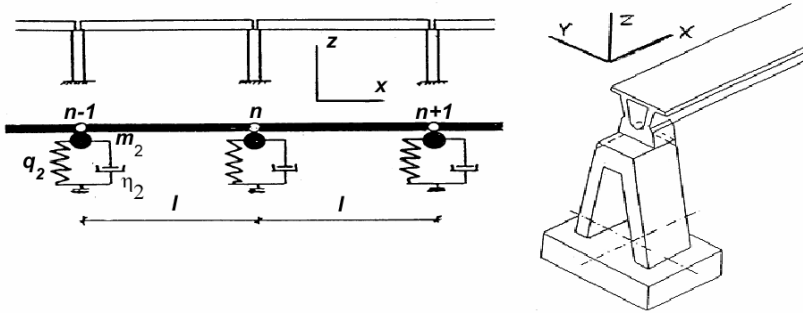
Fig. 6 Track of. Magnetic Levitated Train and its model as periodic structure

Other approach (by the use of perturbation method) for a periodic mass and stiffness distribution along the beam was applied by Popp and Mueller [15] in order to approximate the sleepers spacing in the track. In this case, for the realistic system parameters, the differences were very small. Jezequel studied periodic structures subjected to moving load using Fourier series method, [16]. Also using such approaches as "space harmonic analysis", "energetic method" and "transfer matrix method" were not so successful as the "traveling wave method" used by Mead [17]. The application of Floquet's theorem allows to solve the problem of free and forced vibration of periodic structures subjected to moving load. The motion of harmonic force and traveling waves corresponding to the first and second passing band are studied in [14]. An example of such a study lead to the results for the successive steps of time and assumed parameters. The optimal length of the vehicle is connected with minimum displacement for the operating speed. The magnetic mass-less loading is modeled as many concentrated traveling forces moving with a constant speed. We can see in [14], that in the optimal case maximum displacement take place under the vehicle only. Such a case of study is connected with the magnetic levitated test line realized in Germany .

2. Response of Plates to Moving Load

The more complicated periodical system which is composed of an array of plates vibrating due to moving load is used for modeling the road or an airfield. Such a model is a relatively complicated two or three dimensional periodic system. In the case of the airfield an array of single small plates, which are coupled by appropriate boundary conditions and by a common foundation in form of big supporting plate, with a visco-elastic sliding layer between supporting plate and array of plates.

In the beginning the problem of single plate on an elastic foundation was studied. Then system of plates which creates array of plates [6], which is studied with various boundary condition between small plates and sliding layer.
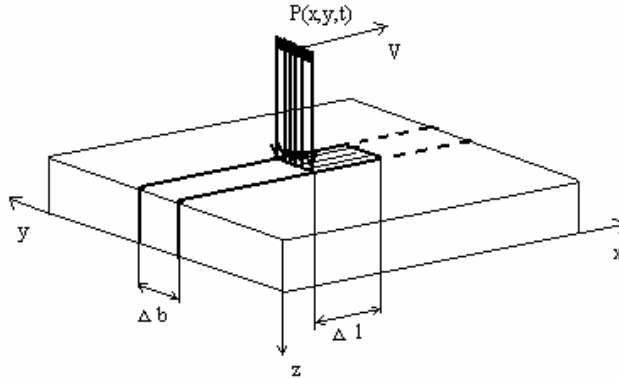
Fig. 7. Scheme of the coordinate system of the upper plate

The large plate in turn is placed on a Winkler foundation and fixed on its boundary. Such a system constitutes a periodic structure, however, in two space dimensions instead of linear, one dimensional studied previously. Equation of motion of each plates has hence the form:

$$\rho\, W,_{tt}(x,y,t) + D\, \Delta\Delta\, W(x,y,t) = g(x,y,t) + F(t)\delta\,(x - V_x t)\delta\,(y - V_y\, t) \qquad (2.12)$$

where ρ is the mass density per unit of area, D - the stiffness of the plate, W - deflection of middle plane. The force $g(x,y,t)$ couples support and top layer. It is assumed proportional to difference of vertical positions. F(t) is the normal load and V_x and V_y are components of velocity of moving load. Looking for the dynamics of the array of plates subjected to moving forces acting at several interaction points also non-symmetric case maybe considered. The majority of consideration deals with simply supported plates or free boundary (without forces). In the real case there are acting non-conservative friction forces and bending moment with value depending on temperature and other parameters. In general case the problem is non-linear due to friction low and contact forces in lateral and vertical directions.

In order to solve the problem use of the analytical methods is inefficacious. That is why the numerical technique is an alternative approach in this case. Promising in the case of moving loads is the time-space element method or finite differences method. From engineering point of view we are interested in rectangular array of plates, hence the finite differences method is easy to apply, [6]. The initial results of simulation shows that the viscosity of the thin layer between upper and bottom plates is very important. In the

symmetric and rectangular case when the load is moving with relatively small speed also analytical orthogonalization methods can be accepted. The results obtained using analytical method are shown in Fig. 6, see ref. [21].

Similar investigations devoted to problems of dynamics of array of plates can be find in ref. [20, 22]. The high speed motion of the load excite disturbances in the system of plates in the form of waves which are visible in Fig. 7. Wavy phenomena of the disturbances is specially important in the case of periodical property of the air plate or array of plates subjected to the following moving load or a set of similar loads [6].

$$F(x,y,t) = F(t)\delta\,(x - V_x t)\delta\,(y - V_y t) \tag{2.13}$$
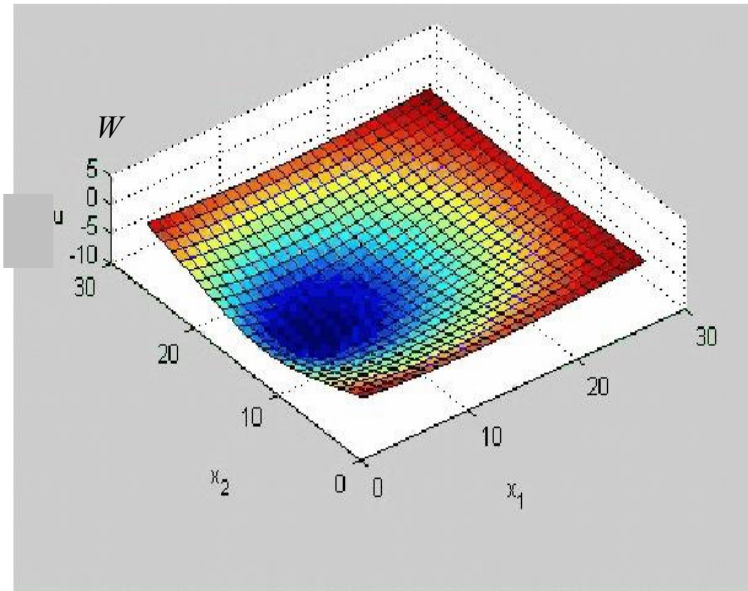
Fig. 6. Displacements of the simply supported plate on an elastic foundation subjected to the force moving at lower speed along symmetry line at x_2

The two dimensional problem in general case is very complicated. The symmetric and rectangular case as shown in Fig. 6 can be easy discretized conventionally by the method of finite differences, [21]. With the discretization of the spatial derivates, we rewrite the second order equation of motion *(2.12)* as a first order system for the nodal positions and velocities. Initial conditions required for equation *(2.12)* we assume as a trivial one (state of rest before the external load is applied).

In the case of plate subjected to the concentrated force moving at high speed along the line $x_2 = 3$ (symmetry line) the wave phenomenon dominate the dynamics of the plate. Such situation is visible on Fig. 7.
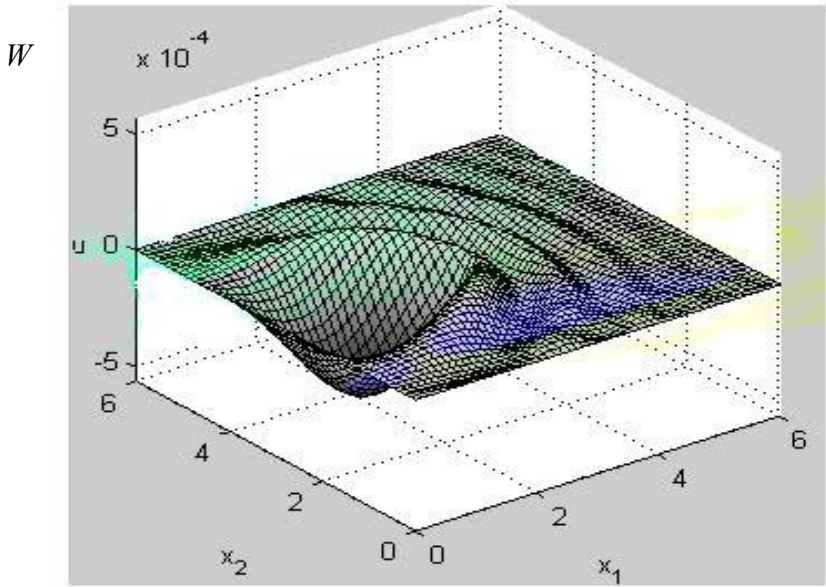
Fig. 7. Displacement of plate subjected to the force moving at high speed along line $x_2 = 3$
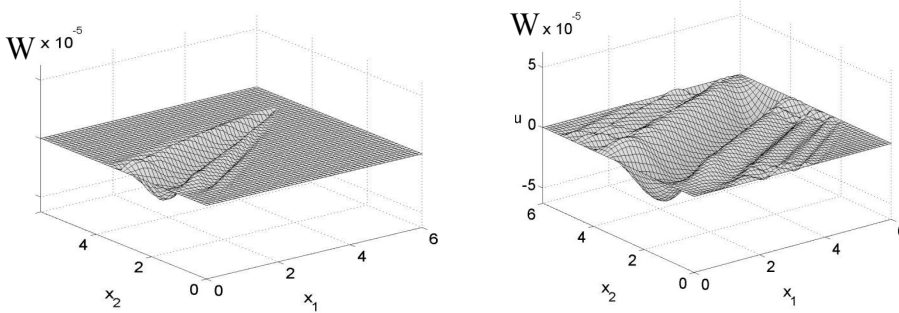
Fig. 8. Displacement of plate under skew motion of concentrated load

3. Conclusions

Several cases of dynamical problems, where the motion of elastically supported beams or plates subjected to moving load was investigated in the paper. Particular attention was paid to the periodic excitation or periodic structures. The application of Floquet's theorem allows to solve the problem of free and forced vibration of periodic systems (guideway) when the system is linear (one dimensional). The periodic structure subjected to harmonic load is connected with an infinite number of travelling waves, whereby the crucial contribution to the solution have the waves corresponding to the passing and stopping bands. Much more complicated case, the two dimensional problem of array of rectangular plates subjected to traveling load was formulated and partly solved in this paper. The results of farther investigation will be presented in the next publications.

References

1. S. Timoshenko, *Method of analysis of static and dynamical stresses in rail*. Proc. 2nd Int. Congr. Appl. Mech., Zurich, (1926), pp. 407-418.
2. K. Ludwig, *Deformation of rail elastically supported of infinite length by loads moving at a constant horizontal velocity*. Proc. 5th Int. Congress Appl. Mech., (1938), pp. 650-655.
3. P.M. Mathews, *Vibration of beam on elastic foundation*. Z. angew. Math. u. Mech. **38**.(1958), pp. 105-115
4. R. Bogacz and T. Krzyżyński, *On the Bernoulli-Euler beam on a visco-elastic foundation under moving oscillating load.* Inst. Fund. Technol. Res. Report Nr **38**.(1986).
5. R. Bogacz, T. Krzyzynski, K. Popp, *Wave propagation in two dynamically coupled periodic systems*, Proc. International Symposium on Dynamic of Continua, Proc. International Symposium on Dynamics of Continua, Bad Honnef, Shaker Verlag (1998), 55-64.
6. R. Bogacz, K. Frischmuth, *Vibration of array of plates induced by moving load.* Simulation in R&D. Eds. L. Bobrowski, Z. Łukasik and Z. Strzyzakowski , Radom, 2006 (2008), pp. 41-46.
7. A.D. Kerr, *The continuously supported rail subjected to axial force and moving load.* Int. J. Mech. Sci.**14**.(1972). 71-78.
8. R. Bogacz, T. Krzyżynski and K. Popp, *On generalization of Mathews' problem of the vibration of a beam on elastic foundation*. Z. angew. Math. Mech. **69**, (1989), 243-252.
9. R. Bogacz and Z. Rozenbajgier, *Steady state vibration of beam on a viscoelastic semi-space under moving load* (in Polish). Proc. of Warsaw Univ. of Technology. **63**, (1979), 63-71.
10. N.Z. Yakushev, *Dynamics of elastic systems subjected to dynamic loads. In: Investigation of Theory of Plates and Shells*. (in Russian). Publ. of Kazan University,1972.
11. L. Fryba , *Vibration of Solids and Structures under Moving Loads*. Noordhoff, 1972.
12. I.D. Achenbach and C. T. Sun, *Moving load on flexibly supported Timoshenko beam.* Int. J. Solid & Structures.1. (1965), 353-370.
13. R. Bogacz, *On dynamics and stability of continuous systems subjected to distributed moving load*. Ing. Archiv.(1983), 57-69.
14. R Bogacz, T. Krzyżynski and K. Popp, *On vertical and lateral dynamics of periodic guideways for maglev vehicle.* Dynamical Problems in Mechanical Systems. Warszawa (1993). 219-233.
15. K. Popp and P. C. Mueller, *Ein Beitrag zur Gleisdynamik.* Z. angew. Math. Mech. **62** (1982), T65-T67.

16. L. Jezequel, *Response of periodic systems to moving load*. Journal of Appl. Mech. **48**. (1981), 613-618

17. D. J. Mead, *A new method of analyzing wave propagation in periodic structures; Application to periodic Timoshenko beams and stiffened plates*. J. Sound Vibr., **104(1),** (1986), 9-27.

18. R. Bogacz, T. Krzyżyński, K. Popp, *On the dynamics of linearly extended and cyclic periodic structures*, in: Proc. of the 4th German-Polish Workshop on Dynamical Problems in Mechanical Systems, Berlin, 1995.

19. K. Frischmuth, *Regularization methods for non-smooth dynamical problems*, in: R. Bogacz, G. P. Ostermeyer and K. Popp (Editors), *Dynamical Problems in Mechanical Systems IV*, Proceedings of the 4th Polish-German Workshop, 1995. Berlin, IPPT-PAN, Warsaw, 99–108, 1996.

20. R. Bogacz, J. S. Worobjew, M.W. Czernobriwko, L. Kruszka, *Influence of moving impulse load on the plate on elastic inertial foundation*. *In Simulation in R&D*. Eds.L. Bobrowski, Z. Łukasik and Z. Strzyzakowski , Radom, 2006 (2008), pp. 47-52.

21. R. Bogacz, K. Frischmuth, *Analysis and computer simulation of systems with traveling and follower loads. Simulation in R&D*.Eds. L. Bobrowski and A. Grzyb, Kraków (2007), pp.47-54.

22. T. Szolc, R. Bogacz, *Analysis of the airport runway vibration excited by motion of heavy aircrafts.* Proc. Int. Symposium WAVES AND VIBRATION, Poznań (2006), pp. 343-348.

23. T. Szolc, *Dynamics of plates system under moving load*. Machine Dynamics Problems. (2006).Vol.**30**.No.1, pp.73-95.

EVOLUTIONARY COMPUTING IN OPTIMIZATION AND IDENTIFICATION OF DYNAMICAL PHYSICAL SYSTEMS

Tadeusz BURCZYŃSKI

Department for Strength of Materials and Computational Mechanics,
Silesian University of Technology, ul.Konarskiego 18a, 44-100 Gliwice, Poland
Institute of Computer Modelling, Artificial Intelligence Department,
Cracow University of Technology, Warszawska 24, 31-455 Cracow, Poland
+48322371204, Tadeusz.Burczynski@polsl.pl

Abstract

The paper id devoted to applications of evolutionary algorithms to optimization of dynamical physical systems. Identification of internal defects are also considered. Several numerical examples of shape and topology optimization for various criteria and crack or void detection are presented.

Key words: evolutionary algorithms, optimization, defect identification

1. Introduction

Applications of classic algorithms in optimization of dynamical system is restricted by limitations referring to the continuity of an objective function and the necessity of gradient or hessian evaluation. These methods give substantial probability of finding a local optimum. Therefore new optimization methods, free from limitations mentioned above, have been still looked for. The optimization methods inspired by biological mechanisms have become very popular in last few decades. Most of them give good results in optimization problems where a multimodal objective functional appears. The paper describes a computational intelligence method - evolutionary algorithm (EA) in optimization of vibrating physical systems. The evolutionary algorithms (EAs) are based on mechanisms taken from biological evolution of species. This mechanism similar to biological one like a mutation, a crossover and a selection are used in EAs. EAs operate on population of chromosomes (individuals with one chromosome). EAs have found several application in optimization of mechanical structures [2].

2. Formulation of the optimization problem

Consider an elastic isotropic body which occupies a domain Ω bounded by a boundary Γ:

$$\mu\nabla^2\mathbf{u}+(\lambda+\mu)grad\ div\mathbf{u}+\mathbf{Z}=\rho\ddot{\mathbf{u}}(\mathbf{x},t),\quad \mathbf{x}\in\Omega, t\in T\in[0,t_f] \tag{1}$$

where:

$\mu,\ \lambda$ – Lame constants;

$\mathbf{Z}$ – body forces.

Equation (1) is supplemented by boundary conditions:

$$\mathbf{u}(\mathbf{x},t)=\overline{\mathbf{u}}(\mathbf{x},t),\quad \mathbf{x}\in\Gamma\equiv\partial\Omega$$
$$\mathbf{p}(\mathbf{x},t)=\overline{\mathbf{p}}(\mathbf{x},t),\quad \mathbf{x}\in\Gamma\equiv\partial\Omega \tag{2}$$

and initial conditions:

$$\mathbf{u}(\mathbf{x},t)\big|_{t=0}=\mathbf{u}^o(\mathbf{x}),\qquad \dot{\mathbf{u}}(\mathbf{x},t)\big|_{t=0}=\mathbf{v}^o(\mathbf{x}),\quad \mathbf{x}\in\Omega \tag{3}$$

The direct initial-boundary value problem is solved by the boundary element method [1]. The problem of the shape and topology optimization of elastic structures being under dynamical loads can be formulated as the minimization of the volume of the structure

$$J\equiv\int_{\Omega}d\Omega \tag{4}$$

subjected to the constraints imposed on equivalent stresses and displacements

$$\sigma_{eq}(\boldsymbol{x},t)-\sigma_o\le 0,$$
$$\big[\boldsymbol{u}(\boldsymbol{x},t)\big]-u_o\le 0, \tag{5}$$

where: $\big[\boldsymbol{u}\big]=\sqrt{\boldsymbol{u}\cdot\boldsymbol{u}}$ $\mathbf{x}\in\Gamma$ or $\mathbf{x}\in\Omega$, $t\in T=[0,t_f]$, σ_o and u_o are admissible equivalent stresses and displacement, respectively.

There is also an alternative formulation in which one minimizes a functional:

$$J\equiv\int_T\int_\Omega\Psi(\sigma,\varepsilon,\boldsymbol{u})d\Omega dt+\int_T\int_\Gamma\Phi(\boldsymbol{u},\boldsymbol{p})d\Gamma dt \tag{6}$$

with the constraints imposed on the volume of the structure:

$$J\equiv\int_\Omega d\Omega-Vo\le 0 \tag{7}$$

Integrands Ψ and Φ are the arbitrary functions of their arguments. Using the evolutionary algorithms, the minimization of (4) and (6) is performed with respect to shape design variables. The dual reciprocity boundary element method [1] enables evaluation of the functional (6) and constraints (5).

The boundaries in 2-D structure are modeling as the NURBS curves. In the case of 3-D structure the boundaries as the NURBS surfaces are modeled. Due to using the NURBS curves and surfaces, the number of optimized parameters can be decreased.

The voids in 2-D structure are modeling as the: (i) – circular, (ii) – elliptical, and (iii) – using the closed NURBS curve. In the case of 3-D structure the void as the: (i) – spherical, (ii) – ellipsoidal and (iii) – using the closed NURBS surface is modeled.

Due to introduction the special types of chromosomes the evolutionary algorithm finds the optimum very easy.

3. Formulation of identification problem

In identification problems one assumes that a body contains some defects as cracks or voids. The number, shapes and sizes of the defects are unknown.

The identification problem is expressed as the minimization of the special objective function. This function contains the physical values which can be measured in the special selected sensor points. The sensor points are located on the surface of the body. As the measured values are considered here: (i) – displacements under static loading, (ii) – displacements under dynamical loading, (iii) – eigenfrequencies. Therefore the function takes the forms:

- for displacements under static loading:

$$J = \sum \int_{\Gamma} \left[\hat{\mathbf{u}}(\mathbf{x}_i) - \mathbf{u}(\mathbf{x}_i) \right]^2 \delta(\mathbf{x} - \mathbf{x}_i) d\Gamma = \sum_i \left(\hat{\mathbf{u}}_i - \mathbf{u}_i \right)^2 \qquad (8)$$

- for displacements under dynamical loading:

$$J = \sum_i \sum_j \int_{\Gamma} \left[\hat{\mathbf{u}}(\mathbf{x}_i,t) - \mathbf{u}(\mathbf{x}_i,t) \right]^2 \delta(\mathbf{x} - \mathbf{x}_i) \delta(t - t_j) dt d\Gamma = \sum_i \sum_j \left(\hat{\mathbf{u}}_i^j - \mathbf{u}_i^j \right)^2 \qquad (9)$$

- for eigenfrequencies:

$$J = \sum_k \left(\hat{\omega}_k - \omega_k \right)^2 \qquad (10)$$

- and for all information:

$$J = \alpha \sum_i \left(\hat{u}_i - u_i \right)^2 + \beta \sum_i \sum_j \left(\hat{u}_i^j - u_i^j \right)^2 + \gamma \sum_k \left(\hat{\omega}_k - \omega_k \right)^2 \qquad (11)$$

where: $\hat{\mathbf{u}}_i$ - measured displacement in i-th sensor point, $\hat{\mathbf{u}}_i^j$ - measured displacement in i-th sensor point in j-th time step, $\hat{\omega}_k$ - measured k-th eigenfrequency. The analogous values without the hat mean adequate values computed by evolutionary algorithm. The parameters: α, β and γ are the weights.

The shape and topology parameters of the body are modelled in the similar way as in the optimization problem.

4. Evolutionary computing

Evolutionary algorithms are well known and applied in many areas of optimization problems [3]. The main disadvantage of these algorithms is the long time needed for computation. The parallel evolutionary algorithms perform an evolutionary process in the same manner as the sequential evolutionary algorithm. The difference is in a fitness function evaluation. The parallel evolutionary algorithm evaluates fitness function values in the parallel way. Theoretically, maximum reduction of time needed to solve the optimization problem using parallel evolutionary algorithms is equal to the number of used processing units. The flowchart of the parallel evolutionary algorithm is shown in Fig. 1. The starting population of chromosomes is created randomly. The evolutionary operators change chromosomes and the fitness function value for each chromosome is computed. The server/master transfers chromosomes to clients/workers. The workers compute the fitness function and send it to server. The workers operate on different processing units. The selection is performed after computing the fitness function value for each chromosome. The selection decides which chromosomes will be in the new population. The selection is done randomly, but the fitter chromosomes have bigger probability to be in the new population. The next iteration is performed if the stop condition is not fulfilled. The stop condition can be expressed as a maximum number of iterations. The evolutionary operators used in the presented algorithms are a crossover and a Gaussian mutation. The crossover chooses randomly two parent chromosomes and creates a new one containing a part of genes from the first and a part from the second parent. The Gaussian mutation creates chromosome based on a randomly chosen one. The part of the genes in a new chromosome have values changed by adding random numbers with the Gaussian distribution. The selection is performed by the use of the ranking method. The probability of being in the new population does not depend on the fitness function value, but on the number of chromosomes ordered accordingly to the fitness function values.
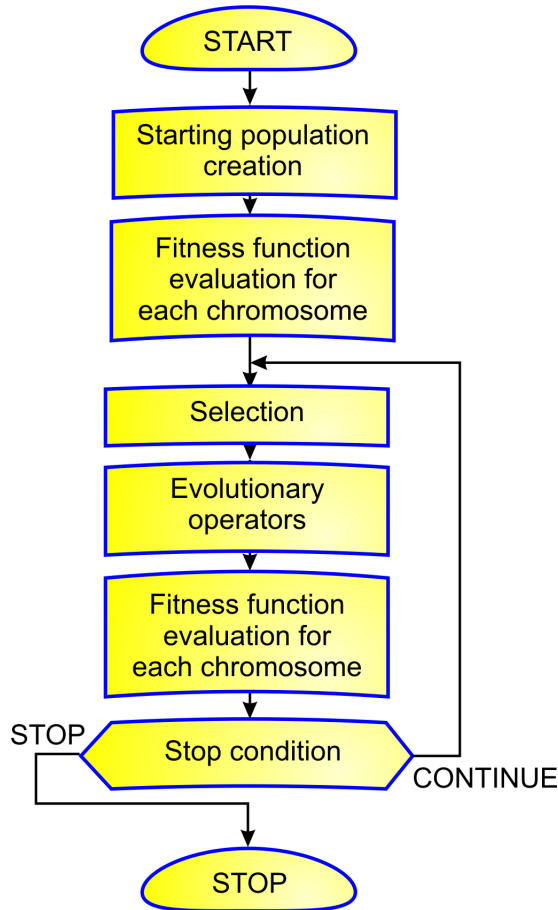
Figure 1. The flowchart of evolutionary algorithm

5. Example 1 – Shape optimization

The example concerns the minimization the mass of the support (Fig. 2). The support is loaded by dynamical loading $F(t)=F_0\sin(\omega t)$, F_0=10kN. The optimization fitness function (4) was used. The constraints on the values of the displacements were imposed. The surface of the support was modeled using the NURBS surface. The coordinates of the marked points (Fig. 3) (control points of the NURBS surface) were modified. The following parameters of the evolutionary algorithms were applied: *pop_size*: 50, *max_life*: 400. The optimal structure on the Fig.4 was shown.
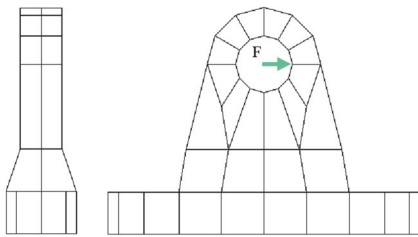
Fig.2. The support
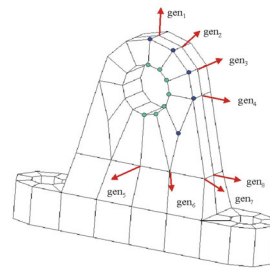
Fig.3. The NURBS control points
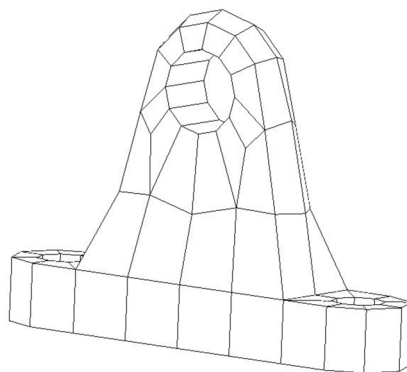
Fig.4. The support after optimization

6. Example 2 – Topology optimization

A shape and topology optimization problem of the structure presented in Fig.5 is considered for criterion (6). The evolutionary algorithm searched the optimal topology and shape of the structure.
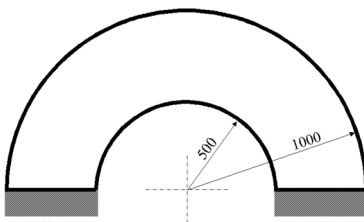
Fig.5. The structure before the optimization
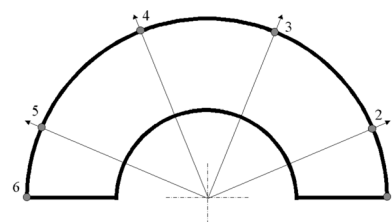
Fig.6. The parametrization of the structure

The upper part of the boundary was modelled using the 6-point NURBS curve, additionally 4 circular holes could be introduced to the structure. The population size of the evolutionary algorithm was equal to 200. The number of generations was equal to 100. After the optimization the fitness function was decrased from 2226 to 2271 s^{-1}. The Fig. 7 shows the optimal topology and shape after the optimization.

Fig.7. The structure after the optimization

7. Example 3 – Shape identification

Consider a two-dimensional elastic body (plane strains) with a circular hole (Fig.8).
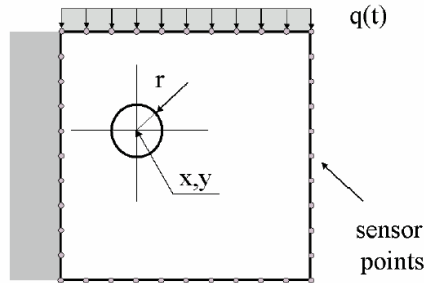
Fig.8. The plate with the circular defect

The body (1 cm × 1 cm) is loaded dynamically by a traction field $q(t) = qH(t)$, where q =100kN, $H(t)$ – Heaveside function. The coordinates x, y and the radius r of the hole are unknown. The aim of the test is the identification of the parameters of the hole through the minimization of the objective functional (9).

The actual parameters of the hole are: $x = 0.30$, $y = 0.60$ and $r = 0.10$. The parameters of the EA are as follows: the probability of the mutation: $pro\_mut = 0.2$, the probability of the crossover: $pro\_cro = 0.2$, population size: $pop\_size = 100$. The number of generations is equal to 150.

The found values are equal to: $x = 0.29$, $y = 0.62$ and $r = 0.10$.

8. Example 4 – Topology identification

A 2-D structure, shown in the Fig. 9 contains two internal defects. The actual parameters of an elliptic void are: $z_2=z(2)=\{50, 25, 5, 2.5, 2.5\}$, where the first two parameters are co-ordinates of the ellipse center, next - two radii of the ellipse and the last one – the angle between the x_1 axis and first radius. The actual crack parameters are: $z_1=z(1)=\{20, 30, 5, 0, 0.25\}$ and are defined as for the ellipse. The identification task is to find a number of defects and their shape having displacements $\hat{\mathbf{u}}(\mathbf{x},t)$ in 33 sensor points, shown in the Fig. 9.
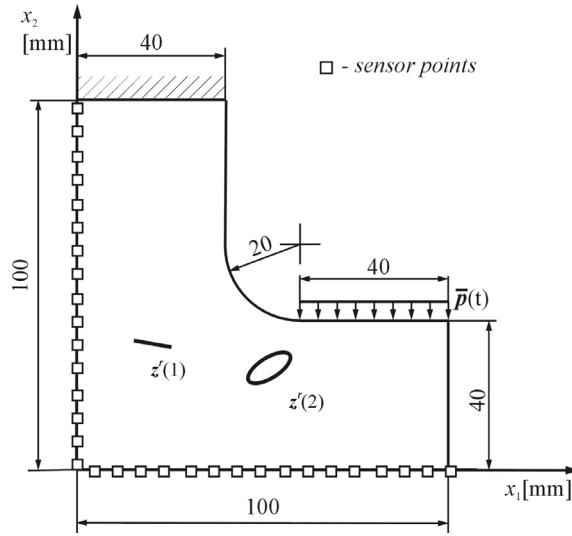
Fig. 9. The 2D structure with an internal crack and void

The structure is loaded by $p(t)=p_0\sin\omega t$ (p_0=40 kN/m, ω=15708 rad/s) in time $t\in[0,600]$ μs. The following parameters of the evolutionary algorithms are applied: *pop_size*: 2000, *max_life*: 100. Fig.10 presents the best solution of the first and the last generation.
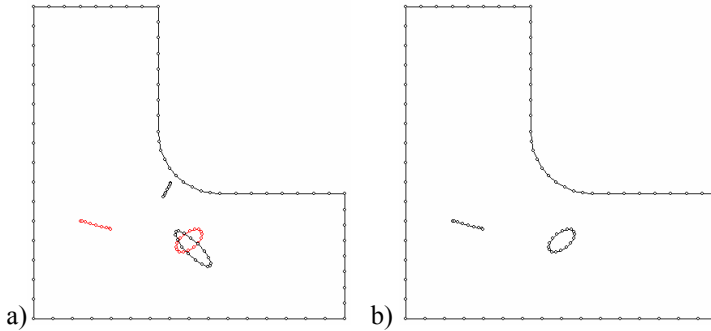
Fig.10. Results of defect identification :
a) 1st generation, b) 100th generation

9. Example 5 – Topology optimization based on the different informations

The last discussed problem concerns the different type of information in the sensor points. Consider the plate presented in the Fig.11. The few possibility of distance between the defects was considered: distance R={1, 3, 5, 7 and 9}mm. For each distance the identification problem was solve on basis the different information. In order to checking the influence the measured information to the identification process, the many test has been carried out. One of them is presented in this paper.
The aim of presented test is to find the circular defects in the plate (Fig. 11). The plate is constrained on the left side. The plate is loaded by q (static case) and q(t) = qH(t), where q =100kN, H(t) – Heaveside function (dynamic case). The minimized function has the following forms (8)-(11).
The following parameters of the evolutionary algorithms are applied: *pop_size*: 200, *max_life*: 500.
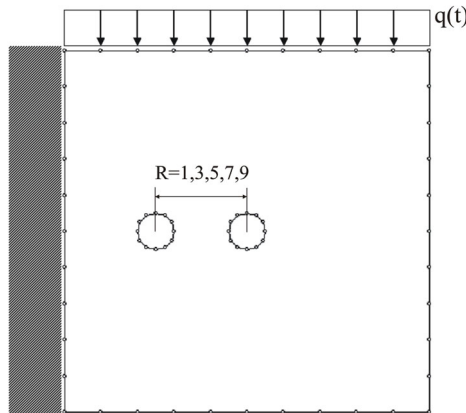
Fig.11. The plate the with the circular defects

The results of the identification process for following fitness functions (8)-(11) were presented in the Fig. 12-15.
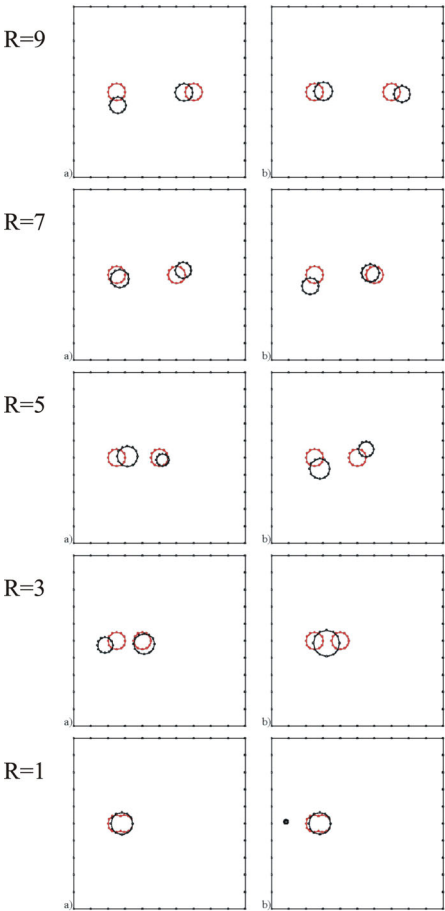
Fig.12. The results obtained for the fitness functions expressed by the displacement in static problem (8)
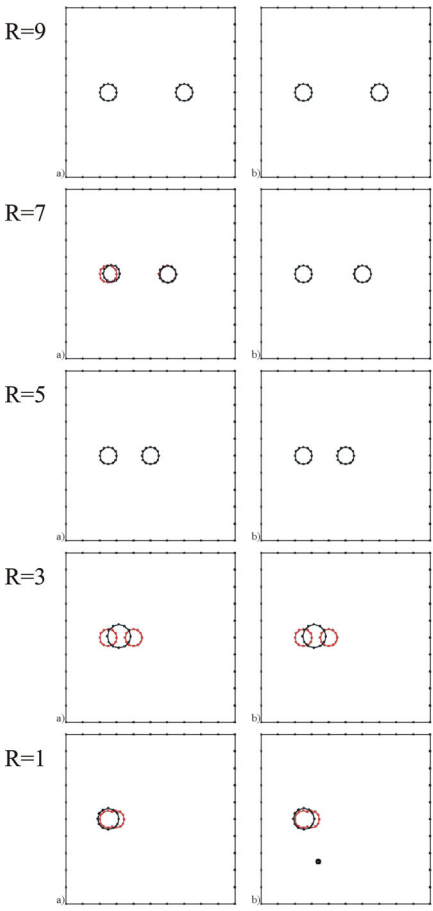
Fig.13. The results obtained for the fitness functions expressed by the displacement in dynamic problem (9)
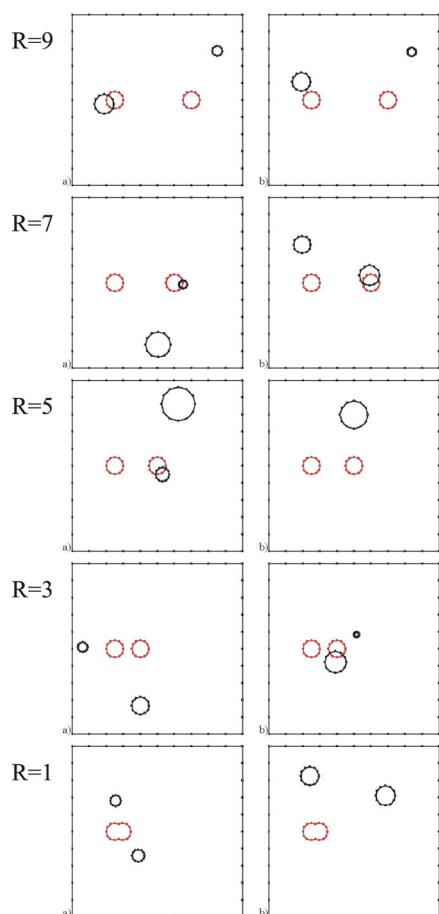
Fig.14. The results obtained for the fitness functions expressed by the frequencies in eigenvalue problem (10)
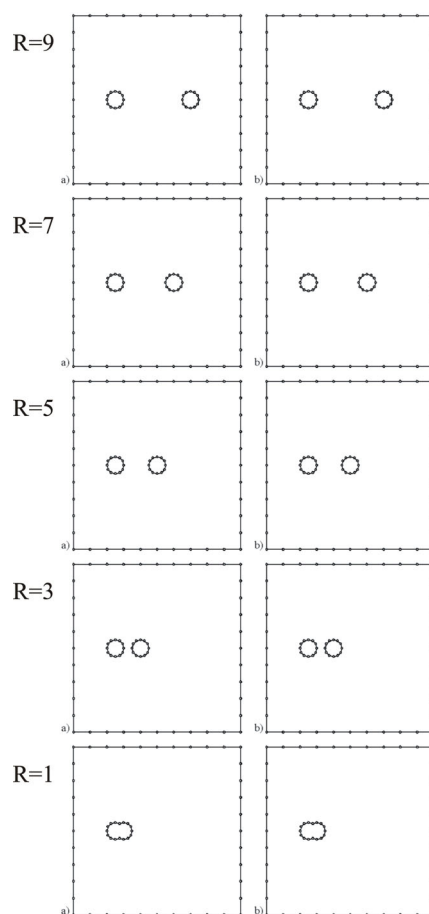
Fig.15. The results obtained for the fitness functions expressed by the sum of previous informations (11)

10. Conclusions

Evolutionary computing can be considered as an efficient approach for solving the shape and topology optimization and defect identification in dynamical physical systems.
Using NURBS curves allows modeling complicated shapes with a relatively small number of design variables. This method of parameterization decreases the time of computation.

Evolutionary algorithms are very time-consuming, but applications of different variants of parallel and distributed computing can speed up the optimization process.

References

1. T. Burczyński, *Metoda elementów brzegowych w mechanice*. WNT, Warszawa 1995.
2. T. Burczyński, A.Osyczka, (eds), *Evolutionary Methods in Mechanics*. Kluwer, Dordrecht 2004.
3. Z.Michalewicz, *Genetic Algorithms + Data Structures = Evolutionary Programs*, Springer-Verlag, Berlin 1996.

DYNAMICS OF A KINEMATICALLY EXCITED SYSTEM
WITH CHOSEN FRICTION MODELS

Jan AWREJCEWICZ, Dariusz GRZELCZYK, Yuriy PYRYEV
Department of Automatics and Biomechanics, Technical University of Łódź
ul. Stefanowskiego 1/15, Łódź
awrejcew@p.lodz.pl, dariusz.grzelczyk@p.lodz.pl, jupyrjew@p.lodz.pl

Abstract

Stick-slip vibrations in a mechanical system with dry friction and kinematical excitation with chosen friction models in a stick phase are studied in this work. Although there are numerous works in the scientific literature dedicated to stick-slip vibrations, a rigid body lying on a belt which moves at non-constant velocity is less investigated. A novel friction model is used and its advantages, in comparison to the often applied friction models, are illustrated. The behavior of the system is monitored via standard motion analysis in the system's phase space.

Key words: dry friction, stick-slip vibrations.

Introduction

Dry friction belongs to one of the most known phenomena in mechanical systems. Its proper mathematical modeling is not an easy task, because friction force is a complex process and in general depends on various parameters, e.g. slip velocity, normal load, temperature and time. An extensive literature review on applied friction models can be found in the works [1, 5, 6, 7, 9] and others.

Many practical engineering problems are related to vibrations caused or influenced by physical discontinuities, e.g. dry friction or impacts. In view of mechanical aspects, the authors of many publications are mainly concerned with dry friction stick-slip oscillations with different models of friction. Even in the last decade stick-slip vibrations were the aim of research of many authors, for example in the works [3, 4, 8]. In these works, stick-slip induced vibrations are studied for cases where body or bodies are riding on a driving belt as a foundation that moves at a constant velocity.

In this work, as the example of a mechanical system which exhibits stick-slip vibrations, the mechanical model with non-constant belt (foundation) velocity is studied. One degree-of-freedom model with dry friction is presented in Section 1, whereas numerical methods to calculate solutions in the system's phase space and results can be found in Section 2. Conclusions of our study are presented in the last Section 3.

1. Model with kinematical excitation

Consider a simple mechanical system with 1-dof and with kinematical excitation. The model of this system is shown in Figure 1. Disc II is characterized by mass moment of

inertia B, linear stiffness k and the coefficient of damping c. This disc is fixed to the frame. The second disc II is coupled with driving first disc I and dry friction occurs between the discs, which generates the moment of friction force M_{fr} (the maximum static moment of friction force is equal to M_s).
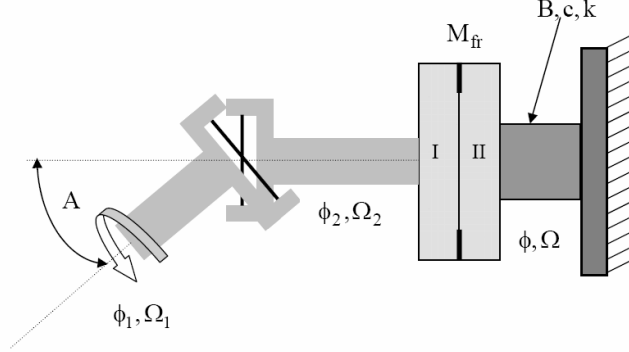
Fig. 1 One degree-of-freedom model with dry friction and kinematical excitation.

The excitation of the first disc is realized by Cardan mechanism with angle A between input shaft and output shaft, whose angular displacements are described by angles ϕ_1 and ϕ_2, respectively. Angular velocity Ω_2 is non-constant and not equal to angular velocity Ω_1 and is governed by the equation

$$\Omega_2 = \Omega_1 \frac{\cos A}{1 - \sin^2 \phi_1 \sin^2 A} . \tag{1}$$

The relative velocity of the second disc with respect to the first disc is denoted by $\Omega_{rel} = \Omega_2 - \dot{\phi}$. In this work we study non-constant maximum friction force M_s between coupled discs as a result of wear of these discs and its influence on our model dynamics. The additional static friction force is a function of the relative angular displacement between discs. For example, a model of the multi discs brakes has been studied in the works [10, 11]. For these reasons in our model a maximum static friction is the sum of constant moment of friction force M_H and additional moment with amplitude M_B. Therefore, in our model $M_s = M_H + M_B \sin(\phi_2 - \phi)$. It has been shown in reference [11] that term M_B depends on the wear of discs. The motion of the second disc is governed by the following second order differential dimensional equation

$$B\ddot{\phi} + c\dot{\phi} + k\phi = M_{fr} . \tag{2}$$

Let us introduce coefficient t_* and the following dimensionless parameters: $\tau = t/t_*$, $\varphi = \phi$, $\varphi_1 = \phi_1$, $\varphi_2 = \phi_2$, $\alpha = A$, $\omega = \dot{\phi}t_*$, $\omega_1 = \Omega_1 t_*$, $\omega_2 = \Omega_2 t_*$, $\omega_r = \omega_2 - \dot{\varphi}$, $d = ct_*/B$, $\omega_d^2 = kt_*^2/B$, $F_H = M_H t_*^2/B$, $F_B = M_B t_*^2/B$, $F_s = F_H + F_B \sin(\varphi_2 - \varphi)$. In our calculations we take $t_* = \sqrt{B/k}$. Then, vibrations of the second disc are governed by the following non-dimensional second order equation

$$\ddot{\varphi} + d\dot{\varphi} + \varphi = F_{fr}, \qquad (3)$$

where a dot denotes the differentiation with respect to non-dimensional time τ. The proposed continuous friction model has the following form

$$F_{fr}(\omega_r, F_{ex}) = \begin{cases} F(|\omega_r|)\operatorname{sgn}\omega_r, & V_1 \\ F_s \operatorname{sgn} F_{ex}, & V_2 \\ (2A_3 - 1)F_s \operatorname{sgn}\omega_r, & V_3 \\ A_3(-F_{ex} + F_s \operatorname{sgn}\omega_r) + F_{ex}, & V_4 \end{cases}, A_3 = \frac{\omega_r^2}{\varepsilon^2}\left(3 - 2\frac{|\omega_r|}{\varepsilon}\right), \quad (4)$$

where
$V_1 : |\omega_r| > \varepsilon$,
$V_2 : [(0 \le \omega_r \le \varepsilon) \cap (F_{ex} > F_s)] \cup [(-\varepsilon \le \omega_r \le 0) \cap (F_{ex} < -F_s)]$,
$V_3 : [(0 < \omega_r \le \varepsilon) \cap (F_{ex} < -F_s)] \cup [(-\varepsilon \le \omega_r < 0) \cap (F_{ex} > F_s)]$,
$V_4 : (|\omega_r| \le \varepsilon) \cap (|F_{ex}| \le F_s)$.

This model of friction has been already used by the authors in studies [2, 12]. In this model of mechanical system we have $F_{ex} = d\omega + \varphi$ and kinetic friction $F(|\omega_r|)$ is given by

$$F(|\omega_r|) = \frac{F_s}{1 + \delta|\omega_r|}. \qquad (5)$$

2. Numerical Computations and Results

Let us take the following dimensionless parameters: $d = 0.01$, $F_H = 1$, $\omega_1 = 0.2$, $\alpha = 0$, $\delta = 30$. The differential equations of motion are solved via the Runge-Kutta-Fehlberg (RKF 45) method with varied time step h ($h_{min} = 10^{-5}$, $h_{max} = 10^{-1}$) and with a Runge-Kutta-Fehlberg tolerance of $\eta = 10^{-6}$ and steepness parameter $\varepsilon = 10^{-3}$. The system dynamics is monitored via standard time histories in the system's phase space.

Let us consider the first solution without an additional term in the moment of friction force, i.e. for $F_B = 0$. Figure 2 shows phase portraits obtained with the two compared friction models (the standard approximation using a signum function modeled by the

second-order polynomial in the stick phase and the proposed model). For the first friction model the computation took 84533 integrations points to obtain the orbit with the non-dimensional period time 13.5. Small time steps are not necessary near the transitions, but during the whole stick phase, as Figure 2a shows. For our friction model the computation took only 231 integrations points to obtain the same orbit (Figure 2b).

a)   b)
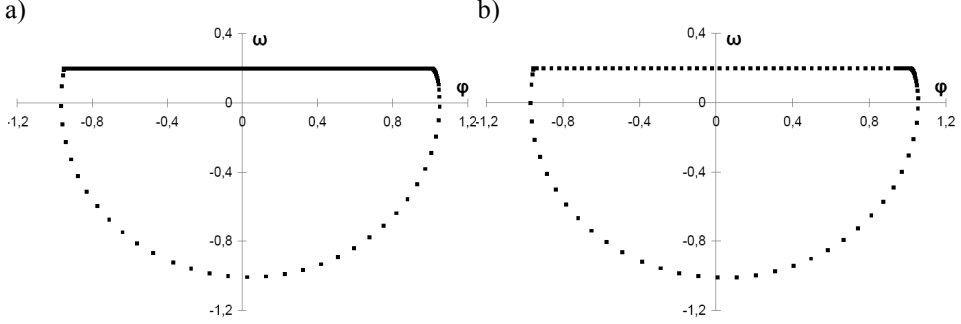
Fig. 2 Points of trajectories of motion in the system's phase space for different models of friction:
a) smoothing approximation, b) the proposed model.

In this case small time steps are taken only near the transitions between stick and slip phases and time step in the stick phase is bounded by maximum time step h_{max}. Consequently, we show that in this case smoothing approximation of classical signum function is clearly more expensive than the proposed model. The differential in the first friction model is extremely large for relative velocity equal to zero, whereas in our model it is equal to zero and this is an advantage for numerical computations.

Figure 3 shows time histories in the system's phase space in the neighborhood of zero value of the relative velocity.

a)   b)
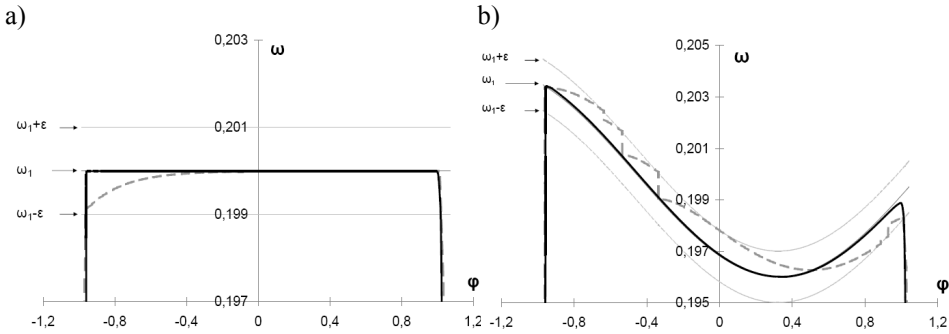
Fig. 3 Trajectories of motion in the stick phase for different models of friction: switch model
(dashed line) and the proposed model (solid line) for a) $\alpha = 0$ and b) $\alpha = 0.2$.

Our continuous friction model was compared with the so called switch model [8]. We are focused now on the near-zero relative velocity because the periodic stick-slip

oscillations have the sliding velocity almost the same (both for the switch model and continuous friction model) and in the sticking phase some differences are observed.

Below, the investigated system dynamics is reported for $F_H = 0.2$ (Figure 4) and for $F_H = 1$ (Figure 5) related to various parameters F_B and α in the time interval (50, 150).

$F_B = 0$, $\alpha = 0$.

$F_B = 0$, $\alpha = 0.5$.

$F_B = 0.01$, $\alpha = 0$.

$F_B = 0.01$, $\alpha = 0.5$.
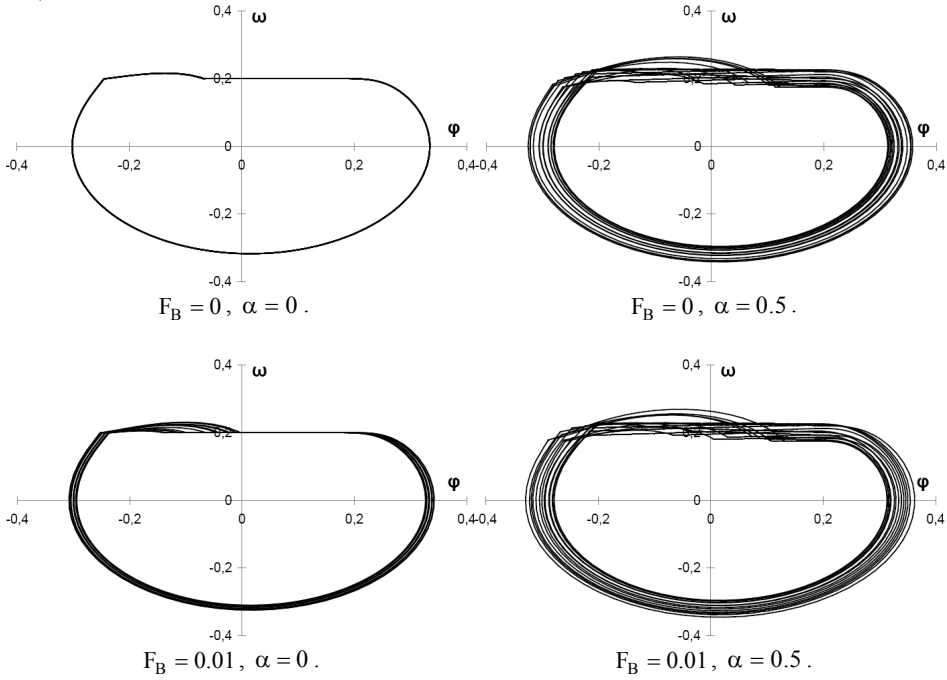
Fig. 4 Phase portraits for $F_H = 0.2$ and various parameters F_B and α .
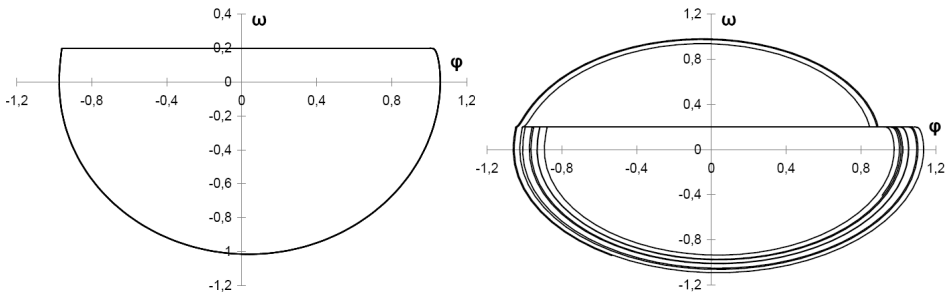
Fig. 5 Phase portraits for $F_B = 0$ (on the left) and for $F_B = 0.1$ (on the right).

Phase portraits in Figures 4 and 5 indicate that dynamical behavior depends both on uneven of velocity of the first disc as a result of non-zero α angle and on the process of wear of discs, which strongly influences the system dynamics.

3. Conclusions

A continuous friction model suitable for simulation of stick-slip vibrations is proposed and validated using a one-degree-of-freedom mechanical system with dry friction. The model yields engineering accepted results and has some advantages in comparison to other friction models. Contrary to the smoothing methods, our calculations are less expensive from the computational point of view. Our results indicate better numerical accuracy of the proposed continuous model. Contrary to the switch model results, the results obtained using the continuous friction model are better. We have obtained almost exact solutions (high precision numerical computations). In addition, some interesting dynamic behaviors are reported and analyzed, including stick-slip periodic and non-periodic motions.

References

1. J. Awrejcewicz, P. Olejnik, *Analysis of dynamics systems with various friction laws*, Applied Mechanics Reviews, **58**(6) (2005) 389 – 411.
2. J. Awrejcewicz, D. Grzelczyk, Yu. Pyryev, *On the stick-slip vibrations continuous friction model*, Proceedings of the 9th Conference on Dynamical Systems – Theory and Applications, Eds: J. Awrejcewicz, P. Olejnik, J. Mrozowski, Łódź, Poland, December 17-20 (2007) 113 – 120.
3. U. Galvanetto, S. Bishop, *Dynamics of a Simple Damped Oscillator Undergoing Stick-Slip Vibrations*, Meccanica, **34** (1999) 337 – 347.
4. N. Hinrichs, M. Oestreich, K. Popp, *Dynamics Oscillators with Impact and Friction*, Chaos, Solitons and Fractals, **8**(4) (1997) 535 – 558.
5. R.A. Ibrahim, *Friction-induced vibration, chatter, sequeal, and chaos. Part I: Mechanics of contact and friction*, Applied Mechanics Reviews, **47**(7) (1994) 209 – 226.
6. I.V. Kragelsky, V.S. Shchedrov, *Development of the science of friction*, Izd. Acad. Nauk SSSR, Moscow 1956 (in Russian).
7. S.P. Kuznecov, *Dynamical chaos* , Moskva Fizmatlit 2001, in Russian.
8. R.I. Leine, D.H. Van Campen, A. De Kraker, Van den Steen, *Stick-Slip Vibrations Induced by Alternate Friction Models*, Nonlinear Dynamics, **16**(1) (1998) 41 – 54.
9. J.A.C. Martins, J.T. Oden, F.M.F. Simoes, *A study of static and kinetic friction*, Int. J. Engng. Sci., **28**(1) (1990) 29 – 92.
10. J. Osiński, M. Sadowski, *Dynamical behavior of a multi-disks brake made from composite C/C*, II International Conference Modeling and Simulation of the Friction Phenomena in the Physical and Technical Systems "Friction 2002", December (2002) 176 – 182, in Polish.
11. L. Prochowski, *Vibrations generated by discs brakes*, Scientific Bulletin of Vehicle Institute of the Warsaw University of Technology, **1**(44)/2002, Warszawa 2002, in Polish.
12. Yu. Pyryev, D. Grzelczyk, J. Awrejcewicz, *On a novel friction model suitable for simulation of the stick-slip vibration*, Khmelnitskiy State University Bulletin, **1**(4) (2007) 86 – 92.

MOVING INERTIAL LOAD AND NUMERICAL MODELLING

Czesław BAJER and Bartłomiej DYNIEWICZ
Institute of Fundamental Technological Research, Polish Academy of Sciences,
Świętokrzyska 21, 00-049 Warsaw, Poland

Abstract

The paper presents the numerical approach to the moving mass problem. We consider the string and beam discrete element carrying a mass particle. In the literature efficient computational methods can not be found. The same disadvantage can be observed in commercial codes for dynamic simulations. Classical finite element solution fails. The space-time finite element approach is the only method which now results in convergent solutions and can be successfully applied in practice. Characteristic matrices and resulting solution scheme are briefly described. Examples prove the efficiency of the approach.

Keywords: moving mass, time integration, space-time finite element

Introduction

Classical problems of structures subjected to a moving force were intensively treated in recent years. Closed analytical solutions can be found for example in [1]. We must mention here that numerous publications deal with the problem, starting from the 18th century. Numerical application of the moving force is also relatively simple. The force for example can be distributed between neighbouring nodes in the mesh with the ratio varying in time and depending on the position of the particle. The problem of inertial moving load applied to discrete systems and efficiently solved unfortunately is practically not reported. Inertial force, which should be considered as a couple of a force and a mass is usually replaced by a spring-mass system. Finally the problem is solved as a problem with a massless force. This approach is characteristic of significant error, which raises to the ratio 1:3 comparing with the accurate solution, in the case of the speed between 0.8 and 1.0 of the wave speed (Fig. 1). We must also emphasize that the ad-hoc mass distribution between neighbouring nodes simply fails. In the case of the beam at low speed ranges and low ratio of the moving mass to the beam mass results exhibit errors. Unfortunately, Such formulations exist in spite of a wrong formulation and analysis.

In the paper we present the numerical approach to the moving inertial load problem. Classical finite element method with Newmark time integration scheme mentioned in [2, 3] fails. The space-time finite element method is the only method which enables us to describe the mass passing through the spatial finite element in a continuous way. We present the solution in the case of a string and a Bernoulli-Euler beam. The reader should be familiar with the basics of the space-time finite element approach described in velocities [4, 5].
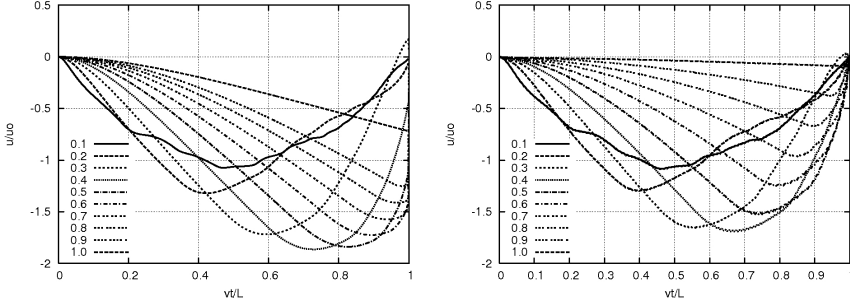
Figure 1: Displacements under the moving mass from the semi-analytical solution (left) and under the rigid oscillator (right).

The motion equation of a string under a moving inertial load with a constant speed v has a form

$$-N\,\frac{\partial^2 u(x,t)}{\partial x^2}\ +\ \rho A\,\frac{\partial^2 u(x,t)}{\partial t^2}\ =\ \delta(x-vt)\,P\ -\ \delta(x-vt)\,m\,\frac{\partial^2 u(vt,t)}{\partial t^2}\ . \quad (1)$$

We assume initial conditions $u(x,0)=0$, $\dot u(x,0)=0$ and boundary conditions $u(0,t)=u(l,t)=0$.

1.   String element carrying moving mass

The last term $\delta(x-vt)\,m\,\partial^2 u(vt,t)/\partial t^2$ in the motion equation (1) describes the inertial moving mass. $\partial^2 u(vt,t)/\partial t^2$ is the vertical acceleration of the moving mass and at the same time the acceleration of the point of the string in which the mass is temporarily placed (it is $x=x_0+vt$). The acceleration of the mass $\partial^2 u(vt,t)/\partial t^2$ moving with a constant velocity v, according to the Renaudot formula (which in fact is the chain rule of differentiation), results in three terms:

$$\frac{\partial^2 u(vt,t)}{\partial t^2}\ =\ \left.\frac{\partial^2 u(x,t)}{\partial t^2}\right|_{x=vt} +\ 2v\left.\frac{\partial^2 u(x,t)}{\partial x\partial t}\right|_{x=vt} +\ v^2\left.\frac{\partial^2 u(x,t)}{\partial x^2}\right|_{x=vt}. \quad (2)$$

Thus we can separate the transverse acceleration, the Coriolis acceleration, and the centrifugal acceleration, respectively. This is the so-called Renaudot notation for the constant speed v. Another one, the so-called Jakushev notation (or approach) finally gives the same result in our case of the constant mass m.

In our space-time finite element method we formulate equations in terms of velocities. The mass acceleration $\partial^2 u(vt,t)/\partial t^2$ is expressed in terms of velocities as well:

$$\frac{\partial^2 u(vt,t)}{\partial t^2}\ =\ \frac{\partial v(vt,t)}{\partial t}\ =\ \left.\frac{\partial v(x,t)}{\partial t}\right|_{x=vt} +\ v\left.\frac{\partial v(x,t)}{\partial x}\right|_{x=vt}. \quad (3)$$

The first term on the right-hand side of (2) states the real inertia (when multiplied by m) and the second term (also multiplied by m) expresses forces similar to damping forces.

In the final stage three resulting matrices are responsible for transverse inertia (the matrix has the form of the inertia matrix), damping forces (the matrix multiplied by the velocity vector has a form similar to the Coriolis forces) and stiffness (potential) forces (the matrix, if multiplied by the velocity vector, has a form similar to the centrifugal forces). The third matrix appears as a result of initial displacements in the time interval.

Let us now follow this idea and treat numerically the right-hand side inertial term of (1). The same mathematical steps as in the case of pure string enables us to integrate the inertial term

$$\int_0^h \int_0^b \mathbf{N}^* m \, \delta(x - vt) \frac{\partial^2 u(x_0 + vt, t)}{\partial t^2} \, dx, dt \; . \tag{4}$$

First we must formulate the virtual power equation. Then it is integrated in the space-time domain. The resulting virtual work equations allows us to derive required metrices in the time stepping scheme. We use the linear interpolation of the velocity in space and in time. The virtual velocity v^*:

$$v^*(x, t) = \mathbf{N}^* \dot{\mathbf{q}}_p = \delta(t - \alpha h) \begin{bmatrix} 1 - \frac{x}{b} \\ \frac{x}{b} \end{bmatrix} \dot{\mathbf{q}}_p \tag{5}$$

Figure 2: Mass path in the space-time finite element domain.

Consequent integration results in two matrices: the moving mass inertia matrix $\mathbf{K}_m$

$$\mathbf{M}_m = \frac{m}{h} \left[\begin{array}{cc|cc} -(1 - \kappa)^2 & -\kappa(1 - \kappa) & (1 - \kappa)^2 & \kappa(1 - \kappa) \\ -\kappa(1 - \kappa) & -\kappa^2 & \kappa(1 - \kappa) & \kappa^2 \end{array} \right] , \tag{6}$$

where $\kappa = (x_0 + v\alpha h)/b$, x_0 is a starting position of the mass in the space-time element (at $t = t_0$) (see Fig. 2), and the moving mass damping matrix $\mathbf{C}_m$

$$\mathbf{C}_m = \frac{mv}{b} \left[\begin{array}{cc|cc} -(1 - \kappa)(1 - \beta) & (1 - \kappa)(1 - \beta) & -(1 - \kappa)\beta & (1 - \kappa)\beta \\ -\kappa(1 - \beta) & \kappa(1 - \beta) & -\kappa\beta & \kappa\beta \end{array} \right] . \tag{7}$$

Let us now consider the contribution of $u(x, 0)$ being the constant term of the integration in time. We integrate by parts the virtual work

$$v^2 \int_0^h \int_0^b v^* \frac{\partial^2 u_0}{\partial x^2} dxdt = -v^2 \int_0^h \int_0^b \frac{\partial v^*}{\partial x} \frac{\partial u_0}{\partial x} dxdt \tag{8}$$

Since displacements of the left and right node of the element are expressed by $u_L = u_L^0 + h[\beta v_1 + (1-\beta)v_3]$ and $u_R = u_R^0 + h[\beta v_2 + (1-\beta)v_4]$, we can derive the required $\mathrm{d}u_0/\mathrm{d}x$

$$\frac{\mathrm{d}u_0}{\mathrm{d}x} = \frac{u_R - u_L}{b} = \frac{u_R^0 - u_L^0}{b} + \frac{h}{b}[-\beta v_1 + \beta v_2 - (1-\beta)v_3 + (1-\beta)v_4] \quad (9)$$

Matrix $\mathbf{K}_m$ is the stiffness mass matrix

$$\mathbf{K}_m = \frac{hmv^2}{b^2} \left[\begin{array}{cc|cc} \beta & -\beta & 1-\beta & -(1-\beta) \\ -\beta & \beta & -(1-\beta) & 1-\beta \end{array} \right] \quad (10)$$

The term $(u_R^0 - u_L^0)/b$ in (9) multiplied by mv^2/b results in initial nodal forces $\mathbf{e}$ in the space-time layer.

2. Beam element carrying moving mass

We remember that virtual time function v^* in the hat shape is constant in time and in the case of the Bernoulli-Euler beam has the following form

$$v_m^*(x,t) = \left(1 - 3\frac{x^2}{b^2} + 2\frac{x^3}{b^3}\right) v_3 + \ldots \dot{\varphi}_3 + \ldots v_4 + \ldots \dot{\varphi}_4 \quad (11)$$

We recognize here the well known shape functions that describe displacements (or velocities) in terms of nodal displacement and nodal rotations. The same interpolation formulas are applied as real spatial shape functions. Then the the elements of the matrix $\mathbf{M}_m$ can be computed. We present here the analysis in the case of the first element $(\cdot)_{11}$ of the inertia matrix only.

$$\begin{aligned} (\mathbf{M}_m)_{11} &= -\frac{m}{h} \int_0^h \int_0^b \delta(x - x_0 - vt) \left(1 - 3\frac{x^2}{b^2} + 2\frac{x^3}{b^3}\right)^2 \mathrm{d}x\mathrm{d}t = \\ &= -\frac{m}{h} \int_0^h \int_0^b \left[1 - 3\frac{(x_0 + vt)^2}{b^2} + 2\frac{(x_0 + vt)^3}{b^3}\right]^2 \mathrm{d}x\mathrm{d}t \end{aligned} \quad (12)$$

We introduce the substitution:

$$s = \frac{x_0 + vt}{b} \quad \text{and} \quad \mathrm{d}s = \frac{v}{b}\mathrm{d}t . \quad (13)$$

The coefficient $(\mathbf{M}_m)_{11}$ can be written then

$$(\mathbf{M}_m)_{11} = -\frac{m}{h} \int_0^h \left(1 - 3s^2 + 2s^3\right)^2 \mathrm{d}s = -\frac{m}{h}\frac{b}{v} \left(\frac{4}{7}s^7 - 2s^6 + \frac{9}{5}s^5 + s^4 - 2s^3 + s\right)\Big|_0^h \quad (14)$$
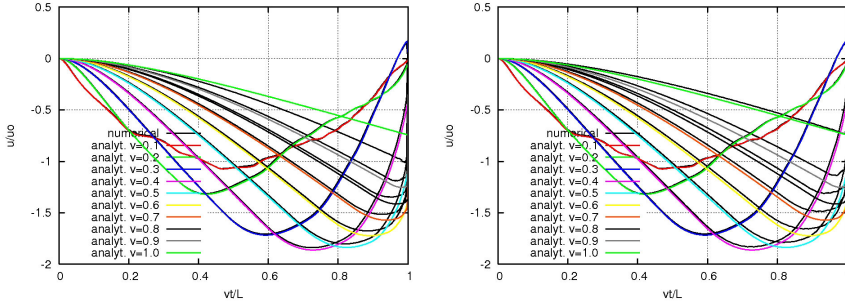
Figure 3: Displacements under moving mass – space-time finite element solution for $\alpha = 0.5$ (upper) and $\alpha = 1.0$ (lower) compared with analytical solution.

3. Numerical results

In our tests the string was discretized by a set of 200 finite elements. The time step h was equal to $b/40v$. It means that the mass passes from joint to joint in 40 time steps. Results obtained by the space-time finite element method are presented in Fig. 3.

Higher velocity can also be considered. Fig. 4 presents displacements in time of the particle for $0.9 \leq v/c \leq 1.2$. We notice a good coincidence of the plot with the expected zero line. We can recall only for information the plot of oscillator displacements moving over the span. The oscillator spring stiffness was assumed to be high enough, to simulate a rigid contact of the mass with the string. Results are depicted in Fig. 1. The solution is significantly worse than results obtained with the method presented in this paper.
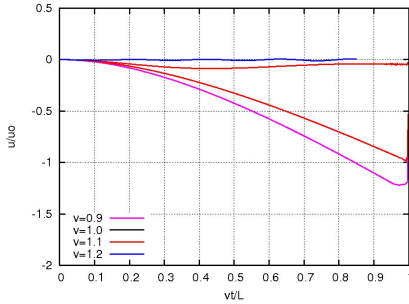
Figure 4: Displacements under the mass moving on a string for v equal to 0.9, 1.0, 1.1 and 1.2 c.
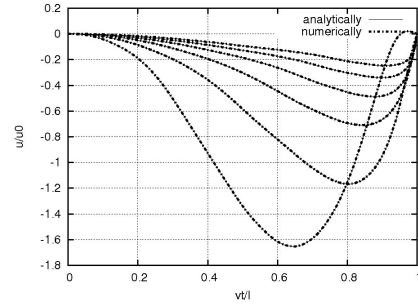
Figure 5: Displacements under the mass moving on the Bernoulli-Euler beam at the speed v=0.1, 0.2, ..., 0.6 (numerical and semi-analytical results).

Numerical results of displacements in time of the Bernoulli-Euler beam are presented in Fig. 5. The following data were applied: E=1.0, A=1.0, I=0.01, l=1.0, ρ=1.0, m=1.0, and P=1.0. We emphasize here that numerical results perfectly coincide with semi-analytical solution in a wide range of the mass velocity. We applied non-dimensional speed v up to 0.6, which corresponds with the 0.4 of the critical speed. The critical speed means the speed of the force travelling in a cyclic way through a beam and increases the vertical deflection to infinity. In the case of the moving mass the critical speed has considerably lower value and in our example we approaches to it.

4. Conclusions

We deal with the problem of the numerical treatment of the moving mass problem. The solution presented in the paper shows the way of mathematical analysis which results in a universal time stepping procedure. It enables us to solve the problem with the arbitrary speed. The solution in the case of the string exhibits discontinuous mass trajectory [6, 7] at the end support. This fact influences high gradients of the solution at the final stage of the motion. This phenomenon is the paradoxical property of the differential equation (1) since considering boundary conditions we intuitively expect smooth curves. Numerical results of the string vibrations exhibit good accuracy, comparing with semi-analytical solution. In the case of the beam the coincidence of both curves is perfect.

The solution presented in the paper is the only correct end efficient numerical solution of the moving mass problem in the literature.

References

1. L. Frỳba. *Vibrations of solids and structures under moving loads.* Academia, Prague, 1972.
2. F.V. Filho. Finite element analysis of structures under moving loads. *The Shock and Vibration Digest*, 10(8):27–35, 1978.
3. E.C. Ting, J. Genin, and J.H. Ginsberg. A general algorithm for moving mass problems. *J. Sound Vib.*, 33(1):49–58, 1974.
4. C. Bajer. Space–time finite element formulation for the dynamical evolutionary process. *Appl. Math. and Comp. Sci.*, 3(2):251–268, 1993.
5. C.I. Bajer and C. Bohatier. The soft way method and the velocity formulation. *Comput. and Struct.*, 55(6):1015–1025, 1995.
6. B. Dyniewicz and C.I. Bajer. Paradox of the particle's trajectory moving on a string. *Arch. Appl. Mech.*, 2008. in print.
7. C.I. Bajer and B. Dyniewicz. Space-time approach to numerical analysis of a string with a moving mass. *Int. J. Numer. Meth. Engng.*, 2008. in print.

ON THE APPLICATION OF THE MATHEMATICA ENVIRONMENT FOR SOLVING THE PROBLEMS OF DYNAMICS OF MECHANISMS OF THIRD CLASS

Jacek BUŚKIEWICZ
Politechnika Poznańska
Instytut Mechaniki Stosowanej
Tel. 061-6652-177
Jacek.buskiewicz@put.poznan.pl

Abstract

The paper presents the solution of a chosen dynamic problem, i.e. determination of the engine power to drive a mechanism, by means of the Mathematica environment for numerical and symbolic computations. It was done on the example of a third class mechanism. The author's intention is to show the advantages of replacing the classes on "Mechanism Theory" with the computer laboratory.

Keywords: numerical methods, mechanism theory, kinematics and dynamics of mechanisms

1. Introduction

The complexity and strong nonlinearity of dynamics problems preceded by the kinematic and geometric analyses arise from the technical applicability of the mechanisms theory. Analytical solutions are restricted to simple mechanisms of well-chosen geometry since, in general, they are time-consuming and cumbersome. It contributed to the development of graphical methods that are robust to the mechanism geometry. The solutions obtained for a few time instants are approximated on the whole operating cycle. The graphical methods do not allow the full kinematic analysis: singular position avoidance, movement simulation, optimum transfer of driving torque, etc. Then, it prevents from mechanism design. The growth of the computer technology causes the graphical methods to have been replaced with the numerical-analytical ones. It forces the changes in teaching Mechanism Theory, i.e. necessity of introducing computer laboratory, which allows to solve effectively problems of dynamics of mechanisms.

The dynamical analysis requires determination of mechanism position from a system of non-linear algebraic equations. In general, many solutions are possible [1-6]. Complexity of the issue depends on the structure of mechanism, mainly on the class of Assur groups included in it. The method of changing active link in a mechanism allows decreasing its class but cannot be used in all the cases of higher class mechanisms. The method of modification of kinematic units was proposed by Mlynarski [5] to convert groups of higher class into groups of second class and illustrated using the four class mechanism of so-called Walking Machine. The paper [2] presents an interesting way of searching all possible positions of Assur group of third class and third order with four links and six prismatic/revolute joints when the positions of external joints are given. The presented procedure leads from geometric equations to one polynomial equation the

real roots of which are related to all possible positions of the internal joints. The authors extended the applicability of the method to the group of four class with one prismatic and five revolute joints [3]. The sixth-order polynomial is obtained which leads, in an extreme case, to six different configurations.

The dimension of the system of kinematic equations depends strongly on the type of chosen coordinates. Cartesian coordinates lead to less coupled and easy to formulate constraint equations, however, the number of unknowns is greater in comparison with the choice of natural or relative coordinates [7].

The paper presents the solution of a chosen dynamic problem in Mathematica environment for symbolic and numerical computations [8]. It is done on the example of the mechanism shown in Fig. 1. The advantage of the approach is that it contains general algorithm for solving problems of this type.

2. Problem formulation

The mechanism of third class RS-SR-RR is considered. The active link is the crank O_1A rotating at given rotational speed $n=120 obr/\min$. The problem is to determine the engine output torque and engine power to drive the mechanism assuming the slider F is subject to the external load $P_U = \begin{cases} 1000N; v_F > 0 \\ -1000N; v_F < 0 \end{cases}$. The mechanism dimensions are:

$l_1 = 30cm$, $l_{31} = 2.4m$, $l_{32} = 2.4m$, $l_4 = 1.6m$, $l_5 = 1.5m$, $\alpha = 25°$, $\beta = 125°$, $\gamma = 140°$. The initial position is assumed to be known. Mass of the link BCD is essential, the others are neglected: $m_3 = 7.2$ kg, $I_3 = 3.456 \, kgm^2$. The flywheel is to be determined also when the admissible coefficient of the speed fluctuation $\eta = 1/40$.

Geometric analysis

The review of literature shows that the methods of the position determination depend on the class and type of kinematic pairs of a mechanism. Therefore, in general case the iterative methods have to be applied [12]. The presented approach does not take the use of the classical vector equations for kinematics. The vector equations for so-called closed independent loops [7, 10] are written. Then, there is need to distinguish among motions the plane motion, rectilinear translation and rotational motion, which is required in graphical methods. The position and orientation of the revolute pair is described by the angles measured anticlockwise from the positive direction of the Ox axis to the link. The position of the slider in the prismatic pair describes its displacement with respect to one of joints. Following this rules unknown angles f_2, f_5 and displacements s_1, s_2 are introduced. The equation $f_3 = f_2 + \beta - \alpha$ relates the angles f_2, f_3 in prismatic pair. The equations for independent loops are the minimum number of vector equations allowing to compute these coordinates. In the considered example they are

$$\overrightarrow{O_1A} + \overrightarrow{AB} + \overrightarrow{BC} = \overrightarrow{O_1O_3} + \overrightarrow{O_3F} + \overrightarrow{FC}, \quad \overrightarrow{O_3F} + \overrightarrow{FC} + \overrightarrow{CD} = \overrightarrow{O_3O_2} + \overrightarrow{O_2D} \quad (1)$$

which leads to four scalar equations. The constant vectors (time independent) are neglected as vanishing at differentiating.

```
Cos[f2[t]] s1[t] + Cos[f1[t]] l₁ - Cos[β + f2[t]] l₃₁ == -Cos[γ] s2[t] + Cos[φ] l₄
```

```
s1[t] Sin[f2[t]] + Sin[f1[t]] l₁ - Sin[β + f2[t]] l₃₁ == -s2[t] Sin[γ] + Sin[φ] l₄ (2)
```

```
-Cos[γ] s2[t] + Cos[φ] l₄ + Cos[α - β - f2[t]] l₃₂ == Cos[f5[t]] l₅
```

```
-s2[t] Sin[γ] + Sin[φ] l₄ + Sin[α - β - f2[t]] l₃₂ == Sin[f5[t]] l₅
```
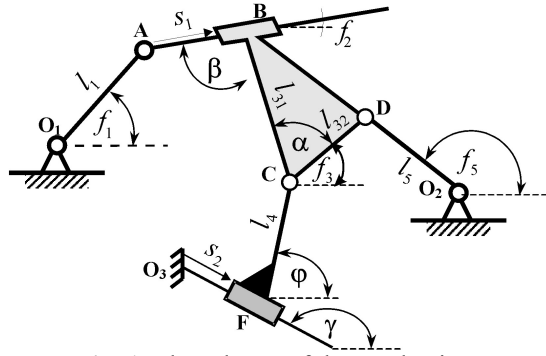

Fig. 1. The scheme of the mechanism.

The initial values for $f_1 = 0$ are: $s_1 = 2m, f_2 = 15°, s_2 = 1.5m, f_5 = 140°$.

Kinematic analysis

The kinematic equations are obtained after differentiating Eqs. (2) with respect to time. The second differentiation relates the accelerations. This is done by the program automatically and no user activity is expected. The manual computations of accelerations and velocities are not sophisticated but much time – consuming. The initial position is known and the iterative method is applied for determining the subsequent ones. The cycle is divided into n – time instants $t_j = \dfrac{j}{n}T$, $T = \dfrac{2\pi}{\omega}$, $\omega = \dfrac{\pi}{30}120rad/s$.

Due to limited size of the paper the basic instructions of Mathematica are not explained, the exceptions are special functions. The separate quantities are collected in so-called lists. A user enters the following lists: : *wsp* – the coordinates s_1, f_2, s_2, f_5 describing the positions and orientations of the links, *wartp* – the values of the coordinates at the initial position, *Loop1* – the x components of the loop equations. Mathematica itself generates the subsequent lists: *dwsp* – the first derivative of the *wsp* derived by means of instruction *D[wsp,t]*, *d2wsp* – the second derivative of the *wsp* derived by means of instruction *D[dwsp,t]*, *Loop2* – the y–component of loop equations that are produced by replacing cosine with sine in the *loop1*, *Loop* – all the scalar

equations for positions, **Eqv** - velocity equations computed as derivatives of the loop equations **D[loop,t]**, **Eqa** – acceleration equations computed as the derivative of the **Eqv** **D[eqv,t]**.

The first fragment of the algorithm computes these lists. The input values are in boxes.

```
wsp={s1[t],f2[t],s2[t],f5[t]};
lzm=Length[wsp];
wartp={2.0,15*Pi/180,1.5,140*Pi/180};
dwsp=D[wsp,t];
d2wsp=D[dwsp,t];
loop1 =
  {l₁ * Cos[f1[t]] + wsp[[1]] * Cos[wsp[[2]]] + l₃₁ * Cos[β + π + wsp[[2]]] ==
    wsp[[3]] * Cos[γ + Pi] + l₄ * Cos[φ],
   wsp[[3]] * Cos[γ + Pi] + l₄ * Cos[φ] + l₃₂ * Cos[β + π + wsp[[2]] - π - α] ==
    l₅ * Cos[wsp[[4]]]};
loop2 = loop1 /. {Cos → Sin};
loop = Join[loop1, loop2]
eqv=D[loop, t];
eqa=D[eqv, t];
```

The below sequence of instructions rewrites the velocity equations into matrix forms: $Av = b$

```
Needs["LinearAlgebra`MatrixManipulation`"]
MF=LinearEquationsToMatrices[eqv,dwsp];
AA=MatrixForm[MF[[1]]] ;
X=MatrixForm[dwsp];
bb=MatrixForm[MF[[2]]];
AAp=MatrixForm[D[MF[[1]],t]];
bbp=MatrixForm[D[MF[[2]],t]];
Y=MatrixForm[d2wsp];
```

$$
A = \begin{pmatrix}
\text{Cos[f2[t]]} & -\text{s1[t] Sin[f2[t]]} + \text{Sin}[\beta+\text{f2[t]]} \, l_{31} & \text{Cos}[\gamma] & 0 \\
0 & \text{Sin}[\alpha-\beta-\text{f2[t]]} \, l_{32} & -\text{Cos}[\gamma] & \text{Sin[f5[t]]} \, l_5 \\
\text{Sin[f2[t]]} & \text{Cos[f2[t]] s1[t]} - \text{Cos}[\beta+\text{f2[t]]} \, l_{31} & \text{Sin}[\gamma] & 0 \\
0 & -\text{Cos}[\alpha-\beta-\text{f2[t]]} \, l_{32} & -\text{Sin}[\gamma] & -\text{Cos[f5[t]]} \, l_5
\end{pmatrix},
$$

$$
v = \begin{pmatrix} \text{s1}'[t] \\ \text{f2}'[t] \\ \text{s2}'[t] \\ \text{f5}'[t] \end{pmatrix}, \quad
b = \begin{pmatrix} \text{Sin[f1[t]]} \, l_1 \, \text{f1}'[t] \\ 0 \\ -\text{Cos[f1[t]]} \, l_1 \, \text{f1}'[t] \\ 0 \end{pmatrix}. \tag{3}
$$

The matrices are filled with the numerical values at each time instant and velocities are derived as $v = A^{-1}b$. The matrix equation for accelerations has a form $\dot{A}v + Aa = \dot{b}$. Then, $a = A^{-1}(\dot{b} - \dot{A}v)$. The successive positions are computed as $x(t+dt) \approx x(t) + vdt + \frac{1}{2}adt^2$. It is denoted in the program $x = pol \ (=\{s_1, f_2, s_2, f_5\})$, $v = pred$, $a = przys$, $\dot{A} = Ap$, $\dot{B} = Bp$. The instant values are added to the lists

listasolp$_i$ (positions), *listasolv$_i$* (velocities), *listasola$_i$* (accelerations), subscript i corresponds with a coordinate placed on the *i-th* position in the lists **wps**. The *j-th* element of a relevant list contains the value computed at the time instant t_j. The code computing positions, velocities and accelerations is presented below.

```
pol = wartp;
Do[
 listasolpᵢ = {};
 listasolvᵢ = {};
 listasolaᵢ = {}, {i, 1, lzm}]
listaalpha = {};
Do[
 listap = {};
 Do[AppendTo[listap, wsp[[i]] → pol[[i]]], {i, 1, lzm}];
 lista1 = {f1[t] → alpha, f1'[t] → w, f1''[t] → 0};
 B = N[MF[[2]] /. lista1];
 A = N[MF[[1]] /. listap];
 pred = N[Inverse[A].B];
 listav = {};
 Do[AppendTo[listav, dwsp[[i]] → pred[[i]]], {i, 1, lzm}];
 B = N[MF[[2]] /. lista1];
 A = N[MF[[1]] /. listap];
 Ap = N[D[MF[[1]], t] /. Join[listap, listav]];
 Bp = N[D[MF[[2]], t] /. Join[lista1, listav]];
 przys = Inverse[A].(Bp - Ap.pred);
 pol = pol + pred * dt + przys * dt^2 / 2;
 alpha = alpha + w * dt;
 AppendTo[listaalpha, N[alpha]];
 Do[AppendTo[listasolpᵢ, pol[[i]]], {i, 1, lzm}];
 Do[AppendTo[listasolvᵢ, pred[[i]]], {i, 1, lzm}];
 Do[AppendTo[listasolaᵢ, przys[[i]]], {i, 1, lzm},
 {lp}]
```

The instruction of substitution */.* requires the explanation. The *MF*[[2]] contains vector of constants in velocity equation in which formulae are written symbolically. Then, substituting numerical values into it causes replacement of the formulae with specific values. Therefore, due to instruction $B = MF[[2]]/.lista1$ the instantaneous numerical value of the vector is computed and stored in B after substituting into *MF*[[2]] the specific values in accordance to the scheme of *lista*1. The following example is presented for illustrative purpose only: the result of the instructions $B = \{Sin[x], Cos[y]\}$; $ValueofB = B/.\{x- > 0, y- > \pi\}$ is $ValueofB = \{0,0\}$.

The kinematic unit is the heart of the program, therefore discussed in detail. The rest of the code is not included in the text.
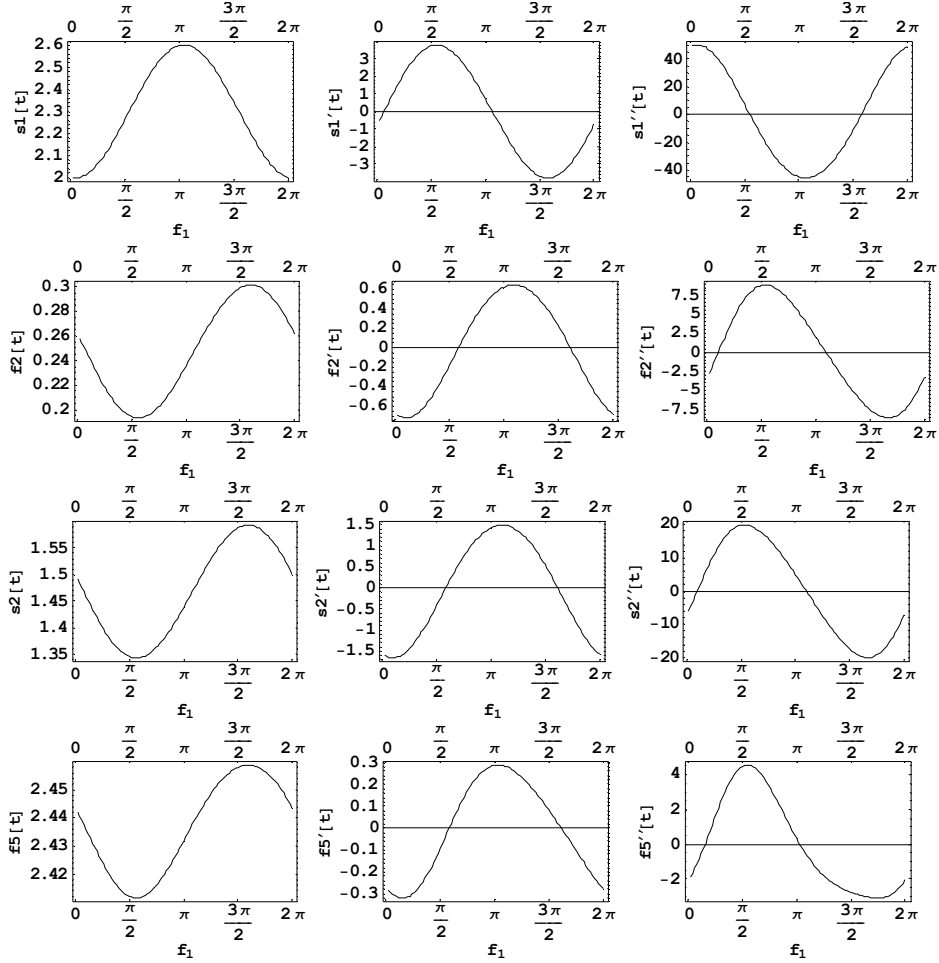
Fig 2. The coordinates describing the mechanism position, their velocities and accelerations.

The results of the computation are presented in Fig. 2. For each time instant t_j, the instantaneous powers of the load force $N_{0j} = -P_{Uj}\dot{s}_{2j}$ and of the inertia forces $N_{Bj} = m_3\left(\dot{x}_{C3j}\ddot{x}_{C3j} + \dot{y}_{C3j}\ddot{y}_{C3j}\right) + I_3\dot{f}_{3j}\ddot{f}_{3j}$ as well as the driving torque

$$M_j = \frac{N_{Bj} - N_{0j}}{\omega_1}$$ are computed and stored up in the lists. In the foregoing equations

x_{C3}, y_{C3} are the coordinates of the mass centre of the link 3. The user has to enter these coordinates.

```
x₃ = wsp[[3]] * Cos[γ] + l₄ * Cos[φ] + l₃₂ * Cos[f2[t] + β - α / 2]
y₃ = x₃ /. Cos → Sin
```

The velocities and accelerations are computed by Mathematica by using the instruction $D[\cdot, t]$. Subsequently, the mean value of the output engine torque M_{MN} =**79.3766** Nm and the engine power $N = $ **997.475** W are computed.
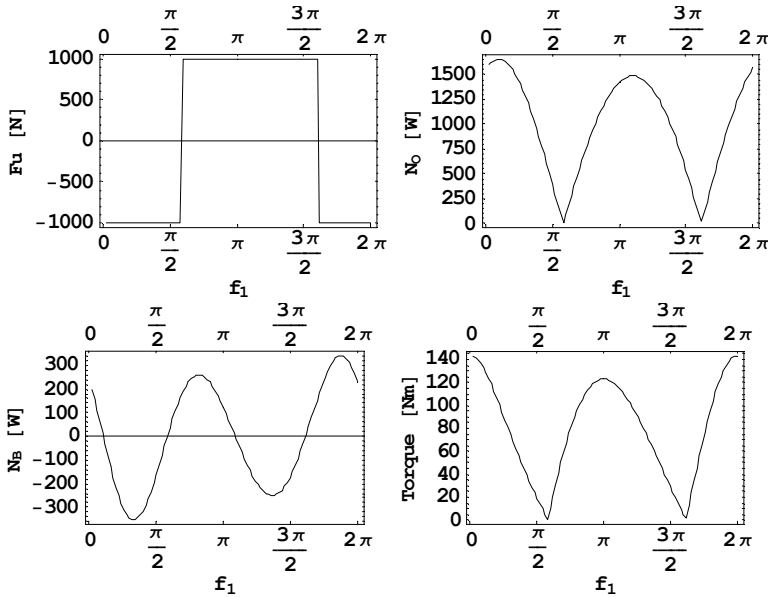
Fig. 3. The load force, power of the load force N_O, power of the inertia forces N_B and output driving torque during one operating cycle.

Finally, the program computes the flywheel. The mass moment of inertia of the flywheel is determined by the approximate method [9, 11] and expressed by the formula $I_{KZ} = \frac{\Delta W}{\omega^2 \eta} = 16.8 kgm^2$, where ΔW is the difference between the extreme values of the work done by the excess of the engine torque (difference between the torques instantaneous and mean).

3. Conclusions

The tool for analysis of the plane mechanisms is presented. The method discussed on the example of the mechanism of third class can be applied to mechanisms of higher classes. The algorithm minimizes the number of manually derived equations. The laboratory classes on Mechanism Theory allow to solve complex problems of kinematics and dynamics of mechanisms as well as give the opportunity to learn a widely used environment Mathematica. The laboratory teaching enables also presentation of the commercial products for kinematic and dynamic simulation of mechanical systems: WorkingModel, NX / Recurdyn.

References

1 S. Mitsi, *Position analysis in polynomial form of planar mechanisms with a closed chain of the Assur group of class 4*, Mechanism and Machine Theory **34** (1999) 1195–1209.

2. S. Mitsi, K.-D. Bouzakis, G. Mansour, I. Popescu, *Position analysis in polynomial form of planar mechanism with Assur groups of class 3 including revolute and prismatic joints*, Mechanism and Machine Theory **38** (2003) 1325-1344.

3. S. Mitsi, K.-D. Bouzakis, G. Mansour, *Position analysis in polynomial form of planar mechanism with an Assur group of class 4 including one prismatic joint*, Mechanism and Machine Theory **39** (2004) 237-245.

4. C. Innocenti, *Position analysis in analytical form of the 7-link Assur kinematic chain featuring one ternary link connected to ternary links only*, Mechanism and Machine Theory **32** (1997) 501–509.

5. T. Młynarski, *Position analysis of planar linkages using the method of modification of kinematic units*, Mechanism and Machine Theory **31** No. 6 (1996) 831-838.

6. T. Młynarski, *Generalized analytical method of kinematic analysis of planar mechanisms*, WPKr, Krakow, 1994 (in polish).

7. B. Paul, K. Krajcinovic, *Computer analysis of machines with planar motion. Part 1— Kinematics. Part 2— Dynamics*, ASME Journal of Applied Mechanics **37** (1970) 697–712.

8. Mathematica, *Mechanical Systems*, WOLFRAM RESEARCH, 1995.

9. Z. Parszewski, *Teoria Maszyn i Mechanizmów*, WNT, Warszawa 1983.

10. A. Morecki, J. Knapczyk, *Teoria mechanizmów i manipulatorów. Podstawy i przykłady zastosowań w praktyce*, WNT 2001.

11. V. Ramamurti, *Mechanics of Machines*, Alpha Science International Ltd., Harrow, U.K., 2005.

12. J. Buśkiewicz, *A method of optimization of solving a kinematic problem with the use of structural analysis algorithm (SAM)*, Mechanism and Machine Theory **41** (2006) 23–837.

INFERRING THE GLOBAL AND PARTIAL SYSTEM CONDITION BY MEANS OF MULTIDIMENSIONAL CONDITION MONITORING[1]

Czesław CEMPEL[2]

Poznan University of Technology

Institute of Applied Mechanics

Division of Vibroacoustics and Biodynamics of Systems

Piotrowo 3 Street

60-965 Poznań, POLAND

Phone: 0048-61-665-2328

E-mail: Czeslaw.Cempel@put.poznan.pl

Abstract

Machines have many faults which evolve during its life (*operation*). If one observe some number of symptoms during the machine operation it is possible to capture needed fault oriented information. One of the methods to extract fault information from such symptom observation matrix (SOM) is to apply the singular value decomposition (SVD), obtaining in this way the generalized fault symptoms. The problem of this paper is to use the total damage symptom, being a sum of all generalized symptoms, and the first generalized symptom to infer better on machine condition. There was some new software created for this purpose, and some cases of machine condition monitoring have been considered as examples. Considering these it seems to the author, that both generalized symptoms should be used for the inference on machine condition. They are complimentary each other in some way, and should be use together to increase the reliability of diagnostic decision.

Key words: condition monitoring, multidimensional observation, singular value decomposition, generalized fault symptoms.

1. Introduction

The most machines in operation, even performing simple operations, have many modes of failure. Hence their diagnostics have to be multidimensional. From the other side, the contemporary advancement in measurement technology allows us to measure almost any component of phenomenal field, inside or outside of the working machine. The only condition for symptoms in such multidimensional diagnostics is some kind of proportionality to gradual worsening of the machine condition which takes place during it operation. If it is so, we can name the measured component of machine phenomenal field as the **symptom**[3] of condition. In this way we are measuring a dozen of '*would be*' symptoms, and our condition monitoring is multidimensional from the beginning. Due to

---

[1] Paper intended to DUF08 (*ISMA08*)

[2] ul. Piotrowo 3, 60-965 Poznań, Poland, email: czeslaw.cempel@put.poznan.pl

[3] Measured physical quantity being proportional to the condition of the machine.

this situation, the application of multidimensional machine condition observation is now well established fact, see [Cempel 99], [Korbicz 04], [Tumer 02], [Jasiński 04] - for example. And there exist some difference in application and processing of the multidimensional signals and/ or symptom observation matrix. For a diagnostic signals and symptoms one can apply also so called data fusion [HallLlinas 97], [RoemerKacprzyńskiOrsagh 01], [Korbicz 04], and similar techniques developed lately.

In case of multi symptom observation one can apply principal component analysis (PCA), or singular value decomposition (SVD), looking for principal or singular components, which may have some diagnostic meaning. For the case of SVD method (*Singular Value Distribution*), there exists the body of experimental evidence [Cempel 04], [CempelTabaszewski 07], for example, that singular components and the quantities created from them, can be treated as **generalized** fault symptoms.

All these transformation and symptom processing starts from the data base called symptom observation matrix (SOM). Let us explain now how the SOM is structured and may be obtained.

During the machine life θ we can observe its condition by means of several symptoms $S_m(\theta)$ physically different and measured at some moments of life θ_n , $n=0,1,\dots p > r$, $\theta_p<\theta_b$, (θ_b – *anticipated breakdown time*). This creates sequentially the symptom observation matrix (SOM), the only source of information on condition evolution of machine in its life time $\theta < \theta < \theta_b$. We assume additionally that real condition degradation is also multidimensional, and is described by semi independent faults $F_t(\theta)$, $t=1,..u < r$, which are evolving in the machine body, as the expression of gradual degradation of the overall machine condition. This degradation proceeds from the **not faulty condition**[4] up to its near breakdown state. Generalizing, one can say now, that we have m dimensional symptom space for condition observation, and $r < m$ dimensional fault space, which we try to extract from the observation space, by using SVD or PCA.

Moreover, some of '*would be*' symptoms contained in SOM are redundant; it means not carrying enough information on the evolving faults during the machine life. But of course there is not unique criterion of the redundancy. During the course of our research, several measure of redundancy has been applied, the volume of observation space (*Vol1*), pseudo Frobenius norm (*Frob1*) of SOM [CempelTabaszewski 07], and others. But they seem to be not good enough with respect of the quality of the final diagnostic decision. This means additionally, when optimizing the observation space, we should take into account the adequate assessment of the **current** and the **future machine condition**. The paper considers this problem, and it is done on the level of previous SVD works of the author. As the forecasting technique with minimal error, the **grey system model** with rolling window [YaoChi 04] was adopted for diagnostic purposes, and has been applied here according to [CempelTabaszewski 07].

---

[4] We assume machine is new, or after the overhaul and repair process.

But having the multidimensional problem of fault assessment, it is important now what type of generalized symptom we use for the forecasting and condition inference. Do we use the overall degradation symptom of the machine, or some specified generalized symptom proportional to one fault only, or both of these. The results of such new approach to multidimensional diagnosis presented here were verified on the real data of machine vibration condition monitoring. Concerning the software, some modification of last programs for the data processing was needed as well. As a result is was found, that this approach seems to be promising enabling a better understanding of machine condition, and also the better current and future condition assessment.

2.   Extraction method of partial faults from the SOM

As it was said in the introduction, our information on machine condition evolution is contained in $p \bullet r$ symptom observation matrix (SOM), where in r columns are presented p rows of the successive readings of each symptom, made at equidistant system lifetime moments θ_n, $t=1,2,\ldots p$. The columns of such SOM are next centered and normalized to three point average of the three initial readings of every symptom. This is in order to make the SOM dimensionless, to diminish starting disturbances of symptoms, and to present the evolution range of every symptom from zero up to few times of the initial symptom value $\mathbf{S_{on}}$, measured in the vicinity of lifetime $\theta_I = 0$.

After such preprocessing we will obtain the dimensionless symptom observation matrix (**SOM**) in the form;

$$SOM \equiv \boldsymbol{O_{pr}} = [\boldsymbol{S_{nm}}], \qquad \boldsymbol{S_{nm}} = \frac{\mathbf{S}_{nm}}{\mathbf{S}_{0m}} - 1, \tag{1}$$

where bold non italic letters indicate primary measured dimensional symptoms.

It was said in the introduction, we apply now to the dimensionless **SOM** (1), the Singular Value Decomposition (**SVD**) [Golub83], [Will05], to obtain singular components (*vectors*) and singular values (*numbers*) of **SOM** , in the form

$$\boldsymbol{O_{pr}} = \boldsymbol{U_{pp}} * \boldsymbol{\Sigma_{pr}} * \boldsymbol{V_{rr}^{T}}, \qquad (\boldsymbol{T}\text{- matrix transposition }), \tag{2}$$

where $\boldsymbol{U_{pp}}$ is p dimensional orthonormal matrix of left hand side singular vectors, $\boldsymbol{V_{rr}}$ is r dimensional orthonormal matrix of right hand side singular vectors, and the diagonal matrix of singular values $\boldsymbol{\Sigma_{pr}}$ is defined as below

$$\boldsymbol{\Sigma_{pr}} = \boldsymbol{diag} \, (\, \sigma_1, \, \ldots, \, \sigma_l\,), \; with \; nonzero \; s. \; v.: \quad \sigma_1 > \sigma_2 > \ldots > \sigma_u > 0, \tag{3}$$

and zero s. v. ; $\sigma_{u+1} = \ldots \sigma_l = 0$, $l = max \, (p, r)$, $u \leq min \, (\, p, r)$, $u < r < p$.

In terms of machine condition monitoring the above (3) means, that from the r primarily measured symptoms (*dimension of observation space*) we can extract only $u \leq r$ nonzero independent sources of diagnostic information, describing the evolving generalized

faults $F_t(\theta)$, $t=1,..u$, and creating in this way the less dimensional **fault space**. But only a few faults developing currently in a machine are making essential contribution to total fault information (*are enough developed*). The rest of potential generalized faults, symbolized here by small σ_u value, are usually below the standard 10% level of noise. What is important here, that such **SVD** decomposition can be made currently, after each new observation (*reading)* of the symptom vector $[S_m]$; $n = 1 \ldots p$, and in this way we can trace the faults evolution, and their advancement, in any operating mechanical system.

3. Diagnostic interpretation of SVD

From the current research and implementation of this idea [Cempel 03], one can say, that the most important fault oriented indices obtained from **SVD;** is the generalized fault symptom SD_t, $t=1,2$, and also the sum of all generalized fault symptoms $SumSD_i$, as some equivalent symptom of total (*cumulated*) machine damage. In another way, the generalized fault symptom SD_t can be named also as discriminant, or the generalized symptom of the fault order t, and one can obtain this as the **SOM** product and singular vector v_t, or in general in matrix notation as below:

$$SD = O_{pr}*V = U*\Sigma,$$

$$and\ in\ particular;\quad SD_t = O_{pr} * v_t = \sigma_t \cdot u_t\ ,\quad t=1,...u < r. \tag{4}$$

We know from **SVD** theory [Golub83], [Will05], that all singular vectors v_t, and u_t, as the components of singular matrices, are normalized to one, so the energy norm of this new discriminant (*generalized fault symptom*) gives simply the respective singular value σ_t:

$$Norm\ (SD_t) \equiv ||SD_t|| = \sigma_t\ ,\ t = 1, ...,u. \tag{5}$$

The above defined discriminant $SD_t(\theta)$ can be also named as lifetime fault profile, and the respective singular value $\sigma_t(\theta)$ as a function of the lifetime seems to be its life advancement of damage (*energy norm*) and the same the measure of importance of the fault. That is the main reason why we use dimensional or dimensionless singular values for the ordering of importance of generalized symptoms (*faults*).

The similar fault inference can be postulated to the meaning, and the evolution of summation quantities, the total damage profile $SumSD_i(\theta)$ as below

$$SD_t(\theta) \propto F_t(\theta),\ with:\ ||SD_t(\theta)|| = \sigma_t\ ,\ t=1,2,$$

$$SumSD_i(\theta) = \sum_{i=1}^{u} SD_i(\theta) = \sum_{i=1}^{u} \sigma_i(\theta) \cdot u_i(\theta) \propto F(\theta),\ with:||SumSD_i(\theta)|| \cong \Sigma\,\sigma_i(\theta) \tag{6}$$

Currently it seems to be, that the condition inference based on the first summation damage measure; $SumSD_i$, (*total damage measure*) may stand as the first approach to multidimensional condition inference, as it was lately shown in the previous papers (*see*

for example [Cempel 04; 05; 06]). The similar inference based on the first (*dominating*) generalized fault SD_1 is valuable and complimentary, as it was shown lately [CempelTabaszewski 08].

Going back to SVD itself it is worthwhile to show some mathematical metaphor of (5), that every perpendicular matrix has such decomposition, and it may be interpreted also as the product of three matrices [Will 05], namely

$$O_{pr} = (\textbf{\textit{Hanger}}) \text{ x } (\textbf{\textit{Stretcher}}) \text{ x } (\textbf{\textit{Aligner}}^{T}). \tag{7}$$

This is very metaphorical description of **SVD** transformation, but it seems to be useful analogy for the inference and decision making in our case. The diagnostic interpretation of formulae (7) one can obtain very easily. Namely, using its left hand side part we are stretching our **SOM** over the life (*observations*) dimension, obtaining the matrix of generalized symptoms as the columns of the matrix **SD** (*see below*). And using its right hand side part of (7) we are stretching **SOM** over the observed symptoms dimension, obtaining the assessment of contribution of every primary measured symptoms in the matrix **AL**, assessing in this way the contribution of each primary symptom to the generalized fault symptom SD_i.

$$SD = O_{pr}*V_{rr} = U_{pp}*\Sigma_{rr}\,; \quad and \quad AL = U^{T}_{pp}*O_{pr} = \Sigma_{rr}*V^{T}_{rr}\,. \tag{8}$$

This means that SD matrix is stretched along the life coordinate giving us the life evolution of the weighted (σ_i) singular vectors. And AL matrix is aligned along the symptom dimension with the same way of weighting by σ_i, giving the assessment of information contribution of each primary symptom.
We will calculate numerically the above matrices and use them for the better interpretation of monitoring results (**SD**), and optimization of dimension of the observation space (**AL**).

4.   The SOM information measure and optimization

Having in mind the redundancy of some primary symptoms, i.e. the primary observation space, some additional considerations should be made concerning **SOM** information assessment. In terms of previous findings this can be done by calculating the Frobenius norm (**Frob**) of this matrix, and the volume (**Vol**) created by **u**-dimensional generalized fault space identified by application of (**SVD**). One can calculate easily both information indices as the sum and the product of singular values in the following way [Golub83], [Kiełbasiński92];

$$\textbf{\textit{Frob(SOM)}} \equiv \{\Sigma\,\sigma_i^{2}\}^{1/2}; \text{ and } \textbf{\textit{Vol(SOM)}} \equiv \Pi\,\sigma_i, \quad i = 1,\dots u$$

But squaring the small singular values of σ_i (*less than one*) make them much smaller, giving seemingly smaller contributions to the matrix information asset, and to the volume of the observation space. Due to this we can propose to use not the exact Frobenius norm but its modification as below

$$\textbf{\textit{Frob1}} = \Sigma\,\sigma_i\,; \text{and: } \textbf{\textit{Vol1}} = \Pi\,\sigma_i. \qquad i = 1,\dots u \tag{9}$$

This will give us possibility to look for the small, just evolving faults, and not omit them when we try to reduce the redundancy of the observation vector. Consequently one can get less redundancy of new optimized SOM, with less number of columns but also keeping in observation the small just evolving fault information (σ_i).

The use of Frobenius measure for a matrix has also mathematical validation. In general, one can understand this as the problem of approximation of matrix B, by so called k-rank approximation. Following the paper [Berry 99] we can make the quantitative assessment of such k-rank approximation of a matrix B as the difference below

$$\| B - B_k \|_F = \{ \sigma^2_{k+1} + \dots \sigma^2_u \}^{1/2} , \tag{10}$$

where the subscript u stands for maximal dimension of nonzero singular value, i.e. the rank of our primary **SOM.**

This means also, that instead of (9), we will write simplified measure of approximation of SOM in the form of deviation from primary **SOM** rank, as below

$$\Delta_k Frob1 \equiv Frob1_o - Frob1_k = \{ \sigma_{k+1} + \dots \sigma_u \}, \tag{11}$$

Using this quality index of matrix approximation measure we, can form additional objective measure of the SOM redundancy. And minimization of **SOM** rank may be carried by excluding some primary measured symptoms S_m with low information contribution, which produce mainly small (*less than one*) singular vales σ_u.

Such criteria of redundancy minimization we have used quite recently. But following the last papers [CempelTabaszewski 07], one may notice that after some symptom rejection, which gives expected increase in the volume of information space (Vol1). Also the rank approximation of **SOM** gives only some drop in Frob1 measure, but the result of prognosis is not enough good, *giving erroneous future values*, sometimes less than the previous one. How to avoid such errors in forecasting?

There seem to be one possibility more, to make the symptom rejection more objective and anticipating the goodness of the condition forecast. We have to consider the contribution of primary measured symptoms to the creation of first generalized symptoms SD_1 , and also the creation of total damage generalized symptom *SumSDi*. The first overall information contribution measure, can be calculated separately to each primary symptom, from the correlation matrix of our SOM (*with appended lifetime in the first column*), as the centered and normalized sum of column elements. The second measure one can obtain if we append additionally to the previous matrix the vector *SumSDi*, as a first column. When calculating covariance matrix from these and in the first row we will have needed information. After needed normalization to the first element of this row this will give us the contribution of every primary symptom to the total damage symptom *SumSDi*.

5. The global and partial fault inference

We have gathered above all necessary analytical and inference knowledge concerning processing of symptom observation matrix, the extraction of fault information, and optimization of SOM rank. So, there is a right moment to validate these finding and proposal by some experimental data taken from real situations of vibration condition monitoring. In order to do this the last Matlab® program **svdopt1gs.m** presented in [CempelTabaszewski 07] has been modified to **svdoptInt.m**. The inference basis for the first program was the total damage generalized symptom *SumSDi*, while in the modified program such inference basis is the first generalized symptom SD_1. Just to catch the the way of inference and the followed diagnostic decision difference we will take some uneasy case of heavy fan (3MW) working in unstable and load uncontrolled regime (*random supply of the air to the mine shaft*), serving as the source of fresh air for ventilation at the deep copper mine. The main troubles with this fun were unbalance and nonalignment between the fan and the driving electric motor, due to that the unit was constantly monitored.

Figure 1 presents below the six pictures as the result of fan data processing by specially prepared program **svdoptint.m** made in the Matlab® environment, where the main stream of inference follows the evolution of the first generalized symptom SD_1. The first top left picture, gives the results of 30 weeks measurements of symptom life curves of vibration velocity at a five points located on the fan aggregate structure. One may notice here the great instability of symptom readings, symptom No 4 in particular. This is better seen at the picture middle left when data are centered and normalized to the average value of the three initial symptom readings. We can notice here the negative values of symptom as an effect of load instability and normalization. The picture bottom left presents the *generalized symptoms* as the result of SVD processing, indicating also the symptom limit value calculated for the generalized symptom of total damage *SumSDi* (*red line*) denoted there as S_{lc}, and also symptom limit value S_{ll} calculated from the first generalized symptom SD_1.

The picture top right shows the relative amounts of information obtained as percentage of given singular value σ_i normalized to the sum of all singular values. As it follows from (5) this indicates at the same time the advancement of the given fault evolution in the machine life. As the legend to this picture we have indication of two redundancy measure, the **Frob1** and the **Vol1**, which will serve as some guidance in the optimization process of the observation space.

The middle right picture presents the contribution of primary measured symptoms (*the first = lifetime*) to the creation of the dominating three generalized symptoms. One can notice here, that symptoms No 4 and 5 give minimal contribution and can be rejected in a process of optimization of the observation space. The last picture, the bottom right, of the Figure 1 shows the evolution of symptom limit value as calculated from the first generalized symptom SD_1, indicating also the value of symptom limit value as calculated from the sum of generalized symptoms *SumSDi*. One can notice from the both bottom

pictures, that in this case the difference between symptom limit values is a small one, but the value obtained from SD_1 gives better indication of the coming machine breakdown.
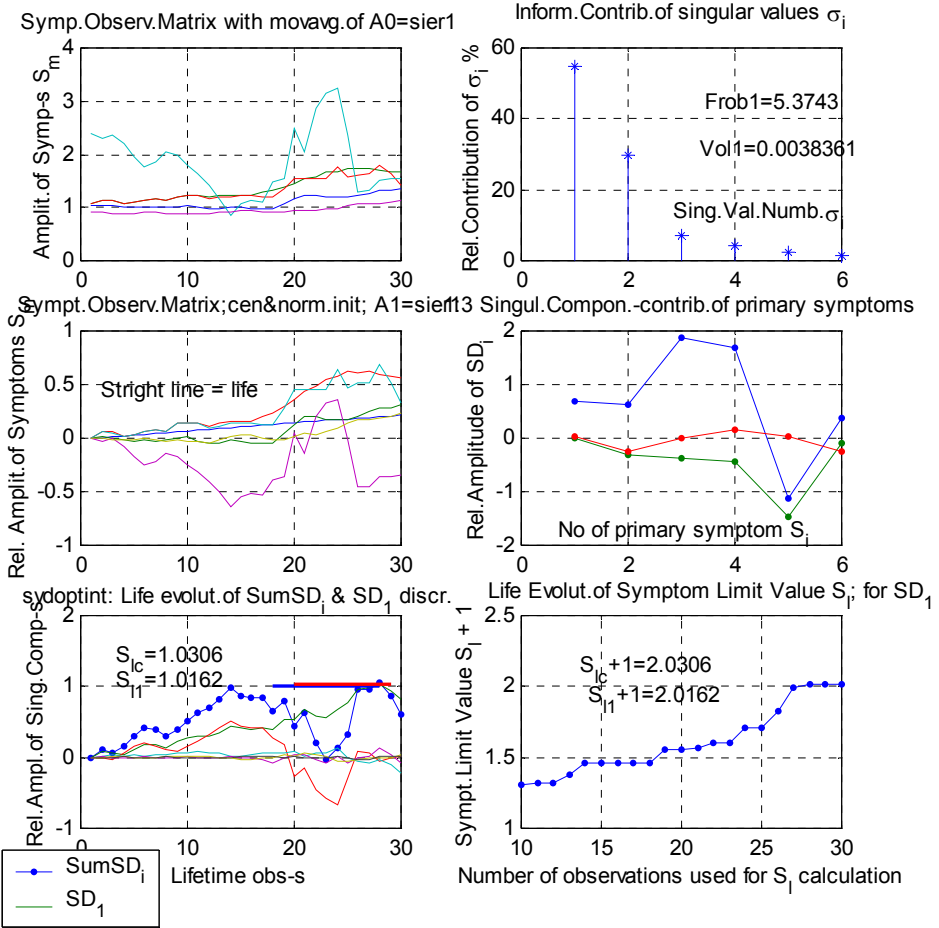
Fig.1 The results of SVD processing of vibration data of a huge fan pumping air into the copper mine shaft, with the inference according to dominating generalized symptom SD_1.
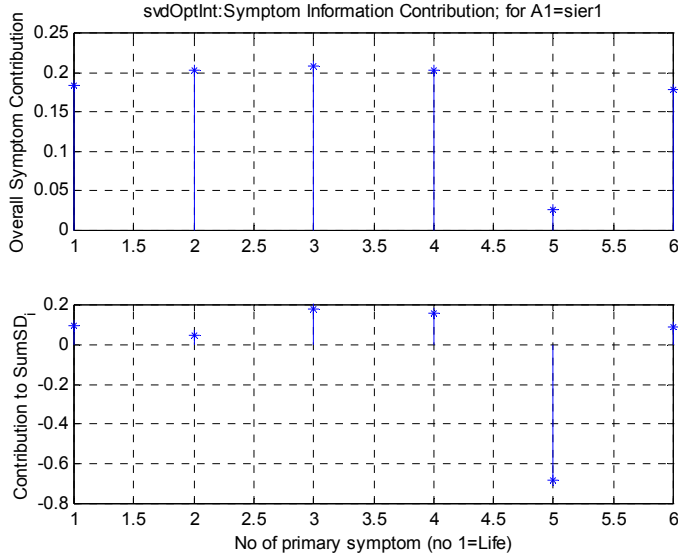
Fig.2. The Correlation measure of overall and particular contribution of primary symptoms.

As it was mentioned before, the program **svdoptint.m** contains not only the matrix ***AL*** (8) (*picture middle left*), but also some correlation assessment of individual and overall information contribution of every primary symptom in SOM. Figure 2 presents these data, and we can see there, really symptom No4 has minimal overall contribution, and a negative one to generalized symptom SD_1.

Having such strong indication of the two symptoms redundancy (*No 4 and No5*), let us begin a gradual rejection of these symptoms contained in SOM. As a first step we rejected symptom No 4, however its contribution is not minimal in this case. The effect of such rejection is shown in a Figure 2, organized in the same manner as a previous one. Comparing the both we can notice the radical change in the symptom behavior, mainly we have rejected the most unstable primary symptom No 4. As the result of such rejection we have much clear situation of symptom evolution, primary symptom (*picture top left*) and generalized (*picture bottom left*), and the values of symptom limit values have change slightly, differing more than previously. Also the Frobenius redundancy measure drops significantly, and the volume of the fault space increased a little. But the most important effect of this rejection is the increased stationarity of remaining symptoms, the primary and generalized as well. Looking at the picture middle right one can notice very low contribution of primary symptom No 5. Hence next motion will be the rejection of this symptom together with previously rejected No 4. The results of such double rejection operation and subsequent processing one can find on the Figure 4.
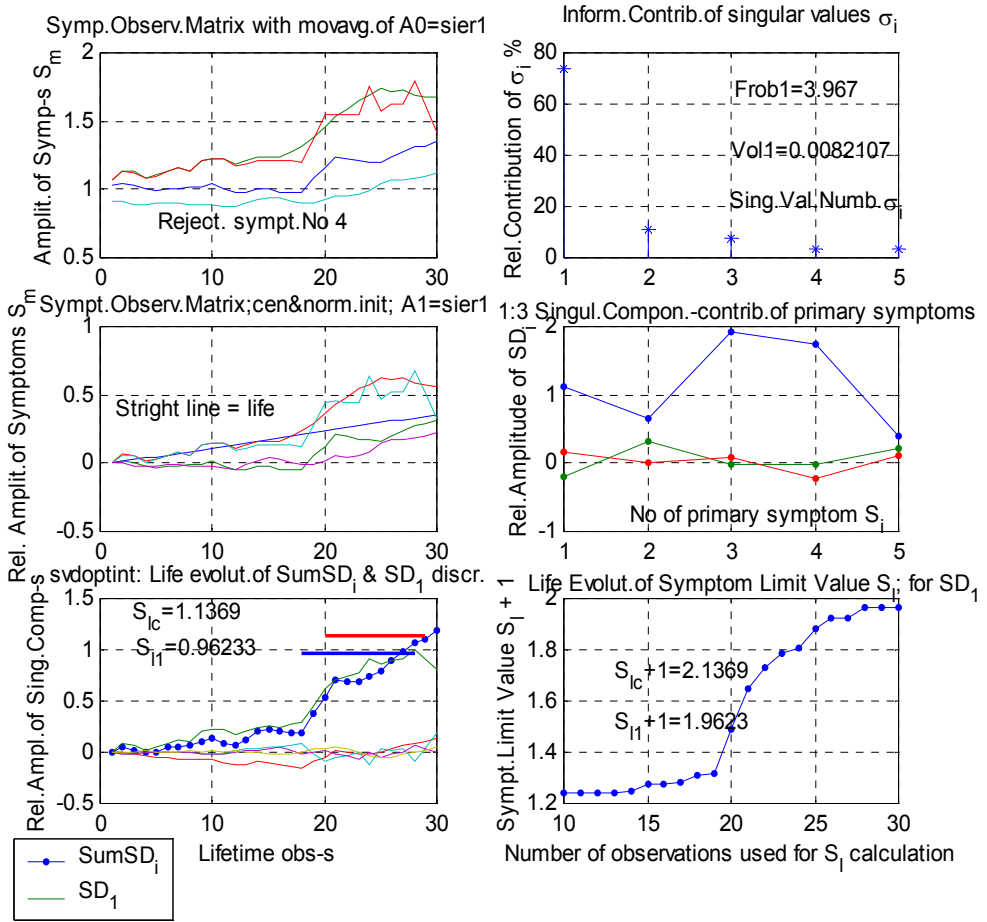
Fig.3 The vibration symptom observation matrix of the huge fan (see Fig.1) after the rejection of unstable symptom No 4.

Looking at the difference between Figures 3 and 4 one can notice much more clear situation on the right hand pictures of Fig 4. Now we can infer on fan condition using both symptom limit values S_{lc} and S_{l1}, however with S_{l1} diagnosis seems to be more reliable. The top right picture indicate that Frobenius measure does not change much, but the volume of fault space increases almost ten times. This may mean that for the condition inference of the fan we should take into consideration the remaining three primary symptoms No 1, 2, 3, and due to this we will have the relative stable and reliable situation for the inference. This conclusion is validated more by the picture middle right,

where one can see that the contribution of all remaining symptoms and the life symptom to the generalized symptom SD_1 is valuable, being almost of the same order.

One can notice also that the calculation of limit value using first generalized symptom $\boldsymbol{SD_1}$ gives us lower value and this can give us more safe assessment of lifetime moment for machine shut down and renewal. From the point of view of reliability of diagnostic decision, this seems to be important to have two different sources of symptom limit vale assessment, and to confront these values and the associated knowledge.
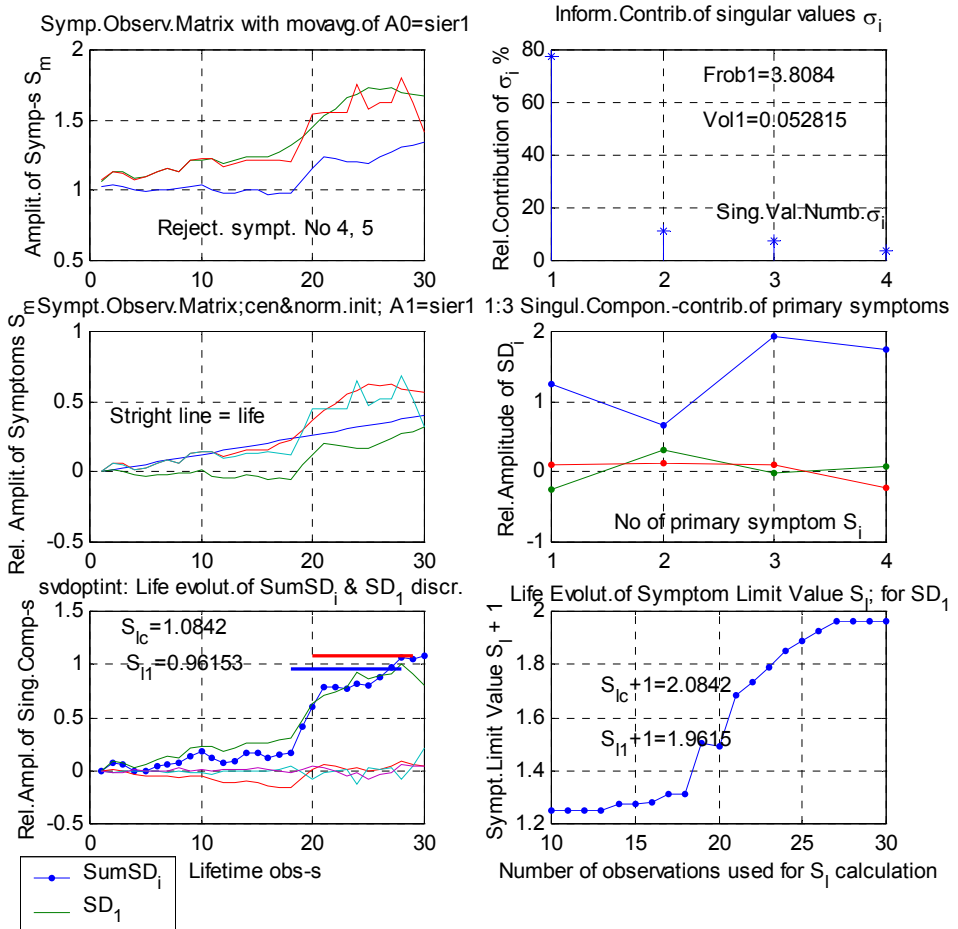
Fig. 4 The vibration symptom observation matrix of the huge fan (see Fig.1) after the rejection of unstable and the redundant symptoms No 4 and No 5.

6.   Forecasting of global system damage and a partial faults advancement

The final quality of diagnostic decision one may judge making the forecast of the future condition in terms of total damage symptom *SumSDi* , and the first generalized fault symptom SD_1. It was said in the introduction, that the forecast will be made by grey system theory (**GST**) [Deng 89], together with the rolling window method using the first order grey model **GM**(1,1) [YaoChi 04].

In general **GST** assumes that our incomplete and uncertain observation can be the output of some dynamic multi input system of high order, described by the grey differential or difference model [Wen 05]. In condition monitoring, we assume it is enough to take the first order system described by the grey differential equation, and one forcing or control input only. This simplest case in **GST** is denoted as **GM**(1,1), means the grey model of order 1 with one input only. The output of the system is the series of discrete observations (*our symptom readings*) denoted here as

$$\mathbf{x^{(0)}} = \{ x^{(0)}(1),\, x^{(0)}(2),\dots x^{(0)}(n)\}, \tag{12}$$

 where $n \geq 4$ is the number of observation made on a system (*machine*).

We will not present GST theory here, but only using the final formulae for the forecasting, and the rolling window concept, which is implemented into the forecasting software.

The application of GST to the above symptom readings gives the possibility to forecast the future one step symptom value, starting from very small number observation, and using the formula

$$\hat{x}^{(0)}(k+1) = \left[x^{(0)}(1) - u/a\right]\!\left(e^{-ak} - e^{-a(k-1)}\right), k=2,3,..n, \tag{13}$$

where *u* and *a* are parameters to be estimated by special least square matrix procedure using the observed data (12), and the hat ^ in (13) means future value of the forecasted quantity.

This concept was adjusted to the purposes of vibration condition monitoring in one of the earlier paper [CempelTabaszewski 07, 08]. One can notice here from the bottom left picture of Fig. 3 and 4, that the total damage generalized symptom ***SumSDi*** (*line with dots*) after rejection the primary symptom No **4 and 5** is evolved well, enabling good forecast even without the rolling window. But of course, as usually in case of grey system modeling, the rolling windows forecast gives the smallest error. This error can be even smaller if we diminish the span of window (*w*), as it is clearly seen from the picture bottom right of the Fig. 5.

It is worthwhile also to remark on the other pictures of this figure. Picture top left presents clearly, that the rejection of No4 symptom was a good idea allowing us to determine symptom limit value S_{ll} and having this information do act properly to shut down the fan ahead of breakdown time. The picture top right present the total forecast of total damage symptom SD_1 with the model *GM(1,1)*. It seems to be good forecast with

the small average error, but the picture bottom left with the rolling windows forecast have he smaller error and the actual forecast adapts smoothly to the course of SD_1.
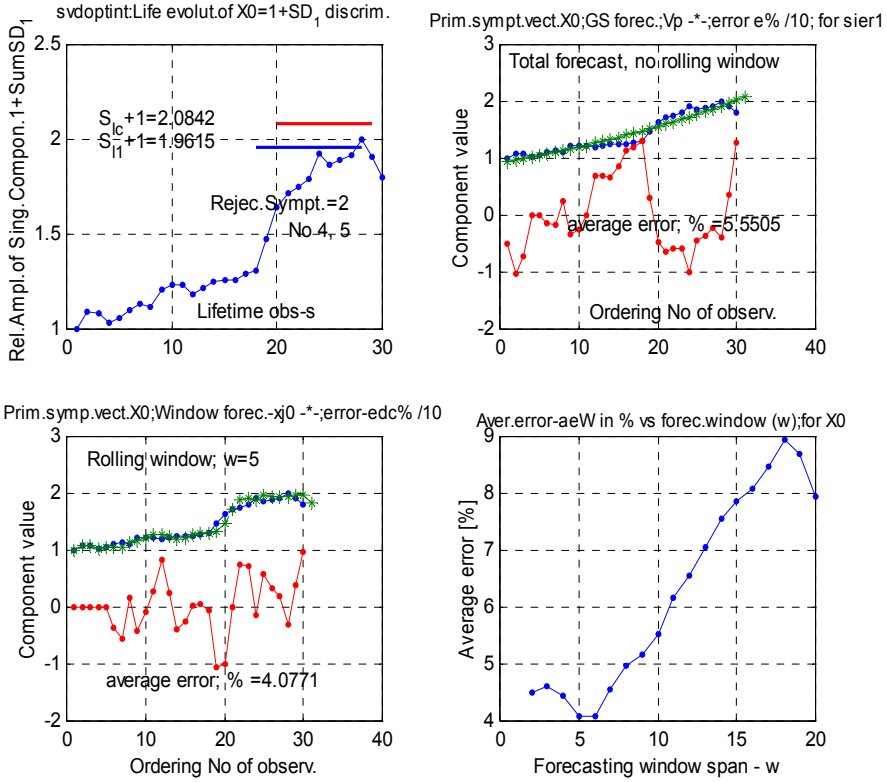
Fig. 5 Grey rolling forecast of the fan condition using the first generalized symptom SD_1, together with the both symptom limit values and the error of the forecasts, with and without rolling window.

It is seen from the Fig. 5 left top picture, that the course of SD_1 symptom is decreasing at the end of fan life, but both assessed symptom limit values S_{lc} and S_{ll} warns in advance enough to undertake shut down decision, just on time. However, comparing the both symptom limit values shown on the picture top right of the last figure, and Fig.4, it is good to know that the global damage symptom limit value S_{lc} can be used only with a global damage symptom $SumSDi$.

Summing up the results of our calculation one can say, that the idea to calculate all limit values for the global damage symptom $SumSDi$, and for the first dominating generalized symptom SD_1 has proved its usefulness. This integration seems to be needed both in the

main calculation and observation space optimization (*Fig 1-4*), as well as in the grey system forecasting *(Fig.5)*.

7. Conclusions

The premise to write this paper was the supposition that the integral inference basing on the first generalized machine symptom and the total damage generalized symptom of machine condition can bring us valuable reliable diagnostic information. As usually in multidimensional condition monitoring we have used the singular value decomposition to extract the fault information from the symptom observation matrix. After the first round of calculation it was possible to optimize observation space using some measures of fault space, such as *Frob1* and *Vol1*. Having just mentioned generalized symptoms calculated, the symptom reliability and the symptom limit values S_{lc}, S_{ll} were assessed on that basis for the total damage symptom *SumSDi*, and for the dominating generalized symptom SD_1. The last stage of inference was the forecast of the future value of the both symptoms made by grey system theory and **GM(1,1)** model. As an example we have used the most unstable case of condition monitoring, of the huge fan working in ventilation system of deep copper mine. It was shown here that the optimization procedure can reject unstable symptom, and more over we are able to calculate two symptom limit values, and infer more effectively on the basis of such integral software.

8. References

1. Cempel C., Innovative developments in systems condition monitoring, Keynote Lecture, Proceedings of DAMAS'99, Dublin 1999, **Key Engineering Materials,** Vols. 167-168 (1999) pp. 172-189.

2. Cempel C., Implementing Multidimensional Inference Capability in Vibration Condition Monitoring, Proceedings of Conference: **Acoustical and Vibratory Surveillance,** Senlis - France, October 2004.

3. Cempel C., Natke H. G., Yao J. P. T., Symptom Reliability and Hazard for Systems Condition Monitoring, **Mechanical Systems and Signal Processing**, Vol. 14, No 3, 2000, pp 495-505.

4. Korbicz J., et all, (*eds*.), **Fault Diagnosis – Models, Artificial Intelligence, Applications**, Springer Verlag, Berlin - Heidelberg, 2004, p828.

5. Tumer I. Y., Huff E. M., Principal component analysis of tri-axial vibration data from helicopter transmission, **56th Meeting of the Society of Machine Failure Prevention Technology,** 2002.

6. Jasiński M., Empirical models in gearbox diagnostics (*in Polish*), **PhD Thesis**, Warsaw University of Technology, Warsaw, December 2004.

7. Cempel C., **Vibroacoustic Condition Monitoring**, Ellis Horwood Press, New York, 1991, p212.

8. Cempel C., Simple condition forecasting techniques in vibroacoustical diagnostics, **Mechanical Systems and Signal Processing**, 1987, pp 75 – 82.

9. Berry M. W., Drmac Z., Jessup E. R., "Matrices, Vector Spacer, and Information Retrieval", **SIAM Review**, 1999, Vol. 41 No 2, pp 335-362.

10. Wen K. L., Chang T. C., The research and development of completed GM(1,1) model toolbox using Matlab, **International Journal of Computational Cognition**, 2005, Vol. 3, No 3, pp 42-48.

11. Zhang L., Wang Z., Zhao S., Short-term fault prediction of mechanical rotating parts on the basis of fuzzy-grey optimizing method, **Mechanical Systems and Signal Processing,** 2007, Vol.21, pp 856-865.

12. Yao A. W. L., Chi S.C., Analysis and design of a Taguchi-Grey based electricity demand predictor for energy management systems, **Energy Conversion& Management,** 2004, Vol.45, pp 1205-1217.

13. Deng J-L., Control Problems of Grey Systems, **Systems and Control Letters**, Vol. 1, No 5, North Holland, Amsterdam, 1982.

14. Deng J-L., Introduction to grey system theory, **The Journal of Grey System,** 1989,Vol. 1, No 1, pp 1-24.

15. Deng J-L., **The Course on Grey Systems Theory**, Publishing House, Huazhong University of Technology, Wuhan, (in Chinese), 1990.

16. Zhang H., Li Z., Chen Z., Application of grey modeling method to fitting and forecasting wear trend of marine diesel engines, **Tribology International,** 2003,Vol.36, pp 753 – 756.

17. Wang T. C., Liou M. C., Hung H. H., Application of grey theory on forecasting the exchange rate between TWD and USD, **Internet** 2005, pp 1 – 8.

18. Tabaszewski M. Forecasting of residual life of the fan mill by means of neural nets (*in Polish*), **Diagnostyka**, vol. 3, (39), 2006, s. 149-156.

19. Cempel C., Tabaszewski M., Multidimensional condition monitoring of the machines in non-stationary operation, **Mechanical Systems and Signal Processing**, Vol. 21, 2007, pp 1233-1247.

20. Cempel C., Tabaszewski M., Grey System Theory in Application to Modeling and Forecasting in Machine Condition Monitoring, (*sent to* **Bulletin of PAN – Technical Sciences***, January 2008).*

21. Hall D. L., Llinas J., An introduction to multisensor data fusion, **Proceedings of the IEEE**, Vol. 85, Jan. 1997, pp 6-23.

22. Roemer M. J., Kacprzyński G. J., Orsagh R. F., Assessment of data and knowledge fusion strategies for prognostic and health management, **Internet**, http://www.impact-tex.com/data/Publications/f054_gjk.pdf

23. Will T., Hanger matrix, two-thirds theorem, **Internet**; **http://www.uwlax.edu/faculty/will/svd/svd/index.html** , June 2005; (*see also: SVD ingredients Mathematica, April 2004*)

APPLICATION OF COMPLEX METHODS FOR OPTIMUM DESIGNING MOBILE VEHICLES

Bohdan DIVEYEV, Igor VIKOVYCH
Lviv Politechnic National University
S. Bandery Str., 12, Lviv, 79013, Ukraine
Igor BUTYTER
Pidstryhach Institute for Applied Problems of
Mechanics and Mathematics, NASU
Naukova Str., 3 b, Lviv, 79053, Ukraine
Phone: 380 (032) 239-99-28, e-mail: tkim@iapmm.lviv.ua

Abstract

The main task of this work is to analyze CAD-system for the bearing systems of mobile wheeled machines and develop new CAD-component. The algorithm and program packages for construction of variety of cars with mounted and trailing equipment should be analyzed and developed on the basis of modern numerical methods of dynamics of continual-discrete systems. The calculation procedure of machine dynamics, resting on the synthesis of block-variational, modal and adaptive schemes, should be applied. The optimal designs were obtained for the boom suspension of boom sprayer with increased stabilizing and vibroprotecting properties.

Keyword: mobile vehicle, sprayer boom, optimal design, vibroprotection.

One of important problems of designing modern bearing systems of transport, in particular mobile vehicles, is providing the bearing power of a body at saving technical-economic optimum indices, namely such as economy, energy and material capacity, operation expenses, expenses on repair et al. A primary task in this direction is the necessity of improvement the analytical method for calculation of effect of dynamic loading with the purpose of approaching the theoretical results to the experimental data and achievement the rational and effective designing of frames, joined wide overall dimension elements: booms, towers etc. Such a task, obviously, can be fulfilled with the help of modern computer programs.

Now there are enough programs for conducting calculations on durability of volume and plane bearing systems on the basis of the finite element method. These are the programs of diverse class. They can have a narrow specialized direction or be universal for a wide class of problems. One of the most powerful design package for calculation the engineering designs on durability is Pro/Engineer, or, briefly – Pro/E. Similar to it according to the properties is the design package ADAMS. For implementation of calculations on durability we can also apply the universal program NASTRAN, ANSYS, COSMOS, for using of which it is necessary to construct a geometrical model (a finite-element model). As a geometrical model we mean construction of points, lines, surfaces and volumes, which in the aggregate describe the design of framework of a body. In the

process of decomposing these geometrical constituents into smaller and giving them physical properties (parameters of cross-section of power elements, thickness of plates, mechanical properties of materials et al.) a finite element model is created. This model can be created on the basis of specialized programs of technical drawing : AUTOCAD, Solid Works, Solid Edge, ParaSolid et al. However complex designs, for example, a body in assembly due to complication of construction not always is transferred from the packet AUTOCAD in the packets ANSYS, NASTRAN, that is why converting models of volume assembly units is to be executed by component-wise. Russian-language programs of such type are, for example, the program Compass, Russian analogue of AUTOCAD, APM WinMashin – that reminds a little Pro/E. The last has such modules which can be used for calculation of design of a body. These programs are less universal, than, for example, NASTRAN, or Pro/E, however they are relatively simple in utilization. Their licensed versions with an educational purpose were bought, similarly as "Compass", by the Lviv Politechnic, and during a long time are studied by students and used by them for writing the diplomas papers. We can also mark the programs "Lyre", "Zenith", "Proton", that also serve for calculation the stress-strain state, stability, dynamics of natural and forced vibrations of three-dimensional frame designs. We will also mark such simple program as "Analisys" – a system for calculation of the stress-strain state of three-dimensional frame designs.

At constructing a finite element model more than 50% of the whole work occupies creation of geometrical model of design (its bearing system). With the purpose of keeping down expenditure on construction of geometrical model it is expedient to transfers a design model into a more comfortable one for construction of geometrical model. It will enable us to facilitate the task of exchange between the systems of CAD and CAE (AutoCAD → ANSYS, NASTRAN), which is carried out by the IGES format. If converting is not executed or we fail to decompose into separate parts, it is recommended to correct a geometrical model in the system CADFIX and to transfer the corrected model by a body or surfaces with the next revision of the model in ANSYS. If correction of inaccuracies and errors does not give a positive result, it is recommended to simplify a model. Because of complexity of design of the bearing system of mobile vehicle and imperfection of the IGES converter, the model of design of mobile vehicle can not fully transfer AMD in the system ANSYS as a solid body geometry. That is why we need to form the bar system maximally close to the design of mobile vehicle. The bar elements of design must be formed on the axes of overall sizes of the cross section and the bar elements which intersect must meet at the point. Geometrical data communication from the CAD system in CAE is carried out with the help of the IGES converter.

In accordance with the requirements which are imposed on the worked out model of mobile vehicle, in the file of drafting model together with a designer model there is a calculation (bar) model. The elements of design in the system ANSYS are decomposed into finite elements for calculation of the stress-strain state. At implementation of calculation of elements of the body it is necessary to bear in mind, that for an acceptable result it is necessary to break up bodies with exactness at which an element contains up

to 100000 finite elements, one linear meter of pipe – more than 8000 finite elements. According to the previous calculation of the model of body of a large mobile vehicle, without the elements of edging, it contains approximately 1500000-2000000 finite elements.

The known numerous methods of modeling such a complex design as the boom-sprayer belong to foreign authors [1-5]. We will note that application only these programs is often insufficient. At first, the dynamics loadings, which act on a frame under the real exploitation conditions, are not exactly known, and the use for this purpose a model "suspension - rigid body" is scarcely correctly. Secondly, we need not only a peak instantaneous value of stress in the elements of design, but their resource estimation. And it requires the account of difficult processes of fatigue and corrosion of metal. The real effective optimization of multielement model is not really. The algorithms of condensation a model are here usually used to a littlesize model on which it is possible to make optimization [6-9]. A possible program complex that is partly able to solve these problems is shown in Fig.1.

Es example considers now the boom-sprayer. It is the sprayer's boom that is the main unit of the agricultural machine. Its design peculiarities influence the basic characteristics of the machine, i. e. uniformity of spraying. At the same time, the boom is the unit of the machine that fails most frequently due to dynamic overloading. Therefore, optimization of the boom design is the main step in the process of rational construction the sprayer. One solution for this problem is to provide significantly improved suspension for the centre vehicle section so that the centre vehicle section moves upwardly and downwardly at a relatively slow rate in response to changing the ground level thus reducing the shock loading to the boom. Undesirable movements of the boom result from its connection to a vehicle rolling over uneven, rough soil and consequently subject to vibrations such as roll and yaw. Conventional suspensions of the boom through pivots or twin link suspensions provide protection from the rolling motion to some extent and are widely used in commercially available machines.

The numerical schemes (NS) row is considered for the complex vibroexited construction. Methods of decomposition and the NS synthesis are considered on the basis of new methods of modal synthesis. Traditional design methodology, based on discontinuous models of structures ore FEM programs is not effective for three-dimension boom nonlinear vibration analysis. The program packages are based on condensed mathematical models. The computer models of aggregates are tested by adequate real time procedure. The optimality criteria for boom constructions are formulated for various field and exploitation conditions. The optimal design decisions are found by genetics algorithms for boom section construction, vertical and horizontal damping and stabilization complex vibroprotecting and vibroabsorbing systems.

The flow chart complex of programs
for definition of dynamic characteristics
complicated designs

The principal program
(data input, organization
of calculations, a
conclusion of outcomes)

The basic program
solutions of the
dynamic equations
processes

Discrete elements: springs,
hidro-, pneumoshock-absorbers,
elements of dry friction

Dynamic
visualization
processes
of Calculation

Continual elements: rods,
plates, shells

Preservation
Outcomes in
different formats
for connection with
programs of
visualization CAD,
CAM, FEM

Influence hydrodynamic,
aerodynamic processes

Programs of calculation
rigidities connecting
elements and strains in them

Control
processes
calculation,
workplace
of the designer

Local
Web and
Internet

For receiving of optimum projects the algorithms of genetic optimization were used in a great number of structural parameters. In Fig. 2 the chart of the combined pendulum-resilient suspension of a boom sprayer and dialog box of the complex of the optimization programs of this suspension are presented.
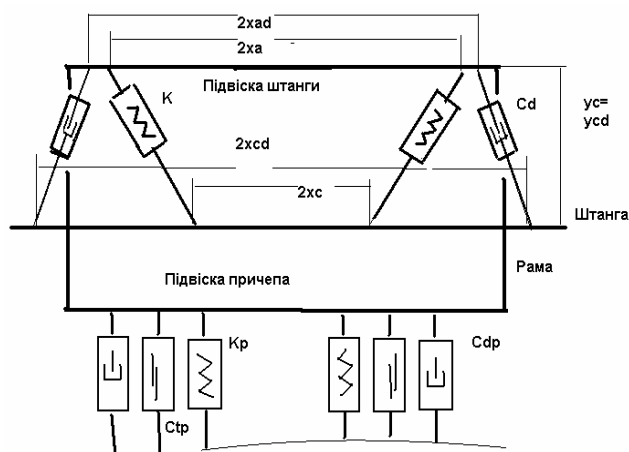
Fig.2a. Scheme of stringing the frame and sprayer boom

Fig.2b. The interface element of the optimization program

In Fig. 3a resulted the surfaces of vibroprotection levels of combined suspension depending on parameters K (rigidity) and C (damping) are presented. The function of angular deviation from a horizontal position is taken. In Fig. 3b the character of vibration process of boom is presented on the combined suspension with various parameters.
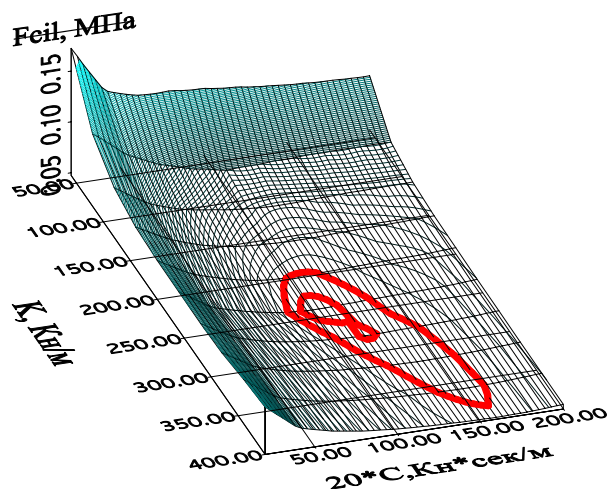
Fig.3a. The level surface of vibro protection of optimized suspension of a sprayer boom
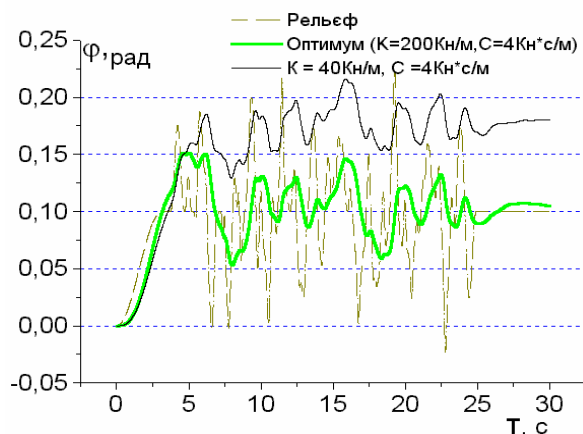
Fig.3b. Realization of stochastic loading of sprayer boom for the optimal and non-optimal values of parameters

Conclusions

At present the problem of developing of the automated complexes of designing of such types of vehicles, as large-profile software's packages of ADAMS, CATIA, Pro-Engineer, Nastran et al. is solving. The discrete-continue models of wheeled land-machines and processes related to their functioning are offered. On the basis of research

of mechanical processes, these models are realized in a number of programmatic complexes. On their basis the algorithms for optimum planning of boom-sprayer suspension are obtained. We will note that the mathematical models, numerical algorithms and programmatic facilities developed for this class of vehicles are adapted and for other vehicles.

References

1. Hobson, P.A., Miller, P.C.H., Walklate, P.J., Tuck, C.R., Western, N.M.,. *Spray drift fromhydraulic spray nozzles: the use of a computer simulation model to examine factors influencing drift*, J. Agri. Eng. Res. **54** (1993), 293–305.

2. Kaul, P., Gebauer, S., Neukampf, R., Ganzelmeier, H., *Modellierung der direkten Abtrift von Pflanzenschutzmitteln-Pflanzenschutzgeraete fuer Flaechenkulturen,* Nachrichtenblatt Deutschen Pflanzenschutzdienst, **48** (1996), 21–31.

3. Miller, P.C.H., Hadfield, D.J., *A simulation model of the spray drift from hydraulic nozzles,* J. Agri. Eng. Res. **42** (1989), 135–147.

4. Oeseburg, F., Van Leeuwen, D., *Dispersie van spray en damp van bestrijdingsmiddelen bij gewasbespuiting met vliegtuigen. Deel 2: Model en berekeningen,* Report No. PML 1984–44, TNO, 1984.

5. Reichard, D.L., Zhu, H., Fox, R.D., Brazee, R.D., *Computer simulation of variables that influence spray drift*, Trans. ASAE **35** (1992), 1401–1407.

6. I. Vikovych, B. Divejev, I. Butyter, D. Ivaschuk *Sprayer boom suspension construction optimization in frequensy domain* // Bulletine of State Technical University of Ternopil. – Ternopil: TSTU. – 2002. – Vol. 7, No. 2. – P. 65–70.

7. Divejev B.M *Automatic design system for boom-sprayers. 1.Main numerical and optimization approach* // Preprint of Mathematical Modelling Center of Pidstryhach Institute for Applied Problems of Mechanics and Mathematics of NAS of the Ukraine. – Lviv.– 1995.– 40p.

8. Diveyev B., Vajda I., Vicovych I. *Design of girder booms for sprayers of increased durability and high quality of agent aplication.* // Proceeding of XIX symposium „Vibration in physical systems". – Poznan-Blazejewsko, 2000. – P. 134–135.

9. Butyter Igor, Diveyev Bogdan, Vikovych Igor *Optimization and design of the girder spray booms of inereased durability and quality of an agent spraying* // XX Symposium „Vibrations in physical systems". – Poznan-Blazejewsko, May 21-25, 2002. – Abstract and invited lectures. – P. 120–121.

ENERGY MODEL OF A SPATIAL HUMAN BEING – DEMOLITION HAMMER SYSTEM WITH WOSSO VIBROISOLATION

Marian Witalis DOBRY, Małgorzata WOJSZNIS
Institute of Applied Mechanics
Poznan University of Technology
3 Piotrowo Street, 60-965 Poznan,
e-mail: Marian.Dobry@put.poznan.pl, Malgorzat.Wojsznis@put.poznan.pl,

Abstract

The paper concerns the problem of energy modeling of a spatial Human Being – Demolition Hammer system with WoSSO vibroisolation (C-MWzWoSSO). For this purpose, first, new spatial physical and mathematical models of the system were developed with the use of the data presented in the ISO 10068 standard. Then, a model of energy flow in a dynamic structure of the investigated system was built.

Keywords: energy modeling, vibroisolation, bio-dynamics

Introduction

The energy investigations carried out at the Laboratory of Dynamics and Ergonomics of the Metasystem: Human being – Technical object – Environment aim at reduction of flow of energy coming from power driven tools into the dynamic structure of a Human Being. This energy is a holistic measure of harmfulness of tool influence on a being and of a risk of appearance of vibration induced white finger disease [1]. In order to minimize the energy flow from the tool into a human being the tool was equipped with a spatial vibroisolation system with a constant reactive force. The advanced energy analysis of the energy flow phenomenon and its optimization required development of an energy model. Such a model is shown in this paper for the case of spatial vibrations of a Human Being – Big Power Driven Hand Tool system with vibroisolation WoSSO (C-DZNR with WoSSO). The modeled bio-mechanical system is shown in Figure 1 [2].

The energy model of the C-DZNR system with WoSSO in the energy flow domain first requires dynamic modeling of the system. Then, with the use of the First Principle of Energy Flow in Mechanical Systems it is possible to pass on to the energy flow domain [1]. The development of the dynamic model of a Human Being – DZNR (demolition hammer) system with the WoSSO vibroisolation was preceded by definition of simplifying assumptions concerning a real object, in which the patented method of spatial vibroisolation WoSSO was used [1, 2]. The WoSSO vibroisolation separates the tool engine from the tool body to which the handles for both operator's hands are fixed. The vibroisolation has spatially diverse efficiency of vibration reduction. The highest efficiency is along the main direction 'z' of vibrations caused by impulse recoil forces, reverse impacts and impacts of the ram on the engine body, and along the perpendicular directions 'x' and 'y' it is such, that the requirements of vibration standards are fulfilled. The model takes into consideration spatial, translational vibrations of a hammer

assuming the influence of rotational vibrations of the tool to be negligible [2]. A dynamic nine degrees of freedom model of a Human Being subjected to hand arm vibrations acting the upper limb [ISO 10068] was used to build the dynamical model of the system. The final model was obtained by synthesis of physical models of two subsystems: a human-operator using two hands during work with a tool and a tool – a demolition hammer [2].
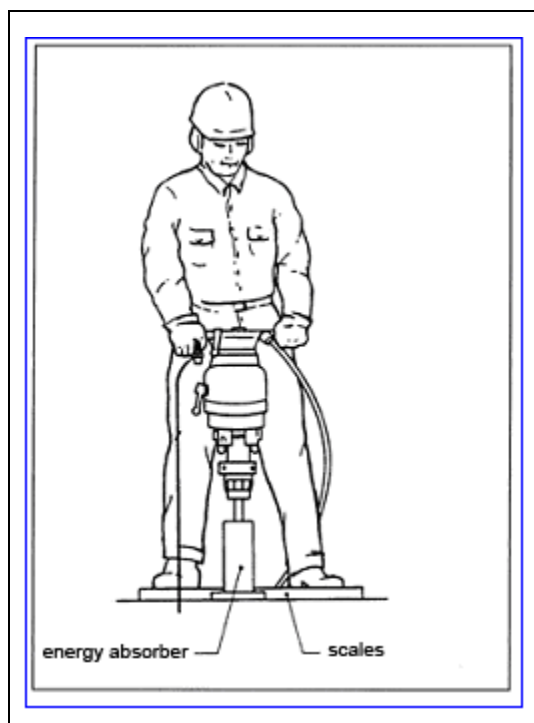
Figure 1. The energy modeled Human Being – Big Power Driven Tool system with the innovative, spatial vibroisolation WoSSO [1, 2]

1. Physical model of the Human Being – Demolition Hammer system with the WoSSO vibroisolation (C-MW with WoSSO)

The physical model of the investigated bio-mechanical system is shown in Figure 2 [2]. The applied physical models of Human Being for vibrations penetrating into one upper limb (presented in the ISO 10068 standard) enables dynamic analysis in the structure of a human body. It is possible in this way to determine dynamic effects of the influence of the tool during work. Forces exciting the demolition hammer to vibrations will be identified experimentally at the laboratory when the hammer will be acting on an energy absorber, see Figure 1 [2]. During research the coordinate system was assumed to be oriented in such a way that the 'z' direction is vertical (along the main axis of symmetry of the tool and working motions of its ram – the direction of the biggest vibrations), the 'y' direction is parallel to the handles, and the 'x' direction is perpendicular to the handles.

The assumed working position of the Human Being is consistent with the description presented in the ISO 10068 standard, which enables the use of substitute parameters for all directions 'x', 'y' and 'z', which are given therein. In the spatial physical model of

the whole structure C-DZNR with WoSSO the following points of reduction were assumed: Tool engine – reduced substitute mass m_s (S), Tool body-Hands (both) – mass $m_{zk} = m_k + m_{1L} + m_{1P}$ (K-D), Forearm-Elbow for the left hand – mass m_{2L} (P_L-L) and for the right hand – mass m_{2P} (P_P-L), Arm-Shoulder for the left hand – mass m_{3L} (R_L-B) and for the right hand – mass m_{3P} (R_P-B).
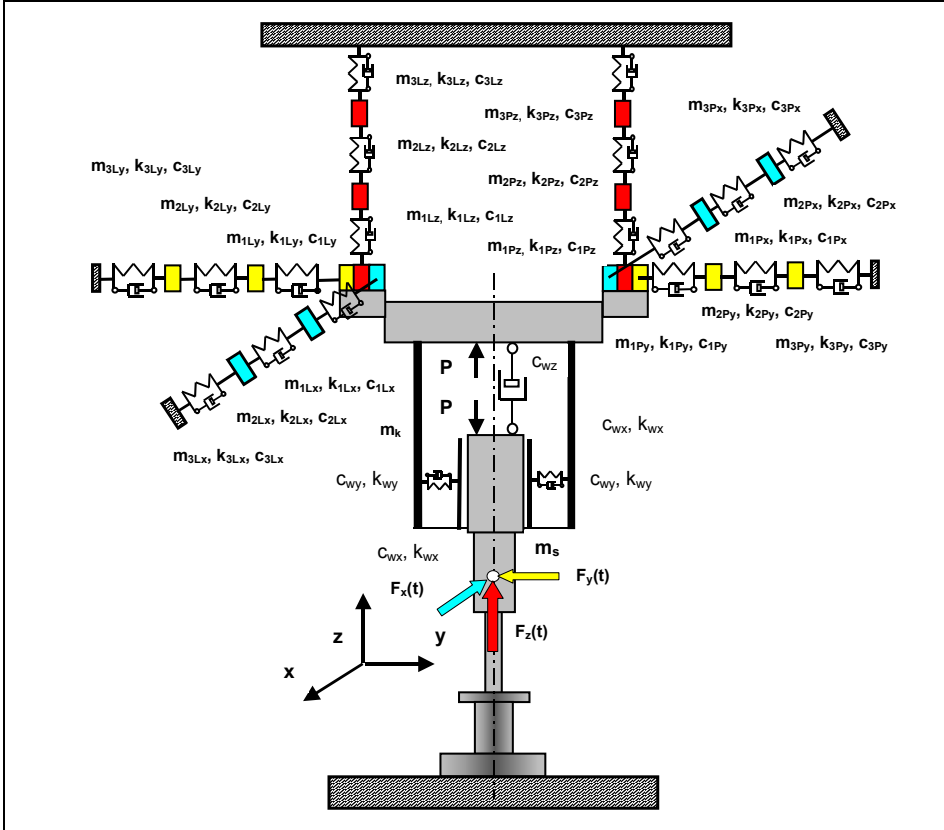
Figure 2. Physical model of a Human Being – Big Power Driven Hand Tool (e.g. demolition hammer) system with the spatial vibroisolation WoSSO [2]

The description of the points of reduction and the reduced substitute parameters for individual directions contains additional information about the directions, i.e. 'x', 'y' and 'z' to be subscripts. Independent consideration of both upper limbs of the Human Being decides about its universality, because it is possible to take other positions of a human body into consideration, for which the reduced substitute parameters are different.

2. Mathematical model of dynamics end energy model of the investigated system

A mathematical model of dynamics of the C-DZNR system with WoSSO was built up using Lagrange equations. The modeled system has 18 degrees of freedom. General coordinates, listed in Table 1, were assumed to describe their motion.

Table 1. The assumed generalized coordinates for description of motion of the C-DZNR system with WoSSO and their notation

Direction 'x'
$x_s(t)$ – displacement of the hammer engine in the x direction,
$x_k(t)$ – displacement of the hammer body in the x direction,
$x_{2Lx}(t)$ – displacement of the P-L point of reduction for the left hand in the x direction,
$x_{3Lx}(t)$ – displacement of the R-B point of reduction for the left hand in the x direction,
$x_{2Px}(t)$ – displacement of the P-L point of reduction for the right hand in the x direction,
$x_{3Px}(t)$ – displacement of the R-B point of reduction for the right hand in the x direction,
Direction 'y'
$y_s(t)$ – displacement of the hammer engine in the y direction,
$y_k(t)$ – displacement of the hammer body in the y direction,
$y_{2Ly}(t)$ – displacement of the P-L point of reduction for the left hand in the y direction,
$y_{3Ly}(t)$ – displacement of the R-B point of reduction for the left hand in the y direction,
$y_{2Py}(t)$ – displacement of the P-L point of reduction for the right hand in the y direction,
$y_{3Py}(t)$ – displacement of the R-B point of reduction for the right hand in the y direction,
Direction 'z'
$z_s(t)$ – displacement of the hammer engine in the z direction,,
$z_k(t)$ – displacement of the hammer body in the z direction,
$z_{2Lz}(t)$ – displacement of the P-L point of reduction for the left hand in the z direction,
$z_{3Lz}(t)$ – displacement of the R-B point of reduction for the left hand in the z direction,
$z_{2Pz}(t)$ – displacement of the P-L point of reduction for the right hand in the z direction,,
$z_{3Pz}(t)$ – displacement of the R-B point of reduction for the right hand in the z direction.

In order to obtain a **mathematical energy model** of the investigated system two energy principles were used: the **First Principle of Power Distribution in a Mechanical System** and the **First Principle of Energy Flow in a Mechanical System** [1]. The results of dynamic analysis, i.e. accelerations, velocities and displacements of all points of reduction and the identified dynamic parameters ensuring correct motion of the modeled system are the input values for this model. The energy model of the C-DZNR system with WoSSO consists of 18 equations defining the streams of energy flowing in the whole dynamic structure of the investigated system – Equations (1), (2) and (3). In these equations forces $F_{sx}(t)$, $F_{sy}(t)$, $F_{sz}(t)$ are the components of the sum of forces causing the motion of the tool engine and reactive forces of the foundation for the individual directions 'x', 'y' and 'z'. The reduced substitute values of dynamic parameters appearing in the above mentioned equations were determined basing on literature research, see Table 2. They concern hand-arm vibrations penetrating into one upper limb of the Human Being modeled by a discrete model with nine degrees of freedom, as in the developed physical model – Figure 1. The remaining parameters will be identified at the Laboratory of Dynamics and Ergonomics of the Metasystem: Human Being – Technical object – Environment [2].

3. Conclusions and summary

The developed energy model of a C-DZNR system with WoSSO describes dynamics of energy flow in a bio-mechanical system, which takes the spatial motion of the system, both upper limbs and real forces causing the motion generated by the tool engine into consideration. The energy investigations concerning this system will be continued [2].

A) for 'x' direction: (1)

$$j=1; \quad \int_{t_1}^{t_2}\left[m_s\left(\overset{\circ\circ}{x}_s\right)+2c_{wx}\overset{\circ}{x}_s+(2k_{wx})x_s\right]\left(\overset{\circ}{x}_s\right)dt=\int_{t_1}^{t_2}\left[2c_{wx}\overset{\circ}{x}_k+(2k_{wx})x_k+F_{sx}(t)\right]\left(\overset{\circ}{x}_s\right)dt;$$

$$j=2; \quad \int_{t_1}^{t_2}\left[(m_{ks}+m_{1Lx}+m_{1Px})\left(\overset{\circ\circ}{x}_k\right)+(c_{1Lx}+c_{1Px})\overset{\circ}{x}_k+(k_{1Lx}+k_{1Px})x_k\right]\left(\overset{\circ}{x}_k\right)dt=$$
$$=\int_{t_1}^{t_2}\left[c_{1Lx}\overset{\circ}{x}_{2Lx}+k_{1Lx}x_{2lx}+c_{1Px}\overset{\circ}{x}_{2Px}+k_{1Px}x_{2Px}\right]\left(\overset{\circ}{x}_k\right)dt;$$

$$j=3; \quad \int_{t_1}^{t_2}\left[m_{2Lx}\left(\overset{\circ\circ}{x}_{2Lx}\right)+(c_{1Lx}+c_{2Lx})\overset{\circ}{x}_{2Lx}+(k_{1Lx}+k_{2Lx})x_{2lx}\right]\left(\overset{\circ}{x}_{2Lx}\right)dt=\int_{t_1}^{t_2}\left[c_{1Lx}\overset{\circ}{x}_k+k_{1Lx}x_k+c_{2Lx}\overset{\circ}{x}_{3Lx}+k_{2Lx}x_{3Lx}\right]\left(\overset{\circ}{x}_{2Lx}\right)dt;$$

$$j=4; \quad \int_{t_1}^{t_2}\left[m_{3Lx}\left(\overset{\circ\circ}{x}_{3Lx}\right)+(c_{2Lx}+c_{3Lx})\overset{\circ}{x}_{3Lx}+(k_{2Lx}+k_{3Lx})x_{3Lx}\right]\left(\overset{\circ}{x}_{3Lx}\right)dt=\int_{t_1}^{t_2}\left[c_{2Lx}\overset{\circ}{x}_{2Lx}+k_{2Lx}x_{2Lx}\right]\left(\overset{\circ}{x}_{3Lx}\right)dt;$$

$$j=5; \quad \int_{t_1}^{t_2}\left[m_{2Px}\left(\overset{\circ\circ}{x}_{2Px}\right)+(c_{1Px}+c_{2Px})\overset{\circ}{x}_{2Px}+(k_{1Px}+k_{2Px})k_{2Px}\right]\left(\overset{\circ}{x}_{2Px}\right)dt=$$
$$=\int_{t_1}^{t_2}\left[c_{1Px}\left(\overset{\circ}{x}_k\right)+k_{1Px}(x_k)+c_{2Px}\left(\overset{\circ}{x}_{3Px}\right)+k_{2Px}(x_{3Px})\right]\left(\overset{\circ}{x}_{2Px}\right)dt;$$

$$j=6; \quad \int_{t_1}^{t_2}\left[m_{3Px}\left(\overset{\circ\circ}{x}_{3Px}\right)+(c_{2Px}+c_{3Px})\overset{\circ}{x}_{3Px}+(k_{2Px}+k_{3Px})x_{3Px}\right]\left(\overset{\circ}{x}_{3Px}\right)dt=\int_{t_1}^{t_2}\left[c_{2Px}\overset{\circ}{x}_{2Px}+k_{2Px}x_{2Px}\right]\left(\overset{\circ}{x}_{3Px}\right)dt;$$

B) for 'y' direction: (2)

$$j=7; \quad \int_{t_1}^{t_2}\left[m_s\left(\overset{\circ\circ}{y}_s\right)+(2c_{wy})\overset{\circ}{y}_s+(2k_{wy})y\right]\left(\overset{\circ}{y}_s\right)dt_s=\int_{t_1}^{t_2}\left[2c_{wy}\overset{\circ}{y}_k+2k_{wy}y_k+F_{sy}(t)\right]\left(\overset{\circ}{y}_s\right)dt;$$

$$j=8; \quad \int_{t_1}^{t_2}\left[(m_k+m_{1Ly}+m_{1Py})\left(\overset{\circ\circ}{y}_k\right)+(2c_{wy}+c_{1Ly}+c_{1Py})\left(\overset{\circ}{y}_k\right)+(2k_{wy}+k_{1Ly}+k_{1Py})y_k\right]\left(\overset{\circ}{y}_k\right)dt=$$
$$=\int_{t_1}^{t_2}\left[2c_{wy}\left(\overset{\circ}{y}_s\right)+2k_{wy}y_s+c_{1Ly}\left(\overset{\circ}{y}_{2Ly}\right)+k_{1Ly}y_{2Ly}+c_{1Py}\left(\overset{\circ}{y}_{2Py}\right)+k_{1Py}y_{2Py}\right]\left(\overset{\circ}{y}_k\right)dt;$$

$$j=9; \quad \int_{t_1}^{t_2}\left[m_{2Ly}\left(\overset{\circ\circ}{y}_{2Ly}\right)+(c_{1Ly}+c_{2Ly})\left(\overset{\circ}{y}_{2Ly}\right)+(k_{1Ly}+k_{2Ly})y_{2Ly}\right]\left(\overset{\circ}{y}_{2Ly}\right)dt=$$
$$=\int_{t_1}^{t_2}\left[c_{1Ly}\left(\overset{\circ}{y}_k\right)+k_{1Ly}(y_k)+c_{2Ly}\left(\overset{\circ}{y}_{3Ly}\right)+k_{2Ly}(y_{3Ly})\right]\left(\overset{\circ}{y}_{2Ly}\right)dt;$$

$$j=10; \quad \int_{t_1}^{t_2}\left[m_{3Ly}\left(\overset{\circ\circ}{y}_{3Ly}\right)+(c_{2Ly}+c_{3Ly})\left(\overset{\circ}{y}_{3Ly}\right)+(k_{2Ly}+k_{3Ly})y_{3Ly}\right]\left(\overset{\circ}{y}_{3Ly}\right)dt=\int_{t_1}^{t_2}\left[c_{2Ly}\left(\overset{\circ}{y}_{2Ly}\right)+k_{2Ly}(y_{2Ly})\right]\left(\overset{\circ}{y}_{3Ly}\right)dt;$$

$$j=11; \quad \int_{t_1}^{t_2}\left[m_{2Py}\left(\overset{\circ\circ}{y}_{2Py}\right)+(c_{1Py}+c_{2Py})\left(\overset{\circ}{y}_{2Py}\right)+(k_{1Py}+k_{2Py})y_{2Py}\right]\left(\overset{\circ}{y}_{2Py}\right)dt=$$
$$=\int_{t_1}^{t_2}\left[c_{1Py}\left(\overset{\circ}{y}_k\right)+k_{1Py}(y_k)+c_{2Py}\left(\overset{\circ}{y}_{3Py}\right)+k_{2Py}(y_{3Py})\right]\left(\overset{\circ}{y}_{2Py}\right)dt;$$

$$j=12; \quad \int_{t_1}^{t_2}\left[m_{3Py}\left(\overset{\circ\circ}{y}_{3Py}\right)+(c_{2Py}+c_{3Py})\left(\overset{\circ}{y}_{3Py}\right)+(k_{2Py}+k_{3Py})y_{3Py}\right]\left(\overset{\circ}{y}_{3Py}\right)dt=\int_{t_1}^{t_2}\left[c_{2Py}\left(\overset{\circ}{y}_{2Py}\right)+k_{2Py}(y_{2Py})\right]\left(\overset{\circ}{y}_{3Py}\right)dt;$$

C) for 'z' direction: (3)

$$j=13; \quad \int_{t_1}^{t_2}\left[m_s\left(\overset{\circ\circ}{z}_s\right)+c_{wz}\left(\overset{\circ}{z}_s\right)\right]\left(\overset{\circ}{z}_s\right)dt=\int_{t_1}^{t_2}\left[c_{wz}\left(\overset{\circ}{z}_k\right)+F_{sz}(t)-P\right]\left(\overset{\circ}{z}_s\right)dt;$$

$$j=14; \quad \int_{t_1}^{t_2}\left[(m_k+m_{1Lz}+m_{1Pz})\left(\overset{\circ\circ}{z}_k\right)+(c_{1Lz}+2c_{wz}+c_{1Pz})\left(\overset{\circ}{z}_k\right)+(k_{1Lz}+k_{1Pz})z_k\right]\left(\overset{\circ}{z}_k\right)dt=$$
$$=\int_{t_1}^{t_2}\left[(c_{1Lz})\left(\overset{\circ}{z}_{2Lz}\right)+k_{1Lz}z_{2Lz}+(c_{1Pz})\left(\overset{\circ}{z}_{2Pz}\right)+k_{1Pz}z_{2Pz}+P\right]\left(\overset{\circ}{z}_k\right)dt;$$

$$j=15; \quad \int_{t_1}^{t_2}\left[m_{2Lz}\left(\overset{\circ\circ}{z}_{2Lz}\right)+(c_{1Lz}+c_{2Lz})\left(\overset{\circ}{z}_{2Lz}\right)+(k_{1Lz}+k_{2Lz})z_{2Lz}\right]\left(\overset{\circ}{z}_{2Lz}\right)dt=\int_{t_1}^{t_2}\left[c_{1Lz}\left(\overset{\circ}{z}_k\right)+(k_{1Lz})(z_k)+c_{2Lz}\left(\overset{\circ}{z}_{3Lz}\right)+(k_{2Lz})(z_{3Lz})\right]\left(\overset{\circ}{z}_{2Lz}\right)dt;$$

$$j=16; \quad \int_{t_1}^{t_2}\left[m_{3Lz}\left(\overset{\circ\circ}{z}_{3Lz}\right)+(c_{2Lz}+c_{3Lz})\left(\overset{\circ}{z}_{3Lz}\right)+(k_{2Lz}+k_{3Lz})z_{3Lz}\right]\left(\overset{\circ}{z}_{3Lz}\right)dt=\int_{t_1}^{t_2}\left[c_{2Lz}\left(\overset{\circ}{z}_{2Lz}\right)+(k_{2Lz})(z_{2Lz})\right]\left(\overset{\circ}{z}_{3Lz}\right)dt;$$

$$j=17; \quad \int_{t_1}^{t_2}\left[m_{2Pz}\left(\overset{\circ\circ}{z}_{2Pz}\right)+(c_{1Pz}+c_{2Pz})\left(\overset{\circ}{z}_{2Pz}\right)+(k_{1Pz}+k_{2Pz})z_{2Pz}\right]\left(\overset{\circ}{z}_{2Pz}\right)dt=\int_{t_1}^{t_2}\left[c_{1Pz}\left(\overset{\circ}{z}_k\right)+(k_{1Pz})(z_k)+c_{2Pz}\left(\overset{\circ}{z}_{3Pz}\right)+(k_{2Pz})(z_{3Pz})\right]\left(\overset{\circ}{z}_{2Pz}\right)dt;$$

$$j=18; \quad \int_{t_1}^{t_2}\left[m_{3Pz}\left(\overset{\circ\circ}{z}_{3Pz}\right)+(c_{1Pz}+c_{3Pz})\left(\overset{\circ}{z}_{3Pz}\right)+(k_{2Pz}+k_{3Pz})z_{3Pz}\right]\left(\overset{\circ}{z}_{3Pz}\right)dt=\int_{t_1}^{t_2}\left[c_{1Pz}\left(\overset{\circ}{z}_{2Pz}\right)+(k_{2Pz})(z_{2Pz})\right]\left(\overset{\circ}{z}_{3Pz}\right)dt.$$

Table 2. Values of dynamic parameters of a physical model of a human operator for three directions x, y and z according to the ISO 10068 standard

Unit	Reduced dynamic parameters of a model of a human being Direction of vibrations		
	X	Y	Z
kg	$m_{1Lx}=m_{1Px}=0.0267$	$m_{1Ly}=m_{1Py}=0.0086$	$m_{1Lz}=m_{1Pz}=0.0299$
kg	$m_{2Lx}=m_{2Px}=0.486$	$M_{2Ly}=m_{2Py}=0.3565$	$M_{2Lz}=m_{2Pz}=0.6623$
kg	$m_{3Lx}=m_{3Px}=3.0952$	$M_{3Ly}=m_{3Py}=3.2462$	$M_{3Lz}=m_{3Pz}=2.9023$
N/m	$k_{1Lx}=k_{1Px}=4368$	$K_{1Ly}=k_{1Py}=27090$	$k_{1Ly}=k_{1Py}=5335$
N/m	$k_{2Lx}=k_{2Px}=132$	$k_{2Ly}=k_{2Py}=300$	$k_{2Lz}=k_{2Pz}=299400$
N/m	$k_{3Lx}=k_{3Px}=1565$	$k_{3Ly}=k_{3Py}=6415$	$k_{3Lz}=k_{3Pz}=2495$
Ns/m	$c_{1Lx}=c_{1Px}=207,5$	$c_{1Ly}=c_{1Py}=68$	$c_{1Lz}=c_{1Pz}=227,5$
Ns/m	$c_{2Lx}=c_{2Px}=18,93$	$c_{2Ly}=c_{2Py}=51,75$	$c_{2Lz}=c_{2Pz}=380,6$
Ns/m	$c_{3Lx}=c_{3Px}=9,10$	$c_{3Ly}=c_{3Py}=30,78$	$c_{3Lz}=c_{3Pz}=30,30$

References

1. Dobry M. W. (1998), Optymalizacja przepływu energii w systemie Człowiek - Narzędzie - Podłoże (CNP), Rozprawa habilitacyjna, Seria „Rozprawy" nr 330. ISSN 0551-6528, Wyd. Politechniki Poznańskiej, Poznań 1998
2. Dobry M. W., Wojsznis M*., Innowacyjna metoda redukcji przepływu energii do człowieka-operatora od dużych zmechanizowanych narzędzi ręcznych.* Raport z etapu I. Projekt badawczy nr N503 017 32/2558. Politechnika Poznańska, Instytut Mechaniki Stosowanej, Poznań 2008

UNEXPECTED PROPERTIES OF SH-WAVES IN SUPERCONDUCTING HETEROSTRUCTURE

Andrzej DRZEWIECKI
Bogdan MARUSZEWSKI
Roman STAROSTA
Institute of Applied Mechanics
Poznan University of Technology
andrzej.drzewiecki@put.poznan.pl, bogdan.maruszewski@put.poznan.pl, roman.starosta@put.poznan.pl,

Abstract

The paper provides confrontation of a surface wave of SH polarization propagating in a superconducting layer (type II superconductor) located in a superconducting halfspace of similar material properties. It was found that the wave in the determined heterostructure is distinguished by the properties significantly different from classical Love wave propagating in similar elastic structure. Among more important differences first of all should be mentioned occurrence of only one mode and changed direction of the inequality that determines allowable range of phase velocity of propagating wave. Both waves are subject to normal dispersion.

Keywords: superconductivity, thermomechanics, surface waves,

Introduction

Surface wave SH propagating in a superconducting heterostructure possess unexpected properties as compared to the ones of classical Love wave in a similar elastic structure [1]. In order to discuss this problem a classical solution is shortly presented below.
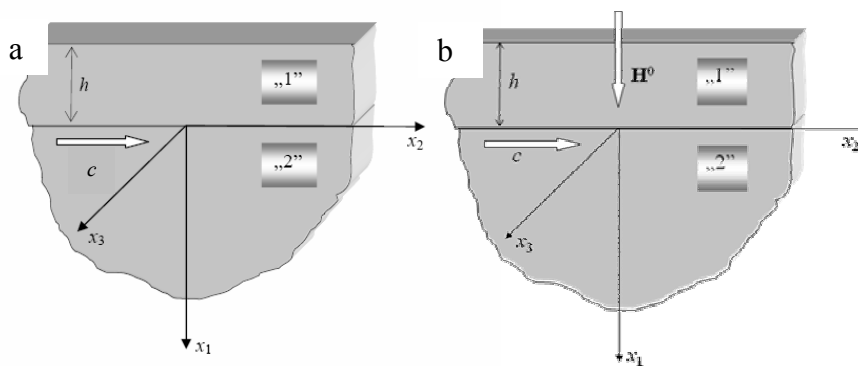
Fig. 1 Geometry of the problem.

Geometry of discussed classical problem is presented in Fig.1a. It is assumed that the displacement vector is a function of x_1, x_2, and time t,

$$\mathbf{u} = \mathbf{u}(x_1, x_2, t). \tag{1}$$

It is conducive to uncoupling of the displacement equations of theory of elasticity. Especially we have

$$\mu \nabla_1^2 u_3 = \rho \ddot{u}_3 \tag{2}$$

where

$$\nabla_1^2 = \frac{\partial^2}{\partial x_1^2} + \frac{\partial^2}{\partial x_2^2}.$$

Solution of (2) is sought in the form of surface wave

$$u_3 = f(x_1) \exp[ik(x_2 - ct)] \tag{3}$$

The solutions and material constants are specified by low indexes "1" or "2", according to Fig.1

Ordinary differential equation is obtained in a layer

$$\frac{d^2}{dx_1^2} f_1(x_1) + k^2 \beta_1^2 f_1(x_1) = 0; \quad \beta_1^2 = \frac{c^2}{c_{T1}^2} - 1 \tag{4}$$

for

$$-h < x_1 < 0$$

In a halfspace

$$\frac{d^2}{dx_1^2} f_2(x_1) + k^2 \beta_2^2 f_2(x_1) = 0; \quad \beta_2^2 = \frac{c^2}{c_{T2}^2} - 1 \tag{5}$$

for

$$x_1 > 0$$

For Love wave to propagate the following assumption should be made

$$\beta_1^2 = \frac{c^2}{c_{T1}^2} - 1 > 0 \quad \beta_2^2 = 1 - \frac{c^2}{c_{T2}^2} > 0 \tag{6}$$

This leads to the following set of inequalities

$$c_{T2} > c > c_{T1} \tag{7}$$

Hence, the equations (4) and (5) take the form

$$f_1(x_1) = A \sin(k\beta_1 x_1) + B \cos(k\beta_1 x_1), \quad -h < x_1 < 0 \tag{8}$$

$$f_2(x_2) = C \exp(-k\beta_2 x_1), \quad x_1 > 0 \tag{9}$$

The solutions should meet the following boundary and seam conditions
- the stress-free boundary

$$\left. \frac{d}{dx_1} f_1(x_1) \right|_{x_1 = -h} = 0 \tag{10}$$

- continuity of displacements

$$f_1(x_1)\big|_{x_1 = 0^-} = f_2(x_1)\big|_{x_1 = 0^+} \tag{11}$$

- continuity of the stress vector

$$\mu_1 \frac{d}{dx_1} f_1(x_1)\bigg|_{x_1=0^-} = \mu_2 \frac{d}{dx_1} f_2(x_1)\bigg|_{x_1=0^+} \tag{12}$$

Appropriate substitutions provide a system of algebraic equations with A, B, C, constants

$$\begin{cases} A\cos(\beta_1 kh) + B\sin(\beta_1 kh) = 0 \\ B - C = 0 \\ A\mu_1\beta_1 + C\mu_2\beta_2 = 0 \end{cases} \tag{13}$$

The system has non-trivial solutions if

$$\mu_2\beta_2 = \mu_1\beta_1 \tan(k\beta_1 h) \tag{14}$$

The equation (14) is a dispersion equation.
The dispersion curves are shown below for the following material constants

$$\mu_2 = 6\cdot 10^7 \frac{N}{m^2}, \quad \mu_1 = 3\cdot 10^7 \frac{N}{m^2}, \quad \rho_2 = \rho_1 = 3\cdot 10^3 \frac{kg}{m^3}, \quad h = 0.001m$$
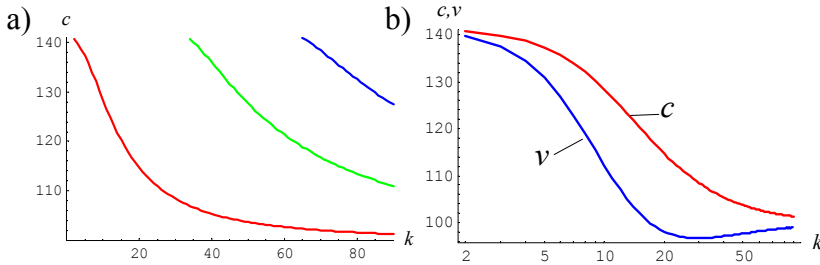
Fig.2 Dispersion curves for Love's wave

Characteristic feature of Love wave consists in occurrence of many modes (Fig. 2a). Relationship between the phase and group velocities on the wave number for the first mode is shown in Fig. 2b.

Surface wave SH in superconducting heterostructure

Basic equations describing elastodynamical properties of the vortex field type II superconductor are proposed in the paper [6]. The problem of surface wave propagation of SH polarization in the considered heterostructure is described by the equations

$$\mu\left(u_{3,11} + u_{3,22}\right) + \mu_0\, h_{3,1}\, H_1^0 - \rho\ddot{u}_3 = 0$$
$$\lambda_0^2\left(h_{3,11} + h_{3,22}\right) - h_3 + u_{3,1}\, H_1^0 = 0 \tag{15}$$

Similarly to classical case the solution is sought in the form

$$f(x_1, x_2, t) = \tilde{f}(x_1) \exp[i\,k\,(x_2 - ct)] \tag{16}$$

Further consideration is carried out in dimensionless form. In order to introduce

dimensionless coordinates x,y,z and dimensionless time τ a characteristic dimension h and characteristic time T are used.

$$x_1 = h\,x, \ x_2 = h\,y, \ x_3 = h\,z, \ t = T\,\tau, \ T = h\sqrt{\frac{\rho_1}{\mu_1}}$$

The dimensionless amplitudes of sought physical fields $u_z(x)$, $h_z(x)$ and dimensionless magnetic field H_0 meet the relationships

$$\widetilde{u}_3(x_1) = h\,u_z(x), \ \widetilde{h}_3(x_1) = H_1\,h_z(x), \ H_1^0 = H_1\,H_0$$

where H_1 is critical field of the layer material..

The dimensionless angular frequency Ω and the phase velocity c meet the relationships

$$\Omega = \omega\,T, \ k = \frac{2\pi}{\lambda} = \frac{\Omega}{c\,T} = \frac{\Omega}{v\,h}, \ v = c\sqrt{\frac{\rho_1}{\mu_1}}$$

while the dimensionless material constants and the universal constants (the symbols with tilda) are related to corresponding dimension constants with the relationships

$$\widetilde{\rho}_1 = \frac{\rho_1\,h^2}{T^2\,\mu_1} = 1, \ \widetilde{\rho}_2 = \frac{\rho_2\,h^2}{T^2\,\mu_1}, \ \widetilde{\mu}_1 = \frac{\mu_1}{\mu_1} = 1, \ \widetilde{\mu}_2 = \frac{\mu_2}{\mu_1}$$
$$\widetilde{\lambda}_{01}^2 = \frac{\lambda_{01}^2}{h^2}, \ \widetilde{\lambda}_{01}^2 = \frac{\lambda_{01}^2}{h^2}, \ \widetilde{\mu}_0 = \frac{\mu_0\,H_1^2}{\mu_1}$$

Proper substitutions lead to the following system of ordinary differential equations met by the amplitudes

$$\widetilde{\mu}_i\,\frac{d^2 u_z}{dx^2} + \frac{\Omega^2}{v^2}\left(v^2\,\widetilde{\rho}_i - \widetilde{\mu}_i\right)u_z + \widetilde{\mu}_0\,H_0\,\frac{dh_z}{dx} = 0,$$
$$\widetilde{\lambda}_{0i}^2\,\frac{d^2 h_z}{dx^2} - \left(\widetilde{\lambda}_{0i}^2\,\frac{\Omega^2}{v^2} + 1\right)h_z + H_0\,\frac{du_z}{dx} = 0, \quad i = 1, 2 \tag{17}$$

The characteristic equation of the above system takes a form

$$\widetilde{\lambda}_{0i}^2\,\widetilde{\mu}_i\,p^4 + \left[\lambda_{0i}^2\,B_i(\Omega,v) - F_i(\Omega,v)\widetilde{\mu}_i - \widetilde{\mu}_0\,H_0^2\right]p^2 - F_i(\Omega,v)B_i(\Omega,v) = 0 \tag{18}$$

where

$$B_i(\Omega,v) = \frac{\Omega^2}{v^2}\left(v^2\,\widetilde{\rho}_i - \widetilde{\mu}_i\right), \ F_i(\Omega,v) = \widetilde{\lambda}_{0i}^2\,\frac{\Omega^2}{v^2} + 1 > 0$$

Squares of the roots of the above equation should meet the relationships

$$p_{1i}^2\,p_{2i}^2 = -F_i(\Omega,v)B_i(\Omega,v)$$
$$-p_{1i}^2 - p_{2i}^2 = \left[\lambda_{0i}^2\,B_i(\Omega,v) - F_i(\Omega,v)\widetilde{\mu}_i - \widetilde{\mu}_0\,H_0^2\right] \tag{19}$$

General integrals of the equations (17) should meet the following jump and seam conditions

for $x = -1$

- Continuity of tangential component of the magnetic field strength
- The stress-free boundary. The stress vector is equal zero
for $x = 0$
- Continuity of tangential component of the magnetic field strength
- Continuity of displacements
- Continuity of stresses

Conditions of the task may be satisfied provided that the number of arbitrary constants used for formulating general integrals (17) is equal to the number of above specified number of the jump conditions. This means that one of squares of the roots of the characteristic equation (18) met in halfspace ($i=2$) should be purely imaginary. In this case an improper condition (i.e. requirement for amplitude to approach zero for $x\to\infty$) ensures equal number of the constants and conditions.

According to the above

$$\left(p_{12}^2 > 0 \ \wedge \ p_{22}^2 < 0\right) \Rightarrow \ B_2\left(\Omega,v\right) > 0 \Rightarrow v^2 > \frac{\widetilde{\mu}_2}{\widetilde{\rho}_2} \ . \tag{20}$$

The result differs from the one obtained in the classical theory (7).

In the ($i=1$) layer the squares of both roots of the characteristic equation (18) should be positive. Other options preclude the relationships (19).

$$\left(p_{11}^2 > 0 \ \wedge \ p_{21}^2 > 0\right) \ \Rightarrow \ B_1\left(\Omega,v\right) < 0 \Rightarrow v^2 < \frac{\widetilde{\mu}_1}{\widetilde{\rho}_1} = 1 \tag{21}$$

Hence

$$\frac{\widetilde{\mu}_2}{\widetilde{\rho}_2} < v^2 < \frac{\widetilde{\mu}_1}{\widetilde{\rho}_1} \ , \tag{22}$$

i.e. direction of the inequality opposite to the one resulting from the classical theory (7). Moreover, as a consequence of the exponential form of the solutions both for the layer and halfspace, the dispersive relationship admits propagation of only one mode.

In accordance with the assumptions the solutions of the equations (17) in the layer have the following form

$$u_z = S_1 \exp(p_{11} x) + S_2 \exp(-p_{11} x) + S_3 \exp(p_{21} x) + S_4 \exp(-p_{21} x)$$
$$h_z = -W_1\left(p_{11},\Omega,v\right)S_1 \exp(p_{11} x) + W_1\left(p_{11},\Omega,v\right)S_2 \exp(-p_{11} x) - \qquad , \tag{23}$$
$$-W_1\left(p_{21},\Omega,v\right)S_3 \exp(p_{21} x) + W_1\left(p_{21},\Omega,v\right)S_4 \exp(-p_{21} x)$$

while in halfspace

$$u_z = S_5 \exp(-p_{12} x), \quad h_z = W_2\left(p_{12},\Omega,v\right)\exp(-p_{12} x) , \tag{24}$$

where

$$W_i\left(p_{\alpha i},\Omega,v\right) = \frac{\widetilde{\mu}_i \ p_{\alpha i}}{\widetilde{\mu}_0 \ H_0} + \frac{\Omega^2}{v^2} \ \frac{v^2 \ \widetilde{\rho}_i - \widetilde{\mu}_i}{\widetilde{\mu}_0 \ H_0 \ p_{ai}} , \quad p_{\alpha i} \text{ is a root of the characteristic equation}$$

(18) (the first index denotes the root number, the other corresponds to the layer or halfspace, according to Fig. 1)..

The seam conditions lead to the dispersive relationship

$$f(\Omega, v; \xi) = 0 \, , \tag{25}$$

where ξ is for the set of material parameters.

In particular case of ceramic material of the layer La… and YbaCuO ceramic material of halfspace, the plot of the dispersive relationship is shown in Fig. 3 (the material constants are drawn from [3])
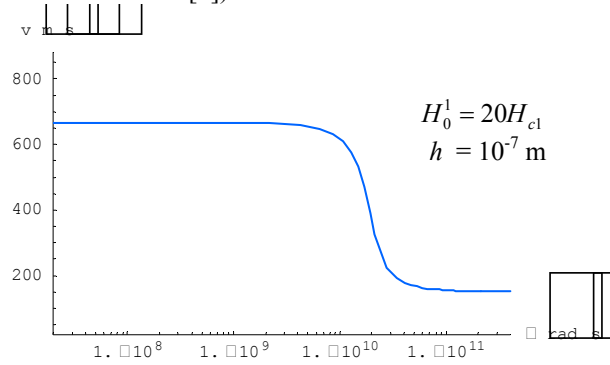
Fig. 3 Dispersion curve.

Conclusions

Elastodynamical properties of the vortex fields in superconducting heterostructure prove to be quite different as compared to the ones commonly known for surface Love wave. In the structure here considered only one mode of the dispersive relationship occurs. Moreover, the inequalities (22) are valid that, according to the notes made above, corresponds to the arrangement opposite to classical one.

References

1. A. C. Eringen, E. S. Suhubi, Elastodynamics, Akademic Press, 1975
2. T.P. Orlando, K.A. Delin, Foundations of applied superconductivity, Addison-Wesley Publ. Co., Reading 1991.
3. M. Cyrot, D. Pavuna, Introduction to superconductivity and high-T materials, World Scientific, Singapore 1992.
4. G. Blatter, M.V. Feigelman, V.B. Geshkenbein, A.I. Larkin, V.M. Vinokur, Vortices in high-temperature superconductors, Rev. Mod. Phys., vol. 66, pp. 1125-1388, 1994.
5. E.H. Brandt, The flux-line lattice in superconductors, Rep. Prog. Phys., vol. 58, pp. 1465-1594, 1995.
6. B. T. Maruszewski, On a Nonclassical Thermoviscomechanical Stress in the Vortex Field in the Type-II Superconductor, physica status solidi (b),vol. 244, p. 919, 2007.
7. B. Maruszewski, A. A. F. van de Ven, Plasmomagnetoelastic waves In a semiconducting heterostructure. II. SH-magnetoelastic modes, in: Nonlinear waves in solids, ed. By J. L. Wegner, F. R. Norwood, ASME Book No AMR 137, 1995.

STRING-BEAM UNDER MOVING INERTIAL LOAD

Bartłomiej DYNIEWICZ and Czesław BAJER
Institute of Fundamental Technological Research, Polish Academy of Sciences,
Świętokrzyska 21, 00-049 Warsaw, Poland

Abstract

The paper deals with the original analytical-numerical approach to the Bernoulli-Euler beam with additional tensile effect under a moving inertial load. The authors applied the 2nd kind Lagrange equation to derive a motion differential equation of the problem. The moving mass can travel through the string-beam with a whole range constant speed, also overcritical. The analytical solution requires a numerical calculation in the last stage and is called a semi-analytical one.

Keywords: moving mass, inertial load, string, beam

Introduction

The problem of bridge spans under a moving inertial load has existed since the beginning of the railways development. The turning point in the literature devoted to moving loads was established by two historical publications [1, 2]. These analytical papers were elaborated with significant mathematical simplifications. The authors considered the complex acceleration of the moving mass. Its geometrical interpretation was presented by Renaudot [3]. Although the number of publications on the moving mass problem exceeded thousand items, still we do not have its detailed and fully analytical solutions. The approach given by Smith [4] seems to be a positive exception. He considered, however, the massless string only. There exist numerous review papers [5, 6, 7, 8] which discuss problems presented in hundreds of other publications. For a long time the main stream of works treated the problem in an analytical-numerical way [9, 10, 11, 12] or strictly numerically [13, 14, 15].

Together with increasing velocity of trains, the influence of the wave phenomenon is rising as well. Dynamic effects are generated by the load of train current collectors, travelling through the power supply cable of the overhead contact line. In this paper, we consider a cable as the string-beam model, since it has a certain flexible stiffness.

Figure 1: A string-beam under the moving mass.

The Bernoulli-Euler beam with additional tensile effect comprises this phenomenon (Fig. 1). In the paper the differential equation of the motion of a string-beam is derived from the Lagrange equation of the 2nd kind.

1. The 2nd kind Lagrange equation

The motion equation of the string-beam under a moving mass m coupled with a force P can be written as follows

$$EI \frac{\partial^4 u(x,t)}{\partial x^4} - N \frac{\partial^2 u(x,t)}{\partial x^2} + \rho A \frac{\partial^2 u(x,t)}{\partial t^2} = \delta(x-vt)\, P - \delta(x-vt)\, m \frac{\partial^2 u(vt,t)}{\partial t^2}, \tag{1}$$

where EI is the beam stiffness, N is a tensile force and ρA is a linear mass density. Taking into account beam terms, we impose four boundary conditions

$$u(0,t) = 0, \qquad u(l,t) = 0, \qquad \left. \frac{\partial^2 u(x,t)}{\partial x^2} \right|_{x=0} = 0, \qquad \left. \frac{\partial^2 u(x,t)}{\partial x^2} \right|_{x=l} = 0 \tag{2}$$

and two initial conditions

$$u(x,0) = 0, \qquad \left. \frac{\partial u(x,t)}{\partial t} \right|_{t=0} = 0 . \tag{3}$$

The kinetic energy of a string-beam and a travelling mass is described by

$$E_k = \frac{1}{2} \rho A \int_0^l \left[\frac{\partial u(x,t)}{\partial t} \right]^2 \mathrm{d}x + \frac{1}{2} m \left[\frac{\partial u(vt,t)}{\partial t} \right]^2 . \tag{4}$$

The potential energy of a string-beam and a moving force is

$$E_p = \frac{1}{2} N \int_0^l \left[\frac{\partial u(x,t)}{\partial x} \right]^2 \mathrm{d}x + \frac{1}{2} EI \int_0^l \left[\frac{\partial^2 u(x,t)}{\partial x^2} \right]^2 \mathrm{d}x - P\, u(vt,t) . \tag{5}$$

In order to separate variables, the displacement can be written in a form of the infinite series and then integrals in space x in Eqns. (4) and (5) can be computed

$$u(x,t) = \sum_{i=1}^{\infty} U_i(x)\xi_i(t) . \tag{6}$$

According to (6) the displacement under a moving load has the following form

$$u(vt,t) = \sum_{i=1}^{\infty} U_i(vt)\xi_i(t) . \tag{7}$$

The velocity of the displacement is determined by a chain rule

$$\frac{\partial u(vt,t)}{\partial t} = v \sum_{i=1}^{\infty} U_i'(x)\xi_i(t) \Bigg|_{x=vt} + \sum_{i=1}^{\infty} U_i(x)\dot{\xi}_i(t) \Bigg|_{x=vt} . \tag{8}$$

It is the function of general coordinates as well as their velocities

$$\frac{\partial u(vt,t)}{\partial t} = f\left(\xi_i, \dot{\xi}_i \right) . \tag{9}$$

After calculation of required derivatives of (6) with respect to t and x, the kinetic and potential energy can be written in the following forms

$$
E_k \;=\; \frac{1}{2}\,\rho A \sum_{i,j=1}^{\infty} \dot{\xi}_i(t)\dot{\xi}_j(t) \int_0^l U_i(x)U_j(x)\mathrm{d}x \;+\; \frac{1}{2}\,m\left[\frac{\partial u(vt,t)}{\partial t}\right]^2 \;, \qquad (10)
$$

$$
E_p \;=\; \frac{1}{2}\,N \sum_{i,j=1}^{\infty} \xi_i(t)\xi_j(t) \int_0^l U_i'(x)U_j'(x)\mathrm{d}x +
$$
$$
+\frac{1}{2}\,EI \sum_{i,j=1}^{\infty} \xi_i(t)\xi_j(t) \int_0^l U_i''(x)U_j''(x)\mathrm{d}x - P\sum_{i=1}^{\infty} U_i(vt)\xi_i(t)\,. \qquad (11)
$$

We assume orthogonal functions (12) which fulfil boundary conditions (2)

$$
U_i(x) \;=\; \sin\frac{i\pi x}{l} \quad. \qquad (12)
$$

The orthogonality of functions $U_i(x)$ allows us to write

$$
\int_0^l U_i(x)U_j(x)\mathrm{d}x \;=\; \begin{cases} \frac{1}{2}l & \text{if } i=j, \\ 0 & \text{if } i\neq j \end{cases} \quad. \qquad (13)
$$

With respect to (6), (12) and (13) the kinetic energy of the hole system is given by

$$
E_k \;=\; \frac{1}{4}\,\rho A l \sum_{i=1}^{\infty} \dot{\xi}_i^2(t) \;+\; \frac{1}{2}\,m\left[\frac{\partial u(vt,t)}{\partial t}\right]^2 \quad. \qquad (14)
$$

The term of the moving mass is not an integral, so we can't use the property of orthogonality. On this stage, the kinetic energy of the travelling load is left in the original form. According to (12) we have $U_i''(x) = -i^2\pi^2/l^2\,U_i(x)$. After integration by parts and taking into account the recent relation, the potential energy can be written in the form

$$
E_p \;=\; \frac{1}{2}\,N \sum_{i,j=1}^{\infty} \frac{i^2\pi^2}{l^2}\xi_i(t)\xi_j(t) \int_0^l U_i(x)U_j(x)\mathrm{d}x +
$$
$$
+\;\frac{1}{2}\,EI \sum_{i,j=1}^{\infty} \frac{i^2 j^2\pi^4}{l^4}\xi_i(t)\xi_j(t) \int_0^l U_i(x)U_j(x)\mathrm{d}x \;-\; P\sum_{i=1}^{\infty} U_i(vt)\xi_i(t) \quad. \qquad (15)
$$

Finally, the orthogonality of (13) allows us to write

$$
E_p \;=\; \frac{1}{4}\,Nl \sum_{i=1}^{\infty} \frac{i^2\pi^2}{l^2}\xi_i^2(t) \;+\; \frac{1}{4}\,EIl \sum_{i=1}^{\infty} \frac{i^4\pi^4}{l^4}\xi_i^2(t) \;-\; P\sum_{i=1}^{\infty} \xi_i(t)\sin\frac{i\pi vt}{l} \quad. \qquad (16)
$$

The motion equation of the string-beam under a moving inertial load is obtained from the 2nd kind Lagrange equation, of which a general form is given by the equation

$$\frac{\mathrm{d}}{\mathrm{d}t}\left(\frac{\partial E_k}{\partial \dot{\xi}_i}\right) - \frac{\partial E_k}{\partial \xi_i} + \frac{\partial E_p}{\partial \xi_i} = 0 \ . \tag{17}$$

This method results in the differential equation of variable coefficients (18).

$$\rho\, A\, \ddot{\xi}_i(t) + \frac{2m}{l}\sum_{j=1}^{\infty}\ddot{\xi}_j(t)\sin\frac{i\pi vt}{l}\sin\frac{j\pi vt}{l} + \frac{4m}{l}\sum_{j=1}^{\infty}\frac{j\pi v}{l}\dot{\xi}_j(t)\sin\frac{i\pi vt}{l}\cos\frac{j\pi vt}{l} +$$

$$+ \ N\frac{i^2\pi^2}{l^2}\xi_i(t) + EI\frac{i^4\pi^4}{l^4}\xi_i(t) - \frac{2m}{l}\sum_{j=1}^{\infty}\frac{j^2\pi^2 v^2}{l^2}\xi_j(t)\sin\frac{i\pi vt}{l}\sin\frac{j\pi vt}{l} =$$

$$= \ \frac{2P}{l}\sin\frac{i\pi vt}{l} \quad . \tag{18}$$

The equation (18) can not be easily solved and we must integrate it in a numerical way. We use the matrix notation here

$$\mathbf{M}\begin{bmatrix}\ddot{\xi}_1(t)\\\ddot{\xi}_2(t)\\\vdots\\\ddot{\xi}_n(t)\end{bmatrix} + \mathbf{C}\begin{bmatrix}\dot{\xi}_1(t)\\\dot{\xi}_2(t)\\\vdots\\\dot{\xi}_n(t)\end{bmatrix} + \mathbf{K}\begin{bmatrix}\xi_1(t)\\\xi_2(t)\\\vdots\\\xi_n(t)\end{bmatrix} = \mathbf{P} \tag{19}$$

which results in a short form $\mathbf{M}\ddot{\boldsymbol{\xi}} + \mathbf{C}\dot{\boldsymbol{\xi}} + \mathbf{K}\boldsymbol{\xi} = \mathbf{P}$, where $\mathbf{M}$, $\mathbf{C}$ and $\mathbf{K}$ are square matrices for $i = j = 1, 2, ..., n$.

When we calculate the value of general coordinates $\xi_i(t)$ for each i to n. Finally we can compute displacements of the string-beam $u(x, t)$

$$u(x, t) = \sum_{i=1}^{\infty}\xi_i(t)\sin\frac{i\pi x}{l} \tag{20}$$

Displacements given in the example below are dimensionless. They were calculated in relation to the static deflection u_0 of the string-beam loaded in the midpoint by the point force P: $u_0 = u_{0s}\, u_{0b}/(u_{0s}\, u_{0b})$. u_{0s} and u_{0b} are static deflections in the case of a string and a beam, respectively.

Example Let us assume the following data: $E = 1$, $I = 0.01$, $N = 1$, $\rho = 1$, $A = 1$, $P = -1$ and $m = 1$. We solve the problem for different speeds v of the moving load. The mass trajectory is depicted in Fig. 2. The simulation of the string-beam motion is depicted in Fig. 3.

2.   Conclusions

In the paper the Bernoulli-Euler beam with additional tensile effect under moving inertial load was presented. The proposed semi-analytical approach can be applied
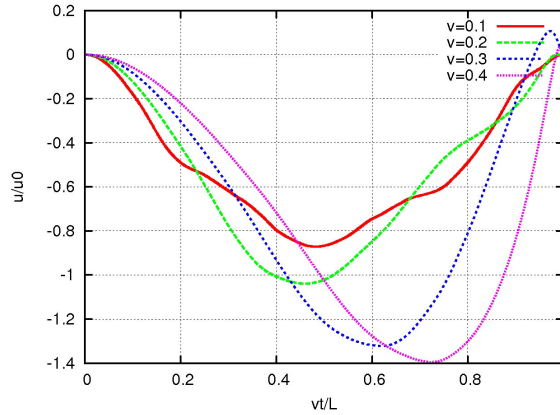
Figure 2: Mass trajectory for different speeds v.

in a hole range of the speed and for all points of the string-beam span. The accuracy of the solution (20) depends on the number of terms in the infinite series. The examined series of displacements is convergent, so it allows us to assume a limited number of terms in our example to $i = 130$.

If we reduce the flexural stiffness of the system, we observe the discontinuity near the end support. It was broadly presented and proved in [11]. The discontinuity had appeared also in the case of the Timoshenko beam [12]. In the matrix form (19) we can use classical numeric methods for the integration of the final differential motion equation, for example Newmark method.

References

1. C.E. Inglis. *A Mathematical Treatise on Vibrations in Railway Bridges*. Cambridge University Press, 1934.
2. A. Schallenkamp. Schwingungen von Trägern bei bewegten Lasten. *Arch. of Appl. Mech. (Ingenieur Archiv)*, 8(3):182–198, June 1937.
3. Renaudot. Etude de l'influence des charges en mouvement sur la resistance, des ponts metallique a poutres droites. *Annales des Ponts et Chausses*, 1:145, 1861.
4. C.E. Smith. Motion of a stretched string carrying a moving mass particle. *J. Appl. Mech.*, 31(1):29–37, 1964.
5. J. Panovko. Historical outline of the theory of dynamic influence of moving load (in Russian). *Engineering Academy of Air Forces*, 17:8–38, 1948.
6. N.Z. Jakushev. Certain problems of dynamics of the beam under moving load (in Russian). *Publisher of the Kazan Univ.*, 12:199–220, 1974.
7. A.S. Dmitrijev. The analysis of solutions of problems with lateral oscillatory vibrations of various beam structures under the motion of non spring point load (in Russian). *Machine Dynamics Problems*, 24:18–28, 1985.
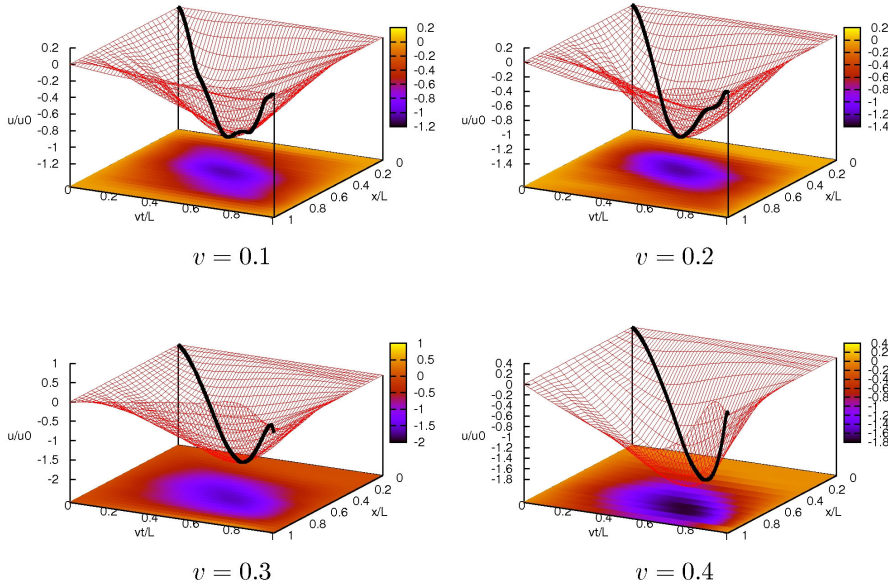
Figure 3: Simulation of the string-beam motion under the mass moving at v=0.1, 0.2, 0.3 and 0.4.

8. W. Szcześniak. Inercyjne obciążenia ruchome na belkach. Prace Naukowe, Politechnika Warszawska, budownictwo 112, 1990.

9. S. Sadiku and H.H.E. Leipholz. On the dynamics of elastic systems with moving concentrated masses. *Ing. Archiv*, 57:223–242, 1987.

10. E.C. Ting, J. Genin, and J.H. Ginsberg. A general algorithm for moving mass problems. *J. Sound Vib.*, 33(1):49–58, 1974.

11. B. Dyniewicz and C.I. Bajer. Paradox of the particle's trajectory moving on a string. *Arch. Appl. Mech.*, 2008. in print.

12. B. Dyniewicz and C.I. Bajer. Discontinuous trajectory of the mass particle moving on a string or a beam. *Machine Dyn. Probl.*, 31(3), 2007.

13. F.V. Filho. Finite element analysis of structures under moving loads. *The Shock and Vibration Digest*, 10(8):27–35, 1978.

14. J.R. Rieker, Y.-H. Lin, and M.W. Trethewey. Discretization considerations in moving load finite element beam models. *Finite Elements in Analysis and Design*, 21:129–144, 1996.

15. C.I. Bajer and B. Dyniewicz. Space-time approach to numerical analysis of a string with a moving mass. *Int. J. Numer. Meth. Engng.*, 2008. in print.

DISCRETE MODEL OF A ROPE WITH SCLERONOMIC AND RHEONOMIC CONSTRAINTS

Paweł FRITZKOWSKI[1], Henryk KAMIŃSKI[2]
[1] Field of study: Computational Mechanics of Structures
[2] Institute of Applied Mechanics
Poznań University of Technology
Phone number, e-mail

Abstract

A preliminary discrete model of a rope with scleronomic and rheonomic constraints is considered. Numerical experiments are performed and advantages of the applied algorithm are discussed in terms of total energy of the system. In case of the non-conservative model the work-energy relation is used to assess the computation efficiency. The next directions of the model development are outlined.

Keywords: multibody dynamics; discrete model; differential-algebraic equations.

Introduction

Analysis of the rope dynamics may serve as an introduction to research on various physical phenomena. One of such examples is a cracking whip, whose amazing dynamics has been drawing attention of scientists for over a hundred years. In the twentieth century different laboratory experiments were performed, giving a significant insight into the phenomenon. On the other hand, theoretical works were based mostly on kinematic models and certain conservation principles.

However, nowadays such a problem may be studied not only experimentally and theoretically but also numerically. Works focus on behaviour of some class of similar bodies such as chains, ropes and whips. For example, Pierański and Tomaszewski [3] analyze dynamics of a falling chain on the basis of laboratory and numerical experiments. Goriely and McMillen [2] consider a dynamical model for propagation of waves in the motion of whips and obtain numerical solutions too.

We concentrate on a simple preliminary model, which actually is a rigid, chain-like one – closer to a rope than a whip. Applying the Lagrange's formulation, we present the equations of motion for the system with scleronomic as well as rheonomic constraints. Approximate solutions to the initial value problems are obtained with the use of computational methods. In some numerical experiments the results and the simulated behaviour of the body are analyzed mostly in respect of time dependence of the total energy.

1. Mechanical system and equations of motion

As a discrete model we use the one described by Pierański and Tomaszewski in [3], which actually is a multiple physical pendulum. Thus, the system consists of n elements – rigid, cylindrical rods – connected by ideal joints (without friction). Each segment has

a length l and mass m. Classically, the motion is restricted to take place in a vertical plane only.

One end of the body is attached to a point denoted by its Cartesian coordinates (x_0, y_0), whereas the other one moves freely. It is important that we focus on the mechanical system moving in a gravitational field, with no external forces acting on it. Consequently, the excitation studied here has purely a kinetic character.

However, let us consider a model with scleronomic constraints at first, that means the one suspended to a fixed point. The state of the system may be simply specified with the use of the angular generalized coordinates – position of ith element is described by a variable φ_i which defines the angle from Y downward axis. The position of each segment (its mass centre) in the Cartesian coordinate system may be written as follows:

$$x_i = \sum_{j=1}^{i-1} l \sin\varphi_j + \frac{1}{2} l \sin\varphi_i \,, \qquad y_i = \sum_{j=1}^{i-1} l \cos\varphi_j + \frac{1}{2} l \cos\varphi_i \qquad (1.1)$$

Having calculated terms for the velocities of the ith segment in the X and Y directions, one may obtain formulas expressing the kinetic and the potential energy of the system:

$$T = ml^2 \sum_{i=1}^{n} \frac{3(n-1)+1}{6} \dot{\varphi}_i{}^2 + ml^2 \sum_{i=1}^{n} \sum_{j=i+1}^{n} \frac{2(n-j)+1}{2} \dot{\varphi}_i \dot{\varphi}_j \cos(\varphi_i - \varphi_j) \qquad (1.2)$$

$$V = -mg \sum_{i=1}^{n} y_i = -mgl \sum_{i=1}^{n} \frac{2(n-i)+1}{2} \cos\varphi_i \qquad (1.3)$$

Using the terms above for the Lagrangian $L=T-V$ we can apply the Euler-Lagrange equations to describe behaviour of the system:

$$\frac{d}{dt}\left(\frac{\partial L}{\partial \dot{\varphi}_i}\right) - \frac{\partial L}{\partial \varphi_i} = 0, \qquad i = 1, 2, \ldots, n \qquad (1.4)$$

After substitutions and simplifications we obtain the equations in the final form:

$$\sum_{j=1}^{n} a_{ij} \ddot{\varphi}_j \cos(\varphi_i - \varphi_j) + \sum_{j=1}^{n} a_{ij} \dot{\varphi}_j{}^2 \sin(\varphi_i - \varphi_j) + b_i \frac{g}{l} \sin\varphi_i = 0, \qquad i = 1, 2, \ldots, n \quad (1.5)$$

where:

$$a_{ij} = \begin{cases} \dfrac{2(n-i)+1}{2} & \text{for } j < i \\[2mm] \dfrac{3(n-i)+1}{3} & \text{for } j = i \\[2mm] \dfrac{2(n-j)+1}{2} & \text{for } j > i \end{cases} \qquad b_i = \frac{2(n-i)+1}{2} \qquad (1.6)$$

Let us turn now to the case involving rheonomic constraints. We assume that one end of the rope is attached to a moving point, whose position expressed in the Cartesian coordinates depends explicitly on time:

$$x_0 = x_0(t), \qquad y_0 = y_0(t) \tag{1.7}$$

Obviously, the dependencies affect the transformation equations (1.1):

$$x_i = x_0 + \sum_{j=1}^{i-1} l \sin \varphi_j + \frac{1}{2} l \sin \varphi_i , \qquad y_i = y_0 + \sum_{j=1}^{i-1} l \cos \varphi_j + \frac{1}{2} l \cos \varphi_i \tag{1.8}$$

Hence, the terms for the kinetic and the potential energy of the system have more complex form and involve the time explicitly, too. Still using the Lagrange's formulation (1.4), we find the following equations of motion for $i = 1, 2, \ldots, n$:

$$\sum_{j=1}^{n} a_{ij} \ddot{\varphi}_j \cos(\varphi_i - \varphi_j) + \sum_{j=1}^{n} a_{ij} \dot{\varphi}_j^2 \sin(\varphi_i - \varphi_j) +$$

$$+ b_i \frac{1}{l}(g \sin \varphi_i + \ddot{x}_0 \cos \varphi_i - \ddot{y}_0 \sin \varphi_i) = 0 \tag{1.9}$$

where the coefficients a and b are defined in (1.6).

2. Numerical experiments

To solve the systems of differential equations (1.5) and (1.9) approximately, we have applied the MEBDFV code developed by Abdulla and Cash (Imperial College, London). They implemented Modified Extended Backward Differentiation Formulas (MEBDF) of Cash. The algorithm is designed to solve stiff Initial Value Problems for systems of linearly implicit Differential Algebraic Equations (DAEs) of the form:

$$\boldsymbol{M(q)\dot{q} = f(t,q)} \tag{2.1}$$

where the matrix $\boldsymbol{M}$ depends on $\boldsymbol{q}$, which is a vector of dependent variables, and t is the independent variable.

As typical for computational methods, the system of dynamic equations should be reformulated into a system of first-order differential equations. Therefore, the problem consists of $2n$ differential equations and $2n$ initial conditions written in a general form as follows:

$$\begin{cases} \dot{\varphi}_1 = \omega_1 \\ \quad \ldots \\ \dot{\varphi}_n = \omega_n \\ \sum_{j=1}^{n} \left[m_{1j}(t, \varphi_1, \varphi_2, \ldots, \varphi_n) \dot{\omega}_j \right] = f_1(t, \varphi_1, \varphi_2, \ldots, \varphi_n, \omega_1, \omega_2, \ldots, \omega_n) \\ \quad \ldots \\ \sum_{j=1}^{n} \left[m_{nj}(t, \varphi_1, \varphi_2, \ldots, \varphi_n) \dot{\omega}_j \right] = f_n(t, \varphi_1, \varphi_2, \ldots, \varphi_n, \omega_1, \omega_2, \ldots, \omega_n) \end{cases} \tag{2.2}$$

$$\varphi_i(t_0) = \varphi_{i0} , \qquad \omega_i(t_0) = \omega_{i0} \qquad \text{for} \quad i = 1, 2, \ldots, n$$

Firstly, let us concentrate on the scleronomic system. We confronted results obtained in our numerical simulations with the ones described in [3] and based on the RADAU5 code developed by Hairer and Wanner. As it was supposed, for the same parameters (n, l, m) and initial conditions there was no difference between the compared configurations of the model in certain moments of time. The time dependencies of the linear velocity of the tip were compatible too. What is more, the authors of the paper [3] confirmed their numerical results by laboratory experiments.

However, the choice of the solver seems to be justified by the energy principle. For instance, using the RADAU5 without any significant modifications would be inefficient when researching long-lasting motion of such a complex mechanical system. After a short period of "good performance" a problem arises with energy conserving by the chain. On the other hand, the MEBDFV code gives results which meet the energy conservation law.

To show the difference, we performed a numerical experiment using both the codes, starting from the same initial conditions: catenary curve, $\dot{\varphi}_i = 0$ (for $i = 1, 2, \ldots, n$), and the same parameters: $n=20$, $nm=0.5$kg, $nl=1$m. The time dependencies of the total energy of the system are presented in Fig. 1.
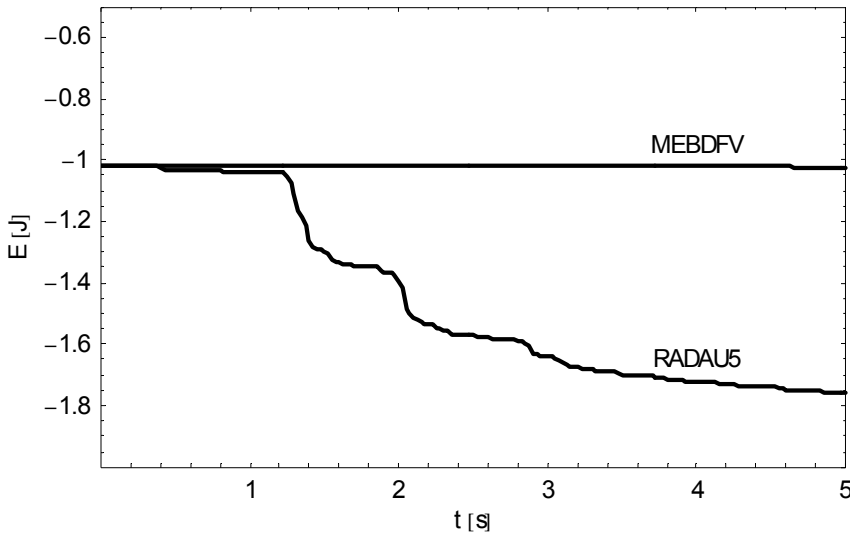
Fig. 1: The total energy based on results from the RADAU5 code and the MEBDFV.

As visible above, the energy calculated from the results given by the MEBDFV may serve as a reference level. When it comes to the other solver, there is a rapid decrease in the energy around $t=1.3$s and the difference between the dependencies increases with time. Obviously, the numerical dissipation impacts on configurations of the chain.

It is necessary to remark that no procedure designed for testing fulfillment of the conservation principle is embedded in the solvers. Both the codes perform the integration process using some internal, numerical convergence tests, which do not refer to mechanics. The user gives the physical sense to the solution and involves it in computation of such quantities as the total energy.

Now we will analyze the dynamics of the rheonomic system. We will consider here a free-hanging chain at a start point, so that $\varphi_i = 0$ and $\dot{\varphi}_i = 0$ for $i = 1, 2, \ldots, n$. The simulation is performed for a model of total length nl=1m and total mass nm=0.5kg, where n=30. Moreover, we focus only on the function $x_0(t)$ referring to the horizontal direction – the body will be brought into motion with the use of the following constraint function:

$$x_0(t) = \begin{cases} A \sin^2(\pi B t) & \text{for} \quad t \leq \dfrac{1}{B} \\ 0 & \text{for} \quad t > \dfrac{1}{B} \end{cases} \qquad (2.3)$$

where A and B are some constants. Here we take:

$$A = 0.1\,[\text{m}], \qquad B = 5\,[1/\text{s}]$$

In this case the evolution of the rope's shape seems to be very interesting. The applied excitation leads to arising a kind of wave-like effects. Visually, a fold created from the upper segments is traveling along the rope. The propagation disappears gradually with the successive direction changes. Actually, such a specific behaviour turns out to be a result of energy transfer between the elements of the discrete model. The fold's flow along the body involves consecutive segments providing additional energy to them. As it may be supposed, the greatest increase of the function occurs at the last element and causes sharp peaks in time dependencies of velocity and acceleration of the tip.

At the end, we will pay attention to the total energy of the whole mechanical system. It should be noted that due to the rheonomic constraints the system is a non-conservative one. In fact, the energy increases initially and then remains constant at the level forced by the applied constraints. All in all, the conservation principle cannot be a test for the approximate solution to the problem.

However, we decided to apply the work-energy principle for a rigid body. Thus, the analysis consists in comparing changes in the kinetic energy of the system over time with the work done by all forces during the same actual displacements. To define "all forces" we take into account the components of the equations (1.9), which come strictly from the gravity and the rheonomic constraints. After consideration appropriate units one may obtain the expressions equivalent to generalized forces – the potential and non-potential ones:

$$Q_i = -b_i m l \left(g \, \sin \varphi_i + \ddot{x}_0 \cos \varphi_i - \ddot{y}_0 \sin \varphi_i \right), \qquad i = 1, 2, \ldots, n \qquad (2.4)$$

Alternatively, the work-energy relation is formulated in [4] as the principle of action and counteraction. The first one is defined as the action of (active) forces, whereas the latter

one refers to the kinetic energy of the system and is named the action of the inertia force. Fig. 2 shows the comparison of these two quantities based on numerical integration.
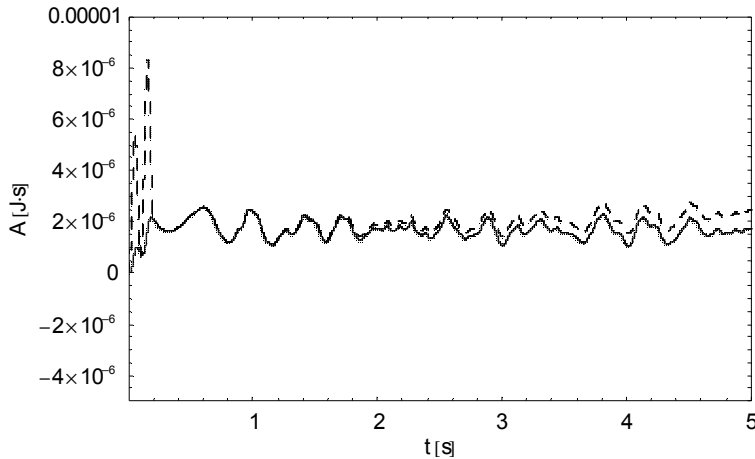
Fig. 2: Time dependence of the action of the active forces (dashed) and the action of the inertia force (solid).

3. Conclusions

Although we have focused on the simple discrete model of the rope, the multibody approach produces an expanded system of second order differential equations, which actually need to be solved numerically. The choice of the solver is justified by the energy principle. The code of Abdulla and Cash manages to give reliable approximate solutions to the Lagrange-Euler equations for the conservative as well as the rheonomic system.

The results inspire to develop the model by including such aspects as elasticity, damping and air-resistance. All in all, the problem provides many possibilities of dynamics analysis, so we feel that the potential directions of development are worth efforts and will be realized successively.

References

1. J.R. Cash, S. Considine, *An MEBDF Code for Stiff Initial Value Problems*, ACM Transactions on Mathematical Software, 18 (1992) 142-155
2. A. Goriely, T. McMillen, *Shape of a cracking whip*, Physical Review Letters, 88 (2002) 244301
3. W. Tomaszewski, P. Pierański, *Dynamics of ropes and chains: I. the fall of the folded chain*, New Journal of Physics, 7 (2005) 45
4. V.A. Vujičić, *The action of force and counteraction principle*, Facta Universitatis, Series: Mechanics, Automatic Control and Robotics, 5 (2006) 59-70

DISCRETE MODEL OF A ROPE WITH MEMBERS
OF A CHANGEABLE LENGTH

Paweł FRITZKOWSKI[1], Henryk KAMIŃSKI[2]

[1] Field of study: Computational Mechanics of Structures
[2] Institute of Applied Mechanics
Poznań University of Technology
Phone number, e-mail

Abstract

A discrete model of a rope with elements of a changeable length is considered. Scleronomic and rheonomic constraints are given to the system. Dynamic equations of motion are formulated and their complexity is presented from the computational point of view. Numerical experiments are performed and the obtained results are discussed in terms of the total energy of the system.

Keywords: multibody dynamics; discrete model; differential-algebraic equations.

Introduction

Dynamics of a rope as a classical problem of mechanics can be significant in research on motion of other real objects. Actually, various works focus on behaviour of some class of similar bodies such as chains, ropes, fly lines and whips. The last one is extremely interesting because of very fast motion of its tip. Laboratory experiments are connected with different difficulties and the complexity of the problem makes the analytical approach also hard to perform.

However, nowadays implementation of numerical methods may produce approximate but satisfactory results, giving considerable insight into the phenomenon. Pierański and Tomaszewski in [5] consider dynamics of a falling chain and base on laboratory as well as numerical experiments. Goriely and McMillen [4] study – both theoretically and numerically – propagation and acceleration of waves in the motion of whips. Gatti and Perkins [3] present mathematical model of fly line and discuss numerical solutions too.

In the previous paper [2] we considered a simple discrete model of the rope with scleronomic and rheonomic constraints. Now the rigid, chain-like system is complemented with some flexibility aspects. We formulate its Lagrange's equations of motion and use computational methods to solve them. In several experiments the behaviour of the given body is simulated and analyzed in terms of the mechanical energy.

1. Mechanical system and equations of motion

Let us modify the model assumptions specified in [2]. The system consists of n elements, but now each segment includes a rigid, cylindrical rod and a spring at the end. More precisely, the ith spring plays a role of a lengthening part – belongs to the ith rod and retains its orientation. The elements as a whole are still linked by ideal joints (without friction), but it should be noted that the connection "bar-bar" is replaced with the "bar-

128

spring" type. Every rod has a length l and mass m. The springs are assumed to be linear and identical – their free length is denoted by l_s and the stiffness by k_s. Their mass is neglected.

The mechanical system is placed in a gravitational field. One end of the body is attached (by the first spring) to a point (x_0, y_0), whereas the other one moves freely. Classically, the motion is restricted to take place in a vertical plane only.

The applied approach means increasing the number of degrees of freedom. Consequently, apart from the angular generalized coordinates φ_i defining the angle between the ith segment and the Y downward axis, we introduce some additional set of variables z_i for $i = 1, 2, \ldots, n$ denoting the springs elongations.

To make our considerations more general, we focus on the rheonomic system at once. Thus, the position of the moving support expressed in the Cartesian coordinates depends explicitly on time:

$$x_0 = x_0(t), \qquad y_0 = y_0(t) \tag{1.1}$$

The position of each segment (its mass centre) in the Cartesian coordinate system may be written as follows:

$$x_i = x_0 + \sum_{j=1}^{i-1}(h_j + l)\sin\varphi_j + \left(h_i + \frac{1}{2}l\right)\sin\varphi_i$$

$$y_i = y_0 + \sum_{j=1}^{i-1}(h_j + l)\cos\varphi_j + \left(h_i + \frac{1}{2}l\right)\cos\varphi_i \tag{1.2}$$

where $h_i = l_s + z_i$ for $i = 1, 2, \ldots, n$. Having calculated terms for the velocities of the ith segment in the X and Y directions, one may obtain formulas expressing the kinetic and the potential energy of the system (T and V respectively).

We apply the Euler-Lagrange equations to describe behaviour of the system:

$$\frac{d}{dt}\left(\frac{\partial L}{\partial \dot{\varphi}_i}\right) - \frac{\partial L}{\partial \varphi_i} = 0, \qquad i = 1, 2, \ldots, n$$

$$\frac{d}{dt}\left(\frac{\partial L}{\partial \dot{z}_k}\right) - \frac{\partial L}{\partial z_k} = 0, \qquad k = 1, 2, \ldots, n \tag{1.3}$$

where $L = T - V$ is the Lagrangian. After substitutions and simplifications we obtain the equations in the final and possibly concise form:

- for $i = 1, 2, \ldots, n$

$$\ddot{\varphi}_i\left(b'_{ii}\frac{h_i^2}{l^2}+2b_{ii}\frac{h_i}{l}+a_{ii}\right)+\sum_{j=1}^{i-1}\left(a'_{ij}\frac{h_i}{l}+a_{ij}\right)\left(\frac{h_j}{l}+1\right)\ddot{\varphi}_j\cos(\varphi_i-\varphi_j)+$$

$$+\sum_{j=i+1}^{n}\left(a'_{ij}\frac{h_j}{l}+a_{ij}\right)\left(\frac{h_i}{l}+1\right)\ddot{\varphi}_j\cos(\varphi_i-\varphi_j)-\frac{1}{l}\sum_{j=1}^{i-1}\left(a'_{ij}\frac{h_i}{l}+a_{ij}\right)\ddot{z}_j\sin(\varphi_i-\varphi_j)+$$

$$-\frac{1}{l}\sum_{j=i+1}^{n}a'_{ij}\left(\frac{h_i}{l}+1\right)\ddot{z}_j\sin(\varphi_i-\varphi_j)+\sum_{j=1}^{i-1}\left(a'_{ij}\frac{h_i}{l}+a_{ij}\right)\left(\frac{h_j}{l}+1\right)\dot{\varphi}_j^2\sin(\varphi_i-\varphi_j)+$$

$$+\sum_{j=i+1}^{n}\left(a'_{ij}\frac{h_j}{l}+a_{ij}\right)\left(\frac{h_i}{l}+1\right)\dot{\varphi}_j^2\sin(\varphi_i-\varphi_j)+\frac{2}{l}\sum_{j=1}^{i}\left(b'_{ij}\frac{h_i}{l}+b_{ij}\right)\dot{\varphi}_j\dot{z}_j\cos(\varphi_i-\varphi_j)+$$

$$+\frac{2}{l}\sum_{j=i+1}^{n}b'_{ij}\left(\frac{h_i}{l}+1\right)\dot{\varphi}_j\dot{z}_j\cos(\varphi_i-\varphi_j)+\frac{1}{l}\left(b'_{ii}\frac{h_i}{l}+b_{ii}\right)(g\sin\varphi_i+\ddot{x}_0\cos\varphi_i-\ddot{y}_0\sin\varphi_i)=0$$

- for $k=1,2,\ldots,n$

$$\sum_{j=1}^{k-1}a'_{kj}\left(\frac{h_j}{l}+1\right)\ddot{\varphi}_j\sin(\varphi_k-\varphi_j)+\sum_{j=k+1}^{n}\left(a'_{kj}\frac{h_j}{l}+a_{kj}\right)\ddot{\varphi}_j\sin(\varphi_k-\varphi_j)+$$

$$+\sum_{j=1}^{n}b'_{kj}\ddot{z}_j\cos(\varphi_k-\varphi_j)-\sum_{j=1}^{k-1}b'_{kj}\left(\frac{h_j}{l}+1\right)\dot{\varphi}_j^2\cos(\varphi_k-\varphi_j)+$$

$$-\sum_{j=k}^{n}\left(b'_{kj}\frac{h_j}{l}+b_{kj}\right)\dot{\varphi}_j^2\cos(\varphi_k-\varphi_j)+2\sum_{j=1}^{n}a'_{kj}\dot{\varphi}_j\dot{z}_j\sin(\varphi_k-\varphi_j)+$$

$$+\frac{1}{l}b'_{kk}\left(-g\cos\varphi_k+\ddot{x}_0\sin\varphi_k+\ddot{y}_0\cos\varphi_k\right)+\frac{1}{l}\frac{k_s}{m}z_k=0$$

where:

$$a_{ij}=\begin{cases}\dfrac{2(n-i)+1}{2} & \text{for } j<i \\[2mm] \dfrac{3(n-i)+1}{3} & \text{for } j=i \\[2mm] \dfrac{2(n-j)+1}{2} & \text{for } j>i\end{cases}\qquad b_{ij}=\begin{cases}\dfrac{2(n-i)+1}{2} & \text{for } j\le i \\[2mm] \dfrac{2(n-j)+1}{2} & \text{for } j>i\end{cases}\qquad(1.4)$$

$$a'_{ij}=a_{ij}+\frac{1}{2}\qquad\qquad\qquad b'_{ij}=b_{ij}+\frac{1}{2}$$

It should be emphasized that the summation convention is not applied in the presented equations of motion.

2. Numerical experiments

As mentioned in [2], in order to solve the system of differential equations approximately, we have applied the MEBDFV code developed by Abdulla and Cash [1]. It should be noted that from the numerical point of view broadening of the problem description gives in fact $4n$ first-order differential equations:

$$
\begin{cases}
\dot{\varphi}_1 = \omega_1 \\
\quad \dots \\
\dot{\varphi}_n = \omega_n \\
\dot{z}_1 = u_1 \\
\quad \dots \\
\dot{z}_n = u_n \\
\sum_{j=1}^{n} m_{1,j}\, \dot{\omega}_j + \sum_{j=n+1}^{2n} m_{1,j} \dot{u}_j = f_1\big(t, \varphi_1, \dots, \varphi_n, z_1, \dots, z_n, \omega_1, \dots, \omega_n, u_1, \dots, u_n\big) \\
\quad \dots \\
\sum_{j=1}^{n} m_{2n,j}\, \dot{\omega}_j + \sum_{j=n+1}^{2n} m_{2n,j} \dot{u}_j = f_{2n}\big(t, \varphi_1, \dots, \varphi_n, z_1, \dots, z_n, \omega_1, \dots, \omega_n, u_1, \dots, u_n\big)
\end{cases}
\tag{2.1}
$$

where $m_{i,j}$ are non-constant coefficients which depend explicitly on the generalized coordinates:

$$
m_{i,j} = m_{i,j}\big(t, \varphi_1, \dots, \varphi_n, z_1, \dots, z_n\big)
\tag{2.2}
$$

Obviously, we have also $4n$ initial conditions:

$$
\varphi_i(t_0) = \varphi_{i0}, \quad \omega_i(t_0) = \omega_{i0}, \quad z_i(t_0) = z_{i0}, \quad u_i(t_0) = u_{i0} \qquad \text{for} \quad i = 1, 2, \dots, n
\tag{2.3}
$$

In the considered numerical experiments we will focus on the examination of the results provided by the solver in terms of the total energy of the mechanical system. It is essential because the code performs the integration process using some internal, numerical convergence tests, which do not refer to mechanics. Thus, giving the physical sense to the solution and involving it in computation of the kinetic and potential energy seems to be an independent and objective test.

Firstly, let us consider the scleronomic system. For instance, we will show the time dependence of the energy for a model consisted of $n=20$ segments with the following parameters: $nm=0.5$kg, $nl=1$m. We have also taken $l_s/l=1/3$ and $k_s=10^4$ N/m. The initial configuration of the rope is specified by catenary curve, where the position of the tip is: $x=0.2$m, $y=-0.5$m. The rest of the initial conditions:

$$
\dot{\varphi}_i(0) = 0, \quad z_i(0) = 0, \quad \dot{z}_i(0) = 0 \qquad \text{for} \quad i = 1, 2, \dots, n
$$

In Fig.1 we present the potential, kinetic and total energy of the rope. As visible, it may be said that these quantities are well-behaved during the simulation. However, the initial conditions do not make the integration easy. The fall of the rope from a relatively high

level causes that the motion of such a discrete system starts to be chaotic very quickly. It is noticeable in the graph – the dependencies $T(t)$ and $V(t)$ look smoothly just up to t=1s.
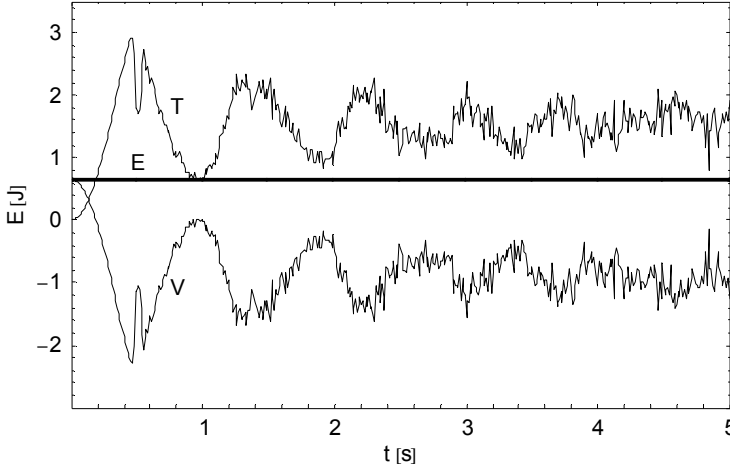
Fig. 1: Kinetic energy (T), potential energy (V) and total energy (E) of the scleronomic system

Now we will deal with the rheonomic system. We will consider here a free-hanging rope, that means $\varphi_i(0) = 0$ for $i = 1, 2, \ldots, n$. The parameters of the model are the same as before. Additionally, zero generalized velocities are assumed at t=0 and also $z_i(0) = 0$ for $i = 1, 2, \ldots, n$. The body will be brought into motion with the use of the following constraint function:

$$x_0(t) = \begin{cases} A \sin^2(\pi B t) & \text{for} \quad t \le \dfrac{1}{B} \\ 0 & \text{for} \quad t > \dfrac{1}{B} \end{cases} \qquad (2.3)$$

where:

$$A = 0.1\,[\text{m}], \qquad B = 5\,[1/\text{s}]$$

To assess the obtained results one may apply the work-energy principle for a rigid body formulated. Thus, the changes in the kinetic energy of the system over time may be compared with the work done by all forces during the same actual displacements. Here we present a graph of the total energy (Fig. 3), which coincides with the intuitive approach. The total energy of the system rises as long as the rheonomic constraints "act". Afterwards the energy remains constant at the level forced by the constraint function.
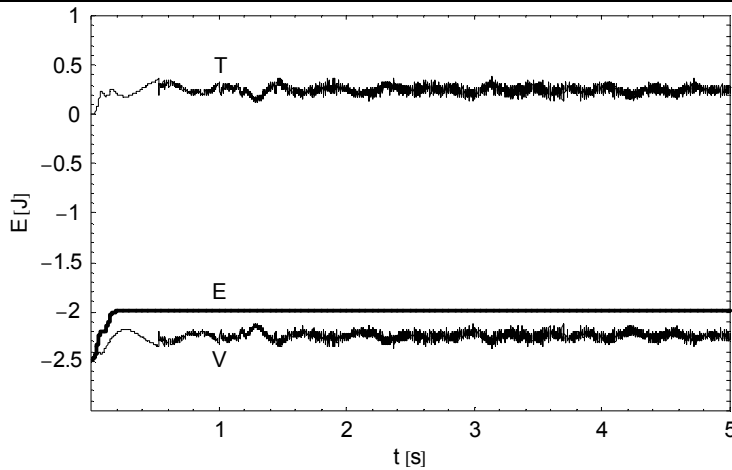
Fig. 2: Kinetic energy (T), potential energy (V) and total energy (E) of the rheonomic system

3. Conclusions

We have focused on the discrete model of the rope with elements of a changeable length. From the numerical point of view the approach produces an expanded system of differential equations. The performance of the algorithm has been tested on the basis of the energy principles, which indicates that the code MEBDFV gives reliable approximate solutions to the Lagrange-Euler equations for the scleronomic as well as the rheonomic system. Thus, the results provide many possibilities of dynamics analysis and we feel that lots of aspects merit further attention.

References

1. J.R. Cash, S. Considine, *An MEBDF Code for Stiff Initial Value Problems*, ACM Transactions on Mathematical Software, 18 (1992) 142-155
2. P. Fritzkowski, H. Kamiński, *Discrete model of a rope with scleronomic and rheonomic constraints* (in print)
3. C. Gatti, N.C. Perkins, *Numerical analysis of flycasting mechanics*, Bioengineering Conference ASME (2001)
4. A. Goriely, T. McMillen, *Shape of a cracking whip*, Physical Review Letters, 88 (2002) 244301
5. W. Tomaszewski, P. Pierański, *Dynamics of ropes and chains: I. the fall of the folded chain*, New Journal of Physics, 7 (2005) 45

APPLICATION OF THE 2D-STATIX ENVIRONMENT TO SOLVE BASIC STATICS PROBLEMS

Paweł FRITZKOWSKI
Institute of Applied Mechanics
Poznan University of Technology
Computational Mechanics of Structures
Piotrowo 3, 60-965 Poznan
061 665 21 77, pawel.fritzkowski@gnail.com

Tomasz WALCZAK
Institute of Applied Mechanics
Poznan University of Technology
Piotrowo 3, 60-965 Poznan
061 665 21 77, tomasz.walczak@put.poznan.pl

Abstract
The paper presents the 2D-Statix environment which was developed for upgrading teaching of statics. The program is designed to solve any statically determinate problem. There is a possibility to deal with a system with different constraints such as simple support and roller support, pin joint and some elements like beams, curved beams, rods and polygonal rigid bodies. Various loads may be applied – concentrated as well as distributed. As a result the program provides values of constraints reactions and information about compression or tension of some elements. The program presented by the authors is unique because there is no similar widely available application. In the paper some classical problems of statics are solved to visualize capabilities of the 2D-Statix.

Introduction

The main aim of the authors was to create a simple application that is useful in didactic process. A lot of statics problems may be solved by some popular programs like WorkingModel 2D or SolidWorks. However, the costs of their simple versions are huge and in fact they are not appropriate to deal with such problems. The presented program is able to determine the solution to every 2D static problem if the considered system is statically determinate. Otherwise, a message is generated to inform that the system is statically indeterminate or improperly constrained.

For planar single rigid body there are possible two cases of loading. In first case several forces act on particle. Then we can write two equilibrium conditions. In second case the considered rigid body is loaded by any system of forces and then we can write three equilibrium equations. In both cases conditions usually leads to linear system of equations with respectively two and three unknown reactions. For system of several connected rigid bodies we can apply equilibrium conditions according to any rigid body and then we can obtain the system of linear equations.

The aim of the paper is presentation of computer implementation of traditional system of equilibrium equations, which can determine reaction forces for single rigid body and for system of connected rigid bodies. In this implementation user define geometry, constrains and loading of considered system. Those data allow to make linear system of equations and to solve it.

The developed environment includes a graphical interface which allows to build any statical system in a very simple way. The whole environment was designed in Fortran 90 language with the use of Winteracter library [4,5].

1. Basic elements of 2D-Statix

To derive a solution to a given statics problem, it is necessary to define basic constraints, elements and loads. Pictures presented below are printed screens of the main 2D-Statix window.

Constraints which may be defined by a user:

- Simple support and roller support. Both can be placed at various angles.

- Fixed support. It can be placed at various angles.

- Pin joint. It may connect different types of elements.

Elements which may be defined by a user:

- Beams (straight and curved) and rigid bodies (polygons)
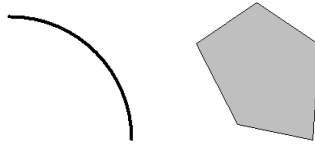
Loads which may be applied to the elements: concentrated forces, moments and distributed loads (defined as a linear, quadratic or cubic function).
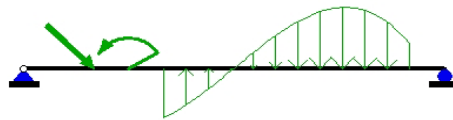
2. Test problems

Problem 1: Determine the forces in all of the members of the truss shown below [2]:
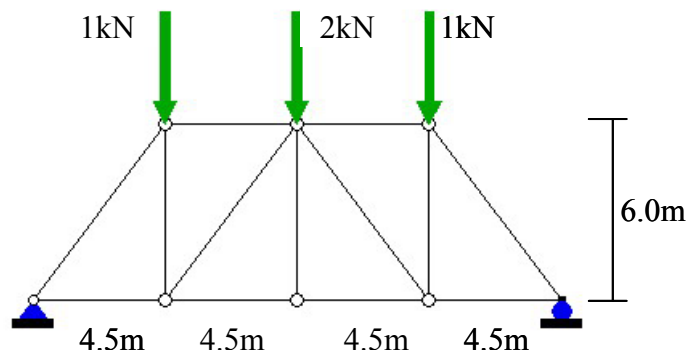
Fig. 1. Example of truss loaded by three forces - picture was made in 2D-Statix.

In classical approach the problem could be solved by solving the system of 2N equations, where N is number of pin joints. The 2D-Statix generates this system and determines all unknowns by solving it. Solution of the given problem is always presented on the screen with the picture of numbered truss members and drawn reaction forces in supports as in the fig. 2.
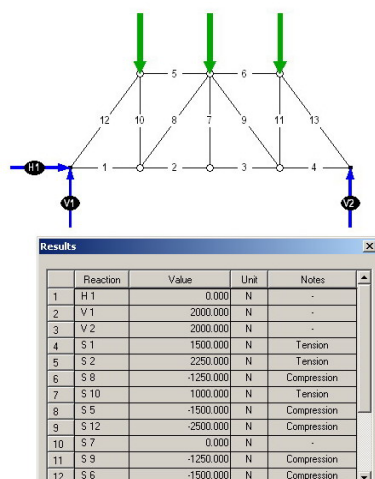
Fig. 2. Considered truss with numbered members and table of unknown reaction forces.

As it may be seen above, apart from the values of the forces in all the bars, 2D-Statix provides information about the character of the forces (tension or compression). The program also draws reaction forces (blue vectors in fig. 2).

Problem 2: Determine the reactions and the force in the bar taking into account mass of the two rigid polygonal bodies $m_1=m_2=1$kg [1].
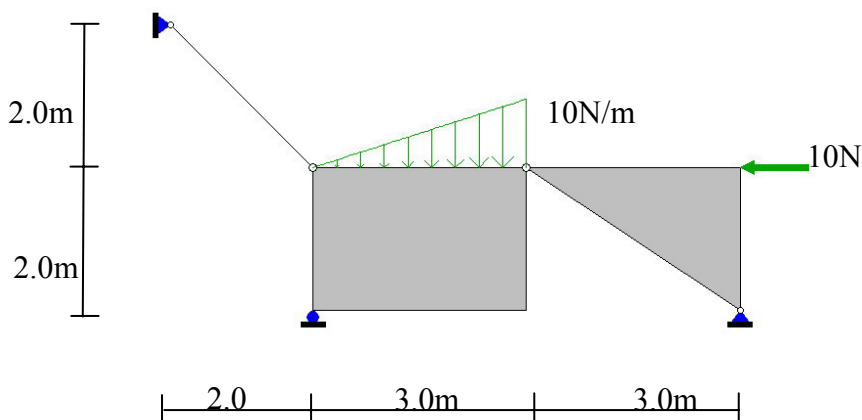
Fig. 3. Two connected polygonal rigid bodies. - picture was made in 2D-Statix.

Solution of problem 2 from fig. 3 is generated by the system in main window of the environment as table of unknown reaction forces and information about tension or compression of rods or beams in considered system of rigid bodies fig. 4.

	Reaction	Value	Unit	Notes
1	H 1	27.263	N	-
2	V 1	27.263	N	-
3	V 2	37.168	N	-
4	H 3	-27.263	N	-
5	V 3	24.715	N	-
6	S 1	-38.555	N	Compression
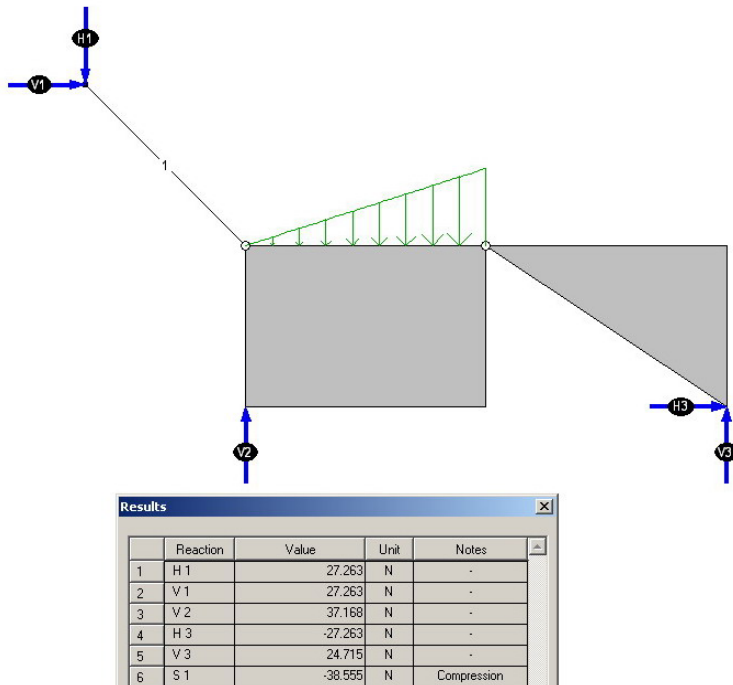
Fig. 4. Two connected polygonal rigid bodies. - picture was made in 2D-Statix.

The 2D-Statix does not draw the reaction forces vectors in pin joints. We can find them in the result table that is always visible under the main picture. There is no limit set for the program for number of connected rigid bodies and forces so it is possible to build really complicated systems and effectively determine all unknown reaction forces.

Problem 4: We consider improperly constrained polygonal rigid body presented in the fig. 5. The message generated by the program informs user about statical indeterminacy of considered system [3].
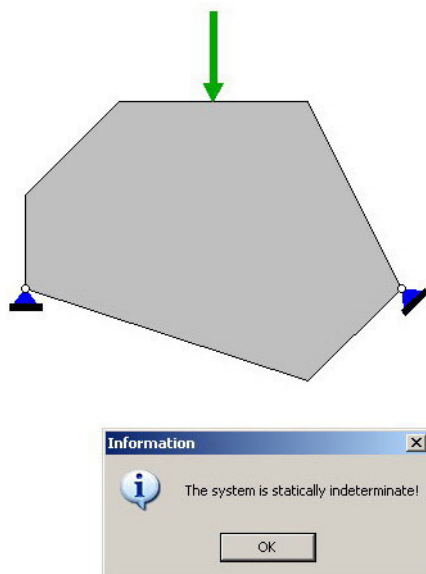
Fig. 5. Two connected polygonal rigid bodies. - picture was made in 2D-Statix.

2D-statix seems to be very useful environment and it could be perfect tool to teach statics in engineering fields of study. The application should be upgraded and there are plans to add to the program some elements of strength of materials in the future.

References

1. F.P. Beer, E.R. Johnston Jr., E.R Eisenberg, *Vector Mechanics for Engineers - Statics,* McGraw Hill, New York, 2007
2. D.J. McGill, W.W. King, *Engineering Mechanics: Statics and An Introduction to Dynamics,* PWS Publishers, Boston, 1985
3. J. Leyko, *Mechanika Ogólna – Statyka I Kinematyka,* PWN, Warszawa, 2004
4. J.D. Hoffman, *Numerical Methods for Engineers and Scientists,* Marcel Dekker, New York, 2001
5. D. Chrobak, *Fortran – Praktyka Programowania,* MIKOM, Warszawa, 2003

**ELIMINATION OF MECHANICAL VIBRATION WITH THE USE OF
RESONANCE-TYPE VIBRATION ELIMINATORS**

Zdzisław GOLEC, Maria GOLEC

Poznań University of Technology

Institute of Applied Mechanics

Vibroacoustics and Biodynamics Group

Piotrowo3, 60-965 Poznań

+48616652302, zdzislaw.golec@put.poznan.pl , maria.golec@put.poznan.pl

Abstract

The paper is devoted to analysis of effectiveness of vibration reduction with the use of resonance-type vibration eliminators, viz. the frictional and viscous-type ones. Their usefulness for vibration minimization in the extra-resonance range has been shown. The resonance-type eliminators, i.e. the frictional and viscous-type ones, are distinguished by similar ability to reduce vibration. Nevertheless, effectiveness of vibration elimination of these eliminators is lower as compared to the effect achieved by increasing the mass of the protected system.

Keywords: dynamics, vibration minimization, vibration eliminators

Introduction

The aim of elimination of mechanical vibration is very important from the point of view of durability and reliability of technological equipment. The most effective method of reduction of dynamical response of a mechanical object consists in elimination of its reasons, i.e. changing amplitudes or spectral composition of excitations. In case the use of such a method (often referred to as a direct method) becomes impossible the intermediate methods are used instead, that consist in interference into mechanical properties of the considered object. Three such methods may be mentioned here

- change of mass – elastic – dissipative parameters, with unchanged object structure;
- introduction of an additional mechanical system into the object, located at the disturbance path, i.e. vibroinsulation;
- introduction of an additional mechanical system – vibration elimination

The paper discusses the problem of vibration in case of a particular coupling between the protected system and the eliminator.

1. Physical and mathematical model of resonance type vibration eliminator

Ability of mechanical vibration minimization depends on the type of vibration eliminator. High effectiveness of vibration reduction is characteristic for dynamical and impact eliminators. The paper describes researching of vibration reduction effectiveness of one of resonance-type eliminators, in which the coupling with the protected object is of dissipative character. Hence, the forces acting in it depend on relative velocity of both sub-systems, i.e. the main, the vibration of which is to be minimized, and the eliminator itself. Two types of eliminators may be mentioned:

- a viscous-type one, in which the interactive force is proportional to odd powers of relative velocity of both bodies;
- a frictional one, in which the interactive force depends on relative velocity of both bodies and is referred to as a dry friction force.

The present paper describes analytical & numerical research of effectiveness of both eliminator types. The consideration is carried out with the assumption that a protected object may be modeled by a non-linear system of one degree of freedom (M, K*, C*) with force harmonic excitation F(t). The vibration eliminator is modeled as a material point of the mass m coupled with the mass M by a force depending on relative velocity of both bodies $S(\dot{x} - \dot{y})$. Physical model of such a system is shown in Fig. 1.
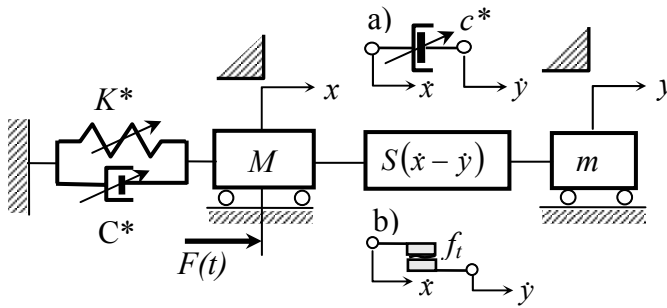
Fig. 1. Physical model of protected system with resonance-type vibration eliminator
a) viscous-type eliminator; b) frictional eliminator

Equation of motion of the mechanical system MK*C* provided with a resonance-type eliminator may be formulated in the form [2,5,6]:

$$M\ddot{x} + C^{*}\dot{x} + K^{*}x + S(\dot{x} - \dot{y}) = F_0 \, sin(\omega t),$$
$$m\ddot{y} - S(\dot{x} - \dot{y}) = 0 \tag{1}$$

where stiffness and damping coefficients of the protected system are assumed in the form: $K^{*} = K(1 + Bx^2)$, $C^{*} = C(1 + W\dot{x}^2)$.

In case of a viscous-type eliminator (a) the coupling force between the protected system and the eliminator is assumed in the form

$$S(\dot{x} - \dot{y}) = c(\dot{x} - y)\left[1 + w(\dot{x} - \dot{y})^2\right] \tag{2}$$

where c and w are constants that describe the nonlinear resisting force.

For a friction eliminator (b) the model of dry friction force is of the form
$S(v_w) = f_t Q(v_w)$, where f_t is a constant, $Q(v_w)$ is dimensionless shape function, and $v_w = \dot{x} - \dot{y}$ is relative velocity of both bodies. According to [1,3,4] the shape function should satisfy the following conditions:

- the function Q is continuous in the whole range of relative velocity v_w;

- $lim(Q) = 1, \ lim(Q) = -1$
  $v_w \to \infty \qquad v_w \to -\infty$

- $min(Q) = -f_s / f_k$, $max(Q) = f_s / f_k$, where f_s / f_k is the ratio of static to kinematic friction force.

In case of dimensionless relative velocity $v_{w1} = v_w \dfrac{2\pi}{g}, \sqrt{\dfrac{K}{M}}$ the shape function is proposed in the form

$$Q(v_{w1}) = \begin{cases} c_1 v_{w1} \ \text{for} \ -v_1 \geq v_{w1} > v_1 \\ c_1 v_{w1} - c_2 sign[v_{w1}]\{abs[v_{w1}] - v_1\}^n \ \text{for} \ -v_1 > v_{w1} \geq -v_2 \ \text{or} \ v_2 > v_{w1} \geq v_1 \\ sign(v_{w1})\left\langle 1 + \left(\dfrac{f_s}{f_k} - 1\right) \cdot exp\left\{-c_3[abs(v_{w1}) - v_2]^m\right\}\right\rangle \ \text{for} \ v_{w1} < -v_2 \ lub \ v_{w1} \geq v_2 \end{cases} \quad (3)$$

where

$$v_{w1} = \dfrac{dx_1}{d\tau} - \dfrac{dy_1}{d\tau}, \ \tau = \dfrac{t}{T_0}, \ x_1 = x\dfrac{K}{Mg}, \ y_1 = y\dfrac{K}{Mg}, \ n, m \geq 2 \text{ - even numbers}$$

Boundaries of subdomains of the function Q have been determined from the conditions:

$$c_1 v_1 = 1 \Rightarrow v_1 = \dfrac{1}{c_1},$$

$$Q(v_2) = \dfrac{f_s}{f_k}, \ \dfrac{dQ(v_{w1})}{dv_{w1}}\Big|_{v_{w1} = v_2} = 0 \Rightarrow v_2 = \dfrac{1}{c_1} \cdot \dfrac{n\dfrac{f_s}{f_k} - 1}{n - 1}, \ c_2 = \left(\dfrac{c_1}{n}\right)^n \cdot \dfrac{(n-1)^{(n-1)}}{\left(\dfrac{f_s}{f_k} - 1\right)^{(n-1)}} \quad (4)$$

Example patterns of the function $S(v_{w1})$ for the viscous-type eliminator and function $Q(v_{w1})$ for the frictional one are shown in Figure 2.
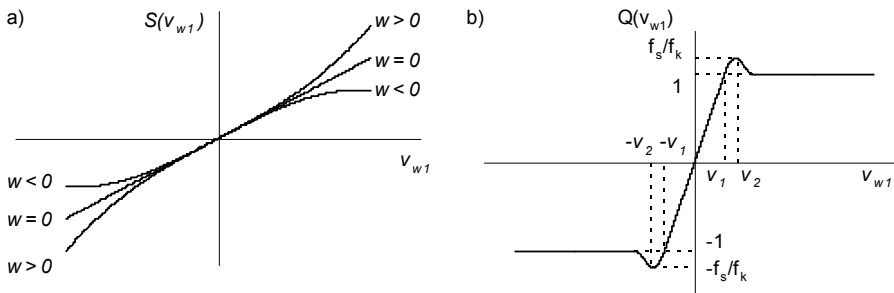
Fig. 2. Coupling forces between the protected system and vibration eliminator:
a) viscous friction; b) shape function of dry friction force

Behaviour of the systems has been researched based on dimensionless equations of motion obtained with the use of the equation (1) and the relationships (2) and (3):

$$\frac{d^2 x_1}{d\tau^2} + 4\pi\xi \frac{dx_1}{d\tau}\left[1 + \alpha_M\left(\frac{dx_1}{d\tau}\right)^2\right] + 4\pi^2\left(1 + \beta x_1^2\right) + S_1(v_{w1}) = 4\pi^2 F_{01}\sin(2\pi\delta\tau)$$

$$\frac{d^2 y_1}{d\tau^2} - \frac{1}{\mu}S_1(v_{w1}) = 0$$

(5)

where $S_1(v_{w1}) = \begin{cases} 4\pi\xi\gamma\left(\dfrac{dx_1}{d\tau} - \dfrac{dy_1}{d\tau}\right)\left[1 + \alpha_m\left(\dfrac{dx_1}{d\tau} - \dfrac{dy_1}{d\tau}\right)^2\right] & \text{for viscotic eliminator} \\[3mm] 4\pi^2 f_{t1} Q\left(\dfrac{dx_1}{d\tau} - \dfrac{dy_1}{d\tau}; n,m,c_1,c_3,\dfrac{f_s}{f_k}\right) & \text{for friction eliminator} \end{cases}$

while the dimensionless values describing dynamics of the main system and the vibration eliminator are given in the form:

$$\xi = \frac{C}{2\sqrt{KM}}, \ \alpha_M = W*\left(\frac{Mg}{KT_0}\right)^2, \ \beta = B\left(\frac{Mg}{K}\right)^2, \ F_{01} = \frac{F_0}{Mg}, \ \delta = \frac{\omega}{\omega_0}, \ \omega_0 = \sqrt{\frac{K}{M}} = \frac{2\pi}{T_0}$$

$$\gamma = \frac{c}{C}, \ \ \alpha_m = w\left(\frac{Mg}{KT_0}\right)^2, \ \mu = \frac{m}{M}, f_{t1} = \frac{f_t}{Mg}$$

The equations of motion (5) have been solved numerically, with the help of a simulation model developed with the use of the SIMULINK package in the MATLAB environment.

2. Investigation of effectiveness of vibration elimination

Effectiveness of elimination of mechanical vibration of a mechanical object MK*C* with a resonance-type eliminator has been assessed based on the value of the effectiveness function defined as the ratio of mean-square amplitudes of vibration displacements of the protected system without the eliminator to the one provided with such an eliminator

$$E = \frac{x_{1RMS}(\mu = 0)}{x_{1RMS}(\mu \neq 0)},$$

(6)

where $x_{1RMS} = \sqrt{\dfrac{1}{T}\displaystyle\int_{\tau_z}^{\tau_z+T} x_1^2(\tau)d\tau} \approx \sqrt{\dfrac{1}{n}\displaystyle\sum_{i=z}^{z+n} x_1^2(\tau_i)}, \ \ \tau_z = z\Delta\tau$ – dimensionless time to

stabilization of the system vibration, counted from the beginning of the simulation , $T = n\Delta\tau$ – dimensionless averaging time, $\Delta\tau$ - time step of the simulation.

Simulation of the system motion has been carried out with the following parameters:
- excitation
  - dimensionless part of the excitation $\delta = 0.95$ - 1.05 with the step $\Delta\delta = 0.01$ for the viscous-type eliminator and $\Delta\delta = 0.005$ for the frictional one;

- o dimensionless excitation amplitude $F_{01}=1$;
- the protected system
  - o damping degree $\xi=0.01$;
  - o coefficient of damping non-linearity $\alpha_M=0$;
  - o coefficient of stiffness non-linearity β
- eliminator
  - o dimensionless mass of the eliminator $\mu=0.1$
- coupling
  - o dimensionless damping coefficient $\gamma=0, 1, 2, 5, 10, \infty$ for a viscous-type eliminator;
  - o coefficient of damping non-linearity $\alpha_m=0$;
  - o dimensionless amplitude of dry friction force $f_{tl}=0.1–0.8$ with the step $\Delta f_{tl}=0.1$ and $f_{tl} = \infty$ for a frictional eliminator;
  - o parameters of the shape function $n = m = 2$, $c_1 = 100$, $c_3 = 1000$, $f_s/f_k = 1.2$.

In case the damping coefficient $\gamma=\infty$ (viscous-type eliminator) and the dry friction force $f_{tl}=\infty$ (frictional eliminator) no relative motion occurs between the two masses M and m. This is equivalent to change in the mass of the protected system. The assumption that the protected system is linear allows to write down the effectiveness of the changes in vibration amplitude E_m according to the relationship (6):

$$E_m = \sqrt{\frac{\left[1-(1+\mu)\delta^2\right]^2 + (2\xi\delta)^2}{(1-\delta^2)^2 + (2\xi\delta)^2}} \tag{7}$$

Effectiveness of vibration elimination of a protected object with the use of a linear viscous-type eliminator is shown in Fig. 3a, while for a frictional vibration eliminator – in Fig. 3b.
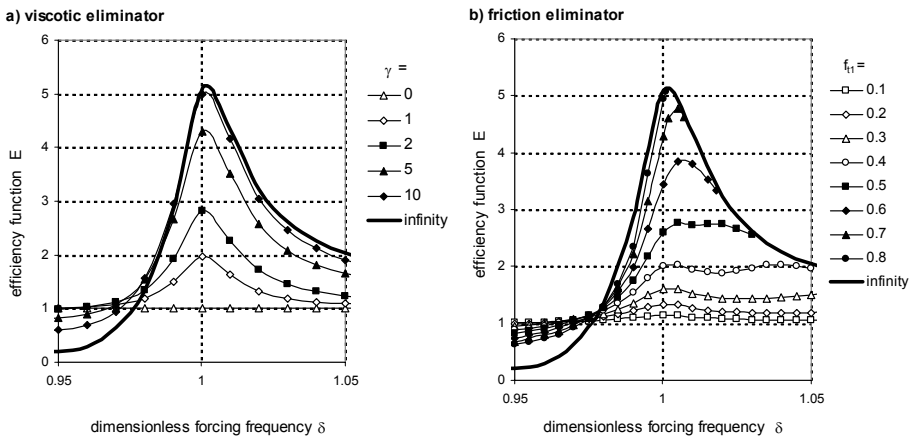
Fig. 3. Effectiveness of vibration elimination of a mechanical object with the use of:
a) viscous-type eliminator; b) frictional eliminator

3. Summary

The research of effectiveness of both types of the vibration eliminators allows to draw the following conclusions:

- The functions of effectiveness of vibration elimination are of equalized variability in the range of dimensionless excitation frequency.
- Value of the function of effectiveness of vibration elimination exceeds one (reduction of vibration amplitude of a protected system) for $\delta > \delta_g$ where δ_g for definite values of μ and ξ are specified below:

  for a viscous-type eliminator

γ	1	2	5	10
δ_g	0.932	0.953	0.967	0.971

  for a frictional eliminator

f_{t1}	0.1	0.2	0.3	0.4	0.5	0.6	0.7	0.8
δ_g	0.941	0.951	0.957	0.961	0.964	0.967	0.969	0.971

- in the range $\delta < \delta_g$ the function E meets the conditions $0 < E > E_m \leq 1$,
- in the range $\delta > \delta_g$ the function E meets the condition. $0 < E < E_m > 1$

The numerical research presented here gives evidence that the use of resonance-type eliminators enables several-fold reduction in vibration amplitude. Nevertheless, effectiveness of vibration elimination achieved this way is lower than in case of simple increase in the mass of the protected system.

References

1. Zbigniew Osiński, *Tłumienie drgań mechanicznych*, PWN, Warszawa 1986,
2. Zdzisław Golec, *Shot Dampers for Mechanical Vibrations Reduction*, The International Workshop on Machine Dynamics and Production Automation, 22 – 25 April, 1995, Szczecin, Poland, Wydawnictwo Uczelniane Politechniki Szczecińskiej, Szczecin 1995, pp. 139 – 151.
3. Karol Grudziński, Bogdan Jacek Warda, Marek Zapłata, *Simulated and Experimental Mass – Spring – Damping System Parameters on Self – Excited Vibrations Induced by Friction*, The International Workshop on Machine Dynamics and Production Automation, 22 – 25 April, 1995, Szczecin, Poland, Wydawnictwo Uczelniane Politechniki Szczecińskiej, Szczecin 1995, pp. 153 – 166.
4. Zbigniew Osiński [red], *Tłumienie drgań*, Wydawnictwo Naukowe PWN, Warszawa 1997.
5. Zdzisław Golec, *Modelling of Impact Vibration Eliminators by means of Matlab – Simulink* Packet, Virtual Design and Automation, Publishing House of Poznan University of Technology, Poznań 2005, pp. 367 – 374,
6. Zdzisław Golec, Maria Golec, *Eliminacja drgań mechanicznych z wykorzystaniem eliminatora ciernego; inny opis tarcia suchego*, Otwarte Seminarium Zakładu Wibroakustyki i Bio-dynamiki Systemów IMS PP, Poznań, 26.11.2007.

DYNAMICS OF COIN TOSSING – INFLUENCE OF AIR RESISTANCE Juliusz

GRABSKI, Jarosław STRZAŁKO, Tomasz KAPITANIAK
Technical University of Łódź
Machines Dynamics Division
Poland, 90-924 Łódź, ul. Stefanowskiego 1/15
phone: +48 42 631-24-22, e-mail: julgrabs@p.lodz.pl

Abstract

In following paper some aspects of tossed coin dynamics are presented. Firstly: one-, two-, and three-dimensional coin models are presented. More general case of nonsymmetric or nonhomogenous coin is described. It is assumed that the coin is released above a plain floor. Free fall of the coin as well as the coin motion including air resistance forces and moments are analysed. Some results of numerical solution simulations are shown.

Keywords: coin tossing, coin dynamics, air resistance, numerical simulation

Introduction

The study of flipped coins was begun by Keller [1]. He assumed that the coin spins about vertically moving horizontal axis (Fig. 1a). Similar problem – plane motion of the coin model – was presented in papers of Vulović, Prange [2] and Mizuguchi, Suwashita [3].
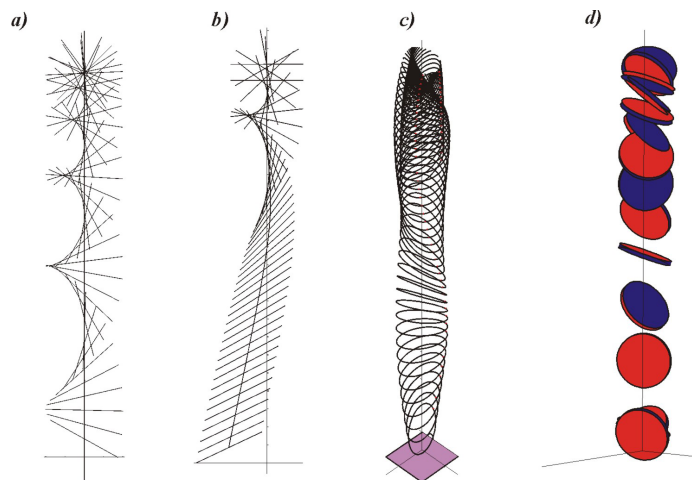
Figure 1. Basic coin models: *a*) one dimensional model (plane motion of thin disk), *b*) one dimensional model including air resistance, *c*) two dimensional model (spatial motion of thin disk), *d*) three dimensional model (spatial motion of thick cylinder) including air resistance

Analysis of spatial motion of thin coin model (Fig. 1c) taking precession into account and results of coin tossing are thoroughly described by Diakonis, Holmes and Montgomery [4]. Special emphasis of this work was put on the probability of heads in the process of flipping a coin, which is caught in the hand (for natural flips, the chance of coming up as started is about 0.51). Previous literature on the dynamics of coin tossing was also presented in [4].

In our previous paper [5] three-dimensional model of coin was shown. Euler parameters (normalised quaternions) used to describe orientation of the body as well as dynamics of the coin. Collisions with flat surfaces were also analysed.

In this paper air resistance forces and moments are included in the model.

1. Kinematics of coin

Any arbitrary position of a rigid body with respect to the fixed reference frame *Oxyz* (Fig. 2) can be described by a combination of the position of the origin of the local reference frame *x'y'z'* and the orientation (angular position) of this frame $\xi\eta\zeta$. The local reference frame *x'y'z'* is rigidly attached to the body and its axes are parallel to the *xyz* frame and $\xi\eta\zeta$ is the frame embedded and fixed in the body.

It is convenient to choose the centre of mass of the body (*C*) or geometric centre of the body model (*B*) as the origin of local frames. (A real coin is in fact nonsymmetric body, therefore to describe its motion we will use the geometric centre of the cylinder modelling the coin (*B*) and the centre of mass of the coin (*C*)).

1.1. Euler parameters

An alternative to Euler angles and similar conventions of body orientation description are Euler parameters called Euler symmetric parameters and known in mathematics as normalized quaternions [6], [7]. They are very useful in representing rotations due to some advantages above the other representations. The main advantage of Euler parameters is that they do not produce any singularities in numerical solutions of body motion equations.

In the matrix notation Euler parameters are represented by a column matrix

$$\mathbf{p} = \begin{bmatrix} e_0 \\ \mathbf{e} \end{bmatrix} = \begin{bmatrix} cos\dfrac{\phi}{2} \\ \mathbf{v}\, sin\dfrac{\phi}{2} \end{bmatrix}, \tag{1}$$

where $\begin{bmatrix} e_0 & \mathbf{e} \end{bmatrix}^T = \begin{bmatrix} e_0 & e_1 & e_2 & e_3 \end{bmatrix}^T$.
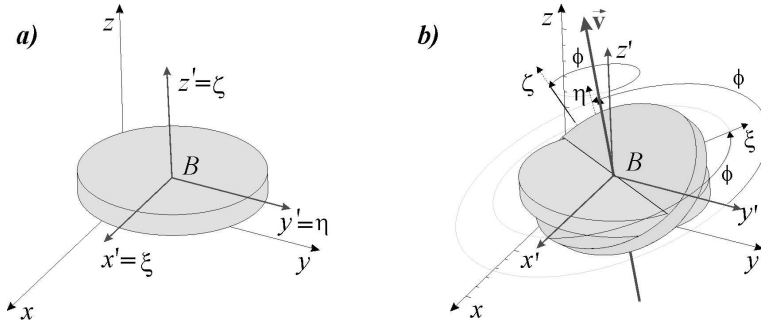
Figure 2. Coin rotation by ϕ – with respect to the vector $\vec{\mathbf{v}}$

The rotation matrix $\mathbf{R}$ – expressed by unit quaternions $\left(e_0,...,e_3\right)$ has following form

$$\mathbf{R} = \begin{bmatrix} -1 + 2e_0^2 + 2e_1^2 & 2e_1e_2 - 2e_0e_3 & 2e_0e_2 + 2e_1e_3 \\ 2e_1e_2 + 2e_0e_3 & -1 + 2e_0^2 + 2e_2^2 & -2e_0e_1 + 2e_2e_3 \\ -2e_0e_2 + 2e_1e_3 & 2e_0e_1 + 2e_2e_3 & -1 + 2e_0^2 + 2e_3^2 \end{bmatrix}. \tag{2}$$

Antysymmetric matrix $\mathbf{\Omega}$ containing scalar components of coin angular velocity vector – in the body embedded frame $\xi\eta\zeta$ – has the form

$$\mathbf{\Omega} = \dot{\mathbf{R}}\mathbf{R}^T = 2 \begin{bmatrix} 0 & -\dot{e}_3e_0 + \dot{e}_2e_1 - \dot{e}_1e_2 + \dot{e}_0e_3 & \dot{e}_2e_0 + \dot{e}_3e_1 - \dot{e}_0e_2 - \dot{e}_1e_3 \\ & 0 & -\dot{e}_1e_0 + \dot{e}_0e_1 + \dot{e}_3e_2 - \dot{e}_2e_3 \\ asym. & & 0 \end{bmatrix}. \tag{3}$$

The angular velocity vector of the coin in the body embedded frame $\xi\eta\zeta$ is expressed by following column matrix

$$\mathbf{\omega} = \begin{bmatrix} \omega_\xi \\ \omega_\eta \\ \omega_\zeta \end{bmatrix} = 2 \begin{bmatrix} \dot{e}_1e_0 - \dot{e}_0e_1 - \dot{e}_3e_2 + \dot{e}_2e_3 \\ \dot{e}_2e_0 + \dot{e}_3e_1 - \dot{e}_0e_2 - \dot{e}_1e_3 \\ \dot{e}_3e_0 - \dot{e}_2e_1 + \dot{e}_1e_2 - \dot{e}_0e_3 \end{bmatrix}. \tag{4}$$

The column matrix containing *xyz* scalar components of the coin angular velocity vector (i.e. components in fixed spatial frame) has the form of

$$\mathbf{\omega}_0 = \begin{bmatrix} \omega_x \\ \omega_y \\ \omega_z \end{bmatrix} = 2 \begin{bmatrix} \dot{e}_1e_0 - \dot{e}_0e_1 + \dot{e}_3e_2 - \dot{e}_2e_3 \\ \dot{e}_2e_0 - \dot{e}_3e_1 - \dot{e}_0e_2 + \dot{e}_1e_3 \\ \dot{e}_3e_0 + \dot{e}_2e_1 - \dot{e}_1e_2 - \dot{e}_0e_3 \end{bmatrix}. \tag{5}$$

2. Dynamics of tossed coin

2.1. Free fall of the coin

Rigid body dynamics equations can be expressed as two equations in matrix form that describe:

– motion of the body mass centre

$$\mathbf{M}\left(\mathbf{a_B} + \dot{\Omega}\mathbf{r}_C + \Omega\Omega\mathbf{r}_C\right) = \mathbf{f}, \tag{6}$$

– spatial orientation of the body

$$\mathbf{J}_B\dot{\boldsymbol{\omega}} + \Omega\mathbf{J}_B\boldsymbol{\omega} + \mathbf{M}\mathbf{R}_C\,\mathbf{a}_C = \mathbf{m}_B. \tag{7}$$

In the mentioned equations $\mathbf{M}$ is the mass matrix of the coin ($\mathbf{M}=diag\,[m;\,m;\,m]$), $\mathbf{a_B}$ denotes absolute acceleration of the point B, $\mathbf{r}_C$ and $\mathbf{R}_C$ include coordinates of the vector $\mathbf{r}_C$, describing the position of centre mass (C) relative to the origin B, $\mathbf{J}_B$ is the body moment of inertia matrix (determined with respect to the body embedded frame $\xi_B\eta_B\zeta_B$ – parallel to the $\xi\eta\zeta$ and with origin B), and $\mathbf{m}_B$ is the body force moment with respect to the B, $\boldsymbol{\omega}$ and Ω are the body angular velocity vector in the form of column and antisymmetric matrices. In general case, for nonsymmetric or nonhomogenous coin, the matrix $\mathbf{J}_B$ is not diagonal, because the axes ξ_B, η_B, ζ_B are not principal axes (some nonzero inertia products in $\mathbf{J}_B$ appear).

The column matrices $\mathbf{a}_B$ and $\mathbf{f}$ are expressed by vector components with respect to the fixed frame (xyz): $\mathbf{a}_B = \begin{bmatrix} \ddot{x} & \ddot{y} & \ddot{z} \end{bmatrix}^T$, $\mathbf{f} = \begin{bmatrix} f_x & f_y & f_z \end{bmatrix}^T$.

On the other hand it is more convenient to describe rotations of the body (equation (7)) by their components with respect to the body embedded frame ($\xi\eta\zeta$).

The equations (6) and (7) are coupled equations even though free fall of a coin is considered, i.e. even if the air resistance is neglected.

2.2. Air resistant forces and moments

It is assumed that total air resistance force ($\mathbf{f}_r$) can be divided into two components: normal ($\mathbf{f}_n$), and tangential ($\mathbf{f}_\tau$) to the coin surfaces i.e. head (1) and tail (2) circles and cylindrical surface (3)

$$\mathbf{f}_r = \mathbf{f}_n + \mathbf{f}_\tau = \mathbf{f}_{1n} + \mathbf{f}_{2n} + \mathbf{f}_{3n} + \mathbf{f}_{1\tau} + \mathbf{f}_{2\tau} + \mathbf{f}_{3\tau}. \tag{8}$$

For thin model (coin thickness $h=0$) air resistance force acting on cylindrical surface is neglected ($\mathbf{f}_{3n} = \mathbf{f}_{3\tau} = \mathbf{0}$) and normal and tangential forces components on both circles are described as

$$\mathbf{f}_{in} = -\lambda_n \int_0^r \left(\int_0^{2\pi} |\mathbf{v}_{Ain}|^b \mathbf{v}_{Ain}\, \rho\, d\theta \right) d\rho, \tag{9}$$

$$\mathbf{f}_{i\tau} = -\lambda_\tau \int_0^r \left(\int_0^{2\pi} |\mathbf{v}_{Ai\tau}|^b \mathbf{v}_{Ai\tau}\, \rho\, d\theta \right) d\rho \,, \tag{10}$$

where λ_n, λ_τ are air force coefficients, $\mathbf{v}_{Ain}$ and $\mathbf{v}_{Ai\tau}$ are normal (outer) and tangential total velocity components of a point on the coin surface, and b is the value of air force velocity exponent $(0 \le b \le 1)$.

As results of (8)–(10) it was found that for thin coin

$$\mathbf{f}_n = -\pi\, r^2 \lambda_n \begin{bmatrix} s\vartheta\, s\psi\left(\xi_C\omega_\eta - \eta_C\omega_\xi + s\vartheta\, s\psi\, \dot{x} - s\vartheta\, c\psi\, \dot{y} + c\vartheta\, \dot{z}\right) \\ -s\vartheta\, c\psi\left(\xi_C\omega_\eta - \eta_C\omega_\xi + s\vartheta\, s\psi\, \dot{x} - s\vartheta\, c\psi\, \dot{y} + c\vartheta\, \dot{z}\right) \\ c\vartheta\left(\xi_C\omega_\eta - \eta_C\omega_\xi + s\vartheta\, s\psi\, \dot{x} - s\vartheta\, c\psi\, \dot{y} + c\vartheta\, \dot{z}\right) \end{bmatrix}, \tag{11}$$

and

$$\mathbf{f}_\tau = -2\pi\, r^2 \lambda_\tau \begin{bmatrix} \dot{x} \\ c\vartheta\left(c\vartheta\, \dot{y} + s\vartheta\, \dot{z}\right) \\ s\vartheta\left(c\vartheta\, \dot{y} + s\vartheta\, \dot{z}\right) \end{bmatrix}, \tag{12}$$

where $s\vartheta \equiv \sin\vartheta$, $c\vartheta \equiv \cos\vartheta$, $s\psi \equiv \sin\psi$, $c\psi \equiv \cos\psi$.

Moment of the air resistance force with respect to the coin centre (C) for thin symmetrical coin (and $\omega_\eta = 0$, $\omega_\zeta = 0$) was described as

$$\mathbf{m}_C = -\frac{\pi\, r^2}{4} \lambda_n \begin{bmatrix} \left(r^2 + 4\,\eta_C^2\right)\omega_\xi + 4\eta_C\left(s\vartheta\, \dot{y} - c\vartheta\, \dot{z}\right) \\ 0 \\ 0 \end{bmatrix}. \tag{13}$$

3. Results and conclusion

As an example of numerical results a comparison of coin tossing results for three models is presented in the Fig. 4. Black regions denote that end result is "head" and white ones mean "tail". These results are obtained using Mathematica system [8].
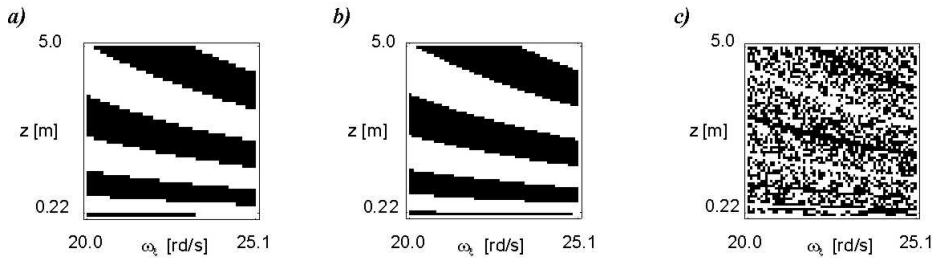
Figure 4. Coin tossing results: a) free fall of coin, b) air resistance included,
c) air resistance and bouncing included

In the Fig. 5 comparison of tossed coin motion for two models of coin (bar model [4] – Fig. 5a, 5b and thin plate model of coin – Fig. 5c, 5d) is shown.
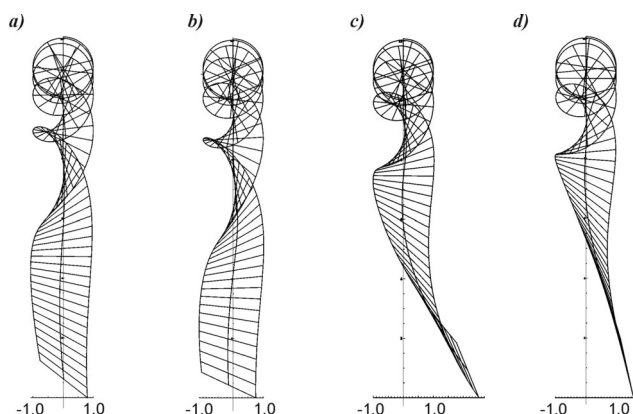
Figure 5. Motions of tossed coin for two models of coin ($\Lambda_n = \lambda_n = 0.3$):
bar model a) $\Lambda_\tau = 0.075$, b) $\Lambda_\tau = 0$; thin plate model c) $\lambda_\tau = 0$, d) $\lambda_\tau = 0.075$

Presented in the paper more realistic mechanical model of coin tossing allow examining whether the initial states leading to "head" or "tail" are distributed uniformly in phase space.

References

[1]   J.B. Keller, *The probability of heads*, American Mathematical Monthly, 93, 3 (1986) 191 – 197.

[2]   P. Diaconis, S. Holmes, R. Montgomery, *Dynamical Bias in the Coin Toss*. Society for Industrial and Applied Mathematics, 49, 2 (2007) 211 – 235.

[3]   V.Ž. Vulović, R.E. Prange, *Randomness of true coin toss*. Physical Review A, 33/1 (1986) 576 – 582.

[4]   T. Mizuguchi, M. Suwashita, *Dynamics of Coin Tossing*. Progress of Theoretical Physics Supplement, 161 (2006) 274 – 277.

[5]   J. Grabski, J. Strzałko, P. Perlikowski, T. Kapitaniak, *Wykorzystanie kwaternionów do opisu dynamiki ciała. Analiza ruchu rzucanej monety.* Materiały Kongresu Mechaniki Polskiej (2007).

[6]   P.E. Nikrevesh, *Computer-Aided Analysis of Mechanical Systems*. Prentice-Hall International, Inc., Englewood Cliffs 1988.

[7]   J. Diebel*, Representing Attitude: Euler Angles, Unit Quaternions, and Rotation Vectors.* http://ai.stanford.edu/~diebel/ (May, 2007).

[8]   Mathematica 4. Standard Add-on Packages. Wolfram Media, 1999.

SURFACE EFFECTS OF COUPLED FIELDS IN MICROPOLAR CONTINUOUS MEDIA

Tadeusz J. HOFFMANN, Marta CHUDZICKA-ADAMCZAK

Poznan University of Technology Institute of Applied Mechanics
ul. Piotrowo 3, 60-965 Poznań
phone:+48 616652301, e-mail: tadeusz.hoffmann@put.poznan..pl
e-mail: martachudzicka@wp.pl

Radoslaw PYTLIŃSKI

Higher Vocational State School in Kalisz Institute of Technology ul. Częstochowska 140, 62-800 Kalisz

Michał POŚPIECH Pratt &Whitney Kalisz
ul. Elektryczna 4a, 62-800 Kalisz
phone: 509-523-888, e-mail: mpospiech@poczta.onet.pl

Abstract

In mechanics of continuous media, one of the sub areas is the coupled field theory describing interactions of mechanical, thermal, diffusion and electromagnetic field. All this physical fields are represented in the tensors introduced in this theory. Taking into consideration the momentum and angular momentum of the electromagnetic field in medium requires introduction of the fields: couple stress, mass angular momentum and mass couple in balance equations. From the vectorial nature of momentum, angular momentum, force and couple it appears that the stress tensor and couple stress tensor are the second order. Bearing in mind the importance for modern technology of the physical properties of the surface and surface layer of a solid, the conception of balance equations will be applied to describe the material surface interacting with an electromagnetic field.
Keywords: coupled fields, micropolar medium, angular momentum, couple stress

Introduction

In the coupled field theory understood as the phenomenological theory of the material bodies, the mass as a quantity typically mechanical becomes a carrier of the electric charge and the magnetic moments. In this way the electromagnetic fields join the interactions in the model medium as typically mechanical or thermo-mechanical. In this case the physical laws considering all the occurring fields should be used. The convenient forms of the physical law in the continuous medium are the balance equations derived from the field theory. The physical fields in the continuous medium are connected with the impact, what determined the form of the theory of the coupled field theory in the theory of the continuous media. From the utilitarian needs of the mechanical engineering point of view the impact of the physical reasons different from

the mechanical load on the stress field in the continuous medium is essential. It cost the advent of the approximate theory aiming these considerations. The quantity relations of the tested effect in used the applied approximations in vital. A good example of such proceedings can be uncoupled thermo-elasticity where the impact of the strain field on the distribution of the temperature in the medium studying only influence on the displacement field and further on the stress fields is omitted.

The theory of coupled field is very successful and there are many interesting problems which have not been worked out yet. The examples of such cases can be the influence of momentum and the angular momentum of the electromagnetic field on the balances of these qualities in the continuous medium.

1. The Geometry of Surface

Let us assume that a material surface is described by the Gaussian method, using curvilinear coordinates , by the fundamental form [1]

$$ds^2 = a_{\alpha\beta} \, du^\alpha \, du^\beta , \quad \alpha,\beta = 1,2, \qquad (1)$$

where, $s, a_{\alpha\beta}, u^\beta$ are the length, the metric tensor, and the assumed Gaussian curvilinear coordinates of the surface respectively. The covariant and contravariant components of the metric tensor satisfy the relation

$$a_{\alpha\beta} a^{\beta\gamma} = \delta_\alpha^\gamma , \quad (2)$$

where, δ_α^γ is the Kronecker's delta.

The natural basis of the surface $S : \mathbf{x}(u^\alpha)$ is $(\mathbf{x}_1, \mathbf{x}_2, \mathbf{m})$, where the vectors $\mathbf{x}_\alpha$ are tangent to the coordinate lines and $\mathbf{m}$ is normal.

Let a vector field $\mathbf{v}(u^\alpha)$, $\mathbf{v} = v^\alpha(u^\beta)\mathbf{x}_\alpha$ defined on the surface $\mathbf{x}(u^\alpha)$. The covariant derivative of the vector $\mathbf{v}(u^\alpha)$ is the mixed tensor of the second order

$$\nabla_\alpha v^\beta = \partial_\alpha v^\beta + \begin{Bmatrix} \beta \\ \gamma,\alpha \end{Bmatrix} v^\gamma ,$$

$$\nabla_\alpha v_\beta = \partial_\alpha v_\beta + \begin{Bmatrix} \gamma \\ \beta,\alpha \end{Bmatrix} v_\gamma , \qquad (3)$$

$\begin{Bmatrix} \beta \\ \gamma, \alpha \end{Bmatrix}$ being the Christoffel symbol of the second kind and $\partial_\alpha(\bullet) = \dfrac{\partial}{\partial u^\alpha}(\bullet)$. If a

tensor field of the second order $S^{\alpha\beta}\left(u^\beta\right)$ is determined on the surface $\mathbf{x}\left(u^\alpha\right)$, the covariant derivative of the components of that tensor is determined, in agreement with [1], by the formulae

$$\nabla_\gamma S^{\alpha\beta} = \partial_\gamma S^{\alpha\beta} + \begin{Bmatrix} \alpha \\ \delta, \gamma \end{Bmatrix} S^{\delta\beta} + \begin{Bmatrix} \beta \\ \delta, \gamma \end{Bmatrix} S^{\alpha\delta} \ ,$$

$$\nabla_\gamma S_{\alpha\beta} = \partial_\gamma S_{\alpha\beta} - \begin{Bmatrix} \delta \\ \alpha, \gamma \end{Bmatrix} S_{\delta\beta} - \begin{Bmatrix} \delta \\ \beta, \gamma \end{Bmatrix} S_{\alpha\delta} \quad , \quad (4)$$

$$\nabla_\gamma S_\beta^\alpha = \partial_\gamma S_\beta^\alpha + \begin{Bmatrix} \alpha \\ \delta, \gamma \end{Bmatrix} S_\beta^\delta - \begin{Bmatrix} \delta \\ \beta, \gamma \end{Bmatrix} S_\delta^\alpha \ .$$

A theory of balance equations will now be formulated for such a surface.

2. Balances of Momentum and Angular Momentum

The momentum balance in the continuous medium is written in the form:

$$\frac{d}{dt}\int_V \rho v_k dV = \int_V \left(\partial_l t_{kl} + \rho f_k\right) dV \qquad (5)$$

where the first integral on the right side describes the contact forces applied to the surfaces limiting the considered area, while the second integral describes far-reaching forces derived from gravitational and electromagnetic external fields [2].

These forces are called volume of mass because they reach every unit of the body and act on every unit of the mass of body. The integral o these forces are show as the sum of the interactions of both fields:

$$\int_V \rho f_k \, dV = \int_V \rho f_k^{elm} dV + \int_V \rho f_k^{mec} dV. \qquad (6)$$

According to [2], [3], [4] balance of momentum of electromagnetic field gets a form:

$$\frac{d}{dt}\int_V \rho(\mathbf{D}\times\mathbf{B})_k \, dV = \int_V (\partial_l T_{kl} + \rho f_k^{elm}) \, dV, \qquad (7)$$

where: $\mathbf{D}, \mathbf{B}$ are vectors of electric induction and magnetic induction, T_{kl} is the Maxwell stress tensor. Let substitute (7) and (6) to equation (5), we will get

$$\frac{d}{dt} \int_V \rho \left[v_k + (\mathbf{D} \times \mathbf{B})_k \right] dV = \int_V \left[\partial_l (t_{kl} + T_{kl}) + \rho f_k^{mec} \right] dV \tag{8}$$

According to [3], [4] the Maxwell stress tensor has a form:

$$T_{kl} = D_k E_l + B_k H_l - \frac{1}{2} \delta_{kl} (D_s E_s + B_s H_s), \tag{9}$$

To facilitate we will introduce notation:

$$V_k = v_k + (\mathbf{D} \times \mathbf{B})_k , \quad \mathfrak{I}_{kl} = t_{kl} + T_{kl} , \tag{10}$$

then

$$\frac{d}{dt} \int_V \rho V_k dV = \int_V (\partial_l \mathfrak{I}_{kl} + \rho f_k^{mec}) dV \tag{11}$$

The differential balance of momentum will be shown as follows

$$\rho D_t V_k = \partial_l \mathfrak{I}_{kl} + \rho f^{mec}, \tag{12}$$

where: D_t is material derivative..

The balance of angular momentum has a form

$$\frac{d}{dt} k_i = m_i, \tag{13}$$

where: angular momentum and moment of the force have the forms [2], [5]

$$k_i = \int_V \left(\rho \in_{ijk} x_j V_k + \rho \kappa_i \right) dV, \tag{14$_a$}$$

$$m_i = \int_V [\partial_l \left(\in_{ijk} x_j \mathfrak{I}_{kl} + m_{il} \right) + \left(\in_{ijk} x_j \rho f_k^{mec} + \rho b_i \right)] dV, \tag{15$_b$}$$

κ_i - is a mass angular momentum, m_{il} - couple stress tensor, b_i - mass moments of the force. The local form of balance of angular momentum can be derived while using the law of conservation of the mass and the balance of momentum (12), in a form

$$\rho D_t \kappa_i = \partial_l m_{il} + \rho b_i + \in_{ikj} \mathfrak{I}_{kj}. \tag{16}$$

It is the most general form of this balance, as occurring in it quantities exhaust all the possibilities of mathematical modeling .

3. Surface Effects

Let us consider the following vector and tensor fields on the surface $\mathbf{x}(u^\alpha)$ described by (1) - (4).

$$V^\beta(u^\alpha, t), \ \mathfrak{I}_{\beta\delta}(u^\alpha, t), \ f^\delta(u^\alpha, t), \ \sigma(u^\alpha, t),$$

$$\tag{17}$$

$$\kappa_\beta(u^\alpha, t), \ m_{\beta\delta}(u^\alpha, t), \ b_\beta(u^\alpha, t)$$

where σ denote the surface density.

The balance equations have, in agreement with Eq. (12), (16), the form

$$\sigma D_t V_\beta = \nabla^\alpha \mathfrak{I}_{\alpha\beta} + \sigma f_\beta,$$

$$\tag{18}$$

$$\sigma D_t \kappa_\beta = \nabla^\alpha m_{\alpha\beta} + \sigma b_\beta + \in_{\beta\alpha m} \mathfrak{I}_{\alpha m},$$

Equations (18) constitute a balance description of coupled fields at the surface.

4. Conclusions

The consideration made in this paper show that in the medium the electromagnetic field has an influence on the stresses through the Maxwell tensor. In the medium the

couple stresses and mass moments of the forces occur. The mass angular momentum can be interpreted as the mass moment of inertia and spin of electromagnetic field. The results just presented make it possible to construct a linear and also nonlinear theory of any type of coupled surface effects.

References

1. J. L. Synge, A. Schild, *The Tensor Calculus,* [in polish] PWN Warszawa 1964
2. C. Rymarz .: *Mechanics of continuous media*. [in polish] PWN Warszawa, 1993.
3. J. D. Jacson, *Classical electrodynamics,* [in polish] PWN Warszawa 1997
4. M. Suffczyński, *Classical electrodynamics*. . [in polish] PWN Warszawa, 1966.
5. T.J. Hoffmann, *Tensory naprężenia pól sprzężonych i pól torsyjnych w ośrodkach ciągłych,* I Kongres Mechaniki Polskiej, Warszawa, 28 – 31 sierpnia 2007 r.

SAINT-VENANT'S PRINCIPLE IN STATIC MAGNETOELASTICITY

Tadeusz J. HOFFMANN, Marta CHUDZICKA-ADAMCZAK

Poznan University of Technology

Instytute of Applied Mechanics

ul. Piotrowo 3, 60-965 Poznań, Poland

Phone: 048 061 665 23 02, e-mail: Tadeusz.Hoffmann@put.poznan.pl

Phone: 048 061 665 20 65, e-mail: martachudzicka@wp.pl

Abstract

Toupin's version of Saint-Venant's principle in linear elasticity is generalized to the case of linear magnetoelasticity. That is, it is shown that, for a straight prismatic bar made a linear magnetoelastic material end loaded by a self-equilibrated system at one end only, the internal energy stored in the portion of the bar which is beyond a distance s from the loaded end decreases exponentially with the distance s.

Key words: magnetoelasticity, Saint-Venant's principle

Introduction

There are many mathematical versions of the Saint-Venant's theorem for instance by Mises -Sternberg, Knowles, Zanaboni, Robinson and Toupin. All the mentioned have been discussed by Gertin[1] in his monograph. In this paper we will prove the Saint-Venant's principle analogically to the Toupin's version. For a linear elastic homogeneous prismatic body of arbitrary length and cross-section loaded on one end only by an arbitrary system or self-equilibrated forces, Toupin [4] showed that the elastic energy $U(s)$ stored in the part of the body which is beyond a distance s from the loaded end satisfies the inequality[5]

$$U(s) \le U(0) \exp\left[-\frac{(s-l)}{s_c(l)} \right].$$
(1)

The characteristic decay length $s_c(l)$ depends upon the maximum and the minimum elastic moduli of the material and the smallest nonzero characteristic frequency of free vibration of a slice of the cylinder of length l. Inequalities similar to (1) have been obtained by Batra [5] for linear elastic piezoelectric prismatic bodies and by Borrelli & Patria [6] for a semi-infinite magnetoelastic cylinder on the asymptotic behaviour of the Dirichlet integral of the magnetic field and of the elastic energy.

Here we consider a linear theory of magnetoelasticity (for infinitesimal strain) in which only the ponderomotive force remains non-linear in presence of a magnetic field . We assume that the elastic body is homogeneous, isotropic and electrically conducting [7], [8], [9], [10].

1. Equations for static magnetoelasticity

Let the finite spatial region occupied by the magnetoelastic body be V, the boundary surface of V be S, the unit outward normal of S be n_i, and S be partitioned as

$$S = S_u \cup S_T = S_E \cup S_B,$$
$$0 = S_u \cap S_T = S_E \cap S_B.$$

(2)

Physically, S_u, S_T are, respectively, parts of the boundary S on which mechanical displacements and tractions are prescribed. S_E is the part of S which is in contact with electrode, hence the tangential electric field vanishes on it, and S_B the parts of S on which the magnetic induction is prescribed. The governing equations and boundary conditions for static magnetoelasticity in rectangular Cartesian coordinates in SI units are:

$$\partial_i \Im_{ij} = 0, \qquad \varepsilon_{ijk} \partial_j E_k = 0, \qquad \partial_k D_k = 0, \qquad\qquad in\ V,$$
$$\varepsilon_{ijk} \partial_j H_k = j_k, \qquad \partial_k B_k = 0, \qquad\qquad in\ V,$$
$$j_k = \sigma E_k, \qquad D_k = \varepsilon E_k, \qquad B_k = \mu H_k, \qquad in\ V,$$
$$\bar{T}_{ij} = t_{ij} + T_{ij}, \qquad t_{ij} = c_{ijkl} \varepsilon_{kl}, \qquad T_{ij} = B_i H_j - \frac{1}{2} \delta_{ij} B_k H_k, \qquad in\ V,$$
$$\varepsilon_{ij} = \frac{1}{2}\left(\partial_i u_j + \partial_j u_i\right), \qquad in\ V,$$
$$u_i = \tilde{u}_i \quad on\ S_u, \qquad n_i \bar{T}_{ij} = \tilde{t}_j \quad on\ S_T,$$
$$\varepsilon_{ijk} n_j E_k = 0 \quad on\ S_E, \qquad n_i B_i = 0 \quad on\ S_B,$$

(3)

where u_i is the mechanical displacement, t_{ij} the mechanical stress tensor, T_{ij} the Maxwell stress tensor, ε_{ij} the strain tensor, E_k the electric field vector, D_k the electric displacement vector, H_k the magnetic field vector, j_k the current vector, B_k the magnetic induction vector, ε, μ, σ the electromagnetic material constants, c_{ijkl} the elastic moduli, ε_{ijk} the permutation tensor, δ_{ij} the unit tensor, ∂_k the spatial derivative, $\tilde{u}_i$ and $\tilde{t}_j$ are the prescribed boundary mechanical displacement and traction vectors. The magnetic enthalpy function h is determined by volume and given by:

$$h = \frac{1}{2} \Im_{kl} \varepsilon_{kl} - \frac{1}{2} B_k H_k,$$

(4)

where $\Im_{kl}$ is the magnetoelastic stress tensor.

We assume that the material constants occurring in our considerations are described positively. We will introduce to our deliberations the internal energy density:

$$W = h + B_k H_k = \frac{1}{2} \Im_{kl} \varepsilon_{kl} + \frac{1}{2} B_k H_k.$$

(5)

To facilitate the further considerations the magnetic quantities will be show in the representation of the vector potential:

$$H_r = \varepsilon_{rsq} \partial_s A_q, \qquad \partial_s A_s = 0,$$

$$H_r = \frac{1}{2} \varepsilon_{rsq} H_{sq}, \qquad H_{sq} = \partial_s A_q - \partial_q A_s.$$

(6)

The Maxwell stress tensor in this representation takes the form:

$$T_{kl} = B_{sk} H_{ls}, \qquad B_{sk} = \mu H_{sk}.$$

(7)

The internal energy density will have a form:

$$W = \frac{1}{2} t_{kl} \varepsilon_{kl} + \frac{1}{2} B_{sk} H_{ls} \varepsilon_{kl} + \frac{1}{2} B_{sk} H_{ks}.$$

(8)

If we use the Hook's law for the transformation (8), we will get

$$W = \frac{1}{2} c_{klrs} \varepsilon_{rs} \varepsilon_{kl} + \frac{1}{2} B_{sk} H_{ls} \varepsilon_{kl} + \frac{1}{2} B_{sk} H_{ks}.$$

(9)

The above density of internal energy is positively defined quadratic function of nine variables $\{\varepsilon_{kl}, H_{kl}\}$. If we form arranged pairs $(\varepsilon_{kl}, H_{kl})$ as the components of the nine-dimensional vector $\mathbf{\Gamma}$, we will write the equation (9) in the symbolic form:

$$W = \mathbf{\Gamma} \cdot \breve{C} \mathbf{\Gamma} = \frac{1}{2} \Gamma_k C_{kl} \Gamma_l,$$

(10)

where $\breve{C}$ is a linear transformation from a nine-dimensional linear space into a nine-dimensional linear space the matrix of transformation created. Because of the positive definiteness of W the inequality is fulfilled:

$$\frac{\partial W}{\partial \Gamma_k} \frac{\partial W}{\partial \Gamma_k} = C_{kl} \Gamma_l C_{kl} \Gamma_l = \Gamma_l C_{kl}^2 \Gamma_l \le a_M \Gamma_k C_{kl} \Gamma_l = 2 a_M W,$$

(11)

where: a_M is the biggest eigenvalue of the matrix $\breve{C}$.

2. Formulation of the problem

Now, we consider the prismatic bar. We introduce the Cartesian coordinate system In such a way that the axis x_3 is the axis longitudinal of the bar. The surface x_3 is loaded by a self-equilibrated force system. Let label the area of the cross-section for $x_3 = 0$ as C_0 and $x_3 = s$ as C_s.

The internal energy as a scalar in non-variable relatively to the stiff body motions. The conditions of the mutual equilibrium of loadings gets a form:

$$\int_{C_0} n_i \Im_{ij} dS = \int_{C_0} n_i \frac{\partial W}{\partial \varepsilon_{ij}} dS = -\int_{C_0} \frac{\partial W}{\partial \varepsilon_{ij}} dS = 0,$$

$$\int_{C_0} \varepsilon_{lkj} x_k n_i \frac{\partial W}{\partial \varepsilon_{ij}} dS = -\int_{C_0} \varepsilon_{lkj} x_k \frac{\partial W}{\partial \varepsilon_{ij}} dS = 0.$$

(12)

We will additionally label the total internal energy as:

$$U(s) = \int\limits_{V, x_3 \geq s} W dV,$$

$$U(0) = \int\limits_{V, x_3 = 0} W dV. \tag{13}$$

THEOREM. *If a prismatic body made of a linear magnetoelastic material and with materially uniform cross-section loaded on C_0 by a self-equilibrated force system, then*

$$U(s) \leq U(0) \exp\left[-(s-l)/s_c l\right], \tag{14}$$

Where

$$s_c(l) = 2aM / \lambda_0(l)^{1/2}, \tag{15}$$

$\lambda_0(l)$ *is the smallest nonzero eigenvalue of the following eigenvalue problem*

$$\partial_i\left(\frac{\partial W}{\partial \varepsilon_{ij}}\right) = \lambda u_j, \qquad \partial_i\left(\frac{\partial W}{\partial B_{ij}}\right) = \lambda A_j \quad \text{in} \quad V,$$

$$n_i \mathfrak{I}_{ij} = 0\big|_S,$$

$$\varepsilon_{ijk} n_j A_k = 0\big|_{S \setminus [C_s \cup C_{s+l}]},$$

$$n_i H_{ij} = 0\big|_{[C_s \cup C_{s+l}]}, \tag{16}$$

for the section of the prismatic body put on the axis length l. In the eq. (13) V is the volume between the sections $x_3 = s$ and $x_3 = s+l$, S is the total surface containing V, C_s and C_{s+l} are the areas of the sections. The written equations (16) correspond with the problem of the free vibrations of the magnetoelastic prismatic body with the length l, unit density and the unit density inertia affiliated with the vector potential.

Proof of the theorem: On the strength of (13)$_1$ we can write:

$$U(s) = \frac{1}{2} \int\limits_{V, x_3 \geq s} \left(\frac{\partial W}{\partial \varepsilon_{ij}} \varepsilon_{ij} + \frac{\partial W}{\partial B_{ij}} B_{ij}\right) dV. \tag{17}$$

Taking under consideration that the internal energy as a scalar is non variable relatively to the stiff rotations we ca write

$$\partial_k u_l \approx \varepsilon_{kl}, \qquad \omega_{kl} = \frac{1}{2}\left(\partial_k u_l - \partial_l u_k\right) \approx 0, \tag{18}$$

omitting the rotation tensor. At the same moment

$$B_{ij} = 2\mu \partial_i A_j, \tag{19}$$

Using (18) i (19) we can write (17)

$$U(s) = \frac{1}{2} \int\limits_{V, x_3 \geq s} \left(\frac{\partial W}{\partial \varepsilon_{ij}} \partial_i u_j + 2\mu \frac{\partial W}{\partial B_{ij}} \partial_i A_j\right) dV. \tag{20}$$

On the surface C_s the orthonormal outer vector has a form $n_k = -\delta_{3k}$, we can write the expression

$$U(s) = \frac{1}{2} \int_{C_s} \left[n_i \left(\frac{\partial W}{\partial \varepsilon_{ij}} u_j + 2\mu \frac{\partial W}{\partial l} \right) \right] dS = -\frac{1}{2} \int_{C_s} \left(\frac{\partial W}{\partial \varepsilon_{3j}} u_j + 2\mu \frac{\partial W}{\partial B_{3j}} A_j \right) dS, \qquad (21)$$

which means the internal energy on the surface C_s. Next, we will utilize inequality Schwarza used by Toupin [1965]

$$2 \int_V fg \, dV \le \alpha \int_V f^2 \, dV + \frac{1}{\alpha} \int_V g^2 \, dV, \qquad \alpha > 0, \qquad (22)$$

where f, g are any functions for which the above integrals exist.

Using the inequality (22) to the surface integrals we will obtain:

$$-\frac{1}{2} \int_{C_s} \frac{\partial W}{\partial \varepsilon_{3j}} u_j \, dS \le \frac{1}{4} \left(\alpha_1 \int_{C_3} \frac{\partial W}{\partial \varepsilon_{3j}} \frac{\partial W}{\partial \varepsilon_{3j}} \, dS + \frac{1}{\alpha_1} \int_{C_s} u_j u_j \, dS \right). \qquad (23)$$

Similarly

$$-\frac{1}{2} \int_{C_s} \frac{\partial W}{\partial B_{3j}} A_j \, dS \le \frac{1}{4} \left(\alpha_2 \int_{C_3} \frac{\partial W}{\partial B_{3j}} \frac{\partial W}{\partial B_{3j}} \, dS + \frac{1}{\alpha_2} \int_{C_s} A_j A_j \, dS \right). \qquad (24)$$

Hence

$$U(s)_{x_3 = s} \le \frac{1}{4} \left[\beta \int_{C_s} \left(\frac{\partial W}{\partial \varepsilon_{ij}} \frac{\partial W}{\partial \varepsilon_{ij}} + \frac{\partial W}{\partial B_{ij}} \frac{\partial W}{\partial B_{ij}} \right) dS + \frac{1}{\beta} \int_{C_s} \left(u_j u_j + A_j A_j \right) dS \right], \qquad (25)$$

because it was assumed $\alpha_1 = \alpha_2 = \beta$. Substituting from (11) into (25) we get

$$U(s)_{x_3 = s} \le \frac{1}{4} \left[\beta \int_{C_s} 2 a_M W \, dS + \frac{1}{\beta} \int_{C_s} \left(u_j u_j + A_j A_j \right) dS \right], \qquad (26)$$

integrating on both sides (26) in respect to x_3 in the boundaries from $x_3 = s$ to $x_3 = s + l$ for $l > 0$ and labeling

$$Q(s, l) = \frac{1}{l} \int_s^{s+l} U(y) \, dy, \qquad (27)$$

we will obtain

$$Q(s, l) \le \frac{\beta a_M}{2l} \int_{C_{s,l}} W \, dV + \frac{1}{4\beta l} \int_{C_{s,l}} \left(u_j u_j + A_j A_j \right) dV, \qquad (28)$$

where $c_{s,l}$ is the volume between the sections $x_3 = s$ and $x_3 = s + l$. In his volume $c_{s,l}$ we will consider the following eigen problem:

$$\partial_i\left(\frac{\partial W}{\partial \varepsilon_{ij}}\right) = \lambda \rho u_j, \qquad \partial_i\left(\frac{\partial W}{\partial B_{ij}}\right) = \lambda \gamma A_j,$$

$$n_i \mathfrak{I}_{ij} = 0\Big|_S, \qquad \varepsilon_{ijk} n_j A_k = 0\Big|_{S\backslash(C_s \cup C_{s+l})}, \tag{29}$$

$$n_i H_{ij} = 0\Big|_{C_s \cup C_{s+l}}.$$

In the equations (29) and the earlier (10) the conditions formulated on the boundary should be understood as the conditions of the jump regarding to the continuity of the quantity of the electromagnetic field. It needs to be like this because the polar quantities are present in the self-equilibrating force system. Introduced in (29) quantities ρ and γ are not important in the static problem which we consider and were introduced in aiming obtaining the uniformity of the physical dimensions of the unit of the eigenvalues λ. In the problem of the free vibrations on which Toupin[1965] invokes ρ and γ mean respectively the mass density and the inertia density of the medium contained in the volume between $x_3 = s$ and $x_3 = s + l$. In the further considerations we assume them as equal to one. Multiplying $(29)_1$ by u_j and $(29)_2$ by A_j, adding these equations and integrating after volume $C_{s,l}$ using the conditions in the boundary $(29)_{3,4,5}$ we obtain

$$\lambda = \frac{2\int\limits_{C_{s,l}} W dV}{\int\limits_{C_{s,l}} \left(u_j u_j + A_j A_j\right) dV}. \tag{30}$$

The density on the internal energy is non negative and get the zero value $W = 0$ only if $\varepsilon_{ij} = 0$ and $B_{ij} = 0$, then $\lambda = 0$. The deformation tensor $\varepsilon_{ij} = 0$ when the displacement concerns the stiff motion. $B_{ij} = 0$ concerns the case when there is lack of magnetizing. Omitting these cases as non physical we assume that the integral in the denominator of the equation (30) is always different from zero. The smallest eigenvalue $\lambda_0(l)$ must be positive and fulfill the inequality

$$\lambda_0(l) \leq \frac{2\int\limits_{C_{s,l}} W dV}{\int\limits_{C_{s,l}} \left(u_j u_j + A_j A_j\right) dV}. \tag{31}$$

Using in (31) expression (28) we get the following result

$$Q(s,l) \leq \frac{s_c(l)}{l} \int\limits_{C_{s,l}} W dV, \tag{32}$$

where

$$s_c(l) = \frac{1}{2}\beta a_M + \frac{2}{\lambda_0 \beta}. \tag{33}$$

In our considerations β is any positive constant. If we opt

$$\beta = \frac{2}{a_M \lambda_0} \tag{34}$$

on the strength of (33) we will obtain

$$s_c(l) = 2\left(\frac{a_M}{\lambda_0}\right)^{\frac{1}{2}}, \tag{35}$$

in accordance with (15).

Differentiating (27) relative to s we get

$$\frac{dQ}{dS} = \frac{1}{l}[U(s+l) - U(s)] = -\frac{1}{l}\int_{C_{s,l}} W dV. \tag{36}$$

If we combine (36) with the inequality (32) the result is as follows:

$$s_c(l)\frac{dQ}{ds} + Q \leq 0. \tag{37}$$

In our considerations the quantity $Q(s,l)$ defined as (27) means the density of the internal energy averaged along the segment l therefore it Has to fulfill the obvious inequality:

$$U(s+l) \leq Q(s,l) \leq U(s). \tag{38}$$

Next, we will integrate the inequality (37) taking into account that $U(s)$ is non rising function, with the effect:

$$\frac{U(s_2 + l)}{U(s_1)} \leq \exp[-(s_2 - s_1)/s_c(l)]. \tag{39}$$

Assuming that $s_1 = 0$, $s_2 = s - l$ we proved the inequality (14), which ends the proof.

Remarks

In this paper, analogically to the Toupin's version Saint-Venant's principle we have proved is that the energy stored In the portion of the bar beyond a distance s from the loaded end decreases exponentially with the distance s. It is generally difficult to find the optimum decay rate unless one considers specific cross-sections.

References:

1. M. E. Gurtin. *The Linear Theory of Elasticity, Handbuch der Physik*, Vol.VIa/2, ed. C. Truesdell, Springer-Verlag, Berlin, Heidelberg, New York, 1972.
2. C. O. Horgan, J. K. Knowles, *Recent developments concerning Saint-Venant's principle*, Advances in Applied Mechanics, Vol. 23, edited by J. W. Hutchinson and T. Y. Wu, Academic Press, New York, 179-269, 1983.
3. C. O. Horgan, *Recent developments concerning Saint-Venant's principle: an update,* Appl. Mech. Rev. (1989) 295-303.

4.   R. A. Toupin, *Saint-Venant's principle*, Arch. Rat,l Mechanics Anal. **18** (1965) 83-96.

5.   R. C. Batra, J. S. Yang , *Saint-Venat's Principle in Linear Piezoelectricity*, J. of Elasticity **38** (1995) 209-218.

6.   A. Borrelli, M. C. Patria, Decay and other estimates for a semi-infinite magnetoelastic cylinder: Saint-Venant's Principle, Int. J. Non-Linear Mech. **32** (1997) 1087-1099.

7.   W. Nowacki, *Dynamic Problems of Thermoelasticity* (in Polish), PWN Warszawa 1966.

8.   G. A. Maugin, *Continuum Mechanics of Electromagnetic Solids*, North Holland, 1988.

9.   A. C. Eringen, G. A. Maugin, *Electrodynamics of Continua*, Vol. 1. Springer-Verlag, 1990.

10. T. J. Hoffmann, *Mechanical Aspects of Magnetoelasticity* (In Polish), Wydawnictwo Politechniki Poznańskiej, Poznań, 2002.

MODAL ANALYSIS OF PHYSIOLOGICAL MODEL OF AVIAN EMBRYOS - IDENTIFICATION EXPERIMENT (PART I)

Joanna IWANIEC[1], Marek IWANIEC[2], Krzysztof PAWLAK[3]
[1] Department of Robotics and Mechatronics,
[2] Department of Mechanics and Vibroacoustics,
AGH University of Science and Technology,
Mickiewicz Alley 30, 30-059 Krakow, Poland
[1] +48 (12) 617-31-28, jiwaniec@agh.edu.pl
[2] +48 (12) 617-35-09, iwaniec@agh.edu.pl
[3] Laboratory of Animal Hygiene,
Department of Poultry and Fur Animals Breeding and Animal Hygiene,
Agricultural University of Cracow,
Mickiewicz Alley 24/28, 30-059 Krakow, Poland
[3] +48 (12) 662-41-09, rzpawlak@cyfronet.pl

Abstract

Avian embryos are commonly used as ethically acceptable physiological models for research into prenatal live. Although easily available, avian embryos are difficult objects for investigation. The main difficulties result from the presence of shell separating the embryo from environmental influences and, what is more important, from the presence and interference of many biomechanical, chemical, electrical and other phenomena. The tiny changes in the object parameters of different nature are hardly measurable by means of the indirect methods. Investigation into the embryo prenatal life requires application of the non-invasive methods, which complicates the measurements. Taking into account the fact that as early as in the second day of incubation the avian embryo hart begins to work being by itself at the beginning of mutual conversions, it is easy to become conscious of the scale of the measurements and resulting identification problems. In the process of forming and growth, the heart of avian embryo undergoes constant biomechanical modifications. This aspects of embryogenesis are correlated to electrical and hydro-dynamical activity. Only mechanical vibrations and acoustical effects can be analysed on the basis of the indirect non-invasive measurements. The research carried out by authors is presented in the series of two papers. The current paper (part I) concerns the innovative non-invasive method dedicated for measurements of low-amplitude vibrations induced by the work of cardiac muscles while in the second paper (part II) there is presented vibration analysis carried out by means of the classical LSCE modal analysis method. Although the biomechanical model of developing heart is characterized by significant nonlinearity of observed parameters resulting from rapid increase in the cardiac muscle mass, during a given measurement session the changes in the object parameters are negligible and the assumptions of modal analysis are valid.

The changes in the proportions and organ masses as well as in time histories and values of forces generated by beating heart are the source of changes not only in the estimated modal model parameters but also in the model order. Some natural frequencies and corresponding mode shapes evolve and change their values, decay or appear. This variability can be observed in the longer time scale (e.g. days). In a single identification experiment lasting up to tens of minutes per day, after elimination of disturbances, the measured vibroacoustical signal can be treated as quasi stationary. Modal model parameters and the model order were determined for each separate measurement session lasting 10 to 40 minutes. Parameter values estimated for the consecutive measurement sessions made it possible to track the changes in modal model in the consecutive days of incubation.

Key words: influence of detrimental substances on biotic functions, non-invasive ethical measurement method, ballistocardiography, modal analysis.

Introduction

Pollutions of natural environment have a detrimental influence on mutual, formed for thousands of years interactions between human kind and the environment. Medicines, rubbish, industrial discards, pollutions of rivers, lakes, seas and the air are the most noticeable forms of environmental pollutions that are dangerous to human health and, in the extreme, to human life. The state of our health is also influenced by changes in environmental conditions determined by physical quantities such as temperature, humidity, air pressure, intensity of magnetic, electric and acoustical fields, etc. Therefore the prevention and early identification of hazards are of great importance.

Carried out research aimed at inventing sensitive and non-invasive method making it possible to examine in ethical way the influence of chemical substances (e. g. medicines, pollutions) and physical factors on the growth of organisms as early as in the prenatal phase. Such formulated objective is especially important since young, still forming organisms are especially sensitive to changes in environmental conditions. The knowledge of influence of chemical substances on the course of embryogenesis makes it possible to test new medicines and, on the other hand, to learn the teratogenous influence of chemical substances already present in the natural environment on alive organisms. Elaborated research methodology aims at life protection in its early period. Results of research carried out on animals are frequently the only base for early assessment of teratogenous influence of environmental pollutions on human health and life. In these research, for the ethical purposes, the experiments are frequently carried out on tissue cultures [2, 15]. In the view of the fact that proper organism functioning is influence by many, connected with each other factors, such as hormones, enzymes, psyche, charge and electromagnetic balance, it seems that far more reliable are the results obtained in research carried out on laboratory animals by the use of non invasive methods.

Chick embryo as a biological model system

The chick embryo has a long history as the biological model system [5, 12] that is frequently used in medical and environmental research. Numerous publications concerns the usage of a chick embryo as a model in research into infectious disease, viral (influenza 14, 30], toxoplasmosis [29], cowpox [16], Kaposi's sarcoma [34], AIDS [22]) as well as bacterial [1, 31], different types of turmous, such as glioma [6, 27], melanoma [26, 32], myeloma [9] and testing various pharmacological substances, such as Pseudolaric acid B [18], Baicalein [20], Apigenin [10]. Due to easiness of carrying out surgical manipulations and vast amount of information concerning chicken embryogenesis, the chic embryo has also served as a model in physiological studies of eye lens [5], genitals [21] and nervous system [25]. Spanel [33] reported applications of chick embryos to biomaterials testing. For years chick embryos have served as a model in research into influence of detrimental chemical substances, such as heavy metals (Cu-sulphate, Cd-sulphate [4], mercury [13], lead [7] or chlorine compounds (PCB 126 [11], TCDD [28]) and electromagnetic field (EMF) [17] on alive organisms. Such works are of great importance since people in the industrialized countries live in an environment of

ubiquitous EMF exposure, both natural and anthropogenic. The intensity, variety, and geographic distribution of anthropogenic EMF exposures have grown dramatically since the mid 20th century, with many uses serving, and in close proximity to, human populations, such as electric power distribution, radio and television transmission, and more recently, personal cell phone communication units and transmitting towers [3].

One of the earliest symptoms of biotic functions of the growing avian embryo is its cardiac work. By cardiac work monitoring it is possible to carry out non-invasive observation of the influence of different factors applied *in ovo* on developing embryo cardiac work. Although there exist a few methods of monitoring chick embryo cardiac work, it is non-contact ballistocardiography [8, 23] that seems to be the most accurate and noninvasive method. In this method the mechanical work of the heart is investigated on the basis of graphical registration of body movements induced by the heart [8, 19, 35]. Mechanical impulses resulting from cardiac work make the whole embryo body vibrate, which, in turn, results in micro vibrations of the whole egg.

Identification experiment

The measurements of growing chick embryo cardiac work were carried out by means of the non-invasive method presented in [35]. In this approach an eggshell with electric charges on it represents one capacitor plate, the other being a receiving antenna of the measuring equipment. The cardiac work of chick embryo induces micro-movements of the whole egg, resulting in changes in the distances between the plates and thus in the difference of potentials between the shell and the receiving antenna, which are registered by measuring equipment (Fig. 1).
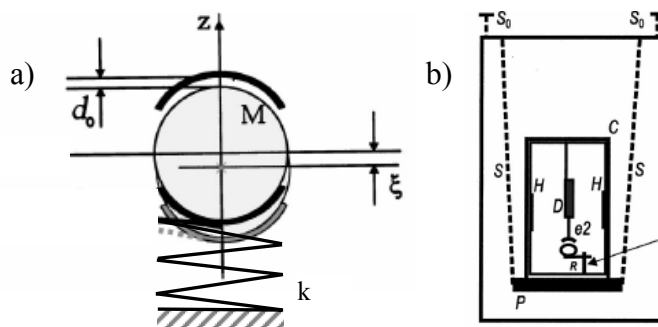
Fig. 1a) Idealized 'egg oscillator' [4], where M: the egg mass approximated by a sphere and firmly cradled at the end of a spring of stiffness k, ξ: displacements of the mass M center in the course of vertical oscillations, d_0: equilibrium distance between the top of the egg shell and the upper electrode, b) measurement set [4]: e_1, e_2: detection system electrodes, D: detector, R: suspension system, C: Faraday cage, H: heaters, P: heavy platform, S: 4 springs, S_0: 4 springs by which the cage is suspended to the laboratory ceiling.

The measuring set consists of the Faraday cage which holds two heaters, detector of electric field and a block of amplifiers, filters and an egg polarization system, supplier, vibration damper and acquisition data system (A/C card for PC computer) [24, 35]. During the measurements, each egg was taken out of the incubator and placed on an elastic suspension in the Faraday cage (Fig. 1b). In order to protect the caged embryo from thermal stress, cage air was heated to the incubator temperature. The measuring antenna of the ballistocardiograph was placed 2 [mm] from the eggshell surface. Each time the measurements were taken 4 minutes after the egg with an embryo was placed in Faraday cage, which aimed at minimization of possible interference in ballistocardiograms resulting from stress of moving an embryo into a new place, position, temperature and other physical conditions. A similar procedure was used by Pawlak et all. [24]. Polarized system was turned on, the signal from each egg was registered for 1,5 minutes, after which the egg was put back into the incubator.

Conclusions and final remarks

The paper concerns the non-invasive measurement method invented and still developed by authors, which is dedicated for measurements of low-amplitude vibrations induced by the work of avian embryo cardiac muscles. Methodology and the results of carried out analysis of signals measured on the chic embryos by means of the proposed method is presented in the paper under the same title (part II) that stands for the continuation of this paper.

Acknowledgements

References

1. R. Adam, S. Mussa, D. Lindemann, T.A. Oelschlaeger, M. Deadman, D.J. Ferguson, R. Moxon, H. Schroten, *The avian chorioallantoic membrane in ovo - a useful model for bacterial invasion assays*, Int. J. Med. Microbiol., **292** (2002) 267 - 75.
2. M. Amidi, S.G. Romeijn, G. Borchard, H.E. Junginger, W.E. Hennink, W. Jiskoot, *Preparation and characterization of protein-loaded N-trimethyl chitosan nanoparticles as nasal delivery system*, J. Control Release, **111** (2006) 107 - 116.
3. C.F. Blackman, *Can EMF exposure during development leave an imprint later in life*, Electromagn. Biol. Med., **25** (2006) 217 - 225.
4. P. Budai, S. Fejes, L. Varnagy, I.M. Somlyay, I. Takacs, *Teratogenicity test of dimethoate containing insecticide formulation and heavy elements (Cu, Cd) in chicken embryos after administration as single compounds or in combination*, Biol. Wet., **66** (2001) 885 - 889.
5. Y.X. Chen, C.E. Krull, L.W. Reneker, *Targeted gene expression in the chicken eye by in ovo electroporation*, Mol, Vis., **17** (2004) 874 - 883.
6. A. Cretu, J.S. Fotos, B.W. Little, D.S. Galileo, *Human and rat glioma growth, invasion, and vascularization in a novel chick embryo brain tumor model*, Clin. Exp. Metastasis, **22** (2005) 225 - 236.

7. I. Diana, A. Lurie, M. Diane, A. Brooks, C. Lincoln, B. Gray, *The effect of lead on the avian auditory brainstem*, Neurotoxicology, **27** (2006) 108 - 117.

8. A. Eblen-Zajjur, *A simple ballistocardiographic system for a medical cardiovascular physiology course*, Advan. Physiol. Edu., **27** (2003) 224 - 229.

9. P. Falardeau, P. Champagne, P. Poyet, C. Hariton, E. Dupont, *Neovastat, a naturally occurring multifunctional antiangiogenic drug, in phase III clinical trials*, Semin. Oncol., **28** (2001) 620 - 625.

10. J. Fang, Q. Zhou, L.Z. Liu, C. Xia, X. Hu, X. Shi, B.H. Jiang, *Apigenin inhibits tumor angiogenesis through decreasing HIF-1alpha and VEGF expression*, Carcinogenesis, **28** (2007) 858 - 864.

11. K.F. Goff, B.E. Hull, K.A. Grasman: *Effects of PCB 126 on primary immune organs and thymocyte apoptosis in chicken embryos*, J. Toxicol. Environ. Health A, **26** (2005) 485 - 500.

12. B.K. Han, J.N. Kim, J.H. Shin, J.K. Kim, D.H. Jo, H. Kim, J.Y. Han, *Proteome analysis of chicken embryonic gonads: identification of major proteins from cultured gonadal primordial germ cells*, Mol. Reprod. Dev., **72** (4) (2005) 521 - 529.

13. G.H. Heinz, D.J. Hoffman, S.L. Kondrad, C.A. Erwin, *Factors affecting the toxicity of methylmercury injected into eggs*, Arch. Environ. Contam. Toxicol., **50**(2) (2006) 264 - 279.

14. A. Helten, M. Marschall, A.J. Reininger, H. Meier-Ewert, *Experimental infection with a persistent influenza C virus variant leads to prolonged genome detection in the chicken lung,* Acta Virol., **40**(4) (1996) 223 - 226.

15. S.I. Kim, K.S. Kim, H.S. Kim, M.M. Choi, D.S. Kim, K.H. Chung, Y.S. Park, *Inhibition of angiogenesis by salmosin expressed in vitro*, Oncol. Res., **14**(4-5) (2004) 227 - 233.

16. G. Kochneva, I. Kolosova, T. Maksyutova, E. Ryabchikova, S. Shchelkunov, *Effects of deletions of kelch-like genes on cowpox virus biological properties*, Arch. Virol., **150**(9) (2005), 1857 - 1870.

17. M.S. Lahijani, M. Ghafoori, *Teratogenic effects of sinusoidal extremely low frequency electromagnetic fields on morphology of 24 hr chick embryos*, Indian J. Exp. Biol., **38**(7) (2000) 692 - 699.

18. M.H. Li, Z.H. Miao, W.F. Tan, J.M. Yue, C. Zhang, L.P. Lin, X.W. Zhang, J. Ding, *Pseudolaric acid B inhibits angiogenesis and reduces hypoxia-inducible factor 1alpha by promoting proteasome-mediated degradation*, Clin. Cancer Res., **10**(24) 2004 8266 - 8274.

19. A. Lindqvist, M. Halme, P. Tukiainen, L.A., *Amplitude variation in static-charge-sensitive bed signal increased in obstructive airways disease*, Clin. Physiol., 18 (1998) 369 - 376.

20. J.J. Liu, T.S. Huang, W.F. Cheng, F.J. Lu, *Baicalein and baicalin are potent inhibitors of angiogenesis: Inhibition of endothelial cell proliferation, migration and differentiation*, Int. J. Cancer, **106**(4) 2003 559 - 565.

21. J. Manner, D. Kluth, *A chicken model to study the embryology of cloacal exstrophy*, J. Pediatr. Surg., **38**(5) (2003) 678 - 681.

22. B. Mitta, C.C. Weber, M. Fussenegger, *In vivo transduction of HIV-1-derived lentiviral particles engineered for macrolide-adjustable transgene expression*, J. Gene. Med., **7**(11) 2005 1400 - 1408.

23. K. Pawlak, J. Niedziółka, *Non-invasive measurement of chick embryo cardiac work*, Czech J. Anim. Sc., **49**(1) (2004) 8–15.

24. K. Pawlak, J. Niedziółka, B. Tombarkiewicz, *The effect of long-term hypo- and hyperthermia on chick embryo cardiac work*, Electronic Journal of Polish Agricultural Universities, Environmental Development, **11**(2) (2007) - in print.

25. V. Pekarik, *Screening for gene function in chicken embryo using RNA and electroporation*, Nat. Biotechnol., **21**(1) (2003) 93 - 96.

26. F. Pernasetti, J. Nickel, D. Clark, P.A. Baeuerle, D. Van Epps, B. Freimark, *Novel anti-denatured collagen humanized antibody D93 inhibits angiogenesis and tumor growth: An extracellular matrix-based therapeutic approach*, Int. J. Oncol., **29**(6) (2006) 1371 - 1379.

27. L. Plasswilm, A. Tannapfel, N. Cordes, R. Demir, K. Hoper, J. Bauer, J. Hoper, *Hypoxia-induced tumour cell migration in an in vivo chicken model*, Pathobiology, **68**(3) 2000 99-105.

28. D.C. Powell, R.J. Aulerich, J.C. Meadows, D.E. Tillitt, J.P. Giesy, K.L. Stromberg, S.J. Bursian, *Effects of 3,3',4,4',5-pentachlorobiphenyl (PCB 126) and 2,3,7,8-tetrachlorodibenzo-p-dioxin (TCDD) injected into the yolks of chicken (Gallus domesticus) eggs prior to incubation*, Arch. Environ. Contam. Toxicol., **31**(3) 1996 404 - 409.

29. X. Que, A. Wunderlich, K.A. Joiner, S.L. Reed, *Toxopain-1 Is Critical for Infection in a Novel Chicken Embryo Model of Congenital Toxoplasmosis*, Infect. Immun., **72**(5) (2004) 2915–2921.

30. T. Saito, W. Lim, M. Tashiro, *Attenuation of a human H9N2 influenza virus in mammalian host by reassortment with an avian influenza virus*, Arch. Virol., **149**(7) (2004) 1397 - 1407.

31. K.H. Schmidt, J. Wiesner, D. Gerlach, W. Reichardt, J.H. Ozegowski, W. Kohler, *Susceptibility of chicken embryos to group A streptococci: correlation with fibrinogen binding*, FEMS Immunol. Med. Microbiol., **7**(3) (1993) 231 - 240.

32. N.V. Soucy, M.A. Ihnat, C.D. Kamat, L. Hess, M.J. Post, L.R. Klei, C. Clark, A. Barchowsky, *Arsenic stimulates angiogenesis and tumorigenesis in vivo*, Toxicol. Sci., **76**(2) 2003 271 - 279.

33. K. Spanel-Borowski, *The chick chorioallantoic membrane as test system for biocompatible materials*, Res. Exp. Med., **189**(1) 1989 69 - 75.

34. J.T. Stine, C. Wood, M. Hill, A. Epp, C.J. Raport, V.L. Schweickart, Y. Endo, T. Sasaki, G. Simmons, C. Boshoff, C. Clapham, Y. Chang, P. Moore, P.W. Gray, D. Chantry, *KSHV-encoded CC chemokine vMIP-III is a CCR4 agonist, stimulates angiogenesis, and selectively chemoattracts TH2 cells*, Blood, **95**(4) (2000) 1151-1157.

35. J.A. Szymański, K. Pawlak, *Capacitive detection of micromotions: Monitoring ballistics of a developing avian embryo*, Review of Scientific Instruments, **73**(9) (2002).

MODAL ANALYSIS OF PHYSIOLOGICAL MODEL OF AVIAN EMBRYOS – MODEL PARAMETER ESTIMATION (PART II)

Joanna IWANIEC[1], Marek IWANIEC[2], Krzysztof PAWLAK[3]

[1] Department of Robotics and Mechatronics,
[2] Department of Mechanics and Vibroacoustics,
AGH University of Science and Technology,
Mickiewicz Alley 30, 30-059 Krakow, Poland
[1] +48 (12) 617-31-28, jiwaniec@agh.edu.pl
[2] +48 (12) 617-35-09, iwaniec@agh.edu.pl
[3] Laboratory of Animal Hygiene,
Department of Poultry and Fur Animals Breeding and Animal Hygiene,
Agricultural University of Cracow,
Mickiewicz Alley 24/28, 30-059 Krakow, Poland
[3] +48 (12) 662-41-09, rzpawlak@cyfronet.pl

Abstract

The research carried out by authors aimed at inventing the sensitive non-invasive method for ethical investigation into the influence of chemical substances and physical factors on the growth of organisms in the prenatal phase. The knowledge of effects of chemical substances on the course of embryogenesis provides the possibility of testing new medicines and assessing the teratogenous influence of chemical substances already present in the natural environment on alive organisms. The results of the research are presented in the form of the series of two papers under the same title. The first paper, denoted as the part I, concerns the invented non-invasive method dedicated for measurements of low-amplitude vibrations induced by the work of cardiac muscles. The current paper (part II) is dedicated to vibration analysis of measured ballistocardiograps carried out by means of the classical LSCE modal analysis method. Due to the rapid increase in the cardiac muscle mass, the parameters of the biomechanical model of developing avian embryo are nonlinear. Nevertheless in a single measurement session the changes in the object parameters are negligible, which enables application of the classical modal analysis methods.

Key words: influence of detrimental substances on biotic functions, non-invasive ethical measurement method, ballistocardiography, modal analysis.

Introduction

Recently, methods of modal analysis [1, 2, 3, 4] are commonly applied to analysis of dynamic signals measured on technical objects such as machines, vehicles and bridges. Estimated results, so called modal models consisted of corresponding system natural frequencies, modal damping factors and mode shapes, are used as a basis for technical state assessing as well as introducing structural modifications aiming at improvement of system dynamic properties. In this paper, for the purposes of identification of natural frequencies of chick embryo heart contractions on the basis of cardiac time histories recorded during consecutive days of incubations, the LSCE (Polyreference **L**east **S**quares **C**omplex **E**xponential) frequency domain method of modal analysis was

chosen. According to the authors' knowledge, the results of modal analysis application to analysis of data measured on biological systems have not been published before.

Polyreference Least Squares Complex Exponential method (LSCE)

Polyreference **L**east **S**quares **C**omplex **E**xponential (LSCE) method is a multiple degree of freedom method providing global estimates of system poles and mode shapes. It consists in approximation of measured characteristics by the use of complex exponential functions [1, 4]. In order to introduce basic formulas used for modal parameters estimation, it is necessary to express the sampled impulse response in the modal coordinates:

$$[h(n\Delta t)] = [V]\left[e^{\lambda n\Delta t}\right][L] \tag{1}$$

where: $[V]$ – modal vector matrix, $[e^{\lambda n\Delta t}]$ – fundamental matrix, $[L]$ – modal participation factor matrix.
Single row of impulse response matrix equals [6]:

$$\{h(n\Delta)\}_m = \sum_{r=1}^{N}\left(\psi_{mr} z_r^n \{L_r\} + \psi_{mr}^* z_r^{n*} \{L_r^*\}\right), \quad z_r = e^{\lambda_r \Delta t} \tag{2}$$

Combinations of exponential function and modal participation factors $z_r\{L_r\}$ or $z_r^*\{L_r^*\}$ are the solution of differential equation of order p:

$$z_r^n \{L_r\}[I] + z_r^{n-1}\{L_r\}[W_1] + \ldots + z_r^{n-p}\{L_r\}[W_p] = \{0\} \tag{3}$$

where: $\left[W_1\right]^{N_i \times N_i}$, $\left[W_2\right]^{N_i \times N_i}$, N_i : number of applied excitations, $p \geq \dfrac{2N_m}{N_i}$: order

of differential equation, N_m : number of identified mode shapes.
Since the system impulse responses measured in the point m are the linear combination of equation (3) solutions, $z_r\{L_r\}$ and $z_r^*\{L_r^*\}$ are also a solution of this equation. Therefore:

$$[h(n\Delta t)]_m [I] + [h((n-1)\Delta t)]_m [W_1] + \ldots + [h((n-p)\Delta t)]_m [W_p] = [0] \tag{4}$$

For the equation (4) written for all the measurement points, by the use of the least squares method, it is possible to determine estimates of $[W_1]$, …, $[W_p]$ matrices. In the next step, estimates of matrices $[W_1]$, …, $[W_p]$ are inserted into the equation (3), resulting in formulation of the eigenvalue problem. System poles and corresponding mode shapes are obtained as a solution of eigenvalue problem. Presented method is one of the most often used methods of modal analysis and serves as a reference point for evaluating other methods [16].

Stabilization diagram method

Stabilization diagram method consists in observing system poles for increasing model order (Fig. 1b). The method allows the user to select poles interactively. It can be stated that a given pole is the true pole of the tested structure if the following conditions are satisfied:

− considered pole is stable with respect to the frequency, damping factor and modal vector (it is marked as 's' on the stabilization diagram),

− considered pole occurs at the frequency corresponding to maximum of the amplitude-frequency characteristic shown in the background.

The meaning of symbols used in the stabilization diagram is as follows: 's'- the pole is stable, 'v' - vibration frequency and modal vector are stable, 'd' - vibration frequency and damping factor are stable, 'f' - vibration frequency is stable, 'o' - the pole is unstable.
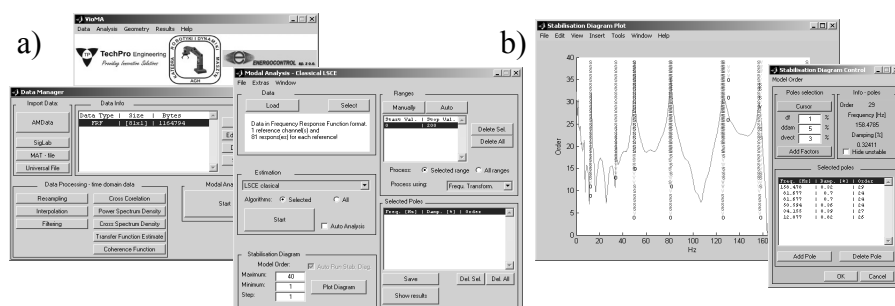
Fig. 1a) VIOMA toolbox for modal analysis, b) example of stabilization diagram.

Accuracy of system poles estimation depends on the measurement data quality, accuracy of the assumed analysis method, correct assumption of the modal model order as well as personal experience and intuition. For instance, as a result of analysis of noisy data or assumption of too high model order, apart from real system poles, so called computational poles can be estimated. Therefore nowadays, for the purposes of interpretation of stabilization diagrams estimated on the basis of data measured on complex systems in the presence of noisy background, supporting methods are used (e. g. balanced realization method used for identification and removing from stabilization diagrams poles that are computational, unstable or poorly represented in the measurement data, fuzzy logic methods applied to assessing which poles belong to a given pole line.

Discussion of obtained results

The analysis of chick embryo cardiac signals measured during consecutive days of incubation was carried out by the use of the procedure realising LSCE method, implemented in the VIOMA (**V**irtual **I**n-**O**peration **M**odal **A**nalysis) toolbox dedicated for Matlab environment (Fig. 1a). Below there are presented results of modal analysis

carried out for data measured on two chick embryos from the 9th day of incubation up to chick hatching in the 21st day of incubation. Values of natural frequencies estimated on the basis of measured ballistocardiographs are gathered in the Table 1.

f	9 day	10 day	11 day	12 day	13 day	14 day	15 day
1	-	-	-	-	-	-	-
2	-	18,800	19,410	17,945	17,132	18,760	17,350
3	21,361	-	-	22,811	20,912	-	22,055
4	-	23,416	23,553	-	-	23,429	-
5	29,019	28,251	28,960	27,401	26,178	26,316	26,613
6	34,373	-	-	36,376	32,061	34,310	-
7	39,114	-	-	-	-	-	-
8	-	-	45,435	-	46,430	44,790	41,250
9	52,814	55,703	-	55,866	56,573	-	56,286
10	58,501	-	57,454	-	-	58,232	-
11	62,920	-	-	63,985	64,834	63,025	61,638
12	-	67,686	67,155	67,952	68,330	65,907	65,810
13	-	71,662	78,824	-	78,268	75,108	-
14	83,615	-	-	-	85,327	80,576	83,164
15	-	-	-	90,098	96,975	92,806	97,530
16	101,843	104,943	99,846	105,531	103,855	102,842	106,59
17	-	-	108,369	115,138	114,253	109,184	111,677
18	-	-	-	-	123,392	121,121	-
	16 day	17 day	18 day	19 day	20 day	21 day	21 day
1	-	12,9083	-	-	-	-	-
2	17,038	17,176	17,100	16,079	15,935	16,191	-
3	20,509	22,0867	21,230	20,021	20,998	22,061	-
4	23,565	24,8278	25,487	23,920	24,952	24,172	-
5	30,486	29,9154	29,952	27,895	27,517	26,748	-
6	37,825	-	-	32,978	32,165	30,226	-
7	-	-	-	-	-	-	-
8	45,359	-	-	-	-	-	-
9	56,779	56,1962	-	53,541	-	52,652	-
10	59,431	-	57,451	-	57,595	56,735	-
11	-	-	62,437	-	-	61,959	-
12	65,579	64,318	68,771	-	65,832	-	-
13	73,677	71,8507	73,472	72,592	71,410	70,947	-
14	83,334	82,4109	84,056	81,647	81,417	87,683	-
15	95,877	98,4129	95,050	93,584	96,714	96,351	-
16	101,127	106,741	105,662	104,548	103,321	100,181	-
17	110,198	-	109,564	115,037	115,667	109,537	-
18	119,996	120,825	121,251	123,201	121,492	124,148	-

Table 1. The first 18 natural frequencies estimated by the LSCE method during consecutive days of incubation.

Graphical interpretation of the estimated results gathered in the Table 1 is presented in the form of Fig. 2a and Fig. 2b.
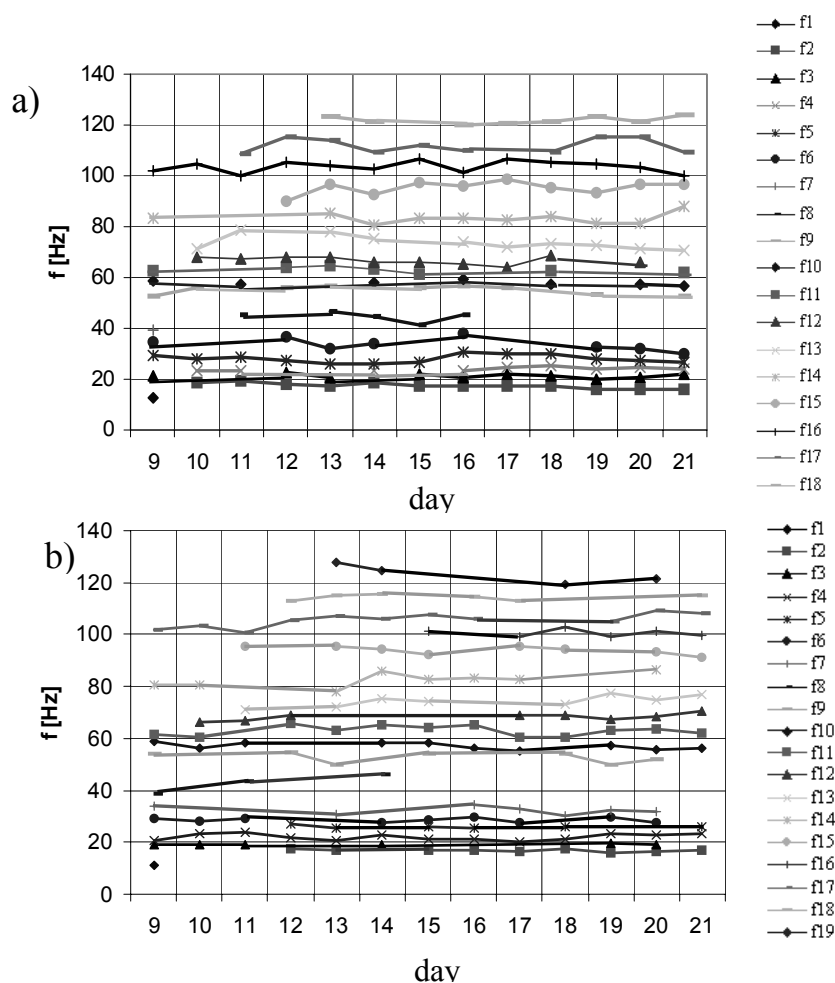
Fig. 2. Changes in natural frequencies during consecutive days of incubation, measurements taken on the chosen 2 eggs.

While analysing the cardiac signals measured on different chick embryos, the examples of which are presented in Fig. 2a and Fig. 2b, the following regularities were observed:

- According to the progress of embryogenesis higher natural frequencies appear,
- Once observed natural frequencies are present in the signal up to the chick hatching in the 21st day of incubation; the only exception to this rule is natural frequency of

40 [Hz], which appears between 9th and 11th day of incubation and fades between 14th and 16th day of incubation.
- Values of low natural frequencies are close to each other while the higher natural frequencies are wider spaced and well separated.
- Values of identified natural frequencies remains almost unchanged during the whole period of incubation; computed 3-point moving average trends are almost linear.

Conclusions and final remarks

The paper concerns analysis of the chick embryo ballistographs measured by means of the method proposed by authors that was presented in the paper under the same title denoted as part I. Analysis was carried out by means of the LSCE classical modal analysis method for cardiac signals registered from 9th to 21st day of incubation in measurement session lasting 10 to 40 minutes.

The changes in the time histories and values of forces generated by beating heart resulted in the changes of modal model parameters estimated in the consecutive days of incubation. Some natural frequencies and corresponding mode shapes evolve and change their values, decay or appear. This variability can be observed in the daily time scale.

Observed regularities of changes in the values of natural frequencies in the consecutive days of incubation can be used as a basis for assessing the influence of tested substances, such as medicines, environmental pollutions and detrimental substances, on avian embryo biotic functions.

The results obtained for many eggs reveled surprisingly small changes in values of observed modal parameters. One of the possible explanations is that the very rapid growth and formation of hart occurs in the early stage of incubation. So the future efforts will be aimed at the improvement of the device sensitivity and moving the observations towards the earlier days of prenatal live.

Acknowledgements

References

1. W. Heylen, S. Lammens, P. Sas, *Modal Anlysis Theory and Testing*, KUL, Leuven, 1997.
2. N.M.M. Maia, J.M.M. Silva, *Theoretical and Experimental Modal Analysis*, Research Studies Press LTD, Taunton, 1997.
3. T. Uhl, W. Lisowski, P. Kurowski, *In–operation modal analysis and its applications* (in Polish), Department of Robotics and Mechatronics, AGH, Krakow, 2001.
4. T. Uhl, *Computer aided identification of mechanical structure models* (in Polish), WNT, Warsaw, 1997.

MOTION EQUATIONS FOR CONTINUOUS MEDIA AND FOR RIGID BODIES

Janusz JANKOWSKI
Poznan University of Technology
Institute of Applied Mechanics
Piotrowo 3, 60- 965 Poznań
061 665-20-21, fax. (061) 665-23-07
E-mail: janusz.jankowski@put.poznan.pl

Abstract

Rigid condition plays an essential role in creating of motion equations for the body. The basic principles of balance, concerned with the global behavior of the body, translate in various forms when they are applied to the rigid body dynamics and to the continuum media theory. On the other hand, just for a rigid body the principles of balance of momentum and moment of momentum take some various forms when are applied to the chosen poles of reduction.

Keywords: rigid body, continuous media, basic principles, stiffness condition

Introduction

The theory of continuous media is concerned with the global behavior of bodies under the influence of external disturbances. A satisfactory training in this field requires the study of the interrelations among external agents and the response of the medium. The external agents that produce changes in the state of the medium may appear in the form of surface and body forces. The nature of these agents, the laws governing them, their mathematical characterization, and the physical measurements of the external effects must be an integral part of study in the rigid body dynamics and in the theory of continuous media. In engineering, the ultimate interest lies in predicting the way in which a medium responds to the external load. In this input-output relationship, the physical model assumed for the constitution of the body occupies a central position. The unified approach to the study of the global behavior of materials consists of, first, a thorough study basic principles common to all media and, second, a clear demonstration of the types of media (such as the solid, rigid body, etc.) within the structure of the theory. The theory so constructed makes available methods, which are useful in the creation of new fields of research. In the exact theories one finds not only a satisfying permanence but also an aesthetic structure that is fundamental to all basic research. Exact theories are frequently criticized for the mathematical difficulties they present in the treatment of nontrivial engineering problems. This objection is balanced, however, by the simplicity of the exact theories. The basic principles are: conservation of mass, balance of momentum and balance of moment of momentum. These are the fundamental axioms essential in the construction of the foundations of the theory.

1. Basic principles of balance

Let a model of the body occupies a region Ω in a 3D space. The position of a place $A \in \Omega$ in this region is denoted by a vector **x** that extends from an origin O of the

coordinate system $O_1 \mathbf{e}_2 \mathbf{e}_3 \mathbf{e}$ to the point A. The manifold $\partial\Omega = \overline{\Omega} \setminus \Omega$ will be called boundary. The position of a place $N \in \partial\Omega$ on the boundary referred to the coordinate system $O_1 \mathbf{e}_2 \mathbf{e}_3 \mathbf{e}$ is denoted by a vector $\mathbf{y}$. Similarly, let a model of the time occupies a range $(0, \infty)$ in a 1D space. The position of an instant $t \in (0, \infty)$ in this range is a real number. The manifold $\{0\} = \overline{(0, \infty)} \setminus (0, \infty)$ will be called initial instant.

In classical mechanics, with each body we associate a measure called mass. It is nonnegative and additive, and it is invariant under the motion. If this measure is absolutely continuous, then there exists a density $\rho(\mathbf{x})$ of the position of a place $A \in \Omega$. The function ρ is called mass density. The total mass m of the body is then found by

$$m = \int_\Omega \rho(\mathbf{x}) \cdot d\mathbf{x}. \tag{1}$$

The axiom of mass conservation states that the mass is invariant under the motion:

$$\dot{m}(t) = 0, \quad t \in (0, \infty),$$
$$m(0) = \widetilde{m}, \tag{2}$$

where $\widetilde{m}$ is initial total mass, and dot defines material derivative.

Velocity is the time rate of change of position of a given place $A \in \Omega$

$$\dot{\mathbf{x}}(A) = \mathbf{g}(\mathbf{x}, t), \quad t \in (0, \infty) \tag{3}$$

Note that the velocity is defined locally. In order to express the momentum $\mathbf{p}$ and moment of momentum $\mathbf{k}$ by the velocity we must take into account the mass density [1]

$$\mathbf{p}(t; \mathbf{0}) = \int_\Omega \rho(\mathbf{x}) \mathbf{g}(\mathbf{x}, t) d\mathbf{x}, \quad t \in (0, \infty) \tag{4}$$

$$\mathbf{k}(t; \mathbf{0}) = \int_\Omega \rho(\mathbf{x}) \mathbf{x} \times \mathbf{g}(\mathbf{x}, t) d\mathbf{x}, \quad t \in (0, \infty) \tag{5}$$

To the basic principle of mass conservation we add two other important axioms of mechanics. The axiom of global momentum conservation states that the time rate of change of momentum is equal to the resultant force $\mathbf{W}$ of both passive and active load on the free- body diagram:

$$\dot{\mathbf{p}}(t; \mathbf{0}) = \mathbf{W}(t; \mathbf{0}), \quad t \in (0, \infty),$$
$$\mathbf{p}(0; \mathbf{0}) = \widetilde{\mathbf{p}}, \tag{6}$$

Here $\widetilde{\mathbf{p}}$ is initial momentum vector of the body, $\mathbf{0}$ is position of an origin O. Axiom (3) constitutes principle of balance of momentum about O.

The axiom of global moment of momentum conservation states that the time rate of change of moment of momentum is equal to the resultant moment $\mathbf{M}$ of both passive and active load on the free-body diagram:

$$\dot{\mathbf{k}}(t; \mathbf{0}) = \mathbf{M}(t; \mathbf{0}), \quad t \in (0, \infty),$$
$$\mathbf{k}(0; \mathbf{0}) = \widetilde{\mathbf{k}}. \tag{7}$$

Here $\widetilde{\mathbf{k}}$ is initial moment of momentum of the body. Axiom (6) constitutes principle of balance of moment of momentum about O. Equation (6), like (7), is a balance equation.

The deep significance of the foregoing two basic principles of continuous media may be better appreciated after the development of the concept of stress.

2. Equations of motion for continuous media

The basic principles are valid for all materials irrespective of their constitution. It is therefore expected that their mathematical expressions are not sufficient to predict uniquely the behaviour of the body. In order to take account of the nature of different materials, we must find additional characteristics of the substance with respect to the response sought. This is done by introducing models appropriate to the particular class of phenomena under scrutiny. There exist certain rules and invariants requirements [1, p. 136], which must be satisfied by such models. It remains acceptable until the phenomena predicted by the theory do not agree with the experiments.

Global mass conservation when applied to an infinitesimal neighbourhood of a place $A \in \Omega$ implies local mass conservation:

$$\frac{\partial}{\partial t}\rho(\mathbf{x},t) + div[\rho(\mathbf{x},t)\mathbf{g}(\mathbf{x},t)] = 0, \quad (\mathbf{x},t) \in \Omega \times (0,\infty),$$

$$\rho(\mathbf{x},0) = \widetilde{\rho}(\mathbf{x}), \quad \mathbf{x} \in \Omega, \tag{8}$$

$$\rho(\mathbf{y},t)\mathbf{g}(\mathbf{y},t) \circ \mathbf{n}(\mathbf{y},t) = \widetilde{j}(\mathbf{y},t), \quad (\mathbf{y},t) \in \partial\Omega \times (0,\infty).$$

Here $\mathbf{n}$ is outside normal to the boundary, $\widetilde{\rho}$ is field of initial mass density distribution in the region, $\widetilde{j}$ is initial mass flow on the boundary, and cross means Cartesian set product. Formula (8) is the initial-boundary value problem for the unknown function ρ.

Forces and moments create load in mechanics, but are not defined. The force $\mathbf{W}$ and the couple $\mathbf{M}$ acting on a body are vector quantities known a priori. The resultant force $\mathbf{W}$ consists of the vector sum of all forces acting on the body. The resultant moment $\mathbf{M}$ is the sum of the moment of the individual forces about O and the sum of all concentrated couples. The internal loads create a system of surface forces $\mathbf{t}(\mathbf{x},t;\mathbf{m})$ called stress vectors. They depend not only on the vector $\mathbf{x}$ of the place $A \in \Omega$ on the surface under consideration and the time instant t, but also on the exterior normal $\mathbf{m}$ to the surface at the place. On the boundary they become external surface tractions $\widetilde{\mathbf{t}}(\mathbf{y},t;\mathbf{n})$.

Let $\mathbf{b}$ be the body force per unit mass. Then the resultant force and the resultant moment acting on the body about the origin O are given by [1, p.96]

$$\mathbf{W}(t;\mathbf{0}) = \int_{\Omega} \rho(\mathbf{x})\mathbf{b}(\mathbf{x},t)d\mathbf{x} + \oint_{S} \mathbf{t}(\mathbf{x},t;\mathbf{m})d\sigma, \quad t \in (0,\infty) \tag{9}$$

$$\mathbf{M}(t;\mathbf{0}) = \int_{\Omega} \rho(\mathbf{x})\mathbf{x} \times \mathbf{b}(\mathbf{x},t)d\mathbf{x} + \oint_{S} \mathbf{x} \times \mathbf{t}(\mathbf{x},t;\mathbf{m})d\sigma, \quad t \in (0,\infty) \tag{10}$$

Here S is material surface. The stress vector acting on any plane through a place is fully characterized as a linear function of the stress tensor $\mathbf{T}$ at the place. Applying the Green- Gauss theorem to convert surface integrals into volume integrals in (9), we get a necessary and sufficient condition for the local balance of momentum:

$$\hat{\rho}\dot{\mathbf{g}}(\mathbf{x},t) = \hat{\rho}\mathbf{b}(\mathbf{x},t) + div\mathbf{T}(\mathbf{x},t), \quad (\mathbf{x},t) \in \Omega \times (0,\infty),$$

$$\mathbf{g}(\mathbf{x},0) = \tilde{\mathbf{v}}(\mathbf{x}), \quad \mathbf{x} \in \Omega, \tag{11}$$

$$\mathbf{T} \circ \mathbf{n}(\mathbf{y},t) = \tilde{\mathbf{t}}(\mathbf{y},t;\mathbf{n}), \quad (\mathbf{y},t) \in \partial\Omega \times (0,\infty).$$

Here $\tilde{\mathbf{v}}$ is field of initial velocity distribution in the region. Partial differential equations in (11) contain some differential operators with respect to time and space. That is why the motion of the body has to be determined from initial boundary value problem (11). Applying the Green- Gauss theorem to convert surface integrals into volume integrals in (10), we get a necessary and sufficient condition for the local balance of moment of momentum, when the momentum is locally balanced:

$$\mathbf{T}^{T}(\mathbf{x},t) = \mathbf{T}(\mathbf{x},t), \quad (\mathbf{x},t) \in \Omega \times (0,\infty). \tag{12}$$

The formulae (11,12) are respectively the first and the second laws of motion of Cauchy. We can see that the necessary and sufficient condition for the local balance of moment of momentum is the symmetry of the stress tensor. Therefore we have only six independent stress components. Consequently the left and right mixed components of the stress tensor are the same.

3. Role of mass center and moment of inertia in rigid body dynamics

Let we consider a body model, which takes the region Ω, and the distance (in Euclidean metric) between places $A, B \in \Omega$ is a time function:

$$d(A,B) = f(t;\ A,\ B), \quad t \in (0,\infty). \tag{13}$$

If f is constant function for any places $A, B \in \Omega$, then body model is called rigid body. The axiom of mass conservation states that the total mass is invariant under the motion:

$$m(t) \equiv \tilde{m}, \quad t \in (0,\infty). \tag{14}$$

Absolute motion in reference system with coordinate system $O_1\mathbf{e}_2\mathbf{e}_3\mathbf{e}$ can be described locally for chosen both place $A \in \Omega$ and instant $t \in (0,\infty)$ with two mathematical objects: rotation matrix $\Re$ and position vector $\mathbf{x}$ connecting point O with the place A Absolute linear velocity $\mathbf{v}(A)$ of the place A is time derivative of $\mathbf{x}$ vector. Following the Chasles theorem [3, p.329] rotation of rigid body can be described by absolute angular velocity $\boldsymbol{\omega}(A)$. Finally the rigid body motion can be determined locally by two functions of time

$$\mathbf{v}(A) = \mathbf{g}(\mathbf{x},t), \quad \boldsymbol{\omega}(A) = \mathbf{h}(\mathbf{x},t), \quad t \in (0,\infty). \tag{15}$$

Global properties of motion can be described kinematically by the stiffness condition:

$$\mathbf{v}(B) = \mathbf{v}(A) + \boldsymbol{\omega}(A) \times \mathbf{AB}, \quad \boldsymbol{\omega}(B) = \boldsymbol{\omega}(A), \quad A, B \in \Omega. \tag{16}$$

Formulae (15,16) exhaust the rigid body kinematics. In particular, if:

$$\mathbf{h}(\mathbf{x},\ t) = 0, \quad t \in (0,\infty), \tag{17}$$

then the rigid body will be called particle. Rigid body dynamics is described by the formulae (4-7). They are of a global character, invariant of the place in the region. Note that the absolute angular velocity does not appear in the formulae (4-7). That means that

the particle dynamics is the same as the rigid body dynamics. Absolute linear velocity is an unknown function in (4,5). That makes impossible to execute an integration procedure. We therefore have the stiffness condition to lead out the unknown vectors in front of integral signs. Let us now denote a set of points in the space that fulfils the stiffness condition (16) by $\hat{\Omega}$. Then the principles of balance of both momentum and moment of momentum about $B \in \hat{\Omega}$ take the form:

$$\mathbf{p}(t;B) = m\mathbf{g}(\widetilde{\mathbf{x}},t) + \mathbf{h}(\widetilde{\mathbf{x}},t) \times \mathbf{S}(B), \quad t \in (0,\infty) \tag{18}$$

$$\mathbf{k}(t;B) = \mathbf{S}(B) \times \mathbf{g}(\widetilde{\mathbf{x}},t) + \mathbf{J}(B) \circ \mathbf{h}(\widetilde{\mathbf{x}},t), \quad t \in (0,\infty) \tag{19}$$

Here $\widetilde{\mathbf{x}}$ is the position vector for the place B, and the notations correspond to:

$$\mathbf{S}(B) \equiv \int_{\Omega} \rho(\mathbf{x})(\mathbf{x} - \widetilde{\mathbf{x}})d\mathbf{x} \tag{20}$$

$$\mathbf{J}(B) \circ \mathbf{h} \equiv \int_{\Omega} \rho(\mathbf{x})(\mathbf{x} - \widetilde{\mathbf{x}}) \times [\mathbf{h} \times (\mathbf{x} - \widetilde{\mathbf{x}})]d\mathbf{x} \tag{21}$$

Formulae (20,21) represent the following mathematical objects: static moment $\mathbf{S}$ and moment of inertia $\mathfrak{I}$ with respect to the reduction pole $B \in \hat{\Omega}$. They are also called the mass moments, first and second kind properly. Note that the moment of inertia is the tensor and only the scalar product gives a vector (21) in result [4, p.382]. The mass moments depend on the time instant, and so is why the motion equations have very complicated coupled form:

$$m\dot{\mathbf{g}}(\widetilde{\mathbf{x}},t) + \frac{d}{dt}[\mathbf{h}(\widetilde{\mathbf{x}},t) \times \mathbf{S}(B)] = \mathbf{W}(t;B), \quad t \in (0,\infty),$$
$$m\mathbf{g}(\widetilde{\mathbf{x}},0) + \mathbf{h}(\widetilde{\mathbf{x}},0) \times \mathbf{S}(B) = \widetilde{\mathbf{p}}, \tag{22}$$

$$\frac{d}{dt}[\mathbf{S}(B) \times \mathbf{g}(\widetilde{\mathbf{x}},t) + \mathfrak{I}(B) \circ \mathbf{h}(\widetilde{\mathbf{x}},t)] = \mathbf{M}(t;B), \quad t \in (0,\infty),$$
$$\mathbf{S}(B) \times \mathbf{g}(\widetilde{\mathbf{x}},0) + \mathfrak{I}(B) \circ \mathbf{h}(\widetilde{\mathbf{x}},0) = \widetilde{\mathbf{k}}. \tag{23}$$

Here the initial conditions are coupled also. For the particle we have:

$$m\dot{\mathbf{g}}(\widetilde{\mathbf{x}},t) = \mathbf{W}(t;B), \quad t \in (0,\infty),$$
$$m\mathbf{g}(\widetilde{\mathbf{x}},0) = \widetilde{\mathbf{p}}, \tag{24}$$

$$\frac{d}{dt}[\mathbf{S}(B) \times \mathbf{g}(\widetilde{\mathbf{x}},t)] = \mathbf{M}(t;B), \quad t \in (0,\infty),$$
$$\mathbf{S}(B) \times \mathbf{g}(\widetilde{\mathbf{x}},0) = \widetilde{\mathbf{k}}. \tag{25}$$

The moment of inertia has no influence on the movement of the particle. Formula (25) describes the changes of the particles moment of momentum that can be caused by the resultant moment acting on the body, or by the initial moment of momentum.

We can choose a moving frames of motion $O_1\mathbf{f}_1\mathbf{f}_2\mathbf{f}_3$ that rotating with the rigid body together. Then the formulae (22,23) take the form:

$$m\dot{\mathbf{g}}(\widetilde{\mathbf{x}},t) + \dot{\mathbf{h}}(\widetilde{\mathbf{x}},t) \times \mathbf{S}(B) = \mathbf{W}(t;B), \quad t \in (0,\infty),$$
$$m\mathbf{g}(\widetilde{\mathbf{x}},0) + \mathbf{h}(\widetilde{\mathbf{x}},0) \times \mathbf{S}(B) = \widetilde{\mathbf{p}}, \tag{26}$$

$$\mathbf{S}(B) \times \dot{\mathbf{g}}(\widetilde{\mathbf{x}}, t) + \Im(B) \circ \dot{\mathbf{h}}(\widetilde{\mathbf{x}}, t) = \mathbf{M}(t; B), \quad t \in (0, \infty),$$
$$\mathbf{S}(B) \times \mathbf{g}(\widetilde{\mathbf{x}}, 0) + \Im(B) \circ \mathbf{h}(\widetilde{\mathbf{x}}, 0) = \widetilde{\mathbf{k}}.$$
(27)

We can remove the coupling of the initial-value problems for the rigid body, if we are writing the principles of balance of both momentum and moment of momentum about $C \in \hat{\Omega}$ so well chosen that $\mathbf{S}(C) = \mathbf{0}$:

$$\mathbf{v}(C) = \frac{d}{d(m \cdot t)} \int_{\Omega} \rho(\mathbf{x}) \mathbf{x} \, d\mathbf{x} = \mathbf{v}(B) + \boldsymbol{\omega}(B) \times \mathbf{BC}, \quad \boldsymbol{\omega}(C) = \boldsymbol{\omega}(B), \quad B \in \Omega. \quad (28)$$

Then the initial-value problems (22,23) become uncoupled:

$$m\dot{\mathbf{g}}(\hat{\mathbf{x}}, t) = \mathbf{W}(t; C), \quad t \in (0, \infty), m\mathbf{g}(\hat{\mathbf{x}}, 0) = \widetilde{\mathbf{p}}, \quad (29)$$

$$\frac{d}{dt} \left[\Im(B) \circ \mathbf{h}(\hat{\mathbf{x}}, t) \right] = \mathbf{M}(t; B), \quad t \in (0, \infty),$$
$$\Im(B) \circ \mathbf{h}(\hat{\mathbf{x}}, 0) = \widetilde{\mathbf{k}}.$$
(30)

Here $\hat{\mathbf{x}}$ is the position vector for the place C. The reduction pole $C \in \hat{\Omega}$ is called mass center. Analogously we get an uncoupled shape of the initial-value problems (26,27). Note that the initial-value problems (24,25) for the particle takes diametrically opposed views, when the reduction pole is the mass center $C \in \hat{\Omega}$:

$$m\dot{\mathbf{g}}(\hat{\mathbf{x}}, t) = \mathbf{W}(t; C), \quad t \in (0, \infty), m\mathbf{g}(\hat{\mathbf{x}}, 0) = \widetilde{\mathbf{p}}, \quad (31)$$

$$\mathbf{0} = \mathbf{M}(t; C), \quad t \in (0, \infty). \quad (32)$$

The equation (32) is the equilibrium equation for the couple resultant about a place $C \in \hat{\Omega}$ for the rigid body.

4. Conclusions

In this paper we have determined the motion equations and the associated mass conservation law to the rigid body and continuous medium. The shapes of the equations follow from the ways of translating the global basic principles of balance for the body into some local ones. It leads to the initial-boundary value problems for the continuous media and to the initial value problems for the rigid bodies.

References

1. A. C. Eringen, *Nonlinear theory of continuous media,* McGraw- Hill Book Co., New York, 1962.
2. W. Kosiński, *Wstęp do teorii osobliwości pola i analizy fal,* PWN Warszawa- Poznań, 1981.
3. S. Banach, *Mechanika,* PWN Warszawa, 1956.
4. E. Karaśkiewicz, *Zarys teorii wektorów i tensorów,* PWN Warszawa, 1975.

DYNAMIC CONSTRAINTS LOAD FOR CONNECTED RIGID BODIES

Janusz JANKOWSKI

Piotr KĘDZIA

Poznan University of Technology

Institute of Applied Mechanics

Piotrowo 3, 60- 965 Poznań

061 665-20-21, fax. (061) 665-23-07

E-mail: janusz.jankowski@put.poznan.pl

piotr.kedzia@doctorate.put.poznan.pl

Abstract

This article presents the foundations of Newton-Euler rigid body dynamics and its generalized forms in the light of the load reduction principle. We prove that most of the features of dynamics may be directly deduced from this principle and that some generalizations on a system of rigid bodies are acceptable.

Keywords rigid body systems, constraints load, moment of momentum

Introduction

The principle of load reduction has played an important role in statics. On the one hand, as soon as we consider the principle of momentum and want to strictly preserve its form, the well-known vector addition is not dependent of the reductions pole. On the other hand, to express the laws of rigid body dynamics with respect to both possible independence motions: translations and rotations necessitates of the effect of a moment of momentum on the mathematical representation of forces and moments appearing to the motion equations. This is actually the role of an axiom stating that momentum and moment of momentum are quantities on equal terms and, in a consistent theory, the motion equations must concern the same reductions pole in the principles of momentum and moment of momentum. The remark extends to dynamics of rigid body systems with Euler equations for rotations. To clarify this matter it is inevitable to return to the interpretation of the motion equations not only for particles but also for realistic models of mechanisms, with forces and torques, what is much more complicated.

1. Rigid body dynamics

Let the body model takes the region Ω in 3D Euclidean space Z. Element $A \in \Omega$ of the region is called the place. Interval $(0, \infty)$ of the real numbers in 1D space R is called time, and its element $t \in (0, \infty)$ is called instant. Set $\{0\} = \overline{(0, \infty)} \setminus (0, \infty)$ will be called initial instant. The distance (in Euclidean metric) between places $A, B \in \Omega$ is a time function:

$$d(A, B) = f(t), \quad t \in (0, \infty). \tag{1}$$

If f is constant function for any places $A, B \in \Omega$, then body model is called rigid body. Ruthless motion in reference system with Cartesian coordinate system $O_{,\mathbf{e}_2\mathbf{e}_3\mathbf{e}}$ can be described locally for chosen both place $A \in \Omega$ and instant $t \in (0, \infty)$ with two mathematical objects: rotation matrix $\mathfrak{R}$ and position vector $\mathbf{x}$ connecting point O with the place A. Absolute linear velocity $\mathbf{v}(A)$ of the place A is time derivative of $\mathbf{x}$ vector. Following the Chasles theorem [1, p.329] rotation of rigid body can be described by absolute angular velocity $\boldsymbol{\omega}(A)$. Finally the rigid body motion can be determined by two functions of time

$$\mathbf{v}(A) = \mathbf{g}(\mathbf{x}, t), \quad \boldsymbol{\omega}(A) = \mathbf{h}(\mathbf{x}, t), \quad t \in (0, \infty). \tag{2}$$

If $\mathbf{h}$ is the zero function, then the body will be called particle.
Global properties of rigid body motion can be described kinematically by stiffness condition

$$\mathbf{v}(B) = \mathbf{v}(A) + \boldsymbol{\omega}(A) \times \mathbf{AB}, \quad \boldsymbol{\omega}(B) = \boldsymbol{\omega}(A), \quad A, B \in \Omega. \tag{3}$$

Inertial properties of the body dynamics is determined with the momentum- velocity relation:

$$\mathbf{p}(t; O) = \int_{\Omega} \rho(\mathbf{x}) \mathbf{g}(\mathbf{x}, t) \, d\mathbf{x}, \quad t \in (0, \infty), \tag{4}$$

$$\mathbf{k}(t; O) = \int_{\Omega} \mathbf{x} \times \rho(\mathbf{x}) \mathbf{g}(\mathbf{x}, t) \, d\mathbf{x}, \quad t \in (0, \infty), \tag{5}$$

where: $\mathbf{p}$ - momentum, $\mathbf{k}$ - moment of momentum, ρ - mass density. Rigid body dynamics can be characterize globally by the influence of all of forces and moments acting in an active and passive way on the model of the body. The definition of equipollent force systems correctly suggests that we may replace any system, no matter how complicated, by a force $\mathbf{W}$ named the total force and a couple $\mathbf{M}$ named the total moment at any place O named the reduction pole. The force-couple pair, $\mathbf{W}$ and $\mathbf{M}$ is called a resultant of load system. The influence all of the passive and active loads on the movement of the body is characterized by a momentum $\mathbf{p}$ and a moment of momentum $\mathbf{k}$ changes:

$$\begin{aligned} \dot{\mathbf{p}}(t; O) &= \mathbf{W}(t; O), \quad t \in (0, \infty), \\ \mathbf{p}(0; O) &= \widetilde{\mathbf{p}}, \end{aligned} \tag{6}$$

$$\begin{aligned} \dot{\mathbf{k}}(t; O) &= \mathbf{M}(t; O), \quad t \in (0, \infty), \\ \mathbf{k}(0; O) &= \widetilde{\mathbf{k}}. \end{aligned} \tag{7}$$

Here $\widetilde{\mathbf{p}}$ is an initial momentum of the rigid body, $\widetilde{\mathbf{k}}$ is an initial moment of momentum and the dot over a vector sign means the time derivative. Rigid body motion is specified here in the place O. The equations (6,7) have got some global character. It means there

are defined place independent for the region. Ordinary differential equations, whose unknowns are vector functions of the single time variable, appear as a side effect. A primary aim of the rigid body dynamics is to find the solutions of initial value problems (6,7). At this point it is reasonable to wonder why there is no absolute angular velocity in the equations (4,5). The reason is that the relationship between linear and angular velocities can be found in the stiffness condition (3).

2. Moments of mass

The set of the points in space Z kinematically connected with the region by the stiffness condition will be denoted by $\hat{\Omega}$. To avoid the procedure of solving integral equations (4,5) we use (3). Thus, we can write the relations (6, 7) in the reduction pole $B \in \hat{\Omega}$:

$$\mathbf{p}(t;B) = m\mathbf{g}(\widetilde{\mathbf{x}},t) + \mathbf{h}(\widetilde{\mathbf{x}},t) \times \mathbf{S}(B), \quad t \in (0,\infty), \tag{8}$$

$$\mathbf{k}(t;B) = \mathbf{S}(B) \times \mathbf{g}(\widetilde{\mathbf{x}},t) + \Im(B) \circ \mathbf{h}(\widetilde{\mathbf{x}},t), \quad t \in (0,\infty), \tag{9}$$

where $\widetilde{\mathbf{x}}$ is the position vector for B. Here we introduced the following denotations:

$$m = \int_{\Omega} \rho(\mathbf{x}) \, d\mathbf{x}, \tag{10}$$

$$\mathbf{S}(B) = \int_{\Omega} (\mathbf{x} - \widetilde{\mathbf{x}}) \rho(\mathbf{x}) \, d\mathbf{x}, \tag{11}$$

$$\Im(B) \circ \mathbf{h}(\widetilde{\mathbf{x}},t) = \int_{\Omega} (\mathbf{x} - \widetilde{\mathbf{x}}) \times [\mathbf{h}(\widetilde{\mathbf{x}},t) \times (\mathbf{x} - \widetilde{\mathbf{x}})] \rho(\mathbf{x}) \, d\mathbf{x}. \tag{12}$$

The formulae (10-12) are mass of the body, static moment and tensor of inertia according to the reduction pole B. It allows us to rewrite the equations of motion (for the rigid body) in the following form

$$m\frac{d}{dt}\mathbf{g}(\widetilde{\mathbf{x}},t) + \frac{d}{dt}[\mathbf{h}(\widetilde{\mathbf{x}},t) \times \mathbf{S}(B)] = \mathbf{W}(t;B), \quad t \in (0,\infty),$$
$$m\mathbf{g}(0) + \mathbf{h}(0) \times \mathbf{S}(B) = \widetilde{\mathbf{p}}, \tag{13}$$

$$\frac{d}{dt}[\mathbf{S}(B) \times \mathbf{g}(\widetilde{\mathbf{x}},t) + \Im(B) \circ \mathbf{h}(\widetilde{\mathbf{x}},t)] = \mathbf{M}(t;B), \quad t \in (0,\infty),$$
$$\mathbf{S}(B) \times \mathbf{g}(0) + \Im(B) \circ \mathbf{h}(0) = \widetilde{\mathbf{k}}. \tag{14}$$

In particular, for the particle we have

$$m\frac{d}{dt}\mathbf{g}(\widetilde{\mathbf{x}},t) = \mathbf{W}(t;B), \quad t \in (0,\infty),$$
$$m\mathbf{g}(0) = \widetilde{\mathbf{p}}, \tag{15}$$

$$\frac{d}{dt}\left[\mathbf{S}(B)\times\mathbf{g}(\widetilde{\mathbf{x}},t)\right]=\mathbf{M}(t;B),\quad t\in(0,\infty),$$

$$\mathbf{S}(B)\times\mathbf{g}(0)=\widetilde{\mathbf{k}}.$$

(16)

We can see that the system of initial value problems is coupled only for the rigid body, but not for the particle.

3. Reduction pole for the system

For the system of n rigid bodies, both models rigid body and particle can be some elements with number i. For chosen element, which encloses the region $_i\Omega$, $i=\overline{1,n}$, the position vector $_i\mathbf{x}$ shows the place $_iA\in{}_i\Omega$. Thus the motion of the element is locally determined by two functions of time:

$$\mathbf{v}(_iA)=\mathbf{g}(_i\mathbf{x},t),\quad \boldsymbol{\omega}(_iA)=\mathbf{h}(_i\mathbf{x},t),\quad t\in(0,\infty),\ i=\overline{1,n}.$$

(17)

Global properties of system element motion can be described kinematically by stiffness condition

$$\mathbf{v}(_iB)=\mathbf{v}(_iA)+\boldsymbol{\omega}(_iA)\times{}_i\mathbf{A}_i\mathbf{B},\quad \boldsymbol{\omega}(_iB)=\boldsymbol{\omega}(_iA),\quad {}_iA,{}_iB\in{}_i\Omega.$$

(18)

Inertial properties of the system element dynamics is determined with the momentum-velocity relation:

$$\mathbf{p}(t;O)=\sum_{i=1}^{n}{}_i\mathbf{p}(t;O),\quad t\in(0,\infty),$$

(19)

$$\mathbf{k}(t;O)=\sum_{i=1}^{n}{}_i\mathbf{k}(t;O),\quad t\in(0,\infty).$$

(20)

We can apply the momentum and moment of momentum principles (6,7), where total force and total moment are taken for the whole rigid body system. But the practical application of these equations is negligible because the linear velocities are unknown. That is why we define the momentum and moment of momentum vectors for the reduction pole $_iB\in{}_i\hat{\Omega}$ as follows

$$_i\mathbf{p}(t;{}_iB)={}_im\mathbf{g}(_i\widetilde{\mathbf{x}},t)+\mathbf{h}(_i\widetilde{\mathbf{x}},t)\times{}_i\mathbf{S}(_iB),$$

(21)

$$_i\mathbf{k}(t;{}_iB)={}_i\mathbf{S}(_iB)\times\mathbf{g}(_i\widetilde{\mathbf{x}},t)+{}_i\Im(_iB)\circ\mathbf{h}(_i\widetilde{\mathbf{x}},t).$$

(22)

Here

$$_im=\int_{_i\Omega}{}_i\rho(\mathbf{x})\,d\mathbf{x},$$

(23)

$$_i\mathbf{S}(_iB)=\int_{_i\Omega}(\mathbf{x}-{}_i\widetilde{\mathbf{x}})_i\,\rho(\mathbf{x})\,d\mathbf{x},$$

(24)

$$_i\Im\!\left(_iB\right)\circ\mathbf{h}\!\left(_i\widetilde{\mathbf{x}},t\right)=\int_{i\Omega}\!\left(\mathbf{x}-_i\widetilde{\mathbf{x}}\right)\times\left[\mathbf{h}\!\left(_i\widetilde{\mathbf{x}},t\right)\times\left(\mathbf{x}-_i\widetilde{\mathbf{x}}\right)\right]_i\rho(\mathbf{x})\,d\mathbf{x}. \qquad (25)$$

The influence all of the passive and active loads on the movement of the system element is characterized by a momentum $_i\mathbf{p}$ and a moment of momentum $_i\mathbf{k}$ changes:

$$\begin{aligned}
_i\dot{\mathbf{p}}\!\left(t;\,_iB\right)&=\,_i\mathbf{W}\!\left(t;\,_iB\right),\quad t\in(0,\infty),\\
_i\mathbf{p}\!\left(0;\,_iB\right)&=\,_i\widetilde{\mathbf{p}},\quad i=\overline{1,n},
\end{aligned} \qquad (26)$$

$$\begin{aligned}
_i\dot{\mathbf{k}}\!\left(t;\,_iB\right)&=\,_i\mathbf{M}\!\left(t;\,_iB\right),\quad t\in(0,\infty),\\
_i\mathbf{k}\!\left(0;\,_iB\right)&=\,_i\widetilde{\mathbf{k}},\quad i=\overline{1,n}.
\end{aligned} \qquad (27)$$

We can add above equations and we have the result

$$\begin{aligned}
\sum_{i=1}^{n}{}_i\dot{\mathbf{p}}\!\left(t;\,_iB\right)&=\sum_{i=1}^{n}{}_i\mathbf{W}\!\left(t;\,_iB\right),\quad t\in(0,\infty),\\
\sum_{i=1}^{n}{}_i\mathbf{p}\!\left(0;\,_iB\right)&=\sum_{i=1}^{n}{}_i\widetilde{\mathbf{p}},
\end{aligned} \qquad (28)$$

$$\begin{aligned}
\sum_{i=1}^{n}{}_i\dot{\mathbf{k}}\!\left(t;\,_iB\right)&=\sum_{i=1}^{n}{}_i\mathbf{M}\!\left(t;\,_iB\right),\quad t\in(0,\infty),\\
\sum_{i=1}^{n}{}_i\mathbf{k}\!\left(0;\,_iB\right)&=\sum_{i=1}^{n}{}_i\widetilde{\mathbf{k}}.
\end{aligned} \qquad (29)$$

Since the right-hand sides of the motion equations contain the set of reduction poles, the question is: can we substitute the total force and total moment for the system. Analogously the momentum and moment of momentum have not any reduction pole.

As is coming to see the reaction forces could appear in the equation (29). Our goal is to get the internal forces acting in neighbourhood of a body. We can expect the momentum and moment of momentum principles to be valid for the system of the rigid bodies whenever the interactions of the bodies are negligible. As it is known, the total moment for internal forces is equal to zero [1, p. 300]. That is why the sum of total moments in the formula (29) cannot be the total moment for the system.

5. Concluding remarks

In the paper we have extended the rigid body dynamics on the rigid bodies systems based on the relation velocity-momentum standpoint. In order to gain an intuitive understanding of the effects of the mechanism motions, we have to realize that kinematical quantities are essentially frame-dependent. That is why we called absolute velocities. The possibility of linking absolute velocities to rigid body motion is a consequence of some presumptions that load is an objective quantity and that inertial

forces depend only of absolute quantities in Newtonian mechanics. But the mathematical form of the inertia operators is strictly defined in the configuration with respect to a body fixed frame. But the connected rigid bodies are not a rigid body. That is why we come not into possession of dynamic laws for the rigid bodies systems. Only some mathematical transformations are possible for them.

References

1. S. Banach, *Mechanika,* PWN Warszawa, 1956.
2. C. Kittel, W.D. Knight, M.A. Ruderman, *Mechanika,* PWN Warszawa, 1973.
3. E. Karaśkiewicz, *Zarys teorii wektorów i tensorów,* PWN Warszawa, 1975.

METHODS FOR IDENTIFICATION OF UNCORRELATED FORCES ACTING IN THE MACHINES

Henryk KAŹMIERCZAK

Jacek KROMULSKI

Tadeusz PAWŁOWSKI

Przemysłowy Instytut Maszyn Rolniczych

Poznań, Starołecka 31

(061) 8712279, kazmhenr@pimr.poznan.pl

Summary

In the work presented are methods of identification of uncorrelated operational forces based on orthogonal decomposition of crosspower spectrum matrix. In this purpose were used methods based on eigen- and singular value decomposition of PSD matrix. Except methods in frequency domain were used methods in time domain (ICA - Independent Component Analysis) for identification statistically independent and principal component. The methods were used to identify the number of sources of the exciting forces acting during the work of a real mechanical system..

Key words: force identification, singular value decomposition, independent component analysis.

Introduction

Knowledge of the operational loads is very useful in diagnostic process of mechanical structures and to simulate the response under working condition. In many cases, dynamic forces are not directly measurable and need to be identified using inverse solution method. In the present work presented are methods of identification of uncorrelated operational forces based on orthogonal decomposition of response PSD matrix. Except methods in frequency domain were used methods in time domain (ICA - Independent Component Analysis) for identification statistically independent and principal component. The methods were used to identify the number of sources of the exciting forces acting during the work of a real mechanical system – machine for compostable organic materials processing. Knowledge of impendent principal component could be useful for identification of force application points.

1. Mathematical bases of procedures of separation of uncorrelated components from crosspower spectrum matrices

The relationship between the input x(t), and the output y(t) of a linear system can be written in the following form:

$$[G_{yy}(\omega)] = [H(\omega)]^* [G_{xx}(\omega)] [H(\omega)]^H \tag{1}$$

where: $[G_{xx}(\omega)]$ is the input spectral matrix, $[G_{yy}(\omega)]$ is the output spectrum matrix, and $[H(\omega)]$ is the Frequency Response Function (FRF) matrix.

Computing all crosspower spectra we archiving 3 dimensional crosspower spectrum matrix. This matrix can be considered as a set of square matrix (determined for each frequency). The element $(i,j(\omega))$ of this matrix contained crosspower spectrum between signal x_i and x_j at frequency ω.

A commonly used method of identification the uncorrelated sources of exciting forces is the method of square crosspower spectrum matrix decomposition into eigenvalues:

$$[G_{N \times N}(\omega)] = [U_{N \times N}(\omega)] [\Lambda_{N \times N}(\omega)] [U_{N \times N}(\omega)]^H \qquad (2)$$

The obtained eigenvalues $[\Lambda_{N \times N}(\omega)]$ of $[G_{N \times N}(\omega)]$ in descending order can be considered as the principal component autopower spectra. The principal component spectra are mutually totally uncorrelated (crosspower spectra are zero). The principal autopower spectra, sorted in descending order and plotted as a function of frequency yield a graphical representation of the rank of crosspower matrix, which indicates the number of incoherent phenomena (principal uncorrelated sources of mechanical vibration), observed in the signal set S($x_1, x_2, \ldots, x_N$) at every frequency.

Instead of analysing eigenvalue decomposition of a square matrix one can use its SVs. SVD allows drawing conclusions of the number of uncorrelated sources in the same way as the eigenvalues analysis. The decomposition of crosspower spectrum matrices into singular values can be performed by mean following relationship:

$$[G_{M \times N}(\omega)] = [U_{M \times M}(\omega)] [\Sigma_{M \times N}(\omega)] [V_{N \times N}(\omega)]^H \qquad (3)$$

2. Independent component analysis

Independent component analysis, or ICA, is a statistical technique that represents a multidimensional random vector as a linear combination of nongaussian random variables ('independent components') that are as independent as possible. For nongaussian random vectors, this decomposition is not equivalent to decorrelation as is done by principal component analysis, but something considerably more sophisticated. ICA allows one to separate nongaussian source signals from their linear mixtures 'blindly', i.e. using no other information than the congaussianity of the source signals. ICA can also be used to extract features from image and sound signals according to the principle of redundancy reduction that has its origins in the neurosciences. Independent component analysis (ICA) is a multivariate analysis technique that aims at recovering linearly mixed unobserved multidimensional independent signals from the mixed observable variables. Let x be an m-dimensional observed vector. The ICA model for x is written as:

$$x = As \qquad (4)$$

where: A is called a mixing matrix and *s* is an *n*-dimensional vector of independent components with zero mean and unit variance.

ICA analysis of vibration signals can be used for both assessing the statistical independence of signals and segmenting nondeterministic signal sources for further analysis.

4. Practical example of identification of uncorrelated forces acting in the agricultural machines

The depicted above method were used to identify sources of exciting forces acting during the work of real mechanical system – a machine for compostable organic materials processing (Fig 1).

Fig.1. Machine for compostable organic materials processing

The data used for identification of the operational loads was collected from series measurements in a different operational condition scenario:

- exhaust engine works only,
- exhaust engine and feeders works only,
- all mechanisms of combines work.

The vibration acceleration signals from 21 points were measured simultaneously.

During work of combine for organic materials on idle run when exhaust engine works only or exhaust engine and feeders works totals number of uncorrelated forces identified by decomposition crosspower spectrum matrices were 3. During when all mechanisms of combines work total number of uncorrelated forces were 5 (Fig. 2).
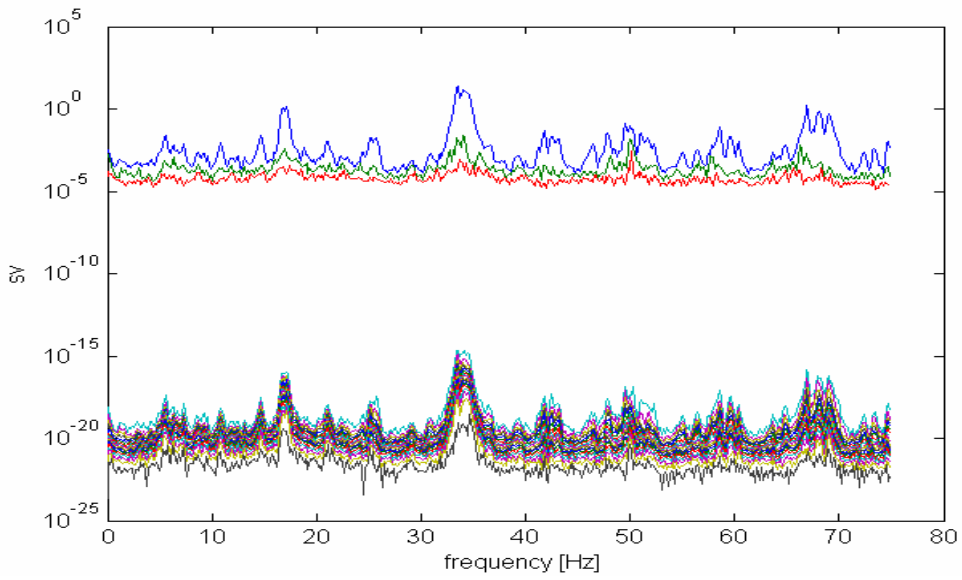
Fig.2. Singular spectra of PSD response matrices - exhaust engine
and feeders works only
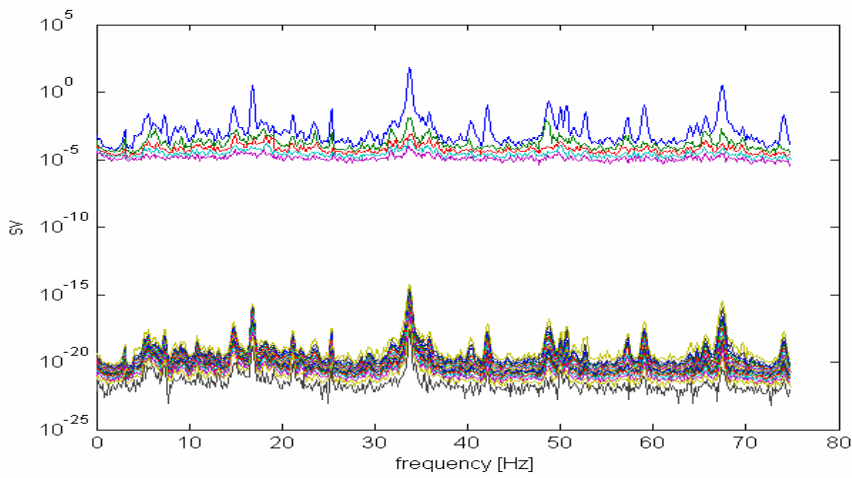
Fig.3. Singular spectra of PSD response matrices- all mechanisms of combines work
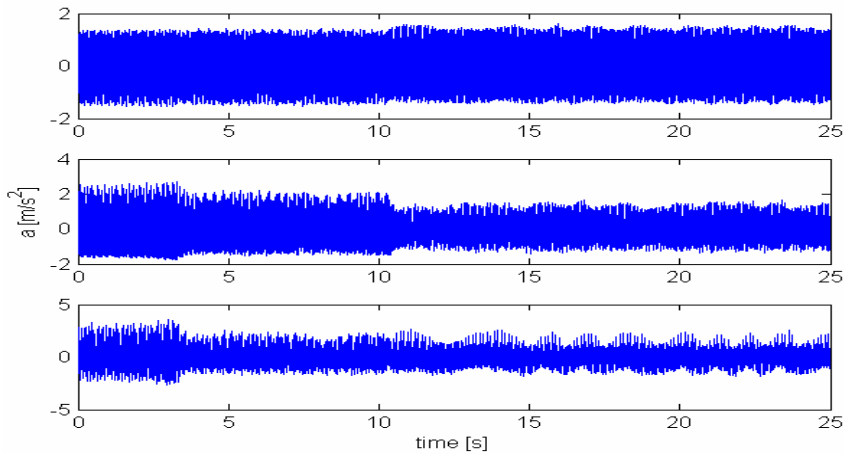
Fig.4. Independent component computed from ICA procedures- exhaust engine and feeders works only
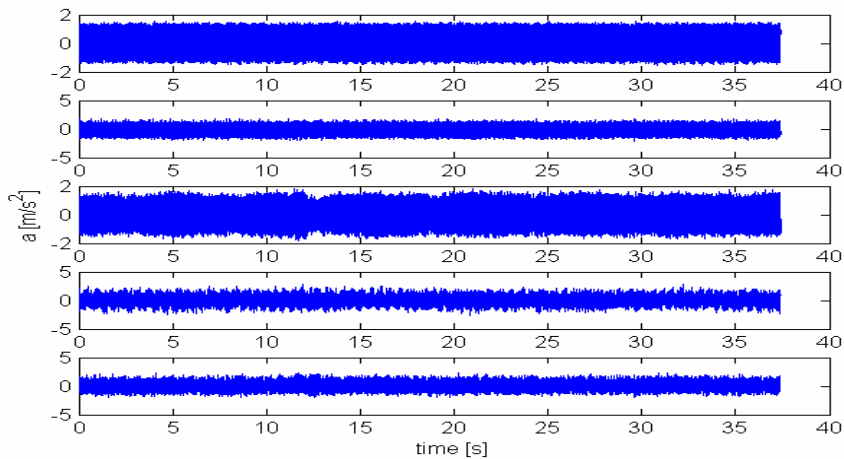
Fig.5. Independent component computed from ICA procedures - all mechanisms of combines work

You can then reduce the dimension of the data by retaining only the subspaces corresponding to the largest eigenvalues of the covariance matrix of the data.

The number of independent component computed from ICA procedures was the same as number of uncorrelated forces identified by decomposition crosspower spectrum matrices (Fig 4-5).

Knowledge of impendent principal component could be useful for identification of force application points.

Bibliography

1. Allemang R. J., Brown D. L., *A unified matrix polynomial approach to modal identification*, Journal of Sound and Vibration (1998) 211(3), 301-322
2. A. Hyvärinen , J. Karhunen, E. Oja, *Independent Component Analysis*, John Wiley & Sons, 2001
3. A. Hyvärinen. *A unifying model for blind separation of independent sources*. Signal Processing, 85(7):1419-1427, 2005.
4. A. Hyvärinen, E. Oja., *Independent Component Analysis:Algorithms and Applications*, Neural Networks, 13(4-5):411-430, 2000
5. M. Joho , H. Mathis, R.H. Lambert*, Overdetermined blind source separation: Using more sensors than source signals in a noisy mixture.* Independent Component Analysis and Blind Signal Separation ICA 2000, June 19–22, 2000, Helsinki, Finland, pp. 81–86
6. J. Kromulski, *Badanie charakterystyk dynamicznych drgań źródeł akustycznych o złożonej strukturze mechanicznej metodą analizy modalnej*, Praca doktorska, UAM Poznań, 1998, Wydział Fizyki.
7. J. Kromulski, *Nowe metody identyfikacji nieskorelowanych sił wymuszających działających w maszynach rolniczych*, Journal of Research and Applications in Agricultural Engineering, Vol. 51(1), 2006.
8. J. Kromulski., *Identification of uncorrelated sources of exciting forces by means of the methods of crosspower spectrum matrix decomposition into singular values and eigenvalues*, Archives of Acoustics 2/1998.
9. S. Shimizu, A. Hyvärinen, Y. Kano, P. Hoyer, A. Kerminen. *Testing significance of mixing and demixing coefficients in ICA*. Proc. International Symposium on Independent Component Analysis and Blind Signal Separation (ICA2006), Charleston, SC, USA, 2006.

PROPAGATION OF SOLITARY WAVES IN ROD MADE OF MATERIAL WITH NEGATIVE POISSON'S RATIO

Piotr KOŁAT

Poznan University of Technology, Institute of Applied Mechanics

Piotrowo 3, 60-965 Poznan

+48 61 665 21 78, piotr.kolat@put.poznan.pl

Abstract

It is found the propagation of longitudinal solitary waves in an elastic rod made of material with negative Poisson's ratio. It is used the difference scheme to solve the non-linear partial differential equation.

Keywords: auxetic, solitary wave, finite difference method

Introduction

Many physical systems are modeled by nonlinear partial differential equations, which are not exactly integrable. The numerical investigations of solitary waves in an elastic rod made of auxetic material is presented. Existence of solitary waves is provided by a balance between non-linearity and dispersion. Non-linearity in the elastic rod is caused by the finite stress values and the elastic material properties while the dispersion results from finite transverse size of the rod [1]. The solitons can propagate as long bell-shaped strain waves with permanent form and transfer energy long distance along. Recently the successful experiments on solitary waves observation in a transparent polystyrene rod have caused the interest on propagation of solitary waves in solids.

Auxetics or auxetic materials, both names are related to materials with negative Poisson's ratio v, exhibit the unusual behavior; becoming wider when stretched and narrowed when compressed. A wide range of auxetic materials and structures have been discovered in the last decade [2,3]. Auxetics possess many extraordinary properties, consequently the interest of them increases. Areas of application are seen in the biomedical field as prosthetic materials or surgical implants. Auxetic fibre reinforcements should also enhance the failure properties of composites. Fibre pull-out is a major failure mechanism in composites.

The negative Poisson's ratio, has been treated as an abnormal elastic parameter. In conventional isotropic materials the range of Poisson's ratio varies from 0 to 0.5, but generally the possible range of v for isotropic case varies from –1 to 0.5, based on thermodynamic consideration of strain energy in the theory of elasticity [4,5].

From theoretical and experimental point of view the study of non-linear strain waves in rod made of auxetics seems attractive, because these new materials can have many practical applications and may be the part of any construction. Recently isotropic elastic materials with negative Poisson's ratio have been produced. Consequently, many theoretical and experimental results of the theory dealing with positive Poisson's ratio have to be reexamined on auxetics.

1. Governing equation

Taking into account the geometrical and physical nonlinearties leads to nonlinear mathematical models. There are many equations describing the propagation of solitary waves in the elastic rod. One of the most popular is Boussinesq equations with one dispersive term:

$$\frac{\partial^2 u}{\partial x^2} - \frac{\partial^2 u}{\partial t^2} + \frac{1}{2}\frac{\partial^2}{\partial x^2}\left(u^3\right) + \frac{\partial^4 u}{\partial x^2 \partial t^2} = 0 \,, \tag{1}$$

$$\frac{\partial^2 u}{\partial x^2} - \frac{\partial^2 u}{\partial t^2} + \frac{1}{2}\frac{\partial^2}{\partial x^2}\left(u^2\right) + \frac{\partial^4 u}{\partial x^2 \partial t^2} = 0 \,, \tag{2}$$

there are terms with cubic (1) and quadratic nonlinearity (2).

Let us consider a nonlinear infinite elastic rod of a radius R. The structural element has been defined in the cylindrical Lagrangian coordinates (x, r, φ). The torsion was neglected, then the displacement vector is $\vec{V} = [u, w, 0]$. Murnaghan developed the energy as a power series in the invariants of the strain tensor. The density of potential energy is:

$$\Pi = \frac{\lambda + 2\mu}{2} I_1^2 - 2\mu I_2 + \frac{l + 2m}{3} I_1^3 - 2m I_1 I_2 + n I_3 \,, \tag{3}$$

λ, μ are Lamé constants, l, m, n are the Murnaghan moduli, I_1, I_2, I_2 are invariants of the deformation tensor.

The density of kinetic energy have a form:

$$K = \frac{\rho_0}{2}\left[\left(\frac{\partial u}{\partial t}\right)^2 + \left(\frac{\partial w}{\partial t}\right)^2\right], \tag{4}$$

where ρ_0 is the rod material density.

The single governing equation has been obtained in [1] using the Hamilton's principle in variational form:

$$\delta S = \delta \int\limits_{t_0}^{t_1} dt\, 2\pi \int\limits_{-\infty}^{+\infty} dx \int\limits_0^R rL\, dr = 0 \,, \tag{5}$$

where the Lagrangian density per unit volume is defined as $L = K - \Pi$, as follows:

$$\frac{\partial^2 u}{\partial t^2} - a\frac{\partial^2 u}{\partial x^2} - c_1 \frac{\partial^2}{\partial x^2}\left(u^2\right) - b_1 \frac{\partial^4 u}{\partial x^2 \partial t^2} + b_2 \frac{\partial^4 u}{\partial x^4} = 0 \,, \tag{6}$$

$a = \dfrac{E}{\rho_0}$, $c_1 = \dfrac{\beta}{2\rho_0}$, $b_1 = \dfrac{\nu(\nu-1)R^2}{2}$, $b_2 = -\dfrac{\nu E R^2}{2\rho_0}$, β is the coefficient of nonlinearity, $u(x,t)$ is the longitudinal strain function.

The equation (6) is called double dispersive equation (DDE), because it has two dispersive terms. The coefficients b_1, b_2 in case of materials with negative Poisson's ratio are always negative, consequently changing the form of the solutions equation (6).

The numerical simulations of the equation (6) has been performed to show how the solitary waves in an elastic rod made of auxetic materials propagate.

2. Solitary wave solution

Using the central-difference formula the equation (6) with space step Δx and time step Δt takes the form:

$$
\begin{aligned}
&b_1 U_{j-1}^{n+1} - (\Delta x^2 + 2b_1) U_j^{n+1} + b_1 U_{j+1}^{n+1} = \Delta x^2 (U_j^{n-1} - 2U_j^n) - \\
&a\Delta t^2 (U_{j-1}^n - 2U_j^n + U_{j+1}^n) - c_1 \Delta t^2 ((U_{j-1}^n)^2 - (2U_j^n)^2 + (U_{j+1}^n)^2) - \\
&b_1 (U_{j-1}^{n-1} - 2U_{j-1}^n - 2U_j^{n-1} + 4U_j^n + U_{j+1}^{n-1} - 2U_{j+1}^n) + \\
&\frac{b_2 \Delta t^2}{\Delta x^2} (U_{j-2}^n - 4U_{j-1}^n + 6U_j^n - 4U_{j+1}^n + U_{j+2}^n),
\end{aligned}
\tag{7}
$$

$$
u(x,t) = U(p\Delta x, q\Delta t) = U_j^n, \quad p = 0,1,2,...,M, \quad q = 0,1,...
$$

The result of discretization is Crank-Nicolson system with a tridiagonal matrix, which is solve by the Gauss elimination with initial conditions:

$$
\begin{aligned}
U_j^0 &= f(j), \\
U_j^1 &= g(j),
\end{aligned}
\tag{8}
$$

and numerical boundary conditions [6]:

$$
U_0^n = U_M^n = 0.
\tag{9}
$$

The figures below show the propagation of solitary waves from bell-shaped initial pulse.
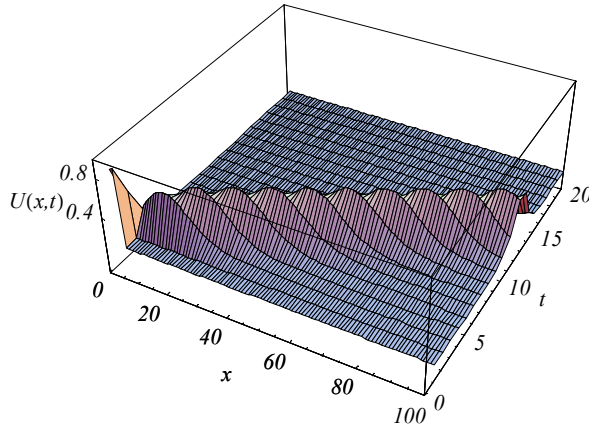
Figure 1. Formation of solitary waves in a rod made of material with negative Poisson's ratio ($\nu = -0.8$)

$U(x,t)$
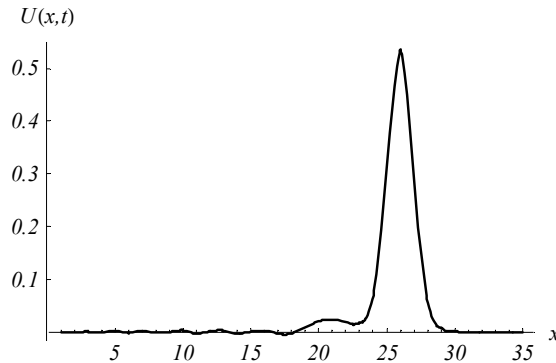
Figure 2. Formation of solitary waves in a rod made of material with negative Poisson's ratio ($\nu = -0.8$)

The stability analysis of equation (7) base on method developed by John von Neumann [7] was done. The finite difference scheme is "conditionally stable".

4. **Conclusion**

The double dispersive equation (6) was solved using the finite difference method. The propagation of solitary waves in the rod made of auxetic materials is possible. The value of the amplitude in the material with negative Poisson's ratio decreases, when ν is less than 0.

References

1. A. V. Porubov, *Amplification of Nonlinear Strain Waves in Solids*, World Scientific, Singapore, 2003.
2. A. William Lipsett, A. I. Beltzer, *Reexamination of Dynamic Problems of Elasticity for Negative Poisson's Ratio*, J. Acoust. Am., **84** (1988) 2179 – 2186.
3. B. Lüthi, *Physical Acoustics in the Solid State*, Springer, Berlin, 2005.
4. L. Landau, E Lifszic, *Mechanika Ośrodków Ciągłych*, PWN, Warszawa, 1958.
5. W. Nowacki, *Teoria Sprężystości*, PWN, 1969.
6. V. Y. Belashov, S.V. Vladimirov, *Solitary Waves in Dispersive Complex Media*, Springer Berlin 2005.
7. J. L. Davis, *Finite Difference Methods in Dynamics of Continuous Media*, MCP New York 1986.

VIBRATIONS DUE TO THE PASSAGE OF A RAILWAY VEHICLE ON STRAIGHT AND CURVED TRACKS

Robert KONOWROCKI, Czesław BAJER

Institute of Fundamental Technological Research (IPPT PAN)

Świętokrzyska 21, 00-049 Warsaw

rkonow@ippt.gov.pl, bajer@ippt.gov.pl

Abstract

The paper presents the results of vibration measurements on line of railway during passages of a train at a constant speed. The measurements have been performed on a railway track at straight and curve sections as well as and inside the train on the floor. The experimental results exhibited higher amplitudes of vibrations on the curve of the track than on its straight segments. The lateral slip in rail/wheel contact zone is considered as a possible reason of such a phenomenon.

Keywords: railway vibrations, dynamic train-track interaction, ground borne vibrations, moving load.

Introduction

There is an increasing interest in the scientific world in the issue of ground borne vibrations from railway tracks, and in the vibration control by means of the track structure modification [1]. A wide range of different track and train structures is available, characteristic of different levels of performance. A train generates vibrations which are transmitted through the track to the ground, resulting in vibration and re-radiation noise in nearby building. The amplitude of vibrations depends on several factors, such as roughness of wheels and rails, dynamic properties of a train, a vehicle speed, characteristics of a railway track, a soil damping and a propagation of waves thought the soil [2, 3, 4].
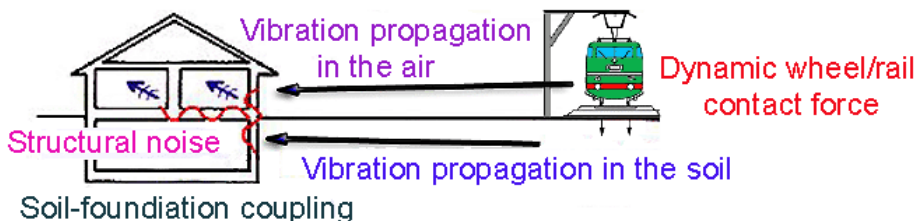
Fig. 1. The mechanism of the ground borne noise generation .

The main objective of the paper is to present results of experimental measurements of vibrations within the train and on the sleeper at straight and curve segments of track and to compare experimental data with numerical simulation results. The paper is focused on the influence of the lateral slip in rail/wheel contact zone on the generation of vibrations and a noise [5].

1. Measurement system

Our measurement system can be divided into two subsystems. The first one allows us to measure vibrations on the railway track, the second one can measure vibrations on the floor inside the train car-body. The external measurement system included: two-axis vibration transducer, geophone, infrared gate system, analog-digital converter of 12 bit/20kHz and data acquisition computer (Fig. 2). The two-axial accelerometer and geophone were fixed in the middle of railway sleeper (Fig. 3). The sensors were connected with the data acquisition computer through the A/D converter. The measurement was initialized and stopped when the infrared gate system gave an impulse to the converter. The first infrared gate switched on the converter when the train arrived at the measuring area while the second gate stopped measurements when the train was leaving this area.
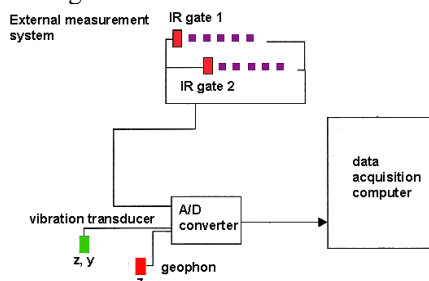
Fig. 2. Scheme of measurement system.   Fig. 3. Sensors placed on a railroad.
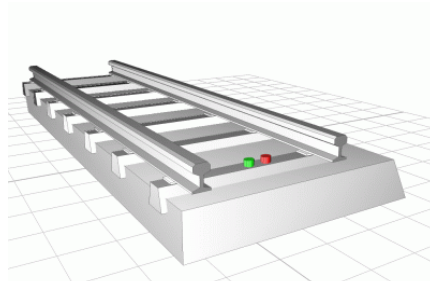
The second measuring system included two one-axis transducers and the mobile A/D converter of 12bit/10kHz. The converter contained data acquisition system (Fig. 4). The transducers was fixed to a steel bar in vertical and horizontal direction. The steel bar was placed on the train floor (Fig. 5).
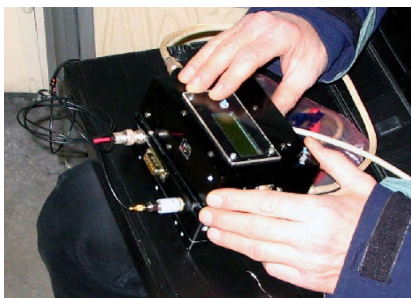
Fig. 4. Mobile converter with self data   Fig. 5. Vibration transducers placed
         acquisition system.   on the train floor.
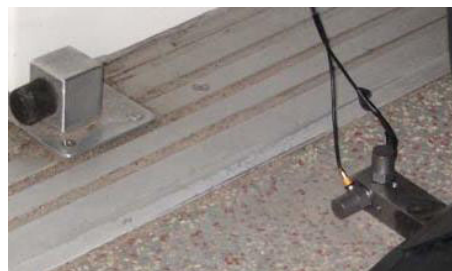
The average speed of the train has been estimated from two sources. The first one was a portable GPS module located in the train. The infrared system was the second source of information. The infrared gates measured time between the passage of the first and the

last wheelset. The time interval and the distance between both axles allowed us to estimate the train speed.

2. Characteristic of the rolling stock

The investigated train of type EN 71-100 consisted of four coaches (Fig. 6). Each coach had two bogies with two wheelsets. Two final coaches had motor bogies while two middle coaches had trailer bogies. The length of motor car was 20.70 m, while the length of the trailer cars was 21.57 m. The total length of the train was 85 m. The distance between axles on the bogie was 2.70 m. The dead weight of the trailer car was 34 T whereas of the motor car was 57 T. The total mass of the train was 182 T. The traction and trailer wheels were of monobloc type and had a diameter of about 0.94 m and 1.00 m, respectively.
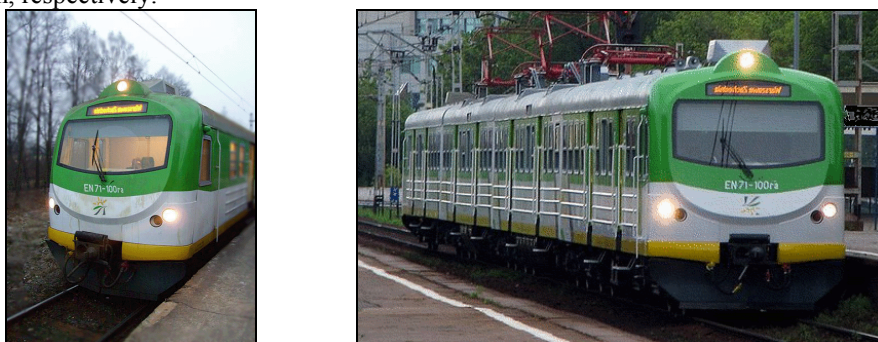
Fig. 6. Investigated train of type EN71-100.

3. Experimental results

The vibration measurements were performed during rush hours (10 am ÷ 16 pm) for 10 passages of EN 71-100 type trains on straight and curve test segments of a track and in the train in the same places. The radius of the curvature of the tested track segment was about 1000 m. The average speed of the railway vehicle was equal to 58 km/h on the curve segment of the track and the average speed of the train was equal to 61 km/h on the straight segment. The vertical and horizontal accelerations and vertical velocity were measured by two-axial accelerometer and one-axial geophone (Fig. 3).

Vibrations were analyzed in terms of accelerations, velocities or displacements as a function of time and frequency. The displacements were obtained by double integration of acceleration results. Displacements were checked by integrated velocity results obtained by measurements by the geophone.

Comparison of experimental results demonstrated higher amplitudes of vibrations generated on curves of the track than on straight segments (Fig. 7, 9). Measurements on curves exhibited eight characteristic predominant groups of vibrations (Fig. 7). These groups confirmed the passage of respective wheelsets of bogies by the point of measurement. In Fig. 8 the spectral analysis of experimental results of vibration are
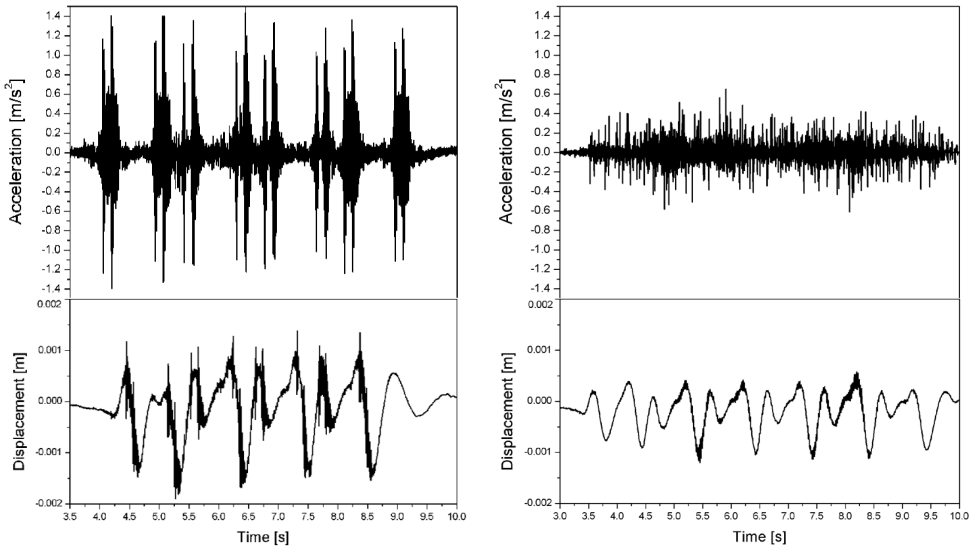
Fig. 7. Time history of the vertical accelerations and displacements measured
on the sleeper: curve segment (left), straight segment of a track (right).
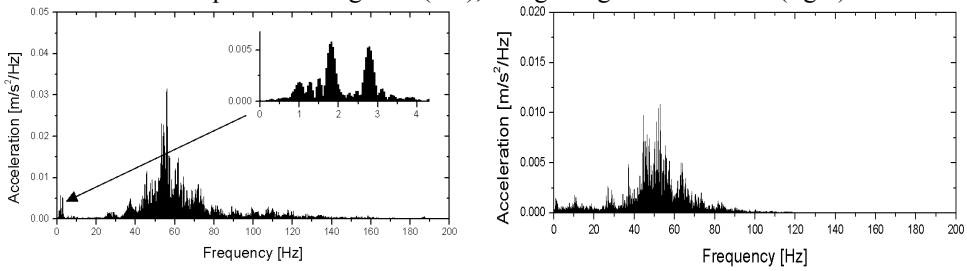
Fig. 8. Spectra of vertical accelerations measured on the sleeper:
curve segment of a track (left), straight segment of a track (right).
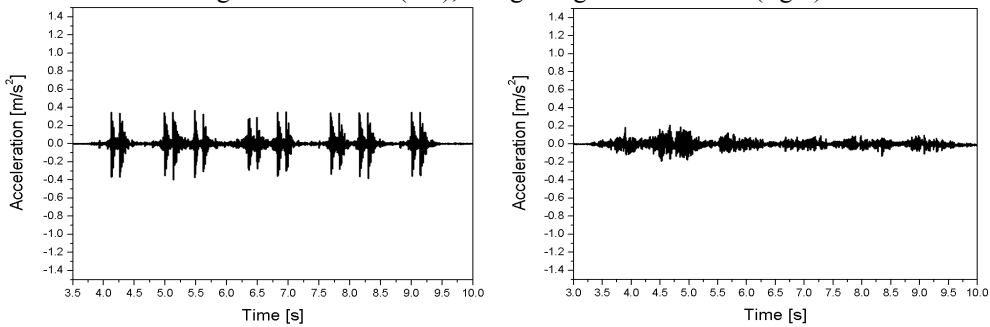
Fig. 9. Time history of lateral accelerations measured on the sleeper:
curve segment of track (left), straight segment of track (right).

depicted. Frequencies from ranges 1÷2 Hz and 40÷80 Hz on the curve segment of the track can be noticed whereas on the straight the respective frequency is equal to 30÷75 Hz. The predominant frequency on the curve and straight segments of track is equal to 53 Hz and 58 Hz, respectively.

Fig. 10 shows the time history of vertical and horizontal vibration measured inside a car body on the floor for a period of time corresponding to the passage of approximately one train length. The measurements were performed during the passage in the place of investigation on the track. The comparison of the graphs in Fig. 10 exhibits higher intensity of horizontal vibrations (in transversal direction) for the curve segment than for the straight segment. Moreover, in this case we have about 2 times higher amplitude. Differences in amplitudes of vibration in the vertical direction are significantly lower than in the transversal direction.

Fig. 11. shows the spectra of vertical and horizontal acceleration measured inside a car body. It can be noticed that vibrations with higher range frequencies occur on the straight track than on the curve segments. The spectral analysis of vibrations (Fig. 11) shows the frequencies of ranges 2÷60 Hz and 300÷600 Hz on the curve segment whereas on the straight segment the frequency was 500÷700 Hz for transversal direction and 400÷750 Hz for vertical direction. The predominant frequency on the curve and straight segments is equal to 43, 400, 700 Hz and 52, 83, 550, 630 Hz, respectively.
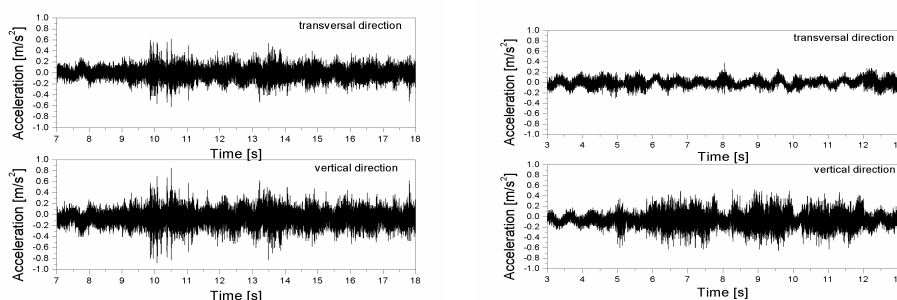
Fig. 10. Time history of vertical and horizontal acceleration measured inside car body on the floor: curve segment of track (left), straight segment of track (right).

4. Numerical results

Intensive numerical modelling of vibrations generated by a travelling vehicle was performed by the space-time finite element models. It was the only method which allowed us to analyze the moving mass problem. In classical approaches the track was subjected to a moving system of massless forces. The wave phenomena could not be considered with a sufficient accuracy in higher ranges of a speed. In reality the moving wheel or wheelset considered as an inertial point is bound with the track or simply with the rail. It significantly influences the dynamic response of the trail-track system. This problem, however, will not be considered in the present paper.
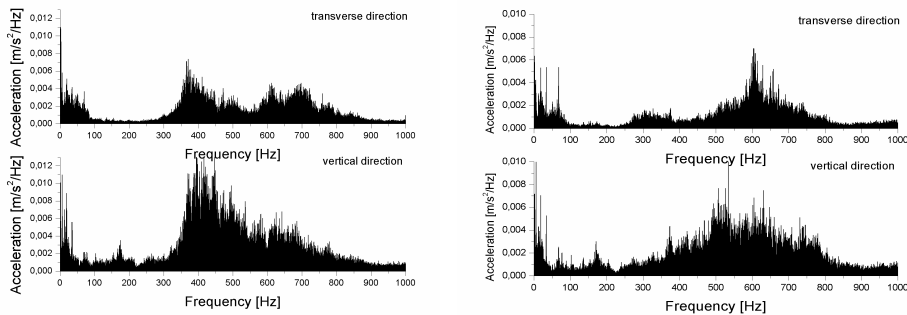
Fig. 11. Spectra of vertical and horizontal acceleration measured inside a car body on the floor: curve segment of track (left) and straight segment of track (right).

5. Conclusions

Higher vibrations on curves can be resulted from the wear of railway track which was caused by centrifugal forces influenced by the passages of the train, deformations of wheels, wheelsets and rails, different linear velocity of wheels on curves and rotary oscillations of wheelsets. Plane of the wheel skewed to the direction of the rolling resulted in lateral slip in rail/wheel contact zone. The rail/wheel system oscillates and generates noise.

In the future the experimental data presented here as well as results of measurements in the Metro tunnel will be used for validation of numerical prediction models, being under development. Model development, calibration and validation will benefit from the available data set. In further stage of the project the obtained models of vibration source and models of soil will be applied to describe vibration propagation through the soil to the buildings in the environment.

References

1. M. Heckl, G. Hauck and R. Wettschureck, Structure-borne sound and vibration from rail traffic. *Journal of Sound and Vibration.* 193:175–184, 1996.
2. R. Konowrocki, R. Bogacz and Cz. Bajer, Study of wheel/road interaction with lateral slip. *Simul. in R&D*. Eds. M. Nader and A. Tylikowski, Warsaw, 2005.
3. D. Clouteau, M. Arnst, T.M. Al-Hussaini, G. Degrande, Free field vibrations due to dynamic loading on a tunnel embedded in a stratified medium, Journal of Sound and Vibration. 283 (1–2):173–199, 2005.
4. R. Bogacz, Cz. Bajer, Rolling contact with wave phenomena. - Numerical investigation. In: *Proc. of VIII Pan -American Congress of Applied Mechanics*. Havana, Cuba, pp. 346-349, 2004.
5. R. Konowrocki, Cz. Bajer. Investigation of the friction phenomenon in the wheel-road interaction. XXII Symposium-Vibrations in physical systems, 12:173–178, 2006.

ACOUSTIC SH WAVES IN DEFORMED FOAM RUBBER

Sławomir KOSIŃSKI

Łódź University of Technology, Faculty of Civ. Eng., Arch. & Env. Eng.

90-924 Łódź, al. Politechniki 6

(042) 631-35-71, e-mail: kosislaw@p.lodz.pl

Abstract

The purpose of this paper is to consider the reflection-refraction problem of plane 2-D acoustic SH waves at a plane interface between two initially deformed nonlinear rubberlike materials. The standard procedure for the linearisation of the equations of motion was used. This approach bases on the assumption that small, time depending motions are superimposed on large static deformations. The initial deformations induce additional effects essential for the calculations of the reflection and refraction coefficients.

Key words: acoustic SH waves, initially deformed rubberlike materials, reflection-refraction problem, small motions superimposed on large static deformations

Introduction

Paper reports the results of an examination of the reflection-refraction plane wave problem. The interaction of harmonic SH-type waves with a plane boundary between two different isotropic half-spaces, which are perfectly welded along the plane X_2=0 (Fig. 1) is investigated. It is assumed that the half-spaces have different mechanical properties and that the static deformations in both material regions are also distinct. In spite of a simplicity, the problem illustrates some new phenomena characteristic for the nonlinear initially deformed materials. Results are presented for a specific elastic compressible Blatz-Ko rubberlike material and a general discussion of the limitations of the solutions is presented. The obtained results differ very strong from the results of the same problem in the linear theory. In the regions with inital deformation the speed of propagation of the shear waves is not constant, it depends on the direction of propagation. Both shear waves propagation speeds $c_{2//}$ and $c_{2\perp}$ in the direction normal and perpendicular to the interface are different. In contrast to the linear theory these both speeds are equal $c_{2//} = c_{2\perp} = c_2\sqrt{\mu/\rho_R}$. The speed of propagation u_n (comp.(15)) in arbitrary direction depends on $c_{2//}$ and $c_{2\perp}$ and also on the unit normal **N** to the plane of the wave front.

1. Basic equations

The general motion to be discussed here is defined by (1). It is assumed that the material has been subjected to an initial static homogeneous deformation with constant principal stretches $\lambda_1, \lambda_2, \lambda_3$ and to a superimposed small motion $u_3 = u_3(X_1, X_2, t)$ characterized by a small displacement field which is time dependent:

$$x_1 = \lambda_1 X_1, \quad x_2 = \lambda_2 X_2, \quad x_3 = \lambda_3 X_3 + u_3(X_1, X_2, t). \tag{1}$$

The final and static deformations are very close. The components of the deformation gradient $\mathbf{F}_0$ and $\mathbf{F}$ (for static and final deformation) and the components of the right Cauchy-Green tensor $\mathbf{C}$, are:

$$[\mathbf{F}_0] = \begin{bmatrix} \lambda_1 & 0 & 0 \\ 0 & \lambda_2 & 0 \\ 0 & 0 & \lambda_3 \end{bmatrix}, [\mathbf{F}] = \begin{bmatrix} \lambda_1 & 0 & 0 \\ 0 & \lambda_2 & 0 \\ u_{3,1} & u_{3,2} & \lambda_3 \end{bmatrix}, [\mathbf{C}] = \begin{bmatrix} \lambda_1^2 + u_{3,1}^2 & u_{3,2} u_{3,2} & \lambda_3 u_{3,1} \\ u_{3,2} u_{3,2} & \lambda_2^2 + u_{3,2}^2 & \lambda_3 u_{3,2} \\ \lambda_3 u_{3,1} & \lambda_3 u_{3,2} & \lambda_3^2 \end{bmatrix}, \tag{2}$$

where $u_3 = w(X_2)u(X_1, t)$.
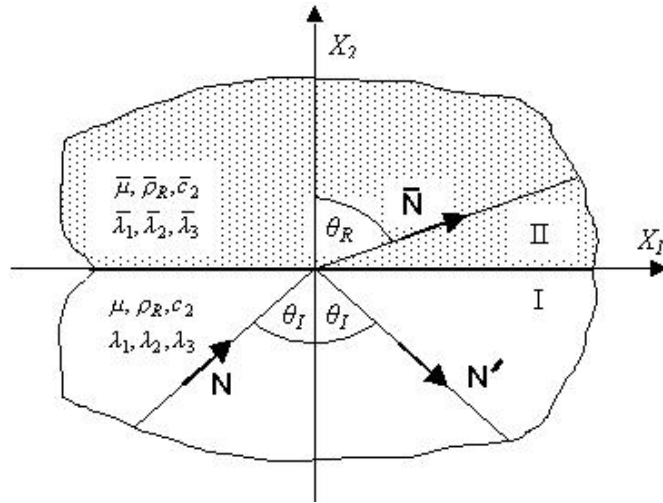
Fig. 1 Reflection and refraction of an SH wave at the interface

For a compressible isotropic hyperelastic material there exists a strain energy function denoted $W = W(\mathbf{F})$, defined on the space of deformation gradients such that, the nominal stress tensor $\mathbf{S}$ (transpose of the first Piola-Kirchhoff tensor (comp.[2], [3])) is defined as

$$\mathbf{S} = [\partial(W(\mathbf{F})) / \partial \mathbf{F}] = 2W_1 \mathbf{F}^T + 2W_2 (I_1 \mathbf{F}^T - \mathbf{C} \mathbf{F}^T) + 2W_3 I_3 \mathbf{F}^{-1}, \tag{3}$$

where I_i invariants of the tensor $\mathbf{C}$ and $W_i = \partial W / \partial I_i$, $i = 1, 2, 3$. The stress tensor components which we need to consider are S_{13} and S_{23}. It follows from (2) and (3) that

$$S_{13} = 2(W_1 + W_2 \lambda_2^2) u_{3,1}, \quad S_{23} = 2(W_1 + W_2 \lambda_1^2) u_{3,2}. \tag{4}$$

Substitution of (4) into the differential equations of motion of finite elasticity gives for the superimposed infinitesimal displacement two trivial one non-trivial equations of motion

$$A_{i3}^{\alpha\beta}(\mathbf{F_0})u_{3,\alpha\beta}=0, \quad A_{33}^{11}(\mathbf{F_0})u_{3,11}+A_{33}^{22}(\mathbf{F_0})u_{3,22}=\rho_R\ddot{u}_3 , \tag{5}$$

where $A_{ik}^{\alpha\beta}=(\partial S_{\alpha i}/\partial F_{k\beta})$, and these derivatives are evaluated at $\mathbf{F}=\mathbf{F_0}$, $u_{3,3}=0$ and for $i,\alpha=1,2$; $\beta=3$ also $A_{i3}^{\alpha\beta}(\mathbf{F_0})=0$. The one nontrivial equation takes the form

$$c_{2//}^2 w(X_2)[u(X_1,t)]_{,11}+c_{2\perp}^2 u(X_1,t)[w(X_2)]_{,22}=\rho_R w(X_2)\ddot{u}(X_1,t) , \tag{6}$$

where $c_{2//}^2=2\left(W_1+W_2\lambda_2^2\right)$ and $c_{2\perp}^2=2\left(W_1+W_2\lambda_1^2\right)$ (comp. (17)). Suppose now that the displacements in both media are given by

$$u_3=w(X_2)\exp[i(kX_1-\omega t)], \quad \bar{u}_3=\bar{w}(X_2)\exp\left[i\left(\bar{k}X_1-\bar{\omega}t\right)\right]. \tag{7}$$

Substituting of $(7)_{1,2}$ into (6) gives two equations for two unknown functions $w(X_2),\bar{w}(X_2)$

$$[w(X_2)]_{,22}+k^2 p^2 w(X_2)=0 \qquad [\bar{w}(X_2)]_{,22}+\bar{k}^2\bar{p}^2\bar{w}(X_2)=0 , \tag{8}$$

where $p^2=\left(\omega^2/(k^2 c_{2\perp}^2)-(c_{2//}/c_{2\perp})^2\right)$, $\bar{p}^2=\left(\bar{\omega}^2/(\bar{k}^2\bar{c}_{2\perp}^2)-(\bar{c}_{2//}/\bar{c}_{2\perp})^2\right)$, and the displacement take the form

$$u_3=\exp[i(kX_1-\omega t\pm kpX_2)], \quad \bar{u}_3=\exp\left[i\left(\bar{k}X_1-\bar{\omega}t\pm\bar{k}\bar{p}X_2\right)\right]. \tag{9}$$

The linearised equations of motion must be complemented with the continuity conditions at the interface. The initial static deformations λ_i and $\bar{\lambda}_i$ (i=1,2,3) in both half-spaces under consideration are different. When two half-spaces are in rigid contact, then the displacement vector and stress vector must be continuous at the interface i.e.

$$S_{2i}(\mathbf{F})=\bar{S}_{2i}(\overline{\mathbf{F}}), \quad i=1,2,3 \text{ and } \lambda_1=\bar{\lambda}_1, \ \lambda_3=\bar{\lambda}_3, \ u_3(X_1,0,t)=\bar{u}_3(X_1,0,t) . \tag{10}$$

The boundary conditions at the interface are meet if and only if $\omega=\bar{\omega}, k=\bar{k}$. Expanding into the power series the components of the stress tensor we obtain

$$S_{2i}(\mathbf{F})=S_{2i}(\mathbf{F_0})+A_{i3}^{21}(\mathbf{F_0})u_{3,1}+A_{i3}^{22}(\mathbf{F_0})u_{3,2} . \tag{11}$$

According to the continuity conditions at the interface, the small wave motion is dynamically admissible if and only if, the static deformations and small wave motions satisfy the following conditions:

$$S_{21}(\mathbf{F_0})=\bar{S}_{21}(\overline{\mathbf{F}}_0)=0, \qquad S_{22}(\mathbf{F_0})=\bar{S}_{22}(\overline{\mathbf{F}}_0),$$

$$A_{33}^{22}(\mathbf{F_0})u_{3,2}=A_{33}^{22}(\overline{\mathbf{F}}_0)\bar{u}_{3,2} \text{ or } \rho_R c_{2\perp}^2 u_{3,2}=\bar{\rho}_R\bar{c}_{2\perp}^2\bar{u}_{3,2} \tag{12}$$

The relationship $(12)_2$ for $i = 2$ gives the dependency between the components λ_2 and $\overline{\lambda}_2$ in both half-spaces.

3. Reflection – refraction problem

It is assumed that the incident plane SH wave of given amplitude A_1 propagates in the lower medium. Taking into account the solutions (9) it is possible to define the wave motion in both regions I and II in the form:

$$u_3 = A_1 \exp\left[iK(N_1 X_1 + N_2 N_2 - c_n t)\right] + A_2 \exp\left[iK(N_1 X_1 - N_2 N_2 - c_n t)\right],$$
$$\overline{u}_3 = \overline{A}_1 \exp\left[i\overline{K}(\overline{N}_1 X_1 + \overline{N}_2 N_2 - \overline{c}_n t)\right], \tag{13}$$

where $K = k(1 + p^2)^{1/2}$, $\overline{K} = k(1 + \overline{p}^2)^{1/2}$ are wave numbers in respective regions. The above solution will of course change its character according to whether p and $\overline{p}$ are real or imaginary. Let us suppose that both p and $\overline{p}$ are real , i.e. $c = \omega / k > (c_{2//}, \overline{c}_{2//})$. The first and second term in $(13)_1$ are two plane waves in the first medium which propagate respectively, in the directions $\mathbf{N} = [N_1, N_2]$ (*incident wave*) and $\mathbf{N'} = [N_1, -N_2]$ (*reflected wave*) where (comp.(Fig. 1))

$$N_1 = (1 + p^2)^{-1/2}, \; N_2 = p(1 + p^2)^{-1/2} \tag{14}$$

with propagation speed

$$u_n = c\left(1 + p^2\right)^{-1/2} . \tag{15}$$

The expression $(13)_2$ represents the wave refracted in the second medium. The propagation directions and speed of propagation for this wave are obtained by replacing c and p in (14) and (15) by corresponding values $\overline{c}$ and $\overline{p}$ respectively.

The analysis of the reflection-refraction problem for the strain energy function in the general form $W = W(I_1, I_2, I_3)$ is very complicated. For this reason in the further considerations we take the special Blatz-Ko strain energy function adequate for the the foam rubber

$$W(I_2, I_3) = \frac{\mu}{2}\left(\frac{I_2}{I_3} - 3 + \frac{1 - 2\nu}{\nu}\left(I_1^{\frac{\nu}{1 - 2\nu}} - 1 \right) \right). \tag{16}$$

The expressions for the propagation speeds $c_{2//}$ and $c_{2\perp}$ in the directions paralell and perpendicular to the boundary take in this case very simple forms:

$$c_{2\perp}^2 = \frac{\mu}{\rho_R} \frac{1}{\lambda_3^2 \lambda_2^2} , \qquad c_{2//}^2 = \frac{\mu}{\rho_R} \frac{1}{\lambda_1^2 \lambda_2^2} . \tag{17}$$

Additionally the Poisson ratio ν for the foam rubber takes the value $\nu = 0.25$. Substituting this value into $(12)_2$ we obtain the following relationship between the components of the static deformation gradient

$$\frac{\bar{\lambda}_2}{\lambda_2} = \left[\Lambda\left(1 - \frac{\mu}{\bar{\mu}}\right)\lambda_2^3 + \frac{\mu}{\bar{\mu}} \right]^{-1/3} , \tag{18}$$

where $\Lambda = \lambda_1\lambda_3 = \bar{\lambda}_1\bar{\lambda}_3$. The unknown amplitudes A_2 and $\bar{A}_1$ can be determined on using the continuity conditions at the interface $(10)_4$, $(12)_{3,4}$. These yield

$$\frac{\bar{A}_1}{A_1} = \frac{2}{1+\Delta}, \quad \frac{A_2}{A_1} = \frac{1-\Delta}{1+\Delta} , \tag{19}$$

where

$$\Delta = \frac{\bar{\rho}_R}{\rho_R}\frac{\bar{c}_{2\perp}^2}{c_{2\perp}^2}\frac{\bar{p}}{p} = q\frac{\lambda_2^2}{\bar{\lambda}_2^2}\frac{1}{\cos\theta_I}\left(\left(\frac{\bar{\lambda}_2}{\lambda_2}\frac{c_2}{\bar{c}_2}\right)^2\left[\cos^2\theta_I + \frac{\lambda_3^2}{\lambda_1^2}\sin^2\theta_I\right] - \sin^2\theta_I\right)^{1/2} , \quad q = \bar{\mu}/\mu ,$$

θ_I is the incident angle and $c_2 = \sqrt{\mu/\rho_R}$, $\bar{c}_2 = \sqrt{\bar{\mu}/\rho_R}$ are shear wave speeds in initially undeformed medium i.e. when $\mathbf{F}_0 = \mathbf{1}$ and $\bar{\mathbf{F}}_0 = \mathbf{1}$ respectively. The structure of the expressions (19) is similar as in linear theory (comp.[1]), but the term Δ has more complicated form. The amplitude of the reflected waves vanishes wherever $\Delta=1$ or at the following angle of incidence

$$\sin^2\theta_0 = \left[1 - q^2\frac{\lambda_2^6}{\bar{\lambda}_2^6}\frac{c_2^2}{\bar{c}_2^2}\right]\left\{1 + q^2\frac{\lambda_2^4}{\bar{\lambda}_2^4}\left[\frac{c_2^2}{\bar{c}_2^2}\frac{\bar{\lambda}_2^2}{\lambda_2^2}\left(\frac{\lambda_3^2}{\lambda_1^2} - 1\right) - 1\right]\right\}^{-1} . \tag{20}$$

If $\mathbf{F}_0 = \mathbf{1}$ and $\bar{\mathbf{F}}_0 = \mathbf{1}$, then (20) takes the form well known from the linear theory $\sin^2\theta_{0Lin} = (1 - q^2 c_2^2/\bar{c}_2^2)/(1 - q^2)$ The geometrical nonlinearity influents very strong the results known from the linear theory. As a spectacular example it will be considered bellow the analysis of the expression for the incident angle (20) at which the reflected wave vanishes.

4. Numerical results

The numerical analysis will be confined here to define the angles of incidence θ_0 at which the reflected wave vanishes. It is evident, that a real angle θ_0 can be found only for selected combinations of the shear moduli, densities and initial deformations. For the analysis of (20) we assume here the following data representativ for the foam rubber

$q = \bar{\mu} / \mu = 1.1$, $\bar{\rho}_R / \rho_R = 1.07$ and $(c_2 / \bar{c}_2)^2 = 0.964$. For the chosen numerical data the solution θ_{0Lin} in the linear theory exists. Fig. 2 shows the relations between the values of the function $\sin^2 \theta_0$ at which the reflected wave vanishes, as function of the ratio $\bar{\lambda}_2 / \lambda_2$ for three values of the components rate $\Omega = \lambda_3 / \lambda_1$. It is easy to observe the essential dependence of the results on the initial deformations. The angles of incidence θ_0 vary rapidly in a small range of changes of the static deformations. This remark is important also for the analysis of the reflection and refraction coefficients (19).
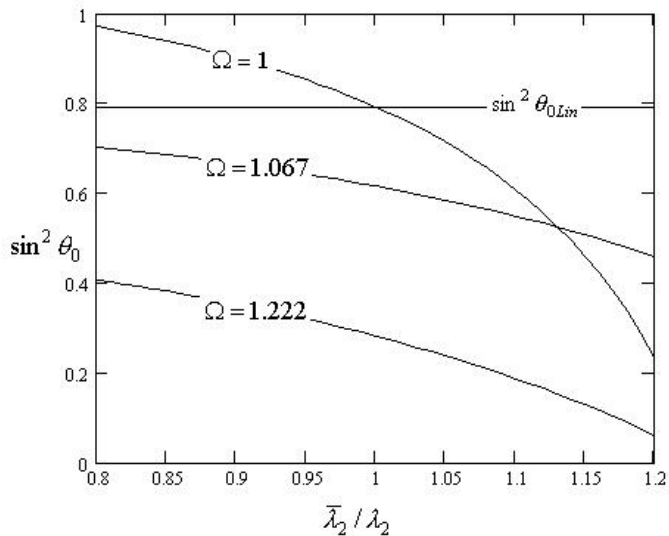
Fig. 2 The incident angle θ_0 at which the reflected wave vanishes
as function of the changing components ratio $\bar{\lambda}_2 / \lambda_2$ and $\Omega = \lambda_3 / \lambda_1$

Literature

1. A. C. Eringen, E. S. Suhubi, *Elastodynamics vol. II*, Academic Press, 1975.
2. R., W. Ogden, *Non-Linear Elastic Deformations*, Ellis Horwood Limited, Publishers Chichester 1984
3. S. Kosiński, *Fale sprężyste w gumopodobnych kompozytach warstwowych*, Monografie Politechniki Łódzkiej, Łódź 2007.

COMPARISON OF SDQM AND FDM IN NONLINEAR FREE VIBRATION ANALYSIS OF BEAM

Artur KROWIAK

Cracow University of Technology, Institute of Computing Science,
Al. Jana Pawła II 37, 31-864 Kraków, Poland
Tel.: +48 (12) 628-36-32; e-mail: krowiak@mech.pk.edu.pl

Abstract

In the paper the formulation of the differential quadrature method based on spline functions as well as the way of determination of the weighting coefficients are presented. The convergence and accuracy of the method in comparison to the finite difference method are studied on the example of the geometrically nonlinear free vibrations of a beam.

Keywords: differential quadrature method, nonlinear vibrations

Introduction

Recently the differential quadrature method (DQM) has become a tool that has been willingly used in solving various computational tasks, especially in mechanical analysis [1]. It is a result of a high rate of convergence and great accuracy provided by the method. With a few sampling points the method allows to obtain much better accuracy then popular discretization techniques as finite element or finite difference method (FDM). Better efficiency of the DQM follows from the way the wanted solution is approximated. In the conventional DQM the solution is searched in the form of the interpolation polynomial, whose nodes are all the sampling points from the entire domain, while in the other mentioned methods a local approximation is used. One can say that the conventional DQM is equivalent to the FDM of the highest order of accuracy. As a global numerical technique the DQM has some limitations and drawbacks. The main of them are difficulties with application to problems with irregular domain and computational instability. In order to overcome these drawbacks some modifications of the conventional method have still appeared. One of them is an approach presented in [2], where the spline interpolation is used to approximate the wanted solution. This approach eliminates unfavorable effects of the polynomial interpolation, especially appearing when the equally spaced nodes are imposed, that lead to instability of the method. It was found that spline-based differential quadrature method (SDQM) gives very accurate results using various grid point distributions and in the problems where the conventional method fails [2,3]. However the rate of convergence of the SDQM is weaker then the conventional method. Therefore the question concerning the efficiency of the SDQM in comparison to low order numerical techniques arises. In the paper the rate of convergence and the accuracy of the method based on spline functions are studied and compared with the results obtained by the FDM. The estimation is done on the example of the geometrically nonlinear free vibrations of a beam. The choice of the computational example has been motivated by the prediction contained in [4], that the efficiency of the DQM should rise with the higher nonlinearity of the problem.

1. Formulation of the problem

In the paper the equation for the geometrically nonlinear free vibrations of a beam with simply supported and immovable ends is analyzed. The equation of motion of the beam can be derived with various assumptions and with the help of several procedures, what is described in detail in [5]. In this paper the equation derived with the assumption of the axial displacement and nonlinear strain-displacement relationship is taken under consideration

$$m\frac{\partial^2 w}{\partial t^2} + EI\frac{\partial^4 w}{\partial x^4} - N\frac{\partial^2 w}{\partial x^2} = 0 \tag{1}$$

where w and m represent the transverse displacement and the mass density per unit length, respectively, E denotes Young's modulus and I is the moment of inertia.

Taking into account that the ends are immovable, the dynamic axial force N can be expressed as

$$N(t) = \frac{EA}{2L}\int_0^L \left(\frac{\partial w}{\partial x}\right)^2 dx \tag{2}$$

where A is the cross-section area of the beam and L denotes its length.

Assuming the solution in Equation (1) in the form

$$w(x,t) = a\upsilon(x)\cos\overline{\omega}t \tag{3}$$

where quantity $\upsilon(x)$ is the so-called nonlinear normal mode and $\overline{\omega}$ is the nonlinear free vibration frequency and applying Ritz-Galerkin procedure one obtains [5]

$$\overline{\omega}^2 m\upsilon + EI\frac{d^4\upsilon}{dx^4} - \frac{3}{4}\left[\frac{EAa^2}{2L}\int_0^L \left(\frac{d\upsilon}{dx}\right)^2 dx\right]\frac{d^2\upsilon}{dx^2} = 0 \tag{4}$$

Further analysis is carried out using the dimensionless form of Equation (4)

$$\omega^2 \upsilon + \frac{d^4\upsilon}{d\xi^4} - \frac{3}{8}\left(\frac{a^2}{r^2}\int_0^1 \left(\frac{d\upsilon}{d\xi}\right)^2 d\xi\right)\frac{d^2\upsilon}{d\xi^2} = 0 \tag{5}$$

where $\xi = \dfrac{x}{L}$, $\omega^2 = \overline{\omega}^2\dfrac{mL^4}{EI}$, $r^2 = \dfrac{I}{A}$

The problem is completed by the boundary conditions which have the following form

$$\upsilon(0) = \upsilon''(0) = \upsilon(1) = \upsilon''(1) = 0 \tag{6}$$

2. Discretization of the problem

To discretize Equations (5) and (6), the SDQM and classic formulation of FDM are used.

2.1. Spline-based differential quadrature method

The idea of the method is similar to the difference method and relies on the approximation of the derivatives in the governing equation by the linear weighted sum of unknown function values. The difference to the FDM lies in the fact that each derivative is expressed with the aid of all function values from the entire domain, what can be put as

$$\frac{d^r f(x)}{dx^r}\Big|_{x=x_i} = \sum_{j=1}^{N} a_j^{(r)}(x_i) f(x_j) = \sum_{j=1}^{N} a_{ij}^{(r)} f_j \quad i = 1,...,N \tag{7}$$

where N denotes the number of grid points and $a_{ij}^{(r)}$ are the weighting coefficients for the rth order derivative.

In the SDQM these coefficients are determined on the base of the piecewise polynomial interpolation. Using odd degree polynomials, the function can be expressed as

$$f(x) \approx \left\{ s_i(x), \ x \in [x_i, \ x_{i+1}], \ i = 1,..,N-1 \right\} \tag{8}$$

where the ith spline section has the form

$$s_i(x) = \sum_{j=0}^{n} c_{ij} x^j \tag{9}$$

The coefficients c_{ij} are determined from the interpolation conditions and the derivative continuity ones described in detail in [2]. These coefficients depend on nodes distribution and unknown function values, what can be generally written as

$$c_{ij} = \sum_{k=1}^{N} C_{ijk}(x_1,...,x_N) f_k, \quad i = 1,...,N-1, j = 0,...,n \tag{10}$$

The weighting coefficients $a_{ij}^{(r)}$ are determined by calculating appropriate derivatives of polynomial piecewise function (8)

$$a_{ik}^{(r)} = \sum_{j=r}^{n} \left(C_{ijk} x_i^{j-r} \prod_{l=j-r+1}^{j} l \right), \quad i = 1,...,N-1, \ a_{Nk}^{(r)} = \sum_{j=r}^{n} \left(C_{N-1jk} x_N^{j-r} \prod_{l=j-r+1}^{j} l \right) \tag{11}$$

In the paper the weighting coefficients obtained from the polynomial piecewise function of the eleventh degree ($n = 11$) are used. Owing to the appropriate formulation of the conditions for the determination of the spline function, the derivative boundary

conditions are introduced on the stage of the calculation of the weighting coefficients (11). Then the discretization of the analyzed Equation (5) according to the differential quadrature rules is done in N-2 interior points of imposed mesh

$$\sum_{j=2}^{N-1} a_{ij}^{(4)} \upsilon_j - \frac{3}{8}\left(\frac{a}{r}\right)^2 \left[\sum_{k=1}^{N} C_k \left(\sum_{r=2}^{N-1} a_{kr}^{(1)} \upsilon_r\right)\left(\sum_{s=2}^{N-1} a_{ks}^{(1)} \upsilon_s\right)\right]\sum_{j=2}^{N-1} a_{ij}^{(2)} \upsilon_j = \omega^2 \upsilon_i, \quad i = 2,...,N-1 \quad (12)$$

where C_k are the coefficients derived by the Newton-Cotes integration formulas.

2.2. Finite difference method

To discretize Equation (5) classic formulation of the FDM (based on the uniform grid distribution) is also used. This approach is well known and does not require detailed description. The difference equation corresponding to Equation (5) has the form

$$\gamma_i - \frac{3}{8}\left(\frac{a}{r}\right)^2\left[\sum_{k=1}^{N} C_k \alpha_k \alpha_k\right]\beta_i = \omega^2 \upsilon_i, \quad i = 2,...,N-1 \quad (13)$$

where α_k, β_i i γ_i are difference formulas for the first, second and fourth order derivatives respectively. In the paper the three-points (first and second order derivative) and five-points (fourth order derivative) central difference formulas are used

$$\alpha_k = \frac{\upsilon_{k+1} - \upsilon_{k-1}}{2h}, \quad \beta_i = \frac{\upsilon_{i-1} - 2\upsilon_i + \upsilon_{i+1}}{h^2}, \quad \gamma_i = \frac{\upsilon_{i-2} - 4\upsilon_{i-1} + 6\upsilon_i - 4\upsilon_{i+1} + \upsilon_{i+2}}{h^4}$$

where $h = 1/(N-1)$ denotes the distance between adjacent nodes.

3. Solution of nonlinear eigenvalue problem

Expressions (12) and (13) are the sets of N-2 nonlinear algebraic equations, which can be written in the following matrix form

$$\mathbf{F}(\upsilon, a) = \lambda \upsilon \quad (14)$$

where $\lambda = \omega^2$, υ is the nodal values vector and $\mathbf{F}(\upsilon, a)$ is the vector whose elements are nonlinear functions of the elements of υ and the parameter a (the amplitude of vibration). In order to determine the fundamental frequency of the beam, Equation (14) has to be solved. To this end, the vector iteration method, described in detail in [6], is used. The iteration scheme related to Equation (14) is as follows

$$\mathbf{F}(\upsilon_{i+1}, a) = \lambda_i \upsilon_i \quad (15)$$

To solve Equation (15), the Newton-Raphson method is applied. As starting values for the nonlinear eigenpair (λ, υ), the values that meet the associated linear problem are

assumed. In each cycle of the iteration, the eigenvector $\mathbf{v}_i$ should be normalized so that $\left\|\mathbf{v}_i\right\|_\infty = \max_j \upsilon_{j,i} = 1$, before using in Equation (15). New approximation of λ is obtained as

$$\lambda_{i+1} = \lambda_i \frac{\left\|\mathbf{v}_i\right\|_\infty}{\left\|\mathbf{v}_{i+1}\right\|_\infty} \qquad (16)$$

The iteration process is broken when $\left|\lambda_{i+1} - \lambda_i\right|/\lambda_{i+1} \le \varepsilon_1$, $\left\|\mathbf{v}_{i+1} - \mathbf{v}_i\right\|_2 / \left\|\mathbf{v}_{i+1}\right\|_2 \le \varepsilon_2$, where ε_1 and ε_2 are assumed accuracies of the calculation.

The percentage relative error of the ratio of the nonlinear frequency to the linear one ω/ω_L versus number of sampling points applied is shown in Fig.1. As a reference values the exact results are chosen. The calculations are carried out for several dimensionless amplitudes. Fig.1 shows that the SDQM gives very accurate results even using only few nodes. One can notice that when the amplitude of vibration rises the rate of convergence of SDQM is higher unlike the FDM. It is clearly seen in Fig.2 when the results for $N = 7, 15$ are presented as a dependence on the amplitude of vibration.

$\Diamond$ - SDQM $\bigcirc$ - FDM
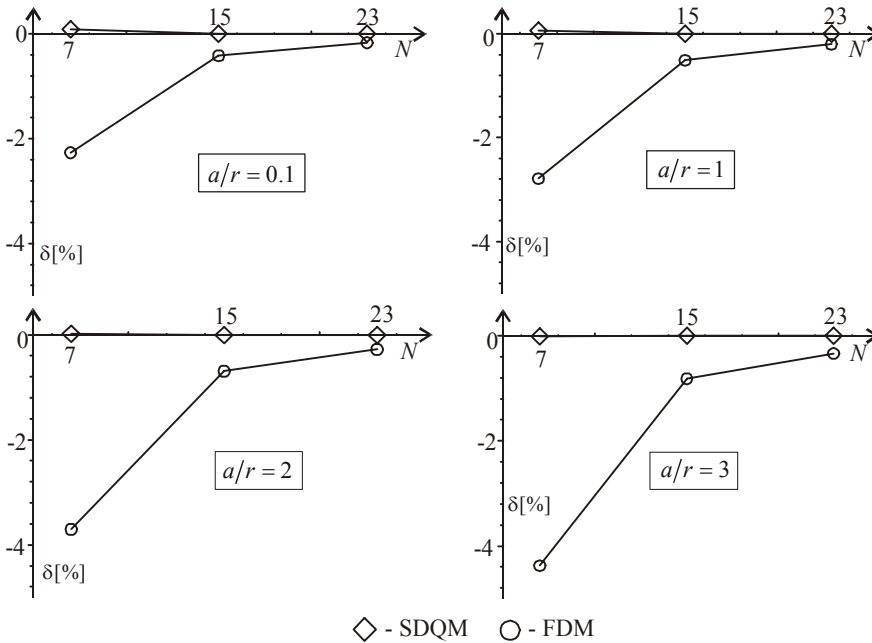
Fig.1. The percentage relative error of the ratio of the nonlinear frequency to the linear one versus number of sampling points
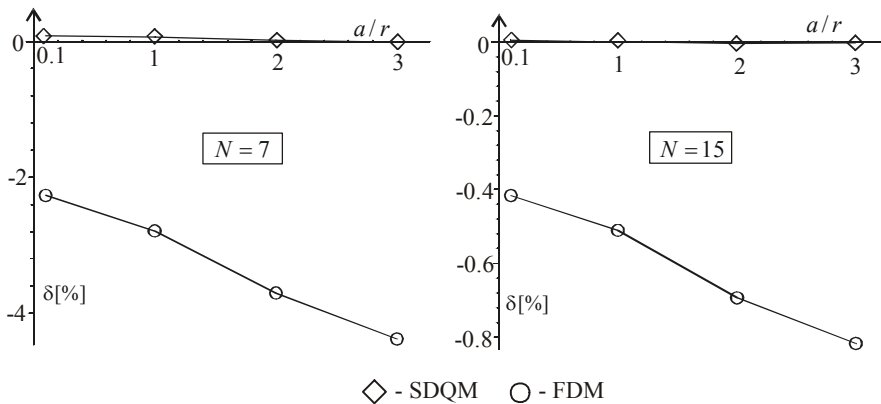
Fig.2. The percentage relative error of the ratio of the nonlinear frequency to the linear one versus dimensionless amplitudes

4. Conclusion

In the paper the convergence and accuracy of the SDQM – the alternative for the known method based on the interpolation polynomial – and classic FDM are compared on the example of the nonlinear vibration of the beam. The results show that the rate of convergence of the SDQM is considerably higher then the FDM and improves when the amplitude of vibration rises. It should be noted that the solution of the nonlinear set of equations (15) takes more time when the differential quadrature discretization is applied. However very accurate results can be obtained using only few discrete points.

Literature

1. C.W. Bert, M. Malik, *Differential quadrature method in computational mechanics*, Applied Mechanics Review, **49** (1996) 1-28
2. A. Krowiak, *Symbolic computing in spline-based differential quadrature method*, Commun. Numer. Meth. Engng, **22** (2006) 1097-1107
3. A. Krowiak, *The Convergence and stability of the spline-based differential quadrature method applied to the vibration analysis of rectangular plates with free corners*", Vibr. physical systems, Poznań – Będlewo 2006, 197-202
4. W. Chen, T. Zhong*, The Study on the Nonlinear Computations of the DQ and DC Methods,* Num. Meth. Partial Diff. Equations, **13** (1997) 57-75
5. G. Singh, A.K. Sharma, G.V. Rao, *Large-amplitude free vibrations of beams – a discussion on various formulations and assumptions*, J. Sound & Vibration, **142** (1990) 77-85
6. R. Lewandowski, *Free vibrations of structures with cubic non-linearity – remarks on amplitude equation and Rayleigh quotient*, Comput. Meth. Appl. Mech. Engrg, **192** (2003) 1681-1709

STOCHASTIC APPROACH TO MOVEMENTS OF A MULTIHULL
ON WAVES

Agnieszka KRÓLICKA

Gdansk University of Technology, Faculty of Ocean Engineering and Ship Technology

Narutowicza 11/12, 80-952 Gdańsk, Poland

Ph. :(58)347-11-46, e-mail: krag@pg.gda.pl

Abstract

Due to difficulties in determining precise initial conditions for the motion of sea waves and the nature of wind undulation, the dynamics of sea waves can be only modelled within the framework of a stochastic theory.

The article presents a method for determining differential equations of motion for multihulls, such as catamaran or trimaran. The catamaran sails at constant translatory velocity and at an arbitrary angle to the undulation direction. The set of differential equations of motion presented in the article models anti-symmetric (lateral) movements of the catamaran. For those movements, stochastic differential equations (*Itô* equations) are constructed in the form of the equation set (8). Using the state vector X and the excitation vector Y, the *Itô* equations take the form (9) and (10).

1. Introduction

With respect to their marine operation, watercraft units can be divided into stationary objects (in the geographic sense) or moving objects. The latter include catamarans and trimarans as the units equipped with their own drive. These units represent extremely complicated dynamic systems and reveal strongly nonlinear characteristics.

A catamaran (**double hull**) is a watercraft unit having two hulls situated parallel to each other and linked with a deck.

Fig.1. Large experimental catamaran built for military purposes

Fig.2. Lagoon Catamaran

Catamarans are built in various sizes, from big ocean-going vessels down to small boats, the length of which does not exceed 5 meters. They can be either equipped with an

engine, or driven by wind or paddles. An advantage revealed by the catamaran is high initial stability, which (in case of sail drive) allows it to reach much higher speeds than those achieved by monohulls of comparable size. It also reveals higher resistance to side-overturning. At the same time its disadvantage is almost inability to restore the correct position when the overturning already takes place, and higher susceptibility to bow-overturning. Both catamarans and trimarans, frequently referred to as *pontonboots*, are flat-bottomed boats with multi-chamber floats, stable and safe.

2. Movements of the catamaran as a linear object

A multihull with non-deformable structure sails freely at constant translatory velocity V_0.

In our studies the examined object is idealised as a linear dynamic system with 6 freedom degrees, which are:

    a)   longitudinal oscillation (surge)- η_1 ,

    b)   lateral oscillation (sway)- η_2 ,

    c)   heaving - η_3 ,

    d)   rolling - η_4 ,

    e)   pitching - η_5 ,

    f)   yawing - η_6 .
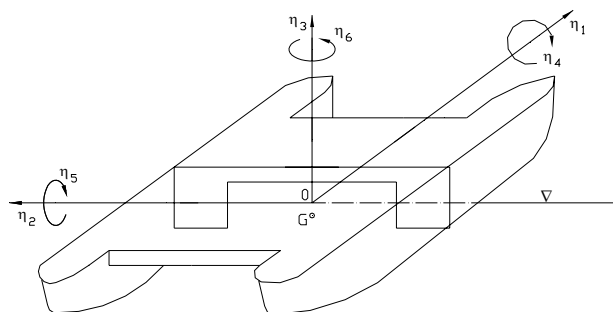
Fig. 3. Scheme of the physical model of a catamaran

Local movements of the vessel around the equilibrium position are its response to the excitations coming from sea undulation.

For the vessel treated as a rigid object moving at constant speed v and an arbitrary angle to the direction of sea waves, its movements are described by the mathematical model having the form of a set of second-order differential equations (1).

If the model of the dynamic system is a linear model of watercraft, then the equations

$$\sum_{i,j=1}^{6} I_{ij}\ddot{\eta}_i + B_{ij}\ \dot{\eta}_i + C_{ij}\ \eta_i = F_i(t) \tag{1}$$

in which:

$I = M + A$ - matrix of inertia,

B - matrix of dynamic damping,

C - matrix of hydrostatic stiffness,

η - vector of displacements,

$F(t)$ - vector of exciting forces,

can be treated as a system of two uncoupled groups of mutually coupled equations. The coupling is assumed to be executed via linear and nonlinear damping coefficients and hydrostatic elasticity coefficients.

The first group of equations represents symmetric (longitudinal) movements. They include η_1 - linear longitudinal movements (surging), η_3 - linear vertical movements (heave) and η_5 - angular longitudinal, movements (pitch). In our discussion we will neglect η_1 - linear longitudinal movements (surging). These movements are usually examined on models with one freedom degree.

The second group consists of the equations describing antisymmetric movements. They include:

η_2 - lateral linear movements (swaying), η_4 - lateral angular movements (rolling) and

η_6 - horizontal angular movements (yawing).

Since our further goal is to construct stochastic differential equations ($It\hat{o}$ equations), let us introduce new variables:

$$\begin{Bmatrix} \eta_1 \\ \eta_3 \\ \eta_5 \\ \eta_2 \\ \eta_4 \\ \eta_6 \end{Bmatrix} = \begin{Bmatrix} z_1 \\ z_2 \\ z_3 \\ z_4 \\ z_5 \\ z_6 \end{Bmatrix} \tag{2}$$

The mutually coupled variables are η_3, η_5 and η_2, η_4, η_6.

Equation (1), taking into account two groups of mutually coupled movements, takes the following form written in new variables:

$$
\begin{bmatrix}
M_{11}+A_{11} & 0 & 0 & 0 & 0 & 0 \\
0 & 0 & M_{23}+A_{23} & 0 & M_{25}+A_{25} & 0 \\
0 & 0 & M_{33}+A_{33} & 0 & M_{35}+A_{35} & 0 \\
0 & M_{42}+A_{42} & 0 & M_{44}+A_{44} & 0 & M_{46}+A_{46} \\
0 & M_{52}+A_{52} & 0 & M_{54}+A_{54} & 0 & M_{56}+A_{56} \\
0 & M_{62}+A_{62} & 0 & M_{64}+A_{64} & 0 & M_{66}+A_{66}
\end{bmatrix}
\begin{Bmatrix}
\ddot{z}_1 \\ \ddot{z}_4 \\ \ddot{z}_2 \\ \ddot{z}_5 \\ \ddot{z}_3 \\ \ddot{z}_6
\end{Bmatrix}+
$$

$$
+\begin{bmatrix}
B_{11} & 0 & 0 & 0 & 0 & 0 \\
0 & 0 & B_{23} & 0 & B_{25} & 0 \\
0 & 0 & B_{33} & 0 & B_{35} & 0 \\
0 & B_{42} & 0 & B_{44} & 0 & B_{46} \\
0 & B_{52} & 0 & B_{54} & 0 & B_{56} \\
0 & B_{62} & 0 & B_{64} & 0 & B_{66}
\end{bmatrix}
\begin{Bmatrix}
\dot{z}_1 \\ \dot{z}_4 \\ \dot{z}_2 \\ \dot{z}_5 \\ \dot{z}_3 \\ \dot{z}_6
\end{Bmatrix}+
\begin{bmatrix}
C_{11} & 0 & 0 & 0 & 0 & 0 \\
0 & 0 & C_{23} & 0 & C_{25} & 0 \\
0 & 0 & C_{33} & 0 & C_{35} & 0 \\
0 & C_{42} & 0 & C_{44} & 0 & C_{46} \\
0 & C_{52} & 0 & C_{54} & 0 & C_{56} \\
0 & C_{62} & 0 & C_{64} & 0 & C_{66}
\end{bmatrix}
\begin{Bmatrix}
z_1 \\ z_4 \\ z_2 \\ z_5 \\ z_3 \\ z_6
\end{Bmatrix}=
\begin{Bmatrix}
F_1 \\ F_4 \\ F_2 \\ F_5 \\ F_3 \\ F_6
\end{Bmatrix}
$$

To get explicit forms of the equations with respect to $\ddot{z}$ we have to solve a set of second-order differential equations with two unknowns.

$$
\ddot{z}_k = \phi_k + \widetilde{F}_k \tag{3}
$$

or

$$
\begin{Bmatrix}
\ddot{z}_1 \\ \ddot{z}_2 \\ \ddot{z}_3 \\ \ddot{z}_4 \\ \ddot{z}_5 \\ \ddot{z}_6
\end{Bmatrix}=
\begin{bmatrix}
\phi_1 \\ \phi_2 \\ \phi_3 \\ \phi_4 \\ \phi_5 \\ \phi_6
\end{bmatrix}+
\begin{bmatrix}
\widetilde{F}_1 \\ \widetilde{F}_2 \\ \widetilde{F}_3 \\ \widetilde{F}_4 \\ \widetilde{F}_5 \\ \widetilde{F}_6
\end{bmatrix} \tag{4}
$$

Here:

$$
\begin{aligned}
\phi_k &= B_k + C_k \\
dla \quad k &= 1, \quad B_k = B_k(\dot{z}_1), \quad C_k = C_k(z_1), \\
dla \quad k &= 2,3, \quad B_k = B_k(\dot{z}_2, \dot{z}_3), \quad C_k = C_k(z_2, z_3), \\
dla \quad k &= 4,5,6, \quad B_k = B_k(\dot{z}_4, \dot{z}_5, \dot{z}_6), \quad C_k = C_k(z_4, z_5, z_6).
\end{aligned} \tag{5}
$$

3. Stochastic equations for a linear object (*Itô* equations)

In the stochastic differential equations (*Itô* equations), making the starting point for examining the nonlinear process of object response with the aid of the method based on

the diffusion process theory, the state vector has components representing construction response and those representing the multidimensional Markov process that models undulation excitation.

Stochastic *Itô* equations are used for modelling dynamic systems with rapidly changing random excitations, for instance those described by white noise. At relatively general assumptions, the solutions to the stochastic *Itô* equations are Markov diffusion processes.

Equations (1) for separated coupled movements η_2, η_4 and η_6 can be written as:

$$\ddot{\eta}_i + b_i(\dot{\eta}_2, \dot{\eta}_4, \dot{\eta}_6) + c_i(\eta_2, \eta_4, \eta_6) = \widetilde{F}_i \tag{6}$$

where:
$$\widetilde{F}_i = \widetilde{F}_i(F_2, F_4, F_6), \quad dla \quad i = 2,4,6$$

In the new variables z_4, z_5 and z_6 adopted by us at the beginning the equations (6) take the form:

$$\ddot{z}_i = \varphi_i(\dot{z}_4, \dot{z}_5, \dot{z}_6) + \psi_i(z_4, z_5, z_6) + f_i(t) \tag{7}$$

where:

$i = 4,5,6$,

φ_i - damping in i-th movement,

ψ_i - stiffness in i-th movement,

f_i - excitation in i-th movement.

Finally, *Itô* equations for z_4, z_5 and z_6 take the form:

$$\left.\begin{aligned}
\ddot{z}_4 &= \varphi_4(\dot{z}_4, \dot{z}_5, \dot{z}_6) + \psi_4(z_4, z_5, z_6) + f_4(t) \\
\ddot{z}_5 &= \varphi_5(\dot{z}_4, \dot{z}_5, \dot{z}_6) + \psi_5(z_4, z_5, z_6) + f_5(t) \\
\ddot{z}_6 &= \varphi_6(\dot{z}_4, \dot{z}_5, \dot{z}_6) + \psi_6(z_4, z_5, z_6) + f_6(t)
\end{aligned}\right\} \tag{8}$$

If the process F(t) can be presented by a multidimensional homogeneous Markov process in the phase space corresponding to the vector

$$Y(y_1, y_2, \ldots y_n), \quad where \quad Y = F(t) \quad then \quad F(t) = \sum_0^3 (a_i y_1^i + b_i y_2^i) = F(y_1, y_2, y_3, y_4).$$

Let X be the state vector, components of which describe the behaviour of the object modelled by the set of second-order differential equations, and let vector Y represent the excitations, then the *Itô* equations take the form:

$$\dot{X} = G(X) + F(t) \tag{9}$$

with:

$$
\left.\begin{array}{ll}
x_1 = z_4 & y_1 = F_4(t) \\
x_2 = \dot{z}_4 & \dot{y}_1 = y_2 \\
x_3 = z_5 & \dot{y}_2 = y_3 \\
x_4 = \dot{z}_5 & \dot{y}_3 = -S_{04} - S_{14}y_1 - S_{24}y_2 - S_{34}y_3 + \xi_4(t) \\
x_5 = z_6 & y_4 = F_5(t) \\
x_6 = \dot{z}_6 & \dot{y}_4 = y_5 \\
\dot{x}_1 = x_2 & \dot{y}_5 = y_6 \\
\dot{x}_2 = \ddot{z}_4 & \dot{y}_6 = -S_{05} - S_{15}y_1 - S_{25}y_2 - S_{35}y_3 + \xi_5(t) \\
\dot{x}_3 = x_4 & y_7 = F_6(t) \\
\dot{x}_4 = \ddot{z}_5 & \dot{y}_7 = y_8 \\
\dot{x}_5 = x_6 & \dot{y}_8 = y_9 \\
\dot{x}_6 = \ddot{z}_6 & \dot{y}_9 = -S_{06} - S_{16}y_1 - S_{26}y_2 - S_{36}y_3 + \xi_6(t)
\end{array}\right\}
\tag{10}
$$

Here:

ξ - white noise,

S_i - coefficients of linear filters (determined from the excitation correlation function, or from its spectral density).

Using relevant linear filters the "white noise" process, for which the spectral density is constant, is substituted by densities corresponding to different undulation spectra.

References

[1]Davis M.R., Holloway D.S. and Watson N.L., *Dynamic wave loads on a high speed catamaran ferry fitted with t-foils and stern* tabs, Transactions of the Royal Institution of Naval Architects, International Journal of Maritime Engineering, Vol. 148, Part A1,
1-16, 2006.
[2]Gichman I.I., Skorochod A.W., *Introduction to the theory of stochastic processes,* Warsaw 1968 (in Polish).
[3]Gutowski R., *Ordinary differential equations,* Warsaw 1971 (in Polish).
[4]Kang D., Hasegawa K., *Prediction method of hydrodynamic forces acting on the hull of a blunt-body ship in the even keel condition*, Journal of Marine Science and Technology, Vol. 12, Number 1, 1-14, 2007.
[5]Królicka A., *Unsymmetrical movements of a multi-hull vessel treated as a linear object*, Marine Technology Transactions, Vol. 18, pp. 63-74, Gdańsk 2007.
[6]Rumianowski A., *Investigating the dynamics of selected marine floating objects*, Gdańsk 2003 (in Polish).
[7]Rumianowski A., *Stochastic approach to the dynamics of marine floating objects,* Marine Technology Transactions Vol. 17, pp. 155-165, Gdańsk 2006.
[8]Sobczyk K., *Stochastic differential equations*, Warsaw 1996 (in Polish).
[9]Sobczyk K, Spencer Jr.,B.F., *Stochastic material fatigue models,* Wydawnictwa Naukowo-Techniczne, Warsaw 1996 (in Polish).
[10]Wu M.K., Moan T., *Numerical prediction of wave-induced long-term extreme load effects in a flexible high-speed pentamaran*, Journal of Marine Science and Technology, Vol. 11, Number 1, 39-51, 2006.

IDENTIFICATION OF PARAMETERS
OF THE FRACTIONAL MAXWELL MODEL
Roman LEWANDOWSKI, Bartosz CHORĄŻYCZEWSKI
Poznan University of Technology, Institute of Structural Engineering
60-965 Poznań, ul. Piotrowo 5
Phone: (+48) 61 6652472, E-mail: roman.lewandowski@put.poznan.pl

Abstract

The passive dampers are often modeled using the either classical or fractional rheological models. An important problem, bounded with the fractional models, is an estimation of the model parameters from the experimental data. The process of parameter identification is an inverse problem which is underdetermined and can be ill conditioned. The new method of parameters identification of the fractional Maxwell model is proposed. The parameters are estimated using results obtained from dynamical tests. Results of example calculation based on artificial and experimental data are presented.

Keywords: dampers, identification of parameters, fractional Maxwell model

Introduction

Viscoelastic (VE) dampers have been often used for control vibration of structures to reduce of oscillations of building structures induced by earthquakes and strong winds. Many applications of VE dampers in civil engineering are listed in [1]. The VE dampers could be divided broadly into the fluid and the solid VE dampers. Analysis of structures supplemented with VE dampers requires the good description of the dynamical behaviour of dampers. The dampers behaviour depends mainly on the rheological properties of the viscoelastic material from which dampers are made.

In a classical approach, the mechanical models consisting of the springs and dashpots are used to describe the rheological properties of VE dampers [2, 3]. A good description of VE dampers requires mechanical models build from a set of appropriately connected springs and dashpots. In this approach the dynamic behaviour of **a** single damper is described by a set of differential equation, (see [3]) what considerably complicate the dynamic analysis of structures with dampers because the large set of motion equation must be solve. Moreover, the nonlinear regression procedure, described for example in [4], must be used to determine parameters of the mentioned above models.

The rheological properties of VE dampers are also described using the fractional mechanical models. Currently this approach received considerable attention and has been used in modeling the rheological behaviour of linear viscoelastic materials [5 – 7]. The fractional models have an ability to correctly describe the behaviour of viscoelastic material using a small number of parameters. A single equation is enough to describe the VE damper dynamics, what is an important advantage of the discussed models. In this case the VE damper equation of motion is the fractional differential equation. The fractional models of VE fluid dampers are proposed in [8, 9].

An important problem, bounded with fractional models is an estimation of model parameters from the experimental data. In the past, many different methods have been tested for estimation of model parameters [2, 10, 11]. The process of parameter identification is an inverse problem which can be ill conditioned (see, [4, 11]).

The aim of this paper is to describe a new method of parameters identification of the fractional Maxwell model. The parameters are estimated using results obtained from dynamical tests. Results of example calculation are further presented.

1. Fractional Maxwell model equation of motion and their steady state solution

In order to construct the fractional models equation of motion, we introduce the fractional element called also the springpot which obey the following equation:

$$u(t) = \widetilde{c}^{\alpha} D_t^{\alpha} q(t) = c \, D_t^{\alpha} q(t) \ , \tag{1}$$

where $c = \widetilde{c}^{\alpha}$ and α, ($0 < \alpha \le 1$), are the springpot parameters and $D_t^{\alpha} q(t)$ is the fractional derivative of order α with respect to time t. There are a few definitions of fractional derivatives which coincide under certain conditions. Here, symbols like $D_t^{\alpha} q(t)$ means the Riemann-Liouville fractional derivatives with the lower limit $-\infty$ (see [12]). The considered element can be understood as an interpolation between the spring element ($\alpha = 0$) and the dashpot element ($\alpha = 1$).

The fractional Maxwell model is build from the spring and the springpot connected in series as it is shown schematically on Fig 1. For the considered model we can write:

$$u(t) = k \, q_1(t) \ , \qquad u(t) = \widetilde{c}^{\alpha} D_t^{\alpha} (q(t) - q_1(t)) \ , \tag{2}$$

where $\widetilde{\tau} \equiv \tau^{\alpha} = \widetilde{c}^{\alpha} / k = c / k$.

Eliminating $q_1(t)$ from above relations we get the motion equation in the form:

$$u(t) + \tau^{\alpha} \, D_t^{\alpha} u(t) = k\tau^{\alpha} D_t^{\alpha} q(t) \ . \tag{3}$$

The considered model has three real and positive value parameters: k, c and α.
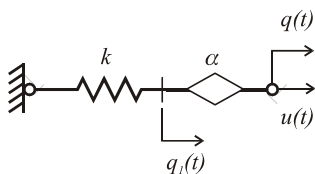
Fig. 1 Scheme of fractional Maxwell model

In a case of harmonically excitation, the steady state solution to motion equation of the Maxwell fractional model is assumed in the following form:

$$u(t) = u_c \cos \lambda t + u_s \sin \lambda t \ , \qquad q(t) = q_c \cos \lambda t + q_s \sin \lambda t \ , \qquad (4)$$

where λ is the excitation frequency.

Introducing relations (4) into equation (3) we obtain that the coefficients q_c, q_s, u_c and u_s are interrelated in the following way:

$$q_c = \phi_1 u_c - \phi_2 u_s \ , \qquad\qquad q_s = \phi_2 u_c + \phi_1 u_s \ , \qquad (5)$$

where

$$\phi_1 = \frac{1}{k(\tau\lambda)^\alpha} \left[(\tau\lambda)^\alpha + \cos(\alpha\pi/2) \right] \ , \qquad \phi_2 = \frac{1}{k(\tau\lambda)^\alpha} \sin(\alpha\pi/2) \ . \qquad (6)$$

2. Identification of parameters of the fractional Maxwell model

In the proposed method, for the given frequency of excitation λ_i, the experimentally measured damper force $u_{ei}(t)$ and the experimentally measured damper displacement $q_{ei}(t)$ are approximated by

$$\widetilde{u}_i(t) = \widetilde{u}_{ci} \cos \lambda_i t + \widetilde{u}_{si} \sin \lambda_i t \ , \qquad \widetilde{q}_i(t) = \widetilde{q}_{ci} \cos \lambda_i t + \widetilde{q}_{si} \sin \lambda_i t \ , \qquad (7)$$

where quantities $\widetilde{u}_{ci}$, $\widetilde{u}_{si}$, $\widetilde{q}_{ci}$ and $\widetilde{q}_{si}$ are determined using the last-square method. When the experimental data concerning damper force are considered the values of $\widetilde{u}_{ci}$ and $\widetilde{u}_{si}$ are obtained from the following equations:

$$I_{cc}\widetilde{u}_{ci} + I_{sc}\widetilde{u}_{si} = I_{cu} \ , \qquad\qquad I_{sc}\widetilde{u}_{ci} + I_{ss}\widetilde{u}_{si} = I_{su} \ , \qquad (8)$$

where

$$I_{cc} = \int_{t_1}^{t_2} \cos^2 \lambda_i t dt \ , \qquad I_{ss} = \int_{t_1}^{t_2} \sin^2 \lambda_i t dt \ , \qquad I_{cs} = I_{sc} = \int_{t_1}^{t_2} \sin \lambda_i t \cos \lambda_i t dt \ , \qquad (9)$$

$$I_{cu} = \int_{t_1}^{t_2} u_{ei}(t) \cos \lambda_i t \, dt \ , \qquad\qquad I_{su} = \int_{t_1}^{t_2} u_{ei}(t) \sin \lambda_i t \, dt \ . \qquad (10)$$

In a similar way the parameters $\widetilde{q}_{ci}$ and $\widetilde{q}_{si}$ are determined.

Next, we assume that the quantities $\widetilde{u}_{ci}$, $\widetilde{u}_{si}$, $\widetilde{q}_{ci}$ and $\widetilde{q}_{si}$ obtained from the experimental data approximately fulfils equations (5) i.e. we can rewrite (5) in the form:

$$\phi_{1i}\widetilde{u}_{ci} - \phi_{2i}\widetilde{u}_{si} = \widetilde{q}_{ci} \ , \qquad\qquad \phi_{2i}\widetilde{u}_{ci} + \phi_{1i}\widetilde{u}_{si} = \widetilde{q}_{si} \ , \qquad (11)$$

where $\phi_{1i} = \phi_{1i}(\lambda_i)$ and $\phi_{2i} = \phi_{2i}(\lambda_i)$. From above equations we have

$$\phi_{1i} = \frac{\widetilde{q}_{ci}\widetilde{u}_{ci} + \widetilde{q}_{si}\widetilde{u}_{si}}{\widetilde{u}_{ci}^2 + \widetilde{u}_{si}^2} \ , \qquad\qquad \phi_{2i} = \frac{\widetilde{q}_{si}\widetilde{u}_{ci} - \widetilde{q}_{ci}\widetilde{u}_{si}}{\widetilde{u}_{ci}^2 + \widetilde{u}_{si}^2} \ . \qquad (12)$$

For a given set of excitation frequencies λ_i ($i = 1,2,..,n$), used in experiments, two sets of values of ϕ_{1i} and ϕ_{2i} are obtained.

The model parameters c, k and α will be determined using the last-square method. The error functional which will be minimized is chosen in the form:

$$J(\bar{c}, \bar{k}, \alpha) = \sum_{i=1}^{n}(r_i^2 + s_i^2) , \qquad (13)$$

where $\bar{k} = 1/k$, $\bar{c} = 1/c$ and

$$r_i = \bar{k} + \bar{c}\lambda_i^{-\alpha}\cos\frac{\alpha\pi}{2} - \phi_{1i} , \qquad s_i = \bar{c}\lambda_i^{-\alpha}\sin\frac{\alpha\pi}{2} - \phi_{2i} . \qquad (14)$$

If we assume that parameter α is known, the stationary conditions of functional (13) with respect to $\bar{k}$ and $\bar{c}$ give us the following system of equations:

$$n\bar{k} + \bar{c}\sum_{i=1}^{n}\lambda_i^{-\alpha}\cos\frac{\alpha\pi}{2} = \sum_{i=1}^{n}\phi_{1i} ,$$

$$\bar{k}\sum_{i=1}^{n}\lambda_i^{-\alpha}\cos\frac{\alpha\pi}{2} + \bar{c}\sum_{i=1}^{n}\lambda_i^{-2\alpha} = \sum_{i=1}^{n}\lambda_i^{-\alpha}\left(\phi_{1i}\cos\frac{\alpha\pi}{2} + \phi_{2i}\sin\frac{\alpha\pi}{2}\right) , \qquad (15)$$

For particular values of α the values of damper parameters, resulting from (15), could be negative. These solutions haven't physical meaning and must be rejected. The right value of α are obtained using the method of systematic searching. The values of α, $\bar{k}$ and $\bar{c}$ for which (13) has a minimal value are the searched parameters of the model.

3. Results of example identification of Maxwell model parameters

First the method is applied to the artificially generated experimental data. The artificial solutions are calculated on a base of steady state solution given by relations (4) and (5). The following data are used: $n = 9$ $q_c = 0$, $q_s = 0.001\,m$, $\alpha = 0.6$ $k = 290.0\,kN/m$, $c = 68.0\,kNs/m$, $\lambda_1 = 0.5\,Hz$, $\lambda_2 = 1.0\,Hz$, $\lambda_3 = 2.0\,Hz$, $\lambda_4 = 4.0\,Hz$, $\lambda_5 = 6.0\,Hz$, $\lambda_6 = 8.0\,Hz$, $\lambda_7 = 10.0\,Hz$, $\lambda_8 = 12.5\,Hz$, $\lambda_9 = 15.0\,Hz$. The obtained data are modified applying random perturbations. After application of the identification procedure the following results are obtained: $\alpha = 0.61$, $k = 284.543\ kN/m$, $c = 68.096\ kNs/m$, when 3 percent noises are randomly introduced to artificial data.

On Fig. 2 the plot of functional (13) versus the α parameter is shown for three levels of noises (3, 5 and 10%). In a range of values of α parameter we have one minima of functional. Results of calculation performed for the artificial data shown that if noises are not too much the results obtained using suggested method of identification is not sensitive to noises. Errors of values of parameters obtained are of order of noises level.

The next step is to apply the identification procedure to real experimental data. The experimental data presented by Makris and Constantinou [9] are chosen and used in this example. Makris and Constantinou were using the damper manufactured by GERB Schwingungsisolierungen GmbH & Co. KG in their investigations. Similar dampers are often used in piping systems or in machine foundations. The following parameters of fractional Maxwell model are determined: $\alpha = 0.77$, $k = 503.350\ kN\,/\,m$, $c = 13.823\ kNs\,/\,m$. On Figs. 3 and 4 the comparison of experimental and approximated storage modulus K' and loss modulus K'' are presented. These quantities can be calculated from:

$$K' = \frac{k(\tau\,\lambda)^{\alpha}\big[(\tau\,\lambda)^{\alpha} + \cos(\alpha\pi\,/\,2)\big]}{1 + (\tau\,\lambda)^{2\alpha} + 2(\tau\,\lambda)^{\alpha}\cos(\alpha\pi\,/\,2)} \ , \quad K'' = \frac{k(\tau\,\lambda)^{\alpha}\sin(\alpha\pi\,/\,2)}{1 + (\tau\,\lambda)^{2\alpha} + 2(\tau\,\lambda)^{\alpha}\cos(\alpha\pi\,/\,2)} \ . \quad (16)$$

The three-parameter fractional Maxwell model satisfactory well describes dynamic properties of the considered damper.
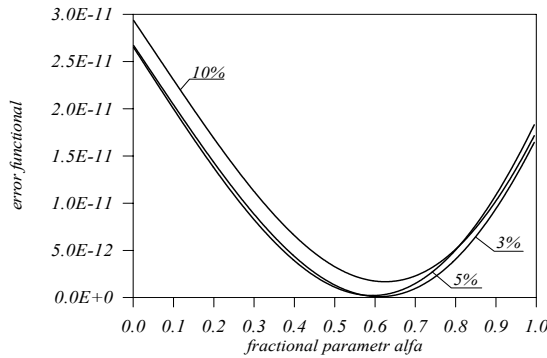
Fig. 2 Error functional (13) of Maxwell model versus the α parameter
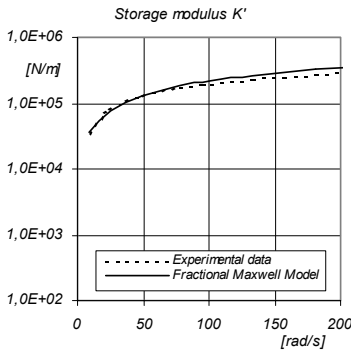
Fig. 3 Storage modulus   Fig. 4 Loss modulus
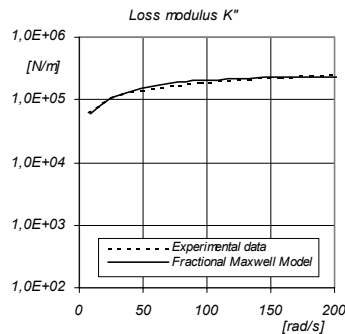
4. Concluding remarks

The presented model is working satisfactory. The identification procedure of parameters of the fractional Maxwell model is simply, well applicable and efficient. After few modifications this procedure can be used to determine parameters of other fractional models, for example, to determine parameters of the fractional Kelvin-Voight model.

However the three-parameter fractional Maxwell has some limitations. There are materials (used in VE dampers) to which this model cannot be fitted in satisfactory way. The other restriction is an impossibility to analyze very low and medium frequencies together. The results are going worse when experimental results for very low frequencies are included.

References

1. Christopoulos C., Filiatrault A., *Principles of passive supplemental damping and seismic isolation*, IUSS Press, Pavia, Italy, 2006.
2. S. W. Park, *Analytical modeling of viscoelastic dampers for structural and vibration control,* Int. J. of Solids and Struct., **38** (2001) 8065 – 8092.
3. A. Palmeri, F. Ricciardelli, A. De Luca, G. Muscolino, *State space formulation for linear viscoelastic dynamic systems with memory,* J. of Engng Mech., **129** (2003) 715 – 724.
4. S. Gerlach, A. Matzenmiller, *Comparison of numerical methods for identification of viscoelastic line spectra from static test data,* Inter. J. for Numer. Meth. in Engng, **63** (2005) 428 – 454.
5. T. Pritz, *Analysis of four-parameter fractional derivative model of real solid materials,* J. of Sound and Vibr., **195** (1996) 103 – 115.
6. R. L. Bagley, P. J. Torvik, *Fractional calculus – a different approach to the analysis of viscoelastically damped structures,* AIAA J., **27** (1989) 1412 – 17.
7. A. Schmidt, L. Gaul, *Finite element formulation of viscoelastic constitutive equations using fractional time derivatives,* J. Nonlin. Dyn., **29** (2002) 37 – 55.
8. A. Aprile, J. A. Inaudi, J. M. Kelly, *Evolutionary Model of Viscoelastic Dampers for Structural Applications,* J. of Engng Mech., **123** (1997) 551 – 560.
9. N. Makris, M. C. Constantinou, *Fractional-derivative Maxwell model for viscous dampers,* J. of Struct. Engng, **117** (1991) 2708 – 2724.
10. J. Honerkamp, *Ill-posed problem in rheology,* Rheol. Acta, **28** (1989), 363 – 71.
11. T. Beda, Y. Chevalier, *New method for identifying rheological parameter for fractional derivative modeling of viscoelastic behavior,* Mech. of Time-Dependent Mater., **8** (2004) 105 – 118.
12. L. Podlubny, *Fractional Differential equations,* Academic Press, 1999.

APPLICATION OF LYAPUNOV EQUATION TO ANALYSIS OF RANDOM VIBRATION OF STRUCTURE WITH TUNED MASS DAMPERS

Roman LEWANDOWSKI, Justyna GRZYMISŁAWSKA

Institute of Structural Engineering, Poznan University of Technology

Piotrowo Street 5, 60-965 Poznan

e-mail: roman.lewandowski@ikb.poznan.pl, justyna.grzymislawska@ikb.poznan.pl

Abstract

In this paper the Lyapunov equation is used to analyse random vibration of building structure. The structures with mass dampers are considered. The excitation forces which are functions of fluctuations of wind velocity are treated as random forces. Lyapunov equation is used to determine root mean square of displacements. Results of example calculation are presented and briefly discussed.

Keywords: tuned mass damper (TMD), multiple-tuned mass damper (MTMD), Lyapunov equation

Introduction

Dynamic analysis of structure with tuned mass dampers (TMD) and multiple-tuned mass dampers (MTMD) have been studied for many years [1-3]. Mainly, the numerical integration have been used to calculate the root mean square of quantities which characterize the structures response.

In this paper it will be studied the possibility of application of Lyapunov equation to dynamic analysis of structure loaded by forces excitated by wind pressure. Wind is treated as white noise random process. Some calculations were made for 20-story building. Results of calculations were compared with ones obtained in classical way. On this basis conclusions concerning effectiveness of using Lyapunov equation are formulated.

1. Designing of multiple tuned mass dampers

The parameters of tuned mass damper (or group of dampers) are chosen in such a way that the damper is tuned to the selected mode of vibration. It means, that the frequency of the damper (or a group of dampers) ω_d, treated as the one degree of freedom of the system, is close to selected vibration mode of structure ω_s $(\omega_d \approx \omega_s)$. The optimal parameters of such damper (or group of dampers) can be determined from formulae given in paper [4]. The optimal frequency ratio is:

$$\frac{\omega_d^2}{\omega_s^2} = \frac{2 + \mu}{2(1 + \mu)^2} \, , \tag{1}$$

where

$$\mu = m_d / M_s \, , \qquad \omega_s^2 = K_s / M_s \, , \qquad \omega_d^2 = k_d / m_d \, . \tag{2}$$

Here M_s and K_s are the modal mass and modal stiffness of the structure of the s-th vibration mode, respectively.

If only one damper is tuned to frequency ω_s, then m_d is the mass of damper, and k_d is the stiffness coefficient of damper. However, if the group of dampers is tuned to the frequency ω_s, then m_d and k_d denote the mass and the stiffness coefficient of selected damper of this group, respectively. Assuming that the mass ratio μ is known, the damper frequency ω_d and the stiffness coefficient k_d can be determined from above formulae.

If excitation forces acting on structure have a random character and can be treated as the white noise process, the optimal value of non-dimensional damping coefficient of damper is determined from formula:

$$\gamma_{opt} = \sqrt{\frac{\mu(4+3\mu)}{8(1+\mu)(2+\mu)}} \ . \tag{3}$$

The value of damping coefficient c_d can be calculated in the following way:

$$c_d = 2\gamma_{opt}\omega_d m_d \ . \tag{4}$$

2. Equation of motion

Equation of motion of the system shown on Fig. 1 can be written in the form:

$$\widetilde{\mathbf{M}}\ddot{\mathbf{q}}(t) + \widetilde{\mathbf{C}}\dot{\mathbf{q}}(t) + \widetilde{\mathbf{K}}\mathbf{q}(t) = \widetilde{\mathbf{P}}(t) \ , \tag{5}$$

where $\widetilde{\mathbf{M}}, \widetilde{\mathbf{C}}, \widetilde{\mathbf{K}}$ are the global matrices of mass, damping and stiffness of the system, $\mathbf{q}(t)$ is vector of displacement of the system $\mathbf{q}(t) = col(\mathbf{y}(t), \mathbf{x}(t))$, $\mathbf{y}(t)$ are horizontal displacements of frame, $\mathbf{x}(t)$ are horizontal displacements of dampers, $\widetilde{\mathbf{P}}(t)$ is vector of excitation forces $\widetilde{\mathbf{P}}(t) = col(\mathbf{P}(t), \mathbf{0})$.

It is assumed that the damping matrix of the structure has the form as follows: $\mathbf{C} = \alpha\mathbf{M} + \kappa\mathbf{K}$. Details concerning the mass and stiffness matrices of structure with multiple mass dampers are given in [7].

If Lyapunov equation is used to analyse random vibration of structure then it is desired to write the equation of motion (5) with a help of state-space variables. Introducing symbols

$$\mathbf{z} = col(\mathbf{q}^T(t), \dot{\mathbf{q}}^T(t)), \ \ \mathbf{p}(t) = \widetilde{\mathbf{P}}(t) \ , \tag{6}$$

$$\mathbf{A} = \begin{bmatrix} \mathbf{0} & \mathbf{1} \\ -\mathbf{M}^{-1}\mathbf{K} & -\mathbf{M}^{-1}\mathbf{C} \end{bmatrix}, \ \ \mathbf{B} = \begin{bmatrix} \mathbf{0} \\ -\mathbf{M}^{-1} \end{bmatrix}, \tag{7}$$

where $\mathbf{z}(t)$ denotes the space-state vector we can rewrite (5) in the following form

$$\dot{\mathbf{z}}(t) = \mathbf{A}\mathbf{z}(t) + \mathbf{B}\mathbf{p}(t) \ , \tag{8}$$
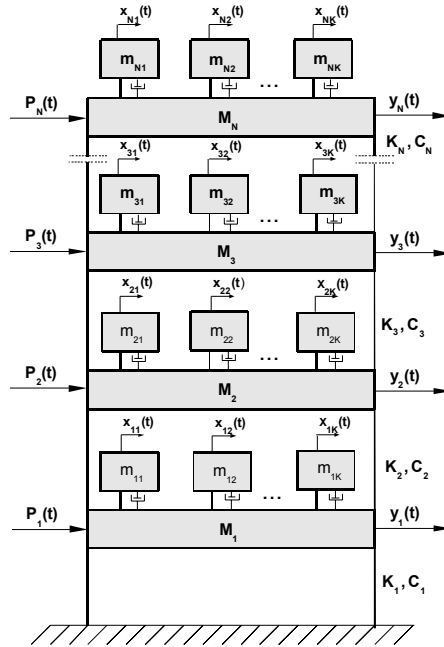
Fig.1. The system with MTMD

3. Modeling of wind load

It is assumed that load is the random, stationary process. Thus, the wind pressure in the arbitrary point of structure can be described in the following form:

$$P_i(t) = C_A A \rho U_i X^2 u_i(t), \tag{9}$$

where: C_A is the aerodynamic drag coefficient, A is the wind-exposed area, ρ is air density, X is the admittance function and $u_i(t)$ are the fluctuations of wind velocity on the level of floors.

Fluctuations of wind velocity are random process and, in this paper, are treated as white noise process. Taken into account the spatial correlation of fluctuations of wind velocity the matrix of spectral density of fluctuations of wind velocity $\mathbf{S}_u(\lambda)$ can be calculated. Elements of the matrix $\mathbf{S}_u(\lambda)$ are calculated from formula:

$$S_{lk}^u = \sqrt{S_{ll}^u(\lambda) S_{kk}^u(\lambda)} \, e^{-\Phi}, \tag{10}$$

where Φ denotes the correlation coefficient. In case of white-noise, elements $S_{ll}^u(\lambda)$ and $S_{kk}^u(\lambda)$ are independent from λ and then $S_{ll}^u(\lambda) = S_{l0} = const$, $S_{kk}^u(\lambda) = S_{k0} = const$.

The relationship between the spectral density matrix of load excited by wind pressure and the spectral density matrix of fluctuations of wind velocity is

$$\mathbf{S}_p = (C_A A \rho U)^2 X^2 \mathbf{S}_u \ . \tag{11}$$

4. Solution to the equation of motion

Solution to the equation of motion (8) has the following form (see [6]):

$$\mathbf{z}(t) - \overline{\mathbf{z}}(t) = \exp\big(\mathbf{A}(t - t_0)\big)\big(\mathbf{z}(t) - \overline{\mathbf{z}}(t)\big) + \int_{t_0}^{t} \exp\big(\mathbf{A}(t - \tau)\big)\mathbf{B}\big(\mathbf{p}(\tau) - \overline{\mathbf{p}}(\tau)\big)d\tau \ . \tag{12}$$

The stochastic properties of response of randomly loaded structures is fully described by covariance matrix $\mathbf{Z}(t)$ and the mean value of response $\overline{\mathbf{z}}(t)$. Here, the mean value of structure displacements is zero because the mean value of excitation is equal zero. The covariance matrix is defined as follows:

$$\mathbf{Z}(t) = E[\mathbf{z}(t), \mathbf{z}^T(t)] \ . \tag{13}$$

Using the theory presented in [6] the covariance matrix can be calculated from the following Lyapunov equation:

$$\dot{\mathbf{Z}}(t) = \mathbf{A}\mathbf{Z}(t) + \mathbf{Z}(t)\mathbf{A}^T + \mathbf{B}\hat{\mathbf{P}}(t)\mathbf{B}^T \ , \tag{14}$$

where $\hat{\mathbf{P}}(t) = 2T\breve{\mathbf{P}}(t)$ and $\breve{\mathbf{P}}(t)$ is the covariance matrix of excitation forces. Moreover, $\hat{\mathbf{P}}(t) = \breve{\mathbf{P}} = P_0\mathbf{I} = const$. Because wind forces are treated as the white noise random process it can be proved that $\mathbf{Z}(t) = \mathbf{Z} = const$ if $t \to \infty$. In this case the $\mathbf{Z}$ matrix can be determined from the following linear algebraic Lyapunov equation:

$$\mathbf{A}\mathbf{Z} + \mathbf{Z}\mathbf{A}^T + \mathbf{B}\hat{\mathbf{P}}\mathbf{B}^T = \mathbf{0} \ , \tag{15}$$

and the covariance matrix of structure response $\mathbf{Z}$ is equal the correlation matrix $\mathbf{R}_q$.

5. Results of calculations

In this section the results of dynamic analysis of the structure using Lyapunov equation are discussed. It is considered structure with TMD and MTMD. Additionally, for comparison it has been made analysis in a classical way.

Parameters of building are given in Table 1. Non-dimensional damping coefficients of first and second vibration mode are equal 1% of critical damping. TMD (tuned to the first mode of vibration) and MTMD (tuned to first three modes of vibration) were located on the top floor. Parameters of dampers are shown in Table 2. The mean wind velocity i-th floor was calculated from formula:

$$U(z) = 2{,}5u_* \ln(z / z_0), \quad u_* = U(10)\sqrt{k} \ , \tag{16}$$

$U(10)$ is the mean wind velocity on the altitude 10m, k is the coefficient depended on type of area, z_0 is the roughness length and z is altitude. Moreover, the following data are used: $\rho = 1{,}226 \, kg/m^3$, $U(10) = 30 \, m/s^2$, $z_0 = 0{,}3$, $k = 12 \cdot 10^{-3}$.

story	mass [kg]	stiffness [N/m]
1	2,83 x10^5	3,31 x10^8
2 - 4	2,76 x10^5	1,06 x10^9
4 - 7	2,76 x10^5	6,79 x10^8
8 - 10	2,76 x10^5	6,79 x10^8
11 – 13	2,76 x10^5	5,84 x10^8
14 - 16	2,76 x10^5	3,86 x10^8
17 – 19	2,76 x10^5	3,47 x10^8
20	2,92 x10^5	2,29 x10^8

Table 1. Parameters of structure

number of mode	mass [kg]	stiffness[N/m]
TMD		
1	36214	472468
MTMD		
1	18107	238870
2	7956	722685
3	8550	2182386

Table 2. Parameters of dampers

The root mean square of *i*-th displacement of the structure is calculated from formula:

$$\sigma_q^2 = R_q , \tag{17}$$

where R_q is *i*-th element from diagonal of the $\mathbf{R}_q$ matrix. Using above formulae the analysis of the structure without dampers, with conventional TMD and with MTMD were made. The classical method of calculation of root mean square of displacement are described in [7] Results of calculation are shown on Fig. 1.
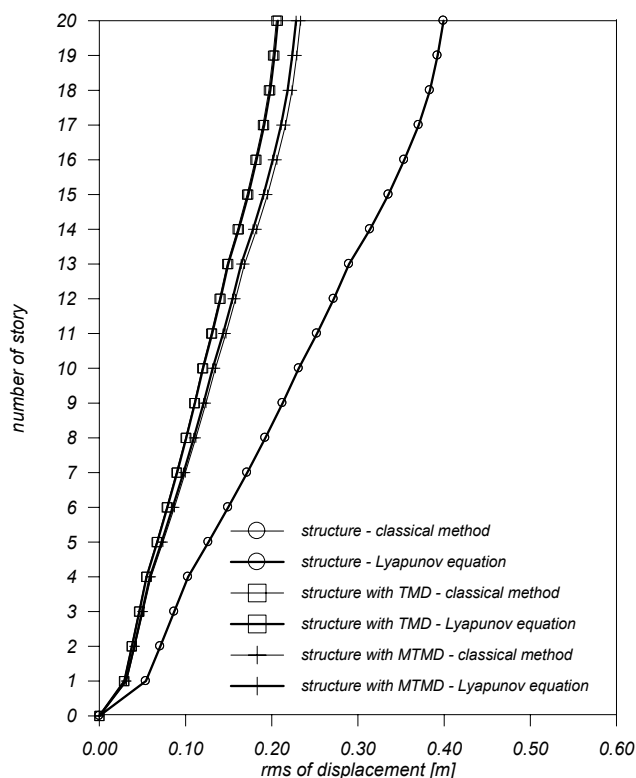
Fig. 1. Root mean square of displacements

It has been observed that in cases of structure without dampers and structure with TMD root mean square of displacements calculated using Lyapunov equation and calculated in a classical way are almost the same.

6. Conclusions

In this paper the possibility of application of Lyapunov equation to analysis of random vibration of structure with tuned mass dampers has been studied. The root mean square of displacement of structure were determined.

The proposed method which use the Lyapunov equation to dynamic analysis of structure can be alternative to the classical method of analysis of random vibrations of structures. However, currently the proposed method can be used only when wind is treated as the white noise process.

References

1. R. J. McNamara, Tuned mass dampers for buildings, *Journal of the Structural Division Proc*., ASCE, **105**(9) (1977) 1785-1798.
2. Y.L. Xu, K.C.S. Kwok, B. Samali, Control of wind-induced tall building vibration by tuned mass dampers, *Journal of Wind Engineering and Industrial Aerodynamics*, **22** (1992) 833-854.
3. G. Chen, J. Wu, Optimal placement of multiple tune mass dampers for seismic structures. *Journal of Structural Engineering*, **127** (2001) 1054-1062.
4. G.B. Warburton, Optimum absorber parameters for various combinations of response and excitation parameters. *Earthquake Engineering and Structural Dynamics*, **10** (1982) 381-401.
5. C. Dyrbye, S.O. Hansen, *Wind Loads on Structures*, John Wiley and Sons, 1999.
6. A.E., Barson, Yu-Chi Ho, *Applied optimal control. Optimization, estimation and control*, John Wiley and Sons, 1975.
7. R. Lewandowski, J. Grzymisławska, *Dynamic analysis of structure with multiple tuned mass dampers*, Proceedings of The 9th Inernational Conference Modern Building Materials, Structures and Techniques, Vilnius, Lithuania, **3** (2007) 981-986.

SPAN'S LOW DAMPED VIBRATIONS AND VIBRATION'S DAMPING BY MODAL DISPARITY INDUCTED BY CABLE STAYS TEMPORAL ADDITION

Krzysztof LIPIŃSKI

Gdansk University of Technology,Mechanical Department
ul Narutowicza 11/12, 80-952 Gdańsk
Tel. 058-347-29-29,   e-mail: klipinsk@pg.gda.pl

Abstract

The paper presents low damped vibrations of a continuous system. Such vibrations are present in many structures, and effective elimination method is requested. In the paper, temporal stiffness modification is proposed in order to distribute the energy amount different modes of the system (for example to these that are better damped). The method is tested with a bridge span numerical model.

Keywords: Continuous system; low damped vibrations; energy transfer

Introduction

The paper concentrates on continuous systems with low damped vibrations. Some alternative, effective elimination method is requested, as additional dampers could be technically difficult to install. Such proposition is presented in the paper. Damping modifications are discarded, and temporal stiffness fluctuations are introduced in the system. Some changes in system's modal characteristic are indicated and energy transfer is possible. Energy of low damped vibrations is distributed amount all modes of the modified system, i.e. to some higher damped vibrations, too. The higher damped vibrations dissipate their energy and the total system energy is reduced. When system's initial parameters are recovered, vibrations amplitudes are lower. Additionally, some energy elimination is associated with deformation of the attached stiffing element. This energy is eliminated quickly, if stiffer vibrations appear after it is disconnected

To verify the method, a test is performed on numerical model of a planar bridge span supported by a cable stay. The span stiffness is low, thus low frequency and low damped forms are present in the system's vibrations. Next, the system is stiffed by addition of an additional cable.

The use of the inter-modes energy transfers was proposed by Diaz and Mukherjee [4, 5]. In their flexible truss-like structure, nine additional cables were introduced. The structure's modes 1 through 6 was observed, but only 1, 3 and 5 was controlled. Total energy in the uncontrolled modes was removed through the process of stiffness switching, i.e. by stiffening and releasing the tension in the cables. The other test was related to some small, non-structural masses added at strategic locations of the structure.

The actual paper is divided in three paragraphs. The first presents the considered structure as well as a method of its mathematical modelling. The second presents results of illustrative tests, done on the structure. The last is devoted for conclusions.

1. CONSIDERED SYSTEM

The physical model corresponds to a planar deformable bridge span supported by a cable stay (Fig 1.a). The span and the stay are modelled with finite elements (FE). Low discretization is considered, as the paper focuses on physical phenomena and not on span modelling precision. The span is discretized by beam elements. Nine elements are used (Fig 1.a). The elements' displacements/deformations are described by nodes' motions, and each of the nodes has two degrees of freedom (vertical and rotational), only. The nodes' longitudinal degrees are locked. The stay is modelled as a tension element. The stiffer is an additional tension bar present between the span and its surroundings.
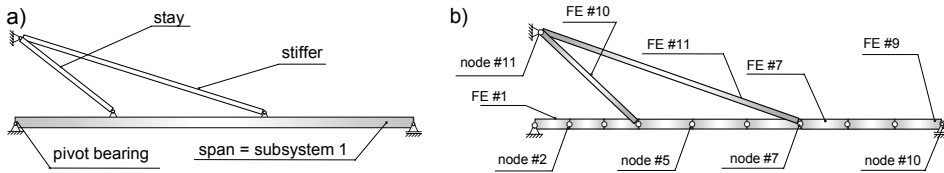
Fig. 1. Considered system: physical model (a), finite elements model (b)

Nodes' vertical and angular positions are system's generalized coordinates. They describe system's deformations. Coordinates: $q_1 \div q_{20}$ describes the span, q_7, q_{13}, q_{21} describes the stays. Independent are: $q_2 \div q_{19}$. The other are fixed in zero position
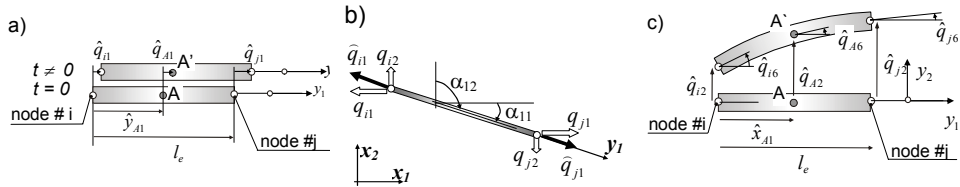
Fig. 2. Details of the finite elements: translations of the bar element (a); transformation between the local and global coordinates (b); displacements of beam element (c)

The global coordinate system is fixed to the reference body. In local (elements') coordinates of beam elements, vertical displacements are performed along y_2 axis, and rotations are about y_3 axis. For bar elements, their displacements are along axis y_1. Then, if the element's nodes are numbered i and j, the elements coordinates are [1-3]:

$$\hat{\mathbf{q}}_{p\mathbf{e}} = col(\hat{q}_{i1}, \hat{q}_{j1}), \qquad \hat{\mathbf{q}}_{b\mathbf{e}} = col(\hat{q}_{i2}, \hat{q}_{i6}, \hat{q}_{j2}, \hat{q}_{j6}), \qquad (1)$$

where: $\hat{q}_{i1}, \hat{q}_{j1}$ - bar translation along y_1 (Fig. 2a), $\hat{q}_{i2}, \hat{q}_{j2}$ - beam translation along y_2 (Fig. 2c), $\hat{q}_{i6}, \hat{q}_{j6}$ - beam rotation about y_3 (Fig. 2c).

Symbol ∧ denotes coordinate measured in local (element's) system of coordinates. System loads could be attached in the nodes, only. Their coordinates are:

$$\hat{\boldsymbol{P}}_{pe} = col(\hat{P}_{i1}, \hat{P}_{j1}) \qquad\qquad \hat{\boldsymbol{P}}_{be} = col(\hat{P}_{i2}, \hat{P}_{i6}, \hat{P}_{j2}, \hat{P}_{j6}) \tag{2}$$

where: $\hat{P}_{i1}, \hat{P}_{j1}$ - bar element's loads (forces) collinear to y_1, $\hat{P}_{i2}, \hat{P}_{j2}$ - beam element's loads (forces) collinear to y_2, $\hat{P}_{i6}, \hat{P}_{j6}$ - beam element's loads (torque) collinear to y_1.

If an internal point of the bar element is considered (as point A in Fig. 2a) its displacements are approximated by linear functions. For a beam element, a cubic function is imposed. Corresponding shape functions are [1-3]:

$$\hat{\boldsymbol{N}}_{pe}(\zeta) = \begin{bmatrix} (1-\zeta) & \zeta \end{bmatrix}, \qquad \hat{\boldsymbol{N}}_{be}(\zeta) = \begin{bmatrix} 2\zeta^3 - 3\zeta^2 + 1 & l_e(\zeta^3 - 2\zeta^2 + \zeta) & -2\zeta^3 + 3\zeta^2 & l_e(\zeta^3 - \zeta^2) \\[4pt] \dfrac{6(\zeta^2 - \zeta)}{l_e} & 3\zeta^2 - 4\zeta + 1 & \dfrac{6(-\zeta^2 + \zeta)}{l_e} & 3\zeta^2 - 2\zeta \end{bmatrix}, \tag{3}$$

where: $\zeta = \hat{x}_1/l_e$ - point's relative position.

Then displacements and velocities of A are obtained if the shape functions are used:

$$col(\hat{q}_{A2}, \hat{q}_{A6}) = \hat{\boldsymbol{N}}_{be}(\zeta) \cdot \hat{\boldsymbol{q}}_{be} , \qquad col(\dot{\hat{q}}_{A2}, \dot{\hat{q}}_{A6}) = \hat{\boldsymbol{N}}_{be}(\zeta) \cdot \dot{\hat{\boldsymbol{q}}}_{be} . \tag{4}$$

Next mass and elasticity matrices are calculated. They are [1-3]:

- for beam element:

$$\hat{A}_{be} = \frac{\rho_e F_e l_e}{420} \begin{bmatrix} 156 & 22l_e & 54 & -13l_e \\ & 4l_e^2 & 13l_e & -3l_e^2 \\ & & 156 & -22l_e \\ sym. & & & 4l_e^2 \end{bmatrix}, \qquad \hat{C}_{be} = \frac{E_e J_e}{l_e^3} \begin{bmatrix} 12 & 6l_e & -12 & 6l_e \\ & 4l_e^2 & -6l_e & 2l_e^2 \\ & & 12 & -6l_e \\ sym. & & & 4l_e^2 \end{bmatrix}, \tag{5}$$

- for bar element:

$$\hat{A}_{pe} = \frac{\rho_e F_e l_e}{6} \begin{bmatrix} 2 & 1 \\ sym. & 2 \end{bmatrix}, \qquad\qquad \hat{C}_{pe} = \frac{E_e J_e}{l_e^3} \begin{bmatrix} 1 & -1 \\ sym. & 1 \end{bmatrix}. \tag{6}$$

Damping matrices are approximated as proportional to mass and elasticity [1-3]

$$\hat{\boldsymbol{B}}_e = \alpha \hat{\boldsymbol{A}}_e + \beta \hat{\boldsymbol{C}}_e . \tag{7}$$

Equations (1÷7) are expressed in element's coordinate systems. They have to be transformed to the global system. It is identity matrix transformation, if the systems are collinear. The case is valid for beam elements. Thus [1-3]:

$$\boldsymbol{q}_{be} = \hat{\boldsymbol{q}}_{be}; \qquad \boldsymbol{P}_{be} = \hat{\boldsymbol{P}}_{be}; \qquad \boldsymbol{A}_{be} = \hat{\boldsymbol{A}}_{be}; \qquad \boldsymbol{C}_{be} = \hat{\boldsymbol{C}}_{be}; \qquad \boldsymbol{B}_{be} = \hat{\boldsymbol{B}}_{be} . \tag{8}$$

For the bar element (Fig. 2b), the transformation matrix is [1-3]

$$\boldsymbol{\Theta}_{pe} = \begin{bmatrix} cos(\alpha_{11}) & cos(\alpha_{12}) & 0 & 0 \\ 0 & 0 & cos(\alpha_{11}) & cos(\alpha_{12}) \end{bmatrix}. \tag{9}$$

And the relation between the local and the global coordinates are [1-3]:

$$\hat{\boldsymbol{q}}_{pe} = \boldsymbol{\Theta}_{pe} \cdot \boldsymbol{q}_{pe} \; ; \quad \hat{\boldsymbol{P}}_{pe} = \boldsymbol{\Theta}_{pe} \cdot \boldsymbol{P}_{pe} \; ; \quad \boldsymbol{A}_{pe} = \boldsymbol{\Theta}_{pe}^{T} \cdot \hat{\boldsymbol{A}}_{pe} \cdot \boldsymbol{\Theta}_{pe} \; ; \quad \boldsymbol{C}_{pe} = \boldsymbol{\Theta}_{pe}^{T} \cdot \hat{\boldsymbol{C}}_{pe} \cdot \boldsymbol{\Theta}_{pe} \; ; \quad \boldsymbol{B}_{pe} = \boldsymbol{\Theta}_{pe}^{T} \cdot \hat{\boldsymbol{B}}_{pe} \cdot \boldsymbol{\Theta}_{pe} \; . \quad (10)$$

The set of independent elements has to be jointed into the common construction. To perform it, vector of nodes' displacements and vector of nodes' loads are collected to:

$$\boldsymbol{q}_{c}^{*} = col(\boldsymbol{q}_{i}) \quad ; \qquad \boldsymbol{P}_{c}^{*} = col(\boldsymbol{P}_{i}) \qquad : \qquad i=1,2,...,w \tag{11}$$

where: $\boldsymbol{q}_{i}$ - vector of ith node's displacements; $\boldsymbol{P}_{i}$ - vector of ith node's loads.

Next, an arrangement of the global matrices $\boldsymbol{A}_{e}^{*}, \boldsymbol{C}_{e}^{*}, \boldsymbol{B}_{e}^{*}$ is performed. For a given element, crossing cells of global matrices are selected, for rows and columns with numbers matching to the element's coordinates. Corresponding blocs of local $\boldsymbol{A}_{e}, \boldsymbol{C}_{e}, \boldsymbol{B}_{e}$ matrices are placed in these cells. The other elements are zero. It can be illustrated as [1-3]:

$$\boldsymbol{A}_{e} = \begin{bmatrix} \boldsymbol{A} & \boldsymbol{B} \\ \hline \boldsymbol{C} & \boldsymbol{D} \end{bmatrix} \begin{matrix} i \\ j \end{matrix} \qquad \boldsymbol{A}_{e}^{*} = \begin{bmatrix} & & \\ & \boldsymbol{A} & \boldsymbol{B} \\ & & \\ & \boldsymbol{C} & \boldsymbol{D} \\ & & \end{bmatrix} \begin{matrix} \vdots \\ i \\ \vdots \\ j \\ \vdots \end{matrix} \tag{12}$$

In the next step, global matrices of the system are obtained by summing matrices of all system's elements [1-3]:

$$\boldsymbol{A}_{c}^{*} = \sum_{e=1}^{n_{e}} \boldsymbol{A}_{e}^{*} \quad , \qquad \boldsymbol{C}_{c}^{*} = \sum_{e=1}^{n_{e}} \boldsymbol{C}_{e}^{*} \quad , \qquad \boldsymbol{B}_{c}^{*} = \sum_{e=1}^{n_{e}} \boldsymbol{B}_{e}^{*} \; . \tag{13}$$

where: n_{e} - number of elements in the considered system. It equals 10 for initial system and 11 for the system with activated stiffer.

Finally rows and columns corresponding to locked nodes are eliminated from the matrices, and final form of dynamics equations is [1-3]

$$\boldsymbol{A}_{c}^{*} \cdot \ddot{\boldsymbol{q}}_{c}^{*} + \boldsymbol{B}_{c}^{*} \cdot \dot{\boldsymbol{q}}_{c}^{*} + \boldsymbol{C}_{c}^{*} \cdot \boldsymbol{q}_{c}^{*} = \boldsymbol{P}_{c}^{*} \tag{14}$$

2. NUMERICAL TESTS

Presented model has been implemented in MATLAB [6]. Then, modal analyses of the system are performed (Table 1) and the lowest damped mode is selected (Fig 3.a). As it is presented in the table, the lowest mode is extremely low damped, as the vibration's reduction rate is lower that 0.2 %. Some initial excitation corresponding to the form of the mode is introduced and numerical time integrations of the model's motion are performed. 20 seconds period of integration is proposed. Motions of its selected points are presented in Fig 4.a for the system without activation of the stiffer. For a comparison, a stiffed system is analyzed in the same conditions. Some additional cable stay is connected to the span at its 7th node vertical displacement. Lowest damped form of vibrations (Table 2) is selected for the stiffed system (Fig. 3.b), and 20 seconds time integration is performed for it. Motions of a selected point are presented in Fig. 4.c for the stiffed system.

When the system's characteristics are determined, the main test is performed for elimination of the low damped vibrations. The tested period is 20 seconds, again. Twice, the stiffing element is connected to the system and twice is disconnected as well. The integration time points are about: 2 s (for first connection); 8 s (for disconnection); 12 s (for second connection); 15 s (for last disconnection). The test results are presented in Fig. 4.b. To insure smooth transitions between the initial and the stiffed periods, additional conditions are set on the transition moments. To avoid any impulsive interactions, the stiffer may be connected only if stiffer/span relative velocity is zero. To increase energy dissipation, the cable is disconnected in the highest span position (the highest compressed cable).

Table 1. Lowest damped modes of the initial system

#	real part	imaginary part	NU(Hz)	ksi(%)	NU0(Hz)
1	-6.8780e-02	-3.7075e+01	5.90	0.19	5.90
2	-1.5377e-01	-5.5448e+01	8.82	0.28	8.82
3	-7.9407e-01	-1.2602e+02	20.06	0.63	20.06
4	-2.9401e+00	-2.4247e+02	38.59	1.21	38.59
5	-7.0918e+00	-3.7654e+02	59.93	1.88	59.94
6	-1.6434e+01	-5.7308e+02	91.21	2.87	91.25

Table 2. Lowest damped modes of the stiffed system

#	real part	imaginary part	NU(Hz)	ksi(%)	NU0(Hz)
1	-1.1531e-01	-4.8012e+01	7.64	0.24	7.64
2	-2.1705e-01	-6.5879e+01	10.48	0.33	10.49
3	-8.6652e-01	-1.3164e+02	20.95	0.66	20.95
4	-2.9416e+00	-2.4253e+02	38.60	1.21	38.60
5	-7.1046e+00	-3.7688e+02	59.98	1.88	59.99
6	-1.6453e+01	-5.7340e+02	91.26	2.87	91.30
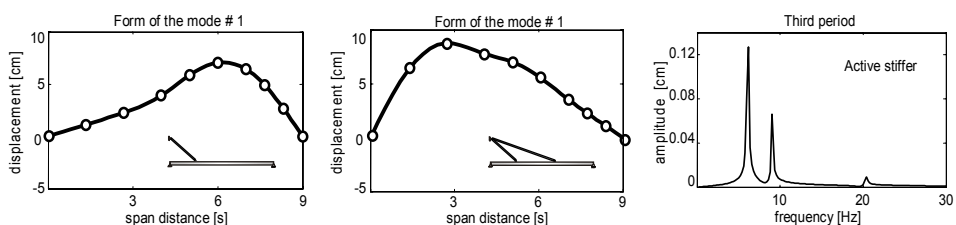
Fig. 3. Forms of vibrations: lowest damped form of the initial system (a); lowest damped form of the stiffed system (b); modal characteristic after recovering initial stiffness (c)

As it is seen in the Fig. 4.b, effective damping was performed for the low damped mode. Final amplitudes are in significantly lower in compare to the initial (Fig.4.a) and to the locked (fig 4.c) systems. Effective inter modes energy transfers are observed. The initial

conditions are compatible with the first (the lowest damped) mode of vibrations. After the firs connecting/disconnecting action (the period between *8 s* and *12 s*) the inter-modes energy transfer can be observed. Fourier transformation procedure indicated frequencies of three dominant modes (Fig. 3.c). They are: f_1= 5.9786 Hz; f_2= 8.7684 Hz; f_3= 20.09676 Hz. They are in closed correlation to free modes indicated by the system's modal analyses.
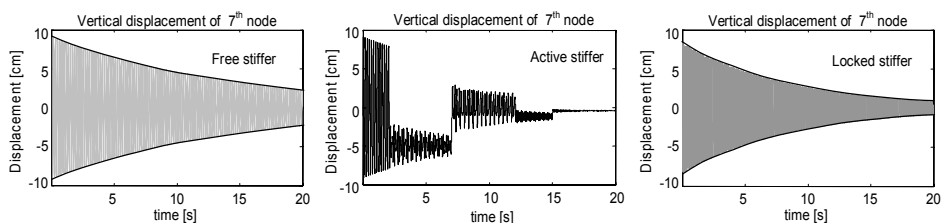
Fig. 4. System's time evolution: initial system (a): controlled system (b); stiffed system (c)

3. CONCLUSIONS

Modal disparity method looks to be an effective active damping method for low damped vibrations present in continuous systems. The method can be employed, if technical reasons preclude installations of additional damping elements. The energy of unrequited vibrations could be easily distributed amount different (including these better damped) modes and there the energy could be dissipated. To avoid unsmooth transitions, the stiffer connecting and disconnecting moments have to be precisely determined. Future test are requires. They should concern about optimal stiffer localization and about parameters of optimal switching conditions, as well.

References

1. R. Hein, K. Lipiński, H. Olszewski, E. Wittbrodt, *Optymalizacja ustawienia odciągów belki wspornikowej z ruchomym pojazdem*, In.: TECHNICON`05, Politechnika Gdańska, (in Polish) Gdańska, 2005, [1-10].
2. W. Gawroński, J. Kruszewski, W. Ostachowicz, J. Tarnowski, E. Wittbrodt, *Metoda elementów skończonych w dynamice konstrukcji*, Arkady, W-wa., 1984.
3. J. Kruszewski, E. Wittbrodt, Z. Walczyk, *Drgania układów mechanicznych w ujęciu komputerowym*, tom 2, WNT, W-wa., 1993.
4. J. Issa, R. Mukherjee, A.R. Diaz, S.W. Shaw, *Modal disparity and its experimental verification*, J. of Sound and Vibr., **311** (2008) 1465–1475.
5. A.R. Diaz and R. Mukherjee: *Methods for control enhancement of flexible structures based on modal disparity*, 6th European Solid Mechanics Conference ESMC 2006, Budapest, 2006, [1-2]
6. http://www.mathworks.com

DISSIPATED ENERGY MINIMIZATION IN A COMBUSTION ENGINE MOUNT SYSTEM BY POSITION DEPENDENT DAMPING COEFFICIENTS

Krzysztof LIPIŃSKI, Zbigniew KNEBA

Gdansk University of Technology,   Mechanical Department

ul Narutowicza 11/12, 80-952 Gdańsk

Tel. 058-347-29-29, 058-347-28-64, e-mail: klipinsk@pg.gda.pl, znkeba@pg.gda.pl

Abstract

Multibody modelling of a combustion engine is presented in the paper. The engine's vibrations are of primary interest as well as energy dissipated in the engine's suspension. System's excitation is proportional to engine's rotational velocity, thus vibration's amplitude converges to some constant, non-zero value for high rotational velocities. With the amplitude being constant, suspension's dissipated energy grows significantly with the velocity. A method to reduce the energy is considered in the paper.

Keywords: Vibrations of combustion engine; forced vibration; energy minimization

Introduction

According to significant masses and to nonlinear motions, combustion engine's elements cause significant inertial effects. Neighbour constructions could be affected, and thus the engines have to be separated from their surrounding. Elasto-damping suspensions are used to fix the engines. They have to be significantly resistant to transmit the engine's inertial effects and stiff to minimize engine's displacements.

The elasto-damping suspension and the periodic loads effect in forced vibrations. The excitation frequencies and the loads depend on engine's rotational velocity. When tuning the suspension parameters some elementary request is to avoid from a coincidence between the engine's rotational velocity and the frequencies of its free vibrations. As the engine's rotational velocity alters within wide range of velocities, the free modes are arranged as lower then the lowest work rotational velocity. According to it, suspension's characteristic has to be soft.

In the engine's suspension, damping elements prevent against its high vibrations. Their role becomes fundamental, if a temporal coincidence is present between the free modes and the rotational velocity (during engine's acceleration). The dampers are active during engine's normal work, too. In [3], the damper's dissipated energy was evaluated and found as significant. As the lonely source of the system's energy is the engine itself, the dissipation reduces the engine's efficiency. A postulate to reduce the dissipation was formulated in [3]. The present paper investigates such elimination by use of segmented dampers or gap dampers, where regions of low and high damped motions are present.

Presented problem is tested by numerical analyses and the tests are presented in the paper. Four parts of the presentation are indicated. The first presents multibody model of

the combustions engine. In the next fundaments of multibody dynamics are presented. In the subsequent, results of numerical test are presented for different models of the main damping elements at the suspension. The last part presents conclusions.
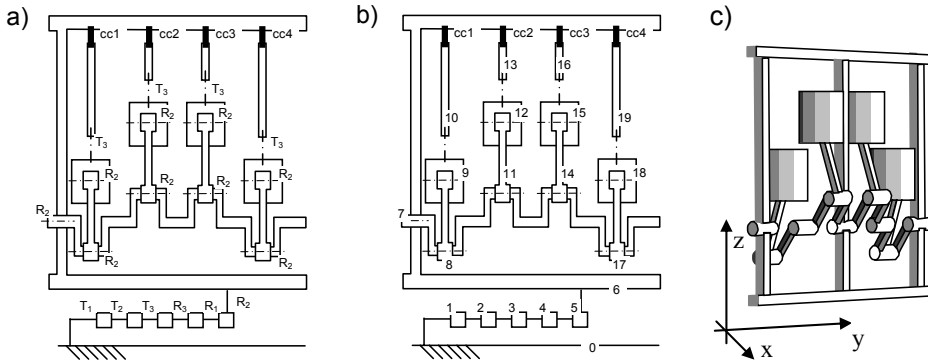
Fig. 1: Multibody model of the engine: bodies' and joint' types (a); bodies' numbering (b); motion of the system (c)

1. CONSIDERED SYSTEM

A multibody model [1] of a four pistons, combustion engine is presented in this section (Fig. 1). It is composed of 19 rigid bodies. Initial five of them are fictitious, point bodies. Together with joints, engine's mobility (complete) between the sixth body and the system reference is modelled. The sixth body models the engine's base. The used sequence of joint mobility is presented in Fig. 1. Translational joints are denoted by T letter. Their indexes indicate direction of translation. It is parallel to corresponding axis of the reference coordinate system. By analogy, rotational joints are denoted by R letter with an index. Seventh body models the crankshaft. A joint connecting it with the engine's base is a rotational joint. Its axis is collinear to y axis of the coordinate system (in non-displaced configuration). Bodies # 8, 11, 14, 17 model connecting-rods. They are connected to the crankshaft by rotational joints. Bodies # 9, 12, 15, 18 model pistons. Remaining bodies # 10, 13, 16, 19 are factious, point bodies used to model translational motion of the pistons in respect to the engine's base. The bodies are connected to the base by use of shadow-body constrains [1].

Table 1: Inertia parameters of bodies

	m	I_{xx}	I_{yy}	I_{zz}
engine's base	300	20	12	28
crankshaft	100	6	1	6
connecting-rods	2	0.007	0.01	0.002
pistons	4	0.05	0.05	0.04

For details, bodies' and joints' numbering is presented in Fig 1.b. Bodies' sizes are presented in fig 2.b, and their inertia parameters are presented in Table 1.

Three elasto-damping elements are used to connect the reference body and the engine. Position of the elements is drawn in Fig. 2.b. The elements are fictitious, point-condensed elements. In non-loaded configurations their terminal points coincide. Only translational deformations are considered for the elements and linear characteristic is assumed between the force and the deformation:

$$f_b = K \cdot u_b + D \cdot \dot{u}_b \quad : \quad \begin{matrix} K = diag(10^5, \quad 10^5, \quad 2 \cdot 10^5) \ N/m \\ D = diag(600, \quad 600, \quad 600) \ Ns/m \end{matrix} \quad ; \quad \begin{matrix} u_b = col(x_x, x_y, x_z) \\ f_b = col(f_x, f_y, f_z) \end{matrix} , \quad (1)$$

where: K – stiffness matrix; D – damping matrix; u_b – vector of deformations; f_b - vector of forces.
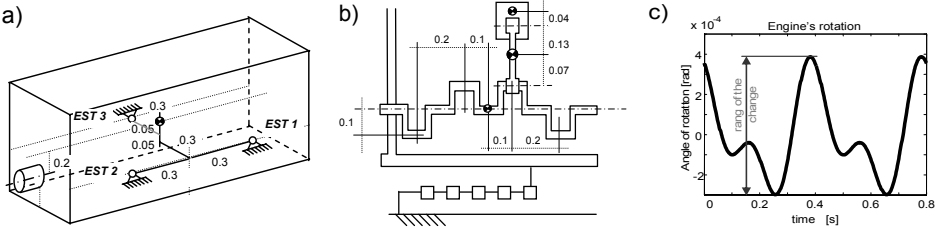
Fig. 2: Model's parameters: positions of elasto-damping elements
and dimensions of the engine' base (a); dimensions of engine's
interior elements (b); time evolution of engine's base (c)

2. DYNAMICS OF MULTIBODY SYSTEM

Multibody systems are composed of rigid bodies and massless connections (Fig. 3b). The system's reference is motionless. Other bodies (with some exceptions) are mobile, have dimensions and inertia properties. Connections are massless, deformable. Structures resulting from body/joints contacts are called kinematical chains (Fig. 3b). Succession order is introduced for such structures. The kinematical chain can have closed structure (Fig. 3b), if the succession leads to a body being its own successor. If not ever one of system's kinematical chains is closed, the system is defined as a tree structure.
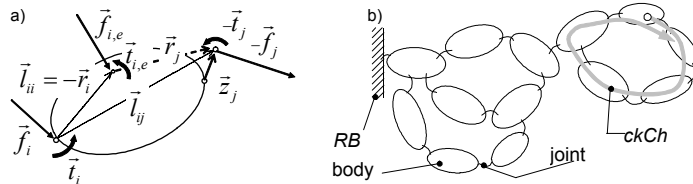
Fig. 3: A multibody system: interactions acting on body i (a); closed system (b)

Bodies are numbered in ascending order with zero at reference. A kinematical chain connecting body i with the reference exists. It is called reference chain, and its bodies are called preceding bodies. Connections are composed of joints and of massless, dimensionless bodies called point bodies. A joint is a restricted connection of translational or rotational type, and if linking body i with its directly preceding body, it has number i.

Velocities of rotations and of translations are described for bodies' centres of mass [1]:

$$\vec{\omega}^{i} = \vec{A}^{2,i} \cdot \dot{q} \quad ; \quad \dot{\vec{x}}^{i} = \vec{A}^{1,i} \cdot \dot{q} \quad ; \quad \dot{\vec{\omega}}^{i} = \vec{A}^{2,i} \cdot \ddot{q} + \dot{\vec{\omega}}^{i,R} \quad ; \quad \ddot{\vec{x}}^{i} = \vec{A}^{1,i} \cdot \ddot{q} + \ddot{\vec{x}}^{i,R} , \quad (2)$$

where: $\vec{A}^{1,i}$, $\vec{A}^{2,i}$ - matrices of vectors; $\dot{\vec{\omega}}^{i,R}$, $\ddot{\vec{x}}^{i,R}$ - reminders free of joint's accelerations

For dynamics, bodies are separated by joint cutting procedure and joints are replaced by interactions. According to it Newton/Euler dynamics equations [1]:

$$\vec{\omega} \times \left(\bar{\bar{I}} \cdot \vec{\omega} \right) + \bar{\bar{I}} \cdot \dot{\vec{\omega}} = \sum_{i=1}^{m} \vec{t}_{i0} + \sum_{i=1}^{k} \vec{r}_{i} \times \vec{f}_{i} \quad ; \quad m \cdot \ddot{\vec{x}}_{0} = \sum_{i=1}^{k} \vec{f}_{i} , \quad (3)$$

where: m –mass, $\bar{\bar{I}}$ - inertia tensor about the mass centre; $\ddot{\vec{x}}_{0}$ - acceleration of the mass centre; $\vec{\omega}$ - body's rotational speed; $\vec{f}_{i}$ - i^{th} force acting on the body (Fig. 3.a); $\vec{t}_{i0}$ - i^{th} torque acting on the body; $\vec{r}_{i}$ - position vector from the mass centre to i^{th} force attaching.

Combining the dynamics Eq. (2) with the kinematics Eq. (1), and separating coefficients in front of joint's accelerations, the dynamics equations obtains form [1]:

$$\vec{B}^{2,i} \cdot \ddot{q} + \vec{\omega} \times \left(\bar{\bar{I}} \cdot \vec{\omega} \right) + \bar{\bar{I}} \cdot \dot{\vec{\omega}}_{R}(q,\dot{q}) = \sum_{i=1}^{m} \vec{t}_{i0} + \sum_{i=1}^{k} \vec{r}_{i} \times \vec{f}_{i} \quad ; \quad \vec{B}^{1,i} \cdot \ddot{q} + m \cdot \ddot{\vec{x}}_{R}(q,\dot{q}) = \sum_{i=1}^{k} \vec{f}_{i} , \quad (3)$$

where: q - column matrix of joint displacements; $\vec{B}^{1,i}$, $\vec{B}^{2,i}$ - square matrices of vectors.

Then, symbols of successors' interactions are eliminated. The dynamics Eqs. (3) are projected into direction of preceding joint's axis and they are collected in [1]

$$M(q) \cdot \ddot{q} + F(\dot{q},q) + Q(\dot{q},q,f_{e},t_{e},t) = 0 , \quad (4)$$

where: M - mass matrix; F - vector of generalised forces set form centrifugal, gyroscopic and Coriolis terms; Q - vector of generalised forces stem form $\vec{f}_{e,l}$, $\vec{t}_{e,l}$; t - time.

If closed kinematical chains are present, then loop cutting procedures are used. It results in a reference tree structure, in its dynamics equations and in algebraic constraint equations. The constraints functions are grouped in a matrix [1] and the equations' differential part is extended with constraints interactions [2]:

$$M(q,t) \cdot \ddot{q} + F(\dot{q},q) + Q(\dot{q},q,f_{e},t_{e},t) + J^{T}(q) \cdot \lambda = 0 ;$$
$$h(q) = 0 ; \qquad \dot{h}(q) = J(q) \cdot \dot{q} = 0 ; \qquad \ddot{h}(q) = J(q) \cdot \ddot{q} + A(q,\dot{q}) = 0 \qquad , \quad (5)$$

where: h - matrix of constraints; J – Jacobian of constraints; λ - Lagrange multipliers.

The vector, q, consists of independent coordinates, v, and of dependent ones, u. The dependent and the Lagrangian multipliers are eliminated, as in [2]. The final form is:

$$M'(v) \cdot \ddot{v} + F'(\dot{v},v) + Q'(\dot{v},v,f_{e},t_{e},t) = 0 \quad (6a)$$

where: $\quad M' = M_{vv} - M_{vu} \cdot J_{u}^{-1} \cdot J_{v} - J_{v}^{T} \cdot \left(J_{u}^{-1} \right)^{T} \left(M_{uv} - M_{uu} \cdot J_{u}^{-1} \cdot J_{v} \right);$

$$F' = F_{v} - M_{vu} \cdot J_{u}^{-1} \cdot \varsigma - J_{v}^{T} \cdot \left(J_{u}^{-1} \right)^{T} \left(F_{u} - M_{uu} \cdot J_{u}^{-1} \cdot \varsigma \right); \quad (6b)$$

$$Q' = Q_{v} - J_{v}^{T} \cdot \left(J_{u}^{-1} \right)^{T} Q .$$

3. NUMERICAL TESTS

Presented model is implemented in MATLAB [5]. The model is used for numerical integrations and time evolution of system's dissipated power is calculated. Its estimation is based on elasto-damping elements' deformations and is calculated as a scalar product of damping forces and velocities of deformations. MATLAB's standard procedure (ode15s) is used for integrations. Integration period corresponds to a singe rotation of the crankshaft. Maximal step of integration is limited to 1/750 of the integrations period.

Calculated energy should correspond to system's steady-state conditions. They are estimated before the integration. Again a singe crankshaft's rotation is considered. The steady state condition is formulated as identity between initial and final state coordinates [5]. The condition depends on 12 parameters, and it is described by 12 nonlinear functions. The system is solved numerically and classical Newton-Raphson's algorithm is employed. Nonlinear equations are linearized about the actual calculation point, and the solution of the linear system is calculated. The step is repeated until a neighbourhood of zero is obtained. Finite differences are used to obtain simplified numerical linearization.

The system's dynamic equations (6) are nonlinear in respect to system's state coordinates. The mass matrix is non-constant and the vector Q is nonlinear, too. It is confirmed in fig 2.c, where time evolution of the base motion is presented for crankshaft rotational velocity of 1.25 rot/s. The evolution differs from a harmonic function of rotation frequency. Frequency domain analyses of linear system become non-useful. The system's evolutions have to be obtained by numerical integration of the dynamics equations.

A set of numerical integrations is performed for velocities from 0.5 to 200 rot/s. In the first test, the damping coefficient equals 600 Ns/m. Resulting base displacements are presented in Fig 4, where relations between the engine's velocity and position's maximal changes (conf. Fig 2.c) are presented.
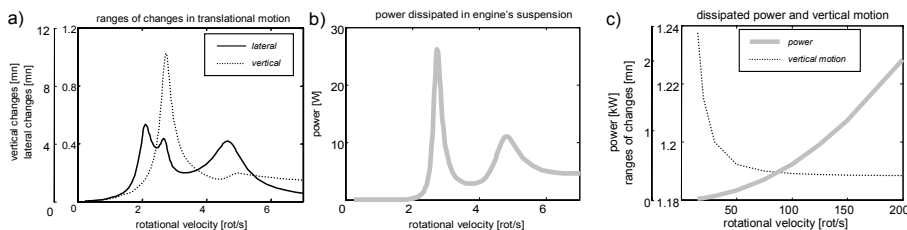
Fig. 4: Results of integration: ranges of change in translational motion for low rotational velocities (a); dissipated power for low rotational velocities (b); ranges of change and dissipated power for high rotational velocities (c)

Few zones of resonance are observed for low rotational velocities (Fig. 4a). It effects in higher dissipated power in the zones. For higher velocities, changes of vertical motions are stabilised about 1.19 mm. The other motions decay. The vertical motion becomes responsible for significant growth of the dissipated power for higher velocities. The power grows parabolically with the velocity and it obtains 2 kW for 200 rot/s.

As the dissipated power obtains significant value, the engine's efficiency is reduced. The dissipated power should be reduced for higher rotational velocities. It can be done if a clearance is present in dampers. In the next model damping coefficient equals 5 *Ns/m* until damper's deformations obtain 1.2 mm. Then it switches to 600 *Ns/m*. New integration results are presented in Fig. 5.
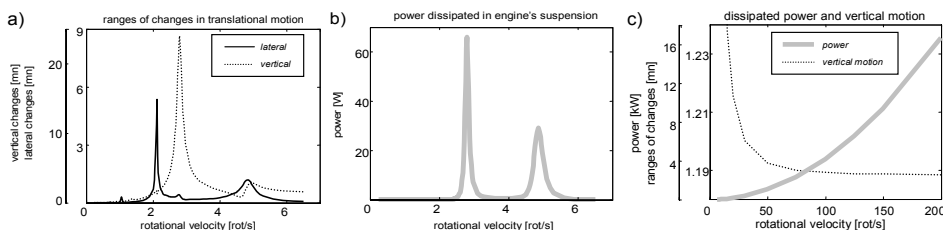
Fig. 5: Results of integration for dampers with clearance: ranges of change for low rotational velocities (a); dissipated power for low rotational velocities (b); ranges of change and dissipated power for high rotational velocities (c)

4. CONCLUSIONS

Multibody modelling looks to be an effective tool for modelling of engine's vibrations. The tests proof that significant damping coefficients are necessary in the suspensions to damp vibrations during low rotational velocities. It prevents against significant amplitudes in zones of resonance with the engine's free vibrations. The damping effects in significant dissipated power for high rotational velocities. It reduces engine's efficiency as the energy source is the engine's power. The dissipated power can be reduced in some clearance is present in the dampers and the clearance size is higher that the vertical vibrations for high velocities. Some low damping coefficient is necessary for low velocities to damp system free vibrations (indicated by initial non-equilibrium conditions). Performed calculations confirm that it the dissipated power can be reduced from 2 kW to 16 W only if the dampers with the clearance are introduced to the engine's suspension.

References

1. P. Fisette, K. Lipiński, J.C. Samin, *Symb. Mod. for the Sim., Contr. and Optim. of Multibody Systems*, Advances in Multibody Sys. and Mechatr., Gratz, (1999).
2. E.J. Haug, J. Yen: *General Coordinate Partitioning. Method for Numerical Integration*, NATO ASI, **69** (1990) 97-114.
3. K. Lipiński, *Modelowanie silnika spalinowego jako układu wielomasowego – wpływ współcz. tłumienia na poziom rozprasz. energii w układzie mocowania silnika*. In: *TECHNICON`06*, Politechnika Gdańska, Gdańsk (2006), [1-10]
4. J. Awrejcewicz: *Drgania deterministyczne układów dyskretnych*, WNT, W-wa, 1996
5. http://www.mathworks.com/

ACOUSTIC ATTENUATION PERFORMANCE
OF HELMHOLTZ RESONATOR AND SPIRAL DUCT

Wojciech ŁAPKA, Czesław CEMPEL

Poznań University of Technology
Institute of Applied Mechanics
Piotrowo 3 Street, 60-965 Poznań, POLAND
+48616652179, e-mail: Wojciech.Lapka@put.poznan.pl

Summary

This work examines a comparison of acoustic attenuation performance of well known Helmholtz resonator and spiral element inserted into circular duct, which creates spiral duct. The paper consists results of numerical computations by the use of Finite Element Method. Here the spiral is a kind of resonant element, which can be applied in circular ducts, mainly for low speed velocity ducts e.g. ventilation, air-conditioning and heat systems. Results are presented as a transmission loss. The sound attenuation performances of Helmholtz resonator and spiral duct depend on their geometrical relationships. The most important observation is that the sound attenuation in both solutions are based on similar phisical phenomenon – resonance.

Keywords: spiral duct, acoustic resonator, sound attenuation.

1. Introduction

There is many silencing applications described in world's famous papers, but authors couldn't find any information about acoustical properties of a spiral element inserted into a duct and used for attenuating sounds. That is a good basis to find out what happen when we do so. This solution is inspired by an Archimedes' screw, historically used for transferring water from a low-lying body of water into irrigation ditches – Fig. 1.
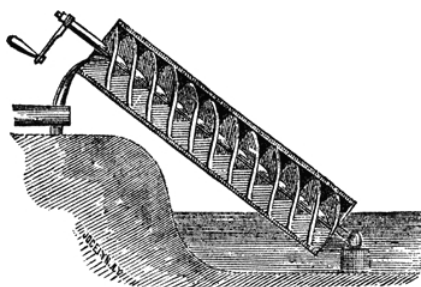
Fig.1. Archimedes' screw from Chambers's Encyclopedia
(Philadelphia: J. B. Lippincott Company, 1875).

Authors expose a different view on this well known and practical solution, presented in Fig.1, by using it in acoustical systems [1-4]. It still requires a lot of research work, but the work already done can be a great basis to formulate fundamental conclusions. The

most important one is that the newly discovered physical phenomenon of a specific sound pressure distribution achieved by inserting spiral element into a circular duct occurs in similar form in well-known Helmholtz resonator. Despite of fact, that construction of both devices is diametrically different. As it is shown in Fig.2 the spiral duct can be made as one spiral turn of Archimedes' screw with a mandrel placed axially. Helmholtz resonator [5] is a kind of simple empty chamber (cavity) connected with duct by a small branch tube - called a neck.
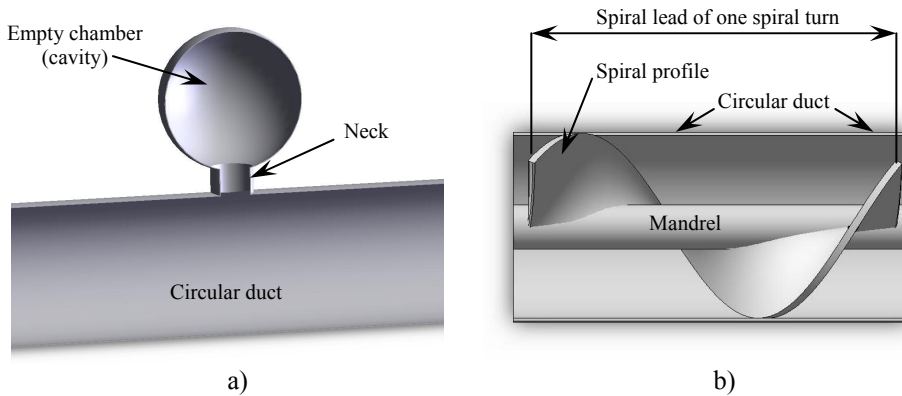
Fig. 2. Examples of resonant elements construction as a part of simple acoustic system (circular duct): a) Helmholtz resonator - outside a circular duct; b) spiral element - inside a circular duct.

Main difference is that the spiral element is situated inside the duct, and Helmholtz resonator stands outside. Whatever, both solutions can be used in series in one acoustic system – Fig. 3.
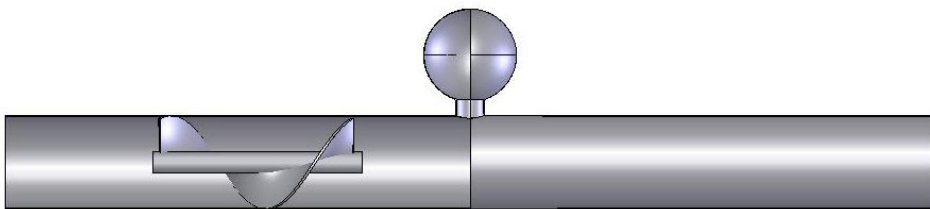
Fig.3. Possible application of Helmholtz resonator and one turn of spiral element inside circular duct used in series in simple acoustic system - circular duct.

2. Simulation

Finite Element Method (FEM) was used to compute three-dimensional (3D) numerical models by the use of time-harmonic analysis in a COMSOL Multiphysics - Acoustics Module [6] computer application. All spiral elements were solidly inserted into circular

ducts and they consisted one spiral turn. The mandrel was placed in axis of each spiral element. The circular ducts are straight and each has the same diameter as spirals – see Fig. 2 b.

Helmholtz resonators were calculated for the same resonance frequency as spirals. The resonance frequency of Helmholtz resonator, at which it would yield very high transmission loss, can be calculated using equation (1) [5]:

$$\omega_H = c\sqrt{\frac{S_n}{l_{eq}V_c}} \tag{1}$$

where:

$l_{eq} = l_n + t_w + 1.7r_n$
$S_n = \pi r_n^2$
V_c – cavity volume,
t_w – thickness of the wall of the propagation circular duct,
r_n – radius of the neck,
l_n – length of the neck,
c – sound speed (343m/s),
$\omega_H = 2\pi f_H$, where f_H [Hz] resonance frequency of Helmholtz resonator.

There isn't such accurate equation for spiral ducts, but authors still work on it. Circular duct length is 6,83m and radius is 0,1839m. Geometrical dimensions of resonators are presented in Tab. 1.

Helmholtz resonator		Spiral duct	
Parameter:	Value:	Parameter:	Value:
V_c – cavity volume - sphere	3,3188e-4 m^3	Spiral lead	0,765m
R – radius of the sphere	0,04295 m	Thickness of the spiral profile	0,0147m
l_n – length of the neck	0,05 m	Diameter of the mandrel	0,0883m
r_n – radius of the neck	0,025 m		
$l_{eq} = l_n + t_w + 1.7r_n$	0,0925 m		
$S_n = \pi r_n^2$	1,9635e-3 m^2		

Tab.1. Geometrical parameters of Helmholtz resonator and spiral duct.

3. Results

The results are shown as the transmission loss (TL) [1,3,5,6]. Calculated resonance frequency for investigated resonators $f_r = 414$Hz. Fig. 4 presents a sound pressure level (SPL) distribution inside silencing system with resonant elements applied to circular duct for the highest value of TL in resonance frequency. There is also shown the shape view of SPL distribution in the distance of 0,1m from the end of resonators.

a) Helmholtz resonator,
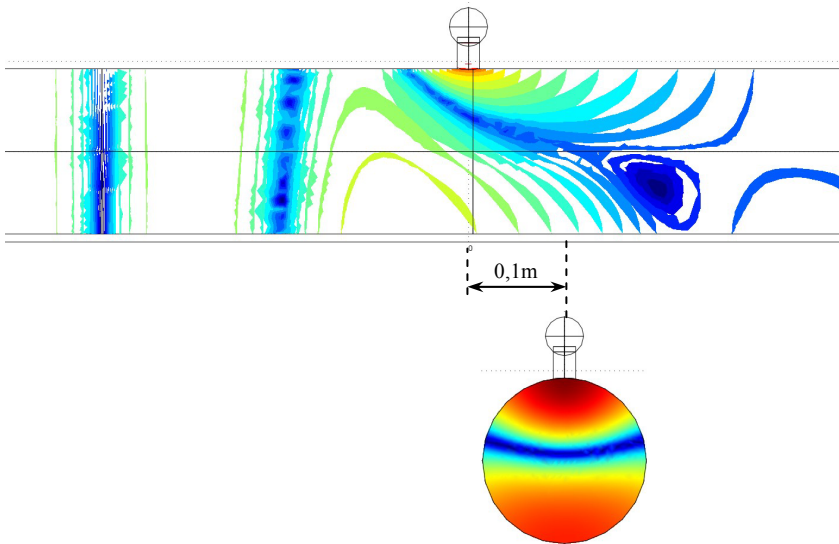
b) spiral duct,
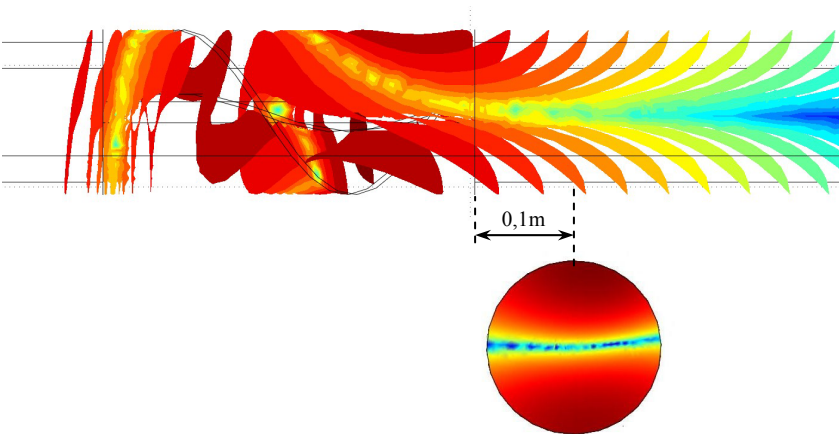
Fig.4. Example views of SPL distribution caused by resonant elements in resonance frequency f_r=414Hz with shape view at the distance of 0,1m from the end of resonators.

TL of investigated Helmholtz resonator and spiral duct is presented in Fig. 5. Higher level of TL in resonance frequency f_r, about 65dB, is achieved by the spiral duct, and Helmholtz resonator reaches almost 20dB of TL.
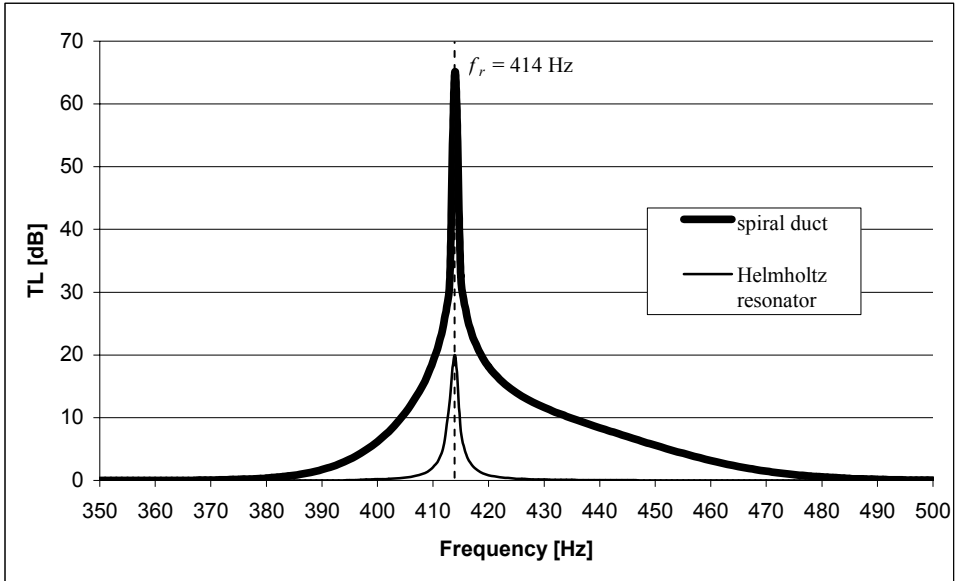
Fig.5. TL of Helmholtz resonator and spiral duct inside investigated simple acoustic system – circular duct; resonance frequency f_r = 414Hz.

In this case the spiral duct seems to be better sound attenuator than Helmholtz resonator. It is also shown in Fig.5 that the spiral duct attenuates wider range of frequency. This is the most important information for practical applications.

4. Conclusions

The spiral duct and Helmholtz resonator can be tuned in frequency band width. That is very important property for practical applications of acoustic Band Stop Filters (BSF) in e.g. heat, ventilation and air-conditioning systems. The best conclusion is that the new type of resonant element has been developed for silencing systems as an alternative substitution of Helmholtz resonator – well known acoustic BSF. The frequency bands of sound attenuation of the spiral ducts are wider than Helmholtz resonator. However, the spiral duct can be applied in large diameter circular ducts silencing systems when Helmholtz resonators do not work properly. This is the most important practical advantage of the spiral ducts.

Acknowledgment

References

1. ŁAPKA W., *„Acoustic attenuation performance of a round silencer with the spiral duct at the inlet",* Archives of Acoustics Vol. 32, No 4 (Supplement), 2007, pp. 247-252.
2. ŁAPKA W., CEMPEL C., „*Noise reduction of spiral ducts"*, International Journal of Occupational Safety and Ergonomics (JOSE), Vol. 13, No. 4, 2007, pp. 419-426.
3. ŁAPKA W., CEMPEL C. *„Spiral waveguide and damper"*, The 36th International Congress & Exhibition on Noise Control Engineering, Global Approaches to Noise Control, Istanbul, Turkey, 28-31 August 2007, p. 8 on CD.
4. ŁAPKA W., CEMPEL C., "Insertion loss of spiral acoustic duct – computational modeling", 35th Winter School on Vibroacostical Hazards Suppressions, Wisła, Poland, February 26 – March 02, 2007, pp. 83-94.
5. MUNJAL M. L., "*Acoustics of Ducts and Mufflers with Application to Exhaust and Ventilation System Design"*, John Wiley & Sons, Inc., Calgary, Canada 1987, p.328.
6. COMSOL Multiphysics version 3.3a, Acoustic Module, COMSOL AB, www.comsol.com, Stockholm, Sweden, 1996-2006.

OPTIMAL ACTIVE SEGMENT DAMPING IN CABLES SUBJECTED TO THE TRAVELING WAVES MOTION

Waldemar ŁATAS

Institute of Applied Mechanics, Cracow University of Technology

Al. Jana Pawła II 37, 31-864 Kraków, Poland

(0-12) 628-33-97, latas@mech.pk.edu.pl

Summary

In the paper the problem of optimal choice of the distributed damping force suppressing the waves traveling along the cable is considered. For the proposed objective function – mean dissipation efficiency - numerical calculations were performed.

Keywords: cable motion, optimal damping, active methods.

Introduction

Cables used in overhead transmission lines and cable-stayed bridges are subjected to large vibrations causing fatigue damages of the cable and assemblies. Long cables are vulnerable to the aerodynamic disturbances due to the low intrinsic damping. The loading process within a span is often imprecisely known through interpretation of displacement response. Wave motion and vibrations occur mainly due to vortex shedding, rivulet formation, galloping and buffeting.

Countermeasures proposed to protect cables can be arranged into:

- Cable surface modifications preventing from the aerodynamic forces induced by the air flow
- Wave energy dissipation methods:
    a) increasing of the cable internal damping,
    b) using the special dampers, damping loops and spacers [2][3][4].

In the paper the problem of optimal distributed damping force necessary to suppress the waves traveling along the cable is considered.

1. Waves induced by the distributed load
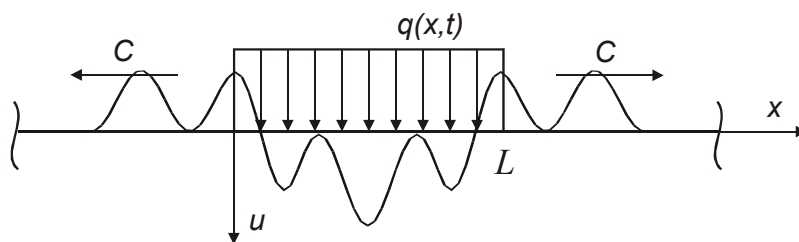
Fig. 1. Distributed force as a source of waves

The equation of motion of the cable excited by load applied to the segment (Fig. 1) can be written in the following form:

$$\mu \frac{\partial^2 u}{\partial t^2} - T \frac{\partial^2 u}{\partial x^2} = \tilde{q}(x,t) \qquad (1)$$

where μ is a linear mass density and T is a tension force,

$$\tilde{q}(x,t) = \begin{cases} q(x,t) & 0 \le x \le L \\ 0 & x<0, \; x>L \end{cases} \qquad (2)$$

The solution of equation (1) without the components dependent on the initial conditions can be written in the integral form [11]:

$$u(x,t) = \frac{1}{2c\mu} \int\limits_0^t \int\limits_{x-c(t-\tau)}^{x+c(t-\tau)} \tilde{q}(\xi,\tau) d\xi d\tau \qquad (3)$$

where c denotes the velocity of traveling waves equal to $\sqrt{T/\mu}$.

In numerical calculations of energies of the traveling waves will be utilized the following expression derived from (3):

$$\frac{\partial u(x,t)}{\partial t} = \frac{1}{2\mu} \int\limits_0^t \left[\tilde{q}(x-c(t-\tau),\tau) + \tilde{q}(x+c(t-\tau),\tau) \right] d\tau \qquad (4)$$

2. Optimal damping distributed force

The damping segment exerts the resisting distributed force applied to the cable which is a source of two secondary waves (Fig. 1): the reflected wave traveling in opposite direction to the original wave and the wave that adds to the original wave forming in result the transmitted wave.

It was shown [8] that for the concentrated force the optimization problem can be solved exactly. The optimal force takes the opposite direction to the component of velocity vector associated with the original wave. The force magnitude is proportional to the magnitude of velocity component. The constant of proportionality is equal to the ratio of the cable tension to the wave velocity. The maximum value of the dissipated energy is equal to the half of the original wave energy.

In order to increase the damping the similar strategy for the distributed damper force was proposed. The damping force is proportional to the component of the cable velocity resulting from the motion of the original wave:

$$q(x,t) = -\alpha \frac{\partial u_0(x,t)}{\partial t} \qquad (5)$$

The original wave used in numerical simulations was assumed in the form of packet wave, described by the expression:

$$u_0(x,t) = \Psi_0 \sin(k_0(x - ct + 4\sigma)) \exp\left(-\frac{(x - ct + 4\sigma)^2}{4\sigma^2}\right) \qquad (6)$$

where: k_0 - wave number; σ - packet width parameter.

This type of wave with amplitude modulation is convenient in modeling of many disturbances observed in cables. The original wave at the moment before it reaches the damping segment is presented in Fig. 2.
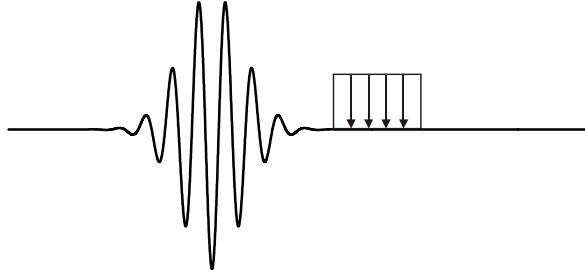
Fig. 2. Original wave before the damping segment

In order to determine the energy E_D dissipated in the active segment the principle of energy conservation can be used:

$$E_D = E_S - (E_R + E_T) \qquad (7)$$

where:

$E_S = \int\limits_0^{\frac{8\sigma}{c}} \sqrt{T\mu} \left(\frac{\partial u_0(0,t)}{\partial t}\right)^2 dt$ - energy of the original wave,

$E_R = \int\limits_0^{\frac{8\sigma+2L}{c}} \sqrt{T\mu} \left(\frac{\partial u(0,t)}{\partial t}\right)^2 dt$ - energy of the reflected wave,

$E_T = \int\limits_{\frac{L}{c}}^{\frac{8\sigma+L}{c}} \sqrt{T\mu} \left(\frac{\partial u(L,t)}{\partial t} + \frac{\partial u_0(L,t)}{\partial t}\right)^2 dt$ - energy of the transmitted wave.

The ratio of the energy dissipated in the active segment to the energy of the original wave is called the dissipation efficiency:

$$\eta = \frac{E_D}{E_S} \qquad (8)$$

In the paper [10] the aim of calculations was to find the optimal value of α/μ which maximizes the energy dissipated in the active segment. Numerical calculations proved benefits of the distributed force damper over the concentrated force damper. When the segment is longer than 0.2λ (where $\lambda = \frac{2\pi}{k_0}$) the optimal distributed force dissipates over 98% of energy of the original wave. With decrease of the segment width the maximal efficiency ratio decreases and approaches 0.5, as for the optimal concentrated force.

It is apparent that the length of the active damping segment is limited due to the technological restrictions. For a given segment length one should adjust the damping so the damper might be efficient in a wide range of the wave length λ and the packet width parameter σ. The optimization problem will be defined using the mean dissipation efficiency:

$$\bar{\eta}(\tilde{\alpha}) = \frac{\iint \eta(\tilde{\alpha}, \bar{\sigma}, \bar{\lambda}) W(\bar{\sigma}, \bar{\lambda}) d\bar{\sigma} d\bar{\lambda}}{\iint d\bar{\sigma} d\bar{\lambda}} \tag{9}$$

where: $\bar{\sigma} = \dfrac{\sigma}{L}$, $\bar{\lambda} = \dfrac{\lambda}{L}$, $\tilde{\alpha} = \dfrac{\alpha}{\mu}$.

The arbitrary weighing function W introduced to the above expression may be related to the probability distribution of packet wave arguments or severity of a packet wave with parameters given. The aim of calculation is to find the optimal value of $\tilde{\alpha}$ which maximizes the mean dissipation efficiency given by expression (9).

3. Numerical results

The Table 1 shows the optimal values of $\tilde{\alpha}\,[1/s]$ altogether with the maximal dissipation efficiency η_{MAX} reached for different values of $\bar{\sigma}$ and $\bar{\lambda}$.

Table 1

	$\bar{\lambda} = 1$		$\bar{\lambda} = 3$		$\bar{\lambda} = 6$	
$\bar{\sigma} = 1$	$\tilde{\alpha}_{OPT} = 80$	$\eta_{MAX} = 0.995$	$\tilde{\alpha}_{OPT} = 71$	$\eta_{MAX} = 0.876$	$\tilde{\alpha}_{OPT} = 55$	$\eta_{MAX} = 0.676$
$\bar{\sigma} = 3$	$\tilde{\alpha}_{OPT} = 80$	$\eta_{MAX} = 0.999$	$\tilde{\alpha}_{OPT} = 69$	$\eta_{MAX} = 0.856$	$\tilde{\alpha}_{OPT} = 48$	$\eta_{MAX} = 0.604$
$\bar{\sigma} = 6$	$\tilde{\alpha}_{OPT} = 80$	$\eta_{MAX} = 0.999$	$\tilde{\alpha}_{OPT} = 68$	$\eta_{MAX} = 0.854$	$\tilde{\alpha}_{OPT} = 47$	$\eta_{MAX} = 0.596$

Assuming the weighing function W equal to one optimization of the following function:

$$\overline{\eta}(\tilde{\alpha}) = \frac{\int\limits_{1}^{6}\int\limits_{1}^{6}\eta(\tilde{\alpha},\overline{\sigma},\overline{\lambda})d\overline{\sigma}d\overline{\lambda}}{25} \qquad (10)$$

gave the results:

$$\tilde{\alpha}_{OPT} = 72[1/s]\,,$$

$$\overline{\eta}_{MAX} = 0.906\,.$$

4. Conclusions

The active segment damper model intended to suppress the traveling waves motion in cables is intuitive and physically motivated. For a given damping segment length when the wave length increases the maximal dissipation efficiency decreases (Table 1), ranging from 1 (when $\overline{\lambda} \to 0$) to 0.5 (when $\overline{\lambda} \to \infty$).

The target was to adjust the damper parameter $\tilde{\alpha}[1/s]$ so the damper could be effective in the given ranges of parameters $\overline{\lambda}$ and $\overline{\sigma}$. For the proposed objective function illustrative optimizing numerical calculations were performed.

References

1. J. J. Burgess, M. S. Triantafyllou, *The elastic frequencies of cables,* Journal of Sound and Vibration, **120** (1988) 153-165.
2. E. A. Johnson, G. A. Baker, B. F. Spencer, Y. Fuyino, *Semiactive damping of stay cables*, Journal of Engineering Mechanics*,* **133** (1) (2007) 1-11.
3. S. Krenk, *Vibration of a taut cable with an external damper*, Journal of Applied Mechanics*,* ASME, **67** (2000) 772-776.
4. B. M. Pachero, Y. Fujino, *Estimation curve for modal damping in stay cables with viscous damper*, Journal of Structural Engineering*,* **119** (6) (1993) 1961-1979.
5. N. C. Perkins, M. Behbahani-Nejad, *Forced wave propagation in elastic cables with small curvature,* ASME, Design Engineering Technical Conferences, **3 – Part B** (1995) 1457-1464.
6. N. C. Perkins, M. Behbahani-Nejad, *Free wave propagation characteristic of elastic cables,* Proceedings International Symposium on Cable Dynamics, Liege 1995.
7. N. C. Perkins, M. Behbahani-Nejad, *Freely propagating waves in elastic cables,* Journal of Sound and Vibration, **2** (1996) 189-202.
8. J. Snamina, *Mechaniczne zjawiska falowe w przewodach elektroenergetycznych linii napowietrznych*, Mechanika **287**, Politechnika Krakowska, Kraków 2003.

9. G. B. Whitham, *Linear and Nonlinear Waves,* John Wiley and Sons Inc., New York 1999.
10. W. Łatas, J. Snamina, *Dissipation of the waves energy in cables by the optimal damper force*, Quarterly Mechanics, AGH, Kraków (printed).
11. W. M. Babicz, M. B. Kapilewicz, *Równania liniowe fizyki matematycznej*, PWN, Warszawa 1970.

NONLINEAR TRAVELING WAVES IN A THIN LAYER

Izabela MAJOR, Maciej MAJOR
Wydział Budownictwa, Politechnika Częstochowska
ul. Akademicka 3, 42-200 Częstochowa
Tel. (34) 3250-984 , e-mail: admin@major.strefa.pl

Abstract

In this paper we consider nonlinear traveling waves in a Mooney – Rivlin elastic layer. By the procedure of averaging the equations of motions over the width of the layer we obtain a system of partial differential equations in one space dimension and time. From analysis follows that obtained wave is a solitary wave of transverse stretch.
Key words: discontinuous surface, traveling waves, hyperelastic materials

We consider the motion of a continuum represented by a set of functions [6]

$$x_i = x_i(X_\alpha, t) \quad \text{where} \quad i, \alpha = 1, 2, 3 \tag{1}$$

We assume that the traveling wave is propagating in the half-infinite elastic layer, which occupies the material region $X_1 > 0$ in the direction of axis X_1. At the frontal area of layer $X_1 = 0$, the boundary conditions for deformations are given (compare [4]). We assume that motion described by equations (2) undergoes without imposing additional contact forces at the lateral planes of layer $X_2 = \pm h$ [8].

Motion of the considered traveling wave is assumed as

$$x_1 = X_1 + u_1(X_1, t) \qquad x_2 = X_2 + X_2 \varepsilon_2(X_1, t) \qquad x_3 = X_3 \tag{2}$$

The strain ε_1, the gradient of the transversal strain κ and speeds of the particle of the medium v_1 and v_2 in both direction of the layer are equal, respectively

$$\varepsilon_1 = u_{1,1} \qquad \kappa = \varepsilon_{2,1} \qquad v_1 = \dot{x}_1 = \dot{u}_1(X_1, t) \qquad v_2 = \dot{x}_2 = X_2 \dot{\varepsilon}_2(X_1, t) \tag{3}$$

For the assumed motion (2), the deformation gradient and the left Cauchy-Green tensor have the form

$$\mathbf{F} = \begin{bmatrix} 1 + \varepsilon_1 & 0 & 0 \\ X_2 \kappa & 1 + \varepsilon_2 & 0 \\ 0 & 0 & 1 \end{bmatrix} \qquad \mathbf{B} = \begin{bmatrix} (1 + \varepsilon_1)^2 & (1 + \varepsilon_1) X_2 \kappa & 0 \\ (1 + \varepsilon_1) X_2 \kappa & (X_2 \kappa)^2 + (1 + \varepsilon_2)^2 & 0 \\ 0 & 0 & 1 \end{bmatrix} \tag{4}$$

For an incompressible material, there is identity $\det \mathbf{F} = 1$, then for the considered material $(1 + \varepsilon_1)(1 + \varepsilon_2) = 1$.

We assume that the layer is made of the Mooney-Rivlin material characterized by the strain-energy function

$$W = \mu[C_1(I_1 - 3) + C_2(I_2 - 3)] \tag{5}$$

where I_1 and I_2 are the invariants of the left Cauchy-Green deformation tensor, C_1 and C_2 are constitutive constants and μ is the shear modulus for infinitesimal deformation.

According to [7] or [2] the Cauchy tensor has the form

$$\mathbf{T} = -q\mathbf{I} + 2\mu\left(C_1\mathbf{B} - C_2\mathbf{B}^{-1}\right) \tag{6}$$

where q is an arbitrary hydrostatic pressure.

The Piola-Kirchhoff tensor $\mathbf{T}_R$ may be expressed by the Caychy tensor $\mathbf{T}$

$$\mathbf{T}_R = \mathbf{T}\mathbf{F}^{-T} \tag{7}$$

For deformation gradient $(4)_1$ the equations of motion are reduced to a system of equations for the plane strain deformation

$$T_{R11,1} + T_{R12,2} = \rho_R u_{1,tt} \qquad T_{R21,1} + T_{R22,2} = \rho_R X_2 \varepsilon_{2,tt} \qquad T_{R33,3} = 0 \tag{8}$$

The boundary conditions at the top and bottom surfaces of the layer have the form

$$T_{R12}\left(X_1, \pm h, X_3\right) = T_{R22}\left(X_1, \pm h, X_3\right) = 0 \tag{9}$$

In pursuance of averaged procedure for equations of motion over the width of the layer, we obtain fundamental equations of traveling waves in Mooney-Rivlin material

$$\left[C_1\left[(1+\varepsilon_1) - (1+\varepsilon_1)^{-3}\right] - \frac{h^2}{6}v_o^{-2}\varepsilon_{2,tt}(1+\varepsilon_1)^{-2} + C_2\left[(1+\varepsilon_1) - (1+\varepsilon_1)^{-3} + \right. \right. \tag{10}$$

$$+ \frac{2}{3}\left(h\varepsilon_{1,1}\right)^2(1+\varepsilon_1)^{-5}\right] - \frac{h^2}{3}\left[2C_2\varepsilon_{1,1}^2(1+\varepsilon_1)^{-5} + \right.$$

$$\left. \left. - (C_1 + C_2)\left[2\varepsilon_{1,1}^2(1+\varepsilon_1)^{-5} - \varepsilon_{1,11}(1+\varepsilon_1)^{-4}\right]\right]\right]_{,1} = \frac{1}{2}v_o^{-2}u_{1,tt}$$

where $v_o = \sqrt{\mu/\rho_R}$ is the speed of infinitesimal shear waves.

The phase ξ is defined by

$$\xi = X_1 - Vt \tag{11}$$

where V is the speed of propagation of traveling wave with a constant profile displaced along the axis X_1. For the traveling wave with any profile, we express motion as a function of one parameter ξ only

$$u_1(X_1, t) = u_1(\xi) \qquad \varepsilon_2(X_1, t) = \varepsilon_2(\xi) \tag{12}$$

Substituting (11), integrating the equation (10) with respect to ξ, multiplying mutually by $\varepsilon_{1,\xi}$ and integrating once more we obtain

$$\frac{1}{2}(C_1 + C_2)\left[(1+\varepsilon_1)^2 + (1+\varepsilon_1)^{-2}\right] + \frac{h^2}{12}v\varepsilon_{1,\xi}^2(1+\varepsilon_1)^{-4} + \tag{13}$$

$$- \frac{h^2}{6}(C_1 + C_2)\varepsilon_{1,\xi}^2(1+\varepsilon_1)^{-4} = \frac{1}{4}v\varepsilon_1^2 + d_1\varepsilon_1 + d_2$$

where $v = V^2/v_o^2$ and d_1 and d_2 are integration constants.

Multiplying the equations of motion in the form (13) by $4/(v - 2C_1)$ and including b_1, b_2, D_1 and D_2 according to [5], we obtain an approximate form

$$(b_1 + b_2)\left[(1+\varepsilon_1)^2 + (1+\varepsilon_1)^{-2}\right] + \frac{h^2}{3}\varepsilon_{1,\xi}^{2}(1+\varepsilon_1)^{-4}(1-b_2) = \varepsilon_1^{2}(1+b_1) + 2D_1\varepsilon_1 + 2D_2 \qquad (14)$$

Now we introduce the following transformation

$$\zeta = \frac{\sqrt{3}}{h}\xi \qquad (15)$$

Apart from a scaling factor, ζ is just the current configuration coordinate X_1 in terms of the phase ξ and (14) takes the form

$$\varepsilon_{1,\zeta}^{2} = F(\varepsilon_1, D_2) \qquad (16)$$

where

$$F(\varepsilon_1, D_2) = \frac{(1+\varepsilon_1)^6\left[2D_1\varepsilon_1 + 2D_2 + \varepsilon_1^{2}(1+b_1)\right] - (b_1+b_2)\left[(1+\varepsilon_1)^8 + (1+\varepsilon_1)^4\right]}{(1-b_2)(1+\varepsilon_1)^2} \qquad (17)$$

In the above equations (16) and (17) D_2 is an argument of F (compare [4]).

The phase point is the equilibrium point if

$$F(\varepsilon_1, D_2) = (1+\varepsilon_1)^6\left[2D_1\varepsilon_1 + 2D_2 + \varepsilon_1^{2}(1+b_1)\right] - (b_1+b_2)\left[(1+\varepsilon_1)^8 + (1+\varepsilon_1)^4\right] = 0 \qquad (18)$$

$$F'(\varepsilon_1, D_2) = 6(1+\varepsilon_1)^5\left[2D_1\varepsilon_1 + 2D_2 + \varepsilon_1^{2}(1+b_1)\right] + 2(1+\varepsilon_1)^6\left[D_1 + \varepsilon_1(1+b_1)\right] +$$
$$- 4(b_1+b_2)\left[2(1+\varepsilon_1)^7 + (1+\varepsilon_1)^3\right] = 0$$

Eliminating D_2 and simplifying, we obtain the polynomial equation

$$\left\{(1+\varepsilon_1)^5\left[D_1 + + \varepsilon_1(1+b_1)\right] + (b_1+b_2)\left[(1+\varepsilon_1)^2 - (1+\varepsilon_1)^6\right]\right\}(1+\varepsilon_1)^2 = 0 \qquad (19)$$

According to Theorem 1 from [2] (compare[5]), we suppose that a center point for function $F(\varepsilon_1, D_2)$ exists for $\varepsilon_1 = \varepsilon_{1c}$ (then $F(\varepsilon_{1c}, D_2) = 0$ and $F'(\varepsilon_{1c}, D_2) = 0$), and we can find D_1 and D_2 as functions of ε_{1c}, which determines this center

$$D_1 = \frac{1}{(1+\varepsilon_{1c})^5}(b_1+b_2)\left[(1+\varepsilon_{1c})^6 - (1+\varepsilon_{1c})^2\right] - \varepsilon_{1c}(1+b_1) \qquad (20)$$

$$D_2 = \frac{\varepsilon_{1c}(b_1+b_2)\left[(1+\varepsilon_{1c})^2 - (1+\varepsilon_{1c})^6\right]}{(1+\varepsilon_{1c})^5} + \frac{(b_1+b_2)\left[(1+\varepsilon_{1c})^6 + (1+\varepsilon_{1c})^2\right]}{2(1+\varepsilon_{1c})^4} + \frac{1}{2}\varepsilon_{1c}^{2}(1+b_1)$$

Substituting D_1 i D_2 according to (20) (replacing ε_{1c} by ε_{1s}), into equation (17) and simplifying we receive

$$\varepsilon_{1,\zeta}^{2} = \frac{(\varepsilon_1 - \varepsilon_{1s})^2(\varepsilon_1 - \varepsilon_{1n})(\varepsilon_1 - \varepsilon_{1m})}{(1-b_2)} \qquad (21)$$

where

$$\varepsilon_{1n,m} = \frac{-1}{\left(1+\varepsilon_{1s}\right)^3 \left(b_2 - 1\right)} \Big(b_1 + b_2 + \left(1+\varepsilon_{1s}\right)^3 \left(b_2 - 1\right) \pm \tag{22}$$

$$\pm \sqrt{\left(b_1 + b_2\right)\left(\varepsilon_{1s}\left(2+\varepsilon_{1s}\right)\left(2+2\varepsilon_{1s}+\varepsilon_{1s}{}^2\right)\left(1-b_2\right)+1+b_1\right)} \Big)$$

ε_1 variable aims to ε_{1s} if $\zeta \to \pm\infty$, the minimal value of ε_1 is $\varepsilon_{1n} > 0$. ζ is just the current configuration in terms of the phase ξ then $\varepsilon_1(\zeta)$ represents solution of single traveling wave, for which $\varepsilon_{1s} > 0$ is the value of axial stretch in the infinity, however $\varepsilon_{1n} > 0$ is the minimum value of axial stretch aims to the cusp point. If the lateral surface of the layer is described by equation $H = \pm h/\left(1+\varepsilon_1\right)$, the wave amplitude h_1 is

$$h_1 = \frac{h}{\left(\varepsilon_{1n}+1\right)} - \frac{h}{\left(\varepsilon_{1s}+1\right)} > 0 \tag{23}$$

and is positive if $\varepsilon_{1s} > \varepsilon_{1n}$.

Taking square root, separating variables, integrating and substituting $\tau^2 = L - \varepsilon_{1n}$ equation (21) takes the form

$$\zeta - \zeta_n = \pm \frac{2\sqrt{1-b_2}}{\left(\varepsilon_{1s}-\varepsilon_{1n}\right)\sqrt{\left(\varepsilon_{1n}-\varepsilon_{1m}\right)}} \int_0^{\tau_1} \frac{d\tau}{\left(1-\beta_1{}^2\tau^2\right)\sqrt{1+m_1{}^2\tau^2}} \tag{24}$$

where

$$\tau_1{}^2 = \varepsilon_1 - \varepsilon_{1n} \qquad \beta_1{}^2 = \frac{1}{\varepsilon_{1s}-\varepsilon_{1n}} \qquad m_1{}^2 = \frac{1}{\varepsilon_{1n}-\varepsilon_{1m}} \tag{25}$$

in (24) ζ_n is the value ζ for which $\varepsilon_1 = \varepsilon_{1n}$.

We assume that both expression $(25)_{2,3}$ are positive. According to (22) ε_{1n} corresponds with sign plus, and ε_{1m} with sign minus, then we receive

$$\varepsilon_{1n} - \varepsilon_{1m} = \frac{-2\sqrt{\left(b_1+b_2\right)\left(\varepsilon_{1s}\left(2+\varepsilon_{1s}\right)\left(2+2\varepsilon_{1s}+\varepsilon_{1s}{}^2\right)\left(1-b_2\right)+1+b_1\right)}}{\left(1+\varepsilon_{1s}\right)^3\left(b_2-1\right)} \tag{26}$$

Above expression fulfill condition $\varepsilon_{1n} - \varepsilon_{1m} > 0$ if $b_2 < 1$. It means that condition $b_2 < 1$ is the necessary condition to existing real solutions for this expression.

Finally equation (24) after transformation takes the form

$$\zeta - \zeta_n = \pm \frac{\beta^2 m\sqrt{1-b_2}}{\phi} \left[ar\, tgh\left(\frac{\beta_1 + m_1{}^2\sqrt{\varepsilon_1-\varepsilon_{1n}}}{\phi\sqrt{1+m_1{}^2\left(\varepsilon_1-\varepsilon_{1n}\right)}} \right) + \right. \tag{27}$$

$$\left. + ar\, tgh\left(\frac{-\beta_1 + m_1{}^2\sqrt{\varepsilon_1-\varepsilon_{1n}}}{\phi\sqrt{1+m_1{}^2\left(\varepsilon_1-\varepsilon_{1n}\right)}} \right) - ar\, tgh\frac{\beta}{\phi} - ar\, tgh\left(\frac{-\beta}{\phi}\right) \right]$$

In the square brackets of above expression there are four elements. From analysis follows that only first of element of equation (27) have the infinite value and the right hand side of expression (27) approach $\pm\infty$ as $\varepsilon_1 \to \varepsilon_{1s}$.

In fig.1 there is a graph of expression (27). From above analysis follows that for $\varepsilon_1 = \varepsilon_{1n} = -0,44$, $\zeta = \zeta_n$, however for $\zeta \to \pm\infty$, $\varepsilon_1 = \varepsilon_{1s} = 0,5$ (according to assumption).

The graph in fig.1 is in $\langle -0,44; 0,5\rangle$ interval. The deformation values correspond to speed $V = 20,5\,m/s$ and constants $b_1 = 0,335$ and $b_2 = 0,047$ (Mooney-Rivlin material). Then this is the graph of solitary wave of transverse stretch, which decrease from the cusp of wave according to tgh function (compare [5]).
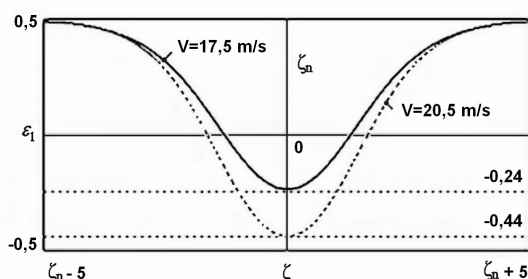
Fig.1. Graph of $\zeta - \zeta_n$ integral according to (27) in the Mooneya – Rivlina material for OKA-1 rubber ($\mu = 1,46\,kG/cm^2$, $\rho = 1190\,kg/m^3$). We assumed $\varepsilon_{1s} = 0,5$ however ε_{1n} (and ε_{1m} except of figure scale) according to (22). For speed $V = 20,5\,m/s$ (broken line), $\varepsilon_{1n} = -0,44$, $b_1 = 0,335$, $b_2 = 0,047$ and $v = 3,49$. For speed $V = 17,5\,m/s$ (solid line), $\varepsilon_{1n} = -0,24$, $b_1 = 0,525$, $b_2 = 0,0739$ and $v = 2,545$

In fig.2.b there is profile of soliton wave corresponding to fig.1 for speed $V = 20,5\,m/s$ (broken line). Assuming $\varepsilon_1 = \varepsilon_{1s} = 0,5$ from $(1+\varepsilon_1)(1+\varepsilon_2) = 1$ we have

$$(1+0,5)(1+\varepsilon_2) = 1 \quad \Rightarrow \quad (1+\varepsilon_2) = 0,66 \tag{28}$$

if the layer high is h', after contraction

$$h' = (1+\varepsilon_2)h = 0,66h \quad \Rightarrow \quad 2h' = 1,32h \tag{29}$$

Similarly, substituting $\varepsilon_1 = \varepsilon_{1n} = -0,44$, in the place of transverse stretching the high of the layer h' will be equal $2h' = 3,57h$.

The range of „hump" we calculate from (15). From fig.1 follows, that the graph quickly disappeared out of area $\Delta = 10$. For ξ this is the area

$$\xi = \frac{h\zeta}{\sqrt{3}} \quad \Rightarrow \quad \Delta\xi = \frac{h\Delta\zeta}{\sqrt{3}} = \frac{10}{\sqrt{3}}h = 5,77h \tag{30}$$

It will be then considerable change of wave thickness h (comp. (23)), because the wave amplitude is $h_1 = (3,57 - 1,32) \cdot 0,5 = 1,12h$ and this changes there are in the small area equal $5,77h$. In fig.2.c there is profile of soliton wave corresponding to fig.1 for speed $V = 17,5\, m/s$ (solid line). The layer height after contraction is $2h' = 1,32h$ (comp. (29)), however substituting $\varepsilon_1 = \varepsilon_{1n} = -0,24$, in the place of transverse stretch, the layer height is $2h' = 2,63h$. The range of „hump" is $\Delta\xi = 5,77h$ (comp. (30)). If the speed is smaller the change of wave thickness h is smaller too, the wave amplitude is $h_1 = (2,63 - 1,32) \cdot 0,5 = 0,655h$, the changes there are in the area equal $5,77h$.
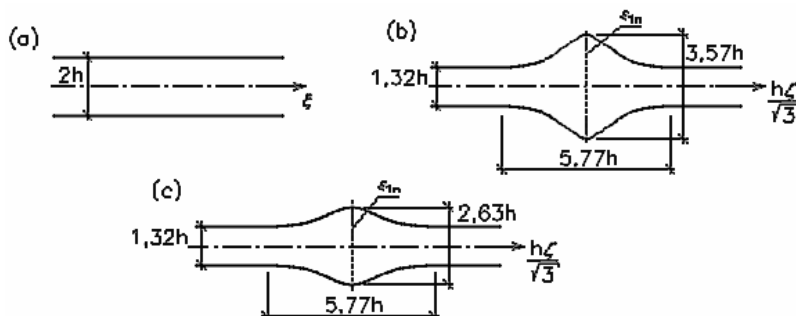
Fig.2. Profiles of solitary waves of transverse stretch for the layer, $\varepsilon_{1s} = 0,5$, $\Delta = 10$, the value h' according to (28) and (29). (a) reference configuration, (b) for the parameters like in Fig.1 and the speed $V = 20,5\, m/s$, (c) for the parameters like in Fig.1 and the speed $V = 17,5\, m/s$

References

1. Braun M., Kosiński S., *Evolution behavior of transverse shocks in a nonlinear elastic layer*, Internationa Series of Numerical Mathematics, **129**, (1999), 119-128.
2. Dai H.-H., *Nonlinear dispersive waves in a circular rod composed of a Mooney–Rivlin material*, *Nonlinear elasticity: Theory and applications*, London Mathematical Society Lecture Note Series **283**, (2001), 392-432.
3. Fu Y.B., Scott N.H., *Acceleration waves and shock waves in transversely isotropic elastic non-conductors*, Int. J. Engng. Sci., **22**, 11, (1989), 1379-1396.
4. Major I., Major M., *Phase plane analysis for nonlinear traveling waves in incompressible hyperelastic circular rod*, Vibrations in physical system, **XXII**, (2006), 243-249.
5. Major I., Major M., N*onlinear traveling waves in a thin layer composed of the Mooney-Rivlin material*, Journal of Theoretical and Applied Mechanics, **45**, 2, (2007), 259-275.
6. Truesdell C. and Toupin R.A., *The classical field theories*, Handbuch der Physik, **III/1**, Springer-Verlag, Berlin 1960.
7. Wesołowski Z., *Wprowadzenie do nieliniowej teorii sprężystości,* Wydawnictwo Uczelniane Politechniki Poznańskiej, Poznań 1972.
8. Wright T.W., *Nonlinear waves in rods*, Proc. of the IUTAM Symposium on Finite Elasticity, D.E. Carlson and R.T. Shields (eds.), (1981), 423-443, Martinus Nijhoff The Hague.
9. Zahorski S., *Doświadczalne badania niektórych własności mechanicznych gumy*, Rozprawy inżynierskie, tom **10**, 1, (1962), 193-207.

FREE VIBRATION ANALYSIS OF THIN-WALLED FRAMES WITH USE OF NODE SUPERELEMENTS

Tomasz MIKULSKI

Gdansk University of Technology

80-952 Gdańsk ul. Narutowicza 11/12, tel. 48 58 3472051, e-mail : tomi@pg.gda.pl

Czesław SZYMCZAK

Gdansk University of Technology

80-952 Gdańsk ul. Narutowicza 11/12, tel. 48 58 3472538, e-mail : szymcze@pg.gda.pl

Summary

The paper deals with free vibration analysis of frames made of thin-walled members. The investigations are based upon assumptions of classical theory of thin-walled beams of non-deformable cross-section. The warping effects are included into the consideration. It should be observed that in the vicinity of the nodes the stresses and deformations are in inconsistency with these assumptions. To take into account these inconsistencies the stiffness and mass matrices of nodes necessary in the finite element method applied are determined with aid of the superelement concept. Some numerical examples related to the frame made of I-beams are presented. The frequencies and modes of free vibration determined by the method proposed are show and compared with results of the analysis carried out by the system NASTRAN and with aid of the classical frame model without the warping effect.

Key words : free vibrations, thin-walled frames, finite element analysis

Introduction

Thin-walled frames are widely used in various civil engineering constructions, like industrial or shopping halls, island station (umbrella) roofs or high buildings. Such constructions consist of many beams, columns, lateral or wind bracings connected in nodes. The classical thin-walled beam theory [1] is adopted to carry out the static, dynamic and stability finite element analysis of these structures. The stiffness, geometric and mass matrices of the beam element are available in many papers (see for example [2], [3] and [4]). It should be observed that in vicinity of the nodes or stiffeners the stresses and deformations are not in accord with the classical beam theory. To take into account theses inconsistency the superelement concept is adopted and necessary stiffness and mass matrices of the node are derived using the unit displacement method. It is worthy of noticing that these matrices and in results the warping distribution in the node depends on the frame node construction. The free vibration analysis of the frames made of thin-walled members of bisymmetric cross-section is presented in the paper.

1. Node stiffness and mass matrix

Nodes of thin-walled frames are the most significant elements, where the thin-walled beams are connected at different angles. In this case, within one dimensional classic beam theory, it is impossible to determine the warping distribution and bimoments as internal forces. Since the bimoment is a self-equilibrium internal force there are no equilibrium conditions of bimoments in nodes. Moreover, occurrence of significant

deformations of cross section is noted, which is in inconsistency with the assumptions of the thin walled beam theory – non-deformable cross section. The node superelement is thus a suitable model to take all the effects mentioned into account. Figure 1 illustrate typical thin-walled node connecting two I-beam beams. Also the node stiffeners plays an important role in the warping distribution phenomena.
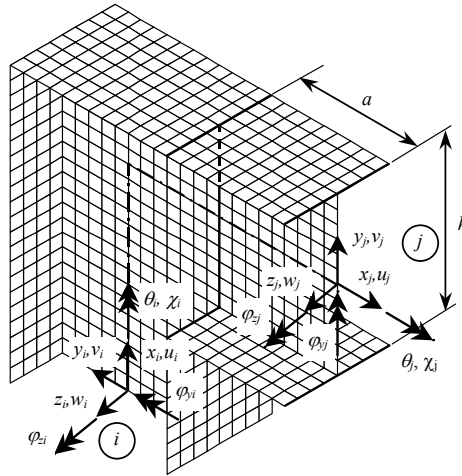
Fig. 1. Node superelement, 14 degrees of freedom

The stiffness matrix of the thin-walled node superelement has been calculated according to the common procedure of the unit-enforced displacements where the resultant 14 reaction forces (example shown in Fig. 2.) for each enforced unit displacement form the corresponding column of the stiffness matrix. Herein the axial stretching, bending and shearing behaviour of the thin-walled superelement node is coupled with torsional performance.
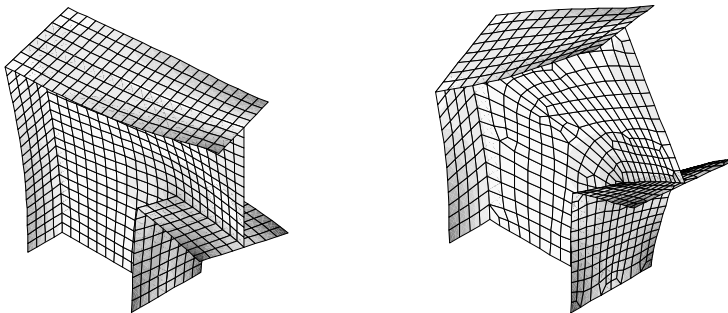
Fig. 2 Example of unit unforced state of two different node type - warping $\chi_j = 1$

Discrete displacement field inside the superelement (shell model) can be written as

$$\mathbf{q} = \mathbf{P} \cdot \mathbf{D} \tag{1}$$

where columns of the **P** matrix are global displacements vector (shell model) for fourteen unit unforcement state and can be treated as shape functions, **D** is the superelement node displacement vector. The kinetic energy of the node can be written also in discrete form using displacement vector inside the superelement for each unit unforcement displacement state

$$T = 0.5 \cdot \dot{\mathbf{D}}^T \left[\mathbf{P}^T \cdot \bar{\mathbf{M}} \cdot \mathbf{P} \right] \cdot \dot{\mathbf{D}} = 0.5 \cdot \dot{\mathbf{D}}^T \cdot \mathbf{M} \cdot \dot{\mathbf{D}} \qquad (2)$$

where **M** is the consistent mass matrix of the node superelement. It should be note that only the masses related to translation displacements are included to the diagonal mass matrix $\bar{\mathbf{M}}$.

The collaboration length parameter a has been defined to describe the dimension of the node superelement (Fig. 1). An appropriate assumption of parameter a is of great significance in the node superelement stiffness and mass matrices generating process. A small value of parameter a gives over-stiffened matrix coefficients, whereas a bigger value of a parameter provides better results. The numerical analysis experience allows to recommend the collaboration length as $0.5h < a < h$, where h stands for the beam height.

2. Free vibration analysis - examples

The free vibration numerical analysis of the frame made of thin-walled I-members shown in Fig. 5 is carried out for three different models:
  A) classic beam theory model, the frame is modelled by FEM elements of 12 degrees of freedom (6 on each node), with warping effect without node superelement (MSC/NASTRAN [5]),
  B) thin-walled elements with node superelement, both the beam and the node elements have 14 degrees of freedom with warping effects (Fig. 3.),
  C) shell model, the frame is modelled using the FEM computer system MSC/NASTRAN [5]. The QUAD4 four-node shell elements with 24 degrees of freedom are implemented (Fig. 4.).
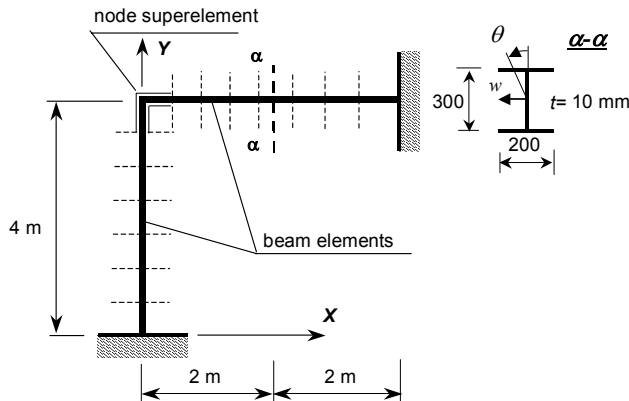
Fig. 3. Frame modelled by thin-walled elements and node superelement
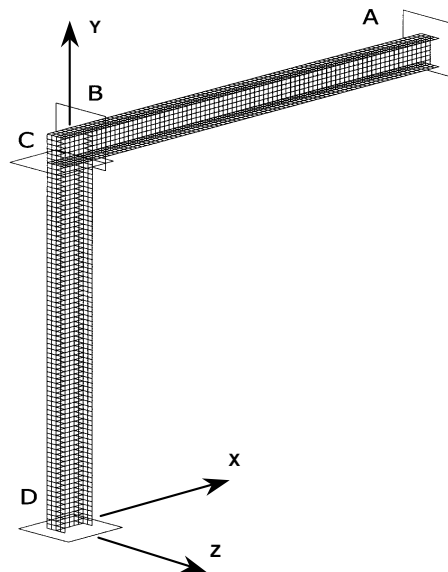
Fig. 4. Shell model of the frame, MSC/NASTRAN, QUAD4 elements

Fig. 5. Second eigenmode of the frame n_2=32.88 Hz

Figures 5 shows the second eigenmode of the frame obtained for the model C. Comparison of the free vibration frequencies and third eigenmode for three different numerical models under consideration is shown in Table 1 and on Fig. 6, 7 and 8.

Table 1. First three free vibrations frequencies – comparison of model A and model C

Model A	Model C
n_{1A} =7.77 Hz	n_{1C} =7.68 Hz
n_{2A} =17.13 Hz	n_{2C} =32.88
n_{3A}=17.14 Hz	n_{3C} =35.79
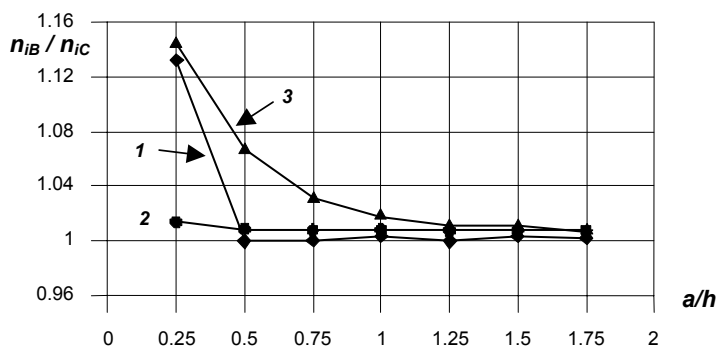
Fig. 6. First three free vibration relative frequency values vs. relative collaboration length parameter *a/h* (Fig.1.) – comparison of model B and model C
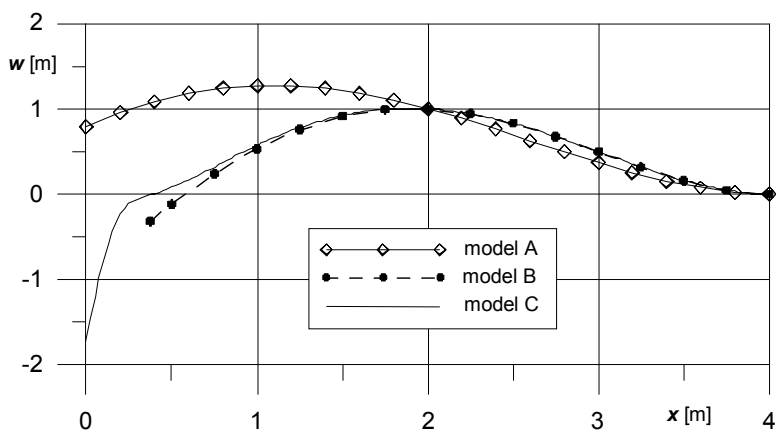
Fig. 7. Third eigenmode - distribution of displacement *w* along the horizontal beam – comparison of three different models
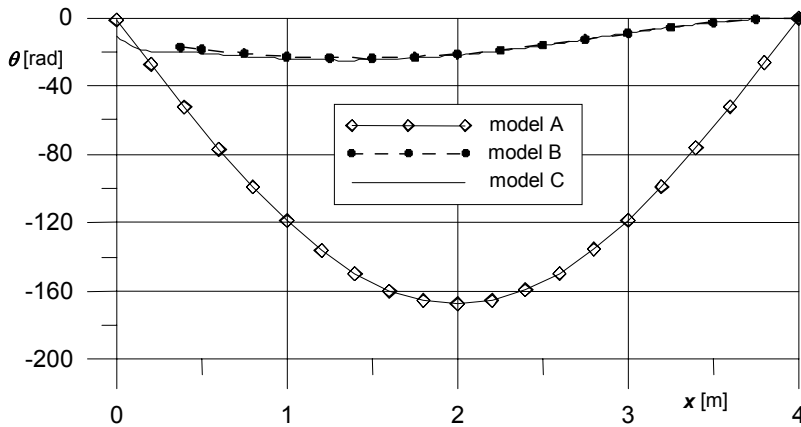
Fig. 8. Third eigenmode - distribution of torsion angle θ along the horizontal beam - comparison of three different models

3. Final conclusions

The numerical free vibration analysis of the simple frame made of thin-walled I-members carried out allows to draw conclusions that the FEM model of the frame consisting of the thin-walled members with the node superelements offers the accuracy comparable with the most exact detailed FEM model. It should be emphasised that the model size of the former is hardly a fraction of the size of the latter. It is worthy noticing considerable effect of the warping on the frequencies and eigenmodes of the frame (see Table 1 and Figs. 7, 8). Additional numerical analysis, not presented here with respect to limited scope of the paper, points out that the bimoment distribution in the node and in result the frame behaviour is very sensitive to the node construction.

References

1. V. Z. Vlasov, *Thin-walled elastic beams*, Fizmatgiz, Moscow 1959, (in Russian).
2. R. Borsoum, R. H. Gallagher, *Finite element analysis of torsional and torsional-flexural stability problems,* Int. J. Numer. Methods Engng., **2** (1970) 335-352.
3. C. Szymczak, *Torsional vibration of thin-walled bars with bisymmetric cross-section*, Engng. Transactions, **26**, (1978) 267-274 (in Polish).
4. C. Szymczak, *Torsional buckling of thin-walled beams of bisymmetric open cross-section*, Engng. Transactions, **26**, (1978) 323-330 (in Polish).
5. MSC Nastran for Windows, Version 2001, MSC Software Corporation, Los Angeles US.

DYNAMIC STABILITY OF SANDWICH BAR COMPRESSED BY PERIODICALLY VARIABLE FORCE

Waldemar MORZUCH

Wrocław University of Science

Wybrzeże Wyspiańskiego 27

tel. 3203393, e-mail: w.morzuch@onet.eu

Abstract

The work presents an analysis of dynamic buckling of a sandwich bar compressed by a periodically variable force. In order to determine the stability of the bar transverse motion, equations of its transverse vibration were formulated. From the equations of motion, differential equations interrelating of the bar dynamic deflection with space and time were derived. The partial differential equations were solved using the method of separation of variables (Fourier's method). Then an ordinary differential equation (Hill's equation) describing the bar vibration was solved. An analysis of the solution became the basis for determining the regions of sandwich bar motion instability. Finally, the critical damping coefficient values at which parametric resonance occurs have been calculated.

Key words: sandwich bar, stability

Introduction

Sandwich constructions are characterized by light weight and high strength. Such features are highly valuable in aviation, building engineering and automotive applications. The primary aim of using sandwich constructions is to obtain properly strong and rigid structures with vibration damping capacity and good insulating properties. Figure 1 shows a scheme of a sandwich construction which is composed of two thin facing plates and a relatively thick core [4,5]. The core, made of plastic and metal sheet or foil, transfers transverse forces and maintains a constant distance between the plates. Sandwich constructions are classified into bars, plates and beams. A major problem in the design of sandwich constructions is the assessment of their stability under axial loads causing their buckling or folding. The existing methods of calculating such structures are limited to the assessment of their stability under loads constant in time [3,5].

There are no studies dealing with the analysis of parametric vibration and dynamic stability (dynamic buckling). This paper presents a dynamic analysis of a sandwich bar compressed by a periodically variable force, assuming that the core is linearly viscoelastic. Differential equations describing the dynamic flexural buckling of bars are derived and regions of instability are identified. The dynamic analysis of sandwich constructions is of great importance for automotive vehicles and aeroplanes, since most of the loads which occur in them have the form of time-dependent forces.
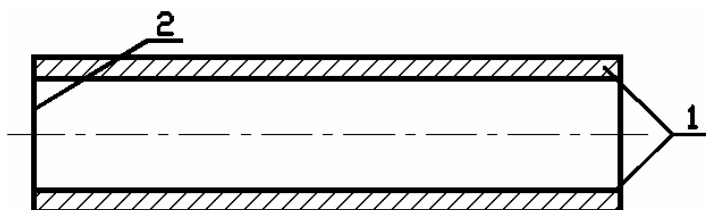
Fig. 1. Scheme of sandwich construction 1 – plates, 2 – core.

Dynamic buckling of a sandwich bar

A simply-supported sandwich bar compressed by time-dependent force F is shown in Fig. 2. Force F can be expressed as follows

$$F = F_1 + F_2 \cos pt \tag{1}$$

where F_1 – constant component of the compressive force, F_2 – amplitude of the variable component of the compressive force, p – frequency of variable component F_2, t – time.
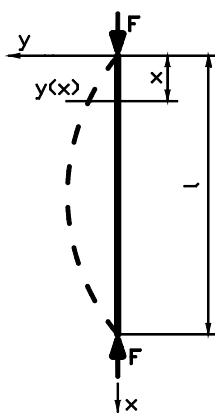
Fig. 2. sandwich bar compressed by force F.

The cross section of the sandwich bar is shown in Fig. 3. The basis for describing the dynamic buckling of the sandwich bar is the differential equation of the sandwich beam centre line. The equation can be written as

$$B \frac{\partial^4 y}{\partial x^4} = q - k \frac{B}{S} \frac{\partial^2 q}{\partial x^2} \tag{2}$$

where B – flexural rigidity of the bar, q – load intensity, k – a coefficient representing the influence of the transverse force on the deflection of the bar, S – transverse rigidity of the bar.
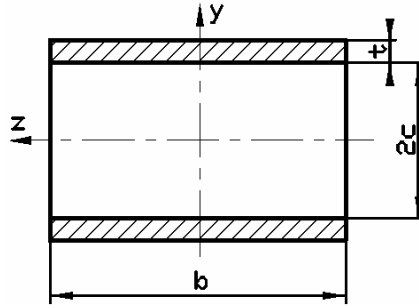
Fig. 3. Cross section of sandwich bar.

In sandwich constructions the core is merely sheared and does not transfer normal stresses whereby coefficient k is equal to one (k = 1).

$$S = 2bcG_c \tag{3}$$

where b, c – dimensions of the core (Fig. 3), G_c – modulus of rigidity of the core material.

Load intensity q can be written in the form:

$$q = q_1 + q_2 + q_3 \tag{4}$$

$$q_1 = -F \frac{\partial^2 y}{\partial x^2}, \quad q_2 = -\mu \frac{\partial^2 y}{\partial t^2}, \quad q_3 = -\eta_r \frac{\partial y}{\partial t} \tag{5}$$

where μ – unit mass of the sandwich bar, η_r – damping coefficient of the core material.

After substituting equations (5) into differential equation (2) the following differential equation is obtained:

$$B\left(1 - \frac{F}{S}\right)\frac{\partial^4 y}{\partial x^4} + F\frac{\partial^2 y}{\partial x^2} - \frac{B}{S}\mu\frac{\partial^4 y}{\partial x^2 \partial t^2} + \mu\frac{\partial^2 y}{\partial t^2} + \eta_r\frac{\partial y}{\partial t} - \frac{B}{S}\eta_r\frac{\partial^3 y}{\partial x^2 \partial t} = 0 \tag{6}$$

The above equation is a fourth-order homogeneous equation with time-dependent coefficients. It was solved by the method of separation of variables (Fourier`s method). The solution can be presented in the form of an infinite series:

$$y = \sum_{n=1}^{\infty} X_n(x) T_n(t) \qquad (7)$$

Eigenfunctions $X_n(x)$, satisfying the boundary conditions at the supports of the bar at its ends, have the following form:

$$X_n(x) = A_n \sin\left(\frac{\pi n x}{l}\right) \qquad (8)$$

Having substituted equations (7) and (8) into the differential equation (6), one gets the following ordinary differential equation describing functions $T_n(t)$:

$$\ddot{T}_n + 2h\,\dot{T}_n + \omega_{on}^2 \left(1 - 2\psi_n \cos pt\right) T_n = 0 \qquad (9)$$

where

$$2h = \frac{\eta_r}{\mu}, \quad 2\psi_n = \frac{F_2\left(\dfrac{\pi n}{l}\right)^2}{\mu \omega_{on}^2} \qquad (10)$$

The square of frequency ω_{on} can be expressed as follows:

$$\omega_{on}^2 = \omega_o^2 - \frac{F_1\left(\dfrac{\pi n}{l}\right)^2}{\mu} \qquad (11)$$

where
$\quad \omega_o$ – the natural frequency of vibration of the bar when $F_1=0$, $F_2=0$, $\eta_r=0$.

The square of frequency ω_o can be expressed as follows:

$$\omega_o^2 = \frac{B\left(\dfrac{\pi n}{l}\right)^2}{\mu\left[1 + \dfrac{B}{S}\left(\dfrac{\pi n}{l}\right)^2\right]} \qquad (12)$$

Differential equation (9) is Hill's equation in the form [1,2]:

$$\ddot{T}_n + 2h\,\dot{T}_n + \Omega_n^2\left[1 - f(t)\right]T_n = 0. \tag{13}$$

If there is no damping in the core (h=0) and assuming f(t)= 2ψcospt, one gets the following classical Mathieu equation:

$$\ddot{T}_n + \omega_{on}^2\left(1 - 2\psi_n \cos pt\right)T_n = 0 \tag{14}$$

In order to solve equation (13), a change of variable was made and the solution was expressed in the form:

$$T_n(t) = e^{-ht}\varphi_n(t) \tag{15}$$

In this way a new differential equation for function $\varphi_n(t)$ was obtained:

$$\ddot{\varphi}_n + \omega_n^2\left[1 - f_1(t)\right]\varphi_n = 0 \tag{16}$$

where

$$\omega_n^2 = \Omega_n^2 - h^2 \tag{17}$$

$$f_1(t) = \frac{\Omega_n^2}{\omega_n^2} f(t) \tag{18}$$

Equation (16) is the Mathieu equation without damping. Therefore for the analysis of this equation one can use the solution of equation (14), substituting $f_1(t)$ for f(t) and $\Omega_n^2 - h^2$ for ω_n^2.

Let us now analyze the stability of the solutions of the differential equation (16), limiting the analysis to the first (most important) region of instability.
By solving of equation (9) the boundary lines of the first region of instability has been obtained (Fig. 4.).

In a similar way as in the case without damping the following relations for the boundary lines of the first region of instability are obtained:

$$\frac{p}{\Omega_n} < 2\sqrt{\frac{\left(1 - \xi_n\right)^2 - \psi_n^2}{1 - 3\xi_n - \sqrt{\psi_n^2 - 4\xi_n + 8\xi_n^2}}} \tag{19}$$

$$\frac{p}{\Omega_n} > 2\sqrt{\frac{\left(1 - \xi_n\right)^2 - \psi_n^2}{1 - 3\xi_n + \sqrt{\psi_n^2 - 4\xi_n + 8\xi_n^2}}} \tag{20}$$

where

$$\xi_n = \left(\frac{h}{\Omega_n}\right)^2 \tag{21}$$

Hence the 'wedge' of the first region of instability has the coordinates:

$$\psi_{wn} = 2\sqrt{\xi_n - 2\xi_n^2} \; , \; \gamma_{wn} = 2\sqrt{1 - 3\xi_n} \tag{22}$$

Relations (19) and (20) describe the upper and lower boundary line, respectively.
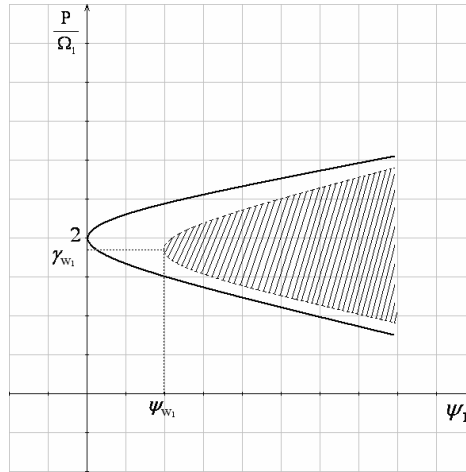
Fig. 4. First region of instability ($\xi_n = 0$, without damping, $\xi_n \neq 0$, with damping).

From formula (22) the boundary value of coefficient ψ_{wn} at which parametric resonance occurs has been obtained.

If $\psi_n < \psi_{wn}$, no parametric resonance arises. It follows from the above that there exist compressive force components F_1 and F_2 at which the bar does not lose stability.

References

1. Dżygadło Z., Kaliski S., Solarz L., Włodarczyk E., *Vibrations and waves*, WAT, Warsaw 1965.
2. McLachlan N. W., *Theory and application of Mathieu Functions*, Oxford 1947.
3. Morzuch W., *Dynamic stability of a sandwich bar compressed by a time-dependent force* [in Polish], Rozprawy Inżynierskie, **37**, 2, 1989.
4. Plantema J.F*., Sandwich construction*, Stanford University, London 1966.
5. Romanów F., Stricker L., Teisseyre J.: *Stability of sandwich structures* [in Polish], Skrypt Politechniki Wrocławskiej, Wrocław 1972.

DYNAMIC STABILITY OF SHAFT LOADED WITH AXIAL COMPRESSION AND MAGNETIC TENSION

Waldemar MORZUCH

Wrocław University of Science

Wybrzeże Wyspiańskiego 27

tel. 3203393, e-mail w.morzuch@onet.eu

Abstract

The analysis of dynamic stability of shaft loaded with magnetic tension and axial compression has been presented. In order to estimate the stability of radial motion of the shaft, the equations of its transverse vibration have been formulated. On the basis of equations of motion the differential equations, connecting the dynamic deflection of shaft with space and time, have been obtained. Partial differential equations were solved by using the method of separation of variables (Fourier's method). Then the ordinary differential equation, describing the vibration of shaft in time, has been solved and the characteristic equation has been drawn. The analysis of solution of this equation becames the basis for estimating the free vibrations frequency of the shaft. Subsequently the critical values of magnetic tension and of axial load have been determined.

Key words: shaft, stability

Introduction

The problem of estimating the stability of shafts loaded with magnetic tension and axial compression is important for example in electrical machines. These machines have small values of the air gaps. For that reason, the basis problem occurring in phase of construction of such machines is to estimate the stability of rotors. The problem of stability of shafts bears a relation to their vibrations. It is especially important in case of long shafts loaded with axial compression, for example for rotors of motors of deep-well pumps. Such pumps operate in deep waters. The rotors of such motors are loaded with large forces.

Problems of estimation of stability of transverse motion of rotors are presented in the papers [3-6] but the influence of axial compression is not considered there. The theories presented in the papers [1] and [2] are based on too much simplified models of rotors without taking into consideration a continuous load distribution on the surface of shaft.

Influence of axial compression and magnetic tension on the free vibration frequency has been determined in the paper. Solution of this problem allows us to determine the critical parameters of magnetic tension or compressive force for which the loss of stability of transverse motion of shaft occurs.

1. Dynamic stability of shaft

In order to estimate the dynamic stability of the shaft, it is necessary to arrange the differential equations connecting the dynamic deflections of the shaft with space and time.

These equations have been derived as in [3]. The force of magnetic tension is continuous load on the surface of shaft and is acting in direction of a shaft's centre deflection. A load intensity of the magnetic tension (Fig. 1.) can be described by following formula [2]:

$$q(x) = Cy(x) \qquad (1.1)$$

where: C – coefficient of the magnetic tension, y(x) – deflection of the shaft

The shaft shown in Fig. 1 is loaded with magnetic tension and axial compression. In order to simplify the considerations a vertical position of the shaft has been assumed (elimination of a dead weight). It agrees with a reality (position of shafts in deep-well pumps).
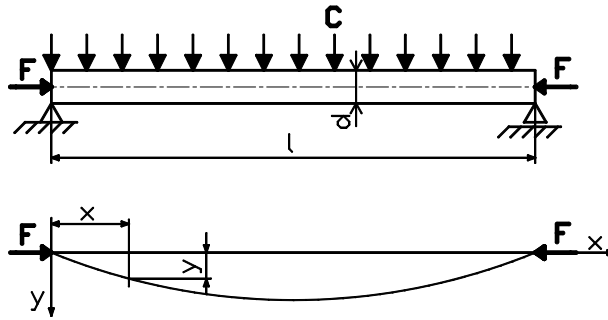
Fig. 1. The shaft loaded by magnetic tension and axial compression.

The differential equations of dynamic deflections of the shaft can be obtained on the basis of the differential equation of a centre line of a beam. This equation can be introduced in the form:

$$S \frac{\partial^4 y}{\partial x^4} = -q_x \qquad (1.2)$$

where: S – flexural rigidity of the shaft, q_x – load intensity

The load intensity q_x can be introduced in the form:

$$q_x = q_{1x} + q_{2x} + q_{3x} \qquad (1.3)$$

where: q_{1x} – load intensity taking into account influence of a compressive force F, q_{2x} – load intensity taking into account influence of forces of inertia, q_{3x} – load intensity taking into account influence of the magnetic tension.

The equation (1.2) can be then introduced in the form:

$$\beta^2 \frac{\partial^4 y}{\partial x^4} + \alpha \frac{\partial^2 y}{\partial x^2} - \gamma y + \frac{\partial^2 y}{\partial t^2} = 0 \tag{1.4}$$

where:

$$\beta^2 = \frac{S}{\mu}, \qquad \alpha = \frac{F}{\mu}, \qquad \gamma = \frac{C}{\mu}, \tag{1.5}$$

μ – unit mass (per unit length) of the shaft section, t – time

Equation (1.4) is a partial differential equation with constant coefficients. It can be solved by means of separation of variables method and presented in form of infinite series:

$$y = \sum_{n=1}^{\infty} X_n(x) T_n(t) \tag{1.6}$$

After a separation of variables and definition of parameter k_n the following equations have been obtained:

$$\beta^2 \overset{IV}{X}_n + \alpha \overset{II}{X}_n - k_n^4 X_n = 0 \tag{1.7}$$

$$\ddot{T}_n + \omega_n^2 T_n = 0 \tag{1.8}$$

where: ω_n denotes the n-order frequency of free vibrations of shaft.
On the basis of above equations the following formula has been obtained:

$$\omega_n^2 = k_n^4 - \gamma \tag{1.9}$$

The equation (1.4) can be introduced in the form:

$$\overset{IV}{X}_n + a\,\overset{II}{X}_n - bX_n = 0 \tag{1.10}$$

The solution of last equation can be introduced in the form:

$$X_n = C_{1n}shmx + C_{2n}chmx + C_{3n}\sin nx + C_{4n}\cos nx \tag{1.11}$$

where:

$$m = \sqrt{\frac{-a + \sqrt{a^2 + 4b}}{2}} \tag{1.12}$$

$$n = \sqrt{\frac{a + \sqrt{a^2 + 4b}}{2}} \tag{1.13}$$

The constants C_{1n}, C_{2n}, C_{3n}, C_{4n} can be determined on the basis of the boundary conditions. On the basis of above conditions the following characteristic equation has been obtained:

$$(m^2 + n^2)shml\,\sin nl = 0 \tag{1.14}$$

A solution of above equation can be introduced in the following form:

$$nl = s\pi \tag{1.15}$$

where: s is an integer number

On the basis of above equations the frequency ω_n has been expressed:

$$\omega_n = \sqrt{\beta^2 \frac{s^2\pi^2}{l^2}\left(\frac{s^2\pi^2}{l^2} - \frac{F}{EJ}\right) - \gamma} \tag{1.16}$$

The critical value of the force F can be found as a solution of the following equation

$$\omega_n = 0 \tag{1.17}$$

in the form

$$F_{cr} = \frac{EIs^2\pi^2}{l^2} - \frac{Cl^2}{s^2\pi^2}$$ (1.18)

2. Example of calculations

Calculations of the shaft loaded with a magnetic tension and axial force (Fig. 1) has been performed for the following data assumed:

$$E = 2.0601 \times 10^5 \; MPa \qquad d = 5 \times 10^{-2} \; m \qquad l = 70 \times 10^{-2} \; m$$

Frequency ω_n has been determined according to formula (16). Figure 2 shows the diagram of frequency ω_n against the axial force F, for different values of magnetic tension coefficients C. The conclusion which can be drawn from these curves is that the axial force has a considerable influence on free vibrations. The increase of this force causes a decrease of free vibrations frequency. The influence of the force is stronger for greater values of the magnetic tension coefficient C. The point of intersection of the curve with the axis of abscissae determines the value of so-called critical force. In the presence of this force instability of the shaft occurs.
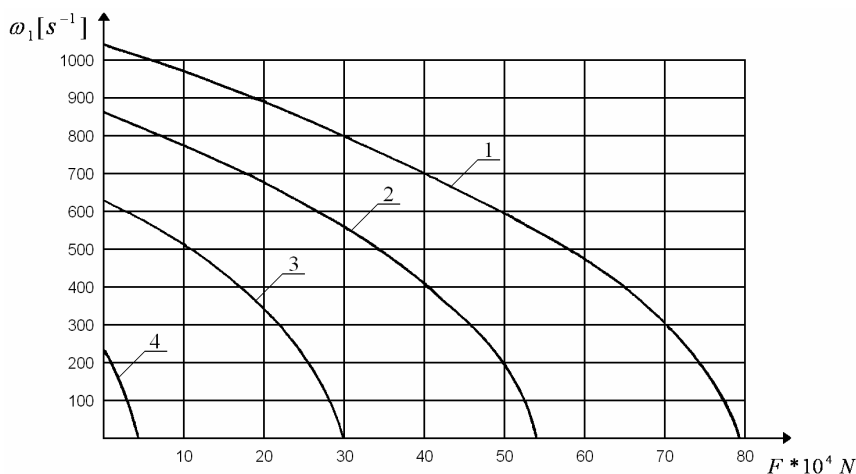
Fig. 2. The diagram of natural frequency ω_1 versus axial force F: 1 – C=9,81 MPa, 2 – C=14,715 MPa, 3 – C=19,62 MPa, 4 – C=24,525 MPa

All the curves shown in Fig. 2 prove that the greatest decrease of the free vibrations frequency takes places in the region where the compression forces occur and approach the critical value. The diagrams shown in Fig. 2 demonstrate that there exist such a mag-

netic tension called the critical one, at which the frequency of free vibrations of the shaft is equal to zero. According to the data from the above example, the critical magnetic tension has a value of $C_{cr} = 25,57\,MPa$.

Summarising the considerations, it is necessary to state that the shaft can lose the stability of transverse motion when magnetic tension and the compression force take certain values. These values are called the critical ones.

It has to be mentioned that the presented analysis is valid for the case of the shaft with undeformable stator. The deformability of the stator will certainly have an influence on the decrease of the value of the critical force, due to increase of the load introduced by the magnetic forces.

3. Conclusions

The magnetic field (described by the coefficient of magnetic tension C) and the axial compression have a great influence on the free vibrations frequency of the shaft. The increase of magnetic tension as well as the increase of the axial compression causes the decrease of the frequency of free vibrations of the shaft.

The formula defining the dependence of free vibrations frequency of the shaft on the axial compression is a decreasing function. The diagram of this function is a parabola, whose axis of symmetry is horizontal.

There exist a critical magnetic tension and a critical force of compression at which the shaft loses stability of the transverse motion. This critical force is relative to the coefficient tension C. The increase of the coefficient of magnetic tension causes the decrease of the critical force. The relation between the critical force and the magnetic tension is non-linear. The non-linearity is very significant when the magnetic tension approaches its critical value.

References

1. Aleksiejev A.E.: *Konstrukcja maszyn elektrycznych (Design of electrical machines* – in Polish). Warszawa, PTW, 1953.
2. Dąbrowski M.: *Konstrukcja maszyn elektrycznych (Design of electrical machines* – in Polish). Warszawa, WNT, 1977.
3. Gabryszewski Z., Morzuch W.: *Analiza dynamiczna wirników silników asynchronicznych klatkowych (Dynamic analysis of squirrel-cage asynchronous motors* – In Polish). Archiwum Elektrotechniki, Vol. XXX, No. 1, 1981.
4. Morzuch W.: *Stateczność dynamiczna wirników dwubiegunowych silników asynchronicznych (Dynamic stability of rotors of two-pole asynchronous motors* – In Polish). Archiwum Elektrotechniki, Vol. XXXII, No. 3-4, 1983.
5. Morzuch W.: *Obszary niestateczności wirników klatkowych dwubiegunowych silników asynchronicznych (Instability areas of squirrel-cage rotors of two-pole asynchronous motor* – In Polish). Archiwum Budowy Maszyn, Vol. XXXIII, No. 2, 1986.
6. Morzuch W.: *Stateczność dynamiczna wirników klatkowych silników asynchronicznych z odkształcalnym stojanem (Dynamic stability of squirrel-cage rotors of asynchronous motors with deformable stators* – In Polish). Archiwum Budowy Maszyn, Vol. XXXV, No. 1-2, 1988.

FREE TRANSVERSE VIBRATION ANALYSIS OF AN ANNULAR MEMBRANE

Stanisław NOGA

Faculty of Mechanical Engineering and Aeronautics,
Rzeszów University of Technology, ul. W. Pola 2, 35-959 Rzeszów, Poland
(17) 8651348, noga@prz.edu.pl

Abstract

In the paper, transversal vibration of an annular membrane is studied using analytical methods and numerical simulation. The two mathematical models are analysed. The first model is treated as a continuous system. The general solution of the free vibrations are derived by the Bernoulli-Fourier method and the boundary problem is solved. The second model is formulated by using finite element representations. The natural frequencies and natural mode shapes of vibration of membrane are determined. The FE model is manually tuned to reduce the difference between the natural frequencies of the tuned and continuous models, respectively. It is important to note that the data presented in the paper is brought the practical advice to design engineers.

Keywords: annular membrane, transverse vibration, natural frequencies, mode shapes

Introduction

The problem of free transverse vibration of isotropic membrane systems is a well – known problem in structural dynamics. The majority of previous works in the field presents solutions for the vibration frequencies of the circular, annular and rectangular membrane systems. Fundamental theory of single membrane system is developed in [4]. Free transverse vibrations of double – membrane compound system are studied analytically in the work [7]. In the paper [5] exact solution for free vibrations of circular and annular composite membranes is given by using theory of membrane. The transverse vibrations of the non – homogeneous circular and annular membranes have been investigated in work [3]. In this paper the free transverse vibrations of an annular isotropic membrane system are analyzed using membrane theory and finite element technique. The analytical solution is utilized to manual tuning the finite element model of the system. This work continues the recent author's investigations concerning transverse vibrations of structures [6].

1. Formulation of the problem

The objective of this work is formulation of a dynamic model of an annular membrane. It is assumed that the membrane is thin, homogeneous and perfectly elastic and it has constant thickness. The membrane is uniformly tense by adequate constant tensions applied at the edges (see Fig. 1). The small vibrations with no damping are considered. The partial differential equation of motion for the free transversal vibrations may be written in the form [4]

$$\frac{1}{r}\frac{\partial}{\partial r}\left(r\frac{\partial w}{\partial r}\right)+\frac{1}{r^2}\frac{\partial^2 w}{\partial \varphi^2}-\frac{1}{a^2}\frac{\partial^2 w}{\partial t^2}=0 \tag{1}$$
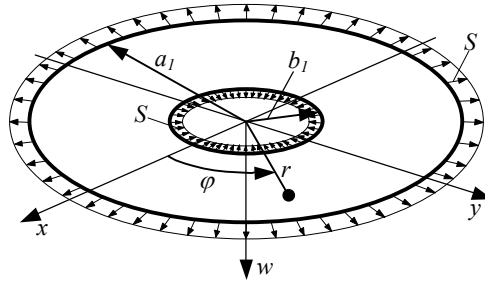
Fig. 1. The physical model of an annular membrane

where $w = w(r,\varphi,t)$ is the transverse membrane displacement, r,φ,t are the polar coordinates and the time, a_1, b_1, h are the membrane dimensions, ρ is the mass density, S is the uniform constant tension per unit length and $a^2 = S/\rho h$. The boundary conditions are

$$w(a_1,\varphi,t) = 0, \quad w(b_1,\varphi,t) = 0, \quad w(r,\varphi,t) = w(r,\varphi + 2\pi, t) \qquad (2a, b, c)$$

The two mathematical models of a membrane have been analysed.

2. Free vibration analysis

2.1. The continuous model

The first model of the membrane is treated as a continuous system. The Bernoulli – Fourier method (separation of variables) is employed to solve the free vibration problem. The general solution of equation (1) takes the form [4]

$$w(r,\varphi,t) = W(r,\varphi)T(t), \quad T(t) = L\cos\omega t + M\sin\omega t \qquad (3a, b)$$

where ω is the natural frequency of the system. Introducing solutions (3) into (1) yields

$$\frac{1}{r}\frac{\partial}{\partial r}\left(r\frac{\partial W(r,\varphi)}{\partial r}\right) + \frac{1}{r^2}\frac{\partial^2 W(r,\varphi)}{\partial \varphi^2} + \left(\frac{\omega}{a}\right)^2 W(r,\varphi) = 0 \qquad (4)$$

Assuming the solution of equation (4) in the form [4]

$$W(r,\varphi) = R(r)U(\varphi) \qquad (5)$$

and introducing it into (4) yields

$$r^2\frac{d^2 R(r)}{dr^2} + r\frac{dR(r)}{dr} - \left(n^2 - \left(\frac{\omega r}{a}\right)^2\right)R(r) = 0, \quad \frac{d^2 U(\varphi)}{d\varphi^2} + n^2 U(\varphi) = 0, \ n = 0,1,2,... \quad (6a, b)$$

The boundary conditions (2) take the form

$$R(a_1) = 0, \quad R(b_1) = 0, \quad U(\varphi) = U(\varphi + 2\pi) \qquad (7a, b, c)$$

The general solutions of equations (6) may be written as

$$R_n(r) = A_n J_n(r\,\omega/a) + B_n Y_n(r\,\omega/a), \ U_n(\varphi) = C_n \sin(n\varphi) + D_n \cos(n\varphi) \qquad (8a, b)$$

where J_n and Y_n are the Bessel functions of the first and second kinds, respectively. The constants A_n, B_n are determined from the boundary conditions. Substituting (8a) into the boundary conditions (7) gives

$$A_n J_n(\omega a_1/a) + B_n Y_n(\omega a_1/a) = 0, \quad A_n J_n(\omega b_1/a) + B_n Y_n(\omega b_1/a) = 0 \qquad (9a, b)$$

For non – trivial solutions of equations (9), the cardinal determinant ot the system coefficient matrix must vanish. This gives the following frequency equation

$$J_n(\omega a_1/a) Y_n(\omega b_1/a) - J_n(\omega b_1/a) Y_n(\omega a_1/a) = 0 \qquad (10)$$

where the roots of equation (10) $\omega = \omega_{mn}$ ($m = 1,2,3,...$) are the free frequencies of the membrane. The general solution of the free vibrations of an annular membrane may be written in the following form

$$w(r,\varphi,t) = \sum_{n=0}^{\infty} \sum_{m=1}^{\infty} R_{mn}(r) U_n(\varphi) T_{mn}(t) = \sum_{n=0}^{\infty} \sum_{m=1}^{\infty} T_{mn}(t) B_{mn}\left(C_n W_{mn}^{(1)}(r,\varphi) + D_n W_{mn}^{(2)}(r,\varphi)\right) =$$

$$= \sum_{n=0}^{\infty} \sum_{m=1}^{\infty} B_{mn}\left(L_{mn} \cos \omega_{mn} t + M_{mn} \sin \omega_{mn} t\right) U_n(\varphi)\left(e_{mn} J_n(r\,\omega_{mn}/a) + Y_n(r\,\omega_{mn}/a)\right) \qquad (11)$$

where

$$W_{mn}^{(1)} = \left(e_{mn} J_n(r\,\omega_{mn}/a) + Y_n(r\,\omega_{mn}/a)\right) \sin(n\varphi)$$

$$W_{mn}^{(2)} = \left(e_{mn} J_n(r\,\omega_{mn}/a) + Y_n(r\,\omega_{mn}/a)\right) \cos(n\varphi) \qquad (12)$$

are a two linear – independent mode shapes, and

$$e_{mn} = - Y_n(\omega_{mn} a_1/a) / J_n(\omega_{mn} a_1/a) \qquad (13)$$

2.2. The finite element model

The second model is formulated by using the finite element representations. Introducing the finite element assumption, it leads to the equations of motion of the membrane that may be written in the following form [1]

$$\mathbf{M\ddot{u} + Ku = 0} \qquad (14)$$

where $\mathbf{M}$ and $\mathbf{K}$ are, the global mass and global stiffness matrices (made up by proper assembly of the element matrices); $\mathbf{\ddot{u}}$ and $\mathbf{u}$ are the nodal acceleration and nodal displacement vector, respectively. The global mass and stiffness matrices are assembled from the element matrices that are given by [1]

$$\mathbf{M}^{(e)} = \int_{V^{(e)}} \rho^{(e)} \mathbf{N}^T \mathbf{N} \, dV^{(e)}, \quad \mathbf{K}^{(e)} = \int_{V^{(e)}} \mathbf{B}^T \mathbf{E} \mathbf{B} \, dV^{(e)} \tag{15}$$

where $\rho^{(e)}$ is the mass density coefficient for an element e; $V^{(e)}$ is the volume of the element e; $\mathbf{N}$ is the matrix of the element shape functions; $\mathbf{B}$ and $\mathbf{E}$ are, the element shape function derivatives, and the elasticity matrices, respectively. The natural frequencies of the system may be obtained by solving the eigenvalue problem

$$\left(\mathbf{K} - \omega^2 \mathbf{M}\right)\overline{\mathbf{u}} = \mathbf{0} \tag{16}$$

where ω is the natural frequency and $\overline{\mathbf{u}}$ is the corresponding mode shape vector which can be obtained from equation (16). The number of eigenpairs ($\omega_i, \overline{\mathbf{u}}_i$) corresponds the number of degree of freedom of the system. The block Lanczos method is employed to solve the eigenvalue problem (16) [1].

3. Numerical analysis

Numerical analysis results of the annular membrane free vibration are obtained using the models suggested earlier. For each approach, only the first ten natural frequencies and mode shapes are discussed and compared for these two models. The parameters characterizing the system used in calculations are shown in Table 1.

Table 1. Parameters characterizing the annular membrane

a_I [m]	b_I [m]	h [m]	ρ [kg/m^3]	E [Pa]	v	S [N/m]
0.5	0.1	0.001	$7.85 \cdot 10^3$	$2.05 \cdot 10^{11}$	0.29	1000

In the table, E and v are, the Young's modulus of elasticity and Poisson ratio, respectively. In this paper the continuous model is considered as exact, compared to the finite element model, which is treated as approximation of the precise model.

3.1. The continuous model

The natural frequencies are determined from numerical solution of the equation (10). The results of the calculation of the natural frequencies are shown in Table 2.

Table 2. Natural frequencies of the annular membrane system ω_{mn} [Hz]

		n						
		0	1	2	3	4	5	6
m	1	13.7092	15.2172	18.76	22.9736	27.2692	31.5139	35.6973
	2	27.9711	28.9403	31.6293				

3.2. The finite element model

Numerical solution results are presented using the finite element representation. Like mentioned earlier, the FE model is treated as approximation of the exact system. The quality of the approximation model depends on, the type and density of the mesh, and the manner of the apply a distributed tension force. In this work the impact of the apply the distributed force manner in the FE models on the quality of the accurate model

approximation is analysed. In order to make a comparison of the continuous system analysis results with the FE model solution, two finite element models are prepared and discussed.

(a) The first model

The model consists of the annular membrane divided into 9540 finite elements. The four node quadrilateral element (shell63) with six degree of freedom in each node, and with the element stiffness option *" Membrane only "* is used to solve the problem. The prepared model is shown in Fig. 2. The uniform constant tension per unit length is apply to the outer edge by using the FE code system standard procedure.
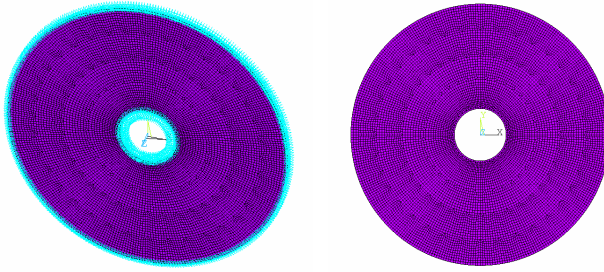
Fig. 2. Finite element model

Table 3. Natural frequencies of the system ω_{mn} [Hz]

		n						
		0	1	2	3	4	5	6
m	1	14.331	15.563	18.637	22.542	26.678	30.825	34.928
	2	29.138	29.882	32.006				

Table 4. Frequency error ε_{mn} [%]

		n						
		0	1	2	3	4	5	6
m	1	4.5356	2.2724	-0.6556	-1.8786	-2.1680	-2.1860	-2.155
	2	4.1718	3.2539	1.1909				

The frequency error is expressed as [2]

$$\varepsilon_{mn} = \left(\omega_{mn}^{f} - \omega_{mn}^{c}\right)/\omega_{mn}^{c} \cdot 100\% \qquad (17)$$

where ω_{mn}^{f} and ω_{mn}^{c} are the natural frequencies of the FE and exact models, respectively. The results of the calculation are presented in Tables 3 and 4. The biggest difference between the analytical results and FE solution can be visible for the frequencies ω_{10}, ω_{20}, and ω_{21}, respectively.

(b) The second model

This dynamic model of the annular membrane is the same as in section 3.2a but the constant tension applying is different. To each node lying on the outer edge is imposed a concentrated tension force S_i. The proper value of the force are selected experimentally to minimize the relation defined by the equation (16). The results of the calculation are shown in Tables 5 and 6, respectively. The results presented in Table 6 are achieved for $S_i = 9.6 \, [\mathrm{N}]$.

Table 5. Natural frequencies of the system ω_{mn} [Hz]

		n						
		0	1	2	3	4	5	6
m	1	14.26	15.486	18.545	22.43	26.546	30.672	34.755
	2	28.994	29.734	31.848				

Table 6. Frequency error ε_{mn} [%]

		n						
		0	1	2	3	4	5	6
m	1	4.0177	1.7664	-1.1406	-2.3661	-2.652	-2.6715	-2.6397
	2	3.6569	2.7425	0.6914				

The smaller difference between the models are observed for the frequencies ω_{10}, ω_{20} and ω_{21}. For the frequencies ω_{12}, ω_{13}, ω_{14}, ω_{15} and ω_{16}, respectively, the frequency error grew slight. The biggest frequency error is observed for the frequency ω_{10}.

4. Conclusions

This work deals with the transverse vibrations of an annular isotropic membrane. The free vibrations are determined by using the Bernoulli – Fourier and finite element methods. Due to space limitation the mode shapes are not presented. The analytical solution is utilized to manual tuning the FE model. Such approach permits to determine the proper value of the radial concentrated tension force imposed to a nodes lying on the outer edge instead of using the distributed constant tension force applied to the edge. To achieve the better fit between the tuned FE model and the continuous system, the further research concerning the type and density of the mesh are needed.

References

1. C. de Silva, *Vibration and shock handbook*, Taylor & Francis, Boca Raton, 2005.
2. M. Friswell, J. Mottershead, *Finite element model updating in structural dynamics*, Kluwer Academic Publishers, Dordrecht, 1995.
3. M. Jabareen, M, Eisenberger, *Free vibrations of non-homogeneous circular and annular membranes*, J. of Sound and Vibration, **240** (2001) 409–429.
4. S. Kaliski, *Vibrations and waves in solids*, IPPT PAN, Warsaw, 1966 (in Polish).
5. P. Laura, C. Rossit, S. Malfa, *Transverse vibrations of composite, circular annular membranes: exact solution*, J. of Sound and Vibration, **216** (1998) 190–193.
6. S. Noga, *Dynamical analysis of the low – power electrical engine rotor*, Proceedings of the 10th European Mechanics of Materials Conference ″ Multi–phases and multi–components materials under dynamic loading ″, Kazimierz, Poland, 2007, 457–465.
7. Z. Oniszczuk, *Vibration analysis of compound continuous systems with elastic constraints*, Publishing House of Rzeszów University of Technology, Rzeszów, 1997 (in Polish).

DYNAMICS OF IMPACTS WITH A TABLE MOVING WITH PIECEWISE CONSTANT VELOCITY

Andrzej OKNIŃSKI[1)], Bogusław RADZISZEWSKI[2)]

Politechnika Świętokrzyska, Wydział Zarządzania i Modelowania Komputerowego

25-314 Kielce, Al. Tysiąclecia PP 7, Poland

[1)] 41 3424382, fizao@tu.kielce.pl, [2)] 41 3424101, boradzi@tu.kielce.pl

Abstract

Dynamics of a ball moving in gravitational field and colliding with a moving table is considered. The motion of the limiter is assumed as periodic with piecewise constant velocity. It is assumed that the table moves up with a constant velocity and then goes down with another constant velocity. The Poincaré map describing evolution from an impact to the next impact, is derived. Several classes of solutions were computed in analytical form.

Key words: non-smooth dynamics, bouncing ball

Introduction

Vibro-impacting systems are very interesting examples of non-smooth and non-linear dynamical systems with important technological applications [1]. Dynamics of such systems can be extremely complicated due to velocity discontinuity arising upon impacts. A very characteristic feature of impacting systems is presence of non-standard bifurcations such as border-collisions and grazing impacts appearing in the case of motion with low velocity after impact, which often leads to complex chaotic motion [1].

The main difficulty with investigating impacting systems is in gluing pre-impact and post-impact solutions. More exactly, the problem consists in finding instant of the next impact. The Poincaré map, describing evolution from an impact to the next impact, is a natural tool to study such systems. In the present paper we investigate motion of a material point in a gravitational field colliding with a moving motion-limiting stop. Typical example of such dynamical system, related to the Fermi model, is a small ball bouncing vertically on a vibrating table. Since evolution between impacts is expressed by a very simple formula the motion in this system is easier to analyze than dynamics of impact oscillators. It is possible to simplify the problem further assuming a special motion of the limiter.

The paper is organized as follows. In the first Section of this article a one-dimensional dynamics of a ball moving in a gravitational field and colliding with a table is considered. It is assumed that velocity of the table is piecewise linear. In Section 2 results of numerical simulations are described while in Section 3 analytical results are presented. We discuss our results in the last Section.

1. Motion with impacts: a simple motion of the limiter

We consider motion of a small ball moving vertically in a gravitational field and colliding with a moving table, representing unilateral constraints. We shall assume that the limiter's mass is so large that its motion is not affected at impacts. Motion of the ball between impacts is described by equation:

$$m\ddot{x} = -mg,$$ (1)

where $\dot{x} = dx/dt$ and motion of the limiter is adopted as:

$$y = y(t),$$ (2)

with a known function y. We shall also assume that y is a continuous function of time. Impacts are modeled as follows:

$$x(\tau_i) = y(\tau_i),$$ (3a)

$$\dot{x}(\tau_i^+) - \dot{y}(\tau_i) = -R(\dot{x}(\tau_i^-) - \dot{y}(\tau_i)),$$ (3b)

where duration of an impact is neglected with respect to time of motion between impacts and impacting bodies are considered perfectly rigid. In Eqs. (3) τ_i stands for time of the i-th impact while $\dot{x}_i^-$, $\dot{x}_i^+$ are left-sided and right-sided limits of $\dot{x}_i(t)$ for $t \to \tau_i$, respectively, and R is the coefficient of restitution, $0 \le R < 1$ [2].

Let us consider Eq. (1) for $t \in (\tau_i^+, \tau_{i+1}^+)$. General solution of this equation reads:

$$x(t) = -\frac{1}{2}gt^2 + c_1^i t + c_2^i.$$ (4)

Applying to Eq. (4) impact conditions (3) the Poincaré map is obtained [3]:

$$\gamma Y(T_{i+1}) = \gamma Y(T_i) - (T_{i+1} - T_i)^2 + (T_{i+1} - T_i)V_i,$$ (5a)

$$V_{i+1} = -RV_i + 2R(T_{i+1} - T_i) + \gamma(1 + R)\dot{Y}(T_{i+1}),$$ (5b)

where T_i, $Y(T_i)$, V_i and γ are non-dimensional time, position, velocity and acceleration, respectively:

$$T_i = \omega\tau_i, \quad Y(T_i) = y(\tau_i)/a, \quad V_i = (2\omega/g)\dot{x}(\tau_i^+), \quad \gamma = 2\omega^2 a/g.$$ (6)

and ω and a determine time and length scales. Let us note that in non-dimensional units velocity of the table is equal to $\gamma\dot{Y}$.

In our previous paper we have assumed limiter's motion in form $Y(T) = \sin(T)$ [3]. This choice leads to serious difficulties in solving Eq. (5a) thus making analytical investigations of dynamics hardly possible. Accordingly, we have decided to choose the

limiter's periodic motion as simple as possible. Very recently we have adopted a very simple motion of the table with piecewise constant velocity:

$$Y(T) = T \ (\text{mod } 1), \tag{7}$$

and we have performed numerical and analytical computations [4]. This motion of the table implies that while the table moves up with a constant velocity, it goes down infinitely fast and hence the model is not physical.

We have decided to investigate dynamics of a ball with a more realistic motion of the table. Let us thus assume that the table moves up with a finite constant velocity $\gamma \dot{Y}_1$ and then goes down with a finite constant velocity $\gamma \dot{Y}_2$. Therefore, displacement of the table is the following periodic function of time:

$$Y(T) = \begin{cases} \dfrac{1}{h}(T - \lfloor T \rfloor), & for \ T - \lfloor T \rfloor < h \\[2mm] \dfrac{-1}{1-h}(T - \lfloor T \rfloor) + \dfrac{1}{1-h}, & for \ h < T - \lfloor T \rfloor \end{cases} \qquad (0 < h < 1) \tag{8}$$

with $\dot{Y}_1 = 1/h$, $\dot{Y}_2 = -1/(1-h)$, where $\lfloor x \rfloor$ is the floor function – the largest integer less than or equal to x, see Fig. 1 where $h = 0.8$:
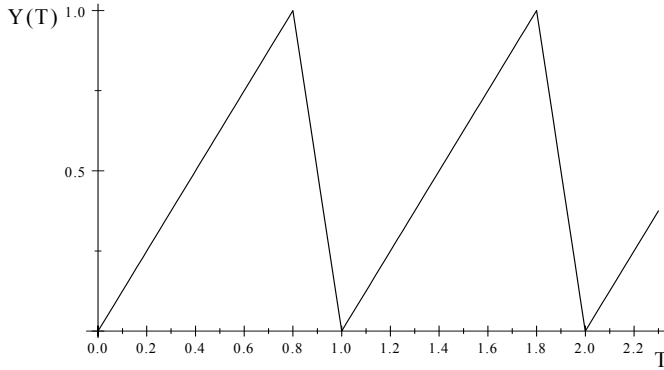
Fig. 1

2. Computational and analytical results

Our model consists of Eqs. (5), (8) with control parameters R, γ, h. Since period of motion of the limiter is equal one the map (5), (8) is invariant under the translation $T_i \to T_i + 1$. Accordingly, all impact times T_i are reduced to the unit interval $[0, 1]$.

Let us observe first that if all impacts occur at times $T_i \in (0, h)$ then all our results obtained for the model described by equations (5), (7) [3] are valid with only small changes. We only have to take into account that fixed points in the present model have to fulfill condition $T_* < h$ and that velocity of the table for $0 < T < h$ is $\dot{Y}_1 = \gamma/h$. For example, there is a manifold of fixed points with one impact per k periods:

$$V_*^{(k/1)} = k, \quad \gamma_{cr}^{(k/1)} = hk\frac{1-R}{1+R}, \quad k = 1, 2, \ldots, \quad T_*^{(k/1)} \in (0, h), \tag{9}$$

and a manifold of fixed points with m impacts per one period:

$$\gamma_{cr}^{(1/m)} = h\frac{(1-R)^2(1+R^m)}{(1+R)^2(1-R^m)}, V_{*1}^{(1/m)} = \frac{(1-R)\left[1+R+2R^2+(1-R)R^m\right]}{(1+R)^2(1-R^m)}, T_{*1}^{(1/m)} \in (0, \tau_m), \tag{10}$$

with

$$\tau_m = h\frac{(1-R)(1+R^m)}{(1+R)(1-R^m)}. \tag{11}$$

Furthermore, condition for initial velocity V_1 and initial time T_1 such that the ball chatters – impacts infinite number of times in time interval $(0, h)$ – and grazes reads:

$$\frac{V_1 - \gamma/h}{1-R} < h - T_1. \tag{12}$$

Analogous condition for infinite number of impacts in time interval $(h, 1)$ is

$$\frac{V_1 + \gamma/h}{1-R} < T_1 - h. \tag{12}$$

It turns out, however, that dynamics is radically different when some impacts occur at times $T_i \in (0, h)$ and some at times $T_i \in (h, 1)$, yet it is still possible to obtain analytical results. Let us first consider the case of two impacts with $T_1 \in (0, h)$ and $T_2 \in (h, 1)$. These means also the following conditions must be fulfilled: $V_{*3} = V_{*1}$, $T_{*3} = T_{*1} + 1$. Substituting all these conditions into Eqs.(5), (8) we obtain the set of equations:

$$\begin{cases} \gamma(-T_2 + 1)/(1-h) = (\gamma/h)T_1 - (T_2 - T_1)^2 + (T_2 - T_1)V_1 \\ V_2 = -RV_1 + 2R(T_2 - T_1) - \gamma(1+R)/(1-h) \\ \gamma T_1/h = \gamma(-T_2 + 1)/(1-h) - (T_1 + 1 - T_2)^2 + (T_1 + 1 - T_2)V_2 \\ V_1 = -RV_2 + 2R(T_1 + 1 - T_2) + \gamma(1+R)/h \end{cases} \tag{13}$$

Since all nonlinear terms in Eq.(13) depend on $T_2 - T_1$ only it is useful to introduce new variables, namely T_1 and $X = T_2 - T_1$. Equations (13), after being expressed in new variables, can be simplified resulting in one quadratic equation only in variable X:

$$AX^2 + BX + C = 0$$
$$A = 2h(1-h)(R+1)/(\gamma(1-R))$$
$$B = (R+1)(2h^2 - 2h - \gamma)/(\gamma(1-R)) \quad (14a)$$
$$C = (h + h\gamma - h^2 + R\gamma + (h + \gamma - h\gamma - h^2)R^2)/(\gamma(1-R^2))$$

where $X = T_2 - T_1$ and V_1, V_2, T_1 are expressed by X

$$V_1 = \frac{2R}{R-1}X + \frac{h\gamma R^2 + (-2h^2 + 2h + \gamma)R + \gamma(1-h)}{(h^2 - h)(R^2 - 1)}$$

$$V_2 = -\frac{2R}{R-1}X + \frac{(h\gamma - \gamma - 2h + 2h^2)R^2 - \gamma R - h\gamma}{(h^2 - h)(R^2 - 1)} \quad (14b)$$

$$T_1 = \frac{h(h-1)(R+1)}{\gamma(R-1)}X^2 + \frac{(2h - 2h^2 + \gamma)R + \gamma}{\gamma(R^2 - 1)} + h$$

Solutions of Eqs.(14) must meet several physical conditions. Variable T_1 must fulfill inequality $0 < T_1 < h$ while $T_2 = T_1 + X$ must obey $h < T_2 < 1$. In Fig.2 below acceptable values of parameters h, γ are shown for $R = 0.85$
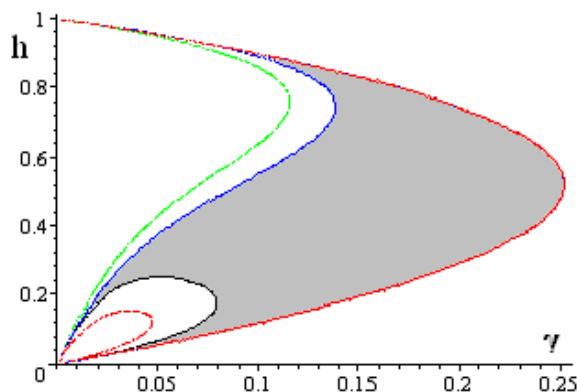
Fig. 2

Blue, black, green and red lines correspond to conditions $T_1 = 0$, $T_1 = h$, $T_2 = h$ and $T_2 = 1$, respectively. The shaded region in Fig. 2 shows physically acceptable values of variables T_1 and T_2. This is, however, only a necessary condition and stability of these solutions must be investigated.

3. Discussion

In the present paper we have investigated dynamics of a ball moving vertically in gravitational field and colliding with a moving table. Motion of the table has been assumed as simple as possible, i.e. periodic with piecewise constant velocity. Motion of the table was assumed in a more realistic form than in our previous work [3]: it is assumed that the table moves up with a finite constant velocity $\gamma \dot{Y}_1$ in time interval $(0, h)$ and then goes down with a finite constant velocity $\gamma \dot{Y}_2$ in time interval $(h, 1)$.

The improved model is still simple and we were able to compute several classes of solutions in analytical form. In the present paper we have found solutions in analytical form for the following modes of dynamics: (1a) one impact per k periods, (1b) m impacts per one period, (1c) infinite number of impacts ending with graze – all in time interval $(0, h)$; (2) infinite number of impacts ending with graze in time interval $(h, 1)$; (3) one impact in time interval $(0, h)$ and one impact in time interval $(h, 1)$.

It follows from our results that dynamics is radically different when some impacts occur at times $T_i \in (0, h)$ and some at times $T_j \in (h, 1)$ and we are going to study this problem in the future.

References

1. M. di Bernardo, C.J. Budd, A.R. Champneys, P. Kowalczyk, *Bifurcations and Chaos in Piecewise Smooth Dynamical Systems. Theory and Applications*. Springer 2006.
2. W.J. Stronge, *Impact mechanics*. Cambridge University Press, Cambridge 2000.
3. A. Okniński, B. Radziszewski, *Grazing dynamics and dependence on initial conditions in certain systems with impacts*, arXiv:0706.0257 (2007).
4. A. Okniński, B. Radziszewski, *Dynamics of a material point colliding with a limiter moving with piecewise constant velocity*, in: *Modeling, Simulation and Control of Nonlinear Engineering Dynamical Systems*, J. Awrejcewicz (ed.), Springer, in print.

DAMPED FORCED VIBRATIONS
OF AN ELASTICALLY CONNECTED DOUBLE-MEMBRANE SYSTEM

Zbigniew ONISZCZUK
Rzeszów University of Technology
ul. W. Pola 2, 35-959 Rzeszów
tel.:(017)8651377, e-mail: zbononka@interia.pl

Abstract

The purpose of the present paper is to consider theoretically damped forced transverse vibrations of an elastically connected rectangular double-membrane system. The system is treated as two viscoelastic membranes joined by a Kelvin-Voigt viscoelastic layer. Applying the modal expansion method, exact analytical solutions of damped forced responses for a simplified model of this system subjected to arbitrarily distributed transverse continuous loads are determined in the case of arbitrary magnitude of linear viscous damping. Nine possible different solutions obtained are described by the combinations of time functions expressing the damped motions for undercritical, critical and overcritical damping cases, according to the mutual relations between physical parameters of the system.

Keywords: double-membrane system, damped vibrations, modal expansion method.

1. Introduction

Paper [1] deals with the damped free transverse vibrations of an elastically connected rectangular double-membrane system. In the present paper, the damped forced vibration theory of this system subjected to arbitrarily distributed continuous loads is developed, and exact analytical general solutions of the problem in the case of arbitrary value of viscous damping are formulated [2]. The damped forced vibration analysis for such a system with light damping is carried out in work [3]. Next a number of papers [4-12] by Oniszczuk [4-7], Nizioł [8,9], Kucuk [10,11], and Liu et al. [12] have been devoted to different aspects of undamped responses of a double-membrane system. Articles [3-6,8,9,12] have shown an interesting feature of the system considered, which allows a double-membrane system to be applied as a continuous dynamic vibration absorber (CDVA). In Refs. [13-18], an analysis similar to this made here, has been performed for arbitrarily damped analogous complex continuous systems of two rectangular plates [13,14], two strings [15,16] and two beams [17,18]. Publications [19-20] referring to the vibration theory of a two-degree-of-freedom (TDOF) discrete system with viscous damping can also be helpful in present considerations because of evident analogy existing between the title system and TDOF one [3,4].

2. Formulation of the problem

The transverse vibration problem of an elastically connected double-membrane system with viscous damping has been exactly formulated in Refs. [1-3]. The investigated vibratory system shown in Fig. 1 constitutes a complex two-dimensional continuous system modelled as a rectangular three-layered structure which is composed of two parallel, homogeneous, uniform, viscoelastic membranes separated by a continuously distributed homogeneous Kelvin-Voigt viscoelastic massless layer. As is well known this

foundation model being a generalized Winkler one is characterized by two parameters: stiffness modulus k and viscous damping coefficient c [3]. Both membranes governed by simply supported boundary conditions are uniformly tight by suitable constant tensions applied at the edges and subjected to arbitrarily distributed transversal continuous loads.
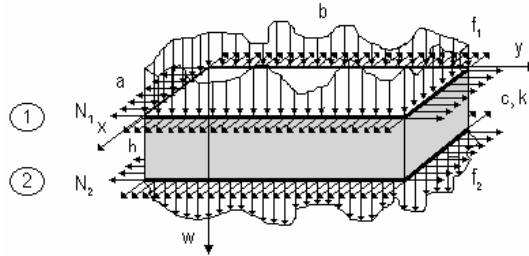
Fig. 1. The physical model of an elastically connected complex rectangular double-membrane system.

According to the Kelvin-Voigt foundation model, the small damped transverse motion of an elastically connected double-membrane system due to general loadings is described by the following set of two non-homogeneous partial differential equations [1-3]

$$m_1 \ddot{w}_1 + c_1 \dot{w}_1 + c(\dot{w}_1 - \dot{w}_2) - N_1 \Delta w_1 + k(w_1 - w_2) = f_1(x,y,t),$$
$$m_2 \ddot{w}_2 + c_2 \dot{w}_2 + c(\dot{w}_2 - \dot{w}_1) - N_2 \Delta w_2 + k(w_2 - w_1) = f_2(x,y,t),$$

(1)

where $w_i = w_i(x,y,t)$ is the transverse membrane displacement; x,y,t are the spatial co-ordinates and the time; $f_i = f_i(x,y,t)$ is the exciting distributed load; c_i is the viscous damping coefficient for the membrane; $c,\ k$ are the viscous damping coefficient and the stiffness modulus of a Kelvin-Voigt viscoelastic layer, respectively; a,b,h_i are the membrane dimensions; N_i is the uniform constant tension per unit length; ρ_i is the mass density; $m_i = \rho_i h_i$, $\Delta w_i = \partial^2 w_i / \partial x^2 + \partial^2 w_i / \partial y^2$, $\dot{w}_i = \partial w_i / \partial t$, $i = 1,2$.

Simply supported boundary conditions for membranes may be written as

$$w_i(0,y,t) = w_i(a,y,t) = w_i(x,0,t) = w_i(x,b,t) = 0, \quad i = 1,2,$$

(2)

and initial conditions are presented in the homogeneous form

$$w_i(x,y,0) = 0, \quad \dot{w}_i(x,y,0) = 0, \quad i = 1,2.$$

(3)

Eqs. (1) constitute a coupled system of two differential equations, which is difficult to solve in a general form. Making certain simplifying assumptions, this system can be easily decoupled, which considerably facilitates finding the solutions. Therefore, the analysis of this problem is performed for a simplified system variant when the physical parameters, namely, the viscous damping coefficients c_i, the unit masses m_i, and the tension forces N_i are the same and assumed to be

$$c_i = C, \quad m_i = \rho_i h_i = m, \quad N_i = N, \quad i = 1,2.$$

(4)

It is seen that the membrane parameters h_i and ρ_i satisfying the corresponding relation (4) can be arbitrary to a certain degree. In the light of the above assumptions, Eqs. (1) can be rewritten in the form

$$m\ddot{w}_1 + C\dot{w}_1 + c(\dot{w}_1 - \dot{w}_2) - N\Delta w_1 + k(w_1 - w_2) = f_1(x,y,t),$$
$$m\ddot{w}_2 + C\dot{w}_2 + c(\dot{w}_2 - \dot{w}_1) - N\Delta w_2 + k(w_2 - w_1) = f_2(x,y,t).$$

(5)

Introducing the new variables being the principal co-ordinates defined as

$$u_1(x,y,t) = \sum_{i=1}^{2} w_i(x,y,t), \quad u_2(x,y,t) = \sum_{i=1}^{2} a_i w_i(x,y,t), \quad a_1 = -a_2 = 1,$$

(6)

allows the decoupling Eqs. (5). The following differential equations are obtained

$$m\ddot{u}_1 + C\dot{u}_1 - N\Delta u_1 = F_1(x,y,t), \quad m\ddot{u}_2 + (C+2c)\dot{u}_2 - N\Delta u_2 + 2ku_2 = F_2(x,y,t),$$

(7)

where

$$F_1(x,y,t) = \sum_{i=1}^{2} f_i(x,y,t), \quad F_2(x,y,t) = \sum_{i=1}^{2} a_i f_i(x,y,t), \quad a_1 = -a_2 = 1.$$

(8)

The equations of motion (7) are now uncoupled, and each of them represents the damped transverse vibrations of a single membrane. Moreove, the second equation describes the oscillations of a membrane resting on viscoelastic foundation. Eqs. (7) are accompanied by appropriate transformed boundary conditions (2)

$$u_i(0,y,t) = u_i(a,y,t) = u_i(x,0,t) = u_i(x,b,t) = 0, \quad i = 1,2,$$

(9)

and can be solved independently of each other to find the principal co-ordinates.
Finally, the unknown solutions of Eqs. (5) can be determined from the relations

$$w_1(x,y,t) = 0,5\sum_{i=1}^{2} u_i(x,y,t), \quad w_2(x,y,t) = 0,5\sum_{i=1}^{2} a_i u_i(x,y,t), \quad a_1 = -a_2 = 1.$$

(10)

3. Solution of the damped forced vibration problem

Damped forced responses of the system due to arbitrarily distributed transverse continuous loads are represented by the particular solutions of the governing non-homogeneous partial differential equations (1). These solutions are formulated after solving a derived auxiliary uncoupled set of equations (3). Applying the modal expansion method [2,3], their solutions are assumed to be in the form:

$$u_1(x,y,t) = \sum_{m,n=1}^{\infty} W_{1mn}(x,y)P_{1mn}(t) = \sum_{m,n=1}^{\infty} W_{mn}(x,y)P_{1mn}(t) = \sum_{m,n=1}^{\infty} \sin(a_m x)\sin(b_n y)P_{1mn}(t),$$

$$u_2(x,y,t) = \sum_{m,n=1}^{\infty} W_{2mn}(x,y)P_{2mn}(t) = \sum_{m,n=1}^{\infty} W_{mn}(x,y)P_{2mn}(t) = \sum_{m,n=1}^{\infty} \sin(a_m x)\sin(b_n y)P_{2mn}(t),$$

(11)

where $P_{1mn}(t)$ and $P_{2mn}(t)$ are the unknown time functions to be determined;

$$W_{1mn}(x,y) = W_{2mn}(x,y) = W_{mn}(x,y) = \sin(a_m x)\sin(b_n y),$$

(12)

$$a_m = a^{-1}m\pi, \quad b_n = b^{-1}n\pi, \quad k_{mn}^2 = a_m^2 + b_n^2 = \pi^2[(a^{-1}m)^2 + (b^{-1}n)^2], \quad m,n = 1,2,3,\ldots$$ (13)

Substituting solutions (11) into Eqs. (7) leads to the following relationships:

$$\sum_{m,n=1}^{\infty} [\ddot{P}_{1mn} + 2h_1\dot{P}_{1mn} + \omega_{1mn}^2 P_{1mn}]W_{mn} = m^{-1}F_1, \quad \sum_{m,n=1}^{\infty} [\ddot{P}_{2mn} + 2h_2\dot{P}_{2mn} + \omega_{2mn}^2 P_{2mn}]W_{mn} = m^{-1}F_2.$$

Multiplying the above relations by the eigenfunction W_{kl}, then integrating them over the membrane surface and applying the corresponding orthogonality condition [1-3]

$$\int_0^a \int_0^b W_{kl} W_{mn} dx dy = \int_0^a \sin(a_k x) \sin(a_m x) dx \int_0^b \sin(b_l y) \sin(b_n y) dy = d\delta_{klmn}, \qquad (14)$$

$$d = \int_0^a \int_0^b W_{mn}^2 dx dy = \int_0^a \sin^2(a_m x) dx \int_0^b \sin^2(b_n y) dy = 0,25 ab,$$

where δ_{klmn} is the Kronecker delta function: $\delta_{klmn} = 0$ for $k \neq m$ or $l \neq n$, and $\delta_{klmn} = 1$ for $k = m$ and $l = n$; one gets the differential equations for unknown time functions

$$\ddot{P}_{imn} + 2h_i \dot{P}_{imn} + \omega_{imn}^2 P_{imn} = K_{imn}(t), \quad i = 1,2, \quad m,n = 1,2,3,..., \qquad (15)$$

where $h_1 = 0,5 C m^{-1}$, $h_2 = 0,5(C+2c)m^{-1} = h_1 + h_0$, $h_0 = c\, m^{-1}$, $M = abm$,

$$\omega_{1mn}^2 = N k_{mn}^2 m^{-1}, \quad \omega_{2mn}^2 = (N k_{mn}^2 + 2k)m^{-1} = \omega_{1mn}^2 + \omega_0^2, \quad \omega_0^2 = 2km^{-1},$$

$$K_{imn}(t) = (dm)^{-1} \int_0^a \int_0^b F_i W_{mn} \, dx\, dy = 4M^{-1} \int_0^a \int_0^b F_i(x,y,t)\, \sin(a_m x)\sin(b_n y) \, dx\, dy.$$

Searching for their solutions, three possible cases [2] depending on the values of damping coefficients should be considered:

(1) *Undercritical damping:* $h_i < \omega_{imn}$,

$$P_{imn}(t) = \Omega_{imn}^{-1} \int_0^t K_{imn}(\tau) e^{-h_i(t-\tau)} \sin[\Omega_{imn}(t-\tau)] d\tau, \quad i = 1,2, \qquad (16)$$

where $\Omega_{imn} = (\omega_{imn}^2 - h_i^2)^{1/2}$,

$$\Omega_{1mn} = (N k_{mn}^2 m^{-1} - 0,25 C^2 m^{-2})^{1/2}, \quad \Omega_{2mn} = [(N k_{mn}^2 + 2k)m^{-1} - 0,25(C+2c)^2 m^{-2}]^{1/2}.$$

(2) *Critical damping:* $h_i = \omega_{imn}$,

$$P_{imn}(t) = \int_0^t K_{imn}(\tau) e^{-h_i(t-\tau)}(t-\tau) d\tau, \quad i = 1,2. \qquad (17)$$

(3) *Overcritical damping:* $h_i > \omega_{imn}$,

$$P_{imn}(t) = \Psi_{imn}^{-1} \int_0^t K_{imn}(\tau) e^{-h_i(t-\tau)} \sinh[\Psi_{imn}(t-\tau)] d\tau, \quad i = 1,2, \qquad (18)$$

where $\Psi_{imn} = (h_i^2 - \omega_{imn}^2)^{1/2}$,

$$\Psi_{1mn} = (0,25 C^2 m^{-2} - N k_{mn}^2 m^{-1})^{1/2}, \quad \Psi_{2mn} = [0,25(C+2c)^2 m^{-2} - (N k_{mn}^2 + 2k)m^{-1}]^{1/2}.$$

Setting solutions (10) for the damped forced vibrations of the system $\qquad (19)$

$$w_1(x,y,t) = 0,5 \sum_{m,n=1}^{\infty} u_i = 0,5 \sum_{m,n=1}^{\infty} W_{mn}(x,y) \sum_{i=1}^{2} P_{imn}(t) = 0,5 \sum_{m,n=1}^{\infty} \sin(a_m x)\sin(b_n y) \sum_{i=1}^{2} P_{imn}(t),$$

$$w_2(x,y,t) = 0,5 \sum_{m,n=1}^{\infty} a_i u_i = 0,5 \sum_{m,n=1}^{\infty} W_{mn} \sum_{i=1}^{2} a_{imn} P_{imn}(t) = 0,5 \sum_{m,n=1}^{\infty} \sin(a_m x)\sin(b_n y) \sum_{i=1}^{2} a_{imn} P_{imn}(t),$$

where $a_{1mn} = a_1 = -a_{2mn} = -a_2 = 1$, the following nine possible cases have to be shown:

{1} $h_1 < \omega_{1kl}$, $h_2 < \omega_{2rs}$, when $C < 2(N k_{kl}^2 m)^{1/2}$, $c < [(N k_{rs}^2 + 2k)m]^{1/2} - 0,5C$,

$$w_{1,2}(x,y,t) = 0,5 \left\{ \sum_{m=1}^{k-1} \sum_{n=1}^{l-1} \Psi_{1mn}^{-1} \sin(a_m x)\sin(b_n y) \int_0^t K_{1mn}(\tau) e^{-h_1(t-\tau)} \sinh[\Psi_{1mn}(t-\tau)] d\tau \right.$$
$$\left. + \sum_{m=k}^{\infty} \sum_{n=l}^{\infty} \Omega_{1mn}^{-1} \sin(a_m x)\sin(b_n y) \int_0^t K_{1mn}(\tau) e^{-h_1(t-\tau)} \sin[\Omega_{1mn}(t-\tau)] d\tau \right\} \qquad (20)$$

$$\pm 0.5 \left\{ \sum_{m=1}^{r-1} \sum_{n=1}^{s-1} \Psi_{2mn}^{-1} \sin(a_m x) \sin(b_n y) \int_0^t K_{2mn}(\tau) e^{-h_2(t-\tau)} \sinh[\Psi_{2mn}(t-\tau)] d\tau \right.$$

$$\left. + \sum_{m=r}^{\infty} \sum_{n=s}^{\infty} \Omega_{2mn}^{-1} \sin(a_m x) \sin(b_n y) \int_0^t K_{2mn}(\tau) e^{-h_2(t-\tau)} \sin[\Omega_{2mn}(t-\tau)] d\tau \right\}, \tag{20}$$

$\{2\}$ $h_1 < \omega_{1kl}$, $h_2 = \omega_{2rs}$, when $C < 2(Nk_{kl}^2 m)^{1/2}$, $c = [(Nk_{rs}^2 + 2k)m]^{1/2} - 0.5C$,

$$w_{1,2}(x,y,t) = 0.5 \left\{ \sum_{m=1}^{k-1} \sum_{n=1}^{l-1} \Psi_{1mn}^{-1} \sin(a_m x) \sin(b_n y) \int_0^t K_{1mn}(\tau) e^{-h_1(t-\tau)} \sinh[\Psi_{1mn}(t-\tau)] d\tau \right.$$

$$\left. + \sum_{m=k}^{\infty} \sum_{n=l}^{\infty} \Omega_{1mn}^{-1} \sin(a_m x) \sin(b_n y) \int_0^t K_{1mn}(\tau) e^{-h_1(t-\tau)} \sin[\Omega_{1mn}(t-\tau)] d\tau \right\}$$

$$\pm 0.5 \left\{ \sum_{m=1}^{r-1} \sum_{n=1}^{s-1} \Psi_{2mn}^{-1} \sin(a_m x) \sin(b_n y) \int_0^t K_{2mn}(\tau) e^{-h_2(t-\tau)} \sinh[\Psi_{2mn}(t-\tau)] d\tau \right. \tag{21}$$

$$+ \sin(a_r x) \sin(b_s y) \int_0^t K_{2rs}(\tau) e^{-h_2(t-\tau)} (t-\tau) d\tau$$

$$\left. + \sum_{m=r+1}^{\infty} \sum_{n=s+1}^{\infty} \Omega_{2mn}^{-1} \sin(a_m x) \sin(b_n y) \int_0^t K_{2mn}(\tau) e^{-h_2(t-\tau)} \sin[\Omega_{2mn}(t-\tau)] d\tau \right\}$$

$\{3\}$ $h_1 < \omega_{1kl}$, $h_2 > \omega_{2rs}$, when $C < 2(Nk_{kl}^2 m)^{1/2}$, $c > [(Nk_{rs}^2 + 2k)m]^{1/2} - 0.5C$,

$$w_{1,2}(x,y,t) = 0.5 \left\{ \sum_{m=1}^{k-1} \sum_{n=1}^{l-1} \Psi_{1mn}^{-1} \sin(a_m x) \sin(b_n y) \int_0^t K_{1mn}(\tau) e^{-h_1(t-\tau)} \sinh[\Psi_{1mn}(t-\tau)] d\tau \right.$$

$$\left. + \sum_{m=k}^{\infty} \sum_{n=l}^{\infty} \Omega_{1mn}^{-1} \sin(a_m x) \sin(b_n y) \int_0^t K_{1mn}(\tau) e^{-h_1(t-\tau)} \sin[\Omega_{1mn}(t-\tau)] d\tau \right\}$$

$$\pm 0.5 \left\{ \sum_{m=1}^{r} \sum_{n=1}^{s} \Psi_{2mn}^{-1} \sin(a_m x) \sin(b_n y) \int_0^t K_{2mn}(\tau) e^{-h_2(t-\tau)} \sinh[\Psi_{2mn}(t-\tau)] d\tau \right. \tag{22}$$

$$\left. + \sum_{m=r+1}^{\infty} \sum_{n=s+1}^{\infty} \Omega_{2mn}^{-1} \sin(a_m x) \sin(b_n y) \int_0^t K_{2mn}(\tau) e^{-h_2(t-\tau)} \sin[\Omega_{2mn}(t-\tau)] d\tau \right\}$$

$\{4\}$ $h_1 = \omega_{1kl}$, $h_2 < \omega_{2rs}$, when $C = 2(Nk_{kl}^2 m)^{1/2}$, $c < [(Nk_{rs}^2 + 2k)m]^{1/2} - (Nk_{kl}^2 m)^{1/2}$,

$$w_{1,2}(x,y,t) = 0.5 \left\{ \sum_{m=1}^{k-1} \sum_{n=1}^{l-1} \Psi_{1mn}^{-1} \sin(a_m x) \sin(b_n y) \int_0^t K_{1mn}(\tau) e^{-h_1(t-\tau)} \sinh[\Psi_{1mn}(t-\tau)] d\tau \right.$$

$$+ \sin(a_k x) \sin(b_l y) \int_0^t K_{1kl}(\tau) e^{-h_1(t-\tau)} (t-\tau) d\tau$$

$$\left. + \sum_{m=k+1}^{\infty} \sum_{n=l+1}^{\infty} \Omega_{1mn}^{-1} \sin(a_m x) \sin(b_n y) \int_0^t K_{1mn}(\tau) e^{-h_1(t-\tau)} \sin[\Omega_{1mn}(t-\tau)] d\tau \right\} \tag{23}$$

$$\pm 0.5 \left\{ \sum_{m=1}^{r-1} \sum_{n=1}^{s-1} \Psi_{2mn}^{-1} \sin(a_m x) \sin(b_n y) \int_0^t K_{2mn}(\tau) e^{-h_2(t-\tau)} \sinh[\Psi_{2mn}(t-\tau)] d\tau \right.$$

$$\left. + \sum_{m=r}^{\infty} \sum_{n=s}^{\infty} \Omega_{2mn}^{-1} \sin(a_m x) \sin(b_n y) \int_0^t K_{2mn}(\tau) e^{-h_2(t-\tau)} \sin[\Omega_{2mn}(t-\tau)] d\tau \right\}$$

$\{5\}$ $h_1 = \omega_{1kl}$, $h_2 = \omega_{2rs}$, when $C = 2(Nk_{kl}^2 m)^{1/2}$, $c = [(Nk_{rs}^2 + 2k)m]^{1/2} - (Nk_{kl}^2 m)^{1/2}$,

$$w_{1,2}(x,y,t) = 0.5 \left\{ \sum_{m=1}^{k-1} \sum_{n=1}^{l-1} \Psi_{1mn}^{-1} \sin(a_m x) \sin(b_n y) \int_0^t K_{1mn}(\tau) e^{-h_1(t-\tau)} \sinh[\Psi_{1mn}(t-\tau)] d\tau \right. \tag{24}$$

$$+\sin(a_k x)\sin(b_l y)\int_0^t K_{1kl}(\tau)e^{-h_1(t-\tau)}(t-\tau)d\tau$$

$$+\sum_{m=k+1}^{\infty}\sum_{n=l+1}^{\infty}\Omega_{1mn}^{-1}\sin(a_m x)\sin(b_n y)\int_0^t K_{1mn}(\tau)e^{-h_1(t-\tau)}\sin[\Omega_{1mn}(t-\tau)]d\tau\Big\}$$

$$\pm 0,5\Big\{\sum_{m=1}^{r-1}\sum_{n=1}^{s-1}\Psi_{2mn}^{-1}\sin(a_m x)\sin(b_n y)\int_0^t K_{2mn}(\tau)e^{-h_2(t-\tau)}\sinh[\Psi_{2mn}(t-\tau)]d\tau \qquad (24)$$

$$+\sin(a_r x)\sin(b_s y)\int_0^t K_{2rs}(\tau)e^{-h_2(t-\tau)}(t-\tau)d\tau$$

$$+\sum_{m=r+1}^{\infty}\sum_{n=s+1}^{\infty}\Omega_{2mn}^{-1}\sin(a_m x)\sin(b_n y)\int_0^t K_{2mn}(\tau)e^{-h_2(t-\tau)}\sin[\Omega_{2mn}(t-\tau)]d\tau\Big\},$$

$\{6\}\ h_1=\omega_{1kl},\ h_2>\omega_{2rs},\ \text{when}\ \ C=2(Nk_{kl}^2 m)^{1/2},\ \ c>[(Nk_{rs}^2+2k)m]^{1/2}-(Nk_{kl}^2 m)^{1/2},$

$$w_{1,2}(x,y,t)=0,5\Big\{\sum_{m=1}^{k-1}\sum_{n=1}^{l-1}\Psi_{1mn}^{-1}\sin(a_m x)\sin(b_n y)\int_0^t K_{1mn}(\tau)e^{-h_1(t-\tau)}\sinh[\Psi_{1mn}(t-\tau)]d\tau$$

$$+\sin(a_k x)\sin(b_l y)\int_0^t K_{1kl}(\tau)e^{-h_1(t-\tau)}(t-\tau)d\tau$$

$$+\sum_{m=k+1}^{\infty}\sum_{n=l+1}^{\infty}\Omega_{1mn}^{-1}\sin(a_m x)\sin(b_n y)\int_0^t K_{1mn}(\tau)e^{-h_1(t-\tau)}\sin[\Omega_{1mn}(t-\tau)]d\tau\Big\} \qquad (25)$$

$$\pm 0,5\Big\{\sum_{m=1}^{r}\sum_{n=1}^{s}\Psi_{2mn}^{-1}\sin(a_m x)\sin(b_n y)\int_0^t K_{2mn}(\tau)e^{-h_2(t-\tau)}\sinh[\Psi_{2mn}(t-\tau)]d\tau$$

$$+\sum_{m=r+1}^{\infty}\sum_{n=s+1}^{\infty}\Omega_{2mn}^{-1}\sin(a_m x)\sin(b_n y)\int_0^t K_{2mn}(\tau)e^{-h_2(t-\tau)}\sin[\Omega_{2mn}(t-\tau)]d\tau\Big\}$$

$\{7\}\ h_1>\omega_{1kl},\ h_2<\omega_{2rs},\ \text{when}\ \ C>2(Nk_{kl}^2 m)^{1/2},\ \ c<[(Nk_{rs}^2+2k)m]^{1/2}-0,5C,$

$$w_{1,2}(x,y,t)=0,5\Big\{\sum_{m=1}^{k}\sum_{n=1}^{l}\Psi_{1mn}^{-1}\sin(a_m x)\sin(b_n y)\int_0^t K_{1mn}(\tau)e^{-h_1(t-\tau)}\sinh[\Psi_{1mn}(t-\tau)]d\tau$$

$$+\sum_{m=k+1}^{\infty}\sum_{n=l+1}^{\infty}\Omega_{1mn}^{-1}\sin(a_m x)\sin(b_n y)\int_0^t K_{1mn}(\tau)e^{-h_1(t-\tau)}\sin[\Omega_{1mn}(t-\tau)]d\tau\Big\}$$

$$\pm 0,5\Big\{\sum_{m=1}^{r-1}\sum_{n=1}^{s-1}\Psi_{2mn}^{-1}\sin(a_m x)\sin(b_n y)\int_0^t K_{2mn}(\tau)e^{-h_2(t-\tau)}\sinh[\Psi_{2mn}(t-\tau)]d\tau \qquad (26)$$

$$+\sum_{m=r}^{\infty}\sum_{n=s}^{\infty}\Omega_{2mn}^{-1}\sin(a_m x)\sin(b_n y)\int_0^t K_{2mn}(\tau)e^{-h_2(t-\tau)}\sin[\Omega_{2mn}(t-\tau)]d\tau\Big\}$$

$\{8\}\ h_1>\omega_{1kl},\ h_2=\omega_{2rs},\ \text{when}\ \ C>2(Nk_{kl}^2 m)^{1/2},\ \ c=[(Nk_{rs}^2+2k)m]^{1/2}-0,5C,$

$$w_{1,2}(x,y,t)=0,5\Big\{\sum_{m=1}^{k}\sum_{n=1}^{l}\Psi_{1mn}^{-1}\sin(a_m x)\sin(b_n y)\int_0^t K_{1mn}(\tau)e^{-h_1(t-\tau)}\sinh[\Psi_{1mn}(t-\tau)]d\tau$$

$$+\sum_{m=k+1}^{\infty}\sum_{n=l+1}^{\infty}\Omega_{1mn}^{-1}\sin(a_m x)\sin(b_n y)\int_0^t K_{1mn}(\tau)e^{-h_1(t-\tau)}\sin[\Omega_{1mn}(t-\tau)]d\tau\Big\} \qquad (27)$$

$$\pm 0,5\Big\{\sum_{m=1}^{r-1}\sum_{n=1}^{s-1}\Psi_{2mn}^{-1}\sin(a_m x)\sin(b_n y)\int_0^t K_{2mn}(\tau)e^{-h_2(t-\tau)}\sinh[\Psi_{2mn}(t-\tau)]d\tau$$

$$+\sin(a_r x)\sin(b_s y)\int_0^t K_{2rs}(\tau)e^{-h_2(t-\tau)}(t-\tau)d\tau$$

$$+ \sum_{m=r+1}^{\infty} \sum_{n=s+1}^{\infty} \Omega_{2mn}^{-1} \sin(a_m x)\sin(b_n y)\int_0^t K_{2mn}(\tau)e^{-h_2(t-\tau)}\sin[\Omega_{2mn}(t-\tau)]d\tau \Big\}, \quad (27)$$

$\{9\}$ $h_1 > \omega_{1kl}$, $h_2 > \omega_{2rs}$, when $C > 2(Nk_{kl}^2 m)^{1/2}$, $c > [(Nk_{rs}^2 + 2k)m]^{1/2} - 0,5C$,

$$\begin{aligned}
w_{1,2}(x,y,t) = 0,5\Big\{ &\sum_{m=1}^{k} \sum_{n=1}^{l} \Psi_{1mn}^{-1} \sin(a_m x)\sin(b_n y)\int_0^t K_{1mn}(\tau)e^{-h_1(t-\tau)}\sinh[\Psi_{1mn}(t-\tau)]d\tau \\
&+ \sum_{m=k+1}^{\infty} \sum_{n=l+1}^{\infty} \Omega_{1mn}^{-1} \sin(a_m x)\sin(b_n y)\int_0^t K_{1mn}(\tau)e^{-h_1(t-\tau)}\sin[\Omega_{1mn}(t-\tau)]d\tau \Big\} \\
\pm 0,5\Big\{ &\sum_{m=1}^{r} \sum_{n=1}^{s} \Psi_{2mn}^{-1} \sin(a_m x)\sin(b_n y)\int_0^t K_{2mn}(\tau)e^{-h_2(t-\tau)}\sinh[\Psi_{2mn}(t-\tau)]d\tau \\
&+ \sum_{m=r+1}^{\infty} \sum_{n=s+1}^{\infty} \Omega_{2mn}^{-1} \sin(a_m x)\sin(b_n y)\int_0^t K_{2mn}(\tau)e^{-h_2(t-\tau)}\sin[\Omega_{2mn}(t-\tau)]d\tau \Big\}
\end{aligned} \quad (28)$$

where $k, l, m, n, r, s = 1,2,3, \ldots$. In those cases where $k, l, r, s = 1$, the corresponding expressions $\sum_{m=1}^{k-1}(\ldots)$, $\sum_{n=1}^{l-1}(\ldots)$, $\sum_{m=1}^{r-1}(\ldots)$, $\sum_{n=1}^{s-1}(\ldots)$ must be assumed equal to zero.

4. Conclusions

The paper is concerned with the theoretical analysis of damped forced transverse vibrations for a system of two viscoelastic rectangular membranes connected by a Kelvin-Voigt viscoelastic layer. This analysis is performed for a certain simplified model of the system. Assumed simplifications permit to decouple the governing equations of motion, which can be solved by application of the classical modal expansion method. Exact analytical solutions for damped forced responses of membranes subjected to arbitrarily distributed continuous loads and due to arbitrary viscous damping are formulated. It is relevant to note that coefficients shaping the solutions are explicitly expressed in terms of the physical parameters characterizing the system. Nine forms of solutions obtained are described by the combinations of time functions relating to three possible cases resulting from magnitude of damping, which are undercritical, critical and overcritical damping. Investigation of all possible solutions of the problem allows a better understanding of the vibration phenomena occurring in damped complex continuous systems. The forced vibration analysis is of great importance in consideration of the possibility of wide engineering applications of a double-membrane system as a continuous dynamic vibration absorber (CDVA) [2-5,8,9,12].

References

1. Z. Oniszczuk, *Damped free vibrations of an elastically connected double-membrane system,* Cracow University of Technology Publishers, Technical Journal, Mechanics 5-M (2004) 265-275.
2. Z. Oniszczuk, *Damped forced transverse vibrations of an elastically connected double-membrane system*, Transactions of the 12th Polish-Ukrainian Seminar „Theoretical Foundations of Civil Engineering", Warsaw-Dnepropetrovsk, I, 2004, pp. 319-326.

3. Z. Oniszczuk**,** *Vibration Analysis of Compound Continuous Systems with Elastic Constraints*, Publishing House of Rzeszów University of Technology, Rzeszów, 1997.

4. Z. Oniszczuk, *Transverse vibrations of elastically connected rectangular double-membrane compound system,* Journal of Sound and Vibration, **221** (1999) 235-250.

5. Z. Oniszczuk**,** *Forced vibration analysis of an elastically connected rectangular double-membrane complex system,* Proceedings of the 4th International Scientific Colloquium CAx Techniques'99, Bielefeld*,* 1999, pp. 393-400.

6. Z. Oniszczuk, *Dynamic vibration absorption in complex continuous systems,* Machine Dynamics Problems, **24** (2) (2000) 81-94.

7. Z. Oniszczuk, *Free transverse vibrations of an elastically connected rectangular plate-membrane complex system*, Journal of Sound and Vibration, **264** (2003) 37-47.

8. J. Nizioł, *Damping of vibrations of continuous systems in probabilistic formulation*, Scientific Works of Cracow University of Technology, Mechanics,**83** (2001) 213-220.

9. J. Nizioł, *Damping of vibrations of plates and membranes in probabilistic formulation,* Cracow University of Technology Publishers, Technical Journal, Mechanics, **5-M** (2004) 233-242.

10. I. Kucuk, *Necessary conditions for the optimal control of the double-membrane system*, WSEAS Transactions on Mathematics, **5** (5) (2006) 589-594.

11. I. Kucuk, *Optimality conditions for the control of a double-membrane complex system by a modal decomposition technique,* Applied Mathematical Modelling, **32** (4) (2008) 562-574.

12. Y. Liu, D. Yu, H. Zhao, X. Wen, *Review of passive dynamic vibration absorbers,* Chinese Journal of Mechanical Engineering, **43** (3) (2007) 14-21.

13. Z. Oniszczuk, *Damped transverse vibrations of an elastically connected double-plate system. Part I: free vibrations,* Proceedings of the XXth Symposium „Vibrations in Physical Systems", Poznań-Błażejewko*,* 2002*,* 240-241.

14. Z. Oniszczuk**,** *Damped transverse vibrations of an elastically connected double-plate system. Part II: forced vibrations*, Proceedings of the XXth Symposium „Vibrations in Physical Systems", Poznań-Błażejewko, 2002, pp. 242-243.

15. Z. Oniszczuk, *Damped free transverse vibrations of an elastically connected double-string system,* Proceedings of the Conference „Polish Mechanics at the Beginning of Twenty First Century", Kazimierz Dolny-Warsaw, 2001, pp. 339-346.

16. Z. Oniszczuk, *Damped vibration analysis of an elastically connected complex double-string system*, Journal of Sound and Vibration, **264** (2003) 253-271.

17. Z. Oniszczuk**,** *Damped forced transverse vibrations of an elastically connected double-beam system,* Transactions of the 10th Polish-Ukrainian Seminar „Theoretical Foundations of Civil Engineering", Warsaw*,* Vol. I, 2002, pp. 331-340.

18. Z. Oniszczuk**,** *Damped forced transverse vibrations of an elastically connected double-beam system,* Proceedings of the XXIth Symposium „Vibrations in Physical Systems", Poznań-Kiekrz, 2004, pp. 283-286.

19. Z. Oniszczuk**,** *Damped vibrations of a two-degree-of-freedom discrete system,* Scientific Works of Cracow University of Technology, Mechanics, **83** (2001) 325-332.

20. Z. Oniszczuk**,** *Damped vibration analysis of a two-degree-of-freedom discrete system,* Journal of Sound and Vibration, **257** (2002) 391-403.

FREE TORSIONAL VIBRATIONS
OF AN ELASTICALLY CONNECTED DOUBLE-SHAFT SYSTEM

Zbigniew ONISZCZUK

Rzeszów University of Technology
ul. W. Pola 2, 35-959 Rzeszów
tel.:(017)8651377, e-mail: zbononka@interia.pl

Abstract

In this article, a theoretical undamped torsional vibration analysis of an elastically connected double-shaft system is presented. The double-shaft system is one of the simplest model of a complex continuous system, which is composed of two concentric, cylindrical circular elastic shafts attached together by a Winkler elastic layer. The free transverse vibration problem of this system is considered by using the separation of variables method. The boundary value and initial-value problems are solved. The natural frequencies and natural mode shapes of vibration are determined. The free vibrations of an elastically connected double-shaft system are realized by synchronous and asynchronous angular displacements.

Keywords: double-shaft system, torsional vibrations, separation of variables method

1. Introduction

In linear vibration theory of simple continuous systems, an analysis of longitudinal vibrations of a straight rod, an analysis of transverse vibrations of a stretched string, and an analysis of torsional vibrations of a uniform shaft are all analogous [1-4]. For this reason, the partial differential equations of motion describing these three vibration problems are similar, and the same mathematical procedures can be used to solve them effectively to find free and forced vibrations. In the present paper, the similarity between the vibrations of mentioned three simple continuous systems is applied to adopt the vibration analysis of an elastically connected complex double-string system [4-7] and double-rod system [8-11] for the formulation and solution of the torsional vibration problem of an elastically connected double-shaft system [12-18]. The undamped free vibrations of this system are analyzed and the complete exact theoretical solutions are formulated. It seems that Refs. [19,20] can be helpful in dynamic analysis of the system.

2. Formulation of the problem

The physical model of an elastically connected double-shaft system shown in Fig. 1 interpreted as a sandwich or layered shaft is represented by a three-layered structure consisting of two concentric, cylindrical circular elastic shafts, in which the middle cylindrical layer is modelled as a Winkler massless elastic foundation [1,4,5,8]. The both shafts of the same length are uniform, homogeneous, isotropic and perfectly elastic. As a whole this layered shaft is governed by corresponding fixed-free boundary conditions.

The shafts are subjected to external exciting loadings in the form of arbitrarily distributed torsional moments. Small undamped vibrations of the system are considered.
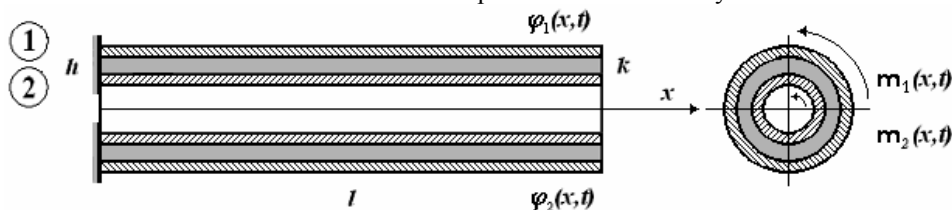
Fig. 1. The physical model of an elastically connected complex double-shaft system.

The torsional vibrations of a generally loaded double-shaft system are governed by the following partial differential equations [4-11]:

$$I_1 \ddot{\varphi}_1 - K_1 \varphi_1'' + k(\varphi_1 - \varphi_2) = m_1(x,t), \quad I_2 \ddot{\varphi}_2 - K_2 \varphi_2'' + k(\varphi_2 - \varphi_1) = m_2(x,t), \qquad (1)$$

where $\varphi_i = \varphi_i(x,t)$ is the torsional (angular) displacement of the shaft; $m_i = m_i(x,t)$ is the external exciting distributed torsional moment applied along the shaft; x, t are the spatial co-ordinate and the time; G_i is the Kirchhoff's shear modulus of elasticity; J_i is the area polar moment of inertia of the shaft cross-section; K_i is the torsional rigidity of the shaft; k is the stiffness modulus of a Winkler elastic layer; l is the shaft length; ρ_i is the mass density; $I_i = \rho_i J_i$, $K_i = G_i J_i$, $\dot{\varphi}_i = \partial \varphi_i / \partial t$, $\varphi_i' = \partial \varphi_i / \partial x$, $i = 1, 2$.

The torsional vibrations of shafts are usually analyzed under fundamental homogeneous geometrical boundary conditions for clamped (C) and free (F) ends

$$\varphi_1(0,t) = \varphi_2(0,t) = \varphi_1'(l,t) = \varphi_2'(l,t) = 0 \qquad (2)$$

Initial conditions for this vibratory system are taken in the general form:

$$\varphi_i(x,0) = \varphi_{i0}(x), \quad \dot{\varphi}_i(x,0) = \omega_{i0}(x), \quad i = 1, 2. \qquad (3)$$

3. Solution of the free vibration problem

The governing equations for undamped free vibrations of the system are the following:

$$I_1 \ddot{\varphi}_1 - K_1 \varphi_1'' + k(\varphi_1 - \varphi_2) = 0, \quad I_2 \ddot{\varphi}_2 - K_2 \varphi_2'' + k(\varphi_2 - \varphi_1) = 0. \qquad (4)$$

These homogeneous partial differential equations may be solved by the Fourier method of separation of variables, for which the general solutions of Eqs (4) are decomposed into products of functions of x and t:

$$\varphi_1(x,t) = \Phi_1(x)T(t), \quad \varphi_2(x,t) = \Phi_2(x)T(t), \qquad (5)$$

where $\Phi_1(x)$ and $\Phi_2(x)$ are the unknown functions of the spatial co-ordinate x representing natural mode shapes of vibration for shafts, and $T(t)$ is the unknown time function. By substituting expressions (5) into Eqs. (4), as a result of separation of variables, one obtains a set of three ordinary differential equations of second order

$$K_1 \Phi_1'' + (I_1 \omega^2 - k)\Phi_1 + k\Phi_2 = 0, \quad K_2 \Phi_2'' + (I_2 \omega^2 - k)\Phi_2 + k\Phi_1 = 0, \qquad (6)$$

$$\ddot{T} + \omega^2\, T = 0\,, \tag{7}$$

where ω is the separation constant denoting the natural frequency of the vibrating system; $\Phi_i^{'} = d\Phi_i\,/\,dx,\ \dot{T} = dT\,/\,dt,\ i = 1,2.$

It is seen that Eq. (7) is independent of two Eqs. (6), and can be solved without any difficulty. Since this equation describes a simple harmonic motion, then its solution has the known form

$$T(t) = A\sin(\omega t) + B\cos(\omega t). \tag{8}$$

Eqs. (6) constitute a coupled system of two linear homogeneous differential equations with constant coefficients, which can be solved by using the classical method [1,3-5] supposing solutions in the form of exponential functions as follows:

$$\Phi_1(x) = Ce^{irx},\quad \Phi_2(x) = De^{irx},\quad i = (-1)^{1/2}\,, \tag{9}$$

where C and D are the arbitrary constants.

Substituting them into Eqs. (6) results in the following system of homogeneous algebraic equations:

$$[K_1\,r^2 + (k - I_1\,\omega^2)]C - kD = 0,\quad kC - [K_2\,r^2 + (k - I_2\,\omega^2)]D = 0, \tag{10}$$

for which non-trivial solutions exist in the case when the cardinal determinant of the system coefficient matrix is equal to zero. Expanding this determinant yields the following characteristic equation:

$$r^4 - [(I_1\,\omega^2 - k)K_1^{-1} + (I_2\,\omega^2 - k)K_2^{-1}]\,r^2 + \omega^2[I_1\,I_2\,\omega^2 - k(I_1 + I_2)](K_1\,K_2)^{-1} = 0. \tag{11}$$

Since the discriminant of the above biquadratic algebraic equation is positive, then it has two distinct real roots

$$\begin{aligned} r_{1,2}^2 = 0,5\{[(I_1\omega^2 - k)\,K_1^{-1} + (I_2\omega^2 - k)\,K_2^{-1}] &\pm ([(I_1\omega^2 - k)\,K_1^{-1} + (I_2\omega^2 - k)\,K_2^{-1}]^2 \\ &- 4\omega^2(K_1\,K_2)^{-1}[I_1\,I_2\,\omega^2 - k(I_1 + I_2)])^{1/2}\}. \end{aligned} \tag{12}$$

The roots r_1^2 and r_2^2 are both positive, when $\omega^2 > \omega_0^2$ ($\omega_0^2 = k(I_1^{-1} + I_2^{-1})$). Eq. (11) has the following four real roots as two pairs of distinct opposite numbers:

$$r_s = +k_1,\ -k_1,\ +k_2,\ -k_2, \tag{13}$$

where

$$\begin{aligned} k_{1,2} = \{0,5[(I_1\omega^2 - k)\,K_1^{-1} + (I_2\omega^2 - k)\,K_2^{-1}] &\pm 0,5([(I_1\omega^2 - k)\,K_1^{-1} + (I_2\omega^2 - k)\,K_2^{-1}]^2 \\ &- 4\omega^2(K_1\,K_2)^{-1}[I_1\,I_2\,\omega^2 - k(I_1 + I_2)])^{1/2}\}^{1/2}. \end{aligned} \tag{14}$$

In view of roots (14), the solutions (9) can be rearranged to a more useful alternative form by introducing the trigonometric functions instead of exponential ones.

Finally, the general mode shapes of vibration for shafts can be presented as follows

$$\begin{aligned} \Phi_1(x) &= \sum_{s=1}^{4} C_s\, e^{ir_s x} = \sum_{i=1}^{2} \Phi_{1i}(x) = \sum_{i=1}^{2}[A_i\sin(k_i\,x) + B_i\cos(k_i\,x)], \\ \Phi_2(x) &= \sum_{s=1}^{4} D_s\, e^{ir_s x} = \sum_{i=1}^{2} \Phi_{2i}(x) = \sum_{i=1}^{2} a_i\Phi_{1i}(x) = \sum_{i=1}^{2} a_i[A_i\sin(k_i\,x) + B_i\cos(k_i\,x)], \end{aligned} \tag{15}$$

where

$$a_i = (K_1 k_i^2 + k - I_1 \omega^2)k^{-1} = k(K_2 k_i^2 + k - I_2 \omega^2)^{-1}, \quad a_1 > 0, \quad a_2 < 0, \tag{16}$$

$$\Phi_{1i}(x) = A_i \sin(k_i x) + B_i \cos(k_i x), \quad \Phi_{2i}(x) = a_i \Phi_{1i}(x) = a_i[A_i \sin(k_i x) + B_i \cos(k_i x)]. \tag{17}$$

Then the free vibrations (5) of a double-shaft system are described by the expressions

$$\varphi_1(x,t) = T(t)\sum_{i=1}^{2}\Phi_{1i}(x) = [A\sin(\omega t) + B\cos(\omega t)]\sum_{i=1}^{2}[A_i\sin(k_i x) + B_i\cos(k_i x)],$$

$$\varphi_2(x,t) = T(t)\sum_{i=1}^{2}\Phi_{2i}(x) = [A\sin(\omega t) + B\cos(\omega t)]\sum_{i=1}^{2}a_i[A_i\sin(k_i x) + B_i\cos(k_i x)]. \tag{18}$$

Solving the boundary value problem the unknown constants A_i, B_i are determined. Substituting the mode shape functions $\Phi_1(x)$ and $\Phi_2(x)$ (15) into the transformed boundary conditions (2)

$$\Phi_1(0) = \Phi_2(0) = \Phi_1'(l) = \Phi_2'(l) = 0$$

gives a set of four homogeneous algebraic equations for the unknown constants

$$B_1 + B_2 = 0, \quad a_1 B_1 + a_2 B_2 = 0,$$

$$k_1 A_1 \cos(k_1 l) + k_2 A_2 \cos(k_2 l) = 0, \quad a_1 k_1 A_1 \cos(k_1 l) + a_2 k_2 A_2 \cos(k_2 l) = 0.$$

For the existence of its non-trivial solutions the cardinal determinant of the coefficient matrix of equations must vanish. This necessary condition leads to the following characteristic equation:

$$\cos(k_i l) = 0, \quad i = 1, 2. \tag{19}$$

From the above relation the unknown eigenvalues k_i can be calculated as

$$k_i = k_{in} = k_n = (n - 0.5)l^{-1}\pi, \quad n = 1, 2, 3, \ldots \tag{20}$$

The frequency equation of a vibration problem considered is obtained by transforming the relationship (14) and taking into account (20)

$$\omega^4 - [(K_1 k_n^2 + k) I_1^{-1} + (K_2 k_n^2 + k) I_2^{-1}]\omega^2 + k_n^2 [K_1 K_2 k_n^2 + k(K_1 + K_2)](I_1 I_2)^{-1} = 0. \tag{21}$$

This equation can be presented as

$$\omega^4 - (\Omega_{1n}^2 + \Omega_{2n}^2)\omega^2 + (\Omega_{1n}^2 \Omega_{2n}^2 - \Omega_0^4) = 0, \tag{22}$$

where $\Omega_{in}^2 = (K_i k_n^2 + k)I_i^{-1}, \quad \Omega_0^4 = \Omega_{10}^2 \Omega_{20}^2 = k^2 (I_1 I_2)^{-1}, \quad \Omega_{i0}^2 = kI_i^{-1}, \quad i = 1, 2.$

Since the discriminant of this biquadratic algebraic equation is positive, then the frequency equation (22) has two different, real, positive roots $\omega_{1,2n}^2$:

$$\omega_{1,2n}^2 = 0.5\{(\Omega_{1n}^2 + \Omega_{2n}^2) \mp [(\Omega_{1n}^2 - \Omega_{2n}^2)^2 + 4\Omega_0^4]^{1/2}\}, \qquad \omega_{1n} < \omega_{2n}. \tag{23}$$

Finally, the two infinite sequences of natural frequencies of the system are obtained

$$\omega_{1,2n}^2 = 0.5\{[(K_1 k_n^2 + k) I_1^{-1} + (K_2 k_n^2 + k) I_2^{-1}] \mp ([(K_1 k_n^2 + k) I_1^{-1}$$
$$+ (K_2 k_n^2 + k) I_2^{-1}]^2 - 4k_n^2 (I_1 I_2)^{-1}[K_1 K_2 k_n^2 + k(K_1 + K_2)])^{1/2}\}. \tag{24}$$

One can now formulate the time functions (8) and the natural mode shapes (17) corresponding to the two sequences of the natural frequencies ω_{in}

$$\Phi_{1in}(x) = \Phi_n(x) = \sin(k_n x), \quad \Phi_{2in}(x) = a_{in}\Phi_n(x) = a_{in}\sin(k_n x), \tag{25}$$

$$T_{in}(t) = A_{in}\sin(\omega_{in}t) + B_{in}\cos(\omega_{in}t), \tag{26}$$

where

$$a_{in} = (K_1 k_n^2 + k - I_1\omega_{in}^2)k^{-1} = k(K_2 k_n^2 + k - I_2\omega_{in}^2)^{-1} = \Omega_{10}^{-2}(\Omega_{1n}^2 - \omega_{in}^2) = \Omega_{20}^2(\Omega_{2n}^2 - \omega_{in}^2)^{-1}, \tag{27}$$

$$k_n = (n - 0,5)l^{-1}\pi, \quad \Phi_n(x) = \sin(k_n x), \quad i = 1,2, \quad n = 1,2,3,\ldots.$$

The mode shapes coefficients a_{in} (27) can be presented as follows

$$a_{1,2n} = 0,5\Omega_{10}^{-2}\left\{(\Omega_{1n}^2 - \Omega_{2n}^2) \pm [(\Omega_{1n}^2 - \Omega_{2n}^2)^2 + 4\Omega_0^4]^{1/2}\right\}, \tag{28}$$

$$a_{1n} > 0, \quad a_{2n} < 0, \quad a_{1n}a_{2n} = -I_1 I_2^{-1} = -\Omega_{10}^{-2}\Omega_{20}^2.$$

It is proved that the coefficient a_{1n}, dependent on lower natural frequency ω_{1n}, is always positive while a_{2n}, dependent on higher frequency ω_{2n}, is always negative.

Finally, the free vibrations of the system considered are described by the following formulae:

$$\varphi_1(x,t) = \sum_{n=1}^{\infty}\Phi_n(x)\sum_{i=1}^{2}T_{in}(t) = \sum_{n=1}^{\infty}\sin(k_n x)\sum_{i=1}^{2}[A_{in}\sin(\omega_{in}t) + B_{in}\cos(\omega_{in}t)],$$

$$\varphi_2(x,t) = \sum_{n=1}^{\infty}\Phi_n(x)\sum_{i=1}^{2}a_{in}T_{in}(t) = \sum_{n=1}^{\infty}\sin(k_n x)\sum_{i=1}^{2}a_{in}[A_{in}\sin(\omega_{in}t) + B_{in}\cos(\omega_{in}t)]. \tag{29}$$

The unknown constants A_{in} and B_{in} are determined from the assumed initial conditions (3) using the classical orthogonality condition of mode shapes of vibration [1-5]

$$\int_0^l \Phi_m(x)\Phi_n(x)\,dx = \int_0^l \sin(k_m x)\sin(k_n x)\,dx = c\delta_{mn}, \quad c = \int_0^l \Phi_n^2(x)dx = \int_0^l \sin^2(k_n x)dx = 0,5l,$$

where δ_{mn} is the Kronecker delta function: $\delta_{mn} = 0$ for $m \neq n$, and $\delta_{mn} = 1$ for $m = n$.

Solving the initial-value problem yields the following formulas making it possible to calculate the unknown constants [4,5,8]:

$$A_{1n} = (c_{1n}\omega_{1n})^{-1}\int_0^l [a_{2n}\omega_{10}(x) - \omega_{20}(x)]\sin(k_n x)\,dx,$$

$$A_{2n} = (c_{2n}\omega_{2n})^{-1}\int_0^l [a_{1n}\omega_{10}(x) - \omega_{20}(x)]\sin(k_n x)\,dx,$$

$$B_{1n} = c_{1n}^{-1}\int_0^l [a_{2n}\varphi_{10}(x) - \varphi_{20}(x)]\sin(k_n x)dx,$$

$$B_{2n} = c_{2n}^{-1}\int_0^l [a_{1n}\varphi_{10}(x) - \varphi_{20}(x)]\sin(k_n x)dx, \tag{30}$$

where

$$c_{1n} = -c_{2n} = (a_{2n} - a_{1n})c = 0,5(a_{2n} - a_{1n})l.$$

Free vibration problem of an elastically connected double-shaft system is finally solved.

4. Conclusions

The torsional vibration theory of an elastically connected complex double-shaft system is developed. This system is represented by a three-layered structure consisting of two concentric, cylindrical, circular, elastic shafts, in which the middle cylindrical layer is modelled as a Winkler elastic foundation. The motion of the system is described by a

coupled set of two non-homogeneous partial differential equations. The solutions of the free vibrations are formulated by the Fourier method of separation of variables. Solving the boundary value and initial-value problems the natural frequencies and natural mode shapes of vibration are found. The free vibrations of a double-shaft system are realized by two kinds of motions: synchronous vibrations ($a_{1n} > 0$) with lower frequencies ω_{1n} and asynchronous vibrations ($a_{2n} < 0$) with higher frequencies ω_{2n} ($\omega_{1n} < \omega_{2n}$).

References

1. S. Kaliski, *Vibrations and Waves in Solids*, IPPT PAN, Warsaw, 1966 (in Polish).
2. S.P. Timoshenko, D.H. Young, W. Weaver Jr., *Vibration Problems in Engineering,* Wiley, New York, 1974.
3. C.W. de Silva, *Vibration: Fundamentals and Practice*, CRC Press, London, 1999.
4. Z. Oniszczuk**,** *Vibration Analysis of Compound Continuous Systems with Elastic Constraints*, Publishing House of Rzeszów University of Technology, Rzeszów, 1997.
5. Z. Oniszczuk, *Transverse vibrations of elastically connected double-string complex system. Part I: free vibrations,* Journal of Sound and Vibration, **232** (2000) 355-366.
6. Z. Oniszczuk, *Transverse vibrations of elastically connected double-string complex system. Part II: forced vibrations,* Journal of Sound and Vibration, **232** (2000) 367-386.
7. Z. Oniszczuk, *Damped vibration analysis of an elastically connected complex double-string system,* Journal of Sound and Vibration, **264** (2003) 253-271.
8. Z. Oniszczuk, *Free longitudinal vibrations of an elastically connected double-rod system,* Proceedings of the XIIth Symposium on Dynamics of Structures, Rzeszów-Bystre. Scientific Works of Rzeszów University of Technology, Mechanics, **222** (65) (2005) 303-310.
9. Z. Oniszczuk, *Longitudinal vibrations of an elastically connected double-rod complex system. Part I: free vibrations*, Proceedings of the XXIInd Symposium „Vibrations in Physical Systems", Poznań-Będlewo, 2006, pp. 291-296.
10. Z. Oniszczuk, *Longitudinal vibrations of an elastically connected double-rod complex system. Part II: forced vibrations*, Proceedings of the XXIInd Symposium „Vibrations in Physical Systems", Poznań-Będlewo, 2006, pp. 297-302.
11. Z. Oniszczuk, *Longitudinal vibration analysis of an elastically connected double-rod system*, Proceedings of the XIth Scientific Conference „The Influence of Vibrations upon Environment", Cracow-Janowice, Cracow University of Technology Publishers, Technical Journal, Mechanics, (2007) (in press).
12. M.E. Drake, *The normal mode vibrations of a system of two elastically connected concentric cylinders,* M.Sc. Thesis, Loughborough University of Technology, 1972.
13. M.E. Drake, *The normal mode vibrations of a system of two elastically connected concentric cylinders*, Journal of Sound and Vibration, **31** (1973) 419-441.
14. M.P. Chandrasekharan, A. Ghosh, *Damping characteristics of elastic-viscoelastic composite shafts*, Journal of Sound and Vibration, **37** (1974) 1-15.
15. T. Irie, G. Yamada, Y. Muramoto, *The axisymmetrical response of a circular cylindrical double-shell system with internal damping*, Journal of Sound and Vibration, **92** (1984) 107-115.
16. T. Irie, G. Yamada, T. Tanaka, *Free vibration of a circular cylindrical double-shell system interconnected by several springs*, Journal of Sound and Vibration, **95** (1984) 249-259.
17. Z. Oniszczuk, *Free transverse vibrations of elastically connected simply supported double-beam complex system*, Journal of Sound and Vibration, **232** (2000) 387-403.
18. Z. Oniszczuk, *Free transverse vibrations of an elastically connected complex beam-string system,* Journal of Sound and Vibration, **254** (2002) 703-715.

THE DYNAMIC RESPONSE OF AN ELASTIC BACKGROUND
UNDER UNDETERMINED VARIABLE LOADS

Andrzej OSSOWSKI

Institute of Fundamental Technological Research, PAS

ul. Świętokrzyska 21, 00-049 Warszawa

826-12-81, (284), aossow@ippt.gov.pl

Abstract

The problem of Lagrange stability of an elastic background excited by undetermined variable loads is considered. A discrete model of the background with bounded excitations is studied. Applying optimal Lyapunov functions, upper bounds on the dynamic response of the background are estimated and interpreted in terms of rough sets. The described approach is useful to estimate vibration transmission in ground as well as to analyze vibration of a road surface or rail-track loaded by moving vehicles.

Keywords: dynamic response, elastic background, Lagrange stability, differential inclusion, rough set

Introduction

In road and rail-track engineering it is important to estimate the dynamic response of a background on variable loads due to moving vehicles. This enables to optimize the structural parameters at the design stage, in order to minimize undesired vibration of ground, road surface or rail tracks. To achieve this goal appropriate models of the background have to be applied. In modeling vehicle dynamics usually a simplified static background model composed of independent mass-less *Winkler springs* is applied as a functional part of the extended dynamical model of a vehicle suspension. The Winkler spring model is convenient but adequate to represent only soil support. More accurate description of a background composed of various materials such as sand or stones requires a dynamical model of the background.

Another drawback of a typical approach to the dynamical response of a background is that the response is usually calculated numerically for a particular excitation e.g. caused by a vehicle of a determined mass and velocity. However, since real loads are rarely uniquely determined, computer simulations are ineffective for studying such a model. To describe the system dynamics, undetermined excitations have to be included into the model and differential inclusions have to be applied instead of differential equations.

The main aim of this work is to solve the problem of Lagrange stability of a dynamical model of the background composed of interacting linear oscillators excited by undetermined bounded forces. There are some algebraic methods of theoretical qualitative analysis of such models [1]. In this work the analytical method of optimal Lyapunov functions is applied [2]. Assuming different types of non-stationary loads and applying appropriate differential inequalities, upper bounds on the dynamic response of the background are estimated and interpreted in terms of rough sets [2]. The described approach is useful to predict vibration of ground, road surface or rail-tracks loaded by moving road vehicles or trains.

1. A discrete model of the elastic background

A background as a physical object is usually a continuous dynamical system that can be modeled by partial differential equations. To build such a model it is necessary to have a detailed physical description of the background. However, in concrete situations we usually want only to estimate the dynamical response of the background on a class of exciting loads. Therefore it is convenient both from the theoretical and practical point of view to apply a discrete simplified phenomenological model that is independent on details of the physical nature of the background. In such a case parameters of the model have to be empirically identified.

In the physical model considered in this work, a horizontal background (e.g. a segment of the road surface or rail track) is divided into finite elements of the same length d and mass m. Each element, interacting with a rigid base and with fixed neighboring elements, can oscillate vertically. This means that the elastic background is modeled by the set of linear oscillators (representing subsequent finite elements of mass m) with attenuation P and stiffness coefficients Q, R, as is shown in Fig.1.
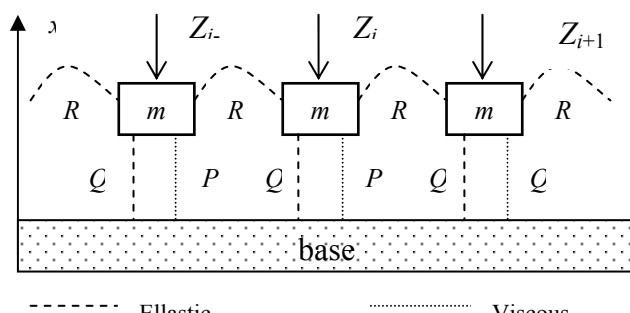
Fig.1. The block scheme of the normalized model of the background

It follows from the above assumptions that the dynamics of the background can be described by the following set of normalized equations:

$$\ddot{x}_1 + 2p\dot{x}_1 + qx_1 + r(x_1 - x_2) = z_1(t),$$
$$\ddot{x}_2 + 2p\dot{x}_2 + qx_2 + r(x_2 - x_3) + r(x_2 - x_1) = z_2(t),$$
$$\dots\dots\dots\dots\dots\dots\dots\dots\dots\dots\dots\dots\dots\dots\dots\dots\dots\dots\dots\dots\dots\dots\dots\dots \quad (1)$$
$$\ddot{x}_{n-1} + 2p\dot{x}_{n-1} + qx_{n-1} + r(x_n - x_{n-1}) + r(x_{n-1} - x_{n-2}) = z_{n-1}(t),$$
$$\ddot{x}_n + 2p\dot{x}_n + qx_n + r(x_n - x_{n-1}) = z_n(t),$$

where $p = P/m$, $q = Q/m$, $r = R/m$ and the time dependent excitations $z_i = Z_i/m$, $i=1,\dots,n$ of the corresponding oscillators represent non-stationary loads of the background. Since the loads are usually due to moving vehicles, it is rational to assume that the excitations are bounded i.e. there is an upper bound $\alpha > 0$ such that $\forall (t > t_0) \; |z_i(t)| \leq \alpha$, for $i = 1,2,\dots,n$. In other words the following relation should be satisfied.

$$\underset{t \geq t_0}{\forall} \; \mathbf{z} = (z_1,...,z_n) \in Z(\alpha) = \{(z_1,...,z_n) \in \underbrace{[0,\alpha] \times \cdots \times [0,\alpha]}_{n} \subset R^n\} . \tag{2}$$

Furthermore, since the excitations are usually unpredictable or undetermined exactly, the model (1) is in fact described by the corresponding set of differential inclusions that can be represented by the following more convenient matrix form [2]:

$$\dot{\mathbf{x}} \in \{\mathbf{Ax} + \mathbf{B}_1 z_1 + \cdots + \mathbf{B}_n z_n : \mathbf{z} = (z_1,...,z_n) \in Z(\alpha)\}, \tag{3}$$

where $\mathbf{x} = [y_1, \dot{y}_1,..., y_n, \dot{y}_n]^{\mathrm{T}}$ is the state vector of the system and the matrix $\mathbf{A}$ and linearly independent vectors $\mathbf{B}_i$, $i = 1,...,n$ are given by the following formulas:

$$\mathbf{A} = \begin{bmatrix} 0 & 1 & 0 & 0 & \cdots & \cdots & 0 & 0 \\ -(q+r) & -2p & r & 0 & 0 & \cdots & & 0 \\ 0 & 0 & 0 & 1 & 0 & \cdots & & 0 \\ r & 0 & -(q+2r) & -2p & r & 0 & \cdots & 0 \\ \vdots & \ddots & \ddots & \ddots & \ddots & \ddots & \ddots & \vdots \\ 0 & \cdots & \ddots & \ddots & \ddots & \ddots & \ddots & 0 \\ 0 & \cdots & \ddots & 0 & 0 & 0 & 0 & 1 \\ 0 & 0 & \cdots & 0 & r & 0 & -(q+r) & -2p \end{bmatrix}, \tag{4}$$

$$\mathbf{B}_i = [0, \delta_{1i}, 0, \delta_{2i},...,0, \delta_{ni}]^{\mathrm{T}}, i = 1,2,...,n. \tag{5}$$

The main aim of this work is to deduce certain dynamical properties of the model and particularly estimate its response to undetermined excitations $\mathbf{z}$.

2. Stability analysis of the model

Let us consider the problem of Lagrange stability of the model (3). Since the matrix $\mathbf{A}$ of the model is stable, there exist a positive definite matrix $\mathbf{S}$ such that the stability index

$$\gamma_0(\mathbf{S}) = -\sup_{\mathbf{x} \neq \mathbf{0}} \left[\frac{\mathbf{x}^{\mathrm{T}}\mathbf{SAx}}{\mathbf{x}^{\mathrm{T}}\mathbf{Sx}} \right] = -\sup_{\|\mathbf{x}\|_{\mathbf{S}} = 1} [\mathbf{x}^{\mathrm{T}}\mathbf{SAx}] \tag{6}$$

is positive. Appropriate matrices $\mathbf{S}$ can be taken as solutions of the matrix Lyapunov equation $\mathbf{A}^{\mathrm{T}}\mathbf{S} + \mathbf{SA} = -\mathbf{Q}$ for any positive definite matrix $\mathbf{Q}$. The condition $\gamma_0(\mathbf{S}) > 0$ means that the norm $\|\mathbf{x}\|_{\mathbf{S}} = \sqrt{\mathbf{x}^{\mathrm{T}}\mathbf{Sx}}$ of any solution $\mathbf{x}(t)$ of the equation

$\dot{\mathbf{x}} = \mathbf{A}\mathbf{x}$ decreases exponentially with the index $\gamma_0(\mathbf{S})$. This obviously means that the system (3) without excitations is globally asymptotically (exponentially) stable.

However, once the excitations are included into the model, it loses asymptotical stability. In such a case one can expect convergence of all system trajectories to a neighborhood X of the origin. In particular, any trajectory starting from X remains in X for any time i.e. X is the region of Lagrange stability of the system. It is clear that X can be interpreted as an estimate of the system response to the undetermined excitations $\mathbf{z}$.

In order to justify the above hypothesis and provide an estimate of the region X let us apply the second method of Lyapunov of stability analysis. It is easy to deduce that the stability index of the non-stationary system (3) should be calculated as follows [1], [2]:

$$\gamma(\mathbf{S},\alpha) = -\sup_{\mathbf{x}\neq\mathbf{0}}\ \sup_{\mathbf{z}\in Z(\alpha)}\left[\frac{\mathbf{x}^{\mathrm{T}}\mathbf{S}\mathbf{A}\mathbf{x}}{\mathbf{x}^{\mathrm{T}}\mathbf{S}\mathbf{x}} + z_1\frac{\mathbf{B}_1^{\mathrm{T}}\mathbf{S}\mathbf{x}}{\mathbf{x}^{\mathrm{T}}\mathbf{S}\mathbf{x}} + ... + z_n\frac{\mathbf{B}_n^{\mathrm{T}}\mathbf{S}\mathbf{x}}{\mathbf{x}^{\mathrm{T}}\mathbf{S}\mathbf{x}}\right]. \tag{7}$$

Let us reformulate the above optimality principle to the more convenient form, namely:

$$\gamma(\mathbf{S},\beta) = -\sup_{\mathbf{x}\neq\mathbf{0}}\ \sup_{\mathbf{w}\in W(\alpha)}\left[\frac{\mathbf{x}^{\mathrm{T}}\mathbf{S}\mathbf{A}\mathbf{x}}{\mathbf{x}^{\mathrm{T}}\mathbf{S}\mathbf{x}} + (w_1+\frac{\alpha}{2})\cdot\frac{\mathbf{B}_1^{\mathrm{T}}\mathbf{S}\mathbf{x}}{\mathbf{x}^{\mathrm{T}}\mathbf{S}\mathbf{x}} + ... + (w_n+\frac{\alpha}{2})\cdot\frac{\mathbf{B}_n^{\mathrm{T}}\mathbf{S}\mathbf{x}}{\mathbf{x}^{\mathrm{T}}\mathbf{S}\mathbf{x}}\right], \tag{8}$$

where $w_i = z_i - \alpha/2$, $i = 1,...,n$, $W(\alpha) = \{\mathbf{w} = [w_1...,w_n]: |w_i| \le \alpha/2,\ i = 1,...,n\}$. If all the transformed excitations w_i are assumed to be independent, then it follows from the above optimality criterion that the anti-optimal excitations are of the form:

$$\hat{w}_i(\mathbf{x}) = (\alpha/2)\cdot sign[\mathbf{B}_i^{\mathrm{T}}\mathbf{S}\mathbf{x}]. \tag{9}$$

Putting (9) into (8) one can obtain the following final formula for the stability index

$$\gamma(\mathbf{S},\frac{\alpha}{2c}) = -\sup_{\|\mathbf{x}\|_{\mathbf{S}}=1}\left[\mathbf{x}^{\mathrm{T}}\mathbf{S}\mathbf{A}\mathbf{x} + \frac{\alpha}{2c}\cdot\left(\left|\mathbf{B}_1^{\mathrm{T}}\mathbf{S}\mathbf{x}\right| + ... + \left|\mathbf{B}_n^{\mathrm{T}}\mathbf{S}\mathbf{x}\right|\right) + \frac{\alpha}{2c}\cdot(\mathbf{B}_1+...+\mathbf{B}_n)^{\mathrm{T}}\mathbf{S}\mathbf{x}\right]. \tag{10}$$

It can be noticed that the index (10) is a continuous and non-increasing function of the parameter $\varepsilon = \alpha/2c$ (see e.g. [1]). It is also clear that $\gamma(\mathbf{S},\varepsilon) \to \gamma_0(\mathbf{S}) > 0$ as $\varepsilon \to 0$ (and $\gamma(\mathbf{S},\varepsilon) \to -\infty$ as $\varepsilon \to +\infty$). Therefore, there is a unique critical value $\varepsilon_{\mathrm{cr}} = \varepsilon_{\mathrm{cr}}(\mathbf{S})$ such that $\gamma(\mathbf{S},0) = 0$, and $\gamma(\mathbf{S},\varepsilon) > 0\ (<0)$ for all $\varepsilon < \varepsilon_{\mathrm{cr}}\ (\varepsilon > \varepsilon_{\mathrm{cr}})$. It is clear that the critical parameter c determines the radius of the stability ellipsoid $X_{\mathbf{S}}(c) = \{\|\mathbf{x}\|_{\mathbf{S}} < c\}$ in the state space. Indeed, it follows from the necessary and sufficient stability condition $\varepsilon < \varepsilon_{\mathrm{cr}}(\mathbf{S})$ that the maximal radius c is equal to

$$c_{\max}(\mathbf{S}) = \frac{\alpha}{2\varepsilon_{\mathrm{cr}}(\mathbf{S})} \ . \tag{11}$$

This means that any trajectory $\mathbf{x}(t)$ of the system starting from the point $\mathbf{x}_0 \notin X_{\mathbf{S}}(c_{\max})$ (or $\mathbf{x}_0 \in X_{\mathbf{S}}(c_{\max})$) converges to (remains in) $X_{\mathbf{S}}(c_{\max})$. Thus the ellipsoid $X_{\mathbf{S}}(c_{\max})$ is the estimate of the Lagrange stability region of the system.

In order to obtain a useful estimate of the stability region let us apply the following estimate of the stability index (10)

$$\gamma(\mathbf{S}, \frac{\alpha}{2c}) \geq \widetilde{\gamma}(\mathbf{S}, \frac{\alpha}{2c}) = \gamma_0(\mathbf{S}) - \frac{\alpha}{2c}(\|\mathbf{B}_1\|_{\mathbf{S}} + ... + \|\mathbf{B}_1\|_{\mathbf{S}} + \|\mathbf{B}_1 + ... + \mathbf{B}_n\|_{\mathbf{S}}) . \tag{12}$$

The sufficient condition of stability $\widetilde{\gamma}(\mathbf{S}, c) > 0$ leads to the following estimate

$$c > \widetilde{c}_{\max}(\mathbf{S}, \alpha) = \alpha \cdot \frac{(\|\mathbf{B}_1\|_{\mathbf{S}} + ... + \|\mathbf{B}_1\|_{\mathbf{S}} + \|\mathbf{B}_1 + ... + \mathbf{B}_n\|_{\mathbf{S}})}{2\gamma_0(\mathbf{S})} . \tag{13}$$

The system (3) is stable (in the sense of Lagrange) in the ellipsoid $X_{\mathbf{S}}(\widetilde{c}_{\max})$.

<u>Example</u> Let us apply to the analysis the regular Lyapunov function of the matrix

$$\mathbf{S} = \begin{bmatrix} q+r & p & 0 & -r & 0 & \cdots & \cdots & 0 \\ p & 1 & 0 & 0 & 0 & \ddots & 0 & \vdots \\ 0 & 0 & q+2r & p & \ddots & -r & \ddots & \vdots \\ -r & 0 & p & 1 & \ddots & \ddots & 0 & 0 \\ 0 & 0 & \ddots & \ddots & \ddots & \ddots & 0 & -r \\ \vdots & \ddots & -r & \ddots & \ddots & \ddots & 0 & 0 \\ \vdots & 0 & \ddots & 0 & 0 & 0 & q+r & p \\ 0 & \cdots & \cdots & 0 & -r & 0 & p & 1 \end{bmatrix} \tag{14}$$

satisfying the following (Malkin) equation [2]:

$$\mathbf{A}^{\mathrm{T}}\mathbf{S} + \mathbf{S}\mathbf{A} = -2p\mathbf{S} . \tag{15}$$

In the sub-critical case $q > p^2$ and sufficiently small parameter r the matrix (14) is positive definite and represents a regular Lyapunov function of the system (3). Then the stability condition $\widetilde{\gamma}(\mathbf{S}, c) > 0$ gives the following estimate of the Lagrange stability region

$$\|\mathbf{x}\|_{\mathbf{S}} < c_{\max}(\mathbf{S}, \alpha) = \frac{\alpha}{2p}(\sum_{i=1}^{n}\|\mathbf{B}_i\|_{\mathbf{S}} + \left\|\sum_{i=1}^{n}\mathbf{B}_i\right\|_{\mathbf{S}}) = \frac{\alpha}{2p}(n + \sqrt{n}) = c_n . \tag{16}$$

It is important to note that estimate (16) is valid for independent (uncorrelated) excitations $\mathbf{z} = [z_1,\ldots, z_n]$. If the correlation (usually observed in the case of long railway vehicles) is taken into account, then better estimate can be obtained, namely:

$$\|\mathbf{x}\|_{\mathbf{S}} \le c_{\max}(\mathbf{S}, \alpha) = \frac{\alpha}{p}(\|\mathbf{B}_1 + \ldots + \mathbf{B}_n\|_{\mathbf{S}}) = \frac{\alpha}{p}\sqrt{n} \; . \qquad (17)$$

Moreover, it is clear that estimate (16) is also applicable when only $j<n$ excitations are active ($\ne 0$) at each time instant. This is usually the case for railway vehicles or relatively small car traffic. Then the discrete function $f(j) = j/n$ for $\|\mathbf{x}\|_{\mathbf{S}} \in [c_{j-1}, c_j)$, $j = 1,\ldots,n, (c_0 = 0)$ is simply the membership function representing the rough boundary of the Lagrange stability region of the system [2].

Conclusions

The results obtained in this work enable to estimate dynamical response of an elastic background excited by any undetermined and bounded loads e.g. those induced by moving vehicles. Moreover, the estimates (16), (17) can be easily generalized to the case of different bounds $\alpha_1,\ldots,\alpha_n$ for the corresponding excitations $z_i, i = 1,\ldots,n$. It is also easy to take into account square geometric nonlinearities of the ground reaction.

It is interesting to continue the presented qualitative approach to study resonance conditions for the elastic background loaded by moving vehicles. Since anti-optimal excitations (9) are *bang-bang*, the system (3) is a piece-wise linear system. It is easy to see that if the system (background) vibrates with an eigen-frequency ω_l, then the excitations (9) vibrate with the same frequency i.e. they ensure the resonance conditions. Such excitations can be induced for example by a multi-axis long (e.g. railway) vehicle moving with a critical speed. Indeed, if the distance between subsequent wheels of the vehicle coincides with the length of k finite elements in the model, then the critical speed of the vehicle coinciding with the ω_l – resonance is equal to $v_l = kd\omega_l/2\pi$.

There is the question of identification of the parameters p, q, r. It can be carried out independently or together with verification of the vehicle models in real circumstances.

References
1. Shahruz S.M., Lords T.R.C., Upper bounds on responses of linear systems under transient loads. Journal of Sound and Vibration **227**(4), 886-894, 1999.
2. A.Ossowski, *Estimation of dynamical response of structures on undetermined excitations*, XV Polish-Ukrainian Conference: Theoretical Problems of Civil Engineering, Warszawa, June 2007.

THE IMPACT RESPONSE OF AN AIRPLANE PNEUMATIC SUSPENSION

Andrzej OSSOWSKI

Institute of Fundamental Technological Research, PAS

ul. Świętokrzyska 21, 00-049 Warszawa

826-12-81, (284), aossow@ippt.gov.pl

Abstract

Pneumatic suspensions, because of their significant advantages in comparison to classical suspension systems containing mechanical springs and hydraulic attenuators, are widely applied in road and railway vehicles. They also seem to be applicable in airplanes due to their advantageous impact properties.

In this paper a simple one-wheel dynamical model of the pneumatic suspension is described. Impact properties of the model are studied in the context of the application in airplanes. Results of theoretical analysis and computer simulations are presented and compared with experimental data.

Keywords: impact response, pneumatic suspension

Introduction

Pneumatic suspensions of vehicles have significant advantages in comparison to classical suspension systems containing steel strings and hydraulic attenuators. Easily adjusted pneumatic devices make it possible to adopt a vehicle suspension to various loads, changing external conditions or user's specific expectations. That is why pneumatic suspensions have been widely applied in lorries and railway vehicles since many years [1], [2]. Recently, pneumatic suspension systems with control are installed in modern cars. They also seem to be applicable in airplanes. However, there are no detailed descriptions of models, theories and experimental data in this subject in the available literature.

Modern pneumatic suspensions are usually complex systems composed of air springs, controlled valves and a compressor. An appropriate control algorithm ensures effective reduction of vibration caused by stationary excitations and enables to achieve optimal compromise between the vehicle stability and the user's comfort. However, one of the important features of pneumatic devices is that a single pneumatic component without control can play the role of a spring and an attenuator simultaneously. This can be achieved for example in an open–cylinder–pneumatic (OCP) device. The typical OCP device is composed of a cylinder, piston and nozzle, as is shown in Fig.1. The working gas (air) compressed by the moving piston causes a nonlinear relation between the displacement of the piston and the reaction force due to the changing gas pressure while the gas flow through the nozzle ensures energy dissipation.

It is clear that an OCP device alone, without a compressor and controlled valves, cannot be applied in suspensions of road vehicles or trains. However, simplicity, reliability and relatively small weight of OCP devices as well as their specific dynamical properties

(e.g. hardening stiffness characteristics) cause that they are an attractive alternative for steel springs and hydraulic attenuators as the main components of airplane suspensions.

In this paper a simple one-wheel dynamical model of the pneumatic suspension with an OCP device is described. Impact properties of the model are studied in the context of the application in airplanes. Results of theoretical analysis and computer simulations are presented and compared with experimental data.

1. A model of a one-wheel OCP suspension

Let us consider the open-cylinder-pneumatic device composed of a cylinder, piston and nozzle as is shown in figure 1. In order to study impulse properties of the device as the main component of the pneumatic suspension of an airplane, we assume that a mass m (representing the half body of the landing airplane) fall down with the speed v_0 on the piston leader. This initializes compression of the working gas (air) in the cylinder and gas flow through the nozzle. Since the gas compression is rapid and the impulse response of the device is of our interest, it is justified to assume the adiabatic (or in general polytropic) process in the physical model of the described device.
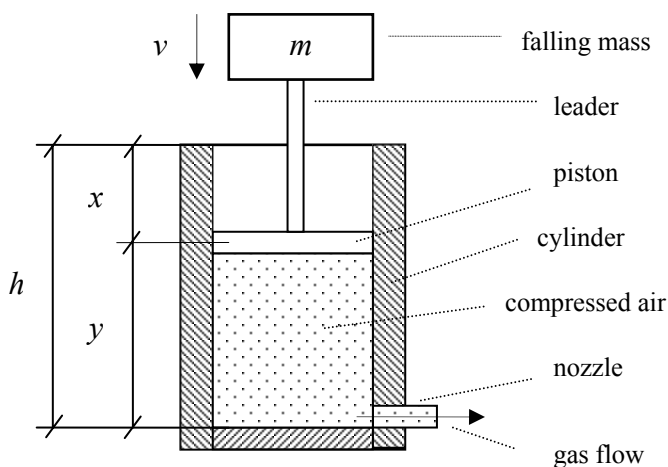
Fig.1. The setup of the open-cylinder-pneumatic device

To describe the dynamics of the device let us also introduce the following notations:

V_0, V – initial and actual cylinder volume, S – section area of the cylinder, n_0, n – initial and actual mol gas contents in the cylinder, h, y – initial and actual position of the piston ($V_0 = hS$, $V = yS$), x – piston displacement ($x = h - y$), v_0, $v = \dot{y}$ – initial and actual velocity of the piston, p_0, p – atmospheric pressure and actual gas pressure in the cylinder, T_0, T – ambient temperature and temperature in the cylinder (^{0}K), η – fixed conductance coefficient of the gas flow through the nozzle.

The system dynamics can be described in terms of the four time dependent functions, namely: x, p, n, T. Appropriate equations (algebraic and differential) deduced directly from the assumptions and physical reasons are listed below.

The equations of motion of the falling mass:
$$m\ddot{x} = mg - (p - p_0)S, \tag{1}$$
The equation of the gas flow
$$dn/dt = -\eta \cdot (p - p_0) \tag{2}$$
The state equation for the ideal gas
$$pV = nRT, \tag{3}$$
The equation of polytropy (with the exponent $\kappa > 1$)
$$pV^{\kappa} = \text{const}, \tag{4}$$

Equation (1), describing the motion of the mass m, is a consequence of the second Newton's dynamical principle. The two main forces are taken into account, namely: gravitation and the force caused by the gas pressure. Equation (2) is based on the assumption that of the gas flow is proportional to the difference between the pressure in the cylinder and the atmospheric pressure. This means that nonlinear effects (e.g. turbulences of the gas flow) are neglected in this model. Moreover, air is assumed to be the ideal gas (Equation (3)) and the general polytorpic process of the gas compression with the exponent $\kappa > 1$ is assumed (Equation (4)).

Taking into account the gas flow one can easily obtain the following equations

$$m\ddot{x} = mg - \left[p_0 \frac{n}{n_0} \left(\frac{h}{h-x} \right)^{\kappa} - p_0 \right] S, \tag{5}$$

$$\dot{n} = -\eta \left[p_0 \frac{n}{n_0} \left(\frac{h}{h-x} \right)^{\kappa} - p_0 \right] \tag{6}$$

The above equations can be finally simplified to the following dynamical model:

$$\ddot{y} = c \frac{n}{y^{\kappa}} - a, \quad \dot{n} = -b \frac{n}{y^{\kappa}} + d, \tag{7}$$

where

$$a = g + \frac{p_0 S}{m}, \ b = \eta \frac{p_0 h^{\kappa}}{n_0}, \ c = \frac{p_0 S}{m}, \ d = \eta \cdot p_0. \tag{8}$$

The non-linear system of differential equations (7), uniquely determined by four parameters (8), is the dynamical model of the pneumatic suspension under consideration.

2. Qualitative analysis of the model

The system of differential equations (7) is interesting from the theoretical viewpoint but difficult to solve and analyze because of the transcendent non-linearity with the exponent $\kappa \in (1,2)$. In particular solutions of (7) cannot be found exactly. However, it is possible to prove certain basic features of the model without solving (7) coinciding with rational predictions based on physical considerations.

First of all, let us notice that the initial acceleration of the piston $\ddot{y}(0)$ is equal to $-g$. However, since the gas pressure p tends to infinity as $y \to 0$ and $\eta = 0$, there must exist a minimal piston position $y_{min} > 0$ at which the sign of the piston speed changes. Similarly, there must exist the maximal piston position y_{max} achievable after the piston reverse.

Rational and physical reasons indicate three types of impulse responses of the pneumatic suspension based on the OCP device for different flow conductance η of the nozzle, as is shown in Fig.2.
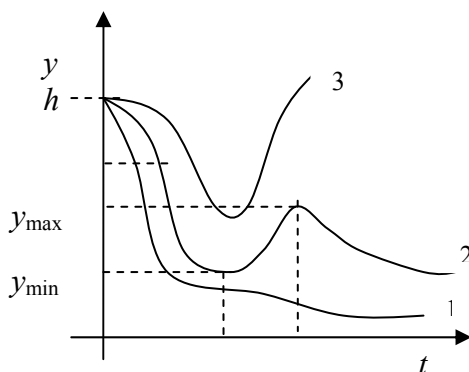
Fig.2. Typical impact responses of the pneumatic suspension

For higher nozzle conductance ($\eta = \eta_1$) the pressure of the compressed gas in the cylinder cannot increase significantly (too soft reaction), to ensure a considerable inverse response. Therefore the piston tends monotonically to its lowest position ($x=h$ or $y=0$). Conversely, for lower conductance ($\eta = \eta_3$) the gas flow is too small to change significantly the qualitative properties of the impulse process of the OCP device in comparison to a closed cylinder pneumatic device (CPD) (i.e. air spring). This results in an undesired inverse response (due to the quickly hardening characteristics of the device) exciding the height h representing the initial piston position (too hard reaction).

It is clear that there is a catastrophic change (bifurcation) of qualitative properties of the impulse response (of the type 1 and 2) for certain critical value $\eta^* \in (\eta_1, \eta_2)$. In order to satisfy basic requirements $y_{min} > 0$, $y_{max} < h$ and achieve significant energy dissipation, certain optimal intermediate value of the conductance $\eta \geq \eta^*$ has to be chosen.

3. Mathematical analysis of the model

The impact response of the model can be studied without the knowledge of general solution to (7). Indeed, it is easy to derive from (7) the following approximate form of the impact response of the system:

$$y(t) \approx h - v_0 t - \frac{g}{2} t^2 + \frac{1}{6} D t^3 - \frac{1}{24} E t^4 , \qquad (9)$$

valid for small time t, where

$$D = \kappa \frac{p_0 S}{h^{\kappa+1}} \frac{n_0 v_0}{m} = \kappa \frac{p_0^2 S^2}{h^{\kappa}} \frac{v_0}{mRT_0} > 0 , \qquad (10)$$

$$E = \kappa \frac{p_0^2 v_0 S}{m h^{\kappa+1}} \left(\eta - \frac{V_0}{RT_0 v_0} \left[g + (\kappa+1) \frac{v_0^2}{h} \right] \right) = \kappa \frac{p_0^2 v_0 S}{m h^{\kappa+1}} \left(\eta - \eta_0 \right). \qquad (11)$$

The higher order terms in (9) with the coefficients D, E (that are due to the mechanical reaction of compressed air in the cylinder) are sufficient to describe basic qualitative properties of the pneumatic device under study.

It is obvious that for sufficiently small values of the parameter η, namely for

$$\eta < \frac{V_0}{RT_0 v_0} \left[g + (\kappa+1) \frac{v_0^2}{h} \right] = \eta_0 \qquad (12)$$

the coefficient E is negative and the response of the system is of the form 3 in Fig.2. Similarly, for sufficiently large η the response (9) is of form (1) in Fig.2. The occurrence of the wavy response of form 2 is dependent on the existence of positive squares of the following third order equation:

$$\dot{y}(t) = -v_0 - gt + \frac{1}{2} D t^2 - \frac{1}{6} E t^3 = 0 . \qquad (13)$$

It is clear that the two positive squares of (13) correspond to y_{min}, y_{max} and can be analytically derived. Similarly, the catastrophic value $\eta*$ (for which the qualitative change 1 => 2 occurs) can be determined from the condition $y_{min} = y_{max}$.

Having in mind practical applications of the described device, it is also important to determine maximal acceleration of the falling mass m. Since the transient acceleration is given by the following formula:

$$\ddot{y}(t) = -g + Dt - \frac{1}{2} E t^2 = 0 , \qquad (14)$$

it reaches its maximal value $\ddot{y}_{max} = -g + \frac{D^2}{2E} > 0$ for $t = \frac{D}{E}$. It is clear that the maximal acceleration should be as small as possible. Therefore, in designing of OCP devices and their parametric optimizations it can be applied the criterion of minimizing the acceleration peak with constraints $y_{min} > 0$ and $y_{max} < h$.

4. Experiments and Computer simulation of the impact response

In order to verify results of qualitative and theoretical analysis the model of a real OCP device with the parameters: h=0.25[m], S= π (0.065[m])^2/4, the nozzle of adjusted conductance $\eta > 0$ and the mass m=15 [kg] falling from the height of 0.5[m] has been considered. On this basis the parameters a, b, c, d of the model have been calculated.

Computer simulations have been carried out. It has been proved that an appropriate choice of the parameters κ, η enables to obtain the results of simulations coinciding with empirical data (for example about 0.2m maximal piston displacement reached in 0.15s after the beginning of the impact) obtained from laboratory experiments with the real OCP device. In particular, the thermodynamic parameters κ = 1.4, corresponding to adiabatic gas process, has proved to be optimal.

5. Conclusions

The described mathematical model of the OCP device renders with an acceptable accuracy the impact response of the real pneumatic device with respect to its quantitative properties while qualitative properties of the device have proved to be suitable for application in modern airplane pneumatic suspensions. In particular, it has been shown that satisfactory energy dissipation can be achieved for a properly adjusted conductance of the nozzle.

The optimal exponent κ of the assumed polytrophic gas process has proved to be about the adiabatic value 1.4. However, this result is valid only for relatively short time in comparison to thermal inertness of the pneumatic device. Thus the described model should be improved in order to describe the process of multi-impact landing. Namely, the heat flow through the cylinder body should be taken into account.

It is possible to generalize the presented studies to the pneumatic suspension with a controlled valve (instead of the nozzle) in order to improve attenuation of vibration induced by the impact excitation. It would be also valuable to study stability of an extended dynamical model of the landing airplane with two independent wheel-sets.

References

1. Docquier-N; Fisette-P; Jeanmart-H, *Multiphysic modelling of railway vehicles equipped with pneumatic suspension*, Vehicle System Dynamics, 45(6): 505-24, June 2007.
2. Wang Yun chao; Gao Xiu hua; Guo Jian hua; Zhang Chun qiu, *Research on virtual prototype of hydro-pneumatic suspension*, Journal of System Simulation, 18(8): 2183-6, Aug. 2006.

INFLUENCE OF THE PIEZOELECTRIC FORCE ON VIBRATIONS OF A TWO-ROD COLUMN

Jacek PRZYBYLSKI, Krzysztof SOKÓŁ

Częstochowa University of Technology
Dąbrowskiego 73 42 200 Częstochowa, Poland
phone number: 034 325 06 32, *e-mail*: jacek.pr@imipkm.pcz.czest.pl

Abstract

This study details the investigation of the non-linear vibrations of a column consisted of two rods, one of which is made of piezoceramic material. The actuator, possessing its flexural stiffness is discretely attached to the main carrying rod. The role of the piezoelectric force generated by the actuator is to moderate the flexural displacement of the column which arises due to an unintensional eccentricity of the external load. The piezoelectric force influences also the natural frequency of the system, which tends to zero for the growing values of the external load.
Keywords: piezoceramic actuator, non-linear system, perturbation method, vibration frequency

Introduction

Piezoelectric materials are widely used in the manufacture of elements responsible for controlling the dynamic or static responses of structures. This development is a direct result of the applied research done in many academic and industrial development centres. The majority of studies have concentrated on the active vibration control of beams and columns, and the shape control of such structures. The problem of buckling enhancement and the flutter capacity of columns has been studied less extensively. Thompson and Loughlan [1] examined experimentally the flexural buckling control of composite cantilever column strips using piezoceramic actuators surface bonded at their mid-heights on both sides of a column. By applying a controlled voltage to the piezoactuators, the lateral deflection caused by the external load was removed, and the column was forced to behave in a straight manner. This could be done because the actuators received an equal but opposite electric field producing tensile and compressive strains. An alternative way of increasing the critical load capacity for columns with different boundary conditions and identically mounted piezoelectrics was considered theoretically by Wang [2]. Here the actuators received an equal field, in both magnitude and sign, to induce the tensile force. It was shown that proper localisation of the piezoelectric layers and an optimal applied voltage could enhance the buckling capacity effectively. Attaching two piezoelectric layers to both sides of a structure not only increases the flexural stiffness locally but also affects the distribution of the mass per unit length along the system, which in turn influences the respective governing lateral vibration equation. In a lot of investigations, the actuators are assumed to be perfectly bonded which means that the bonding layer is so thin that the shear of the layer can be

neglected. The effect of through-width delamination on the vibration characteristics of laminated beams with piezoactuators was studied by Tylikowski [3].

Piezoelectric ceramic linear actuators are produced in a great variety of shapes like bars, tubes, plates, rings as well as different dimensions and possible load range, which reaches 100 kN and even more. Their mechanical properties, especially high Young's modulus, density comparable to constructional materials and maximum compression strength, qualify such actuators to be separate independent parts of engineering structures. This idea was popularised by Chaudhry and Rogers [4] who implemented the concept when considered the flexural and shape control of a simply supported beam with an induced strain actuator attached at two discrete points. It was shown theoretically and experimentally in the paper that the increase in actuator authority achieved by offsetting actuator depended on the beam-actuator thickness and modulus of elasticity ratio.

1. Problem formulation

Most engineering structures are characterised by geometrical imperfections of shapes as a result of inaccurate assembling or quality of manufacturing. It is also practically impossible to achieve precise axial loading of any structure. It is assumed in this work that the main carrying rod of the column is unintentionally eccentrically loaded with eccentricities e_1 and e_2 as it is shown in Fig. 1. This results in initialising the flexural displacements going to large values with the increase the external load. As a counteracting remedy it is proposed an application of an additional piezoceramic rod generating the piezoceramic force and discretely attached with an offset distance denoted by d. The natural vibrations of the system in relation to its static curvilinear shape are influenced by the induced piezoforce also.
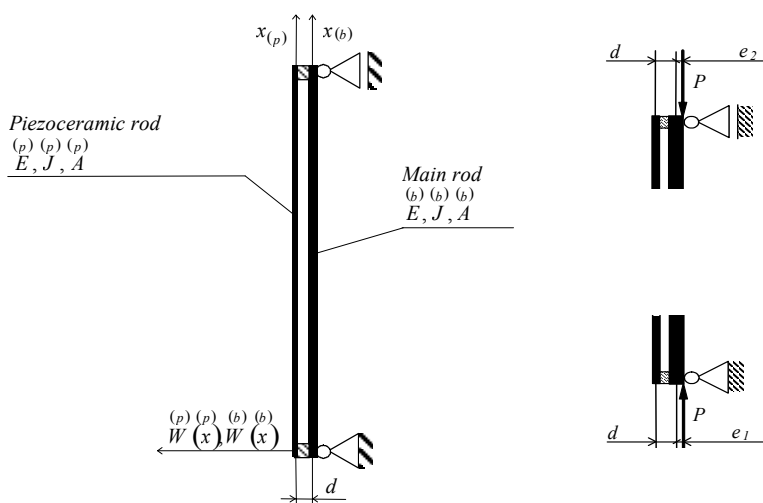

Fig. 1. Scheme of the column

1.1. Piezoelectric force

To formulate the problem of the natural vibrations of the structure, the internal axial forces resulting from the external force P and the piezoelectric force F must be derived. The governing equations for establishing the internal force distribution are obtained by taking the first variation of the total potential energy of the system and setting it to zero. The potential energy of the system can be presented as follows:

$$\Pi = \frac{1}{2}\int_{A_b}\overset{(b)}{\sigma_x}\,\overset{(b)}{\varepsilon_x}\,dA_b + \frac{1}{2}\int_{A_p}\overset{(p)}{\sigma_x}\,\overset{(p)}{\varepsilon_x}\,dA_p - \frac{1}{2}\int_{A_p}D_z\,\overset{(p)}{E_f}\,dA_p \tag{1}$$

where:

- the normal stresses in the particular rods are defined as

$$\overset{(b)}{\sigma_x} = E_b\,\overset{(b)}{\varepsilon_x}\,, \qquad \overset{(p)}{\sigma_x} = E_p\,\overset{(p)}{\varepsilon_x} - e_{31}E_f\,,$$

- the electric displacement D_z caused by the electric field E_f applied to the actuator is expressed as

$$D_z = e_{31}\,\overset{(p)}{\varepsilon_x} + \xi_{33}E_f\,, \tag{3}$$

- the non-linear von Karman strain-displacement relations are as follows

$$\overset{(b)}{\varepsilon_x}(x_b) = \frac{dU_b}{dx_b} - z\frac{d^2W_b}{dx_b^2} - \frac{1}{2}\left(\frac{dW_b}{dx_b}\right)^2, \qquad \overset{(p)}{\varepsilon_x}(x_p) = \frac{dU_p}{dx_p} - z\frac{d^2W_p}{dx_p^2} - \frac{1}{2}\left(\frac{dW_p}{dx_p}\right)^2 \tag{4}$$

and e_{31}, ξ_{33} stand for the piezoelectric and permittivity coefficients, respectively, E_p and E_b are the Young's modulus of piezo and main rod materials, $U(x)$ and $W(x)$ are the longitudinal and lateral displacements, respectively.

Performing necessary variational and integration operations one obtains the set of two differential equations and associated boundary conditions describing the discussed problem.

$$E_b J_b \frac{d^4W_b(x_b)}{dx_b^4} - S_b \frac{d^2W_b(x_b)}{dx_b^2} = 0\,, \qquad E_p J_p \frac{d^4W_p(x_p)}{dx_p^4} + (S_p - F)\frac{d^2W_p(x_p)}{dx_p^2} = 0 \tag{5}$$

where

$$S_b = -E_b A_b\left(\frac{dU_b(x_b)}{dx_b} + \frac{1}{2}\left[\frac{dW_b(x_b)}{dx_b}\right]^2\right), \qquad S_p = E_p A_p\left(\frac{dU_p(x_p)}{dx_p} + \frac{1}{2}\left[\frac{dW_p(x_p)}{dx_p}\right]^2\right)$$

and $F = be_{31}V = S_p - S_b$

The boundary conditions are:

$$W_b(0) = W_p(0) = W_b(l) = W_p(l) = 0 \,,$$

$$W_b^I(x_b)\Big|_{x_b=0} = W_p^I(x_p)\Big|_{x_p=0}\,, \quad W_b^I(x_b)\Big|_{x_b=l} = W_p^I(x_p)\Big|_{x_p=l} \tag{6}$$

$$E_b J_b W_b^{II}(x_b)\Big|_{x_b=0} + E_p J_p W_p^{II}(x_p)\Big|_{x_p=0} = P_w d \pm P e_1 \,,$$

$$E_b J_b W_b^{II}(x_b)\Big|_{x_b=l} + E_p J_p W_p^{II}(x_p)\Big|_{x_p=l} = P_w d \pm P e_1 \,,$$

$$U_b(0) = U_p(0) = 0 \,, \; U_b(l) = U_p(l) - W_b^I(x_b)\Big|_{x_b=0} d + W_b^I(x_b)\Big|_{x_b=l} d$$

On the basis of the performed solution a computer code was prepared for calculation the relation between the axial internal forces in both rods resulting from the external load P and the piezoelectric force F.

1.2. Natural vibrations

The problem of the natural vibrations of the system is described by two pairs of equations having the following non-dimensional form:

$$\frac{\partial^4 \widetilde{w}_i(\xi,\tau)}{\partial \xi^4} + k_i(\tau) \frac{\partial^2 \widetilde{w}_i(\xi,\tau)}{\partial \xi^2} + \omega_i^2 \frac{\partial^2 \widetilde{w}_i(\xi,\tau)}{\partial \tau^2} = 0 \tag{7}$$

where

$$k_i(\tau) = -\lambda_i \left[\frac{\partial u_i(\xi,\tau)}{\partial \xi} + \frac{1}{2}\left(\frac{\partial \widetilde{w}_i(\xi,\tau)}{\partial \xi} \right)^2 \right], \quad (i=1,2)$$

To solve the problem, by using the perturbation method, the transversal ($\widetilde{w}_i(\xi,\tau)$) and axial ($u_i(\xi,\tau)$) displacements, the non-dimensional axial force ($k_i(\tau)$) and the natural frequency (ω_i) are expanded into exponential series with respect to the amplitude parameter ε:

$$\widetilde{w}_i(\xi,\tau) = w_{i0}(\xi) + \sum_{j=1}^{N} \varepsilon^j \widetilde{w}_{ij}(\xi,\tau) + O(\varepsilon^{N+1})\,,$$

$$u_i(\xi,\tau) = u_{i0}(\xi) + \sum_{j=1}^{N} \varepsilon^j u_{ij}(\xi,\tau) + O(\varepsilon^{N+1}) \tag{8}$$

$$k_i^2(\tau) = k_{i0}^2 + \sum_{j=1}^{N} \varepsilon^j k_{ij}^2(\tau) + O(\varepsilon^{N+1})\,, \quad \omega_i^2 = \omega_{0i}^{\,2} + \sum_{n=1}^{N} \varepsilon^j \omega_{ij}^{\,2} + O(\varepsilon^{N+1})$$

By introducing equations (8) into equations of motion and axial force and then equating the terms of respective ε exponents to zero, one obtains an infinite set of equations of motion and longitudinal force. Those equations are associated by the sets of boundary conditions adequate to each power of the amplitude parameter ε. The solution of two

first pair of equations (for ε^0 and ε^1) gives the opportunity to study the influence of the piezoelectric force on the vibration frequency.

2. Results of numerical calculation

Exemplary numerical results, presented in Fig. 2, for columns with different configurations and ways of loading, show courses of the non-dimensional longitudinal forces k_{i0} for ascending values of the external force p up to point C where divergence instability takes place. In Fig. 2a, the courses concern the case without piezoforce and in Fig. 2b they are drawn for two opposite values of the non-dimensional force f. The curves, on which points A and C are placed, are called the buckling envelops. For buckling envelopes drawn in the dimensionless coordinate system as in Fig. 2, the critical points C are placed along the straight line inclined at an angle of $\pi/4$. At these points the following relation holds $k_{10} = k_{20} = p_c$. Buckling phenomenon of two-rod columns is also determined by the axial rigidity ratio E_1A_1/E_2A_2. This ratio sets the location of point A, because they are placed on the straight line OA inclined at an angle $\alpha = arc\,ctg(\mu E_1A_1/E_2A_2)$. Between points A and C the system even when axially loaded applies curvilinear equilibrium shape. Any load eccentricity or the piezoforce disturbs the courses of the internal axial forces as it is shown in Fig.2.
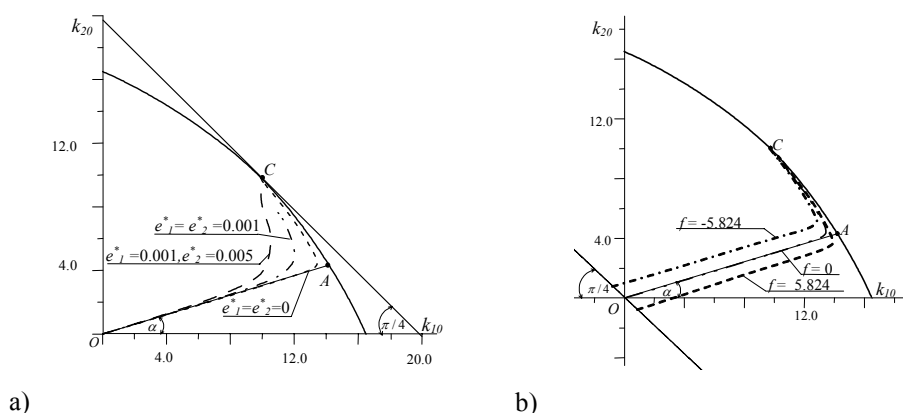
Fig. 2. Change of longitudinal forces for differently loaded and supported two-rod column without piezoforce (a) and with the action of piezoforce (b)

Fig. 3 shows the natural frequency curves obtained for an eccentrically loaded column with and without the participation of the piezoforce. As it is shown, the piezoforce affects the natural frequency but does not modify the value of the critical force. The critical force is established at the level at which the frequency curve crosses the p-axis. In Fig. 4 the influence of the piezoelectric force on the column deflection for the established value of the external load is presented. The column vibrates in regard to those curvilinear static shapes. Induction of the force $f = 2.72$ diminishes the maximal

deflection of the main rod about three times in regard to the case when $f = 0$. The change in frequency is not so significant and not greater then 11%.
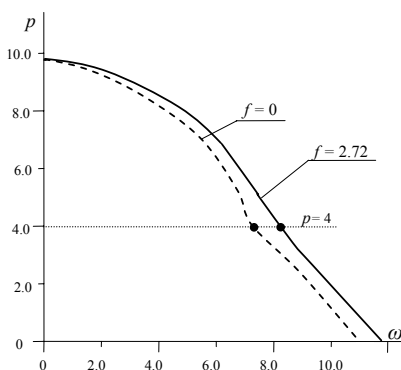
Fig. 3. Effect of the piezoelectric force on the natural vibration curves ($d^* = 0.001$, $e^*_1 = e^*_2 = 0.01$, μ=0.3)
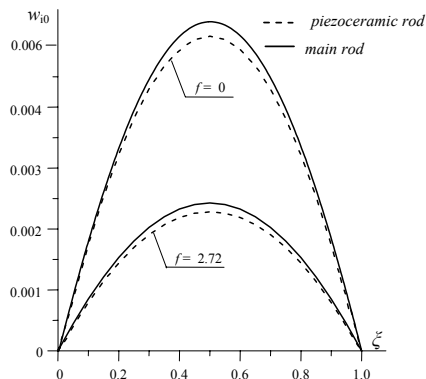
Fig. 4. Transversal rods displacement for the external load $p = 4$ and different piezoelectric force ($d^* = 0.0001$, $e^*_1 = e^*_2 = 0.01$, μ=0.3)

3. Conclusions

A formulation based on the variational principle for the analysis of the role of the piezoelectric force for the static and dynamic responses of a column with an additional piezoceramic rod was presented. It was demonstrated that a piezoceramic rod could be applied to tune the natural frequencies and the transversal displacement of an eccentrically loaded column.

Acknowledgments

References

1. Thompson S., Loughlan J. *The active buckling control of some composite column strips using piezoceramic actuators*. Composite Structures 32 (1995) 59-67.
2. Wang Q. *On buckling of column structures with a pair of piezoelectric layers*. Engineering Structures 24 (2002) 199-205.
3. Tylikowski A. *Effects of piezoactuator delamination on the transfer functions of vibration control systems*. International Journal of Solids and Structures 38 (2001) 2189-2202.
4. Chaudhry Z., Rogers C.A. *Enhancing induced strain actuator authority through discrete attachment to structural elements*. AIAA Journal 31 (1993) 1287-1292.

THE DYNAMIC STABILITY OF BEAMS WITH STEP CHANGES IN CROSS-SECTION

Wojciech SOCHACKI

Institute of Mechanics and Machine Design Foundations,
Częstochowa University of Technology,
ul. Dąbrowskiego 73 , 42–200 Częstochowa
Tel. (048)34 3 250 628, e-mail sochacki@imipkm.pcz.czest.pl

Summary

The influence of step changes in cross-section of beams with different boundary conditions on their dynamic stability was investigated in the paper. The change in the cross-sections took place in an optional location along the beam length. The investigated beams were axially loaded by a force in the form $P(t) = P_0 + S\cos \nu t$. The problem of dynamic stability was solved by applying the mode summation method. The obtained Mathieu equation allowed the dynamic stability of tested systems to be analysed. The analysis relied on testing the influence of step changes in beam cross-sections and their locations on the value of coefficient b in the Mathieu equation. The considered beams were treated as Euler- Bernoulli beams.

keywords : dynamic stability, Mathieu equation, eigenfunctions, beams.

1. Introduction

The research on beam or column dynamics with step changes in cross-sections have been carried out for many years finding justification in their application as parts of machines and equipment. The detailed analysis of fundamental frequency and higher modal frequencies was carried out by Jang and Bert [1,2]. They investigated the influence of step changes in beam sections on their natural frequency for different types of boundary conditions. Naguleswaran [3] presented the results of research on the frequency of an elastically supported Euler-Bernoulli beam with up to three step changes in cross-section. Kukla and Zamojska [4] gave the solution to natural frequency of axially loaded beam with step changes in cross-section. The frequency equation was obtained applying the Green function. Repeated research on the dynamic stability of the beam was mostly applied to the beams with a uniform cross-section. The authors considered an influence of boundary conditions as well as various type of input function on the stability of the systems. Iwatsubo *et al.*[5] analysed the stability regions for the columns loaded by periodical axial force for four typical cases of the boundary conditions. Only a few papers paid attention to an analysis of beams with step changes in the cross-sections taking into account dynamic stability of the beams. For example, Aldraihem and Baz [6] considered dynamic stability of the beams with step changes in the cross-sections under moving loads.

This paper takes into account beams with step changes in the cross-sections at different types of boundary conditions (pinned-pinned P-P and clamped-pinned C-P). Change in the cross-sections took place in an optional place on the beam length. The beams were loaded by $P(t) = P_0 + S\cos \nu t$ force. The considered beams were treated as Bernoulli –

Euler beams. The problem of dynamic stability was solved using the mode summation method. Applied research procedure allowed to describe the dynamics of tested systems with the use of the Mathieu equation. The influence of step changes in the cross-sections of the beams and its position along the beam length on the value of coefficient b in the Mathieu equation was investigated. In this way the possibility of a loss in dynamic stability by the investigated systems was determined.

2. Mathematical model of beam vibrations

A scheme of the considered beams is presented in Fig. 1. Analysis of the solution was carried out for the pinned-pinned beam (P-P Fig. 1.). The vibration equation for two parts of a beam is known and has the following form:

$$E_i J_i \frac{\partial w_i^4(x_i,t)}{\partial x_i^4} + P(t)\frac{\partial w_i^2(x_i,t)}{\partial x_i^2} + \rho_i A_i \frac{\partial^2 w_i(x_i,t)}{\partial t^2} = 0 \qquad (1a,b)$$

where : $P(t) = P_0 + S\cos\nu t$, ν - forcing frequency,
ρ_i – density, A_i – cross-section area, $i = 1,2$ i-th part of the beam
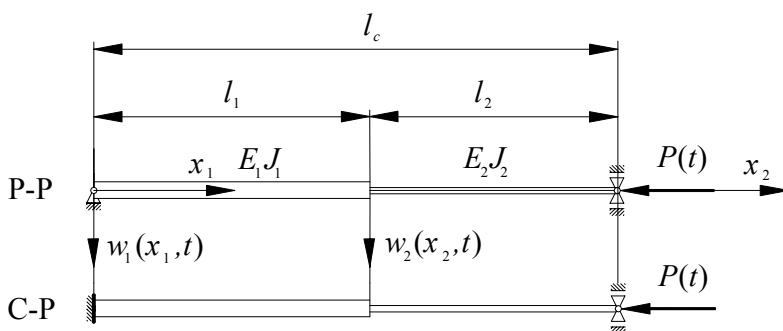
Fig. 1. Models of the beams with step changes in the cross-sections and various boundary conditions: P-P pinned-pinned, C-P clamped-pinned.

Equation (1) is accompanied by the following boundary conditions:

$$w_1(0,t)=0, \quad w_2(l_2,t)=0, \quad w_1^{II}(0,t)=0, \quad w_2^{II}(l_2,t)=0 \qquad (2a\text{-}d)$$

$$E_1 J_1 w_1^{III}(l_1,t) + P(t)w_1^{I}(l_1,t) - E_2 J_2 w_2^{III}(0,t) - P(t)w_2^{I}(0,t) = 0 \qquad (2e)$$

$$w_1(l_1,t)=w_2(0,t), \quad w_1^{I}(l_1,t)=w_2^{I}(0,t), \quad E_1 J_1 w_1^{II}(l_1,t)=E_2 J_2 w_2^{II}(0,t) \qquad (2f\text{-}h)$$

where: the Roman numerals denote differentiation with respect to x.
The solution of equation (1a,b) is assumed to be in the form of eigenfunction series [7].

$$w_i(x_i,t)=\sum_{n=1}^{\infty} W_{in}(x_i)T_n(t) \qquad (i=1,2) \qquad (3a,b)$$

where: $T_n(t)$ are unknown time functions and $W_{in}(x_i)$ are normalized eigenfunctions of free frequencies of i-th parts of the beams which satisfies

$$\sum_{i=1}^{2} \rho_i A_i \int_0^{l_i} W_{im}(x_i) W_{in}(x_i) dx_i = \begin{cases} 0 & \text{for } m \neq n \\ \gamma_n^2 = \sum_{i=1}^{2} \rho_i A_i \int_0^{l_i} W_{in}^2(x_i) dx_i & \text{for } m = n \end{cases} \quad (4)$$

Variables in equation (1) and conditions (2a-h) were separated to determine $W_{in}(x_i)$ by substituting:

$$w_{in}(x_i, t) = W_{in}(x_i) \cos(\omega_n t), \quad (i = 1,2) \quad (5)$$

where: ω_n is n-th natural frequency of the beam with step changes in the cross-section.

Substituting (5) into equations (1a,b) and into conditions (2a-h) one can obtain (for $S=0$)

$$E_i J_i W_{in}^{IV}(x_i) + P_0 W_{in}^{II}(x_i) - \rho_i A_i \omega^2 W_{in}(x_i) = 0, \quad (i = 1,2) \quad (6a,b)$$

and

$$W_{1n}(0) = 0, \quad W_{2n}(l_2) = 0, \quad W_{1n}^{II}(0) = 0, \quad W_{2n}^{II}(l_2) = 0 \quad (7a\text{-}d)$$

$$E_1 J_1 W_{1n}^{III}(l_1) - E_2 J_2 W_{2n}^{III}(0) = 0 \quad (7e)$$

$$W_{1n}(l_1) = W_{2n}(0), \quad W_{1n}^{I}(l_1) = W_{2n}^{I}(0), \quad E_1 J_1 W_{1n}^{II}(l_1) = E_2 J_2 W_{2n}^{II}(0) \quad (7f\text{-}h)$$

The general solution to equations (6a,b) takes the form:

$$W_{in}(x_i) = C_{i1} \sinh(\alpha_{in} x_i) + C_{i2} \cosh(\alpha_{in} x_i) + C_{i3} \sin(\beta_{in} x_i) + C_{i4} \cos(\beta_{in} x_i) \quad (8a,b)$$

where C_{ik} are integration constants ($k = 1, 2, 3, 4$) and:

$$\alpha_{in}^2 = -\frac{\lambda_i}{2} + \sqrt{\frac{\lambda_i^2}{4} + \Omega_{in}}, \quad \beta_{in}^2 = \frac{\lambda_i}{2} + \sqrt{\frac{\lambda_i^2}{4} + \Omega_{in}} \quad (9a,b)$$

where: $\Omega_{in}^2 = \omega_n^2 \dfrac{\rho_i A_i}{E_i J_i}$, $\lambda_i = \dfrac{P_0}{E_i J_i}$, $i=1,2$

The equations of vibrations (6a,b) together with the boundary conditions (7a-h) made the formulation of the boundary value problem of the investigated beam. The natural frequency ω_n and eigenfunctions of the beam $W_{in}(x_i)$ are determined by solving the boundary value problem. Analogical procedure in case of remaining beam C-P after introducing the appropriate boundary conditions, leads to determination of the natural frequency and eigenfunction of this beam.

3. The solution to the problem of the dynamic stability of the beam

The determined eigenfunctions $W_{in}(x_i)$ allowed to solve the problem of the dynamic stability of the considered beams.

Substituting solution (3a,b) into equation (1a,b) one can obtain:

$$\sum_{n=1}^{\infty} \left[E_i J_i W_{in}^{IV}(x_i) T_n(t) + (P_0 + S\cos \nu t) W_{in}^{II}(x_i) T_n(t) + \rho_i A_i W_{in}(x_i) \ddot{T}_n(t) \right] = 0 \quad (10)$$

After multiplying by $W_{im}(x_i)$, one can receive from equation (10):

$$\sum_{n=1}^{\infty}\left[E_i J_i W_{in}^{IV}(x_i)W_{im}(x_i)\, T_n(t) + P_0 W_{in}^{II}(x_i)W_{im}(x_i)T_n(t)+ \right.$$
$$\left. + S\cos\nu t\, W_{in}^{II}(x_i)W_{im}(x_i)T_n(t) + \rho_i A_i W_{in}(x_i)W_{im}(x_i)\ddot{T}_n(t)\right]=0 \tag{11}$$

By analogy, from equations (6a,b), after multiplying by $W_{im}(x_i)$, one can obtain:

$$E_i J_i W_{in}^{IV}(x_i)W_{im}(x_i) + P_0 W_{in}^{II}(x_i)W_{im}(x_i) = \rho_i A_i \omega_n^2 W_{in}(x_i)W_{im}(x_i) \qquad (i=1,2) \tag{12}$$

then (11) takes the following form:

$$\sum_{n=1}^{\infty}\left[\rho_i A_i \omega_n^2 W_{in}(x_i)W_{im}(x_i)T_n(t) + S\cos\nu t\, W_{in}^{II}(x_i)W_{im}(x_i)T_n(t)+ \right.$$
$$\left. \rho_i A_i W_{in}(x_i)W_{im}(x_i)\ddot{T}_n(t)\right]=0 \tag{13}$$

As only basic parametric resonance with the first natural frequency of the beam is taken into account in this paper, further analysis considers the first term of the sum from equation (13). Hence, after integrating equations (13), the following form was obtained for the whole beam and the first term:

$$T_1(t)\left(\omega_1^2 \rho_i A_i \int_0^l W_{i1}^2(x_i)dx_i + S\cos\nu t \int_0^l W_{i1}^{II}(x_i)W_{i1}(x_i)dx_i \right) + \ddot{T}_1(t)\rho_i A_i \int_0^l W_{i1}^2(x_i)dx_i = 0 \tag{14}$$

Appropriate transformations of equation (14) and the substitution of t by a new variable $\tau = \nu t$ lead to the following form of Mathieu equation (the subscripts i and 1 were omitted).

$$\ddot{T}(\tau) + (a + b\cos\tau)T(\tau) = 0 \tag{15}$$

where: $\quad a = \dfrac{\omega_1^2}{\nu^2}, \; b = \dfrac{S}{\nu^2} \dfrac{\displaystyle\sum_{i=1}^{2}\int_0^l W_{i1}^{II}(x_i)W_{i1}(x_i)dx_i}{\displaystyle\sum_{i=1}^{2}\rho_i A_i \int_0^l W_{i1}^2(x_i)dx_i}$ \qquad (16a,b)

The periodical solutions to the Mathieu equation (15) are known (e.g. [8]). These solutions allow us to determine the stable and unstable regions of solutions (Fig.2). The numerical values of a and b each time decide the position of solution in the stable or unstable region. However, it must be stated that the probability of obtaining stable solution is higher in case of lower value of coefficient b, at the determined value of a. In this paper the analysis of changes in coefficient b was carried out assuming $b = |-b|$.
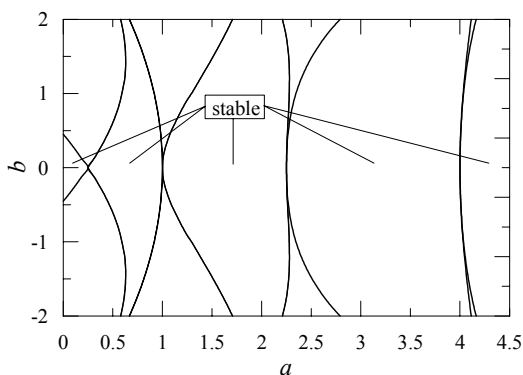
Fig. 2. Stable and unstable regions of solutions for the Mathieu equation [8].

4. The results of numerical computations and discussion

Computations were carried out assuming the following dimensionless quantities:

$$J = \frac{J_2}{J_1}, \quad l = \frac{l_1}{l_c}, \quad p = \frac{P_0}{P_c}, \quad s = \frac{S}{P_c} \tag{17}$$

where: P_c – the critical load of the tested beam with constant cross-section
$p = 0$ and $s = 0.05$ was assumed for computations.
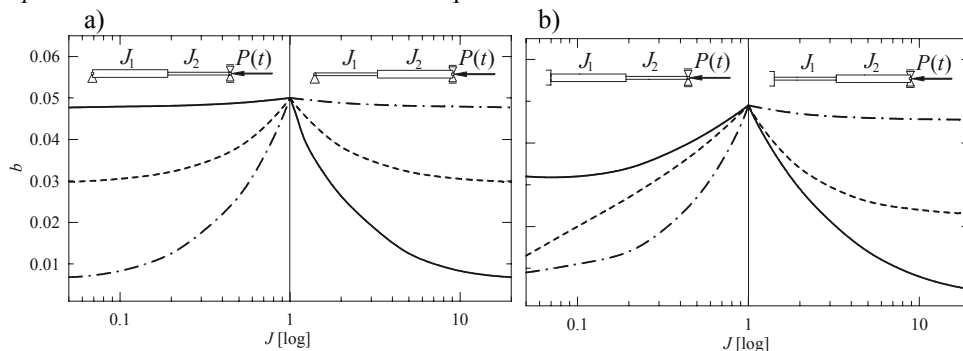
Fig.3. The influence of relation between moments of inertia J for the beams:
a) P-P and b) C-P on the values of coefficient b in the Mathieu equation
for $l = 0.2$ —————, $l = 0.5$ – – – – – , $l = 0.8$ – · – · – · .

The solution to the problem of dynamic stability of the tested beams allowed to deter-mine the values of coefficient b in the Mathieu equation at changeable values of mo ments of inertia J_1 and J_2 for two parts of the beam. In Fig. 3 solutions for both $J > 1$ and $J < 1$ are presented (for $J > 1$ J_2 is constant – beam diameter $d_2 = 0.05$ m, for $J < 1$ J_1 is con-stant – beam diameter $d_1 = 0.05$ m). The shapes of beams for considered relationship of J are presented in Fig. 3 in the shape of simple schemes of the beams. Logarithmic scale

was applied in Fig. 3 to compare the obtained results of research into relation of J for two parts of the beams, when $J<1$ and when $J>1$. The values of J were changed from $J=0.05$ to $J=20$ for the chosen values of l.

The values of coefficient b were also determined for different positions of changeable cross-sections of the beam denoted by l. In Fig. 4 (a-b) the changes in coefficient b in dependence on the position of beam cross-sections for chosen relations $J=0.2, 0.5, 2,$ i 5.

The following conclusions can be drawn from the analysis of the presented results:

- for the beam P-P symmetrical change in J (e.g. from $J = 0.2$ to $J = 5$) and symmetrical change in l in relation to the middle of the beam have no influence on the stability of such systems (curves $l=0.2$ and $l=0.8$ in Fig. 3 are symmetrical in relation to $J=1$ while curves $J=0.2$ and $J=5$ in Figs. 4a are symmetrical towards $l=0.5$)
- similar change in relations between moments of inertia J and similar change in position of cross-section l for beam with different boundary conditions (beam C-P) have influence on their stability, changing courses of coefficient b dependent on J (curves in Figs. 3 are not symmetrical towards $J = 1$) and courses of b dependent on l (curves in Figs. 4b are not symmetrical towards $l = 0.5$)
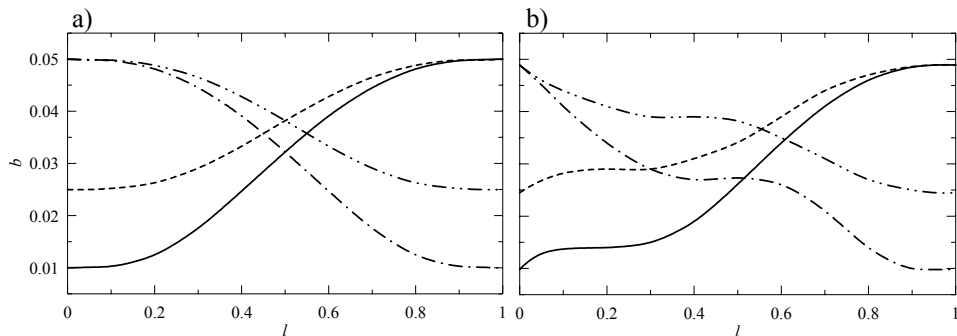
Fig.4. The influence of location of changes in the cross-section l of the beams: a) P-P and b) C-P on the value of coefficient b in Mathieu equation for $J = 0.2$ — · — · — · , $J = 0.5$ — ·· — ·· — , $J = 2$ - - - - - - , $J = 5$ ————.

- the less difference between J_1 and J_2 (higher J for $0<J\leq 1$ and less J for $1\leq J\leq 20$) causes that tested systems could easier loose dynamic stability (higher b)
- an increase in the beam lengths with a higher moment of inertia leads to stabilization of the tested systems (lowers b)
- C-P beam is more stable when $J <1$ (values of coefficient b for determined positions of changes in the cross-section l are lower for most of the tested case).

Acknowledgements

References

1. S. K. Jang, C. W. Bert, *Free vibration of stepeed beams: exact and numerical solutions*, Journal of Sound and Vibration 130 (1989) 342-346.
2. S. K. Jang, C. W. Bert, *Free vibration of stepeed beams: higher mode frequencies and effects of steps on frequency*, Journal of Sound and Vibration 132(1) (1989) 164-168.
3. S. Naguleswaran, *Vibration of an Euler-Bernoulli beam on elastic end supports and with up to three step changes in cross-section*, Mechanical Sciences 44 (2002) 2541-2555.
4. S. Kukla, I. Zamojska, *Frequency analysis of axially loaded stepped beams by Green's function method*, Journal of Sound and Vibration 300 (2007) 1034-1041.
5. T. Iwatsubo, Y. Sugijama, S. Ogino, *Simple and combination resonanses of columns under periodic axial loads*, Journal of Sound and Vibration 33(2) (1974) 211-221.
6. O. J. Aldraihem, A. Baz, *Dynamic stability of stepped beams under moving loads*, Journal of Sound and Vibration 205(5) (2002) 835-848.
7. Craig Jr., R. R., *Structural Dynamics*, New York, Wiley (1981).
8. S. P. Timoshenko, J. E. Gere, *Theory of Elastic Stability*, Mc Graw–Hill – INC. (1961).

MULTIPLE-SCALE METHOD ANALYSIS OF NONLINEAR DYNAMICAL SYSTEM

Roman STAROSTA

Institute of Applied Mechanics

Poznan University of Technology

roman.starosta@put.poznan.pl,

Jan AWREJCEWICZ

Department of Automatics and Biomechanics

Technical University of Łódź

awrejcew@p.lodz.pl

Abstract

The paper concerns analysis of nonlinear vibration of smooth autoparametrical non-autonomous systems of two-degree-of-freedom. A multiple scales method of investigation of small vibrations is applied to the analysis of resonance. The obtained results have been confirmed numerically. Analytical calculation was made with the use of *Mathematica*.

Keywords: nonlinear dynamics, parametrical resonance, asymptotic method

1. Introduction

Autoparametric resonance occurs when a mechanical system consist of two or more coupled vibrating components. In such a case the vibration of one of the component subsystems may destabilize the motion of the other. The investigated problem is very important from engineering point of view. In applications, it is important to understand where the autoparametric resonance occurs. Large vibrations in structures are usually undesirable since they often cause structural failure.

The pendulum of changing length is an example of such a system.

There are many technical applications of the systems containing various types of pendulums. Discussion on such models with a view to damping vibrations may be found in [2,4,5].

In such systems one can observe an auto-parametric resonance phenomena, because of the coupling occurring in the equation of motion. The phenomenon of energy transfer from one of the mode of vibration to the other was widely discussed in [3].

Dynamical analysis of nonlinear vibrations of spring pendulum (Figure 1) was presented in the paper using the multiple scales method. The program in the computer algebra system *Mathematica* was elaborated. It enables automatizing many transformations in the perturbation method use for this purpose [6].

2. Spring pendulum

The kinetic and potential energy of the examined system has the form:

$$T = \frac{1}{2}m\left[\dot{x}^2 + (l+x)^2\,\dot{\theta}^2\right]$$

$$V = mg(l+x)(1-\cos\theta) + \frac{1}{2}kx^2 + \frac{1}{4}k_1x^4 \tag{1}$$

where m – mass of the pendulum, l – the length, k and k_1 – spring stiffness linear and nonlinear parameters, g Earth's acceleration, and x and θ – generalized co-ordinates admitted according to Fig.1.
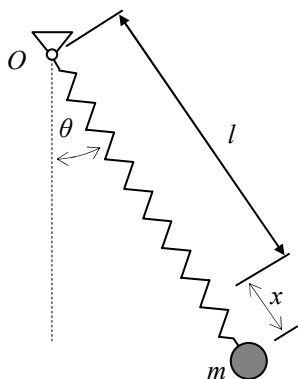
Figure 1. Spring pendulum.

Let us introduce dimensionless generalized co-ordinates (with tilde) $\frac{x}{l} = \varepsilon\widetilde{x}$, $\theta = \varepsilon\widetilde{\theta}$

and the forcing amplitude in the form $f = \varepsilon^2\widetilde{f}$. Applying Lagrangian equation and taking into account external excitation as a force acting on the mass along the pendulum, the equation of motion are obtained in the form:

$$\ddot{\widetilde{x}} + \omega_1^2\widetilde{x} = \varepsilon\left(\dot{\widetilde{\theta}}^2 - G_1\widetilde{\theta}^2 - c_1\dot{\widetilde{x}}\right) + \varepsilon F\cos\Omega t$$

$$\ddot{\widetilde{\theta}} + \omega_2^2\widetilde{\theta} = -\varepsilon\left(2\dot{\widetilde{x}}\,\dot{\widetilde{\theta}} + \widetilde{x}\,\ddot{\widetilde{\theta}} - c_2\dot{\widetilde{\theta}}\right) \tag{2}$$

where $F \equiv \dfrac{\widetilde{f}}{lm}$, $\omega_1^2 \equiv \dfrac{k}{m}$, $\omega_2^2 \equiv \dfrac{g}{l}$, $G_1 \equiv \dfrac{g}{2l}$, c_1, c_2 are damping coefficients $\varepsilon \ll 1$, is a so-called small parameter.

Expansion of trigonometric functions $\sin\theta \cong \theta - \dfrac{1}{3!}\theta^3$ and $\cos\theta \cong 1 - \dfrac{1}{2}\theta^2$, are admitted, assuming that vibrations are small.

In order to simplify the notation, the sign ~ (tilde) is omitted below.

The solution of (2) is sought in the following form

$$x(t;\varepsilon) \approx x_0(T_0,T_1) + \varepsilon\ x_1(T_0,T_1) + O(\varepsilon^2)$$
$$\theta(t;\varepsilon) \approx \theta_0(T_0,T_1) + \varepsilon\ \theta_1(T_0,T_1) + O(\varepsilon^2) \text{,}$$

(3)

where $T_0 = t$, $T_1 = \varepsilon t$ is a scale of time of slowly changing processes.

The original set of equations is transformed to the set of partial differential equations. Substitution of (3) into (2) leads to the equations of the zero and first order, according to the exponent of ε :

$$\frac{\partial^2 x_0}{\partial T_0^2} + \omega_1^2 x_0 = 0$$

(4)

$$\frac{\partial^2 \theta_0}{\partial T_0^2} + \omega_2^2 \theta_0 = 0$$

$$\frac{\partial^2 x_1}{\partial T_0^2} + \omega_1^2 x_1 + 2\frac{\partial^2 x_0}{\partial T_0\, \partial T_1} + G_1\theta_0^2 - \left(\frac{\partial \theta_0}{\partial T_0}\right)^2 + c_1\frac{\partial x_0}{\partial T_0} + -F\cos(\Omega T_0) = 0$$

(5)

$$\frac{\partial^2 \theta_1}{\partial T_0^2} + \omega_2^2 \theta_1 + c2\frac{\partial \theta_0}{\partial T_0} + 2\frac{\partial^2 \theta_0}{\partial T_0\, \partial T_1} + x_0\frac{\partial^2 \theta_0}{\partial T_0^2} + +2\frac{\partial x_0}{\partial T_0}\frac{\partial \theta_0}{\partial T_0} = 0$$

The solution of zero order equation (4) can be written as follows

$$x_0 = A(T_1)e^{i\omega_1 T_0} + \overline{A}(T_1)e^{-i\omega_1 T_0}$$
$$\theta_0 = B(T_1)e^{i\omega_2 T_0} + \overline{B}(T_1)e^{-i\omega_2 T_0} \text{.}$$

(6)

and the first order equation takes the form

$$\frac{\partial^2 x_1}{\partial T_0^2} + \omega_1^2 x_1 = -\frac{1}{2}Fe^{iT_0\Omega} - e^{2iT_0\omega_2}\left(G_1 + \omega_2^2\right)B^2 - 2G_1B\overline{B} + 2\omega_2^2 B\overline{B} - 2ie^{iT_0\omega_1}\frac{dA}{dT_1} + c.c.$$

(7)

$$\frac{\partial^2 \theta_1}{\partial T_0^2} + \omega_2^2 \theta_1 = -e^{iT_0(\omega_1+\omega_2)}\left(-2\omega_1\omega_2 - \omega_2^2\right)AB + -e^{iT_0(\omega_1-\omega_2)}\left(2\omega_1\omega_2 - \omega_2^2\right)A\overline{B} + 2ie^{i\omega_2 T_0}\omega_2\frac{dB}{dT_1} + c.c.$$

where *c.c.* represents the complex conjugates.

In the above equations the arguments of A and B are omitted in order to shorten the notation.

After removal of secular terms in equations (7), its solution has the form

$$x_1 = F\frac{e^{iT_0\Omega}}{2\left(\Omega^2 - \omega_1^2\right)} - \frac{\left(G_1 + \omega_2^2\right)B^2}{-\omega_1^2 + 4\omega_2^2}e^{2iT_0\omega_1} + \frac{\left(-G_1 + \omega_2^2\right)B\overline{B}}{\omega_1^2} + c.c.$$

(8)

$$\theta_1 = -\frac{\omega_2(2\omega_1 + \omega_2)}{\omega_1(\omega_1 + 2\omega_2)}ABe^{i(\omega_1+\omega_2)T_0} + \frac{\omega_2(2\omega_1 - \omega_2)}{\omega_1(\omega_1 - 2\omega_2)}A\overline{B}e^{i(\omega_1-\omega_2)T_0} + c.c.$$

The above solution becomes singular when the primary or internal resonances occurs i.e. when $\omega_1 = \Omega$ and/or $\omega_1 = 2\omega_2$. In order to consider this resonances case, we can

introduce the detuning parameters σ_1 and σ_2 according to:

$$\Omega = \omega_1 + \varepsilon\,\sigma_1, \;\; 2\omega_2 = \omega_1 + \varepsilon\sigma_2\,. \tag{9}$$

The equations (7) can be written now as follows:

$$\frac{\partial^2 x_1}{\partial t_0^2} + \omega_1^2 x_1 =^2 -2G_1 B\overline{B} + 2\omega_2^2 B\overline{B} - e^{iT_0\omega_1}\left(\frac{1}{2}e^{iT_1\sigma_1}F + e^{iT_1\sigma_2}G_1 B^2 + e^{iT_1\sigma_2}\omega_2^2 B^2 + 2i\omega_1\frac{dA}{dT_1}\right) + c.c. \tag{10}$$

$$\frac{\partial^2 \theta_1}{\partial t_0^2} + \omega_2 \theta_1 = e^{3iT_0\omega_2}\left(e^{-iT_1\sigma_2}AB\left(G_2\omega_1\omega_2 + \omega_2^2\right)\right) + e^{iT_0\omega_2}\left(e^{-iT_1\sigma_2}G_2\omega_1\omega_2 A\overline{B} - \omega_2^2 A\overline{B} + 2i\omega_2\frac{dB}{dT_1}\right) + c.c.$$

Removal of secular terms from (10) requires:

$$\frac{1}{2}e^{iT_1\sigma_1}F + e^{iT_1\sigma_2}G_1 B^2 + e^{iT_1\sigma_2}\omega_2^2 B^2 + 2i\omega_1\frac{dA}{dT_1} = 0$$

$$e^{-iT_1\sigma_2}2\omega_1\omega_2 A\overline{B} - e^{-iT_1\sigma_2}\omega_2^2 A\overline{B} + 2i\omega_2\frac{dB}{dT_1} = 0 \tag{11}$$

In order to present the solution of (11) in more familiar form:

$$x = a\cos(\omega_1 t + \alpha)$$
$$\theta = b\cos(\omega_2 t + \beta)\,, \tag{12}$$

the following substitution can be made [1]:

$$A \to \frac{a}{2}e^{i\alpha}, \qquad B \to \frac{b}{2}e^{i\beta} \tag{13}$$

The introduced amplitudes a and b and phases α and β are functions of T_1.
With the use of the above substitution (13), the equations (11) lead to expressions of derivatives of the sought functions:

$$\frac{da}{dT_1} = -\frac{2F\sin\xi + \left(G_1 + \omega_2^2\right)b^2\sin\eta}{4\omega_1}$$

$$\frac{d\alpha}{dT_1} = -\frac{2F\cos\xi + \left(G_1 + \omega_2^2\right)b^2\cos\eta}{4\omega_1 a}$$

$$\frac{db}{dT_1} = \frac{1}{4}\left(2\omega_1 - \omega_2\right)ab\sin\eta \tag{15}$$

$$\frac{d\beta}{dT_1} = \frac{1}{4}\left(2\omega_1 - \omega_2\right)a\cos\eta$$

where

$$\xi = T_1\,\sigma_1 - \alpha(T_1) \text{ and } \eta = T_1\,\sigma_2 - \alpha(T_1) + 2\beta(T_1). \tag{16}$$

Solving the above equations lets to obtain the information about modulations of amplitudes $a(T_1)$ and $b(T_1)$, and phases $\alpha(T_1)$ and $\beta(T_1)$ respectively.

Chaotic motion near resonance

Due to nonlinearities amplitudes and phases are not constant during the motion. Fig.2 presents modulations of amplitudes a and b versus slow time T_1, for simultaneous main and internal resonance: $\Omega=4, \varepsilon=0.1, F=0.1, \omega_1=4, \omega_2=2, c_1=c_2=0$.
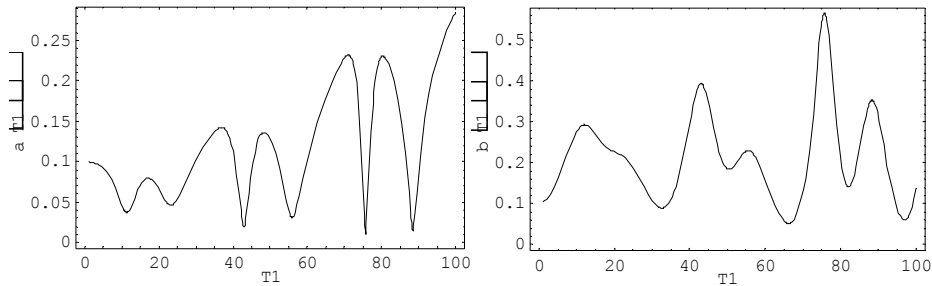
Fig.2 Modulations of amplitudes a and b

The time history of motion of the pendulum for the same numerical data as in the Fig.2 is presented in Fig. 3. For comparison there are shown the results obtained by MS Method and by numerical Runge-Kutta method.
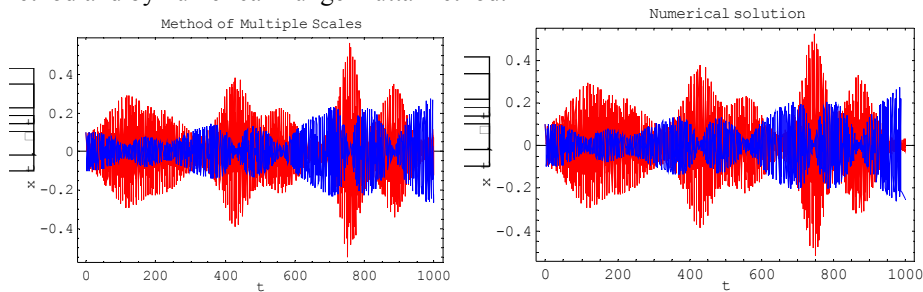
Fig. 3 Time history of motion of pendulum; —— x, —— θ.

Graph in Fig. 3 suggests that the movement is of chaotic type. Let us to drive the largest Lapunov coefficient λ versus frequency of the exciting force (Fig. 4). Fig. 5 presents a chosen Poincare map for the parameter giving negative and positive lambda.
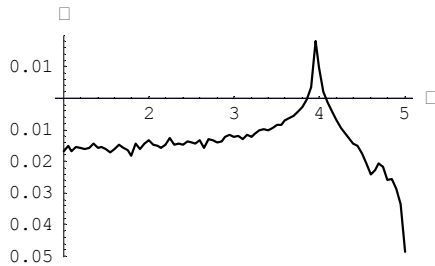
Fig. 5 The largest Lapunov exponent λ
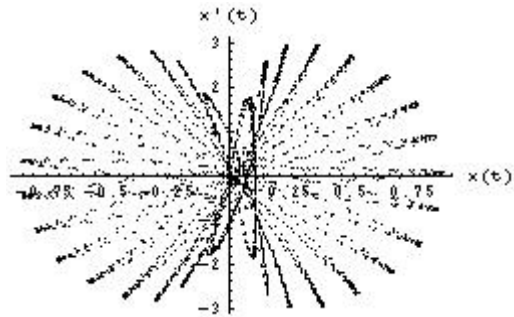
Fig.6 Poincare map of a chosen phase plane for non damped at the main and parametrical resonance $\Omega = 4, \omega_1 = 4, \omega_2 = 2$.

Conclusions

The method allow to recognize the parameters of the system with respect to the occurring resonance. The simultaneous main and internal resonance causes chaotic behavior of the system to chaotic behavior. It was confirmed by the largest Lapunov exponent. The results show that both quantitative and qualitative analyses of nonlinear dynamical systems can be made by the multi-scale-method in time domain.

The transformations within the multiple-scale-method were carried out automatically with the use of a procedure written in *Mathematica.*

References

1. Awrejcewicz J., Krysko V. A., *Wprowadzenie do współczesnych metod asymptotycznych*, WNT, Warszawa, 2004.
2. Genin M. D., Ryabow V. M., *Uprugo–inercjonnyje vibro–izolirujuscie sistemy*, Nauka, Moskwa, 1988.
3. Karamyskin V. V., Dynamiceskoje gasenie kolebanii, *Maszinostrojenie*, Leningrad, 1988.
4. Sado D. Przenoszenie energii w nieliniowo sprzężonych układach o dwóch stopniach swobody, OWPW, Warszawa, 1997.
5. Shivamoggi B. K., *Perturbation methods for differential equations*, Birkhauser Boston,
6. Starosta R., Awrejcewicz J., Analiza układów parametrycznych w obszarach rezonansów, *proceeding, I Kongres Mechaniki Polskiej*, Warszawa, 2007.

ACTIVE CONTROL OF TRANSIENT TORSIONAL VIBRATIONS DUE TO RUN-UP OF A ROTOR MACHINE DRIVEN BY THE ELECTRIC MOTOR

Tomasz SZOLC, Łukasz JANKOWSKI

Institute of Fundamental Technological Research, Polish Academy of Sciences

ul. Świętokrzyska 21, 00-049 Warszawa

phone: +48/22/8261281, e-mail: tszolc@ippt.gov.pl, ljank@ippt.gov.pl

Summary

In the paper active control of transient torsional vibrations induced by the electric motor during run-ups of the radial compressor drive system is performed by means of couplings with the magneto-rheological fluid. The main purpose of these studies is a minimisation of vibration amplitudes in order to increase the fatigue durability of the most responsible elements. The theoretical investigations are based on a hybrid structural model of the vibrating mechanical system and sensitivity analysis of the response with respect to the damping characteristics of the control couplings.

Keywords: active control, transient vibrations, drive system, electric motor

Introduction

Transient torsional vibrations due to start-ups of drive trains driven by electric motors are very dangerous for material fatigue of the most heavily affected and responsible elements of these mechanical systems. Thus, this problem has been considered for many years by many authors, e.g. by [1-3]. But till present majority of these studies reduced to standard transient vibration analyses taking into consideration additional dynamic effects caused by elastic couplings, dry friction in clutches, properties of the gear stage meshings, e.g. backlash, electro-mechanical couplings and others.

Active control of torsional vibrations occurring in the drive systems could effectively minimise material fatigue and in this way it would enable us to increase their operational reliability and durability, e.g. in the form of greater number of admissible safe run-ups and run-outs. Unfortunately, one can find not so many published results of research in this field, beyond some attempts performed by active control of shaft torsional vibrations using piezo-electric actuators, [4]. But in such cases relatively small values of control torques can be generated and thus an application of the piezo-electric actuators has to be reduced to low-power drive systems. In this paper active control is going to be realised by couplings with the magneto-rheological fluid (MRF) applied to attenuate transient torsional vibrations excited during start-ups of the large radial compressor drive system driven by the asynchronous motor.

1. Assumptions for the simulation model and formulation of the problem

In the considered drive system of the radial compressor power is transmitted form the asynchronous motor to the impeller by means of the low-speed and high-speed rigid couplings, multiplication single-stage gear and shaft segments, as shown in Fig. 1.
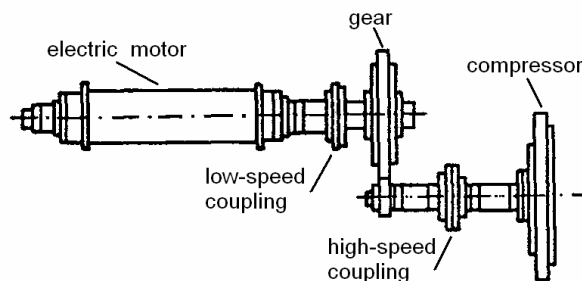
Fig. 1 Mechanical model of the compressor drive system

In order to perform the theoretical investigation of the active control concept applied for this mechanical system a reliable and computationally efficient simulation model is required. In this paper dynamic investigations of the entire drive system are performed by means of the one-dimensional hybrid structural model consisting of continuous visco-elastic macro-elements and rigid bodies. This model is employed here for eigenvalue analyses as well as for numerical simulations of torsional vibrations of the drive train. In this model successive cylindrical segments of the stepped rotor-shaft are substituted by torsionally deformable cylindrical macro-elements of continuously distributed inertial-visco-elastic properties. Since in the drive system of the real compressor the electric motor coils and gears are attached along some rotor-shaft segments by means of shrink-fit connections, the entire inertia of such fragments is increased, whereas usually the shaft cross-sections only are affected by elastic deformations due to transmitted loadings. Thus, the corresponding visco-elastic macro-elements in the hybrid model must be characterized by the geometric cross-sectional polar moments of inertia J_{Ei} responsible for their elastic and inertial properties as well as by the separate layers of the polar moments of inertia J_{Ii} responsible for their inertial properties only, $i=1,2,\dots,n$, where n is the total number of macro-elements in the considered hybrid model. Moreover, on the actual operation temperature T_i can depend values of Kirchhhoff's moduli G_i of the rotor-shaft material of density ρ for each i-th macro-element representing given rotor-shaft segment. In the proposed hybrid model of the compressor drive system with a reasonable accuracy for practical purposes inertias of the impeller and gears can be represented by rigid bodies attached to the appropriate macro-element extreme cross-sections.

Torsional motion of cross-sections of each visco-elastic macro-element is governed by the hyperbolic partial differential equations of the wave type

$$G_i(T_i)J_{Ei}\left(1+\tau\frac{\partial}{\partial t}\right)\frac{\partial^2\theta_i(x,t)}{\partial x^2}-\rho\left(J_{Ei}+J_{Ii}\right)\frac{\partial^2\theta_i(x,t)}{\partial t^2}=q_i(x,t),\qquad(1)$$

where $\theta_i(x,t)$ is the angular displacement with respect to the shaft rotation with the average angular velocity Ω and τ denotes the retardation time in the Voigt model of material damping. The external active, passive and control torques are continuously distributed along the respective macro-elements of the lengths l_i. These torques are described by the two-argument function $q_i(x,t)$, where x is the spatial co-ordinate and t denotes time.

Mutual connections of the successive macro-elements creating the stepped shaft as well as their interactions with the rigid bodies are described by equations of boundary conditions. These

equations contain geometrical conditions of conformity for rotational displacements of the extreme cross sections for $x=L_i=l_1+l_2+...+l_{i-1}$ of the adjacent $(i\text{-}1)$-th and the i-th elastic macro-elements:

$$\theta_{i-1}(x,t) = \theta_i(x,t) \qquad \text{for } x = L_i. \tag{2a}$$

The second group of boundary conditions are dynamic ones, which contain linear equations of equilibrium for external torques $M_i(t)$ as well as for inertial, elastic and external damping moments. For example, the dynamic boundary condition describing a simple connection of the mentioned adjacent $(i\text{-}1)$-th and the i-th elastic macro-elements has the following form:

$$M_i(t) - I_{0i}\frac{\partial^2\theta_i}{\partial t^2} - D_i\frac{\partial\theta_i}{\partial t} - G_{i-1}(T_{i-1})J_{\text{E},i-1}\left(1+\tau\frac{\partial}{\partial t}\right)\frac{\partial\theta_{i-1}}{\partial x} + \tag{2b}$$

$$+ G_i(T_i)J_{\text{E}i}\left(1+\tau\frac{\partial}{\partial t}\right)\frac{\partial\theta_i}{\partial x} = 0 \qquad \text{for } x = L_i, \quad i = 2,3,...,n,$$

where D_i are the external damping coefficients and I_{0i} denotes the mass polar moment of inertia of the rigid body.

In order to perform an analysis of natural elastic vibrations, all the forcing and viscous terms in the motion equations (1) and boundary conditions (2b) have been omitted. An application of the solution of variable separation for Eqs. (1) leads to the following characteristic equation for the considered eigenvalue problem:

$$\mathbf{C}(\omega)\cdot\mathbf{D}=\mathbf{0}, \tag{3}$$

where $\mathbf{C}(\omega)$ is the real characteristic matrix and $\mathbf{D}$ denotes the vector of unknown constant coefficients in the analytical local eigenfuctions of each i-th macroelement. Thus, the determination of natural frequencies reduces to the search for values of ω, for which the characteristic determinant of matrix $\mathbf{C}$ is equal to zero. Then, the torsional eigenmode functions are obtained by solving equation (3).

The solution for forced vibration analysis has been obtained using the analytical -computational approach. Solving the differential eigenvalue problem (1)÷(3) and an application of the Fourier solution in the form of series in the orthogonal eigenfunctions lead to the set of uncoupled modal equations for time coordinates $\xi_m(t)$:

$$\ddot{\xi}_m(t) + \tau\omega_m^2\dot{\xi}_m(t) + \omega_m^2\xi_m(t) = Q_m(t), \quad m = 1,2,..., \tag{4}$$

where ω_m are the successive natural frequencies of the drive system and $Q_m(t)$ denote the modal external excitations. Although each Eq. (4) has its analytical solution, it can be also solved numerically using a direct integration in order to obtain transient torsional response for the passive and actively controlled system.

2. Control of the transient torsional vibrations

The magneto-rheological fluids are functional fluids, whose effective viscosity depends on externally provided magnetic field. This feature makes them perfectly suitable for large couplings with controllable damping characteristic. Besides the ability to generate large damping torques, an important advantage of the MRF-based devices is a low power consumption. External power is needed to supply the electromagnetic coils only, i.e. to modify the dynamic characteristics of the mechanical system, which is the distinguishing feature of the semi-active

control. Moreover, the semi-active damping-based approach eliminates a risk of causing instability, which is intrinsically related to the active control paradigm and can occur in the case of an electrical failure, control time delays or in the case of an inaccurate modelling.

Assume there are N controllable couplings, each with the damping coefficient $c_j k(t)$, $j=1,2,…,N$, where $k(t)$ is the collective control variable and c_j are the coupling-specific multipliers. Each coupling generates the damping torque

$$M_j^D(t) = -c_j k(t) \varpi(x_j,t) = -c_j k(t)\left[\Omega(t) + \sum_{m=1}^{\infty} \dot{\theta}_m(x_j,t)\right], \quad j = 1,2,..., N, \quad (5)$$

where x_j is the location of the j-th coupling. The damping torques $M_j^D(t)$ modify Eqs. (4) by coupling them with each other and with the equation of the rigid body shaft motion. However, by proper determination of the multipliers c_j, the most resonant mode can be decoupled from the influence of the average angular velocity $\Omega(t)$.

The optimum open-loop control $k(t)$ can be determined with respect to the two following objectives:

(1) Maximization of the effectiveness of the damping, which is quantified here as the mean square torque above a given safe level. In practice, this objective can be related to the most resonant eigenvibration mode:

$$F_1[k(t)] = \int \max\left(0, |\xi_r(t)| - \xi_{r(\text{safe})}\right)^2 \, dt. \qquad (6)$$

(2) Minimization of the energy dissipated due to the damping

$$F_2[k(t)] = \sum_{j=1}^{N} \int M_j^D(t)\varpi(x_j,t)\,dt = \sum_{j=1}^{N} \int c_j k(t)\left[\Omega(t) + \sum_{m=1}^{\infty} \dot{\theta}_m(x_j,t)\right]^2 dt. \quad (7)$$

Provided the time history of the control variable $k(t)$ depends on a finite number of parameters, the compound objective function, composed of the weighted objectives (5) and (6), can be minimized using standard numerical approaches. In this paper it is assumed that $k(t)$ is a linear combination of a finite set of base functions, $k(t) = \sum_{i=1}^{K} \hat{k}_i k_i(t),$ which makes it dependent on

K parameters $\hat{k}_i$ and thus suitable for a constrained numerical optimization. A proper choice of the constraints and of the base functions allows also the MRF-specific damping rise and decay rate restrictions to be satisfied. Note that in this way the optimum open-loop control is obtained, which can serve as the best-case reference for possible closed-loop control laws. Moreover, in the case of the asynchronous motor, as the computational example illustrates below, the optimum control is a simple hold-and-release strategy, which can be easily realized using an open-loop control.

3. Computational example and conclusion

In the computational example the start-up of the large radial compressor driven by the 5 MW asynchronous motor is investigated. This system presented schematically in Fig. 1 is accelerated from a standstill to the nominal operating conditions characterized by the rated retarding torque 31831 Nm at the constant rotational speed 1500 rpm. The values of these quantities are reduced to the motor shaft, where the impeller rotational speed is 4.932 times multiplied by the gear

stage. The electromagnetic torque generated by the asynchronous motor has been 'a priori' assumed according to the respective relations contained in [5]. The retarding aerodynamic torque produced by the compressor is described by the parabolic function as proportional to the square of the impeller angular velocity. The time history plots of these torques during run-up are illustrated in Fig. 2a by the black and grey lines, respectively.

a)

b)

time [s]
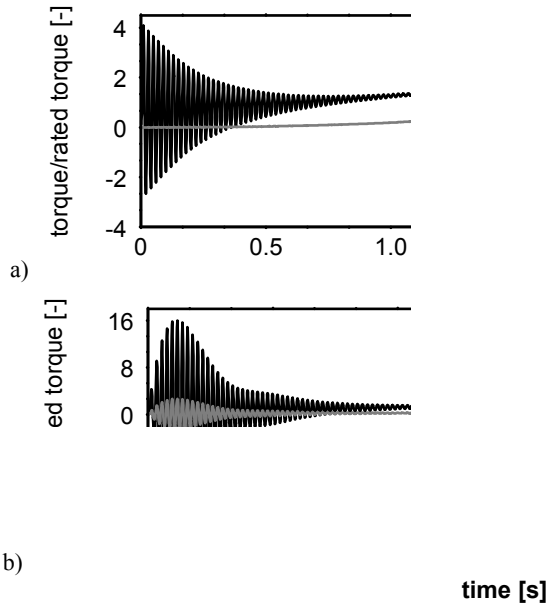
Fig. 2 Time histories of the motor and retarding torques (a) and elastic torques (b)

The passive system transient dynamic response due to the start-up is presented in Fig. 2b in the form of time histories of elastic torques transmitted by the shafts in the vicinity of the low-speed coupling (black line) and the high-speed coupling (grey line). From these plots it follows that the transient component of the asynchronous motor torque in the form of attenuated sinusoid of the network frequency 50 Hz and initial amplitude ca. 3.5 times greater than the rated torque value, Fig. 2a, induces very severe resonance with the first system eigenvibration mode of frequency 47.4 Hz. The maximum amplitudes of the most heavily affected shaft close to the low-speed coupling are almost 16 times greater than the rated torque, Fig. 2b, which is very dangerous for its fatigue durability. Thus, active control of transient torsional vibrations occurring in this drive system during start-ups is very required.
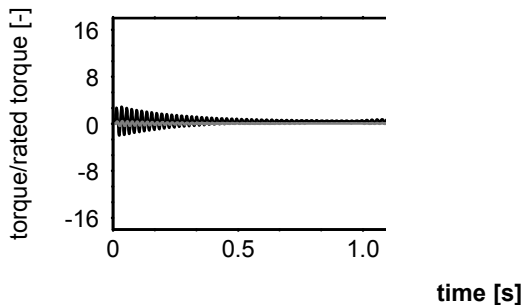
Fig. 3 Time histories of the elastic torques in the actively controlled system

In the same way as above, in Fig. 3 there are depicted plots of the analogous time histories of the elastic torques transmitted by the mentioned shafts and excited due to run-up of the actively controlled system. From these plots it follows that the corresponding extreme values of the elastic torques have been minimised more than 5 times in comparison with these in Fig. 2b. Here, these reduced amplitudes do not exceed dangerously the transmitted nominal torsional moment, where the exact reduction ratio depends on the technological bounds imposed on the control damping coefficient. Nevertheless, it is to remark that the computed optimum active control is a simple hold-and-release strategy and it results in some breaking of the rigid body motion of the system, which leads to a slight run-up retardation in time.

Literature

1. B. F. Evans, A. J. Smalley, H. R. Simmons, *Startup of synchronous motor drive trains: the application of transient torsional analysis of cumulative fatigue assessment,* ASME Paper 85-DET-122 (1985).
2. T. Iwatsubo, Y. Yamamoto, R. Kawai, *Start-up torsional vibration of rotating machine driven by synchronous motor*, Proc. of the International Conference on Rotordynamics, IFToMM, Tokyo 1986, pp. 319-324.
3. P. De Choudhury, *Torsional system design relative to synchronous motor start-up with a variable frequency power supply system*, Proc. of the Int. Conference on Rotordynamics, IFToMM, Tokyo 1986, pp. 325-328.
4. P. M. Przybyłowicz, Torsional vibration control by active piezoelectric system, *J. of Theoretical and Applied Mechanics*, 33(4) 1995, pp. 809-823.
5. A. Laschet, *Simulation von Antriebssystemen,* Springer-Verlag, Berlin, London, New-York, Paris, Tokyo 1988.

VERTICAL AXIS WIND TURBINE VIBROACOUSTICS

Jacek SZULCZYK,
Czesław CEMPEL
Politechnika Poznańska, Instytut Mechaniki Stosowanej,
Zakład Wibroakustyki i Biodynamiki Systemów
ul. Piotrowo 3, 60-965 Poznań, fax: +48 061 665 2307,
e-mail: jacek.szulczyk@doctorate.put.poznan.pl,
e-mail: czeslaw.cepmel@put.poznan.pl

Summary

This report shows the purpose of research undertaken to define occurrences of Vertical Axis Wind Turbines (VAWT). A true threat for natural energy resources depletion, legal requirement for obtaining 7.5% electric energy from renewable sources till 2010, easy installation of vertical axis wind turbines, resistance to high wind speeds, level of knowledge on determining wind energy efficiency factors using two-dimensional discussion (Betz's law – one-dimensional discussion) and likelihood low-frequency characteristics of acoustic spectral of turbine in operation have all become a motive for starting identification research and its accompanying occurrences of VAWT in operation.

Key words: **wind turbine, noise, acoustic climate.**

Introduction

Relatively good wind conditions to our region (Poland) have caused significant interest for obtaining 'green energy' just from wind turbines. The level of knowledge about the use of most common horizontal axis wind turbines (HAWT) is quite extensive. The vertical axis wind turbines on the other hand have low torque moment (possibility of running in wind speed of only 2m/s) easy installation, lack of requirements to building high masts and resistance to strong wind gusts are all interesting alternatives to households requiring little demand for electric energy $(3 - 5 \text{ kW})$. The most probable use of VAWT wind turbines can be considered to be urban and rural areas where the distance between the turbines installed can only be few meters. It is because of that it is worth learning all WA climate characteristics of VAWT in operation.

1. Environment protection

The most important reason for building wind turbine farms is the desire for obtaining electric energy from renewable resources, in other words 'green energy'. European Directive 2001/77/WE about supporting production of electric energy from renewable resources on internal markets (Dz. Urz. WE L 283 z 27.10.2001), which came into effect

in Poland on 4th March 2005 assumes that 7.5% of overall demand for electric energy will come from renewable resources till 2010 in Poland.
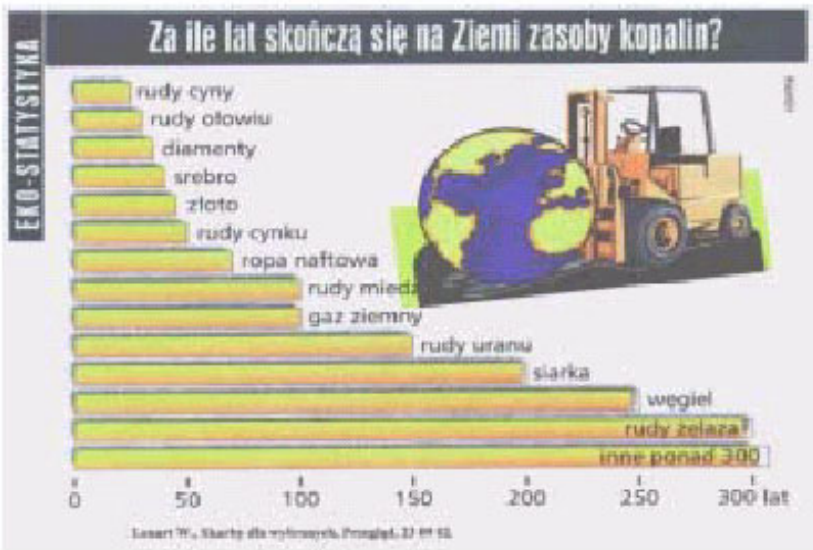
Figure 1. ECO-STATISTICS [source unknown]

2. Why wind farms?

Wind as renewable solar energy source is a movement of air caused by different thickness air masses climbing up. Energetic potential of winds blowing over lands suitable to accept wind power plants (including losses) amounts to 40WT. To compare, inland water energetic potential does not exceed 4WT [Lewandowski 2006]. In Western European countries (Germany, Holland, Denmark) wind energy industry developments have been received with great success, and this is why obtaining the required 7.5% of unconventional sources energy from wind may be a good idea in Poland.
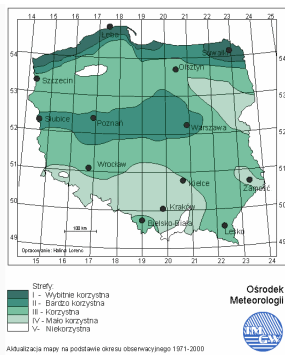
Figure 2. Wind energy zones [http://energiazwiatru.w.interia.pl/walory.htm]

Also tests on winds over the area of country are favorable, for so called wind energetic areas. They show that profitability for building them, especially for northern areas may be economically interesting

3. Wind energy

Wind energy is proportional to wind speed raised to the power cubed, additionally wind speed rise with height and atmospheric pressure and depends on topography.

$$P_A = \frac{1}{2}\rho v^3 \qquad (1)$$

where:
ρ – air thickness, [kg/m3]
v – air speed, [m/s]

At terrain surface wind speed is equal to zero, what is caused by friction forces. Those forces cause that only one quarter of wind kinetic energy fall on winds blowing on heights of 100 m and remaining three quarters on winds blowing higher than 100 m.

The passage of air stream through aero-generator turbine is presented in the following way: initial velocity of wind v_0 as a result of it going through the turbine blades slows down to velocity v_s so to achieve decreased velocity v_k behind the turbine. Decreased velocity v_o before the turbine and v_k behind the turbine and pressures p'_s before the turbine

Figure 3. A passage of air stream through HAWT

and p''_s behind the turbine are causing moment of perimeter forces acting on the turbine's blades which is then transferred on the rotor shaft by gear transmission of the generator.

The value of the largest factor of theoretical efficiency of energy use equates to $\xi_{t\ max} = 16/27 = 0,593$ and that has been named Betz's law after the name of German's physicist Albert BETZ. The efficiency of wind energy conversion of vertical axis wind turbine (VAWT) according to present knowledge is approximately $\xi_{t\ max} = 0,18$ considering Savonius rotor and approximately $\xi_{t\ max} = 0,4$ considering Dariuss's type of rotor taking into account high-speed parameters z.

Considerations which were conducted by Betz were based on wind flow in one-dimensional arrangement.

Currently there are circumstances which lead to believe that the value of efficiency factors of wind energy may be higher, due to the wind flow through wind generators being embraced by two-dimensional arrangement [Agren, Berg, Leijon 2005]. Authors suggest that vertical axis wind turbines have much greater potential of theoretical value of wind energy efficiency.

4. Acoustic characteristics of wind turbines

Source of noise made by wind turbines during exploitation is of mechanical (gearbox, gear transmission, generator) and aero-dynamical origins (movement of propellers causing turbulence in resilient (elastic) medium).

Composition of acoustic spectrum of wind turbine noise not corrected by any frequency characteristics is an example of typical low-frequency and sometimes even infrasound noise. The shape of frequency spectral depends on turbine rotational speed which ranges between 9.0 to 15.0

Figure 4. Sound spectrum Vestas V-80 [Golec2005]
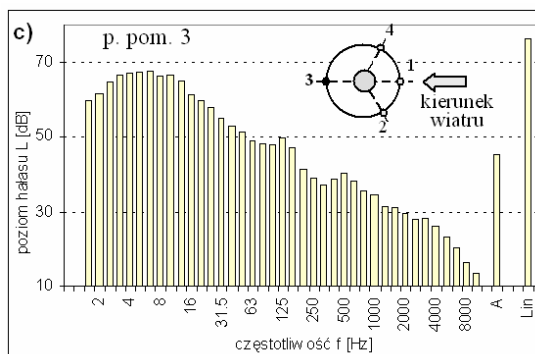
revolutions per minute for horizontal axis wind turbines. Each pass of rotating blades relating to the turbine mast are causing characteristic repeatable hum which in noise spectrum shows at infrasound's level. Mechanically moving part mainly generates noise in hearing range and the elements that influence the level of noise are specific mechanical parts in operation.
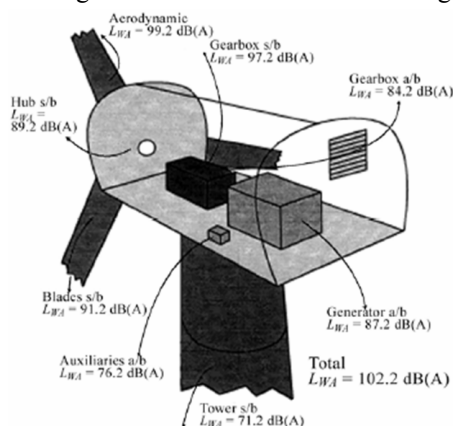
Figure 5. Level of acoustic efficiency of HAWT elements [Wagner1996]

5. Motives for taking up the researches on VAWT by WA

Relatively good wind conditions in our region along with a need for producing renewable energy are causing more interests around wind energy. In a situation when horizontal axis wind turbines were manufactured in a shape of aero-generators with capacities over 4MW, it became necessary to implement smaller capacity wind turbines yet more mobile. Those capabilities can be provided by vertical axis wind turbines, for which wind speed and wind direction are not causing technical and exploitation disturbances.

Sadly, when considering issues on amounts of vibroacoustic emissions of vertical axis wind turbines (VAWT) there is little completed study or even those still in progress.

Taking into consideration the need for describing the occurrences and identification of acoustic climate factors the writers related to basic problems which included:

a) small distance from the place VAWT is being installed to acoustically protected areas
b) infrasound or low-frequency noise generation in respect of jeopardizing people living in urban areas
c) methods for marking levels of acoustic dangers
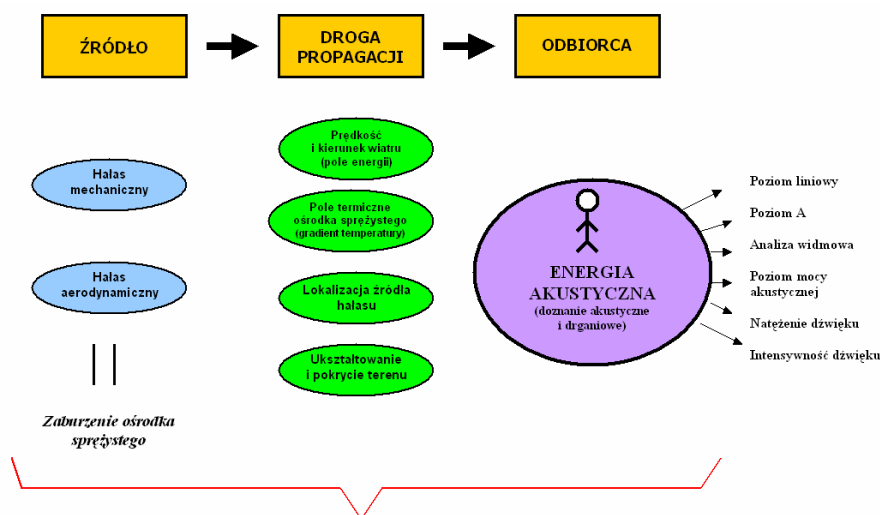
Figure 6. An attempt for defining Acoustic Climate Wind Turbine

Vertical axis wind turbines are being considered as mobile, easy to install and resistant to changing weather condition. It is also being predicted that majority of mini-sized vertical axis wind turbines will be installed in the very urban area, where the distance to potential neighbor can outcome to even few meters. It is though important, that elemental acoustic climate factors are defined for the direct exploitation area.

It is also vital to be able to describe and name factors which are responsible for noise generation process at its source, its ways of propagation and impact on potential receiver in acoustically protected area. Below a proposal for defining Acoustic Climate Wind Turbines (CAWT) has been described (Figure 6.)

The proposal for defining CAWT is the writers' first approximation in describing what happens and what the parameters are during wind turbine operation.

Another important aspect is time a person is being subjected to that work (accidental recipient or even a person that directly uses energy from renewable source of VAWT). In the least favorable model of the working turbine, that is from the low-frequency or infrasound noise influence point of view, a recipient can be subject to 24 hours a day 365 days a year exposition. There are no guidelines in national standards describing levels of

allowable exposition to infrasound or low-frequency noise comparing to constant exposition.

It would also be worth mentioning the economic aspect which could lead to wind efficiencies increase (W/m2) by applying appropriate terrain and building planning. There have already been proposed such plans so to cause the wind speeds increase and to gain improved wind turbines efficiencies [Boczar 2007, p.130].

6. Conclusion

It this study environmental aspects, energy zones and basic relationship describing wind energy have been introduced. It has been noted that considering efficiencies for processing wind energy to electric energy by vertical axis wind turbines based on Betz's law may not be completely correct. It has also been presented what are the sources of noise generated by wind engines in operation and also the need for undertaking vibroacoustic research to identify the behavior of working wind turbine. As an effect a proposal for Acoustic Climate Wind Turbine definition has been introduced which was the writers' first attempt to define behavior and parameters occurring during wind turbine exploitation.

Literature

1. O. Argen, M. Berg, M. Leijon, *A time-dependent potential flow theory for the aerodynamic of vertical axis wind turbine*, **J. of Applied Physics**, 97 (*2005*)
2. M. Golec, Z. Golec, C. Cempel, *Noise of Wind Power Turbine V80 in a Farm Operation,* **First International Meeting On Wind Turbine Noise: Perspectives for Control,** Berlin 17 - 18 October 2005
3. T. Boczar, *Wind energy. Current ways of use*, **PAK**, Warszawa 2007, (*in Polish)*
4. W. Jagodziński, *Wind engines*, **PWT**, Warszawa 1956 (*in Polish*)
5. W. M. Lewandowski, *Pro-environmental renewable energy sources*, **WNT**, Warszawa 2006
6. S. Wagner, R. Bareis, G. Guidati, *Wind Turbine Noise*, **Springer**, 1996
7. Site dedicated to environment changes and renewable energy sources, http://www.biomasa.org/index.php?d=artykul&kat=40&art=35, April 2008,
8. Site dedicated to information about wind power plants, http://www.elektrownie-wiatrowe.org.pl/art_europa.htm, April 2008.

OFRA – VIBRATION SIGNAL SELECTION METHOD
FOR FAST DIAGNOSTICS OF DIESEL ENGINE

Franciszek TOMASZEWSKI

Bartosz CZECHYRA

Poznan University of Technology, Institute of Internal Combustion Engine
ul. Piotrowo 3, 60-965 Poznan
tel.: (+48 61) 665-25-70; fax: (+48 61) 665-22-04
franciszek.tomaszewski@put.poznan.pl
bartosz.czechyra@put.poznan.pl

Abstract

The use of vibroacoustic methods in technical state assessment of mechanical objects is very popular. This fact can be explain by inexpensive acquisition and data collection devices, modern and most efficient signal analysis algorithms, faster computers and signal processing, etc. But in spite of technological advance, the signal selection problem is still permanently unsolved. The paper includes a methodology of vibration signal selection for diesel engine elementary process diagnostics based on OFRA (Operational Frequency Response Analysis) algorithm and auto-excitation of tested machine. Authors propose a new diagnostics method for assessment engine technical state, which is distinguished by high efficiency, fast and easy to use in normal engine operation.

Key words: signal selection, vibrodiagnostic, diesel engine

Introduction

The development of conventional combustion engines is determined by environmental and pro-ecological aspects. Special emphasis is putting on dynamic control of critical engine processes, e.g.: fuel burning, exhaust gas exchanging. The modern engines are equipped with sensors, transducers and computation unit (computer), which are supervisors of loading and running engine parameters. Information about processes occurring during the work-cycle and current engine's technical state are apply to optimization its performance. This information can be use to active prediction of the next term and range of engine maintenance.

However, many boats, heavy vehicles and stationary receivers of previous generation are use to present-day. The reasons of this situation are: very high purchase costs of it, very long life cycle, or others extra-economically cause (e.g.: monumental values). Polish diesel locomotives were made in the 70's and 80's previous century. Mounted diesel engines are without On-Board Diagnostic system (OBD). It is a situation, where unrecognized local defects of engine units have an influence on the reliability and durability of locomotive. Therefore, a modern, fast and easy to application diagnostics method is needed, especially to fault detection of engine critical unit (e.g. in- and outlet valves unit, fuel injector,…). The most critical engine's process is complex fuel burning. The right execution of it determines an efficient chemical to mechanical energy conversion and minimal financial and ecological costs engine operation.

The positive validated idea of diagnostics method, based on Operational Frequency Response Analysis (OFRA), is presented below.

1. Assumptions to OFRA methodology

The phenomenon occurring during the work-cycle of a diesel engine can be described by vibration signal parameters. It is a superposition of dynamic interaction between an engine structures and engine processes connected with fuel injection, preparing a burning mixture, burning of it and exhaust. The vibration effects are manifested in wide frequency range (from 3-5 Hz to 20-30 kHz) [1, 9, 10]. The lowest frequency (half of first rotary crankshaft speed) correspond with valves and injector triggering. And the highest frequency signal component correspond with non-stationary fuel flow in injection moment, and effects of fuel disintegration (Kármán's swirl). Into this very wide range of frequency are included a modal frequency (natural frequency), which are specific for engine structure. It is the reason of complex frequency and amplitude signal modulation, and many troubles with a processing and post-processing of engines' vibration signal. The elaborate a signal decomposition method for separation modal and excitation frequency, was necessary.

Mine assumption to create a diagnostics method was a possibility to use it in the diesel locomotive engines in normal utilization regime. The OFRA (Operation Frequency Response Analysis), basis on Operational Modal Analysis (OMA) and Frequency Response Analysis (FRA). First one can be use to describing the unscalable modal vectors of technical object in situation, where excitation is results of normal object work. Fundamentals of FRA technique are approximation of modal parameters by calculation the Frequency Response Function as a structure answer for appropriate excitation. The excitation force signal, which can be use in individual modal test, is sinus sweep, white noise, chirp sequence signal, Dirrac Delta or pulse (impact) [6]. The OFRA method use a normal work of engine's cam valves, as a self-excitation of compression-ignition engines head. It is a cyclic, dynamic process and can be taken to the analysis, as an impact excitation [5, 8]. Acquisition of vibration signal was preceded by optimization of accelerometer mounting place.

2. Experiment and analysis

The experimental research was done in Institute of Combustion Engines and Transport Laboratory, Poznan University of Technology. Vibration tests were done on a dynamometric stand with one-piston laboratory diesel engine type SB3.1.

Dynamometric stand was adapted to vibroacoustics tests of diesel engine. Main devices of measurement set were:
– accelerometer Brüel & Kjær type 4391,
– transducer of in-chamber pressure AVL type 8QP 505c connected to conditioning amplifier type AVL 3057-A01,
– photoelectric crankshaft rotation marker AMX 210 connected to conditioning amplifier type AVL 3065-A01,
– measurement amplifier Brüel & Kjær type NEXUS 2692.

An appearance of test dynamometric stand are presented on figure 1.

a) b)
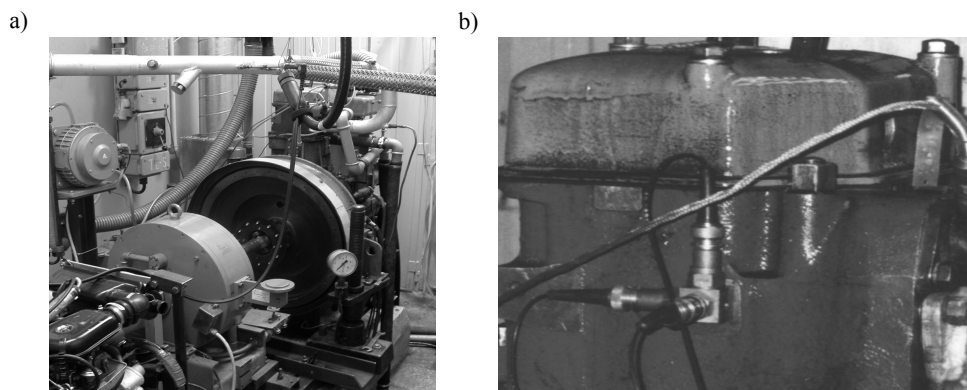
Fig. 1. Dynamometric stand for SB3.1 a) and accelerometers mounted to the SB3.1 engine head b)
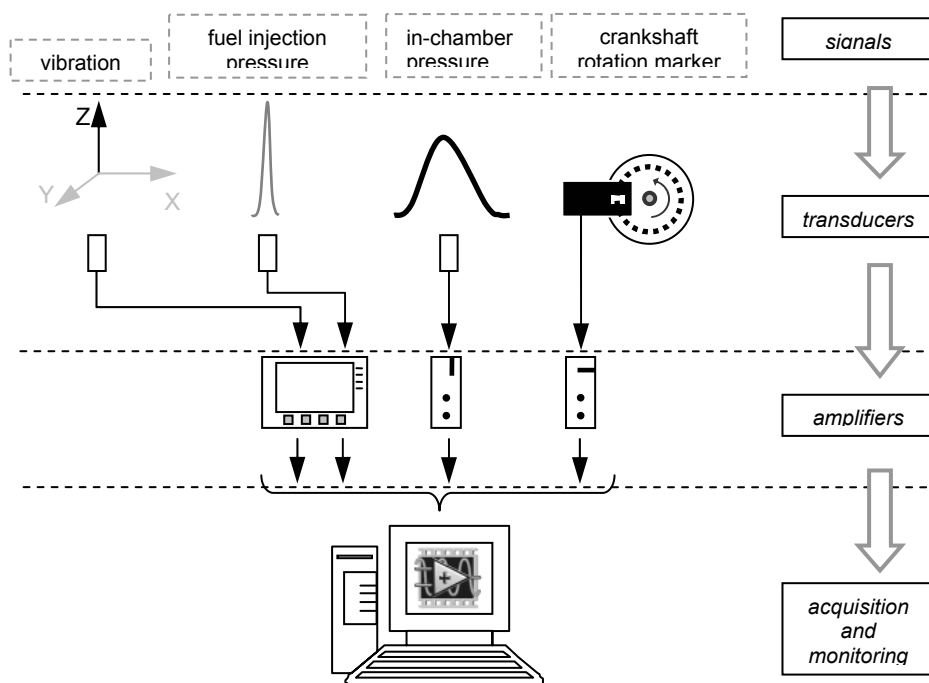
Fig. 2. Diagram of signal acquisition system used in experiment

Acquisition and on-line monitoring system was prepared on PC computer equipped with Dynamic Acquisition Card type NI DAQ PC–4472 and LabView® software made by National Instruments. Schema of acquisition system is shown on figure 2.

In a recorded vibration signal, all engine processes were recognized as a specific signal components, e.g. shutting of cam valves, fuel injection, aggregation of self-ignition and kinetic burning of fuel [3,4,10]. After phase-time selection procedure the vibration effects of cam valves shutting were separated. These parts of signal were synchronous averaged. After this operation a base spectrum was calculated. Comparison of base spectrum and autospectrum of combustion effects provide information about characteristic frequency band, witch are coincide to burning process. Post-processing effects are graphically presents on figure 3.
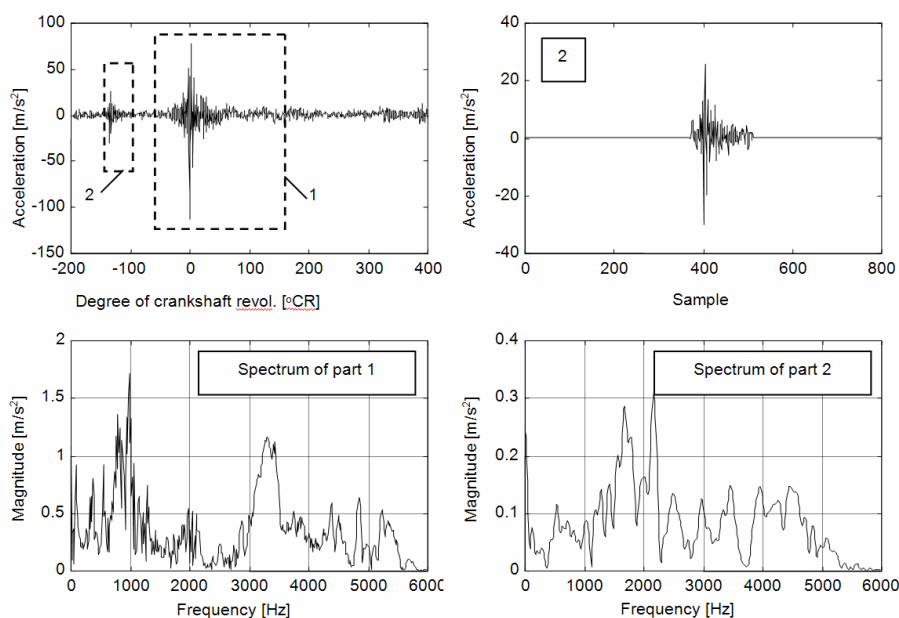
Fig. 3. Signal selection method and analysis of engine head excitation;
1. burning, 2. shut down of outlet valve; engine loading: n=700 RPM, Mt=0 Nm

Typical frequency band of combustion process occurring during work-cycle of SB3.1 type engine, is from 800Hz to 1500Hz approximately. The level of vibration signal energy in this frequency band is a most sensitive to change of engine technical state and its control parameters. Magnitude value for frequency 980 Hz component of vibration signal was accepted as an estimator of engine performance and loading parameter. Validation of loading estimation based on magnitude selected vibration signal was done in wide range of crankshaft rotation speed and load. Developing an engine's loading tests permit to create a vibration engine load map (fig. 4). The prepared Load-Vibration Map can be use for example, to fault detection of fuel injector and detection of misfire process. A misfire process reduces magnitude value from 50% to 80% [1,7].
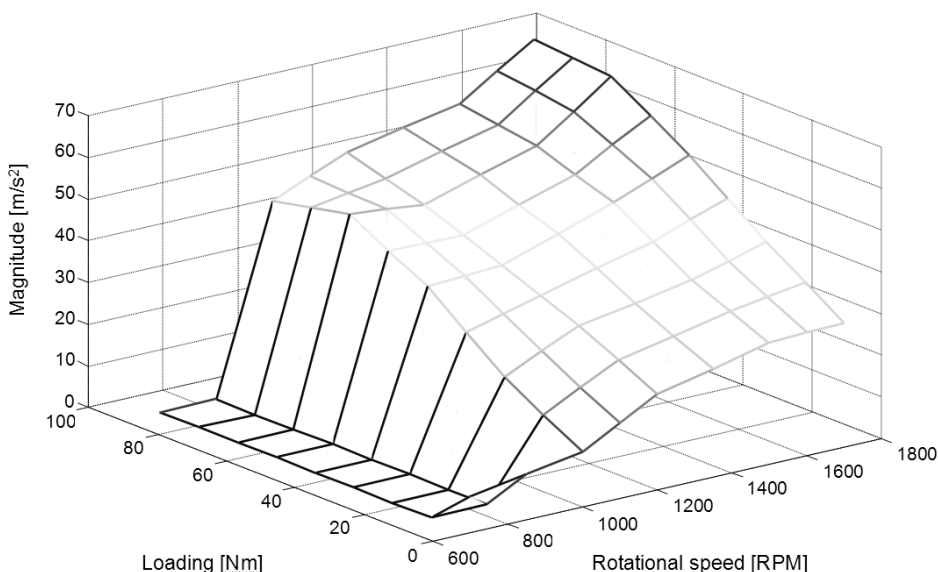
Fig. 4. The Load-Vibration Map of engine type SB3.1

That map is unique, individual description of vibroacoustic activity of engine (here SB3.1 type). The Load-Vibration Map (LVM) can be use as a template for fast technical state diagnostics. In other hand it can be use as a several engine model for load monitoring, control, optimization and fast fault detection, especially critical emission elements – fuel injector [1].

3. Summary

The use of OFRA method to vibration signal selection is very easy to use in normal operation of technical objects. The Load-Vibration Map is a non-invasive, very easy to use diagnostics method and gives new possibilities in engine technical state monitoring and optimal operation. Acquisition of vibration signal doesn't demand especially engine unit preparing and can be executed as an on-line procedure. Spectrum analyzer of engine head vibration signal is useful and can be built-in to OBD/E-OBD systems as a real time monitor, if exist. Possibility of use vibroacoustic activity engine's map to misfire detection was ascertained and confirm at tests, executed on diesel locomotive engine type 2112SSF [2,7]. This method is most sensitive and efficient then organoleptic and experts method used in normal operation. The biggest advantage of LVM is a possibility of using it to technical state monitoring of older engines. This process can be executed as on- or off-line monitoring system.

References

1. Czechyra B.: The use of vibration signal to assess the phenomenon occurring during the work-cycle of a diesel locomotive engine based on identification research carried out on a laboratory test engine. Doctoral dissertation. Department Working Machine and Transport, Poznan University of Technology, Poznan 2006 (in polish)

2. Czechyra B.: The use of vibration signature to assess the propriety of diesel engine running. 27th International scientific conference DIAGO[®] 2008 Technical diagnostics of machines and manufacturing equipment, Roznov pod Radhostem, Czech Republic 5. - 6. February 2008

3. Czechyra B., Szymański G.M., Tomaszewski F.: Analiza możliwości opisu procesów silnikowych za pomocą charakterystyk sygnału drganiowego, Pojazdy Szynowe 3-4/2004

4. Czechyra B., Szymański G.M., Tomaszewski F.: Odwzorowanie procesu spalania w sygnale drganiowym tłokowego silnika spalinowego o zapłonie samoczynnym. 3rd International Congress of Technical Diagnostics, Diagnostics' 2004, 6-9 September 2004, Poznań, Diagnostyka VOL. 30 tom 1 2004

5. Czechyra B., Szymanski G.M., Tomaszewski F.: The assessment of valve clearance in internal combustion engines based on parameters of vibration – methodological assumption. Combustion Engine nr 1/2004(118)

6. Dumping Measurement. Technical Review No.2-1994. Brüel & Kjær, Denmark 1994

7. Merkisz J., Waligórski M., Czechyra B., Gis W.: The application of vibration methods in misfire detection in a compression-ignition engine in the aspect of the OBD system realization in diesel locomotives. Word Automotive Congress FISITA 2006. Yokohama, Japan, 22-27 October 2006

8. Szymański G.M.: Analiza możliwości zastosowania wybranych charakterystyk sygnału drganiowego do diagnostyki silnika spalinowego. Rozprawa doktorska. Politechnika Poznańska, Poznań 2005

9. Tomaszewski F.: Zagadnienia wyznaczania stanu technicznego złożonego obiektu mechanicznego za pomocą sygnału wibroakustycznego; na przykładzie silnika spalinowego pojazdu szynowego. Rozprawy Politechniki Poznańskiej nr 337, Poznań 1998

10. Zabłocki M.: Wtrysk i spalanie paliwa w silnikach wysokoprężnych. Wydawnictwo Komunikacji i Łączności, Warszawa 1976

SPECIFIC LOAD OF SLENDER SYSTEMS –
FREE VIBRATIONS AND STABILITY

Lech TOMSKI, Sebastian UZNY
Technical University of Częstochowa
Intitute of Mechanics and Machine Design Foundations
ul. Dąbrowskiego 73, 42-200 Częstochowa
tel. (034) 3250620, **uzny@imipkm.pcz.czest.pl**

Abstract
Scientific achievements of stability and free vibrations of slender systems subjected to specific load are presented in the paper. Schematic diagrams of heads realising the specific load and boundary conditions in the case of two fundamental types of specific load (generalised load by a force directed towards the positive pole and load by the follower force directed towards the pole) are shown.
Keywords: column, stability, free vibrations

1. Specific load

The specific load was presented for the first time by L.Tomski et al. in [7] in 1994. The specific load is a conservative load, where the static stability criterion is sufficient enough to determine the value of a critical force. It combines in itself features of generalised load [4] or load by the follower force [1] with load by the force directed towards the positive pole (compare [3]) or negative pole (compare [3]). The origin of the nomenclature related to the specific load is presented by means of the diagram given in Figure 1.
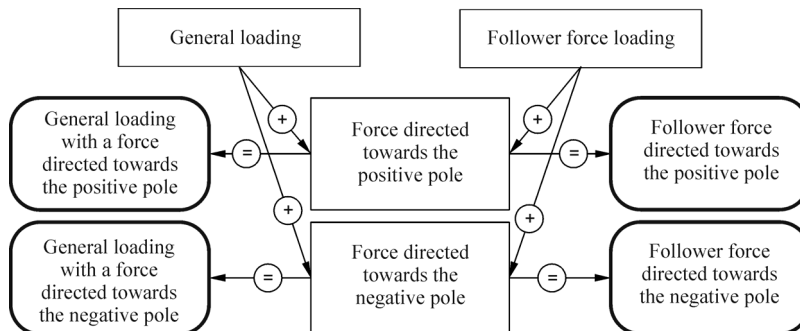
Fig. 1. Diagram illustrating the origin of the nomenclature relating to the specific load [18]

In case of the specific load two variants are distinguished:

− generalised load by a force directed towards the pole (positive or negative). The load by a concentrated force directed towards fixed point (the pole) placed on non-deformed axis of the column. The action of this force does not cause linearly dependent bending moment;

– load by the follower force directed towards the pole (positive or negative). It is realised by the follower force which direction coincides with the tangent to deflection at the free end of the column. The direction of the force passes through the constant point (pole) on non-deformed axis.

The method of formation of the specific load by the follower force directed towards the positive pole (compare [12]) is presented in Fig.2.
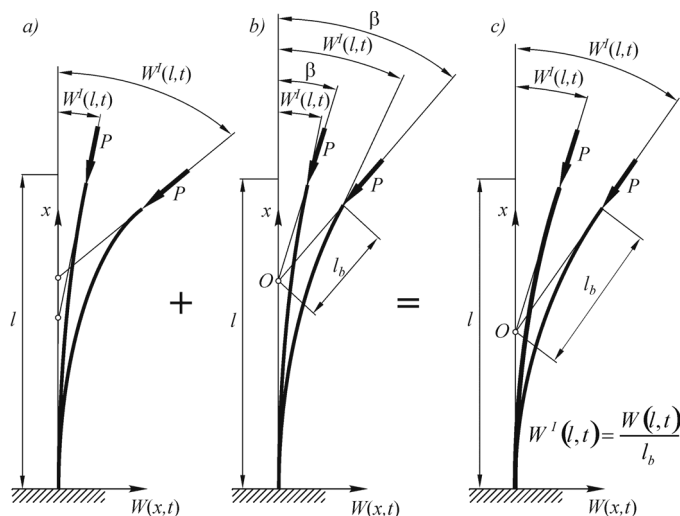
Fig. 2. The method of formation of the load by the follower force directed towards the positive pole: (a) system subjected to the follower force (non-conservative system) [1], (b) system subjected to the force directed towards the positive pole (conservative system) [3], (c) system subjected to the follower force directed towards the positive pole (conservative system) [12].
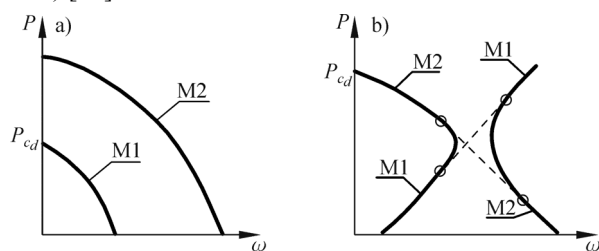
Fig. 3. Load (P) – free vibration frequency (ω) plane curves

Two possible courses of characteristic curves, in dependence on load parameters in the plane: load – natural frequency, are obtained:

– course of the curve presented in Fig. 3a corresponds to divergence system . Column looses its stability due to buckling at the value of the force designated as Pcd, which

corresponds to zero first natural frequency. The first form of natural frequency is present along the first curve,

– course of the curve presented in Fig. 3b corresponds to the pseudo-flutter divergence system. Column looses its stability due to buckling at the value of the force designated in the picture as Pcd. In this case the change of the first form of natural frequency into the second form takes place along the first characteristic curve. The name of "pseudo-flutter divergence system" was given by L.Tomski and R.Bogacz in [2]. In Figure 3, the presence of the first and the second form of natural frequency along characteristic curves were denoted by M1 and M2, respectively..

2. Systems subjected to the specific load (schematic diagrams, boundary conditions)

The considered specific load is realised by application of suitably constructed loading heads (compare [8]). The heads are built from linear or circular elements. The specific load can be realised as active load (loading system) or passive load (bearing system).

Schematic diagrams of the systems realising the specific load are presented in Figure 4. Vertical position of the system axis proves that given construction can realise only active load. Horizontal position of the system axis proves that both active and passive load (bearing) can be realised. In Figure 4 denotation WK( ) is given to every constructional variant. Letter D or U denotes appropriate pole, towards which the loading force is directed (D – positive pole, U – negative pole).

Boundary conditions are given exemplary for constructional variants (WK1D) and (WK6D), whose detailed diagrams are presented in Fig.5:

• generalised load by a force directed towards the positive pole (WK1D):

$$EJ\frac{\partial^2 W(x,t)}{\partial x^2}\bigg|^{x=l} + \frac{P\Psi(r-l_0)}{R-r} = EJ\frac{\partial^3 W(x,t)}{\partial x^3}\bigg|^{x=l} + \frac{P\Psi}{R-r} - m\frac{\partial^2 W(x,t)}{\partial t^2}\bigg|^{x=l} = 0 \quad \text{(1a,b)}$$

• load by the follower force directed towards the positive pole (WK6D):

$$EJ\frac{\partial^3 W(x,t)}{\partial x^3}\bigg|^{x=l} - \frac{1}{R-l_0}EJ\frac{\partial^2 W(x,t)}{\partial x^2}\bigg|^{x=l} - m\frac{\partial^2 W(x,t)}{\partial t^2}\bigg|^{x=l} = \Psi = 0 \qquad \text{(2a,b)}$$

where:
$$\Psi = (R-l_0)\frac{\partial W(x,t)}{\partial x}\bigg|^{x=l} - W(l,t) \qquad \text{(3)}$$

EJ – bending rigidity of the column rod, P – loading force, $W(x,t)$ – transverse displacement of the column corresponding to coordinate x, t – time, R – radius of forcing head, r – radius of receiving head, l_0 – length of rigid bolt.
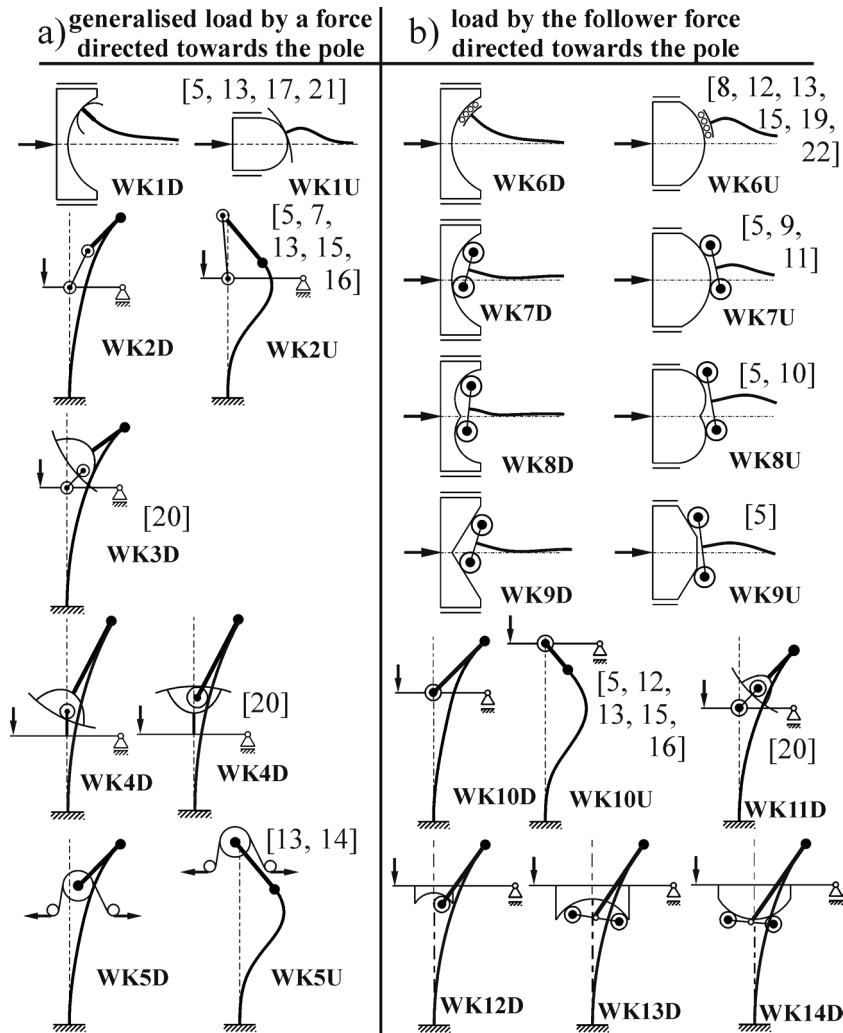
Fig. 4. Realisation of the active and passive specific loads: a) generalised load by a force directed towards the pole, b) load by the follower force directed towards the pole [6]

Important publications dealing with research into the columns subjected to the specific load considering suitable constructional versions are presented in Fig. 4. Theoretical, numerical and experimental research is taken into account in these publications.
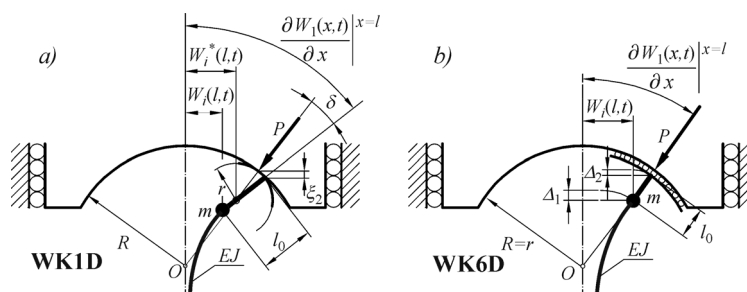
Fig. 5. Schemes of heads realising the specific load in case of constructional variants: a) WK1D [5, 13, 17, 21], b) WK6D [8, 12, 13, 15, 19, 22].

References

1. BECK M.: Die knicklast des einseitig eingespannten tangential gedruckten stabes, ZAMP 4, 1953, 225-228.
2. BOGACZ R., IMIEŁOWSKI SZ., TOMSKI L.: Optymization and Stability of Columns on Example of Conservative and Nonconservative Systems. Machine Dynamics Problems, No. 20, 1998, 35-47.
3. GAJEWSKI A., ŻYCZKOWSKI M.: Optima shaping of an Elastic Homogeneous Bar Compressed by Polar Force, Biulletyn de L`Academie Polonaise des Sciences, Vol. XVII, No. 10, 1969, 479-488.
4. GAJEWSKI A., ŻYCZKOWSKI M.: Optimal Design of Elastic Columns Subject to the General Conservative Behaviour of Loading, ZAMP, 21, 1970, 806-818.
5. Projekt badawczy BG-nr 7T07A01211: Teoretyczne i eksperymentalne badania drgań i stateczności konstrukcji mechanicznych jedno- i dwuwymiarowych, 1996-2000, kierownik pracy L. TOMSKI.
6. TOMSKI L.: Obciążenia układów oraz układy swoiste, rozdział 1, Drgania swobodne i stateczność obiektów smukłych jako układów liniowych lub nieliniowych, Praca zbiorowa wykonana pod kierunkiem naukowym i redakcją L. TOMSKIEGO, Wydawnictwa Naukowo Techniczne, Fundacja „Książka Naukowo-Techniczna", Warszawa 2007.
7. TOMSKI L., GOŁĘBIOWSKA-ROZANOW M., SZMIDLA J.: Free Vibration of a Column Loaded by a Force and Bending Moment, XVI Symposium „Vibrations in Physical Systems", Poznań - Błażejewko, May 26-28, 1994, 317-319.
8. TOMSKI L., KASPRZYCKI A., SZMIDLA J.: Wybrane rozwiązania konstrukcyjne głowic urzeczywistniających potencjalne obciążenie czynne i bierne, XXII Sympozjon Podstaw Konstrukcji Maszyn, Gdynia-Jurata, 2005, 353-358.
9. TOMSKI L., PODGÓRSKA-BRZDĘKIEWICZ I.: Vibrations and Stability of Columns Loaded by Three Side Surfaces of Circular Cylinders Considering Type of Friction in Loaded Heads. International Journal of Structural Stability and Dynamics, 2006, 6, 3, 297-315.

10. TOMSKI L., PODGÓRSKA-BRZDĘKIEWICZ I.: Vibrations and stability of columns loaded by four-side surfaces of circular cylinders, Journal of Theoretical and Applied Mechanics 44, 4, 2006, 907-927.

11. TOMSKI L., PRZYBYLSKI J., GOŁĘBIOWSKA-ROZANOW M., SZMIDLA J.: Vibration and stability of an elastic column subject to a generalized load, Archive of Applied Mechanics 67, 1996, 105-116.

12. TOMSKI L., PRZYBYLSKI J., GOŁĘBIOWSKA-ROZANOW M., SZMIDLA J.: Vibration and stability of a cantilever column subject to a follower force passing through a fixed point, Journal of Sound and Vibration, 214, 1, 1998, 67-81.

13. TOMSKI L., PRZYBYLSKI J., GOŁĘBIOWSKA-ROZANOW M., SZMIDLA J.: Vibration and stability of columns to a certain type of generalised load, Journal of Theoretical and Applied Mechanics, 37, 2, 1999, 283-299.

14. TOMSKI L., PRZYBYLSKI J., PODGÓRSKA I.: Influence of a joint flexibility of a column loaded by a certain type of the loading upon its vibration and stability, Proceedings of the XVIIIth Symposium „Vibrations in physical systems", Poznań 1998, 261-262.

15. TOMSKI L., SZMIDLA J.: Drgania swobodne i stateczność kolumn poddanych obciążeniu swoistemu − sztywne węzły konstrukcyjne układu wymuszającego i przejmującego obciążenie, rozdział 3, Drgania i stateczność układów smukłych, Praca zbiorowa wykonana pod kierunkiem naukowym i redakcją L. TOMSKIEGO, Wydawnictwa Naukowo Techniczne, Fundacja „Książka Naukowo-Techniczna", Warszawa 2004, 68-133.

16. TOMSKI L., SZMIDLA J.: Theoretical and Experimental Investigations of the Natural Vibrations of the Divergence and Divergence Pseudoflutter Type Systems, PAMM 4, 1, 2004, 418-419.

17. TOMSKI L., SZMIDLA J.: Vibration and Stability of Column Subjected to Generalised Load by a Force Directed Towards a Pole, Journal of Theoretical and Applied Mechanics 42, 1, 2004, 163-193.

18. TOMSKI L., SZMIDLA J., GOŁĘBIOWSKA-ROZANOW M.: Drgania swobodne i stateczność układów smukłych poddanych swoistemu obciążeniu konserwatywnemu, Polska Mechanika u progu XXI wieku, Warszawa - Kazimierz Dolny 2001, 503-510.

19. TOMSKI L., SZMIDLA J., GOŁĘBIOWSKA-ROZANOW M.: Vibrations and Stability of a Two-Rod Column Loaded by A Sector of a Rolling Bearing, Journal of Theoretical and Applied Mechanics 42, 4, Warsaw 2004, 905-926.

20. TOMSKI L., SZMIDLA J., GOŁĘBIOWSKA-ROZANOW M., KASPRZYCKI A.: Drgania swobodne kolumn obciążonych poprzez głowice o węzłach obrotowych, XXII Sympozjon Podstaw Konstrukcji Maszyn, Gdynia-Jurata, 2005, 347-352.

21. TOMSKI L., UZNY S.: Vibration and stability of geometrically non-linear column subjected to generalised load with a force directed towards the positive pole, International Journal of Structural Stability and Dynamics, 8, 1, 2008, 1-24.

22. TOMSKI L., UZNY S.: Free vibration and the stability of a geometrically non-linear column loaded by a follower force directed towards the positive pole, International Journal of Solids and Structures, 45, 1, 2008, 87-112.

FREE VIBRATIONS AND STABILITY OF A GEOMETRICALLY NON-LINEAR CANTILEVER COLUMN LOADED BY A FOLLOWER FORCE DIRECTED TOWARDS THE POSITIVE POLE SUPPORTED AT THE LOADED END BY A SPRING

Lech TOMSKI, Sebastian UZNY

Technical University of Częstochowa

Intitute of Mechanics and Machine Design Foundations

ul. Dąbrowskiego 73, 42-200 Częstochowa

tel. (034) 3250620, **uzny@imipkm.pcz.czest.pl**

Abstract

The formulation and solution to stability problem and free vibrations of the geometrically non-linear system loaded by the follower force directed towards the positive pole is presented in the paper. The system is supported at the loaded end by a spring with linear characteristics. The boundary problem was formulated on the basis of Hamilton's principle and, owing to its non-linearity, on the use of the straightforward expansion method. Bifurcation force and characteristic curves (in the plane: load – free vibration frequency) have been determined on the basis solution of boundary value problem. Calculations have been carried out at difference physical and geometrical parameters of considered systems.

Keywords: column, stability, free vibrations

1. Introduction

The considered geometrically non-linear column is built as a planar frame constructed of four rods with symmetrical distribution of flexural and torsional rigidity (Fig. 1b – compare [1, 6]). These systems are characterised by local and global instability [4, 5, 6] and by presence of rectilinear and curvilinear static equilibrium [1, 6]. The considered system is loaded by follower force directed towards the positive pole. This load is the one from a group of specific loads. For the first time the specific load was described and examined (theoretically, numerically and experimentally) by L.Tomski. Formulation of stability problem and free vibrations of column supported at he loaded end by a spring with linear characteristics was the aim of the paper. Supported spring is commonly used as a discrete element by many authors in research into stability and free vibrations of the column (compare [2, 3, 5]). Rigidity of the supported spring has influence – among other things – on change in critical force [2, 3, 5], on change in method of stability loss [3, 5] (flutter or divergence when applying non-conservative load, e.g. Beck's generalised load) and also on the change in characteristic curves in the plane: load – natural frequency [2, 3, 5].

2. Formulation of the boundary problem

Schematic diagram of the considered system is presented in Fig. 1a. The load by follower force directed towards the positive pole is realised by the loading heads constructed of linear elements. The load (Fig. 1a) is developed by infinitely rigid element (bolt) with

l_C in length, directed tangentially to the loaded end. End of the bolt is located on non-deformed axis of the column at point O. Point O determines a direction of the concentrated force P action. The ends of all rods are connected with each other and with the bolt through element with mass m. Spring supported the system is linear , and force recalled by the spring is dependent on deflection of loaded end of the system $W(l,t)$. In the considered case, the boundary problem is formulated on the basis of Hamilton's principle:

$$\delta \int_{t_1}^{t_2} (T-V)dt = 0 \tag{1}$$

Potential energy V and kinetic energy T are defined as follows:

$$V = \frac{1}{2}\sum_{i=1}^{4}(EJ)_i \int_0^l \left[\frac{\partial^2 W_i(x,t)}{\partial x^2}\right]^2 dx + \frac{1}{2}\sum_{i=1}^{4}(EA)_i \int_0^l [\varepsilon_i(x,t)]^2 dx +$$
$$\frac{1}{2}C(W_1(l,t))^2 + PU_1(l,t) + Pl_C \frac{1}{2}\left(\frac{\partial W_1(x,t)}{\partial x}\bigg|^{x=l}\right)^2 \tag{2}$$

$$T = \frac{1}{2}\sum_{i=1}^{4}\int_0^l (\rho_0 A)_i \left[\frac{\partial W_i(x,t)}{\partial t}\right]^2 dx + \frac{1}{2}m\left[\frac{\partial W_1(x,t)}{\partial t}\bigg|^{x=l}\right]^2 \tag{3}$$

where: $W_i(x,t)$, $U_i(x,t)$ – transversal and longitudinal displacement of the i-th rod, respectively, $(EJ)_i$ − flexural rigidity of the i-th rod, $(EA)_i$ − compressive rigidity of the i-th rod, $(\rho_0 A)_i$ − mass per unit length of the i-th rod, C − spring constant.
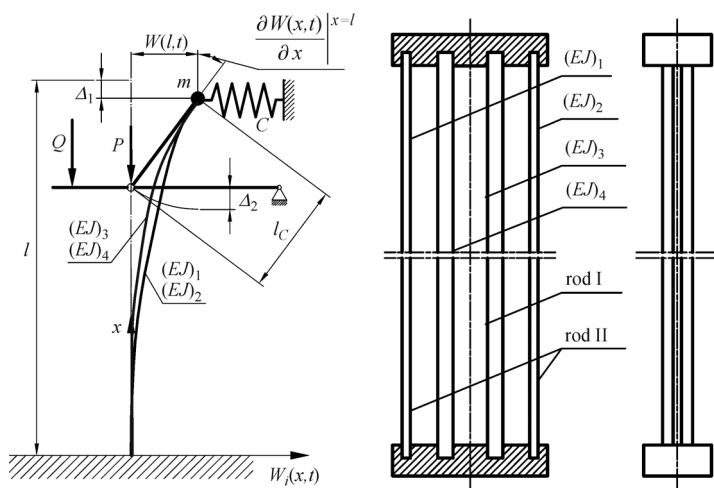
Fig.1. The considered slender system: a) schematic diagram, b) physical model of geometrically non-linear column

Deformation $\varepsilon_i(x,t)$ and axial force of the i-th rod, taking into account the theory of moderately large deflections, is written as:

$$\varepsilon_i(x,t) = \frac{\partial U_i(x,t)}{\partial x} + \frac{1}{2}\left(\frac{\partial W_i(x,t)}{\partial x}\right)^2 ; S_i(t) = -(EA)_i \varepsilon_i(x,t) \qquad (4a,b)$$

Dimensionless quantities are introduced:

$$\xi = \frac{x}{l} , \ w_i(\xi,\tau) = \frac{W_i(x,\tau)}{l} , \ u_i(\xi,\tau) = \frac{U_i(x,\tau)}{l} , \ k_i^2(\tau) = \frac{S_i(\tau)l^2}{(EJ)_i} ,$$

$$\Omega_i^2 = \frac{(\rho_0 A)_i \omega^2 l^4}{(EJ)_i} , \ \tau = \omega t , \ \Theta_i = \frac{A_i l^2}{J_i} , \ i = 1, 2, 3, 4 \qquad (5)$$

where, ω is the natural frequency of the system [rad/s].

Geometrical boundary conditions of the considered column with the use of dimensionless quantities are defined by the following expression:

$$w_1(0,\tau) = w_2(0,\tau) = w_3(0,\tau) = w_4(0,\tau) = 0 \qquad (6a\text{-}d)$$

$$\left.\frac{\partial w_1(\xi,\tau)}{\partial \xi}\right|_{\xi=0} = \left.\frac{\partial w_2(\xi,\tau)}{\partial \xi}\right|_{\xi=0} = \left.\frac{\partial w_3(\xi,\tau)}{\partial \xi}\right|_{\xi=0} = \left.\frac{\partial w_4(\xi,\tau)}{\partial \xi}\right|_{\xi=0} = 0 \qquad (6e\text{-}h)$$

$$\left.\frac{\partial w_1(\xi,\tau)}{\partial \xi}\right|^{\xi=1} = \left.\frac{\partial w_2(\xi,\tau)}{\partial \xi}\right|^{\xi=1} = \left.\frac{\partial w_3(\xi,\tau)}{\partial \xi}\right|^{\xi=1} = \left.\frac{\partial w_4(\xi,\tau)}{\partial \xi}\right|^{\xi=1} \qquad (6i\text{-}k)$$

$$w_1(1,\tau) = w_2(1,\tau) = w_3(1,\tau) = w_4(1,\tau) ; l_C \left.\frac{\partial w_1(\xi,\tau)}{\partial \xi}\right|^{\xi=1} - w_1(1,\tau)l = 0 \qquad (6l\text{-}o)$$

$$u_1(0,\tau) = u_2(0,\tau) = u_3(0,\tau) = u_4(0,\tau) = 0 ; u_1(1,\tau) = u_2(1,\tau) = u_3(1,\tau) = u_4(1,\tau) \qquad (7a\text{-}g)$$

By substituting potential and kinetic energy into Hamilton's principle and carried out appropriate transformation one can obtain:

• differential equation of motion in the transversal direction:

$$\frac{\partial^4 w_i(\xi,\tau)}{\partial \xi^4} + k_i^2(\tau)\frac{\partial^2 w_i(\xi,\tau)}{\partial \xi^2} + \Omega_i^2 \frac{\partial^2 w_i(\xi,\tau)}{\partial \tau^2} = 0 \qquad (8)$$

• differential equation of the longitudinal displacements:

$$\frac{\partial}{\partial \xi}\left[\frac{\partial u_i(\xi,\tau)}{\partial \xi} + \frac{1}{2}\left(\frac{\partial w_i(\xi,\tau)}{\partial \xi}\right)^2\right] = 0 \qquad (9)$$

• the natural boundary conditions:

$$\sum_{i=1}^{4}(EJ)_i\frac{\partial^3 w_i(\xi,\tau)}{\partial\xi^3}\bigg|^{\xi=1} - m\omega^2\frac{\partial^2 w_1(\xi,\tau)}{\partial\tau^2}\bigg|^{\xi=1}l^3 -$$

$$-\frac{l}{l_C}\sum_{i=1}^{4}(EJ)_i\frac{\partial^2 w_i(\xi,\tau)}{\partial\xi^2}\bigg|^{\xi=1} - Cw_1(1,\tau)l^3 = 0 \qquad ; \sum_{i=1}^{4}\left(k_i^2(\tau)\frac{(EJ)_i}{l^2}\right)-P=0 \quad (10a,b)$$

Equations (8) and (9) and boundary conditions (10) are written in dimensionless form after applying equations (5). The equation of longitudinal displacements (9), after having been integrated twice and after considering condition of axial force (4b), takes the form:

$$u_i(\xi,\tau)=-\frac{k_i^2(\tau)}{\Theta_i}\xi-\frac{1}{2}\int_0^\xi\left[\frac{\partial w_i(\xi,\tau)}{\partial\xi}\right]^2 d\xi \qquad (11)$$

The boundary problem presented above is non-linear (non-linearity occurs in relationship (11) – the element of integration). The straightforward expansion method is used to final formulation of the boundary problem. This method relies on expansion of all non-linear expressions $w_i(\xi,\tau)$, $u_i(\xi,\tau)$, $k_i^2(\tau)$ and Ω_i^2 into power series of small parameter. The considered geometrically non-linear system is characterised by rectilinear and curvilinear form of static equilibrium. The expansions into power series of small parameter at rectilinear and curvilinear static form are as follows:

• rectilinear form of static equilibrium:

$$w_i(\xi,\tau)=\sum_{j=1}^{N}\varepsilon^{2j-1}w_{i2j-1}(\xi,\tau)+O\big(\varepsilon^{2(N+1)}\big); u_i(\xi,\tau)=u_{i0}(\xi)+\sum_{j=1}^{N}\varepsilon^{2j}u_{i2j}(\xi,\tau)+O\big(\varepsilon^{2(N+1)}\big)$$

$$k_i^2(\tau)=k_{i0}^2+\sum_{j=1}^{N}\varepsilon^{2j}k_{i2j}^2(\tau)+O\big(\varepsilon^{2(N+1)}\big); \Omega_i^2=\Omega_{i0}^2+\sum_{j=1}^{N}\varepsilon^{2j}\Omega_{i2j}^2+O\big(\varepsilon^{2(N+1)}\big)(12a-d)$$

where: $$w_{ij}(\xi,\tau)=\sum_{z=1}^{\frac{j+1}{2}}\overset{(2z-1)}{w_{ij}}(\xi)\cos[(2z-1)\tau]; u_{ij}(\xi,\tau)=\overset{(0)}{u_{ij}}(\xi)+\sum_{z=1}^{\frac{j}{2}}\overset{(2z)}{u_{ij}}(\xi)\cos[2z\tau]$$

$$k_{ij}^2(\tau)=\overset{(0)}{k_{ij}^2}+\sum_{z=1}^{\frac{j}{2}}\overset{(2z)}{k_{ij}^2}\cos[2z\tau] \qquad (13a-c)$$

• curvilinear form of static equilibrium

$$w_i(\xi,\tau)=w_{i0}(\xi)+\sum_{j=1}^{N}\varepsilon^j w_{ij}(\xi,\tau)+O\big(\varepsilon^{2(N+1)}\big); u_i(\xi,\tau)=u_{i0}(\xi)+\sum_{j=1}^{N}\varepsilon^j u_{ij}(\xi,\tau)+O\big(\varepsilon^{2(N+1)}\big)$$

$$k_i^2(\tau) = k_{i0}^2 + \sum_{j=1}^{N} \varepsilon^j k_{ij}^2(\tau) + O\left(\varepsilon^{2(N+1)}\right); \; \Omega_i^2 = \Omega_{i0}^2 + \sum_{j=1}^{N} \varepsilon^j \Omega_{ij}^2 + O\left(\varepsilon^{2(N+1)}\right) \quad \text{(14a-d)}$$

where: $\quad w_{ij}(\xi,\tau) = \overset{(0)}{w_{ij}}(\xi) + \sum_{z=1}^{j} \overset{(z)}{w_{ij}}(\xi)\cos z\tau \; ; \; u_{ij}(\xi,\tau) = \overset{(0)}{u_{ij}}(\xi) + \sum_{z=1}^{j} \overset{(z)}{u_{ij}}(\xi)\cos z\tau$

$$k_{ij}^2(\tau) = \overset{(0)}{k_{ij}^2} + \sum_{z=1}^{j} \overset{(z)}{k_{ij}^2} \cos z\tau \quad\quad\quad \text{(15a-c)}$$

The expansions into series of small parameter are substituted into the differential equations (8) and (11) and the terms with identical powers of small parameter are being grouped. Thus, the infinite sequence of differential equations of motion in transversal direction and equations of longitudinal displacement have been obtained:

• rectilinear form of static equilibrium

$$\varepsilon^0 : u_{i0}(\xi) = -\frac{k_{i0}^2}{\Theta_i}\xi \; ; \; \varepsilon^1 : \frac{\partial^4 w_{i1}(\xi,\tau)}{\partial \xi^4} + k_{i0}^2 \frac{\partial^2 w_{i1}(\xi,\tau)}{\partial \xi^2} + \Omega_{i0}^2 \frac{\partial^2 w_{i1}(\xi,\tau)}{\partial \tau^2} = 0 \quad \text{(16a,b)}$$

• curvilinear form of static equilibrium

$$\varepsilon^0 : \frac{d^4 w_{i0}(\xi)}{d\xi^4} + k_{i0}^2 \frac{d^2 w_{i0}(\xi)}{d\xi^2} = 0 \; ; \; u_{i0}(\xi) = -\frac{k_{i0}^2 \xi}{\Theta_i} - \frac{1}{2}\int_0^\xi \left[\frac{dw_{i0}(\xi)}{d\xi}\right]^2 d\xi \quad \text{(17a,b)}$$

$$\varepsilon^1 : \frac{\partial^4 w_{i1}(\xi,\tau)}{\partial \xi^4} + k_{i0}^2 \frac{\partial^2 w_{i1}(\xi,\tau)}{\partial \xi^2} + \Omega_{i0}^2 \frac{\partial^2 w_{i1}(\xi,\tau)}{\partial \tau^2} = -k_{i1}^2(\tau)\frac{d^2 w_{i1}(\xi)}{d\xi^2} \quad\quad \text{(17c)}$$

$$u_{i1}(\xi,\tau) = -\frac{k_{i1}^2(\tau)\xi}{\Theta_i} - \int_0^\xi \left[\frac{dw_{i0}(\xi)}{d\xi}\frac{\partial w_{i1}(\xi,\tau)}{\partial \xi}\right] d\xi \quad\quad \text{(17d)}$$

Required equations in case of rectilinear and curvilinear form of static equilibrium, connected to the small parameter in zero and first power, are presented in the paper. The solutions to the equations, connected to small parameter in a power higher than one, are difficult for determination and their influence on total solution is low (small parameter has the value much lower than one ($\varepsilon \ll 1$)). To solve correctly the boundary problem, the expansions into series of small parameter ((12) – at rectilinear and (14) – at curvilinear form of static equilibrium) should be substituted into the boundary conditions given by equations 6), (7) and (10), and should be grouped according to identical powers of small parameter.

3. Solution to the boundary problem

Equation (16a) with the boundary conditions related to longitudinal displacements determines the relationship between internal forces in the rods at rectilinear form of static

equilibrium. Substitution of the solution to equation (16b) into the boundary conditions related to transversal displacement leads into the system of equations, whose determinant of the matrix of coefficients is transcendental equation for free vibration frequency at rectilinear form of static equilibrium. The distribution of internal forces, obtained according to equation (16a), should be considered.

By substituting the solution to equation (17a) into the boundary conditions related to transversal displacements, the system of equations is obtained. Determinant of the matrix of system coefficients is transcendental equation, from which the distribution of internal forces in column rods at curvilinear form of static equilibrium is assigned. The curvilinear form of static equilibrium is present between the bifurcation and critical load. The bifurcation load is computed on the basis on equation (16a) if transcendental equation for internal forces in the rods at the curvilinear form of static equilibrium is fulfilled simultaneously. Free vibration frequency is determined taking into account equation (17c) in case of the curvilinear form of static equilibrium. Equation (17b) is used for a computation of unknown present in the solution to equation (17a).

References

1. TOMSKI L.: Prebuckling Behaviour of Compound Column – Direct Nonlinear Analysis, ZAMM, Z. Angew. Math. U. Mech. 65, 1985, 1, 59-61.
2. TOMSKI L., PODGÓRSKA-BRZDĘKIEWICZ I.: Drgania swobodne i stateczność kolumn poddanych obciążeniu swoistemu – podatne węzły konstrukcyjne układu wywołujacego i przejmującego obciążenie, rozdział 4, Drgania i stateczność układów smukłych, Praca zbiorowa wykonana pod kierunkiem naukowym i redakcją L. TOMSKIEGO, Wydawnictwa Naukowo Techniczne, Fundacja „Książka Naukowo-Techniczna", Warszawa 2004, 134-187.
3. TOMSKI L., PRZYBYLSKI J.: Postbuckling Behavior of the Clamped-Elastically Supported Planar Structure under Follower Force, AIAA Journal, 25(4), 1987, 605-610.
4. TOMSKI L., SZMIDLA J.: Local and global instability and vibration of over-braced Euler's column, Journal of Theoretical and Applied Mechanics 41, 1, 2003, 137-154.
5. TOMSKI L., SZMIDLA J., UZNY S.: The Local and Global Instability and Vibration of Systems Subjected to Non-Conservative Loading, Thin-Walled Structures, 45, 10-11, 2007, 945-949.
6. TOMSKI L., UZNY S.: Free vibration and the stability of a geometrically non-linear column loaded by a follower force directed towards the positive pole, International Journal of Solids and Structures, 45, 1, 2008, 87-112.

EXTERNAL LOADS FOR MULTIHULL WATERCRAFT
Kazimierz TRĘBACKI, Agnieszka KRÓLICKA
Gdansk University of Technology, Faculty of Ocean Engineering and Ship Technology
ul. Narutowicza 11/12, 80-952 Gdańsk, Poland
Ph. :(58)347-22-91, e-mail: katre@pg.gda.pl**,** krag@pg.gda.pl**,**

Abstract
For multihull watercraft, general differential equations of motion were formulated taking into account possible movements of the oceanotechnic construction. These movements are connected with freedom degrees of the construction floating on the undulated sea surface. General formulas given for possible construction movements describe the external loads connected with hydrodynamic reactions, damping forces and hydrostatic reactions. The generalised excitation forces can refer to the case of regular undulation and for this case general formulas are given. Irregular sea undulation, which is a stochastic process, requires using linear filters developed based on parametric wave excitations relating to one of spectra collected in Table 1.

1. Introduction

The stochastic model is the basic model used in analysing sea watercraft subject to water undulation. It is assumed in this case that the sea condition is represented by the superposition of a large number of regular gravitational waves with small progressive amplitudes, for which random variables can be only phases, or both phases and amplitudes. The superposition based solutions obtained for the linear waves can be used for describing irregular undulation. In short time intervals and small areas the stochastic process of undulation can be considered stationary and homogeneous. For large water regions and long time intervals the assumption about homogeneity of the undulation process is not valid.
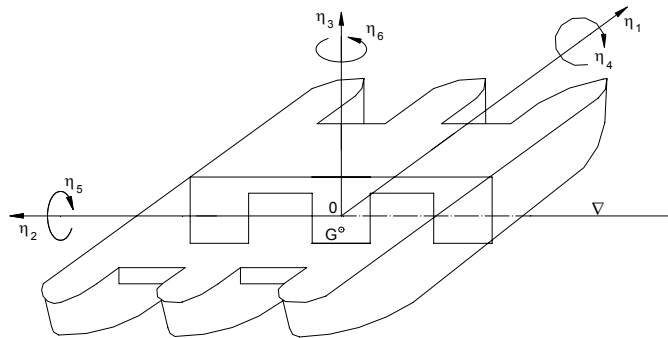
Fig.1. Scheme of the physical model of a multihull - trimaran

2. Equations of motion for the construction

The multihull (Fig.1) is a complex ocean going construction in both strength and hydrodynamic terms. In a general case it is treated as a watercraft consisting of a deck and a number of floats. The mathematical representation of this physical model has the form of six differential equations of motion:

$$A_{mk}\ddot{\eta}_k(t) + B_{mk}\dot{\eta}_k(t) + C_{mk}\eta_k(t) = F_m(t) \qquad (1)$$

for $k, m = 1, 2, 3..6$
where:

$$A_{mk} = M_{mk} + H_{mk} \qquad (2)$$

M_{mk} - elements of matrix of generalised construction masses,

H_{mk} - elements of matrix of generalised hydrodynamic masses,

B_{mk} - elements of matrix of damping coefficients,

C_{mk} - elements of matrix of hydrostatic elasticity,

$F_m(t)$ - generalised excitation forces,

$\eta_k(t)$ - vector of generalised displacements.

When analysing the matrix equation (1) we can separate six equations of motion into two mutually decoupled groups, equal to each other with respect to the number of equations. These two internally coupled groups include: symmetric movements η_k for $k = 1, 3, 5$ and antisymmetric movements η_k for $k = 2, 4, 6$.

3. External forces acting of the watercraft

The form of equation (1) and the type of matrix coefficients depend on the external forces acting on the watercraft. The external forces exerted by water can be divided into hydrodynamic reaction forces and excitation forces, taken into account by matrix coefficients and the free term vector in equation (1).
The generalised external forces acting on the construction are given by relation:

$$P_m = -\int_S (p - p_o)n_m dS \qquad (3)$$

where:

S - wetted surface area,

P_m - orthogonal projections of external forces for $m = 1, 2, 3$ and orthogonal projections of moments of external forces for $m = 4, 5, 6$,

n_m - unit vectors in the direction normal to surface S for $m = 1, 2...6$,

p - pressure at the wetted surface.

If $\phi = \phi(X,t)$ is the water velocity potential induced by watercraft movements and water undulation, then based on the Cauchy-Lagrange integral we can write:

$$p - p_o = -\rho[\phi_t + \frac{1}{2}(\nabla\phi)^2 + gX_3] \tag{4}$$

Substituting (4) into (3) we get:

$$P_m = -\rho\int\limits_S [\phi_t + g(\eta_3 + \eta_4 x_2 - \eta_5 x_1)n_m]dS \tag{5}$$

We search for the velocity potential in the class of additive functions as:

$$\phi = \phi_1(x) + \phi_2(x,t) \tag{6}$$

where:

ϕ_1 -stationary potential induced by floating movement,

ϕ_2 -total potential including water undulation and local movements.

The potential ϕ_2 is given in the following form:

$$\phi_2 = \phi_W + \phi_D + \phi_L \tag{7}$$

where:

ϕ_W -potential of water undulation velocity,

ϕ_D -diffraction potential,

ϕ_L - velocity potential from local movements.

4. Hydrodynamic and hydrostatic coefficients

General formulas for hydrodynamic coefficients from added masses:

$$A_{mk} = \text{Re}[K_{mk}] \tag{8}$$

and for damping coefficients

$$B_{mk} = -\omega\,\text{Im}[K_{mk}] \tag{9}$$

where:

$$K_{mk} = -i\omega\rho\int\limits_S n_m\varphi_k dS \tag{10}$$

for $m,k = 2,3,4,5,6$.

The hydrostatic elasticity coefficients are determined from formula:

$$C_{mk} = -\rho g\int\limits_S n_m(\eta_3 + \eta_4 x_2 - \eta_5 x_1)dS \tag{11}$$

The symmetry of the construction with respect to the vertical longitudinal plane is the reason why the majority of coefficients C_{mk} are equal to zero. The only non-zero coefficients are the following: $C_{33}, C_{44}, C_{55}, C_{35} = C_{53}$.

5. Excitation forces

The excitation forces are generated by water undulation and diffraction of waves. That means that they can be presented as functions of the undulation velocity potential ϕ_W and the diffraction potential ϕ_D in the form:

$$F_m = -i\rho\omega \int_S n_m(\phi_W + \phi_D)dS \qquad (12)$$

for $m = 2,3,..6$.

Instead of (12) we can write another relation for F_m

$$F_m = -\rho \int_S A_m \phi_W dS \qquad (13)$$

where:

$$A_m = i\omega n_m - \varphi_m\left(\frac{\partial}{\partial x_2}n_2 + \frac{\partial}{\partial x_3}n_3\right) \qquad (14)$$

for $m = 2,3,..6$.

When we have to deal with a stochastic process of undulation in long time intervals, then linear filters can be applied to the irregular undulation.

These filters are to be developed in such a way that the parametric excitations from the wave can be described by basic spectra (see Table 1), i.e. Pierson-Moskowitz, ISSC, Jonswap, Striekałow-Massel, and Paszkiewicz spectra.

The most frequently used undulation spectra in the dimensionless form (after parametrisation) are given by the following formula:

$$F = \frac{S_\eta(\omega)}{h_{1/3}^2 T_k} \qquad (15)$$

where:

$S_\eta(\omega)$ - one-dimensional energy spectrum function, T_k -time periods (see Table 2), h - wave height.

The source of information on undulation of seas and oceans are the observations and measurements of the undulation itself, of measurements of the wind that generates the undulation. In stochastic modelling of high importance is proper selection of parameters which describe the phenomenon and finding unique relations between the wind and undulation parameters. When studying the effect of water undulation, the mathematical models of sea watercraft make use of distribution functions of various quantities, obtained from identification carried out by various research centres.

Table 1. Types of undulation spectra

Type of undulation spectrum	Spectral density functions and relations for characteristic time periods
Pierson-Moskowitz spectrum	$F = \dfrac{S_\eta(\omega)}{T_2 h_{1/3}^2} = \dfrac{1}{8\pi^2}\left(\dfrac{\omega T_2}{2\pi}\right)^{-5}\exp\left(-\dfrac{1}{\pi}\left(\dfrac{\omega T_2}{2\pi}\right)^{-4}\right)$ $T_2 = 0,92T_1, \quad T_1 = 0,771T_0, \quad T_2 = 0,71T_0$
ISSC (International Ship Structures Congress) spectrum	$F = \dfrac{S_\eta(\omega)}{T_1 h_{1/3}^2} = \dfrac{0{,}11}{2\pi}\left(\dfrac{\omega T_1}{2\pi}\right)^{-5}\exp\left(-0{,}44\left(\dfrac{\omega T_1}{2\pi}\right)^{-4}\right)$ $T_2 = 0,92T_1, \quad T_1 = 0,771T_0, \quad T_{-1} = 1,11T$ for Northern Atlantic $T_4 = \sqrt{\dfrac{1-\varepsilon}{1,18}}T_1$ ε (spectrum width)-calculated from data obtained during undulation observation $\varepsilon^2 = 1 - \left(\dfrac{N_V}{N_{\max}}\right)^2$ N_V - number of observed waves $N_{\max}$ - number of observed wave maxima
JONSWAP (The Joint North Sea Wave Project) spectrum	$S_\eta(\omega) = \dfrac{AB}{\omega^5}\exp\left(-\dfrac{B}{\omega^4}\right)F^{-1}\gamma^{\exp\left(\frac{1}{2\sigma^2}\left(s\frac{\omega}{\omega_2}-1\right)^2\right)}$ where: $A = 0,25\left(h_{1/3}\right)^2$, $B = 0,32\left(\dfrac{2\pi}{T_2}\right)^4$, $F = 2,049$, $\omega = \dfrac{2\pi}{T_2}$. For $s = 1,406$, $\gamma = 3,3$ $\sigma = \begin{cases} 0,07 & dla \quad \dfrac{\omega}{\omega_2} < 0,711 \\ 0,09 & dla \quad \dfrac{\omega}{\omega_2} > 0,711 \end{cases}$ the undulation model is so- called average JONSWAP spectrum. In the parametrised form: $F = \dfrac{S_\eta}{T_1 h_{1/3}^2} = 0,5AF_{ISSC}$, where: F_{ISSC} - ISSC spectrum, $A = 3,3^{\exp\left(-80\left(0,2069\omega T_1 - 1\right)^{2,5}\right)}$

Paszkiewicz spectrum	$F = \dfrac{S_\eta(\omega)}{T_1 h_{1/3}^2} = 0,812 \cdot 10^{-3} \left(\dfrac{\omega T_1}{2\pi} \right)^{-5} \exp\left(-0,723 \left(\dfrac{\omega T_1}{2\pi} \right)^{-4} \right)$
Striekałow-Massel spectrum	$F = \dfrac{S_\eta(\omega)}{T_1 h_{1/3}^2} = 2,36 \cdot 10^{-2} \exp\left(-35 \left(\dfrac{\omega T_1}{2\pi} - 0,8 \right)^2 \right) +$ $+1,37 \cdot 10^{-2} \left(\dfrac{\omega T_1}{2\pi} \right)^{-5} \exp\left(-1,34 \left(\dfrac{\omega T_1}{2\pi} \right)^{-8} \right)$

Table 2. Averaged wave time periods

Averaged energy period	$T_{-1} = 2\pi \cdot m_{-1} / m_0$
Period connected with the frequency corresponding to spectrum maximum $\omega_m = \omega_0$	$T_0 = T_m = 2\pi / \omega_m$
Average undulation period (characteristic)	$T_1 = 2\pi \cdot m_0 / m_1$
Average period of zero places of the undulation process	$T_2 = 2\pi \sqrt{m_0 / m_2} = T_0^+$
Average period of successive local maxima	$T_4 = 2\pi \sqrt{m_2 / m_4} = T_m$

References

[1] Chakrabarti S.K., *Offshore Engineering*, Offshore Structure Analysis, Inc., Plainfield, Illinois, USA, Vol.1, 2005.
[2] Druet Cz., *Sea dynamics*, Gdansk University Publishing House, Gdańsk 2000 (in Polish).
[3] Kang D., Hasegawa K., *Prediction method of hydrodynamic forces acting on the hull of a blunt-body ship in the even keel condition*, Journal of Marine Science and Technology, Vol.12, Number 1, 1-14, 2007.
[4] Królicka A., *Stochastic approach to the dynamics of a linear floating object*, Marine Technology Transactions-Vol.17, pp.121-130, Gdańsk 2006.
[5] Rumianowski A., *Investigating the dynamics of selected marine floating objects*, Gdańsk 2003 (in Polish).
[6] Rumianowski A., *Dynamics of free weight-displacement rigid offshore float constructions*, Shipbuilding XXXIX, Gdańsk 1984 (in Polish).
[7] Sobczyk K., *Stochastic differential equations*, Warszawa 1996 (in Polish).
[8] Sobczyk K, Spencer Jr.,B.F., *Stochastic models of material fatigue,* Wydawnictwa Naukowo-Techniczne, Warsaw 1996 (in Polish).

STABILITY OF ROTATING SHAFTS IN A WEAK FORMULATION

Andrzej TYLIKOWSKI
Warsaw University of Technology
Narbutta 84, 02-524 Warszawa
phone: +48 22 2348244, e-mail: aty@simr.pw.edu.pl

Abstract
The stability analysis method is developed for a thin-walled rotating shaft with relaxed assumptions imposed on solutions. The problem is motivated by structural vibrations with external time-dependent parametric excitations which are controlled using surface mounted or embedded actuators and sensors. The commonly used strong form of dynamics equations involves irregularities which lead to computational difficulties for estimation and control problems. In order to avoid irregular terms resulting from differentiation of torques the dynamics equations are written in a weak form. The study of stability analysis is based on examining properties of Liapunov functional along a weak solution. Solving the problem is presented for an arbitrary combination of simply supported and clamped boundary conditions. Formulas defining dynamic stability regions are written explicitly.
Key words: weak form, thin-walled shaft, dynamic stability, different boundary conditions.

1. Introduction

Thin-walled, usually angle-ply laminated shafts relatively easy meet requirements of torsional strength and stiffness but are more flexible to bending and have specific elastic and damping properties which depend on the system geometry, physical properties of plies and on the laminate arrangement. Such systems are also sensitive to a lateral buckling. The dynamic stability of rotating composite shaft described by partial differential equations [5] was investigated using the direct Liapunov method. Another important problem of this paper is the description of the global damping of a laminated shaft. Despite the fact that in case of viscoelastic orthotropic plies the resulting constitutive equation is of higher order, the simple Voigt-Kelvin model is assumed. Thin-walled shalls reveal a considerable deformation of cross-section contour during bending. One of the first studies taking into account Brazier's effect was a rotating shaft stability analysis [6] in which the closed form analytical criteria were derived. The influence of thermal activation of hybrid composite shafts on stability domains was examined [7]. Recently, the dynamic stability criterion of rotating viscoelastic shafts with the effect of transverse inertia subjected to a random axial force was determined [4].

In our dynamics study the rotating laminated circular cylindrical shell will be treated as a beam-like structure. The reduction is justified by a symmetric plies arrangement and negligible circumferential stresses in the shaft. The shaft is assumed to be compressed by an axial force. The stability analysis problem of dynamic equations in a weak form is motivated by structural vibrations with external time-dependent parametric excitations

which are controlled using surface mounted or embedded actuators and sensors. The commonly used strong form of dynamics equations involves irregularities which lead to computational difficulties for estimation and control problems. In order to avoid irregular terms resulting from differentiation of torques the dynamics equations are written in a weak form. The direct Liapunov method is used to analyse the uniform stochastic stability of the equilibrium state. Special attention is paid to a positive-definiteness of the appropriate energy-like Liapunov functional. Analysing the positive-definiteness leads to sufficient stability conditions, expressed in terms of the rotation speed, the damping coefficients, the bending stiffness.

2. Weak formulation of shaft dynamics equations

Let us consider a geometrically perfect long cylindrical shell of radius R, length l and total thickness h ($l>>R>>h$). The shaft, treated as a symmetrically laminated shell, contains the conventional (e.g. graphite or glass) fibers oriented at Θ and Θ to the shell axis. The shaft rotates with the constant angular velocity ω and arbitrary combinations of the simply supported and clamped edges is assumed. The shaft is assumed to have a constant circular cross section without initial geometrical imperfections. The mean density is denoted by ρh and the area and the geometrical moment of inertia of the shaft cross-section are denoted by A and J, respectively. The beam-like approach due to Bauchau [2] is used in order to derive the global elastic constant EJ of the shaft. It is assumed that the rotating shaft is loaded by uniformly distributed time-independent centrifugal forces. Displacements of the center shaft line in movable rotating coordinates are denoted by u, v. In order to derive dynamics equations in a weak form we apply Hamilton's principle. Starting from the rotating shaft without damping and axial loading we write an action integral as the time integral of difference of kinetic energy and bending energy

$$A\!\left(\vec{u}\right)=\frac{1}{2}\int_{t_o}^{t}\int_{0}^{l}\!\left[\left(u_{,t}+\omega v\right)^2+\left(v_{,t}-\omega u\right)^2-e\!\left(u_{,xx}^2+v_{,xx}^2\right)\right]\!dx\,dt \tag{1}$$

where $\vec{u}=[u,v]^T \in W=\left(H_b^2(0,l)\right)^2$, the index b denotes the set of functions satisfying the essential boundary conditions, the time interval (t_o,t) is arbitrarily chosen. Consider

$$\hat{u}=\vec{u}+\varepsilon\Theta=\begin{bmatrix}u(t,x)\\v(t,x)\end{bmatrix}+\varepsilon\begin{bmatrix}\eta_1(t)\Phi(x)\\\eta_2(t)\Psi(x)\end{bmatrix} \tag{2}$$

where $\eta_1(t_o)=\eta_2(t)$, $\Theta \in W$. According to Hamilton's principle the shaft motion must have a stationary value to the action integral, therefore

$$\frac{d}{d\varepsilon} A\left(\bar{u} + \varepsilon\Theta\right)\Big|_{\varepsilon=0} = 0 \tag{3}$$

Using equation (2) in equation (3) and integrating by part with respect to time the time-derivatives of functions η_1 and η_2 we obtain the dynamics equations of shaft in a weak form

$$\forall_\Phi \int_0^l \left[\left(u_{,tt} + 2\omega v_{,t} - \omega^2 u\right)\Phi + e u_{,xx}\Phi_{,xx}\right]dx = 0 \tag{4}$$

$$\forall_\Psi \int_0^l \left[\left(v_{,tt} - 2\omega u_{,t} - \omega^2 v\right)\Psi + e v_{,xx}\Psi_{,xx}\right]dx = 0 \tag{5}$$

Adding the internal viscous damping with coefficient β_i, the external viscous damping with coefficient β_e and the axial force as external works the shaft dynamic equations can be written in the weak form as follows

$$\forall_\Phi \int_0^l \left[\left(u_{,tt} + 2\omega v_{,t} - \omega^2 u\right)\Phi + \beta_e\left(u_{,t} + \omega v\right)\Phi + \beta_i u_{,t}\Phi + e u_{,xx}\Phi_{,xx} + f_o u_{,xx}\Phi\right]dx = 0 \tag{6}$$

$$\forall_\Psi \int_0^l \left[\left(v_{,tt} - 2\omega u_{,t} - \omega^2 v\right)\Psi + \beta_e\left(v_{,t} - \omega u\right)\Psi + \beta_i u_{,t}\Psi + e v_{,xx}\Psi_{,xx} + f_o v_{,xx}\Psi\right]dx = 0 \tag{7}$$

where Φ, Ψ are sufficiently smooth test functions satisfying essential boundary conditions. There is no demand of the existence of higher derivatives than the second order. As detailed in [1], the usual integration by parts terms containing derivatives of test functions with respect to the variable x and the assumption of sufficient smoothness of the components of shaft displacements lead to the commonly used strong formulation.

The shaft is assumed to be simply supported or clamped on both ends. Therefore the essential boundary conditions have following form at its ends

$$u(0,t) = u(l,t) = v(0,t) = v(l,t) = 0$$

3. Stability analysis

In order to determine conditions of smooth shaft motion corresponding to the Liapunov stability of of trivial solution $u = v = 0$ we choose the positive-definite Liapunov functional in the energy-like form [5]

$$V = \frac{1}{2}\int_0^l \left[\left(u_{,t} + \omega v + \beta u\right)^2 + \left(u_{,t} + \omega v\right)^2 + \left(v_{,t} - \omega u + \beta v\right)^2 + \right.$$

$$\left. + \left(v_{,t} - \omega u\right)^2 + 2e\left(u_{,xx}^2 + v_{,,xx}^2\right) - 2f_o\left(u_{,x}^2 + v_{,x}^2\right) \right]dx \qquad (8)$$

where $\beta = \beta_i + \beta_e$.

The functional is positive-definite if the constant axial force f_o fulfils a static buckling condition, i.e. is sufficiently small. Therefore, the measure of distance $\parallel \parallel$ of solutions with nontrivial initial conditions from the trivial one needed in stability analysis can be chosen as a square root of the functional. As trajectories of the solution of equations (6) and (7) are physically realizable the classical calculus is applied to calculation of the time-derivative of functional (8). Its time-derivative is given by

$$\frac{dV}{dt} = \int_0^l \left[\left(u_{,t} + \omega v + \beta u\right)\left(u_{,tt} + \omega v_{,t} + \beta u_{,t}\right) + \left(u_{,t} + \omega v\right)\left(u_{,tt} + \omega v_{,t}\right) + \right.$$

$$+ \left(v_{,t} - \omega u + \beta v\right)\left(v_{,tt} - \omega u_{,t} + \beta v_{,t}\right) + \left(v_{,t} - \omega u\right)\left(v_{,tt} - \omega u_{,t}\right) + \qquad (9)$$

$$\left. + 2e\left(u_{,xx}u_{,txx} + v_{,xx}v_{,txx}\right) - 2f_o\left(u_{,x}u_{,tx} + v_{,x}v_{,tx}\right) \right]dx$$

In order to avoid a integration by parts in equations (9) and generation the third and the fourth partial derivatives of displacements we substitute $2u_{,t}$, $2\omega v$, βu as the test functions in equation (6). Therefore, we have three identities, respectively

$$\int_0^l \left[2\left(u_{,tt} + 2\omega v_{,t} - \omega^2 u\right)u_{,t} + 2\beta u_{,t}^2 + 2\beta_e\omega v u_{,t} + 2e u_{,xx}u_{,xxt} + 2f_o u_{,xx}u_{,t} \right]dx = 0$$

$$\int_0^l \left[2\left(u_{,tt} + 2\omega v_{,t} - \omega^2 u\right)\omega v + 2\beta\omega u_{,t}v + 2\beta_e\omega^2 v^2 + 2e\omega u_{,xx}u_{,xxt} + 2\omega f_o u_{,xx}v \right]dx = 0 \quad (10)$$

$$\int_0^l \left[\beta\left(u_{,tt} + 2\omega v_{,t} - \omega^2 u\right)u + \beta^2 u_{,t}u + \beta\beta_e\omega u v + \beta e u_{,xx}^2 + 2\beta f_o u_{,xx}u \right]dx = 0$$

In a similar way we substitute $2v_{,t}$, $2\omega u$, βv as the test functions in equation (7)

$$\int_0^l \left[2\left(v_{,tt} - 2\omega u_{,t} - \omega^2 v\right)v_{,t} + 2\beta v_{,t}^2 - 2\beta_e\omega u v_{,t} + 2e v_{,xx}v_{,xxt} + 2f_o v_{,xx}v_{,t} \right]dx = 0$$

$$\int_0^l \left[2\left(v_{,tt} - 2\omega u_{,t} - \omega^2 v\right)\omega u + 2\beta\omega v_{,t}u - 2\beta_e\omega u v_{,t} + 2e\omega v_{,xx}u_{,xx} + 2\omega f_o v_{,xx}u \right]dx = 0 \quad (11)$$

$$\int_0^l \left[\beta \left(v_{,tt} - 2\omega u_{,t} - \omega^2 v \right) v + \beta^2 v_{,t} v - \beta\beta_e \omega uv + \beta e v_{,xx}^2 + 2\beta f_o v_{,xx} v \right] dx = 0$$

Subtracting identities (10), (11) from the functional time-derivative (9) we obtain the following form

$$\frac{dV}{dt} = -\int_0^l \left[\beta \left(u_{,t}^2 + v_{,t}^2 \right) + \omega^2 \left(\beta_e - \beta_i \right) \left(u^2 + v^2 \right) + 2\omega\beta_e \left(vu_{,t} - uv_{,t} \right) + \right.$$

$$\left. + \beta e \left(u_{,xx}^2 + v_{,xx}^2 \right) - \beta f_o \left(u_{,x}^2 + v_{,x}^2 \right) \right] dx \tag{12}$$

It should be noticed that the way to obtain equation (12) is purely algebraic contrary to systems described by strong equations, where the derivation of stability conditions is based on integrations by parts and manipulations with higher order partial derivatives. Usually the Liapunov stability analysis of shafts was performed for both edges simply supported, cf. [4]. In order to extend the field of possible applications let assume the following combinations of boundary conditions: a) s-s, b) c-s, c) c-c, where s denotes the simply supported edge, and c denotes the clamped edge.

Let assume the following expansions of shaft displacements

$$\begin{bmatrix} u(x,t) \\ v(x,t) \end{bmatrix} = \sum_{n=1,2,\ldots}^{\infty} W_n(x) \begin{bmatrix} S_n(t) \\ T_n(t) \end{bmatrix} \tag{13}$$

where functions $W_n(x)$ are the beam functions [3] depending on the assumed set of boundary conditions. Integrating we have the following equality [8]

$$\int_0^l W_{n,xx}^2(x) dx = \kappa_n \alpha_n^2 \int_0^l W_{n,x}^2(x) dx \tag{14}$$

and

$$\int_0^l W_{n,x}^2(x) dx = \frac{\alpha_n^2}{\kappa_n} \int_0^l W_n^2(x) dx \tag{15}$$

where α_n is an eigen-value of boundary problem. Applying equalities (14) and (15) in equation (12) we have the following upper estimation of the functional time-derivative

$$\frac{dV}{dt} \le -\beta \left(1 + \frac{\beta_e}{\beta_i} \right) \alpha_1^2 \left(e\alpha_1^2 - \frac{f_o}{\kappa_1} \right) \int_0^l \left(u^2 + v^2 \right) dx \tag{16}$$

In Table 1 are given values of κ_n and α_n for the given boundary conditions.

Table 1.

	s-s	s-c	c-c
α_1	π	3.927	4.730
κ_1	1	1.3396	1.8185

Finally, the critical angular velocity is defined as

$$\omega_{cr}^2 = \left(1 + \frac{\beta_e}{\beta_i}\right)^2 \alpha_1^2 \left(e\alpha_1^2 - \frac{f_o}{\kappa_1}\right) \tag{17}$$

4. Conclusions

A method has been presented for analysing the stability of rotating thin-walled composite shafts described by equations in a weak form. The problem is simplified as compared with the strong equations due to the elimination of integration by parts demanding existence of higher order partial derivatives of solutions. The critical rotation speed depends on material parameters and damping coefficients.

Acknowledgement

References
1. H. T. Banks, W. Fang, R. J. Silcox, R. C. Smith, *Approximation methods for control of structural acoustics models with piezoelectric actuators,* Journal of Intelligent Material Systems and Structures, **4** (1993) 98-116.
2. O. A. Bauchau, *Optimal design of high speed rotating graphite/epoxy shafts, J. Composite Materials,* **17** (1983)170 -181.
3. K. F. Graff, *Wave motion in elastic solids*, Dover Publications, New York, 1975.
4. R. Pavlović, P. Rajković, I. Pavlović, *Dynamic stability of the viscoelastic rotating shaft subjected to random excitation*, Intern. J. Mechanical Sciences **50** (2008) 359-364.
5. A. Tylikowski, *Dynamic stability of rotating angle-ply composite shafts,* Machine Dynamics Problems, **6** (1993) 141-156.
6. A. Tylikowski, *Stochastic stability of rotating composite shafts with Brazier's effect*, In: Nonlinear Science, B, **7**, Chaos and Nonlinear Mechanics, (Chua L. O., ed.), World Scientific, Singapore 1994.
7. A. Tylikowski, *Influence of torque on dynamic stability of composite thin-walled shafts with Brazier's effect, Mechanics and Mechanical Engineering*, **1** (1997) 145-155.
8. A. Tylikowski, *Dynamic stability of weak equations of rectangular plates*, J. Theor. Appl. Mech., **46** (2008) (in print).

SOLUTION OF PLATE FREE VIBRATIONS PROBLEM
BY METHOD OF FUNDAMENTAL SOLUTIONS

Anita USCILOWSKA

Poznan University of Technology, Institute of Applied Mechanics
ul. Piotrowo 3, 60-965 Poznan, POLAND
e-mail: anita.uscilowska@put.poznan.pl

Abstract

In this paper, a meshless method for solving the natural vibration of plates problem is proposed. For this particular problem the method of fundamental solutions has been implemented. due to its features, the final resolving system can be solved with the classical approaches by using standard numerical procedures. To asses the formulation, the free vibration of some plates were calculated and the results compared with those obtained using other solution techniques. The present results are in good agreement with those found in the literature showing the accuracy and effectiveness of the proposed approach.

keywords: natural frequencies, free vibrations, method of fundamental solutions

Introduction

In numerical methods, mesh generation of a complicated geometry is always time consuming in the stage of model creation for engineers in dealing with the engineering problems by employing the finite difference method, finite element method and boundary element method. In the last decade, researchers have paid attention to the meshless method without employing the concept of element. The initial idea of meshless method dates back to the smooth particle hydrodynamics method for modeling astrophysical phenomena [1]. Several meshless methods have also been reported in the literature, for example, the domain-based method including the element-free Galerkin method [2], the reproducing kernel method [3], boundary-based method including the boundary node method [4], the meshless local Petrov-Galerkin approach [5], the local boundary integral equation method [6], the radial basis function approach [7], fundamental solution method [8]. These methods are implemented for static, dynamic problems, and natural vibrations as well [9]. The present paper shows the solution of the natural vibration problem of a plate by the method of fundamental solutions.

1. Problem description

A flat plate of thickness h, referred to a Cartesian system of co-ordinates with x_1 and x_2 axes laying on its middle surface and x_3 axis perpendicular to that plane, is considered. The plate domain is denoted by Ω, while its boundary is represented by Γ. The equilibrium equation governing the plate motion is written as

$$D\nabla^4 w(\mathbf{x}, t) + \rho h \ddot{w}(\mathbf{x}, t) = q(\mathbf{x}, t) \text{ for } \mathbf{x} \in \Omega \tag{1}$$

where $w(\mathbf{x},t)$ is the plate deflection, ∇^4 is biharmonic operator, ρ is the mass density of the plate material, D is rigidity of the plate and is given as $D= Eh^3/(12(1\text{-}\nu^2))$, where E and ν are material constants, respectively, young modulus and Poisson ratio. Moreover, $q(\mathbf{x})$ is applied pressure. The boundary conditions for every boundary points are as follows. For the clamped boundary both the deflection and slope of the plate are equal to zero:

$$w(\mathbf{x},t)=0 \qquad \frac{\partial w}{\partial n}(\mathbf{x},t)=0 \qquad \text{for } \mathbf{x} \in \Gamma \tag{2}$$

For simply supported edge of the plate the deflection and bending moment equal zero:

$$w(\mathbf{x},t)=0 \qquad M(\mathbf{x},t)=0 \qquad \text{for } \mathbf{x} \in \Gamma \tag{3}$$

If the edge of the plate is free, the bending moment and transverse force are equal to zero. So the boundary conditions are:

$$M(\mathbf{x},t)=0 \qquad V(\mathbf{x},t)=0 \qquad \text{for } \mathbf{x} \in \Gamma \tag{4}$$

The analysis of the free vibrations of the plate is based on the assumption that the deflection function can be rewritten in the following form:

$$w(\mathbf{x},t)= W(\mathbf{x})T(t)= W(\mathbf{x})e^{i\omega t} \tag{5}$$

where ω is the natural frequency of the plate. Using the formula (5) in the equation (1) gives the free vibration equation:

$$\nabla^4 W(\mathbf{x})- \lambda^4 W(\mathbf{x})= 0 \tag{6}$$

where $\lambda^4 = \omega^2 \rho h/D$. The boundary conditions (2)-(4) are written in a general form and for the equation (6) have the form:

$$B_1 W(\mathbf{x})= 0 \qquad B_2 W(\mathbf{x})= 0 \qquad \text{for } \mathbf{x} \in \Gamma \tag{7}$$

To solve the problem of free vibration the method of fundamental solutions is applied.

2. The method of fundamental solutions

The method of fundamental solutions has been implemented for solving the boundary value problem given by (6) and (7). To write the approximated form of the solutions the set of grid points $\left\{\mathbf{x}_i^g\right\}_{i=1}^{Ng}$ is introduced. The grid points are the points of the region Ω and are shown in Figure 1. The set of boundary points $\left\{\mathbf{x}_i^b\right\}_{i=1}^{Nb}$ is defined and presented in Figure 2. Moreover, the auxiliary boundary so-called source contour (see Figure 2), outside the considered region is introduced. The points laying on the outer contour are called source points and are noted as $\left\{\mathbf{x}_i^s\right\}_{i=1}^{Ns}$.

The solution is assumed to be in form of the sum of linear combination of radial basis functions and linear combination of fundamental solution as:

$$W(\mathbf{x})= \sum_{i=1}^{Ns} c_i f_{S1}\left(r_i^s\right)+ \sum_{i=1}^{Ns} c_{Ns+i} f_{S2}\left(r_i^s\right)+ \sum_{i=1}^{Ng} a_i \phi\left(r_i^g\right)\sum_{i=1}^{Np} b_i \psi_i(\mathbf{x}) \tag{8}$$

In the formula (8) functions f_{S1}, f_{S2} are fundamental solutions of the equation with biharmonic operator. Quantity r_i^s is a distance between arbitrary point of Ω and ith source point, therefore $r_i^s = \left\| \mathbf{x} - \mathbf{x}_i^s \right\|$ for $i = 1,..., N_s$.
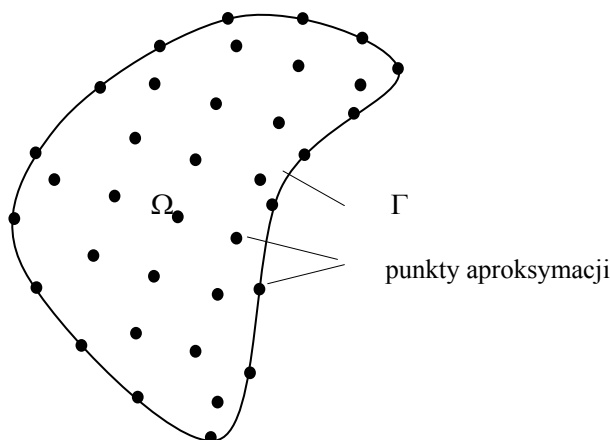
Figure 1. The grid points in the region Ω and on the boundary Γ.

The functions ϕ, ψ_i (for $i = 1,..., N_p$) are the particular solutions of the homogeneous equations:

$$\nabla^4 \varphi(r) = \phi(r) \qquad \nabla^4 \psi_i(\mathbf{x}) = p_i(\mathbf{x}) \text{ for } i = 1,..., N_p \qquad (9, 10)$$

The function ϕ is called Radial Basis Function (RBF), ψ_i (for $i = 1,..., N_p$) are monomials of $\mathbf{x}$. The argument of RBF is a distance between any point of Ω and ith grid point, therefore $r_i^g = \left\| \mathbf{x} - \mathbf{x}_i^g \right\|$ for $i = 1,..., N_g$. Real numbers coefficients c_i (for $i = 1,...,2 N_s$), a_i (for $i = 1,..., N_g$) and b_i (for $i = 1,..., N_p$) are to be calculated. Moreover, the parameter λ, related to natural frequencies, is unknown and is to be calculated.

The equation (6) is written using formula (8) for each grid point. It gives N_g linear equations in the form:

$$
\begin{aligned}
&\lambda^4 \sum_{i=1}^{Ns} c_i f_{S1}\left(r_{ji}^{gs}\right) + \lambda^4 \sum_{i=1}^{Ns} c_{Ns+i} f_{S2}\left(r_{ji}^{gs}\right) \\
&+ \sum_{i=1}^{Ng} a_i \left(\lambda^4 \phi\left(r_{ji}^g\right) - \varphi\left(r_{ji}^g\right)\right) \sum_{i=1}^{Np} b_i \left(\lambda^4 \psi_i\left(\mathbf{x}_j^g\right) - p_i\left(\mathbf{x}_j^g\right)\right) = 0
\end{aligned}
\qquad \text{for } j=1,..., N_g. \qquad (11)
$$

$$\sum_{i=1}^{Ng} a_i p_j\left(\mathbf{x}_i^g\right) = 0 \text{ for for } j=1,..., N_p, \qquad (12)$$

where $r_{ji}^{gs} = \left\| \mathbf{x}_j^s - \mathbf{x}_i^g \right\|$ for $i=1,...,\ N_g$, $j=1,...,\ N_s$, and $r_{ji}^g = \left\| \mathbf{x}_j^g - \mathbf{x}_i^g \right\|$ for $i,j=1,...,\ N_g$.

Next equations are obtained by writing the boundary conditions, described by (7), using form (8) of solution for each of boundary points:

$$\sum_{i=1}^{Ns} c_i B_1 f_{S1}\left(r_{ji}^{bs}\right) + \sum_{i=1}^{Ns} c_{Ns+i} B_1 f_{S2}\left(r_{ji}^{bs}\right) + \sum_{i=1}^{Ng} a_i B_1 \phi\left(r_{ji}^{bg}\right) \sum_{i=1}^{Np} b_i B_1 \psi_i\left(\mathbf{x}_j^b\right) = 0 \tag{13}$$

$$\sum_{i=1}^{Ns} c_i B_2 f_{S1}\left(r_{ji}^{bs}\right) + \sum_{i=1}^{Ns} c_{Ns+i} B_2 f_{S2}\left(r_{ji}^{bs}\right) + \sum_{i=1}^{Ng} a_i B_2 \phi\left(r_{ji}^{bg}\right) \sum_{i=1}^{Np} b_i B_2 \psi_i\left(\mathbf{x}_j^b\right) = 0 \tag{14}$$

for $j=1,...,\ N_b$, where $r_{ji}^{bs} = \left\| \mathbf{x}_j^b - \mathbf{x}_i^s \right\|$ for $i=1,...,\ N_s$, $j=1,...,\ N_b$, and $r_{ji}^{bg} = \left\| \mathbf{x}_j^b - \mathbf{x}_i^g \right\|$ for $i=1,...,\ N_g$, $j=1,...,\ N_b$.
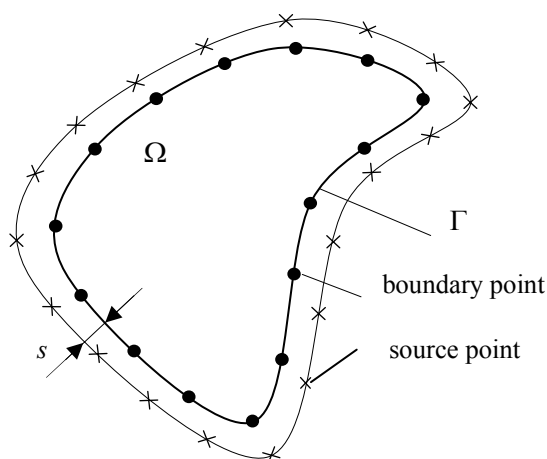

Figure 2. The boundary and source points for the considered region

The equations (11)-(14) form the system of $2N_s + N_g + N_p$ linear equations with $2N_s + N_g + N_p$ unknowns. Moreover the parameter λ is to be obtained. The system of equations (11)-(14) is written in matrix form:

$$\mathbf{A}(\lambda)\mathbf{c} = 0 \tag{15}$$

where $\mathbf{A}(\lambda)$ is a matrix with some elements dependent on unknown parameter λ. This matrix has the form:

$$\mathbf{A}(\lambda) = \begin{bmatrix} \mathbf{A}_{11}(\lambda) & \mathbf{A}_{12}(\lambda) & \mathbf{A}_{13}(\lambda) & \mathbf{A}_{14}(\lambda) \\ \mathbf{A}_{21} & \mathbf{A}_{22} & \mathbf{A}_{23} & \mathbf{A}_{24} \\ \mathbf{A}_{31} & \mathbf{A}_{32} & \mathbf{A}_{33} & \mathbf{A}_{34} \\ \mathbf{A}_{41} & \mathbf{A}_{42} & \mathbf{A}_{43} & \mathbf{A}_{44} \end{bmatrix} \tag{16}$$

and elements of matrix $\mathbf{A}(\lambda)$ are:

$$\mathbf{A}_{11}(\lambda) = \lambda^4 \left[f_{s1}\left(r_{ji}^{gs}\right) \right]_{Ng \times Ns}, \quad \mathbf{A}_{12}(\lambda) = \lambda^4 \left[f_{s2}\left(r_{ji}^{gs}\right) \right]_{Ng \times Ns}, \quad \mathbf{A}_{13}(\lambda) = \left[\lambda^4 \phi\left(r_{ji}^{g}\right) - \varphi\left(r_{ji}^{g}\right) \right]_{Ng \times Ng},$$

$$\mathbf{A}_{14}(\lambda) = \left[\lambda^4 \psi_i\left(\mathbf{x}_j^{g}\right) - p_i\left(\mathbf{x}_j^{g}\right) \right]_{Ng \times Np}, \quad \mathbf{A}_{21} = [0]_{Np \times Ns}, \quad \mathbf{A}_{22} = [0]_{Np \times Ns}, \quad \mathbf{A}_{23} = \left[p_j\left(x_i^{g}\right) \right]_{Np \times Ng},$$

$$\mathbf{A}_{24} = [0]_{Np \times Np}, \quad \mathbf{A}_{31} = \left[B_1 f_{s1}\left(r_{ji}^{bs}\right) \right]_{Nb \times Ns}, \quad \mathbf{A}_{32} = \left[B_1 f_{s2}\left(r_{ji}^{bs}\right) \right]_{Nb \times Ns}, \quad \mathbf{A}_{33} = \left[B_1 \phi\left(r_{ji}^{bg}\right) \right]_{Nb \times Ng},$$

$$\mathbf{A}_{34} = \left[B_1 \psi_i\left(\mathbf{x}_j^{b}\right) \right]_{Nb \times Np}, \quad \mathbf{A}_{41} = \left[B_2 f_{s1}\left(r_{ji}^{bs}\right) \right]_{Nb \times Ns}, \quad \mathbf{A}_{42} = \left[B_2 f_{s2}\left(r_{ji}^{bs}\right) \right]_{Nb \times Ns},$$

$$\mathbf{A}_{43} = \left[B_2 \phi\left(r_{ji}^{bg}\right) \right]_{Nb \times Ng}, \quad \mathbf{A}_{44} = \left[B_2 \psi_i\left(\mathbf{x}_j^{b}\right) \right]_{Nb \times Np}.$$

The vector of unknown coefficients is: $\mathbf{c} = \left[c_1, \ldots, c_{2Ns}, a_1, \ldots, a_{Ng}, b_1, \ldots, b_{Np} \right]^T$

The general notation has been chosen that the subscript j corresponds to the rows, the subscript i indicates the columns. The system of equations (11)-(14) in homogeneous one and the determinant of the matrix given by formula (16) is to be equal to zero. Therefore, the nonlinear algebraic equation

$$\det\left[\mathbf{A}(\lambda)\right] = 0 \tag{17}$$

is solved. The solution of (17) is the parameter λ related to the natural frequencies by formula $\lambda^4 = \omega^2 \rho h / D$. To find the mode shapes the system of equations (15) is solved with λ calculated by solving (17). The system (15) has infinite number of solutions, therefore one of the unknown numbers in $\mathbf{c}$ is treated as parameter and the real value is chosen for this parameter. So, the system (15) is reduced and has $2N_s + N_g + N_p - 1$ unknowns and $2N_s + N_g + N_p - 1$ equations.

3. Numerical example

The natural frequencies and mode shapes of the simply supported plate of thickness $h = 0.01$ m are calculated. The plate material parameters are: $E = 2 \cdot 10^{11}$ Pa, $\nu = 0.3$. The plate is of trapezoid shape, shown in Figure 3.

The numerical experiment has been performed for different values of Δx. The natural frequencies of the plate versus some values of Δx are included in Table 1.
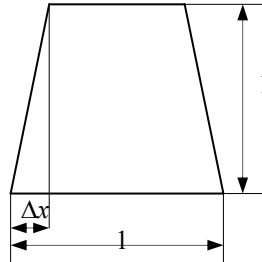

Figure 3. The geometry of the considered plate

The results show that the natural frequency of the plate increases with increasing parameter Δx. The extended discussion about received results will be presented during the Symposium presentation.

Δx	0.0	0.05	0.1	0.15	0.2	0.25
ω	303.137	319.724	339.906	364.005	393.651	429.644

Table 1. Natural frequencies of the simply supported plate.

3. Conclusions

In this paper the method of fundamental solutions has been implemented to find the natural frequencies and mode shapes of the plate. The procedure is prepared for the plate of arbitrary shape and for the arbitrary boundary conditions. The results obtained by numerical experiment show the accuracy and effectiveness of the proposed algorithm

References

1. R. A. Gingold, H. Maragham, *Smoothed particle hydrodynamics: theory and applications to non-spherical stars.* Monthly Notices of the Royal Astronomical Society, **181** (1977) 375-89.
2. T. Belystcho, Y. Lu, L. Gu, *Element free Galerkin methods*. Int J Numer Meth Engng, **37** (1995) 229-56.
3. W. K. Liu, S. Jun, Y. F. Zhang, *Reproducing kernel particle method*, Int J Numer Meth Engng, **20** (1995) 1081-1106.
4. Y. X. Mukherjee, S. Mukherjee, *The boundary node method for potential problems*. Int J Numer Meth Engng, **40** (1997) 797-815.
5. S. N. Atluri, T. A. Zhu, *A new meshless local Petrov-Galerkin (MLPG) approach in computational mechanics.* Comput Mech, **22** (1998) 117-27.
6. V. Sladek, J. Sladek, S. N. Atluri, R. Van Keer, *Numerical integration of singularities in meshless implementation of local boundary integral equations*. Comput Mech, **25** (2000) 394-403.
7. C. S. Chen, Y. F. Rashed, M. A. Golgerg, *A meshless free method for linear diffusion equations*. Numer Heat Transfer, part B, **33** (1998) 469-86.
8. R. L. Hardy, *Multiquadric equations of topography and other irregular surfaces*. Journal of Geophysics Research, **176** (1971) 1905-15.
9. J. T. Chen, I. L. Chen, K. H. Chen, Y. T. Lee, Y. T. Yeh, *A meshless method for free vibration analysis of circular and rectangular clamped plates using radial basis function*, Engineering Analysis with Boundary Elements, **28** (2004) 535-545.

DETERMINING OF STRESSES IN UNPROPPERLY
CURVED CERVICAL SPINE

Tomasz WALCZAK
Institute of Applied Mechanics
Poznan University of Technology
Piotrowo 3, 60-965 Poznań
061 665 21 77, tomasz.walczak@put.poznan.pl

Jacek BUŚKIEWICZ
Institute of Applied Mechanics
Poznan University of Technology
Piotrowo 3, 60-965 Poznań
061 665 21 77, jacek.buskiewicz@put.poznan.pl

Roman JANKOWSKI
Clinic of Neurosurgery and Neurotraumatology
Poznan University of Medical Science
Ul. Przybyszewskiego 49, 60-355 Poznań
klinikanch@op.pl

Abstract
The paper presents the method of determining the stresses in cervical spine vertebrae. It is based on techniques known from strength of materials – the theory of strongly curved beams. It allows to determine normal stresses in vertebrae of cervical part of spine with known characteristic dimensions. The method was tested on three different cases of cervical spine conformation: one properly and two improperly curved spinal line. Obtained information about influence of spine geometry on character and value of stresses could be useful in clinical practice.

Introduction

Degeneration disease of cervical spine touches everybody. It results in change of geometry of cervical vertebrae and intervertebral foramen and also may lead to the dysfunction of the spine and nervous system. Information about intervertebral loads could be very useful, to anticipate the character of disease changes. The paper presents the mechanical model of the cervical spine deformed as a result of degeneration disease. The model allows to determine the normal stresses produced by incorrect loads, which are effects of incorrect curvature of spine line. The main aim of the paper is to find shape of spine line influence on vertebral stresses. The three most common cervical spine
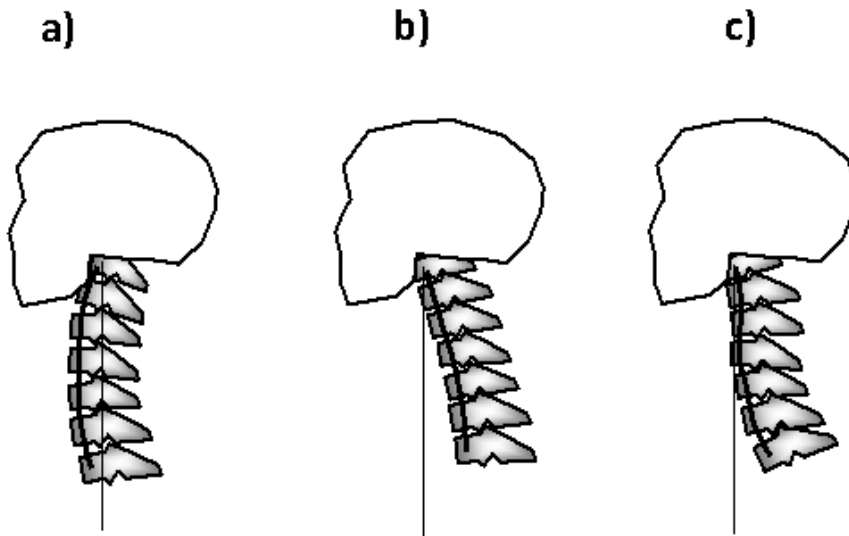
Fig. 1. Three different conformation of cervical spine lines: a) lordosis – properly curved line, b) kyphosis, c) kyphosis in upper segment and lordosis i lower.

conformations are presented in Fig. 1. The lordosis presented in 1a) is properly curved cervical spine line, while the kyphosis in 1b) and S-shape with kyphosis in upper segment of cervical spine and lordosis in lower 1c) are typical spine conformations in degeneration disease [8].

1. Mechanical model of cervical spines

The cervical spine includes seven vertebrae (called from C1 to C7), which six of them (C2-C7) have similar structure. In classical approach the vertebral endplates are shaped like two-layer ellipses, where inside layer is trabecular bone and outside layer is cortical bone [1,2]. The basic assumption for mechanical model is that each of the vertebral body of C2-C7 has an elliptical shell model of cross-section with only cortical bone layer. It involve that cervical spine can be treated as strongly curved elliptical beam with elliptical whole. The loads acting on each vertebra are presented in Fig. 2. Load of the cervical spine becomes from weight of the head Q and vertical component of the extensor muscles S. The resulting axial load applied at C1 is sum of Q and S forces:
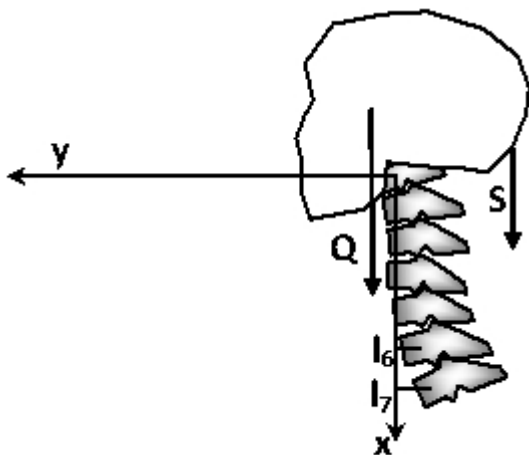
$$F = Q + S \qquad (1)$$

Fig. 2. The Scheme of the loads of cervical spine: Q – the weight of head, S – vertical component of the extensor muscles, l_i – coordinate y of C_i vertebral body center.

The bending moment of each vertebra can be determined as:

$$M_i = l_i(Q + S), \quad i = 2,...,7.$$ (2)

The bending moment (2) acting on C1 is equal to zero. The line of spine $y(x)$ might be approximated by spline-function [7] interpolation on seven vertebral body centers. In next step we can determine the radius of curvature:

$$r_0(x) = \frac{\left[1 + \left(\dfrac{dy}{dx}\right)^2\right]^{\frac{3}{2}}}{\left|\dfrac{d^2y}{dx^2}\right|}.$$ (3)

Then, the placement of neutral axis (the axis, where the normal stresses are equal to zero) we can derive as:

$$e(x) = r_0(x) - \frac{A_i}{\displaystyle\int_{A_i} \frac{dA_i}{r(x)}},$$ (4)

where A_i is the area of cross-section of vertebral body C_i. Both parameters $r_0(x)$ and $e(x)$ are illustrated on Fig. 3.
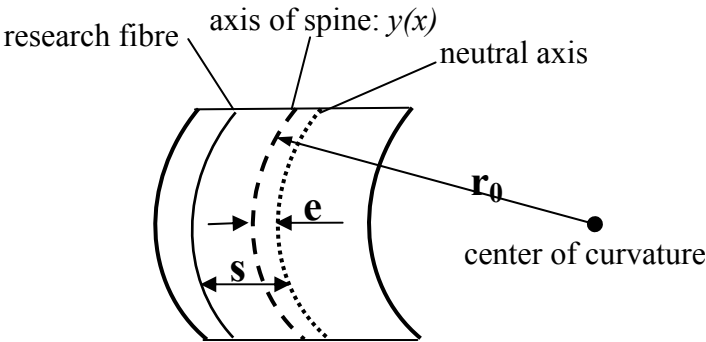

Fig. 3. Basic geometric parameters in sagittal section.

Finally we can determine normal stresses in cross-section of *i*-th vertebra in the distance of *s* from the neutral axis:
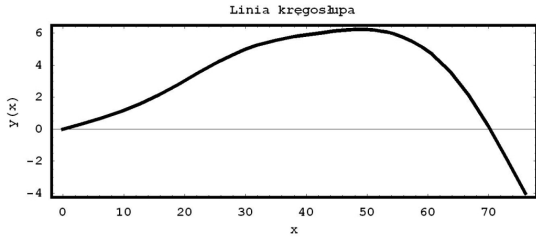
$$\sigma_i = -\frac{F}{A_i} + \frac{M_i}{A_i e}\frac{s}{r} \,, \tag{5}$$

where $r = r_0 - e + s$ is a distance between research fibre and center of curvature $y(x)$ [3].
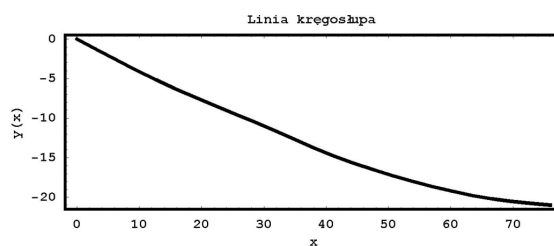
2. Results

The normal stresses of three basic shapes of cervical spine (Fig. 1.) where determined on the anterior and posterior vertebral margins. Interpolated functions $y(x)$ are presented on Fig. 4.
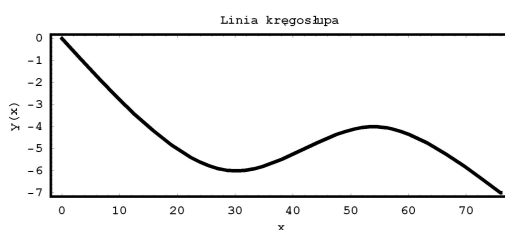
a)

b)

c)

Fig. 4. Interpolated cervical spine lines: a) lordosis b) kyphosis, c) kyphosis in upper segment and lordosis i lower.

To make comparison between all of these cases the calculations where done for the same geometrical parameters of vertebrae and loads. The force Q was assumed as 70N and the force S was derived from literature data [4,5,6]. The results are presented in Tab. 1.

Tab. 1. Normal stresses determined for anterior and posterior C2-C7 vertebral margins.

cervical spine line	place of stresses determining	Normal stresses σ_i [MPa]					
		C2	C3	C4	C5	C6	C7
lordosis (proper line)	anterior body margin	-0.47	0.93	0.98	1.46	0.37	-2.09
	posterior body margin	-1.69	-2.84	-3.10	-3.04	-2.07	-0.04
kyphosis	anterior body margin	-2.90	-4.84	-5.67	-6.00	-5.94	-7.40
	posterior body margin	0.85	2.63	3.81	3.99	4.21	5.33
kyphosis - lordosis	anterior body margin	-2.28	-2.64	-2.76	-2.63	-2.59	-3.16
	posterior body margin	0.21	0.73	0.64	0.23	0.39	1.03

We can observe that the largest normal stresses appears in kyphosis shape. Stresses determined on anterior margins (minus stress value means tension) and posterior margins are bigger than in other shapes. For anterior margins the smallest stresses acting on C2 and C3 vertebrae and the largest for C7. For posterior margins the largest normal stresses we can observe in lordosis shape is on C4 and C5 vertebrae. It is compatible with clinical practice, because most of the deformations and degeneration disease's changes touch C4 and C5 vertebrae.

References

1. Mrozowski J., Awrejcewicz J., Podstawy biomechaniki, Wydawnictwo Politechniki Łódzkiej, Łódź 2004
2. Gzik M., Biomechanika kręgosłupa człowieka, Wydawnictwo Politechniki Śląskiej, Gliwice 2007
3. Zielnica J., Wytrzymałość materiałów, Wydawnictwo Politechniki Poznańskiej, Poznań 1996
4. Harrison D. E., Harrison D. D. Janik T. J., Jones E. W., Cailliet R., Normand M., Comparison of axial and flexural stress In lordosis and three buckled configurations of the cervical spine, Clinical Biomechanics, 16 (2001), 276-284
5. de Zee M., Falla D., Farina D., Rasmussen J., A detailed rigid-body cervical spine model based on inverse dynamics, Journal of Biomechanics, 40 (2007)
6. Vasavada A. N., Li S., Delp S. L., Influence of muscle morphometry and moment arms on the moment-generating capacity of human neck muscle, Spine 23 (1998), 412-422
7. Richard L. Burden, J. Douglas Aires, Numerical Analysis, , PWS-KENT Publishing Company, Boston, 1988
8. Ogawa Y., Chiba K., Matsumoto M., Nakamura M., Takaishi H., Toyama Y., Postoperative factors affecting neurological recovery after surgery for cervical spondylotic myelophaty, J Neurosurg Spine 5:483-487, 2006

EFFECTIVE ALGORITHM OF FLEXIBILITY MATRIX COMPUTATION FOR SHEAR WALL TALL BUILDING

Elżbieta WDOWICKA, Jacek WDOWICKI
Poznan University of Technology
ul. Piotrowo 5, 60-965 Poznań, Poland
tel.: +48 61 665 24 62, e-mail: jacek.wdowicki@put.poznan.pl

Abstract

The dynamic analysis of three-dimensional coupled shear wall structures in tall buildings has been studied. A hybrid approach, based on the analysis of an equivalent continuous medium and a discrete lumped mass system has been used. The algorithm of flexibility matrix computation is presented in this approach. It has been observed that the results of this method are a good match with those obtained using the finite element method.

Keywords: Tall buildings; Dynamic analysis; Coupled shear walls; Continuous connection method

Introduction

The design of multistorey buildings subjected to earthquake ground motion involves the dynamic analysis of the structure. For the dynamic analysis of shear wall tall buildings it is convenient to use a continuous–discrete approach [1], [3], [6], [7]. In this approach the structure mass matrix is found with the lumped mass assumption. To find the flexibility matrix each lumped mass is loaded subsequently with a unit horizontal generalized force and the corresponding horizontal displacement vector to the whole structure is found by the continuous connection method. This paper presents effective algorithm of flexibility matrix computation in the continuous-discrete approach.

1. Governing differential equations

The flexibility matrix is generated from the exact solution of the governing differential equations for three-dimensional continuous model of the shear wall structure [5]. In the case of structures subjected to horizontal concentrated loads, applied at the arbitrary height, the governing differential equations can be stated as follows:

$$
\begin{aligned}
z \in \,<0,h> \qquad & \mathbf{B}N_{ND}''(z) - \mathbf{A}N_{ND}(z) \;=\; f(z), \\
z \in (h,H> \qquad & \mathbf{B}N_{NG}''(z) - \mathbf{A}N_{NG}(z) \;=\; 0
\end{aligned}
\tag{1}
$$

B - n_w x n_w diagonal matrix, containing continuous connection flexibilities,

A - n_w x n_w symmetric, positive semi-definite matrix, dependent on a structure,

n_w - number of continuous connections, which substitute connecting beam bands and vertical joints,

$N_{ND}(z)$ - vector containing unknown functions of the shear force intensity
  in continuous connections below the concentrated load,

$N_{NG}(z)$ - vector containing unknown functions of the shear force intensity in continuous
  connections above the concentrated load,

$f(z)$ - vector formed on the basis of unit concentrated loads P_X, P_Y, M_S:

$$f(z) = C_N^T L (L^T K_Z L)^{-1} T_K, \quad T_K = [P_X, P_Y, M_S]^T = [1, 1, 1],$$

  C_N, L, K_Z - matrices, dependent on a structure [5], [6],

h - the ordinate of point of concentrated loads application,

H - structure height.

The boundary conditions have the following form:

$$
\begin{aligned}
&N_{ND}(0) = 0, \\
&N_{ND}(h) = N_{NG}(h), \qquad N'_{ND}(h) = N'_{NG}(h), \\
&N'_{NG}(H) = 0.
\end{aligned}
\tag{2}
$$

After determining unknown functions of shear force intensity in continuous connections it is possible to obtain the functions of horizontal displacements of the structure as well as its derivatives using the following equations:

$$
\begin{aligned}
&z \in (h, H >, \qquad V_G'''(z) = -V_N N_{NG}(z) \\
&z \in < 0, h >, \qquad V_D'''(z) = (L^T K_Z L)^{-1} T_K - V_N N_{ND}(z)
\end{aligned}
\tag{3}
$$

where:

$V_G(z)$ - vector containing the functions of the horizontal displacements of the structure
  above the concentrated load,

$V_D(z)$ - vector containing the functions of the horizontal displacements of the structure
  below the concentrated load,

$V_N = (L^T K_Z L)^{-1} L^T C_N$.

Boundary conditions have the following form:

$$
\begin{aligned}
&V_D(0) = 0, \qquad V_D'(0) = 0, \\
&V_D(h) = V_G(h), \qquad V_D'(h) = V_G'(h), \qquad V_D''(h) = V_G''(h), \\
&V_G''(H) = 0.
\end{aligned}
\tag{4}
$$

2. Method of solution

In the proposed algorithm the equation systems, described in Eqn (1), are uncoupled by orthogonal eigenvectors of $\mathbf{P} = \mathbf{B}^{-1/2} \mathbf{A} \mathbf{B}^{1/2}$ matrix into n_w sets of two second-order differential equations. Integration constants are determined for each set from the system of four linear equations resulting from boundary conditions. Also, there has been taken

into account the case of zero eigenvalues of $\mathbf{P}$ matrix, allowing for the analysis of the structure with an arbitrary plan.

In order to uncouple differential equation systems auxiliary functions $g_D(z)$, $g_G(z)$, satisfying these relations have been introduced:

$$N_{ND}(z) = \mathbf{B}^{-1/2}\mathbf{Y}g_D(z), \qquad N_{NG}(z) = \mathbf{B}^{-1/2}\mathbf{Y}g_G(z) \qquad (5)$$

where: $\mathbf{Y}$ - n_w x n_w matrix columns of which are eigenvectors of symmetric $\mathbf{P}$ matrix.

One has obtained n_w sets of two second-order differential equations in the following form:

$$\begin{aligned} z \in\, <0, h>, \qquad & g''_{Di}(z) - \lambda_i g_{Di}(z) = F_{Bi}, \\ z \in (h, H>, \qquad & g''_{Gi}(z) - \lambda_i g_{Gi}(z) = 0 \end{aligned} \qquad (6)$$

where:

λ_i - i-th eigenvalue of $\mathbf{P}$ matrix,

$F_{Bi} = Y_i^T \mathbf{B}^{-1/2} f(z)$,

Y_i - eigenvector corresponding to the i-th eigenvalue,

with boundary conditions as follows:

$$g_{Di}(0) = 0, \, g_{Di}(h) = g_{Gi}(h), \quad g'_{Di}(h) = g'_{Gi}(h), \, g'_{Gi}(H) = 0. \qquad (7)$$

Because $\mathbf{A}$ matrix is positive semi-definite, thus $\mathbf{P}$ matrix can also have zero eigenvalues. The solutions of Eqn (6) with boundary conditions (7) in the case of zero eigenvalues have a simple form:

$$\begin{aligned} g_{Di}(z) &= F_{Bi}(z^2/2 - hz), \\ g_{Gi}(z) &= -F_{Bi}h^2/2. \end{aligned} \qquad (8)$$

The form of the solutions corresponding to non-zero eigenvalue λ_i is as follows:

$$\begin{aligned} g_{Gi}(z) &= C_1 e^{\sqrt{\lambda_i}z} + C_2 e^{-\sqrt{\lambda_i}z}, \\ g_{Di}(z) &= C_3 e^{\sqrt{\lambda_i}z} + C_4 e^{-\sqrt{\lambda_i}z} - F_{Bi}/\lambda_i. \end{aligned} \qquad (9)$$

Integration constants are determined from the linear equation system resulting from boundary conditions (7), in the following form:

$$\begin{aligned} R_{Wi}C_i &= P_{Si}, \\ C_i &= [C_1, C_2, C_3, C_4]^T, \end{aligned} \qquad (10)$$

where:

$$R_{Wi} = \begin{bmatrix} 0 & 0 & 1 & 1 \\ e^{\sqrt{\lambda_i}h} & e^{-\sqrt{\lambda_i}h} & -e^{\sqrt{\lambda_i}h} & -e^{-\sqrt{\lambda_i}} \\ \sqrt{\lambda_i}\,e^{\sqrt{\lambda_i}h} & -\sqrt{\lambda_i}\,e^{-\sqrt{\lambda_i}h} & -\sqrt{\lambda_i}\,e^{\sqrt{\lambda_i}h} & \sqrt{\lambda_i}\,e^{-\sqrt{\lambda_i}h} \\ \sqrt{\lambda_i}\,e^{\sqrt{\lambda_i}H} & -\sqrt{\lambda_i}\,e^{-\sqrt{\lambda_i}H} & 0 & 0 \end{bmatrix}, \qquad P_{Si} = \begin{bmatrix} F_{Bi}/\lambda_i \\ -F_{Bi}/\lambda_i \\ 0 \\ 0 \end{bmatrix}.$$

Values of unknown functions $N_{ND}(z), N_{NG}(z)$ of the shear force intensity in continuous connections throughout the building height are obtained after computing all elements of solutions $g_D(z), g_G(z)$ of Eqn (6) and retransforming according to Eqn (5).

3. Horizontal displacement expressions

The next step is to determine functions of horizontal displacements of the system and their derivatives necessary to calculate internal forces and stresses. As a result of integration of Eqn (3) with appropriate boundary conditions (4) the following solution is obtained:

$$V_G''(z) = \int_H^z V_G'''(t)\,dt, \qquad\qquad V_D''(z) = \int_H^h V_G'''(t)\,dt + \int_h^z V_D'''(t)\,dt,$$

$$V_G'(z) = \int_h^z V_G''(t)\,dt + \int_0^h V_D''(t)\,dt, \qquad\qquad V_D'(z) = \int_0^z V_D''(t)\,dt, \tag{11}$$

$$V_G(z) = \int_h^z V_G'(t)\,dt + \int_0^h V_D'(t)\,dt, \qquad\qquad V_D(z) = \int_0^z V_D'(t)\,dt.$$

During the computation of the above-mentioned function values uncoupling of equation systems is used consistently. Equation (3) after introducing auxiliary functions (5) has the following form:

$$\begin{aligned} z \in (h, H >, \qquad & V_G'''(z) = -V_P g_G(z), \\ z \in\, <0, h >, \qquad & V_D'''(z) = F_{POM} - V_P g_D(z) \end{aligned} \tag{12}$$

where: $V_P = V_N \mathbf{B}^{-1/2} \mathbf{Y}, \qquad F_{POM} = (L^T K_Z L)^{-1} T_K = V_T T_K$.

As a result of integration of Eqn (12) according to Eqn (11) the following form of the horizontal displacements function above the concentrated load is obtained:

$$\begin{aligned} z \in (h, H >, \qquad & V_G(z) = V_P CG(z) - V_T(z - h/3)h^2/2, \\ & CG = CG_1 + CG_2 + CG_3 + CG_4 \end{aligned} \tag{13}$$

Where $CG(z)$ – matrix containing integrals of solutions of uncoupled differential equations.

Integrals of solutions corresponding to non-zero eigenvalues (9) have the following form:

$$CG_1 = \int\limits_{h}^{z}\int\limits_{h}^{x}\int\limits_{H}^{y} g_{Gi}(t)\,dt\,dy\,dx = (C_1 e^{sz} - C_2 e^{-sz})/s^3$$

$$(-C_1 e^{sH} + C_2 e^{-sH})(z^2/2 - hz + h^2/2)/s$$

$$+ (C_1 e^{sh} + C_2 e^{-sh})(h-z)/s^2 - (C_1 e^{sh} - C_2 e^{-sh})/s^3,$$

$$CG_2 = \int\limits_{h}^{z}\int\limits_{0}^{h}\int\limits_{h}^{y} g_{Di}(t)\,dt\,dy\,dx = (C_3 e^{sh}(1/s - h)/s + C_4 e^{-sh}(1/s + h)/s$$

$$- (C_3 + C_4)/s^2 + f\,h^2/2)(z-h),$$

$$(14)$$

$$CG_3 = \int\limits_{h}^{z}\int\limits_{0}^{h}\int\limits_{H}^{h} g_{Gi}(t)\,dt\,dy\,dx + \int\limits_{0}^{h}\int\limits_{0}^{x}\int\limits_{H}^{h} g_{Gi}(t)\,dt\,dy\,dx =$$

$$(C_1(e^{sh} - e^{sH}) - C_2(e^{-sh} - e^{-sH}))(z - h/2)h/s,$$

$$CG_4 = \int\limits_{0}^{h}\int\limits_{0}^{x}\int\limits_{h}^{y} g_{Di}(t)\,dt\,dy\,dx = (C_3 e^{sh} - C_4 e^{-sh})(1/s^2 - h^2/2)/s + f\,h^3/3,$$

$$s = \sqrt{\lambda_i}, \quad f = F_{Bi}/\lambda_i.$$

The form of analogous integrals in the case of zero eigenvalues is as follows:

$$CG_1 = F_{Bi}(z^3/6 - Hz^2/2 + hz(h - h/2) + h^3/3 - Hh^2/2),$$

$$CG_2 = F_{Bi}(z-h)h^4 5/24,$$

$$CG_3 = -F_{Bi}(h-H)(z - h/2)h^3/2,$$

$$CG_4 = F_{Bi}h^5 2/15.$$

$$(15)$$

The presented algorithm has been applied to obtain the flexibility matrix used in dynamic analysis for the tall building model in the form of the discrete lumped mass system. The values of the i-th three columns of elements in flexibility matrix for the shear wall structure represent the horizontal displacements (V_x, V_y, Φ) of the system at all levels where lumped masses are located, induced by unit generalized forces (P_X, P_Y, M_S) applied horizontally at the location of the i-th lumped mass. Because of the symmetry only the lower triangular part with a leading diagonal of the flexibility matrix is computed.

Natural frequencies computed using of this method correlate well with the results given in literature, both in the case without connecting beams [4], and with beams [2]. The examples of seismic analysis of shear wall tall buildings based on response spectrum technique were presented in [6], [7], [8].

4. Conclusions

The paper presents effective algorithm of flexibility matrix computation in the continuous-discrete approach applied in dynamic analysis of tall buildings. In the proposed algorithm the equation systems are uncoupled consistently by orthogonal eigenvectors. Also, there has been taken into account the case of zero eigenvalues, allowing for the analysis of the structure with an arbitrary plan. After designing and developing software based on the proposed algorithm a series of tests has been carried out. The conducted tests have confirmed correctness of the algorithm realization. The two advantages of proposed method are the simplicity of data and short computation time.

References

1. Aksogan O.; Bikce M.; Emsen E.; Arslan H.M.: *A simplified dynamic analysis of multi-bay stiffened coupled shear walls*, Advances in Engineering Software, **38**, 8-9 (2007), 552-560.
2. Cheung, Y.K., Hutton, S.G. and Kasemset, C., *Frequency analysis of coupled shear wall assemblies*, Earth. Eng. & Struct. Dyn., **5**, (1977),. 191-201.
3. Li G.-Q., Choo B.S., *A continuous-discrete approach to the free vibration analysis of stiffened pierced walls on flexible foundations,* Int. J. Solids and Structures., **33** (1996) 249-263.
4. Petyt, M. and Mirza, W.H., Vibration of asymmetrical coupled shear walls, *J. of Sound and Vibration*, **27**, (1973.) 573-581.
5. Wdowicki J., Wdowicka E., *System of programs for analysis of three-dimensional shear wall structures*, The Structural Design of Tall Buildings, **2** (1993) 295- 305.
6. Wdowicki J., Wdowicka E., Błaszczyński T., *Integrated system for analysis of shear wall tall buildings*, In: Proc. of the Fifth World Congress "Habitat and High- Rise: Tradition and Innovation". Council on Tall Buildings and Urban Habitat, Amsterdam (1995) 1309-1324.
7. Wdowicki J., Wdowicka E., *Seismic analysis of the shear wall dominant building using continuous-discrete approach,* XXI Sympozjum–*VIBRATIONS IN PHYSICAL SYSTEMS* – Poznań-Kiekrz (2004) 409-412.
8. Wdowicka E.M., Wdowicki J.A., Błaszczyński T.Z.: *Seismic analysis of the "South Gate" tall building according to Eurocode 8*, The Structural Design of Tall and Special Buildings, **14**, 1 (2005) 59-67.

300 – ANNIVERSARY LEONHARD EULER'S BIRTHDAY OF THE GREAT SCIENTIST MATHEMATICIAN, PHYSICIST AND ASTRONOMER AND HIS CONTRIBUTION IN DEVELOPMENT OF CLASSIC MECHANICS

Józef WOJNAROWSKI

Politechnika Śląska

Katedra Mechaniki Stosowanej

Tel. 032-237-24-01

Jozef.wojnarowski@polsl.pl

Abstract

In the presentation epoch-making achievement's Leonhard Euler mainly in the range of classic mechanics were presented and were discussed . The biographical note presents the important aspects with academic Euler's life. Next, it was discussed also certain aspects: mechanics of material point, variational calculus, mechanics of rigid bodies, statics and mechanics of liquids. Besides this it referred to the historical graph of Euler of seven Królewiec bridges on the river Pregole.

Keywords: Biographical note, Euler Publisher the Word, Law of the extremum

1.Introduction

In 2007 year it passes 300 – Anniversary of Birthday of the great scientist Leonhard Euler, whose portraits show with different periods of his life.

Euler's portrait were painted by:
Johanna Georga Brückera   Emanuela Handmanna (1753)

Leonhard Euler was one from five the greatest mathematicians of all times.

He was born in Basel, but he spent most part of life in Berlin and in Petersburg.

When it looks at scientific works of Euler in field of mathematics and mechanics, his rank, wealth, and also on quality of these achievements, it result is imposing. Euler published about 50 books and above 800 research works. What more, this is worthy of attention, so that Euler practically established independently basic equations related to rigid, liquid and also deformed bodies. In this article it will be considered problem related to theory of rigid, liquid and also deformed bodies.

Euler together with other scientists such as e.g. d'Alembert, Daniel Bernoulli, Johann Bernoulli, Alexis Clairaut, Condorcet, Laplace, Lagrange was typical mathematician for the epoch Enlightenment. Therefore achievements of Euler it should became analyzed in relation to development   mechanics and mathematics in this period. Nevertheless, contribution of Euler in the field of science is still considered for fundamental.

Creator of modern mathematics, to which he introduced many used at present signs such as e.g. symbols: **Σ e π and f(x)**.

Born: 15th April, 1707.

Wedding with Katherine Gsell: 7th January of 1734 year. They had 13 sons, childhood survived 8.

He spent in : Switzerland 1707-1727; Berlin 19.06. 1741- 1766; Russia 17.05.1727– 1741, 1766-1783; Poland 10 days in 1766 (at Stanisław August Poniatowski).

Nationality: Swiss.

The fields of researches: mathematics, physics and astronomy.

Institutions: Russian Academy of Sciences, Berlin Academy of Science.

University: Basel.

Religion: Calvinism.

2. Euler- Biographical note

Undoubtedly Leonhard Euler is the greatest mathematician of XVIII century. He was born 15th April of 1707 year near Basel, in north Switzerland, not far of border with France. He was son of Paul Euler and Margaret Bruchner. At the beginning Euler's father was responsible for his science. Next   in age of 13 years he entered   the university, where he showed rare talents in field of mathematics. Euler studied together with Johan Bernoulli, however direct influence on Euler, especially in field of mathematics and philosophy had **Leibniz (1646-1716)** and also **Descartes (1596-1650),** however works of **Newton(1642-1727),** capture coherent arrangement of laws, and giving themselves to apply to significant range of physical phenomena, made the strongest influence on production of Euler in field of mechanics.

Euler applied and used mathematic theory of Leibniz to finite and infinite of small numbers, as well as he accepted the idea of Newton's force, so that yet later to go away from idea of absolute space.

Having thirteen years Euler entered the university in Basel, and in time of studies   he showed mathematical talents.

In age of 17 years, he wrote   article   on subject „ Physical performance of sound". It was first worthy of attention work of Euler, which had unusual influence on researches from the range of acoustics.

In age of 21 years Euler was nominated by Daniel Bernoulli to Petersburg Academy of Sciences. In 1733 year Euler took over post of manager of cathedral mathematics in Academy after Daniel Bernoulli, where he improved integral calculus, developed theory of logarithmic and trigonometric functions In this time he worked unceasingly on simplifying of analytic expressions in mathematics.

Probably because of this intensive effort, in 1735 year Euler stayed partly blind. In 1741 Fryderyk Wielki invited Euler to Berlin Academy. In this year he left Russia and he set out to Berlin, in which he stayed by 25 years. In this period Euler created imposing count of research works.

In 1748 year in article „Introduction to analysis of boundary of infinity" he developed conception of function, which nowadays we know.

In 1755 year he wrote „Differential Calculus", two volumes and also „Integral Calculus", three volumes, from which latest was published in Sankt Petersburg(1768-1770). These all books, by many years were used for guide-book for mathematicians. Therefore it is possible to say, that all front representatives of mathematics of end of XVIII century and also beginning of XIX century were schoolboys of Euler.

In 1766 year Euler returned to Sankt Petersburg on court Katherine II(1729-1796). In this time he was already almost entirely blind. Besides this inconvenience, Euler used his unusual memory to keep this same, superb level of work. Besides this in organization of articles and also manuscripts assistants of Euler helped him. Nevertheless he did not stop his activity, what more, in this time it created much more of his works than whenever. In order to, Euler performed him assistants exact explanations of new tasks. Thanks to this knowledge assistants could start new tasks, which Euler analyzed, and at last these tasks to confirm. In years 1766-1783 created above 400 articles. Above forty years after death of Euler, Russian Academy of Sciences still published his works in yearly remembrance.

Leonhard Euler 7th January of 1734 year married with Katherine Gsell. They had thirteen sons, from what only eight sons survived childhood. One with sons of Euler, Johann Albrecht (1734-1800) analyzed, and next continued works of his father in field of rigid bodies. However one with offspring of Euler, Hans Karl August von Euler-Chelpin (1873-1964) in 1929 year got Nobel's Price in field of chemistry.

Achievements of Euler in field of mathematics are public known. He studied elementary geometry, trigonometric functions. Euler proved, so that every compound number has infinite count of logarithms. He proved formula:

$$e^{i\Theta} = \cos \Theta + i \sin \Theta,$$

from which, after substitution $\Theta = \pi$ it results good known formula:

$$e^{i\pi} + 1 = 0.$$

It is possible to notice, so that the most magnificent numbers appear.

Euler introduced modern terminology known in present mathematics. It were symbols, Σ for summing and also basis of neperian logarithm:

e = 2.71828 18284 59045 23536...

He introduced note **f(x)** describes function of   independent variable **x** and also **i** represents compound numbers. Euler was first person, who used derivative of differentiated function as boundary of relation between two values of variables.

Euler in moment of death   18 September of 1783 year   remained on his   desk manuscripts and also computations concerned problems of aerostatic balloons. It was his latest scientific work.

3. Euler and also Dynamics of Elementary Particles

   Essential conclusion of Euler in field of Dynamics of Elementary Particles it is possible to find in his work entitled „Mechanics of move of bodies-exposition of scientific analysis” (”Mechanica sive motus scientia analitice exposita”), published in 1736   year.

In reality, this work is kind of investigative program. After reading of works of creators of mechanics especially Huyghens (1629-1695) and also Newton (1642-1727), Euler made efforts to transform mechanics into rational science, again to estimate definitions with field of mechanics and also by means of modifications of her theorems. This is necessary to mention, so that idea of force in Euler's mechanics comes from in principle from Galileusz. Besides this Euler distinguished absolute force   from forces of heaviness and these, which depends on relative speeds between bodies.
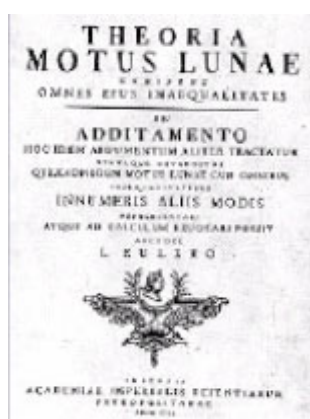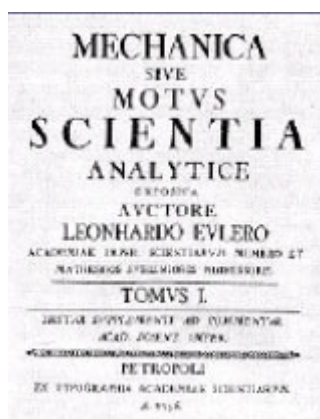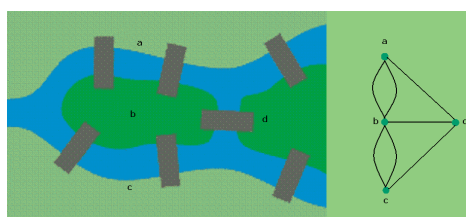
4. Graph of Królewiec Bridges

(a)
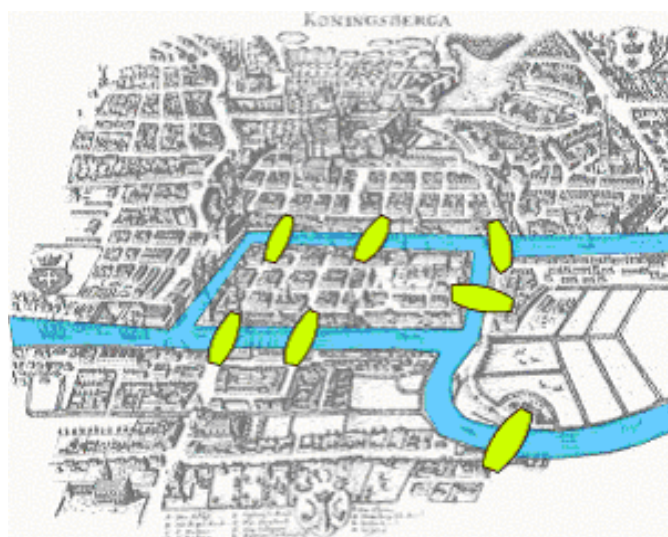
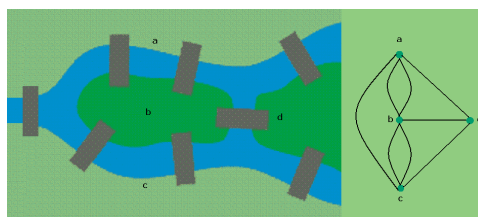

(b)   (c)

Fig. Bridges on the river Pregole (a); Scheme of these bridges and graph (b); Additional bridge is indispensable to creation of Euler's chain (c).

Seven Królewiec bridges on the river Pregole (fig. a) established puzzle for walking for them inhabitants of Królewiec. They established themselves because question, or wanted walker to pass by all bridges can pass every bridge exactly only first time. This problem was inspiration for Euler in order to construct chain with representing districts of city peaks and with edges or lines, which they were subordinated bridges (fig. b).This discussed of situations, multigraph represents graphically, which all peaks have odd degree. Euler in work "Solutio problematis ad geometriam situs pertinentis, Comment Academiae Sci. I. Petropolitane 8", streets 128-140 in work published in 1736 year formulated theorem. Graph is euler if only and only number of peaks about odd degree is equal 0 or 2. We can say either, that in such graph it is possible to separate Euler's

chain. In graph of seven Królewiec bridges it is not possible to distinguish Euler's chain. In moment of addition of eighth bridge in new graph Euler's chain will be made (fig. c). Graph of Królewiec bridges opens history of graphs, at the same time so predominant in scientific papers different disciplines. Euler either ran notation at present known as characteristics of graph under name cyclomatic number, which contains relations between count of edges E, peaks V and walls F. This relation is either for polygons and usually is in form:

$$V - E + F = 2.$$

5. Dynamics of material point in conception of Euler

From times of Newton, Leibniz and Euler to description of liquids, and in essence either all others mechanical systems mathematicians and physicists applies differential equations. Euler in his work published in 1749 year in Berlin „Memoires de l'Academie des Sciences" we find for first time differential equations of move of material point in following form:

$$I. \ \frac{2ddx}{dt^2} = \frac{X}{M} \ ; \ II. \ \frac{2ddy}{dt^2} = \frac{Y}{M} \ ; \ III. \ \frac{2ddz}{dt^2} = \frac{Z}{M}.$$

Later Euler uses note these equations in form used to present times or:

$$m\frac{d^2x}{dt^2} = F_x \ , \ m\frac{d^2y}{dt^2} = F_y \ , \ m\frac{d^2z}{dt^2} = F_z.$$

Researches carried out by Euler gradually showed fertility of mechanics of Newton. At the beginning he investigated no continuous systems, and next state and liquid systems. In 1750 year he discovered, so that principle of linear speed can be applied to all mechanical systems, independently from their form. Other words, independently or are discreet or continuous. In his work entitled „Discovering a New Mechanical Principle", published in 1752 year, he performed equations: where mass M can be finite or infinite small. Next Euler named these equations „ first principles of mechanics". Of course these equations are second law of Newton, therefore we able to name it equations of Newton-Euler.

6. Euler and Law of Extremum

In 1744 year Euler published work entitled „Methodus inveniendi lineas curves maximi minime proprietate gandentes". In enclosure II (appendix) entitled „De motu projectorum in medio non resistente per methodum maximorum ac minimorum determinando" Euler

stated: „If all activities apply to certain laws maximum or minimum, it does not deny, so that trajectories of flight of bullets being under influence of forces will be follow according to properties minimum or maximum".

Euler had essential contribution in development *differential calculus*, which was finished by J.L. Lagrange'a (1736-1813). In his preliminary formulating generalized analytic method was not destination of Euler. Proposed method by Euler is similar to this established by Bernoulli (1700 –1782).

In addition, principle of the smallest of activity was introduced in this times. Author of her was president of Berlin Academy of Sciences French mathematician Maupertuis, who formulated her in sentence:

„When some change follows in nature, this necessary for her achievement of count of work is possible the smallest ".

Euler by remaining principle her name and glory of discovery for Maupertuis, he formulated her new form, practically to application. In his treatise with 1744 year about isoperimetries: entitled „Methodus inveniendi lineas curvas maximi minimive proprietate gaudendes", Euler contains main idea of principle, that in move of body along curve under working of central forces integral of speed multiplied by element of curve always gives maximum or minimum. This means, that in principle body on given surface will run shortest path.

In this manner Euler postulated expression for principle of the smallest working in form:

$$\int m\boldsymbol{v}\mathbf{ds}, \text{ it obtains extremum,}$$

where:
m is mass, $\boldsymbol{v}$ velocity, and $\mathbf{ds}$ infinite small element of trajectory.

Lagrange in his work : „Mecanique analytique" published in 1788 year and referred   to contribution of Euler, he summed up importance of principle of the smallest activity.

7. Euler and Dynamics of State Bodies

In 1760 year, Euler published "Teoria motus corporum solidorum seu rigidorum". This work later was improved by Johanna Albrechta, son of Euler (1790 year). In introduction of original work Euler confirms principles, which he performed in 1736 year, defined main characteristic of rigid bodies by means of invariability distance between two points belonging to body. Besides this for every body Euler defined center of mass, what over he underlined, that center of mass every rigid body implies problem more restrictive than center of mass. Two latest conceptions were defined more correctly by myself in itself inertia, when to system of working forces on state bodies is neglected.

  Euler introduced idea of moment of inertia of rigid body, thanks to he simplified analysis of rotatory and spherical move and also solution of problems from this range. Besides this he computed moments of inertia of some bodies. In addition, Euler admitted system of co-ordinates attributed to rigid bodies, and also he discovered main ax of inertia. Next step was investigation of dynamics of rigid bodies by means of

transformation of move to his analysis in two elements: translation of center of mass and also rotation of body around him.

To description of spherical move he introduces angles of rotation, precession and nutation. In this case motivation were considerations on precession move of Earth.

In addition, Euler dedicates in his works many places astronomy and in particularly move of Moon and Earth.

8. Equations of move of rigid body around state point

Such case takes place in earthly conditions only then when established point 0 is his center of mass. It applies Cardan suspension of rigid body to experimental researches , which enables rotations about every axis passing through chosen in investigated body state point. By means of principle of turning it is possible to obtain equations in analytic form. Euler wrote it as follows:

$$A\dot{\omega}_2 = (B - C)\omega_2\omega_3,$$

$$B\dot{\omega}_2 = (C - A)\omega_3\omega_1,$$

$$C\dot{\omega}_3 = (A - B)\omega_1\omega_2,$$

where: A,B,C are mass moments of inertia.

This system of three differential equations called equations of Euler, enables to determine three co-ordinates of angular speed $\omega_1, \omega_2, \omega_3$ as function of time and by means of given starting conditions describes exactly considered spherical move of rigid body.

In general case when external forces work on body and are described by pair of forces about moment M= $\mathbf{i}M_1+\mathbf{j}M_2+\mathbf{k}M_3$, then equations

$$A\dot{\omega}_2 = (B - C)\omega_2\omega_3 + M_1,$$

$$B\dot{\omega}_2 = (C - A)\omega_3\omega_1 + M_2,$$

$$C\dot{\omega}_3 = (A - B)\omega_1\omega_2 + M_3,$$

are general euler differential equations and describe move of rigid body, or move of rigid body around state point.

These equations are basic in investigation of machine used to realisation of spherical move.

In 1744 year Euler formulates problem of deformation measured by means of analysis of thin resilient rod under working of pressed force P (fig. d) and establishes formula on

critical value of force P_E at which system is unstable: $P > P_E > B\dfrac{\pi}{L^2}$ where B is rigidity

of bending.

9. Euler and Equilibrium of Liquids

In 1755 year Euler made for Berlin Academy work "Principes généraux de d'équilibre des fluidem", in which he referred to problem of equilibrium of liquids . Euler distinguished two types of liquids: compressible and also incompressible, both depends on system of forces. Taken into consideration mass of liquid is contained   three-dimensional parallelepiped about co-ordinates **dx, dy, dz**. If component of working forces on body are **P, Q, R** and thickness of body is equal ρ then   on element of liquid about capacity **dxdydz** component forces   works **Pρdxdydz**, **Qρdxdydz** and also **Rρdxdydz**.

On basis of above considerations Euler formulated generalized equation of equilibrium:

$$\frac{dp}{\rho} = Pdx + Qdy + Rdz$$

Forces **P, Q, R** should be such, so that differential form

Pdx+Qdy+Rdz,

stood integral, thickness will be constant, or unambiguously dependent from resilience, or it will stay integral number, when will be multiplied by given function.

9.1.   Euler's equations in modern form

Basic equations of dynamics of no sticky liquids Euler took out in 1775 year. The starting point is second principle of dynamics, in idea which derivative of speed of system in relation to time is equal of main vector of   external forces, working on this system. It supposes that   liquid in certain limited area V establishes our system. Elementary mass ρdV, distinguished in environment any point in this   area, has momentum $\rho\, v\, dV$

$$\frac{d\,\vec{v}}{dt} = \vec{F} - \frac{1}{\rho} \cdot gradp \qquad / \, d\,\vec{s}$$

$$\frac{d\,\vec{v}}{dt} \cdot d\,\vec{s} = \vec{F} \cdot d\,\vec{s} - \frac{1}{\rho} \cdot dp$$

$$\vec{F} \cdot d\,\vec{s} - \frac{1}{\rho} dp = 0$$

And next after substitution:

$$\vec{F} = F_x \vec{i} + F_y \vec{j} + F_z \vec{k} \qquad F_x{=}P,\ F_y{=}Q\ \text{and}\ F_z{=}R$$

$$d\,\vec{s} = dx \cdot \vec{i} + dy \cdot \vec{j} + dz \cdot \vec{k}$$

we get:

$$\frac{dp}{\rho} = Pdx + Qdy + Rdz.$$

10. Euler and Main Equations of Hydrodynamics

Beginning from higher mentioned document, published in 1755 year, Euler accepted primarily state of liquid for configuration of elementary particles and their speeds. It supposes , that this state, and also forces influenced for this body are known in given time. In order to solve task it is necessary to compute pressure in every point of liquid, thickness as well as speed of crossing elements of liquids by this point. In order to investigate of present state of liquid, Euler applied components of acceleration **P, Q, R**, which are function coming from **x, y, z** and **t**. Thickness ρ, pressure **p** and also components of speed of element liquid **u, v, w**, which find in point **Z,** are unknown values in function time **t**.

In article entitled "Principia motus fluidorum", Euler explains problem of kinematics of continuous centre.

About work of Euler referred to liquids Lagrange wrote: „Thanks to discovery of Euler mechanics of liquids was reduced to analytic form and if values of equations contain problems with field of mechanics of liquids are integers, in all cases of convenience of move and also behaviour of liquids being in move by means of forces, they would be determined. Unfortunately they are such difficult, that to present day it was possible achievement of success in special cases".
Euler proved simplicity, which it takes place, if equation

udx + vdy + wdz

is complete differential. Much later, case, in which is potential of speed, or case of move without of circulation.
It is worthy of emphasis that in 1775 year Euler performed first mathematical formulation of flow of blood in aorta. His work was published posthumously in 1788 year.
In addition, so that with attention on analytic difficulties, Euler could not understand of weight partly-experimental considerations, partly theoretical applied in hydraulics. This is necessary to adding, that in 1752 year Euler undertook researches concerned of water machines, and for verifying of his theoretical results he built in 1754 year carried his name turbine. This was characteristic period for constructing and improvement of machines.

11. The more important works of Euler

-Dissertatio physica de song (Basel, 1727),
-Mechanica sive motus scientia analytice exposita (St. Petersburg, 1736, 2 Vols),

-Ennleitung in die arithmetik (1738 r. 2 Scientia navalis seu tractatus de construendis as dirigendis navibus (St. Petersburg 1749 , 2 Vols),

-Theoria motus lunae (Berlin, 1753),

-Disseratio de principio miniminae actionis uma cum examine objectionum cl. Prof. Koenigii (1753),

-Institutiones calculi differentialis cum ejus usu in analysi intuitorum ac doctrina serierum (1755),

-Constructio lentium objectivarum (St. Petersburg 1762),

-Theoria motus corporum solidorum seu rigidorum (1765),

-Institutiones calculi integralis (St. Petersburg, 1768- 1770, 3 Vols),

-Lettres à une princesse d' Allemagne sur quelques sujects de physique et de philosophie (St. Petersburg,1768-1772, 3 Vols),

-Introduction to algebra (1770),

-Dioptrica (1767- 1771, 3 Vols),

-Opuscula analytica (St. Petersburg, 1783- 1785, 2 Vols),

-Solutio problematis ad geometriam situs pertinentis, Comment Academiae Sci. I. Petropolitane 8, (1736), p. 128- 140,

-Tentamen novae theoriae musicae (1739),

 -Methodus inveniendi lineas curves maximi minimine proprictate gaudentes (Lausanne1744),

-Theoria motuum planetarum et cometarum (Berlin, 1744),

-Opuscula varii argumanti (1745- 1751, 3 Vols),

-Novae et carrectae tabulae ad loco lunae computanda (1746),

-Tabulae astronomicae solis et lunae (ibid),

-Introductio it analysin infinitorum (Lausanne 1746, 2 Vols),

-Scientia navalis seu tractatus de construendis as dirigendis navi bus

(St. Petersburg 1749, 2 Vols),

-Theoria motus lunae (Berlin, 1753),

-Disseratio de principio miniminae actionis uma cum examine objectionum cl. Prof. Koenigii

(1753),

-Institutiones calculi differentialis cum ejus usu in analysi intuitorum ac doctrina serierum

(1755),

-Constructio lentium objectivarum (St. Petersburg 1762),

-Theoria motus corporum solidorum seu rigidorum (1765),

Institutiones calculi integralis (St. Petersburg, 1768- 1770, 3 Vols,

-Lettres à une princesse d' Allemagne sur quelques sujects de physique et de philosophie (St. Petersburg, 1768- 1772, 3 Vols),

-Introduction to algebra (1770),

-Dioptrica (1767- 1771, 3 Vols),

-Opuscula analytica (St. Petersburg, 1783- 1785, Vols).

12. Conclusion

Euler as first wrote second law of Newton in differential form, used this same conception of Newton of force, which describes equations for given systems. This fact connected with effective applications of these equations for many different problems associated with move of points, system of material points and rigid bodies, had fundamental importance in development of mechanics. Mechanics of Newton called philosophy of nature survived intact till until beginning of XX century.

Euler generalized mechanics for point, for rigid body and mechanics of liquids. His mathematical researches directed his to development of variation calculus, which enabled to solve series of unknown problems. This new mathematical tool was further foundation for analytic studies made by Lagrange.

Thus analytic studies of Euler it is possible to accept as one's kind passage between mechanics of d'Alembert and analytic mechanics of Lagrange. In addition we should mention, so that great effort of Euler in development of mechanics of rigid body and among others these studies directed on some new conceptions such as move of center mass, principle of speed and turning. In this equations of Euler for rigid body are the simplest and the most elegant equations in mechanics.

On account of limitation of size of article, force of fact it was necessary to give up with development of some interesting reasoning and papers which are in rich scientific works of Euler. Certainly readers will be can to suspect many lacks and even inaccuracy, therefore it should to treat considerations of author as encouragement to deeper meditation on rich production and it takes into consideration, that scientific works of Euler is worth of it.

13. The place of eternal rest of Euler

Leonhard Euler died in 18 September of 1783 year in St Petersburg, in Russia.
He was buried on the cemetery Alexander Newski (in neighbourhood of orthodox church A. Newski).

References
1. Acheson D. : From Calculus to Chaos. An intoduction to Dynamics Oxford University Press, 1997.
2. Kucharzewski F. Mechanika w swym rozwoju historycznym. Instytut Wydawniczy Warszawa 1924.
3. Oliveira A. R. E. :Euler's Contribution to Classical Mechanics. 12th IFTomm World Congress , Besancon(France) June 18-21 2007.
4. Wróblewski A.K. :Historia fizyki. Wyd. Naukowe PWN.Warszawa 2007.

MEASURING VIBRATION PARAMETERS OF THE REMOTE OBJECTS WITH THE ZIGBEE TECHNOLOGY

Józef WOJNAROWSKI, Bohdan BOROWIK
Akademia Techniczno-Humanistyczna
Bielsko-Białą
tel. 604 875 247, e-mail borowik@tatrynet.pl

Abstract

The paper presents the monitoring and measurement process for the remote object vibration in the plain space. Wireless, RF communication in Tx/Rx duplex mode provides transfer of data with ZigBee transceivers. Presented ZigBee technology operates in many various modes on frequency 2,4 GHz allowing the coordinator node to select certain path and data. Zig Bee technology can be alternative for other vibration research techniques. The vibration displacement is processed further by DSP Digital Signal Processing made with the microcontroller.

Keywords – Microcontroller, Acceleration, Duty Cycle, Accelerometer

Introducion

Contemporary industrial world often creates requirements for microcontroller applications with the measurements of vibrations. Accelerometer applications due to embedded control and I/O digital signal processor DSP play the crucial role in determining vibration and machines fatigue strength testing. It registers, among other, the temporary industrial parameters and monitors plant system parameters such as vibration and/or pressure. Our research, controlled by ZigBee technology can be alternative for other techniques of vibration research.

The paper presents diagnostic procedure and measurements process of the vibration in the plain space. Role of the node play ZigBee transceivers. The vibration monitoring system is gathering information from space through transceivers. The vibration displacement is processed further by DSP Digital Signal Processing made with the microcontroller.

The ZigBee technology are global standard under the IEEE 802.15 working group. IEEE 802.15.4 this is the standard applicable to low-rate wireless Personal Area Networks. ZigBee is the wireless networking standard targeted at low power sensor applications.

1. The acceleration sensor

We use for measurement the dual-axis acceleration measurement system ADXL202E, manufactured by Analog Devices.   It has build in the polysilicon surface-micromachined sensor. The polysilicon springs suspend the structure over the surface of the wafer and provide the resistance against acceleration force. Deflection of the structure is measured using the differential capacitor. The acceleration will deflect the

beam and unbalance the differential capacitor, resulting in an output square wave, whose amplitude is proportional to acceleration. For determining the direction of the acceleration the Phase demodulation techniques are used.

The system can measure both dynamic acceleration like vibration and static acceleration e.g., gravity. The output is digital signal whose pulse is a Duty Cycle modulator. This pulse equals:

$$P = \frac{T1}{T2}$$ (1)

where: T1 denotes pulse width, T2 is a period.

The acceleration is directly proportional to the ratio of P. Subsequently the duty cycle can be directly measured with a counter on board of the microcontroller ds PIC33F256.

The architecture of the integrated circuit also includes the signal conditioning circuitry to implement an open loop acceleration. For each axis an output circuit converts the analog signal to a duty cycle modulated digital signal DCM. Finally, the signal DCM can be decoded by the stand alone microprocessor. In our case we applied the 16 bit microcontroller manufactured by Microchip, dsPIC33FJ256 GP710, operating as the digital signal processor DSP. It is preprogrammed with the firmware to fulfill its function as the digital signal processor for the incoming DCM signal from the sensor. The functional block diagram of the accelerometer is presented on the figure1.
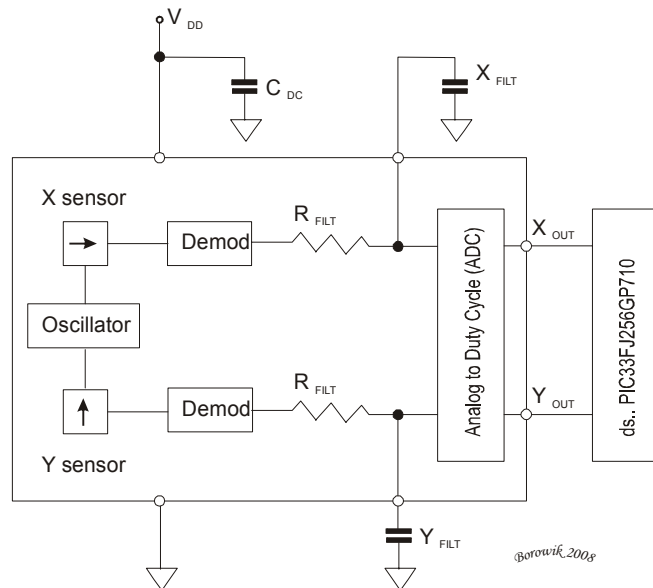

Fig.1. Functional block diagram of the accelerometer

2. Duty Cycle decoding

Acceleration is proportional to the ratio T_1/T_2. The nominal output of the circuit is:

0 g = 50% Duty Cycle. Scale factor = 12,5% Duty Cycle Change per g.

The time period T_2 does not have to be measured for every measurement cycle. It need only to be updated to account for changes due to ambient temperature. Since the T_2 time period is shared by the X and Y channels, it is necessary only to measure it on one channel. The decoding algorithm for the microcontroller dsPIC33F256GP710 was burnt on firmware.

3. Interfacing the Accelerometer with the microcontroller dsPIC

Acceleration circuit is designed especially to work with microcontroller. For the appropriate design of the parameters measured in the object which is endless bandsaw, some preconditions should be observed in the system in term of:

- resolution
- bandwidth
- acquisition time on axis x and y.

These requirements will help to determine the accelerometer bandwidth, the speed of the microcontroller clock and the appropriate Duty Cycle. While the accelerometer is very accurate, it has a wide tolerance for initial offset. The simplest way to clear this offset is with a calibration factor saved on the microcontroller, or by a user calibration for zero g. When the offset is calibrated during manufacturing process, the *one time programmable* microcontroller can be used.

4. Setting the Bandwidth while adjusting the values of C_x and C_y capacitors

Accelerometer has provisions for band limiting the X_{FILT} and Y_{FILT} outputs. Capacitors must be added to the output pins to implement Low-Pass filtering for antialiasing and noise reduction. The equation for the 3 dB bandwidth is

$$F_{-3dB} = \frac{1}{\left(2\pi\left(32\,k\Omega\right)\cdot C\left(x,\,y\right)\right)} \tag{2}$$

simplifying:
$$F_{-3dB} = \frac{5\mu F}{C_{(X,Y)}} \tag{3}$$

A minimum capacitance equals 1000 pF for $C_{(X,Y)}$. The Filter capacitor selection C_x and C_y are shown below

Table 1 Selection Filter Capacitor

Bandwidth [Hz]	C_x, C_y [μF]	rms noise [mg]	Peak-to-Peak Noise [mg]
10	0,47	0,8	0,47
50	0,10	1,8	0,10
100	0,05	2,5	0,05
200	0,027	3,6	0,027
500	0,01	5,7	0,01

5. Seting the DCM Period with R $_{set}$

The analog signal is converted for duty cycle modulated DCM output which is shown on fig.2. Further more impulses of DCM can be decoded by counter/timer included on microcontroller dsPIC33FJ256GP710.
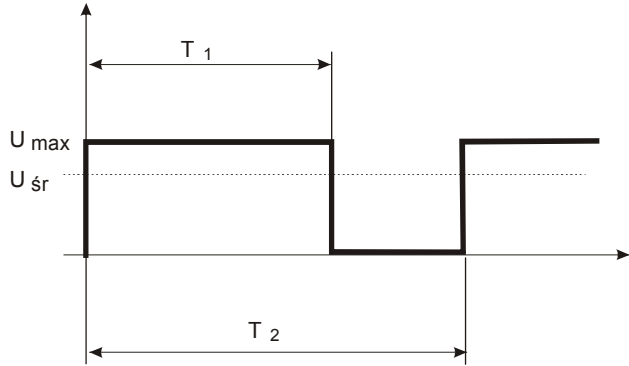
Fig.2. Output of the Duty Cycle

The period of the DCM output is set for both channels by a single resistors from R $_{SET}$ to ground. The equation for the period is:

$$T_2 = \frac{R_{SET}\ (\Omega)}{125\ M\Omega} \tag{4}$$

$$A_{(g)} = \frac{\left(\dfrac{T_1}{T_2} - 0,5\right)}{12,5\%} \tag{5}$$

0 g = 50 % Duty Cycle

A 125 kΩ resistor will set the duty cycle repetition rate to approximately 1 kHz, or 1 ms. The device is designed to operate at duty cycle periods between 0,5 ms – 10 ms.

6. Selection the accelerometer NOISE/BW

In the accelerometer the filtering can be used to lower the noise floor and improve the accelerometer resolution. Resolution is dependent on both the analog filter bandwidth at X $_{FILT}$ and Y $_{FILT}$ and the speed on the microcontroller counter, that can be attained. The analog output of the ADXL202E has a typical bandwidth of 5 kHz while the Duty

Cycle modulator has bandwidth of 500 Hz. In such case the aliasing error appear. Then the signal must be filtered. To minimize DCM errors the analog bandwidth should be less than 1/10 of the DCM frequency. Analog bandwidth may be increased to up to 1/2 the DCM freque

+ncy in most applications. In such cases this will result in greater dynamic error generated at the DCM.

The analog bandwidth may be further decreased to reduce noise and improve resolution. It is recommended to limit bandwidth to the lowest frequency needed by the application to maximize the resolution and dynamic range of the accelerometer. With the single pole roll-off characteristic the typical noise of the mentioned accelerometer is determined by the following equation:

$$Noise_{(rms)} = \left(\frac{200 \, \mu g}{\sqrt{Hz}} \right) \cdot \left(\sqrt{BW \cdot 1{,}6} \right) \qquad (6)$$

then at 100 Hz the noise will be:

$$Noise_{(rms)} = \left(\frac{200 \, \mu g}{\sqrt{Hz}} \right) \cdot \left(\sqrt{100 \cdot 1{,}6} \right) = 2{,}53 \, mg$$

$$(7)$$

Very often the peak value of the noise is desired. Peak-to-peak noise can only be estimated by statistical methods. Table 2 shows estimating the probabilities of exceeding various peak-to-peak values for various rms values.

Table 2
EEstimation of Peak-to-Peak noise

Nominal Peak-to-Peak Value	% of Time that Noise will Exceed Nominal Peak-to-Peak Value
2.0 x rms	32%
4.0 x rms	4.6%
6.0 x rms	0.27%
8.0 x rms	0.006%

7. Mounting the acceleration sensor on the bandsaw.

During the normal operation of the bandsaw there are arousing accompanying vibrations of the chassis, of its sub-assembly and of the bandsaw itself. Because of the teeth geometry those vibrations have the pulse waveform.

In the surveillance as a x, y sensor, the ADXL 202 E accelerometer was used The accelerometer sensor was placed on the passive wheel of the bandsaw (se figure 3).

During the process of cutting metals, the blades of the teeth receive the impulse burden. It applies as well to the endless band saw. The severity of this burden depends on several

factors, such as the clamp between the saw and the stock, thickness of the material, to be cut, or the number of saw's teeth being in contact with the work piece. Especially the clamp of the work piece to the saw has the crucial meaning. It is difficult to protect the teeth of the saw against overloading, when cutting the profiled material, tubes, pipes or contours.
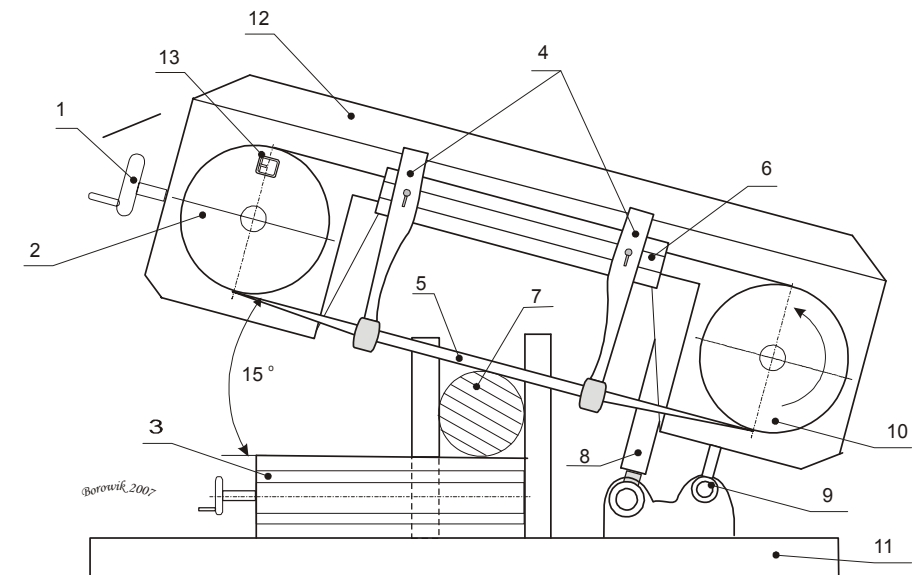

Fig 3. Identification of Basic Cutting Bandsaw Parts during operations

1. Blade tightening screw
2. Stretching wheel
3. Assembling clamping block
4. Stationery blade guard
5. Blade
6. Support of blade guard
7. Material to be cut
8. Hydraulic linear motor
9. Head frame pulley
10. Active wheel
11. Frame of cutting bandsaw
12. Head of cutting bandsaw
13. Accelerometer sensor gathering the impulse burden

In the assumed bandsaw vibration model the oscillations caused by the movement of the mass m_s. are described. The upper constrain of the exploitation speed equals:

$$\beta_0 = v \frac{v_0}{v_{kr,l}} = \frac{v_{eo}}{\sqrt{1 + v_{eo}}} \qquad (8)$$

The critical speed for the parametric resonance equals:

$$v_{0,1}^* = \frac{v_{kr,1}}{\sqrt{1 + \chi_1^{*2}}} \text{ , while: } \chi_1^* = \frac{v_l}{2\pi\sqrt{\chi}} \qquad (9)$$

The equation of the vibration of mass m_s of the stretching wheel is equal:

$$\ddot{x} + 2h_s \cdot \dot{x} + \omega_s^2 x_s - \gamma_{ks}\left(1 - \beta_{ks}\ q_k^2\right)\dot{x}_s = 0 \qquad (10)$$

where: $$\varpi_s = \sqrt{\frac{k_s}{m_s}}, \quad 2h = \frac{c_s}{m_s}, \quad k_s = \left(\frac{k\pi}{l}\right)^2 \cdot \frac{T_0}{m_s\ v_0} \qquad (11)$$

After applying the no-dimensional time: $\tau = \omega_0 t$, $\varpi = \dfrac{v_0}{m_s\ v_0}$, we obtain from (10) as follows:

$$q_k^{''} + \left(a_k^2 + \chi_k\cos\tau\right)q_k + \gamma_{k0}\left(1 - \beta_{ks}q_k^2\right)\ddot{x}_s = 0 \qquad (12)$$

$$\ddot{x}_s + 2h_{s0}\dot{x} + \gamma_{ks0}\left(1 - \beta_{ks}q_k^2\right)\ddot{x}_s = 0 \qquad (13)$$

where: $\gamma_{k0} = \dfrac{\gamma_k}{\varpi_0}, \quad \gamma_{ks0} = \dfrac{\gamma_{ks}}{\varpi_0}, \quad h_{s0} = \dfrac{h_s}{\varpi_{s0}}, \quad k_s = \left(\dfrac{k\pi}{l}\right)^2 \cdot \dfrac{T_0}{m_s\ v_0}$

The border cycle plot for the bandsaw speed of: $v_0 = 0,5$ m/s and the tension of the band **S** equal 400 N is shown on the figure 4.
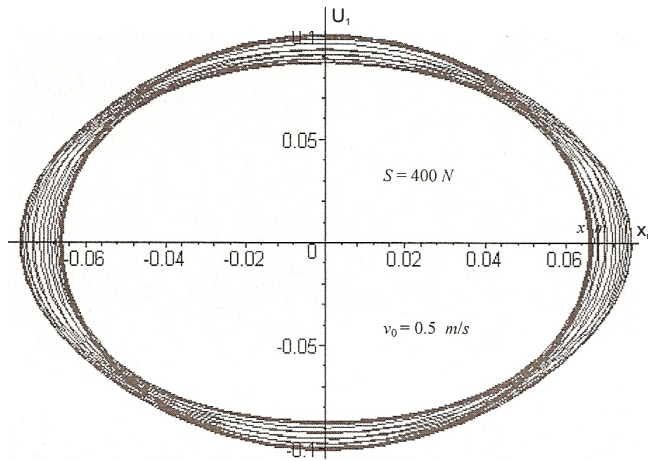
Fig. 4. The border cycle plot (0,5 m/s, 400 N)

The unstable phase portrait for the band saw speed of 4.7 m/s is presented on figure 5.
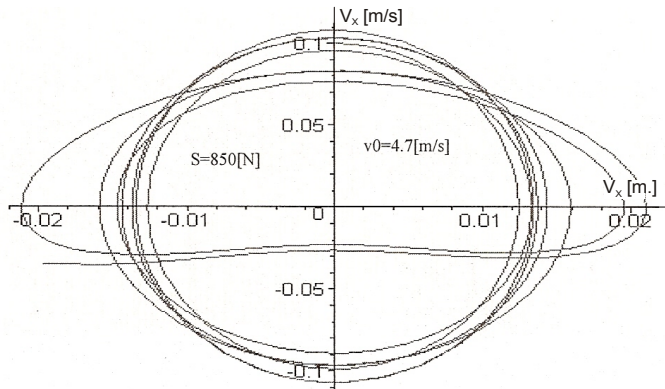

Fig. 5. The unstable phase portrait for the band saw speed $v_0 = 4.7$ m/s

8. Data acquisition and data transfer by means of the ZigBee solution

Zigbee with inherent firmware provides a wireless personal area networking PAN of data from the sensor to microcontroller PIC18F4455. The base of Zigbee hybrid module is IC ZDMAI128-B0. It provides point-to- point communication. A serial port is used to communicate with a host device through an AT command interface, as shown bellow on schematic fig. 6.
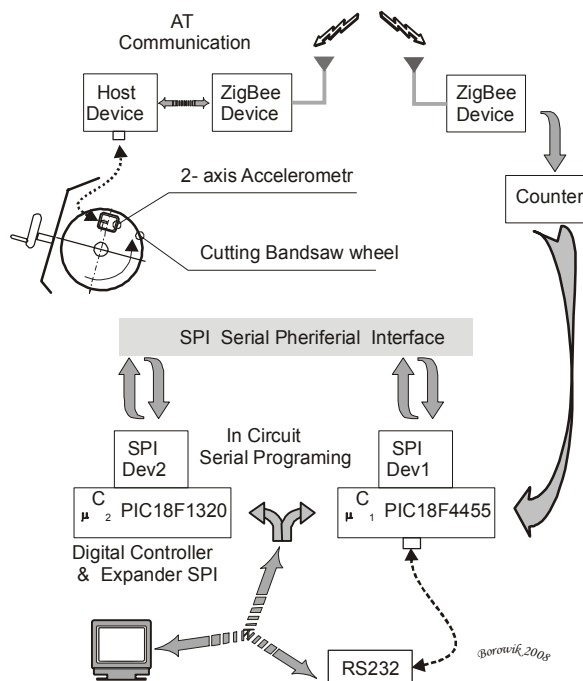
Fig.6. The Zigbee module used for data transfer from the accelerometer sensor

9. Conclusion

The aim of present investigation was to considerer the possibilities of measure   the detachable parts oscillation. The ADXL 202 E accelerometer sensor has been chosen because of its possibility of the dual axis operation. This way the data was acquired during the normal work of the cutting bandsaw. The Aim was achieved by employing the powerful microcontroller PIC18F4455.

Reference

1. J..Wojnarowski: *Ograniczenie Drgań Przecinarek z Taśmowymi Piłami bez Końca*, Politechnika Śląska Wydział Mechaniczny Technologiczny. , Gliwice 2007.
2. www.maxim-ic.com
3. B.Borowik: Mikrokontroler PIC dla praktyków, BTC, Warszawa 2008 (accepted for publishing)
4. www.microchip.com.

ENERGY ANALYSIS OF A MODEL OF A HUMAN BEING-TOOL SYSTEM FOR DIFFERENT ELBOW JOINT INCLINATION ANGLES

Małgorzata WOJSZNIS
Institute of Applied Mechanics
Poznań University of Technology
3 Piotrowo Street, 60-965 Poznań,
e-mail: *Malgorzata.Wojsznis@put.poznan.pl*

Abstract

The paper presents the influence of parameter change of a bio-mechanical Human Being – Machine model on energy quantities. The energy analysis concerned instantaneous power, average power and an energy dose directed into a human operator. The model used consisted of a biological part made up of a hand-arm system (both upper limbs) and a mechanical part made up of a tool (e.g. a demolition hammer). The analysis showed that asymmetric arrangement of upper limbs in the system causes an increase in all measured quantities.

Słowa kluczowe: models, bio-mechanics, energy analysis

Introduction

Among many types of tools commonly used in building engineering there are, for example, demolition hammers, which often are heavier than 10 kg. Such tools are called Big Power-Driven Hand Tools. Their design is closely dependent on the task they are intended to perform. Depending on the type of the grip (Figure 1) the upper limbs may be positioned symmetrically or asymmetrically.

a)   b)

Figure 1. Types of tool grips
a) symmetric b) asymmetric

If the limbs are positioned symmetrically, energy transmission takes place in the same way for each limb. Both the right and the left hands are subjected to the same load, so the levels of acceleration at the point of contact with the tool are the same. This is also true for energy quantities, such as instantaneous power, average power or energy doses determined for the whole system and for the respective points of reduction (hand, elbow, shoulder).

The aim of the investigations was to check how the change of such parameters as rigidity, damping or mass influences the energy quantities at different positioning of arms and whether and how these quantities change for asymmetric positions of arms. Such an analysis enables answering the questions which arrangement of grips should be used at big power driven tools and whether it has a significant influence on energy load of both the whole system and the limbs. Energy values were determined by means of the Principles of Power Distribution and Energy Flow by Dobry [1].

The parameter change was performed by assuming rigidity, damping and mass for two different positions of upper limbs. It was assumed that the elbow joint inclination angle equals 50° for one arm and 120° for the other.

1. Research object

The research object was a bio-mechanical Human Being – Machine system [2,6]. For the selected system a physical model was developed, which assumes a standing, vertically erect operator's working position. As simplifying assumptions the 'z' direction (Figure 2) was assumed to be the main direction of motion of the working tool, and the 'x' and 'y' directions were assumed to be negligible, because of low levels of accelerations in these directions. It was assumed that with symmetrical arm positioning the average elbow joint inclination angle for the population of people working with the tools characterized by the given parameters and having standing, vertically erect posture during work equals 120°. By asymmetrical arrangement of arms it was assumed, that one arm is bent at an angle of 120°, and the other one at an angle of 50°.

2.1. Physical and mathematical models of a Human Being – Machine system
To investigate the influence of arms positioning on energy phenomena a five-degrees-of-freedom model of a bio-mechanical Human Being – Machine system was used – see Figure 2.
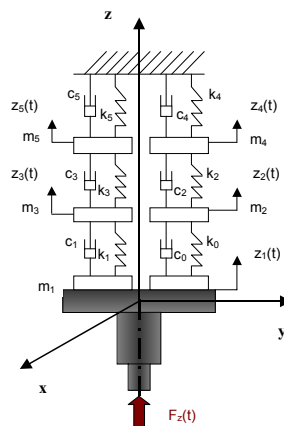

Figure 2. Physical model of a Human Being – Machine system

This model is a synthesis of the model of a human being for hand-arm vibrations developed by Meltzer [3, 4], a model of a human being from the ISO 10068 standard [5], and a model of a tool with mass of 20.3 kg.

In the bio-mechanical model shown in Figure 2 one may distinguish the following points of reduction (from the bottom): Body-Hands (K-D), Forearm-Elbow (P-Ł), Arm-Shoulder (R-B). In the point K-D the substitute mass equals the sum of the mass of the tool and the mass of both hands.

The motion of the structure is described by means of Lagrange equations. In the mathematical model the force $F_z(t)$ is the sum of impulse forces of the ram and the sinusoidal force generated in the chamber over the ram acting the tool body.

2.2. Identification of parameters

Asymmetric arrangement of upper limbs was realized by using the substitute dynamic parameters of the physical model developed by Meltzer in 1979 for the Hand-Arm system. The tool parameters were obtained during identification investigations for a demolition hammer with a mass of 20.3 kg.

Table 1: Values of dynamic parameters of the model given by Meltzer

Substitute dynamic parameters	Meltzer model (elbow joint inclination angle: 120°)	Meltzer model (elbow joint inclination angle: 50°)
m_3 [kg]	1,4	2,0
m_2 [kg]	1,0	0,87
m_1 [kg]	0,13	0,15
k_3 [N/m]	$4,1 * 10^3$	$4,0 * 10^3$
k_2 [N/m]	$7,2 * 10^4$	$9,7 * 10^4$
k_1 [N/m]	$2,1 * 10^5$	$2,7 * 10^5$
c_3 [Ns/m]	145	205
c_2 [Ns/m]	100	150
c_1 [Ns/m]	245	160

2. Influence of hand positioning on global maximum power directed into a human-operator

All the results were obtained by using the PEC-DZNR 2001(Meltzer-1) program written in Matlab/Simulink® environment.

Figure 3 illustrates global (in the whole system) maximum instantaneous power directed into a human-operator by symmetric (both elbow angles equal 120°) and asymmetric (120° and 50°) positioning of arms as a function of time.
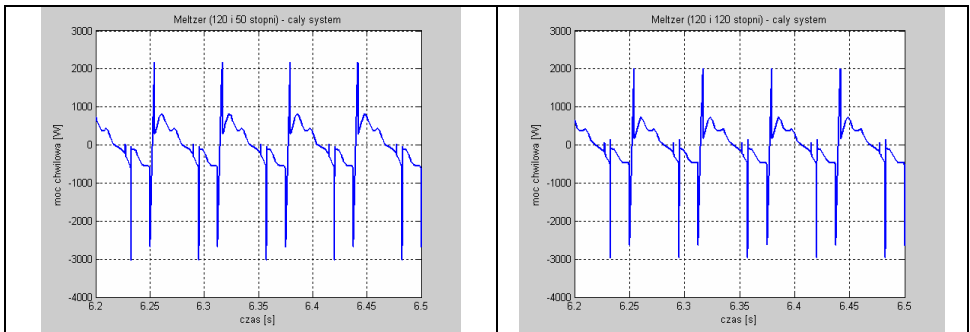
Figure 3. Global instantaneous power directed into a human-operator for asymmetric and symmetric positioning of upper limbs with reference to the whole system

By symmetric positioning of arms during work with the investigated tool both limbs are equally energy loaded. The sum of these loads equals approximately 2900 W of the maximum instantaneous power. When interpreting the results of carried out simulations it was observed that in case of asymmetry of the investigated system all the measuring values increase, including energy quantities (the instantaneous power equals approx. 3000 W).

The determined quantities concern the whole investigated system. Thus, it became important to check, which limb is more energy loaded and whether distribution of these loads is significant for an operator. As a simulation result two graphs of instantaneous power were obtained (Figure 4) for each arm separately by both their symmetric and asymmetric positioning.
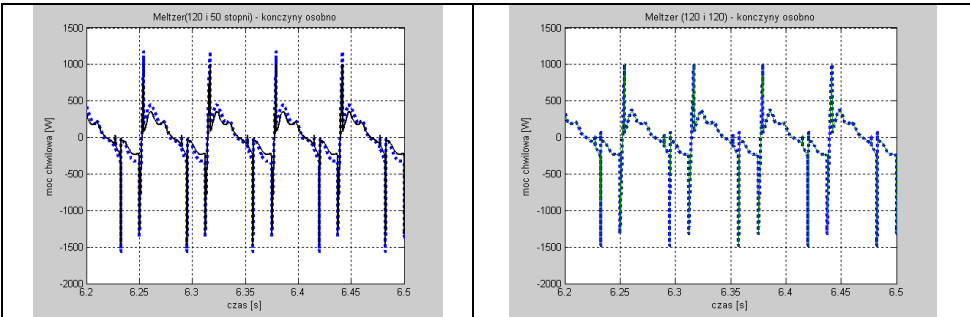

Figure 4. Global instantaneous power directed into a human-operator for asymmetric and symmetric positioning of upper limbs with reference to each limb (•50°, ―120°)

The graph shows values of the instantaneous power for an arm bent at an angle of 50°, for which the maximum instantaneous power equals 1550 W, and for an arm bent at an angle of 120°, for which the maximum instantaneous power equals 1450 W. The

difference between the results obtained for symmetric and asymmetric arrangement of arms equals approximately 100 W.

The research concerned also the differences resulting from asymmetric arrangement of limbs for individual points of reduction – Figure 5.
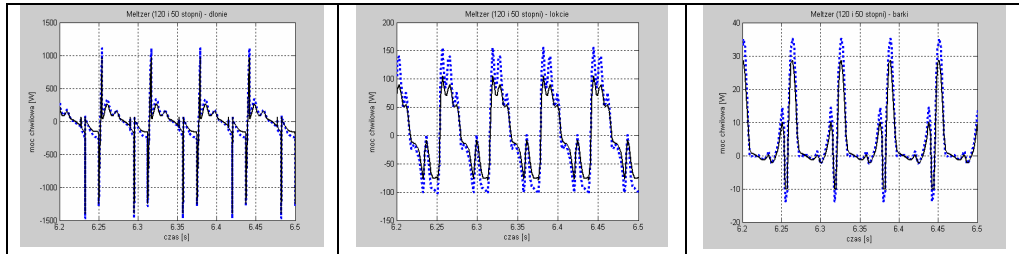

Figure 5. Influence of asymmetry of upper limbs positioning on instantaneous power for the assumed points of reduction

The following values were obtained for the point of reduction K-D (hand): for 50° – 1500 W, and for 120° – 1400 W. The difference between limbs for the point of reduction P-L equals 50 W, with 150 W for 50° and 100 W for 120°. For the point of reduction R-B, for 50^0 were obtained 35 W, and for 120° – 28 W.

The used simulation program enabled also determination of an energy dose for symmetric arrangement of limbs, which equals $D = 4\,040$ J for the simulation time t of 10 s, and a mean value of global power directed into a human-operator Nsr(t) = 404 W. The simulation for asymmetric arrangement of limbs enabled to obtain an energy dose $D = 4\,580$ J and Nsr(t) = 458 W. The results are shown in Table 2.

Table 2: Values of global maximum power directed into a human-operator, an energy dose and average power for different positions of upper limbs (Meltzer model)

Position of upper limbs (elbow joint inclination angle)	Maximum instantaneous power [W]	Energy dose [J]	Average power [W]
symmetric	**2900**	**4040**	**404**
asymmetric	**3000**	**4580**	**458**
limb 120°	1450	2020	202
limb 50°	1550	2560	256

3. Conclusions

The carried out analysis shows that the energy quantities depend on the positions of upper limbs during work, for example, with a demolition hammer. Asymmetry of the system causes an increase in all measured quantities. Hence, the energy load of a human-operator also increases.

This may suggest to design the big power-driven hand-held tools with such handles, which force symmetric positioning of operator's arms. An operator should be limited only to supporting the tool and holding it down to the ground.

References

1. Dobry M. W.; *Optymalizacja przepływu energii w systemie Człowiek - Narzędzie - Podłoże (CNP),* Rozprawa habilitacyjna, Seria „Rozprawy" nr 330. ISSN 0551-6528, Wyd. Politechniki Poznańskiej, Poznań, marzec 1998.
2. Dobry M. W., Wojsznis (Miszczak) M., *Dynamiczny model systemu człowiek- maszyna w przypadku posługiwania się dużymi narzędziami zmechanizowanymi*, Acta of Bioengineering and Biomechanics, Vol. 2, Supplement 1, Oficyna Wydawnicza Politechniki Wrocławskiej, Wrocław, pp. 125-130, 2000
3. Meltzer G., *Vibrational Model for Human Hand-Arm System,* International CISM- IFToMM Symposium: Man under Vibration, Suffering and Protection, April 3-6, Udine, Italy, pp. 210-221, 1979
4. Meltzer G., Melzig- Thiel R., Schatte M., *Ein Mathematiches Schwingungsmodell fur das menschliche Hand-Arm System*, Maschinenbautechnik, 29, 2, pp. 54-58, 1980
5. ISO/FDIS 10068, *Mechanical vibrations and shock – Free, mechanical impedance of human hand- arm system at the driving point*, 1998
6. *Wojsznis M, „Dynamika przepływu energii w systemie biomechanicznym Człowiek – Duże Zmechanizowane Narzędzie Ręczne (C–DZNR)"*, Praca Doktorska, Wydział Budowy Maszyn, Politechnika Poznańska, 2006

SPATIAL MODEL OF A HUMAN BEING - DEMOLITION HAMMER SYSTEM

Małgorzata WOJSZNIS, Marian Witalis DOBRY
Institute of Applied Mechanics
Poznań University of Technology
3 Piotrowo Street, 60-965 Poznań,
e-mail: Malgorzat.Wojsznis@put.poznan.pl , Marian.Dobry@put.poznan.pl

Abstract

The paper presents a model of a Human being – Demolition Hammer system (C-MW) taking into account the motion of the system in three directions x, y, z.. The following models were used to create the model: Meltzer model from 1980, the model from the ISO 10068 standard and authors' own Human Being – Big Power Driven Hand Tool (C-DZNR) model developed in 2000. Dynamic parameters were taken from the ISO 10068 standard for each direction of motion. Identification of tool parameters still needs accurate verification.

Keywords: bio-mechanical models, dynamics of systems

Introduction

For over forty years we found in literature the papers concerning modeling of a hand – arm system. In spite of technological progress and fast growth of numerical methods the problem of modeling of biological, mechanical and bio-mechanical structures still needs investigation.

Taking in mind the need for further investigations in the field of modeling of bio-mechanical systems the authors tried to develop dynamic and energy models of a Human Being – Demolition Hammer (C-MW) system without vibro-isolation. They worked out presumptions concerning dynamic and functional properties. It was assumed that that the system can move in all three directions x, y, z. Models existing in literature were used to create a new physical model. For this purpose the following models were used: Meltzer model from 1980 [2,3], the model from the ISO 10068 standard [4] and the Human Being – Big Power Driven Hand Tool (C-DZNR) unidirectional model developed in 2000 [1, 5] - (Figure 1).
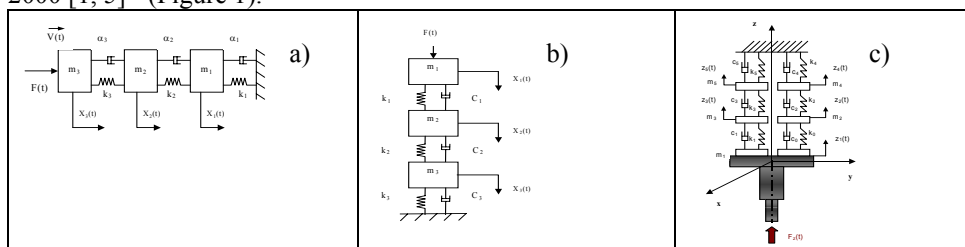

Figure 1. a) Meltzer model b) the model from the ISO 10068 standard
c) the C-DZNR model

The tool which was used may be numbered among so called big power driven hand tools heavier than 10 kg, and which must be operated with two hands.

1. Physical model of the Human Being – Demolition Hammer system

As an object of investigation a system consisting of two subsystems was used: a biological one (a human being) and a mechanical one (a demolition hammer) [2, 6]. It was assumed in the chosen system that the motion is possible in all three directions x, y, z. The z direction is assumed to be the main direction of motion of the working tool, the y axis is along the handle, and the x axis is perpendicular to the handle.

The physical model (Fig. 2) assumes standing, vertically erect operator's working position. For the tools with the given parameters, it was assumed, that with symmetric position of operator's hands the average elbow joint inclination angle equals 120°.
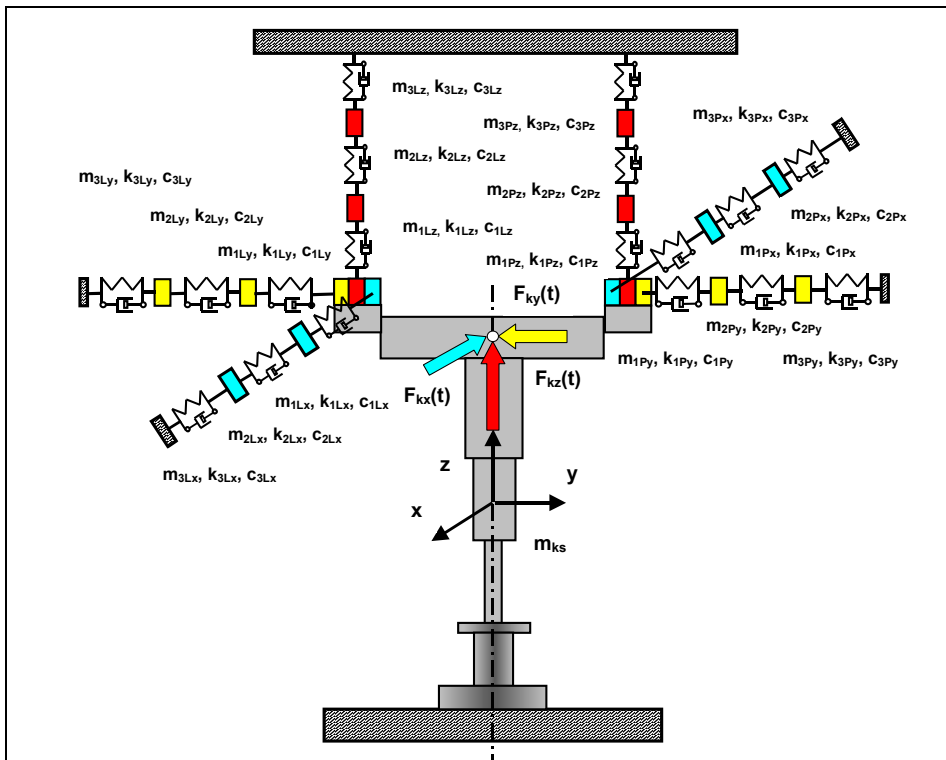

Figure 2. Physical model of a Human Being – Demolition Hammer system [7]

In the physical model of the structure shown in Figure 2, going from the bottom, one can distinguish the following points of reduction for right and left hands, separately: Engine

body with handles – Hands (K-D), Forearm – Elbow (P-L), Arm – Shoulder (R-B). For the K-D point the substitute mass equals the sum of the masses of the tool and both hands for each direction separately.

2. Mathematical model

The motion of the structure was described by means of differential equations, with the use of Lagrange equations for this purpose [6, 7]:

$$\frac{d}{dt}\left(\frac{\partial E}{\partial \dot{q}_j}\right) - \frac{\partial E}{\partial q_j} = Q_j + Q_{jp} + Q_{jR} \qquad [1]$$

where:

$j = 1, 2... s$, s – the number of degrees of freedom,
E – kinetic energy of the investigated system,
q_j – generalized coordinates\,
$\dot{q}_j$ - generalized velocities,

Q_j – generalized external forces,
Q_{jp} – generalized potential forces,
Q_{jR} – generalized non-potential forces.

Table 1 shows symbols assumed for each direction of motion.

Table 1 Symbols describing displacement of the hammer body and individual points of reduction for directions x, y, z [7]

Direction x
$x_{ks}(t)$ – displacement of the hammer engine body in the x direction,
$x_{2Lx}(t)$ – displacement of the P-L point of reduction for the left hand in the x direction,
$x_{3Lx}(t)$ – displacement of the R-B point of reduction for the left hand in the x direction,
$x_{2Px}(t)$ – displacement of the P-L point of reduction for the right hand in the x direction,
$x_{3Px}(t)$ – displacement of the R-B point of reduction for the right hand in the x direction,
Direction y
$y_{ks}(t)$ – displacement of the hammer engine body in the y direction,
$y_{2Ly}(t)$ – displacement of the P-L point of reduction for the left hand in the y direction,
$y_{3Ly}(t)$ – displacement of the R-B point of reduction for the left hand in the y direction,
$y_{2Py}(t)$ – displacement of the P-L point of reduction for the right hand in the y direction,
$y_{3Py}(t)$ – displacement of the R-B point of reduction for the right hand in the y direction,
Direction z
$z_{ks}(t)$ – displacement of the hammer engine body in the z direction,
$z_{2Lz}(t)$ – displacement of the P-L point of reduction for the left hand in the z direction,
$z_{3Lz}(t)$ – displacement of the R-B point of reduction for the left hand in the z direction,
$z_{2Pz}(t)$ – displacement of the P-L point of reduction for the right hand in the z direction,
$z_{3Pz}(t)$ – displacement of the R-B point of reduction for the right hand in the z direction,

Differential equations of motion for the investigated system have the following forms [7]:

1. Direction x

$$(m_{ks} + m_{1Lx} + m_{1Px})\overset{\circ\circ}{x}_k + (c_{1Lx} + c_{1Px})\overset{\circ}{x}_k + (k_{1Lx} + k_{1Px})x_k - c_{1Lx}\overset{\circ}{x}_{2Lx} - c_{1Px}\overset{\circ}{x}_{2Px} - k_{1Lx}x_{2lx} - k_{1Px}x_{2Px} = F_{ksx}(t);$$ [2]

$$m_{2Lx}\overset{\circ\circ}{x}_{2Lx} + (c_{1Lx} + c_{2Lx})\overset{\circ}{x}_{2Lx} + (k_{1Lx} + k_{2Lx})x_{2lx} - c_{1Lx}\overset{\circ}{x}_k - k_{1Lx}x_k - c_{2Lx}\overset{\circ}{x}_{3Lx} - k_{2Lx}x_{3Lx} = 0;$$ [3]

$$m_{3Lx}\overset{\circ\circ}{x}_{3Lx} + (c_{2Lx} + c_{3Lx})\overset{\circ}{x}_{3Lx} + (k_{2Lx} + k_{3Lx})x_{3Lx} - c_{2Lx}\overset{\circ}{x}_{2Lx} - k_{2Lx}x_{2Lx} = 0;$$ [4]

$$m_{2Px}\overset{\circ\circ}{x}_{2Px} + (c_{1Px} + c_{2Px})\overset{\circ}{x}_{2Px} + (k_{1Px} + k_{2Px})k_{2Px} - c_{1Px}\overset{\circ}{x}_k - k_{1Px}x_k - c_{2Px}\overset{\circ}{x}_{3Px} - k_{2Px}x_{3Px} = 0;$$ [5]

$$m_{3Px}\overset{\circ\circ}{x}_{3Px} + (c_{2Px} + c_{3Px})\overset{\circ}{x}_{3Px} + (k_{2Px} + k_{3Px})x_{3Px} - c_{2Px}\overset{\circ}{x}_{2Px} - k_{2Px}x_{2Px} = 0;$$ [6]

2. Direction y

$$(m_{ks} + m_{1Ly} + m_{1Py})\overset{\circ\circ}{y}_k + (c_{1Ly} + c_{1Py})\overset{\circ}{y}_k + (k_{1Ly} + k_{1Py})y_k - c_{1Ly}\overset{\circ}{y}_{2Ly} - k_{1Ly}y_{2Ly} - c_{1Py}\overset{\circ}{y}_{2Py} - k_{1Py}y_{2Py} = F_{ksy}(t);$$ [7]

$$m_{2Ly}\overset{\circ\circ}{y}_{2Ly} + (c_{1Ly} + c_{2Ly})\overset{\circ}{y}_{2Ly} + (k_{1Ly} + k_{2Ly})y_{2Ly} - c_{1Ly}\overset{\circ}{y}_k - k_{1Ly}y_k - c_{2Ly}\overset{\circ}{y}_{3Ly} - k_{2Ly}y_{3Ly} = 0;$$ [8]

$$m_{3Ly}\overset{\circ\circ}{y}_{3Ly} + (c_{2Ly} + c_{3Ly})\overset{\circ}{y}_{3Ly} + (k_{2Ly} + k_{3Ly})y_{3Ly} - c_{2Ly}\overset{\circ}{y}_{2Ly} - k_{2Ly}y_{2Ly} = 0;$$ [9]

$$m_{2Py}\overset{\circ\circ}{y}_{2Py} + (c_{1Py} + c_{2Py})\overset{\circ}{y}_{2Py} + (k_{1Py} + k_{2Py})y_{2Py} - c_{1Py}\overset{\circ}{y}_k - k_{1Py}y_k - c_{2Py}\overset{\circ}{y}_{3Py} - k_{2Py}y_{3Py} = 0;$$ [10]

$$m_{3Py}\overset{\circ\circ}{y}_{3Py} + (c_{2Py} + c_{3Py})\overset{\circ}{y}_{3Py} + (k_{2Py} + k_{3Py})y_{3Py} - c_{2Py}\overset{\circ}{y}_{2Py} - k_{2Py}y_{2Py} = 0;$$ [11]

3. Direction z

$$(m_{ks} + m_{1Lz} + m_{1Pz})\overset{\circ\circ}{z}_k + (c_{1Lz} + c_{1Pz})\overset{\circ}{z}_k + (k_{1Lz} + k_{1Pz})z_k - c_{1Lz}\overset{\circ}{z}_{2Lz} - k_{1Lz}z_{2Lz} - c_{1Pz}\overset{\circ}{z}_{2Pz} - k_{1Pz}z_{2Pz} = F_{ksz}(t);$$ [12]

$$m_{2Lz}\overset{\circ\circ}{z}_{2Lz} + (c_{1Lz} + c_{2Lz})\overset{\circ}{z}_{2Lz} + (k_{1Lz} + k_{2Lz})z_{2Lz} - c_{1Lz}\overset{\circ}{z}_k - k_{1Lz}z_k - c_{2Lz}\overset{\circ}{z}_{3Lz} - k_{2Lz}z_{3Lz} = 0;$$ [13]

$$m_{3Lz}\overset{\circ\circ}{z}_{3Lz} + (c_{2Lz} + c_{3Lz})\overset{\circ}{z}_{3Lz} + (k_{2Lz} + k_{3Lz})z_{3Lz} - c_{2Lz}\overset{\circ}{z}_{2Lz} - k_{2Lz}z_{2Lz} = 0;$$ [14]

$$m_{2Pz}\overset{\circ\circ}{z}_{2Pz} + (c_{1Pz} + c_{2Pz})\overset{\circ}{z}_{2Pz} + (k_{1Pz} + k_{2Pz})z_{2Pz} - c_{1Pz}\overset{\circ}{z}_k - k_{1Pz}z_k - c_{2Pz}\overset{\circ}{z}_{3Pz} - k_{2Pz}z_{3Pz} = 0;$$ [15]

$$m_{3Pz}\overset{\circ\circ}{z}_{3Pz} + (c_{1Pz} + c_{3Pz})\overset{\circ}{z}_{3Pz} + (k_{2Pz} + k_{3Pz})z_{3Pz} - c_{1Pz}\overset{\circ}{z}_{2Pz} - k_{2Pz}z_{2Pz} = 0;$$ [16]

where:

$F_{ksx}(t)$, $F_{ksy}(t)$, $F_{ksz}(t)$, - are components of the sum of the forces actuating the engine and reactive forces of the foundation during work acting the tool body in the x, y, and z directions.

3. Identification of parameters

Substitute values of dynamic parameters of the model of a human being were taken from literature basing on the ISO 10068 standard [5]. The values are shown in Table 2.

Table 2 Values of dynamic parameters of a physical model of a human operator for three directions x, y and z according to the ISO 10068 standard [5]

Unit	Reduced dynamic parameters of a model of a human being Direction of vibrations		
	X	Y	Z
kg	$m_{1Lx} = m_{1Px} = 0.0267$	$m_{1Ly} = m_{1Py} = 0.0086$	$m_{1Lz} = m_{1Pz} = 0.0299$
kg	$m_{2Lx} = m_{2Px} = 0.486$	$M_{2Ly} = m_{2Py} = 0.3565$	$M_{2Lz} = m_{2Pz} = 0.6623$
kg	$m_{3Lx} = m_{3Px} = 3.0952$	$M_{3Ly} = m_{3Py} = 3.2462$	$M_{3Lz} = m_{3Pz} = 2.9023$
N/m	$k_{1Lx} = k_{1Px} = 4368$	$K_{1Ly} = k_{1Py} = 27090$	$k_{1Ly} = k_{1Py} = 5335$
N/m	$k_{2Lx} = k_{2Px} = 132$	$k_{2Ly} = k_{2Py} = 300$	$k_{2Lz} = k_{2Pz} = 299400$
N/m	$k_{3Lx} = k_{3Px} = 1565$	$k_{3Ly} = k_{3Py} = 6415$	$k_{3Lz} = k_{3Pz} = 2495$
Ns/m	$c_{1Lx} = c_{1Px} = 207,5$	$c_{1Ly} = c_{1Py} = 68$	$c_{1Lz} = c_{1Pz} = 227,5$
Ns/m	$c_{2Lx} = c_{2Px} = 18,93$	$c_{2Ly} = c_{2Py} = 51,75$	$c_{2Lz} = c_{2Pz} = 380,6$
Ns/m	$c_{3Lx} = c_{3Px} = 9,10$	$c_{3Ly} = c_{3Py} = 30,78$	$c_{3Lz} = c_{3Pz} = 30,30$

They have been obtained experimentally and they concern hand-arm vibrations of a human being modeled by means of a discrete model with nine degrees of freedom.

Identification of the remaining parameters of the tool being an element of the investigated system still needs final verification [7].

4. Conclusions

The obtained new spatial model of a Human Being – Demolition Hammer system is a synthesis of two models: a human-operator model and a dynamic model of a tool – a demolition hammer in this case. A physical model of a human being with nine degrees of freedom, described in the ISO 10068 standard, into which vibrations come through one limb was used to develop this model. The novelty of the developed model is that it takes into account two ways of propagation of tool vibrations into a human being through both limbs, spatial motion of these limbs and spatial motion of a demolition hammer [7].

Exact matching of the dynamic model of a C-MW system without vibro-isolation with a real object needs further analytical and experimental investigations, including

identification of substitute parameters of a demolition hammer when operated with two hands. A method of digital simulation of dynamics of the investigated system with use of Matlab/Simulink® software will be used for dynamic analysis. Finally, the developed model will be verified basing on the energy criterion of similarity between a real object and a model [7, 8].

References

1. Dobry M. W., Wojsznis (Miszczak) M., *Dynamiczny model systemu człowiek - maszyna w przypadku posługiwania się dużymi narzędziami zmechanizowanymi*, Acta of Bioengineering and Biomechanics, Vol. 2, Supplement 1, Oficyna Wydawnicza Politechniki Wrocławskiej, Wrocław, pp. 125-130, 2000

2. Meltzer G., *Vibrational Model for Human Hand-Arm System,* International CISM-IFToMM Symposium: Man under Vibration, Suffering and Protection, April 3-6, Udine, Italy, pp. 210-221, 1979

3. Meltzer G., Melzig-Thiel R., Schatte M., *Ein Mathematiches Schwingungsmodell für das menschliche Hand-Arm System*, Maschinenbautechnik, 29, 2, pp. 54-58, 1980

4. ISO/FDIS 10068, *Mechanical vibrations and shock – Free, mechanical impedance of human hand- arm system at the driving point*, 1998

5. Wojsznis M., *Dynamika przepływu energii w systemie biomechanicznym Człowiek – Duże Zmechanizowane Narzędzie Ręczne (C–DZNR)*, Praca Doktorska, Wydział Budowy Maszyn, Politechnika Poznańska, 2006

6. Cannon R.H. jr., Dynamika układów fizycznych, WNT, Warszawa, pp. 182- 197, 1973

7. Dobry M. W., Wojsznis M., *Innowacyjna metoda redukcji przepływu energii do człowieka-operatora od dużych zmechanizowanych narzędzi ręcznych.* Raport z etapu I. Projekt badawczy nr N503 017 32/2558. Politechnika Poznańska, Instytut Mechaniki Stosowanej, Poznań 2008

8. Dobry M. W., Optymalizacja przepływu energii w systemie Człowiek - Narzędzie - Podłoże (CNP), Rozprawa habilitacyjna, Seria „Rozprawy" nr 330. ISSN 0551-6528, Wyd. Politechniki Poznańskiej, Poznań 1998

INFLUENCE OF THE POSITION OF AN EXTENSION ARM ON THE DEGREE OF IMPACT IN THE BUCKET'S SERVER OF A LOADER

Sergiusz ZAKRZEWSKI, Zygmunt TOWAREK

Instytut Pojazdów, Konstrukcji i Eksploatacji Maszyn; Katedra Konstrukcji
Precyzyjnych, Politechnika Łódzka
ul. Stefanowskiego1/15, 90-924 Łódź
telefon: 042 631 22 42, 042 631 22 09, e-mail: sergiusz.zakrzewski@p.lodz.pl,
zygtow@p.lodz.pl

Abstract

The study covers the case of driving the loader straight and a symmetric impact of a bucket against a fixed and non-deformable obstacle. The values of impulses of forces that appear in hydraulic servers of a joint-wheel loader's working equipment during an impact were determined. Attention was put on the load of a bucket's server. Numerical calculations were made for geometric units characterizing the working equipment of the loader 560 E (HSW), and the results of the impulses of forces that are transformed by the bucket's hydraulic server have been presented in diagrams.

Key words: joint-wheel loader, hydraulic servers, impact load.

Introduction

Among the many dynamic loads that influence the loader's working equipment there is an emergency load resulting from the impact of a bucket against an obstacle in the gathered load. It is a large momentary load having a disadvantageous influence on the survivability of the equipment's construction elements and the elements of hydraulic system. The elements under the largest load during such uncontrolled impact are the servers of the loader's working system (equipment), especially the bucket's power server.

1. Physical dynamical model of the system

Dynamical description assumed a physical model of a joint-wheel single-bucket loader (pic.1). The following masses were separated in this model: back element mass – m_1, front element mass – m_2, masses of left and right extension arms – $m_3 = m_4$ and bucket's mass – m_5. The model's elements were connected with joints and treated as a system of rigid, non-deformable masses. Hydraulic servers were modeled as discreet rheologic elements of Kelvin – Voit and characterized with substitute susceptibility coefficients K_1, K_2, K_3, and damping C_1, C_2, C_3, respectively for the system of turn, extension arm and bucket. Apart from the masses of the studied system, there were distinguished mass moments of inertia, geometric lengths and angles characterizing the configuration of the working equipment setting. Angular position of the loader's elements resulting from working configuration was defined with angles: α_1 – position of back element in relation to the front one, α_3 – position of extension arms in relation to the level, α_4 – position of the bucket in relation to the level, as presented in pictures 1 and 2.
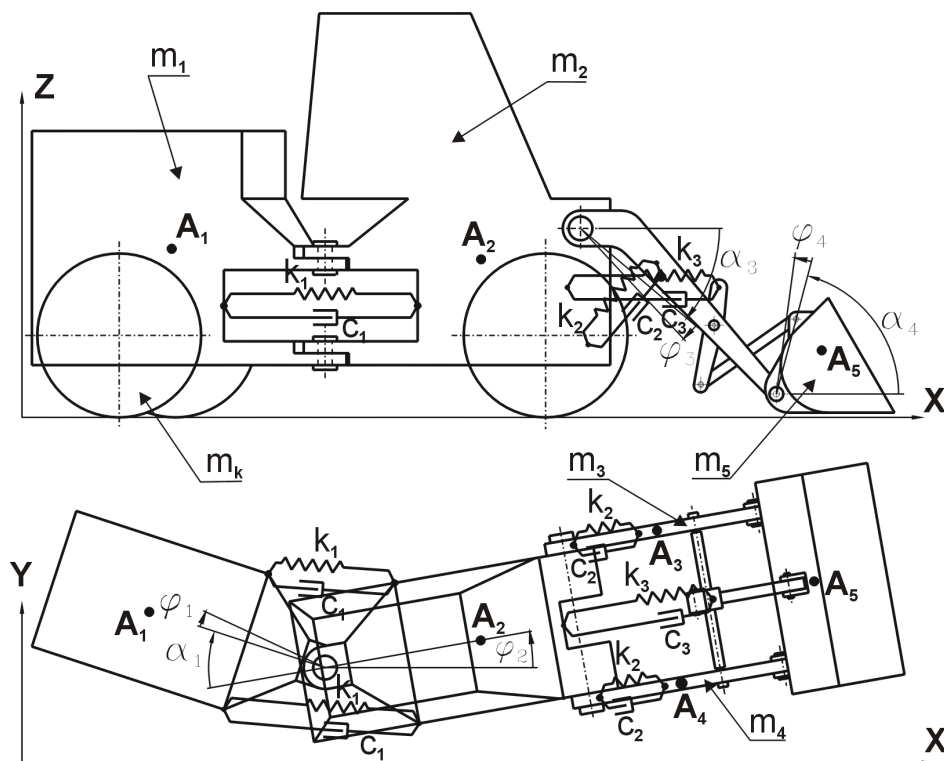
Pic. 1. Model of studied system

The assumed model accepted the power moment imposed to the loader's front wheels as the input function. It did not consider vertical susceptibility of drive wheels and it omitted 'self-alignment' of back axis and ground rheologies. Ground was treated as being non-deformable.

2. Results of numeric calculations

The studied system has six degrees of freedom, however, for the analysis of determining the impulse of force in the servers of equipment in driving the loader straight, the system is reduced to three degrees of freedom.

Dynamic description of the analyzed system was divided into three stages. The first stage concerns the dynamics of the system's movement before the impact, described by the dynamic equations of Lagrange II type; the second one concerns the phenomenon of impact itself and it results from the change of the system's momentum and the restitution coefficient in the place of impact; whereas the third stage describes dynamic behaviour of the studied system after the impact.

Calculations were made for the loader's track speed (model 560 E, producer HSW) v = 1.79 [m/s] against a fixed obstacle and for the restitution coefficient k = 0.4. The case of driving the loader straight and a symmetric impact of a bucket were studied. Angular position of the loader's elements resulting from the configuration of working setting was the following:
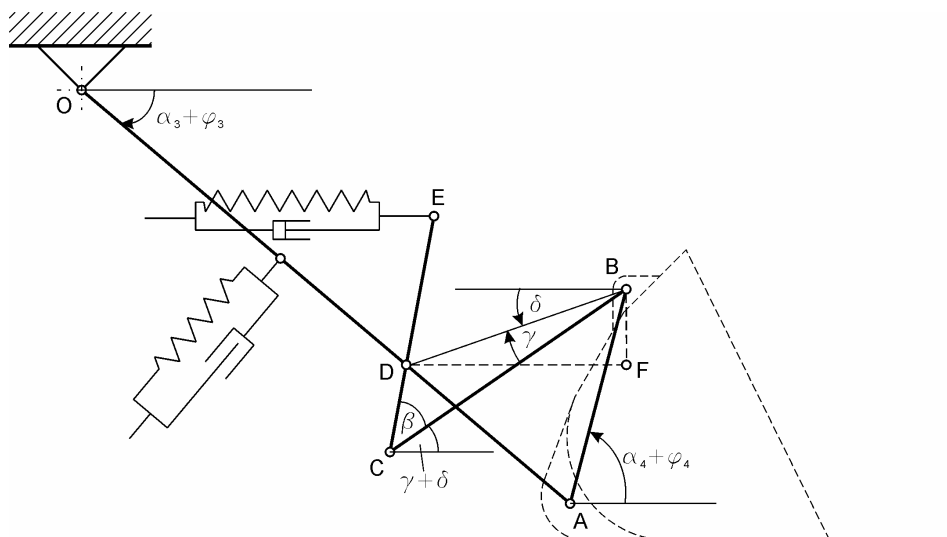
Pic. 2. Model of the loader's working equipment

I	II	III
$_1 = 0$ [rad]	$_1 = 0$ [rad]	$_1 = 0$ [rad]
$_3 = 0,7$ [rad]	$_3 = 0,25$ [rad]	$_3 = -0,7$ [rad]
$_4 = 1,2$ [rad]	$_4 = 1,2$ [rad]	$_4 = 1,2$ [rad]

Calculations were made for the following numerical data, where rigidity and damping were assumed from own experimental studies [2], [3]:

I	II	III
$K_1=1,8\cdot10^8$ [N/m]	$K_1=1,8\cdot10^8$ [N/m]	$K_1=1,8\cdot10^8$ [N/m]
$K_2=3\cdot10^8$ [N/m]	$K_2=1,2\cdot10^8$ [N/m]	$K_2=0,51\cdot10^8$ [N/m]
$K_3=3,6\cdot10^8$ [N/m]	$K_3=2,7\cdot10^8$ [N/m]	$K_3=2,1\cdot10^8$ [N/m]
$C_1=1,2\cdot10^6$ [Ns/m]	$C_1=1,2\cdot10^6$ [Ns/m]	$C_1=1,2\cdot10^6$ [Ns/m]
$C_2=2\cdot10^6$ [Ns/m]	$C_2=0,8\cdot10^6$ [Ns/m]	$C_2=0,34\cdot10^6$ [Ns/m]
$C_3=2,4\cdot10^6$ [Ns/m]	$C_3=1,8\cdot10^6$ [Ns/m]	$C_3=1,4\cdot10^6$ [Ns/m]

where:

K_1 – substitute coefficient of rigidity of the turn system server,

K_2 – substitute coefficient of rigidity of the extension arm server,

K_3 - substitute coefficient of rigidity of the bucket server,

C_1 - substitute coefficient of damping of the turn system server,

C_2 - substitute coefficient of damping of the extension arm server,

C_3 - substitute coefficient of damping of the bucket server.

For the restitution coefficient from the range $0<k<1$ the loader's bucket is several times bounced against an obstacle, then the bucket constantly presses on the obstacle, and then the bucket with the loader bounces off the obstacle. Below are presented values of the loads that the bucket's server of the joint-wheel loader experiences, for different angular positions of the extension arms. Three values of angular position of the extension arms in relation to the level were assumed, and one, unchanged angular position of the bucket.
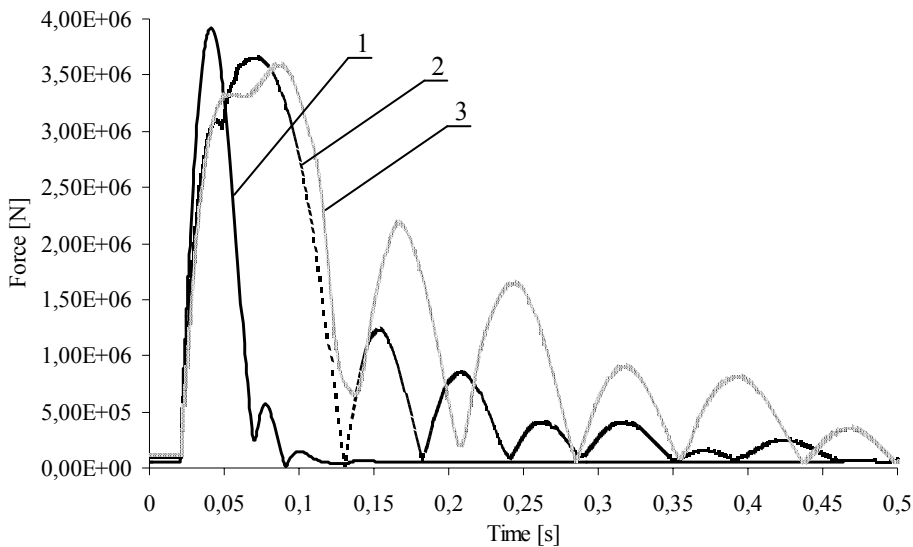
Pic. 3. Force value in the bucket's server for extension arm position: 1 – $_3 = 0.7$ [rad], 2 – $_3 = 0.25$ [rad], 3 – $_3 = -0.7$ [rad]

The diagram presented below illustrates the change of maximum dynamic load of a bucket's hydraulic server in the working system of the joint-wheel loader (data for calculation based on the wheel loader model 560 E) in the function of position change of the extension arms during the drive on a fixed and non-deformable obstacle.
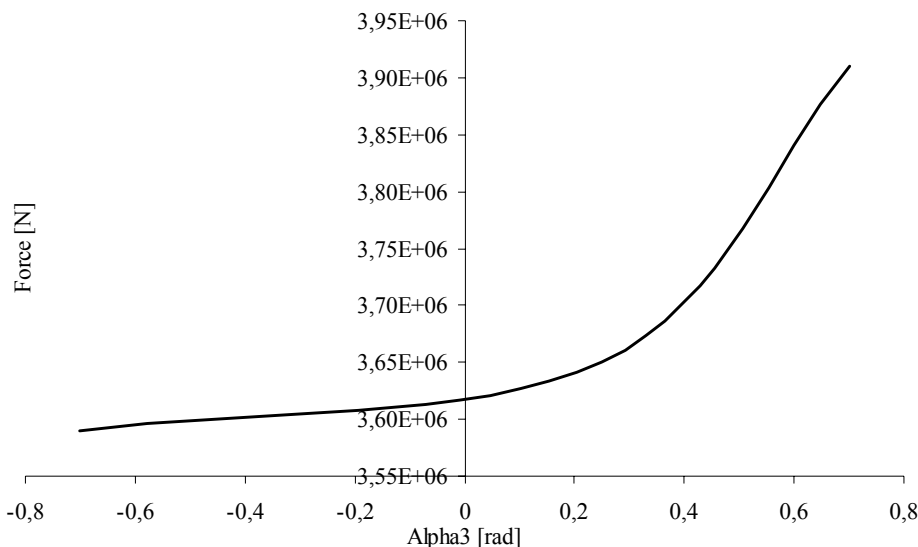
Pic. 4. Force value in the bucket's server in the function of position change of the extension arms

3. Conclusions

It is worth noticing the maximum values of forces generated in the hydraulic server of the loader's bucket during the bucket's impact against a fixed and non-deformable obstacle, for different values of the angular position of extension arms. The difference in the values of force impulse appearing in the loader's bucket server results from the fact that for different settings of the extension arm, there are different lengths of the servers, so there are different values of substitute coefficients of rigidity and damping. Others for a system with lowered extension arm " I ", in comparison to the lifted one " II " and maximally lifted " III ". Substitute rigidity and damping of the hydraulic server depends on the amount of working liquid in the cylinder, that is on the line feed on the piston [2], [3]. The values of those coefficients decrease with the increasing of the amount of hydraulic oil under the piston in the server's cylinder. Substitute susceptibility of server influences also the duration of force impulse. With its increase, the time of impulse duration increases and maximum momentary force value decreases. It means that in the system with lifted extension arm, a considerable part of the force impulse that appears during the impact, is transformed on the bucket's server. This case is most disadvantageous because longer duration of force impulse may lead to a failure of the server and a breakdown of the loader.

References

1. Z. Towarek, S. Zakrzewski, *Wyznaczenie impulsu reakcji w czasie uderzenia łyżki ładowarki o stałą przeszkodę dla różnych prędkości jej najazdu,* Czasopismo Techniczne, 387 – 394, z. 1 – M/2005.

2. M. Krajewski, Z. Towarek, S. Zakrzewski, *Eksperymentalne wyznaczenie charakterystyk siłowników hydraulicznych,* Problemy Maszyn Roboczych, 39 – 48, z. 25/2005.

3. M. Krajewski, Z. Towarek, S. Zakrzewski, *Eksperymentalne wyznaczenie dynamicznych charakterystyk podatności i tłumienia siłowników hydraulicznych obciążonych impulsem siły,* XX Konferencja Naukowa „Problemy Rozwoju Maszyn Roboczych", 181 – 185, 2007

4. Z. Towarek, S. Zakrzewski, *The influence of linearization of nonlinear dynamic equations of motion concerning the impact phenomenon, on the impulse load of working machines,* XXII Symposium Vibrations in Physical Systems "VIBRATIONS and WAVES 2006" 355-360, 2006.

MODAL FREQUENCY SHIFT ANALYSIS FOR PRESTRESSED CONCRETE BEAMS DEVELOPED BY INTEGRITY LOSS

Jerzy ZIELNICA , Roman BARCZEWSKI
Poznan University of Technology Institute of Applied Mechanics
ul.Piotrowo 3, 60-965 Poznań, Poland
tel.+48.61.6652319, e-mail: Jerzy.Zielnica@put.poznan.pl

Summary

The paper presents a method of initial analysis of the modal parameter change (e.g. modal frequency shift) due to progressive integrity loss for prestressed concrete beams (sensitivity analysis). A global rescaling method of the numerical modal frequency set was proposed in order to fit the real vibration components determined experimentally. The aim of simulation is numerical determination of frequency modal components and modes for specific boundary conditions, determined by the tested element support system. On the basis of static and dynamic FEM simulation results the optimal location of excitation points, location of transducers recording structure vibration response can be determined. The presented methodology can be helpful and is necessary for determination of possibilities of application of VA methods for testing the prestressed concrete structures.

Keywords : structure testing, FEM analysis, prestressed concrete, fault detection

Introduction

Prestressed concrete structural elements are commonly used in civil and mechanical engineering. Actually, the new Non Destructive Testing (NDT) methods, based on vibroacoustical (VA) signal analysis [1-6] are developed in order to quick assess the structure condition. These methods are usually used at first stage of the structure testing and allow for initial classification of the elements to the next, more detailed, but more time consuming testing standard techniques.

Elaborated VA methods are based on vibration signal analysis, usually free vibration analysis of the investigated structure, to be the response of the structure on the pulse force excitation. As a result of such excitation the elements respond by their eigenfrequencies and corresponding modes. In the case of VA techniques application, the evaluation of technical condition change of prestressed concrete elements, caused e.g. by structural integrity loss, initial stress loss, microcracks, can be based on: modal frequency shift analysis, vibration mode changes, nonlinearity analysis change [1-4]. If we consider elaboration of VA testing procedure for specific structural element a useful is the initial simulation using the Finite Element Method (FEM). The aim of such simulation is numerical determination of frequency modal components and modes for specific boundary condition (determined by the element support system). On the basis of static and dynamic FEM simulation results one can determine: optimal location of excitation points, location of transducers recording structure vibration response.

Moreover, we can assess the sensitivity of modal parameters caused by destruction of prestressed concrete structure. However, it is to note that FEM simulation results are approximate ones. Differences between numerical and experimental results can be explained by the introduction into calculations the material constants and coefficients not fully verified in the practice, and simplifications in the FEM model. Initially evaluated modal parameters (frequencies and modes) by the FEM method should be verified experimentally. However, it happens in practice that it is difficult to fit the real and numerical modal parameters. The paper presents an example of initial analysis of the modal parameter change due to progressive integrity loss for prestressed concrete beam (sensitivity analysis). A global rescaling method of the numerical modal frequency set was proposed in order to fit the real vibration components determined experimentally.

1. FEM model of prestressed concrete beam

This section describes the application of the FEM method to sensitivity analysis of the modal frequency shift that is developed by the structure disintegrity. We considered the beams with imperfections only (cracks). The observation of the change in the modal parameters provides potential possibilities of their application in the VA evaluation procedures (mentioned in the introduction). Also, we can determine the change of modal parameters (modes and frequencies) caused by imperfections introduced in prestressed beams.

Moreover, the vibration signal transducer location can be fixed on the structure with

Fig. 1. The FEM mesh model of the considered prestressed beam

nonzero amplitudes in order not to use the nodal points for diagnostic observation. Figure 2 presents the model overall view (with dimensions) of the considered prestressed beam.
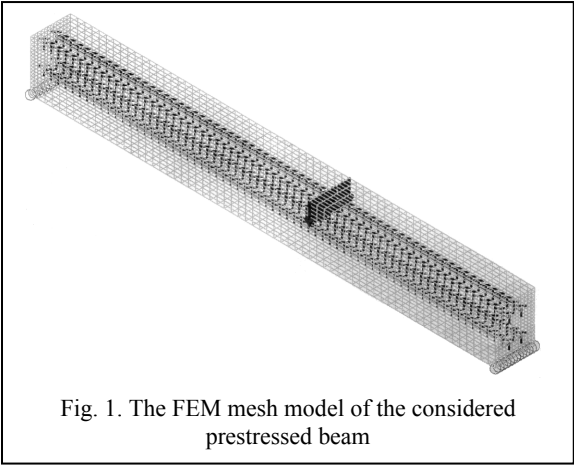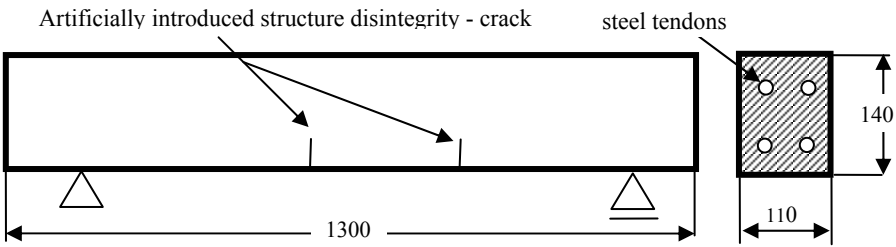

Fig. 2. The model of the considered prestressed beam

The beam was modeled according to the FEM requirements using *brick* and *truss* finite elements. The 3D *brick* elements were used to model the concrete structure, and the *truss* finite elements were used to model the tendons. The material of the matrix is concrete, type C 40/50. The material of tendons is very low relaxation steel C256G grade 270K, with very high ultimate stress equal to about 1900 MPa.

The elaborated FEM model (see Fig.1) consists of 14807 nodes, 12672 *brick* elements, and 264 *truss* elements. The mesh nodes associated with the left hand side support have all three translational degrees of freedom fixed and the right hand side support nodes are fixed against vertical Z displacement only. The effect of the 'prestressing' was simulated in FEM calculations by introducing a negative initial temperature in the respective nodes associated with tendons FEM mesh.

2. Modal frequency shift analysis

The FEM calculation were performed for the first 25 mode shapes for the two cases of the beam. The first case responds to the beam without imperfections and the second case is related with the beam having two vertical imperfections (cracks) introduced artificially into the model. The cracks are assumed to have a different depth, equal to 0%, 27%, and 73 % of the total height of the beam, respectively. The results of numerical simulation are as follows. Table 1 presents percentage values of frequency decrease of beams with imperfection when compared with beams without imperfections.
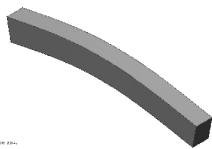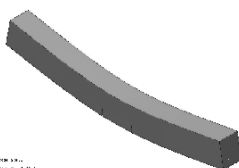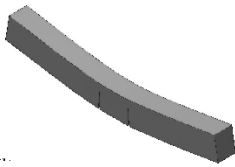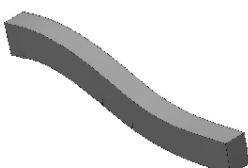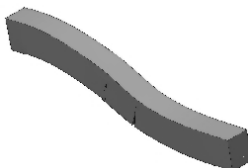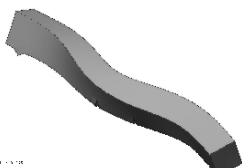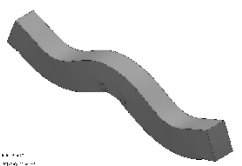
Table 1. Decrease of modal frequencies for the beam developed by imperfections

mode No. (selected)	percent change of modal frequency related to beam with/without imperfections	
	imperfection depth 27 %	imperfection depth 73 %
2	**13.6**	**28.9**
4	0.9	5.1
7	2.1	9.1
8	1.2	12.4
10	**9.1**	**21.0**
13	2.0	14.3
14	6.7	20.1

Table 2 presents the selected mode shapes of prestressed concrete beams without and with imperfections. In addition, the natural frequencies related with the mode shapes are given in the table. We can observe a noticeable decrease in natural frequencies for all modes; also including the modes not presented in the table.

We can conclude that there are possibilities, from practical point of view, to use this phenomenon for detection of disintegration degree of the prestressed structures. Theoretically, the one of most sensitive modal component can be taken in the inspection procedures. However, some difficulties can be expected in a' priori determination which modal component is suitable.

Table 2. Selected mode shapes and corresponding modal frequencies of prestressed concrete beams without and with imperfections [7]

Mode No.	No imperfection	Imperfection depth 27 %	Imperfection depth 73 %
2	172 [Hz]	151[Hz]	122 [Hz]
4	491[Hz]	487 [Hz]	466 [Hz]
8	1108 [Hz]	1095 [Hz]	971 [Hz]
10	1377 [Hz]	1263 [Hz]	1088 [Hz]

Thus, the global frequency shift analysis of all modal components would be easier to realize in the practice. This was confirmed also during experimental tests carried out on the same types of beams.

3. The rescaling problem of modal frequencies

Not all of the modal components determined experimentally in the VA signal are noticeable. This is caused by the influence of boundary conditions, location of force excitation and vibration transducers and other factors. In most cases one can see several modes only
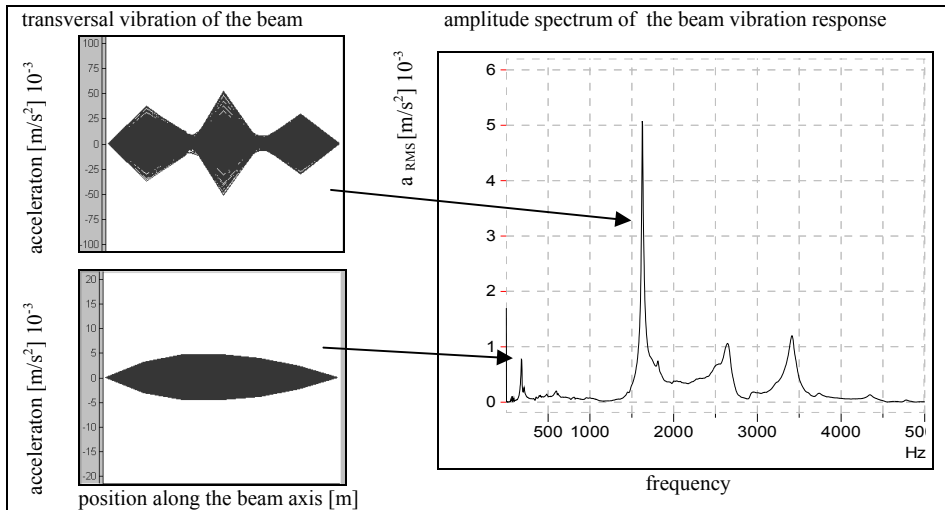
Fig. 3 Experimentally determined vibration modes of prestressed concrete beam
(on the left) and corresponding spectral components.

Table 3. Experimental and numerical modal frequencies and results of rescaling

mode number	modal frequency [Hz]		nearest experimental modal frequency [Hz]	relative error [%]
	simulation FEM	rescaling		
1	32.9	38.9	199.7	80.5
2	**172.7**	**204.2**	**199.7**	**2.3**
3	223.3	264.0	199.7	32.2
4	491.7	581.4		
5	594.9	703.4		
6	709.0	838.3		
7	761.4	900.3		
8	1109	1311		
9	1341	1586	1628	2.6
10	**1377**	**1628**	**1628**	**0.0**
11	1743	2061	1628	26.6
12	1782	2107		
13	2002	2367	2652	10.7
14	**2194**	**2594**	**2652**	**2.2**
15	2477	2929	2652	10.4
16	2676	3164	3231	2.1
17	**2752**	**3254**	**3231**	**0.7**
18	2819	3333	3231	3.2
19	3060	3619		
20	3225	3813		

(usually amplitude dominant, see Fig. 3). For the considered beam in the analyzed frequency band, up to 5 kHz, only four dominant components were good visible. A great care should be taken during assigning the experimental and numerical modal components. Intuitive association is related with those numerical and experimental components that are closest each other, what is not always correct. It results from the fact that creation of the FEM model is an iterative process. It frequently happens that in the first approach we have not full compatibility between numerical and experimental modal frequencies. Table 3 shows differences between numerical and experimental modal frequencies for the beam under consideration, what results from various factors that are not always easy to explain. The proposed rescaling method can be very useful to identify and assign the modal components (numerical and experimental). The first step in rescaling procedure can be pointing out the amplitude predominant components (so called – base mode) and experimental determination of the mode shape for the base mode (see Fig. 3). The second criterion of the base mode chose is physical possibility for mapping the base mode shape. Four transducers were fixed on the considered beam. This configuration allowed for the experimental mapping of the tenth mode shape (corresponding to 1628 Hz). The same mode shape was related with 1366.9 Hz in the FEM analysis. Thus, the global rescaling coefficient equal to about 1.18 could be taken. It is to note that the rescaling process could not always be linear one. Table 3 presents the rescaling results for the first twenty mode frequencies. The components were marked bold for which association of numerical and experimental modal components was possible after rescaling.

References

1. Barczewski R., Application of the Short Time Fourier Transform (STFT) with AFC Correction to Non-linear System Free Vibration Signal Analysis, XIX [th] Symposium Vibration in Physical Systems, Poznań-Błażejewko, May 22-25.2000.
2. Barczewski R., Stress assessment and integrity loss detection of a concrete beam on the basis of backbone curve changes analysis, Proceedings Workshop of COST on NTD Assessment and New Systems in prestressed concrete Structures, NRI Radom -2005, pp.182-187
3. Barczewski R., Short time Rice frequency analysis (STRFA) a method of the time variant vibration signals analysis, XXII Symp. - *Vibrations In Physical Systems* - Poznań-Będlewo 2006
4. Barczewski R., Condition assessment of prestressed concrete structures based on the vibroacoustic signal analysis, Proceedings of the International Symposium *Trends in Continuum Physics* TRECOP'07 Lviv/ Briukhovichi, Ukraine 16-20, September 2007.
5. Kaźmierczak H., Kromulski J., Cempel C., Barczewski R., "Energetic description of the destruction process of steel concrete structures", COST Action 534 New Materials and Systems for Prestressed Concrete Structures, Workshop of COST on NTD Assessment and New Systems in Prestressed Concrete Structures, Radom.
6. Dobry M. W. „Metoda diagnostyki energetycznej w zastosowaniu do rozpoznawania stanu technicznego i obciążenia belek żelbetowych", Diagnostyka Vol. 36 2005 r. Wyd. Polskie Towarzystwo Diagnostyki Technicznej, Uniwersytet Warmińsko – Mazurski w Olsztynie, Olsztyn, pp. 39-44
7. Zielnica J., Barczewski R., Sensitivity analysis of modal frequency shift caused by beam condition change using the FEM simulation New methods for assessment and monitoring of prestressed concrete structures - END PRODUCT of the COST 534 Action, Part III New materials, systems, methods and concepts for durable prestressed concrete structures (in press).